Disease Markers

Biomarkers and Therapeutic Targets of Diabetes Mellitus and its Complications

Lead Guest Editor: Yaoyao Bian
Guest Editors: Hongsheng Zhang and Zhaoqi Dong

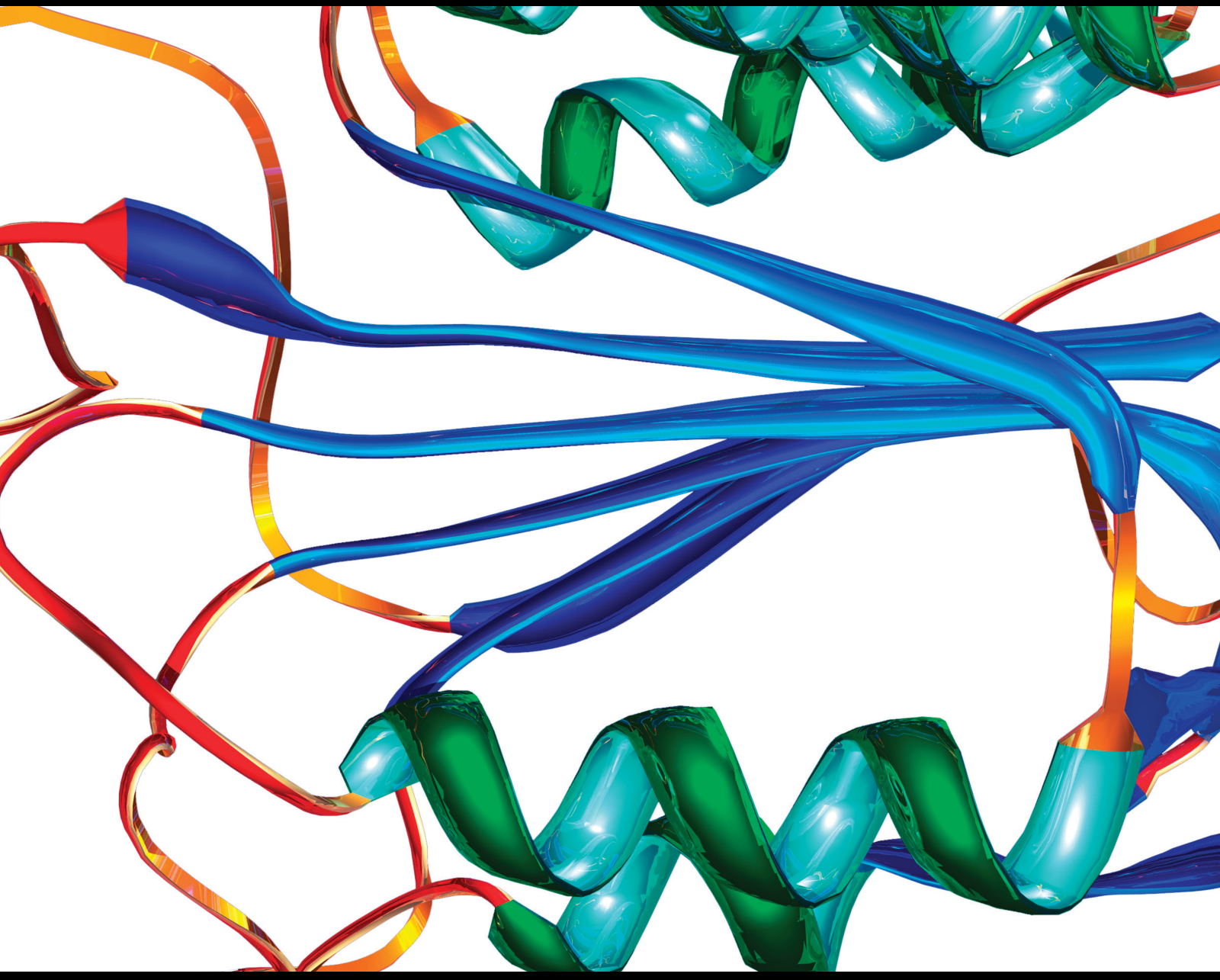

Biomarkers and Therapeutic Targets of Diabetes Mellitus and its Complications

Disease Markers

Biomarkers and Therapeutic Targets of Diabetes Mellitus and its Complications

Lead Guest Editor: Yaoyao Bian
Guest Editors: Hongsheng Zhang and Zhaoqi Dong

Contents

Contents

Study on Correlation between Type 2 Diabetes and No-Reflow after PCI
Su-Rui Zhao, Rui Huang, Fang Liu, Ya Li, Yue Gong, and Jun Xing
Research Article (7 pages), Article ID 7319277, Volume 2022 (2022)

Thyroid-Stimulating Hormone Inhibits Insulin Receptor Substrate-1 Expression and Tyrosyl Phosphorylation in 3T3-L1 Adipocytes by Increasing NF-κB DNA-Binding Activity
Yajing Zhang and Ling Feng
Research Article (9 pages), Article ID 7553670, Volume 2022 (2022)

Analysis of Rehabilitation Effect of Neurology Nursing on Stroke Patients with Diabetes Mellitus and Its Influence on Quality of Life and Negative Emotion Score
Yanhong Yang, Guixia Niu, Qing Mi, Feifei Hong, and Guiqin Zhang
Research Article (7 pages), Article ID 1579928, Volume 2022 (2022)

Glaucocalyxin A Attenuates IL-1β-Induced Inflammatory Response and Cartilage Degradation in Osteoarthritis Chondrocytes via Inhibiting the Activation of NF-κB Signaling Pathway
Weidong Zhu, Yi Zhang, Yueshan Li, and Hao Wu
Research Article (9 pages), Article ID 6516246, Volume 2022 (2022)

Hindawi
Disease Markers
Volume 2022, Article ID 1927688, 12 pages
https://doi.org/10.1155/2022/1927688

Research Article

Exploring Anti-Type 2 Diabetes Mellitus Mechanism of Gegen Qinlian Decoction by Network Pharmacology and Experimental Validation

Weiping Bao,[1] Hongping Sun,[1] Xiang Wu,[2] Juan Xu,[1] Huifeng Zhang,[1] Lin Cao,[1] and Yaofu Fan[1]

[1]*Department of Endocrinology, Affiliated Hospital of Integrated Traditional Chinese and Western Medicine, Nanjing University of Chinese Medicine, Nanjing, Jiangsu, China*
[2]*Department of Geriatrics, Affiliated Hospital of Nanjing University of Chinese Medicine, Nanjing, Jiangsu, China*

Correspondence should be addressed to Lin Cao; guodongcl@163.com and Yaofu Fan; fanyaofu2010@163.com

Received 14 June 2022; Accepted 5 September 2022; Published 15 October 2022

Academic Editor: Atul Kabra

Purpose. Gegen Qinlian Decoction (GGQL) has been employed to treat type 2 diabetes mellitus (T2DM) in the clinical practice of traditional Chinese medicine. However, the underlying mechanism of GGQL in the treatment of T2DM remains unknown. This study was aimed at exploring the pharmacological mechanisms of GGQL against T2DM via network pharmacology analysis combined with experimental validation. *Methods*. The effective components of GGQL were screened, and the target was predicted by using traditional Chinese medicine systems pharmacology database and analysis platform (TCMSP). The candidate targets of GGQL were predicted by network pharmacological analysis, and crucial targets were chosen by the protein-protein interaction (PPI) network. Gene Ontology (GO) and Kyoto Encyclopedia of Genes and Genomes (KEGG) functional enrichment analyses were performed to predict the core targets and pathways of GGQL against T2DM. Then, T2DM mice were induced by a high-fat diet combined with streptozotocin. The model and GGQL groups were given normal saline and GGQL aqueous solution (10 and 20 g/kg/d) intragastric administration, respectively, for 8 weeks. The mice in the GGQLT groups were administered with GGQLT at 10 and 20 g/kg/d, respectively. The pathological changes in liver tissues were observed by hematoxylin-eosin staining. The protein expression of TNF-α and NF-κB was verified by western blotting. *Results*. A total of 204 common targets of GGQL for the treatment of T2DM were obtained from 140 active ingredients and 212 potential targets of T2DM. GO and KEGG enrichment analysis involved 119 signaling pathways, mainly in inflammatory TNF signaling pathways. Animal experiments showed that GGQL significantly reduced the serum levels of body mass, fasting blood glucose, fasting insulin, HOMA-IR, TNF-α, and IL-17. The liver pathological section showed that GGQL could improve the vacuolar degeneration and lipid deposition in the liver of T2DM mice. Mechanistically, GGQL downregulated the mRNA expression of TNF-α and NF-κB. *Conclusions*. This study demonstrated that GGQL may exert antidiabetic effects against T2DM by suppressing TNF-α signaling pathway activation, thus providing a basis for its potential use in clinical practice and further study in treating T2DM.

1. Introduction

More than 90% of people with diabetes are type 2 diabetes mellitus (T2DM), whose pathological characteristics are mainly progressive beta-cell failure or insulin resistance (IR) [1, 2]. According to the International Diabetes Federation (IDF) Global Diabetes Map, the number of T2DM patients worldwide reached 463 million in 2021 [3]. It is estimated that by 2045, there are more than 700 million diabetes patients in the world, which would bring up a large economic burden on society [3]. The goals of diabetes management are to maintain their quality of life by keeping their blood sugar levels as close to normal as possible and within a target range and prevent or delay the development of

various diabetic complications [4]. Over the past decades, a large number of glucose-lowering medications have been approved for clinical use in the control of T2DM, but most drugs have certain adverse reactions, such as hypoglycemia, gastrointestinal symptoms, oedema, osteoporosis, lactic acidosis, and urinary tract infection [5–7]. In addition, the management of complications of T2DM is still a major challenge in clinical practice and a substantial global healthcare burden [8]. Therefore, it is of necessity to explore the safe and effective anti-T2DM drugs for the clinical application.

Since ancient times, various medicinal plants were the first choice to treat diabetes as they are concerned with minimum side effects [9]. In recent years, large-scale clinical trials have confirmed that traditional Chinese medicine (TCM) has made progress in controlling blood glucose levels. An increasing number of studies have shown that Chinese formulae can be used in the prevention and treatment of diabetes through the "Bacteria-Mucosal Immunity-Inflammation-Diabetes" axis [10]. Gegen Qinlian Decoction (GGQL), which consists of *Radix puerariae*, *Radix scutellariae*, *Rhizoma coptidis*, and *Radix glycyrrhizae*, is a famous Chinese medicine prescription. GGQL was first recorded in a famous ancient medicine treatise Shanghan Lun, compiled by Zhong-Jing Zhang in the Han Dynasty of Chinese history (202 BC-220 AD). In previous researches, it has been found that GGQL exerts a range of pharmacological activities, including anti-inflammation, antidiabetic, antioxidant, and immunoregulative effects [11–14]. Our research team has confirmed that GGQL could decrease the fasting blood glucose (FBG) in mice with diabetes and improve the oral glucose tolerance and insulin tolerance in rats with T2DM [15]. These results indicate that GGQL has definite antidiabetic effects. However, the underlying pharmacological mechanisms of action of GGQL and its components in the treatment of T2DM remain unclear. More preclinical evidence is needed.

With the rapid progress of bioinformatics, systems biology, and polypharmacology, network pharmacology has been proven to be a novel strategy to elucidate the active compounds and potential mechanisms of TCM formulas. Therefore, this study was aimed at using network pharmacology to identify potential targets of GGQL as mediators of T2DM, thus providing useful clues for further experimental research. Mice fed a high-fat diet (HFD) combined with streptozotocin were used as a T2DM model to further explore the actions and mechanisms of GGQL against T2DM. This study provides a scientific basis for understanding the effectiveness of multicomponents, multitargets, and compound formulas as well as a new strategy for investigating therapeutic drugs for the treatment of T2DM.

2. Materials and Methods

2.1. Collection and Screening of Bioactive Compounds in GGQL. The active ingredients in GGQL were screened from the traditional Chinese medicine systems pharmacology database and analysis platform (TCMSP) (https://old.tcmsp-e.com/tcmsp.php) by using "Ge Gen", "Huang Qin", "Huang Lian", and "Gan Cao" as keywords to identify targets related to GGQL. Oral bioavailability (OB) ≥ 30% and drug likeness (DL) ≥0.18 were employed to identify the potential active compounds in GGQL. With the help of the UniProt database (https://www.uniprot.org/), the effective compound composition information was converted into the corresponding target gene.

2.2. T2DM Disease Target Collection and Venn Diagram Construction. Using "T2DM" and "type 2 diabetes mellitus" as keywords, details on the human genes associated with T2DM were screened from GeneCards (http://www.genecards.org/), OMIM (https://omim.org/), PharmGkb (http://www.pharmgkb.org/), TTD (http://db.idrblab.net/ttd/), and DrugBank (http://www.drugbank.com/) databases. Repetitive targets were deleted, and all target genes were transformed into human genes by the UniProt database. The harvested GGQL-related targets and T2DM-related targets were subjected to a Venn diagram to determine the intersected targets.

2.3. Construction of GGQL Component-T2DM-Target Interaction Network and Protein-Protein Interaction (PPI) Network. The GGQL-compound-target-T2DM network was constructed by Cytoscape 3.8.2. As previous researches show, intersection targets were imported into the STRING 11.0 database (https://string-db.org/). Species were positioned as "Human," and the confidence threshold was set as >0.90. The selected proteins were introduced into Cytoscape 3.8.2 software to construct PPI networks, and the node connectivity was analyzed to screen out the core targets.

2.4. Gene Ontology (GO) Functional Annotation and Kyoto Encyclopedia of Genes and Genomes (KEGG) Pathway Analysis. R software, a free software environment for statistical computing and graphics, was used to perform GO and KEGG functional enrichment analyses for the key targets. The threshold value was $P < 0.05$. GO analysis analyzed the functional level of potential target genes from three aspects: biological process (BP), cell composition (CC), and molecular function (MF). KEGG analysis showed that GGQL interfered with the biological pathway of T2DM. The top 10 items of GO analysis and the top 20 items of KEGG analysis identified from R software were mapped as bubble plots.

2.5. Animal. 40 C57BL/6J mice, male, SPF grade, 12 weeks old, were purchased from Shanghai Shrek Experimental Animal Co., Ltd., license number: SCXK (Shanghai) 2017-0005, feeding condition, relative humidity 50%, Mel 70%. The feeding and experimental process of the animals involved in the experiment followed the relevant guidelines for the management and protection of experimental animals in the Hospital of Integrated Traditional Chinese and Western Medicine affiliated to Nanjing University of Traditional Chinese Medicine (reference number: AEWC-20190814-81).

2.6. Drugs, Reagents, and Instruments. All pieces of traditional Chinese medicine in GGQL were purchased from the Hospital of Integrated Traditional Chinese and Western Medicine affiliated to Nanjing University of Traditional

Table 1: Active components of GGQL (top 20 of OB).

Mol ID	Active components	OB (%)	DL
MOL002907	Corchoroside A_qt	104.95	0.78
MOL002934	Neobaicalein	104.34	0.44
MOL002311	Glycyrol	90.78	0.67
MOL008647	Moupinamide	86.71	0.26
MOL004990	7,2′,4′-Trihydroxy-5-methoxy-3-arylcoumarin	83.71	0.27
MOL004904	Licopyranocoumarin	80.36	0.65
MOL004891	Shinpterocarpin	80.3	0.73
MOL005017	Phaseol	78.77	0.58
MOL004841	Licochalcone B	76.76	0.19
MOL002932	Panicolin	76.26	0.29
MOL004810	Glyasperin F	75.84	0.54
MOL001484	Inermine	75.18	0.54
MOL000500	Vestitol	74.66	0.21
MOL012246	5,7,4′-Trihydroxy-8-methoxyflavanone	74.24	0.26
MOL005007	Glyasperins M	72.67	0.59
MOL004941	(2R)-7-Hydroxy-2-(4-hydroxyphenyl) chroman-4-one	71.12	0.18
MOL004959	1-Methoxyphaseollidin	69.98	0.64
MOL000392	Formononetin	69.67	0.21
MOL002927	Skullcapflavone II	69.51	0.44
MOL002911	2,6,2′,4′-Tetrahydroxy-6′-methoxychaleone	69.04	0.22

Chinese Medicine. The quality ratio of Gegen (batch number: 20170301), Huangqin (batch number: 1610009), Huanglian (batch number: 1703015), and Gancao (batch number: 170109) was prepared according to the ratio of 8 : 3 : 3 : 2. The preparation of GGQL was made according to the method described in the literature [16]. Pioglitazone hydrochloride tablets (batch number H20110048, Jiangsu Deyuan Pharmaceutical Co., Ltd.). The tumor necrosis factor-α (TNF-α) and interleukin-17 (IL-17) ELISA kits were purchased from Jiangsu Biyuntian Biotechnology Co., Ltd.; the TNF-α, nuclear factor kappa-B (NF-κB), and β actin antibodies were purchased from the American Abcam company; and the second anti-rabbit was purchased from the American CST company. The biospectrum-gel imaging system was from Bio-Rad company, USA; tissue slicer from Leica company, Germany; and optical microscope from Olympus company, Japan.

2.7. Modeling and Drug Delivery. After 1 week of adaptive feeding, 40 C57BL/6J mice were randomly divided into a normal fat diet group (NFD group, $n = 8$) and HFD group ($n = 32$). The HFD group was fed with high-fat diet (purchased from Nantong Tolofei Feed Technology Co., Ltd., batch number 2017416, with a formula of 60% high-fat model feed). After 4 weeks of feeding, 1% streptozotocin solution 45 mg kg-^{1} was injected intraperitoneally (lasting 3 days). 72 hours after injection, random blood glucose ≥ 16.7 mmol/L was detected in the tail vein, and T2DM modeling was successful. HFD group mice were equally divided into 4 groups: HFD group (received saline 10 ml/kg/d), pioglitazone group (PIO group, received pioglitazone 30 mg/kg/d), low-dose GGQL group (GGQLL group, received GGQL 10 mg/kg/d), and high-dose GGQL group (GGQLH group, received GGQL 20 mg/kg/d). The NFD group was also administrated with saline (10 ml/kg/day). All these doses were given via oral gavage daily for 8 weeks. The weight of mice was weighed every week to adjust the dose of intragastric administration.

2.8. Biochemical Analysis and Histopathological Examination. At the end of the experiment, abdominal aortic blood samples were taken after the last dose. The serum sample was used to measure the levels of FBG. Kits were purchased from Nanjing Jiancheng Bioengineering Institute (Nanjing, China). The plasma insulin (FINS), TNF-α, and IL-17 were measured by ELISA Assay Kit (ALPCO, USA). Homeostasis model assessment of insulin resistance index (HOMA-IR) was calculated using the previously described formula: HOMA-IR = FINS × FBG/22.5. 10% formalin-fixed liver tissues were embedded in paraffin, cut into 4 μm thick sections, and then stained with hematoxylin and eosin (H&E) for histopathological examination. Sections were examined, and digital pictures were captured using an Olympus digital camera (BX20, Beijing, China) using NIS Element SF 4.00.06 software (Beijing, China) and photographed at 200× magnification for analysis.

2.9. Western Blotting. Western blotting analysis of proteins was carried out as previously reported [15]. The liver tissue of 100 mg was homogenized, and the total protein was extracted according to the instructions of the whole protein extraction kit. The concentration of total protein was

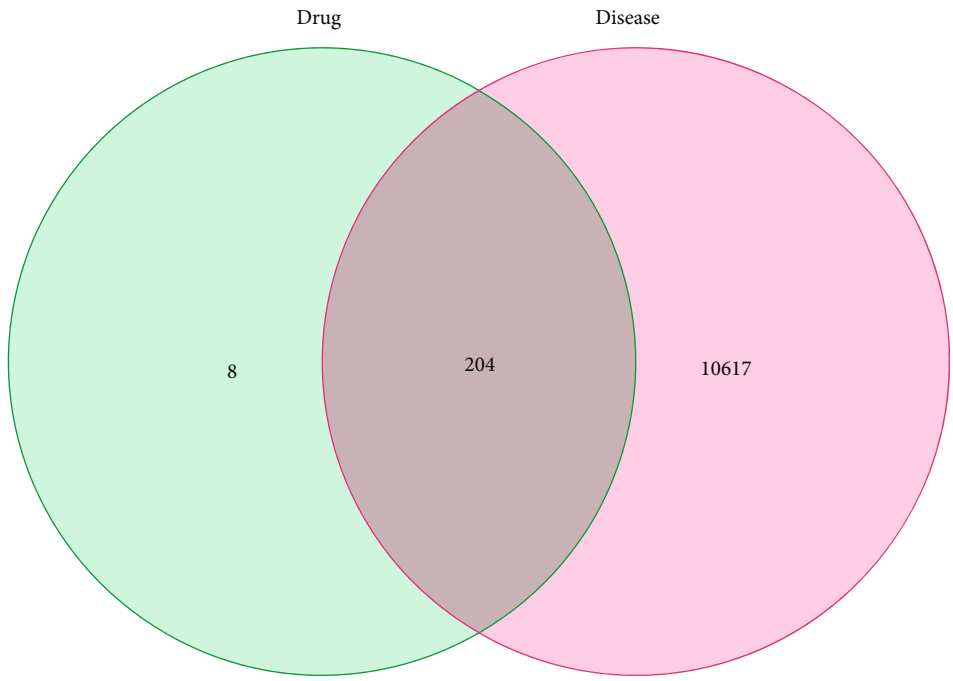

(a)

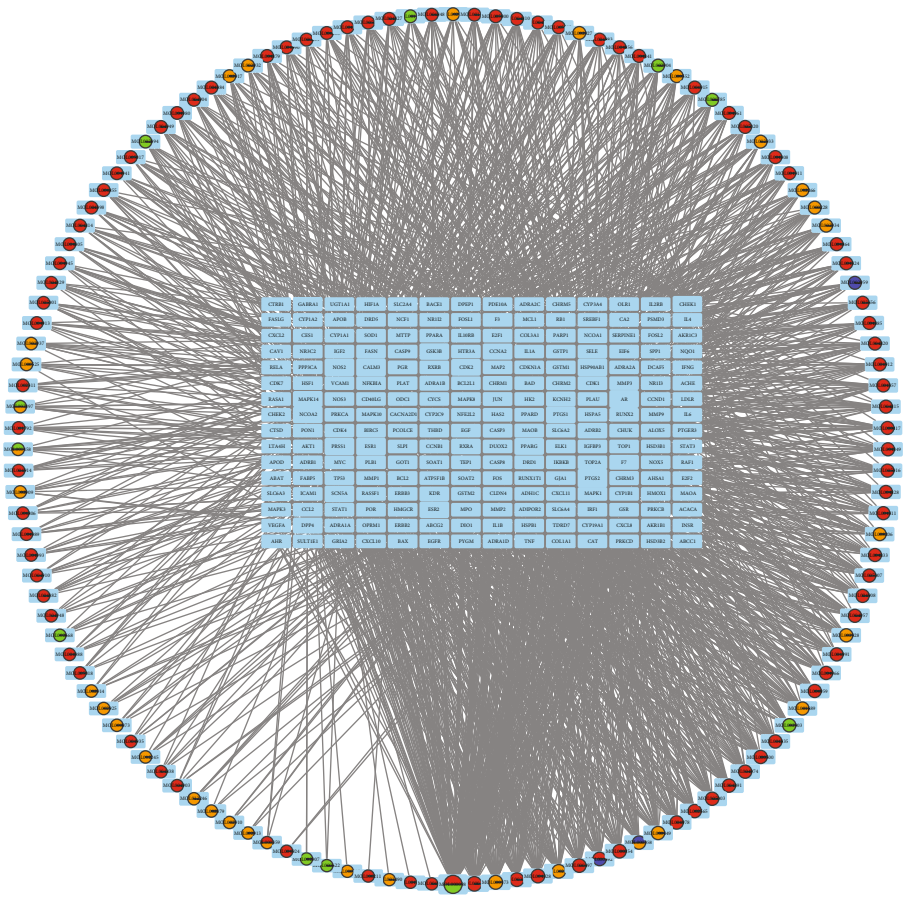

(b)

Figure 1: Potential GGQL targets treat T2DM and network analysis. (a) Venn diagram summarizing the intersection targets of the GGQL and T2DM. (b) Network of targets shared between GGQL and T2DM. The ring represented the composition, and the rectangle represented target genes.

Table 2: The top 10 key active ingredients of GGQL in the treatment of T2DM.

Molecular ID	Ingredient	Degree	Source	OB (%)	DL
MOL000098	Quercetin	135	Gancao Huanglian	46.43	0.28
MOL000422	Kaempferol	54	Gancao	41.88	0.24
MOL000173	Wogonin	40	Huangqin	30.68	0.23
MOL003896	7-Methoxy-2-methyl isoflavone	35	Gancao	42.56	0.20
MOL004328	Naringenin	34	Gancao	59.29	0.21
MOL002714	Baicalein	31	Huangqin	33.52	0.21
MOL000392	Formononetin	30	Gancao Gegen	69.67	0.21
MOL000497	Licochalcone A	30	Gancao	40.79	0.29
MOL000354	Isorhamnetin	29	Gancao	49.60	0.31
MOL002565	Medicarpin	26	Gancao	49.22	0.34

determined by BCA kit, and the same amount of protein was electrophoretic by 10%SDS-PAGE. After being transferred to polyvinylidene fluoride (PVDF) membrane, 5% skim milk was used to seal the protein at room temperature for 2 hours. Protein gel electrophoresis was carried out according to the western blot method, and a gel imaging analysis system was used to detect protein bands.

2.10. Statistical Analysis. All data were expressed as mean ± SEM. Results were tested for normal distribution, then were analyzed using ANOVA followed by Bonferroni post hoc test using GraphPad Prism 5.01 (GraphPad Software Inc., San Diego, CA, USA). P values < 0.05 were considered as statistically significant.

3. Results

3.1. GGQL Active Compound Network Analysis. GGQL obtained a total of 146 chemical components after searching the TCMSP database, with 4 compounds from Gegen, 36 compounds from Huangqin, 14 compounds from Huanglian, and 92 compounds from Gancao. There are 140 components after deleting the duplicate value, and the top 20 items of active components are shown in Table 1. Correcting based on the UniProt database, we obtained 212 targets in total.

3.2. Potential GGQL Targets Treat T2DM and Network Analysis. To elucidate the mechanism and pharmacodynamics of GGQL, 10821 target genes of T2DM were obtained from GeneCards, OMIM, PharmGkb, TTD, and DrugBank databases. Further analysis with Venn diagrams identified 204 targets associated with both T2DM and GGQL that are displayed in Figure 1(a). Then, to elucidate the relationship between active ingredients and potential targets as well as T2DM, an ingredient-target-disease network was constructed by Cytoscape 3.8.2 software, consisting of 349 nodes and 1989 edges (Figure 1(b)). The top 10 key active ingredients of GGQL in the treatment of T2DM are enumerated in Table 2.

3.3. PPI Network Construction and Key Targets. To elucidate the potential mechanism by which GGQL protects against T2DM, PPI relationships of the 204 target genes were obtained using the STRING tool, and the results are displayed in Figure 2(a). Then, we used the Cytoscape software to calculate the topological parameters, and 18 core targets were obtained. The top 10 key targets in the core position were JUN, AKT1, STAT3, MAPK3, FOS, MAPK1, MYC, MAPK14, ERS1, and TP53, as shown in Figure 2(b).

3.4. Pathway and GO Term Enrichment Analysis. The drug-disease common targets were processed by R language for GO function and KEGG pathway enrichment analysis. The GO enrichment bubble chart was formed by selecting the top 10 significant biological process (BP), cellular components (CC), and molecular function (MF), as shown in Figure 3.

To explore the signal pathway mechanism of GGQL in the treatment of T2DM, we performed KEGG enrichment analysis. As shown in Figure 4, it shows the first 20 signal pathways, which involve the TNF signaling pathway, IL-17 signaling pathway, and so on. The key KEGG pathway and the location of T2DM and overlapping genes of enriched pathways are listed in Figure 5.

3.5. GGQL Ameliorated IR in HFD Mice. Figure 6(a) shows that within HFD-fed mice, treatment with GGQLL or GGQLH could alter body weight compared with HFD mice, but these were not statistically significant. The HFD-fed group mice led to a marked elevation in the levels of fasting glucose, fasting insulin, and HOMA-IR in the serum region compared with those of the control group, as shown in Figures 6(b)–6(d).

3.6. Effects of GGQL on Hepatic Tissue. The HE staining of the liver tissue of mice in each group is shown in Figure 7. The results showed that, compared with the NFD group, lipid deposition, vacuolar degeneration, and watery degeneration were observed in the liver of the HFD group.

3.7. Effects of GGQL on the TNF Signaling Pathway in T2DM Mice. The network pharmacology results demonstrated that

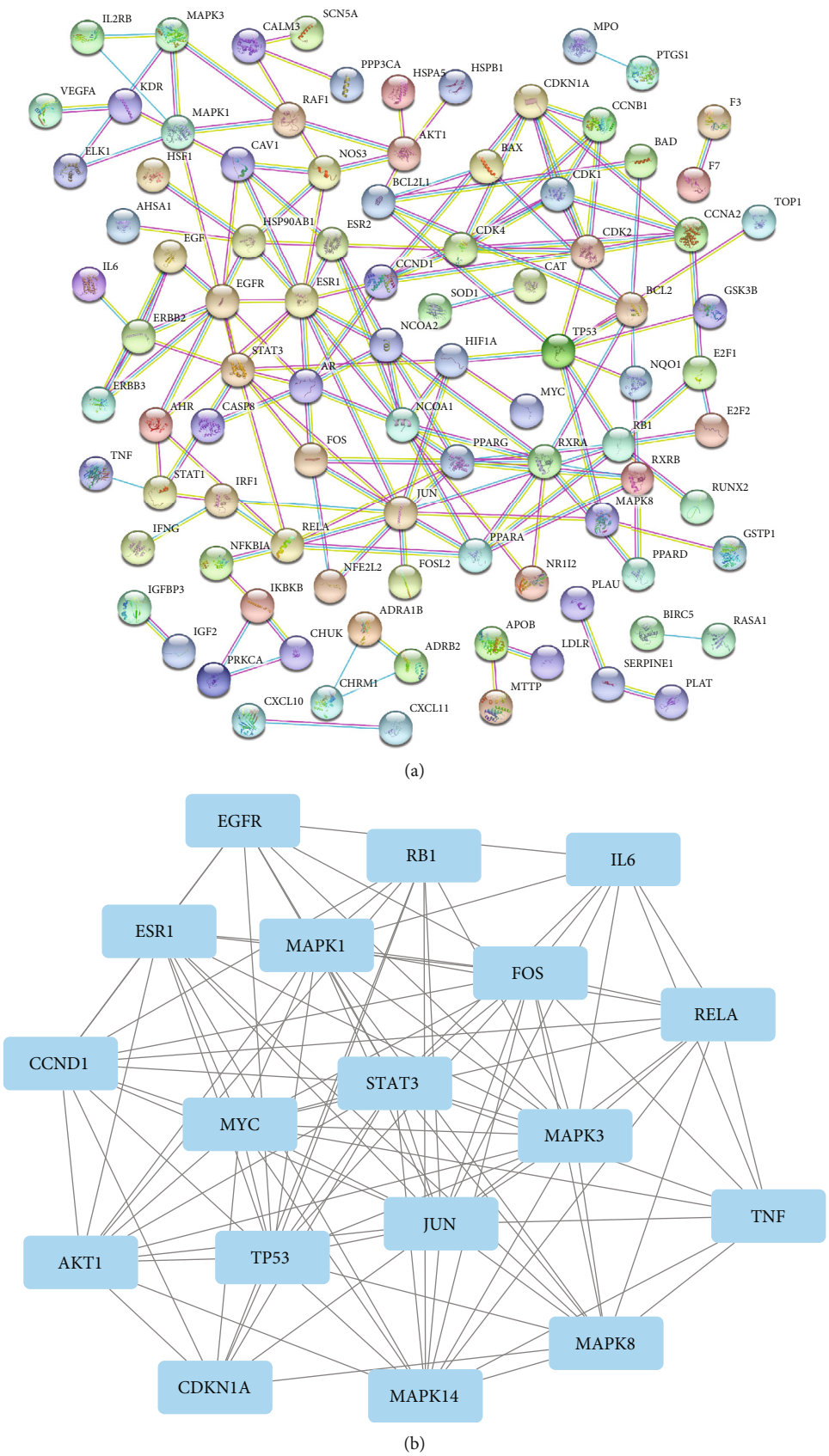

Figure 2: PPI network construction and key targets. (a) PPI network of potential targets of GGQL for the treatment of T2DM. (b) Obtaining 18 core proteins of GGQL for T2DM.

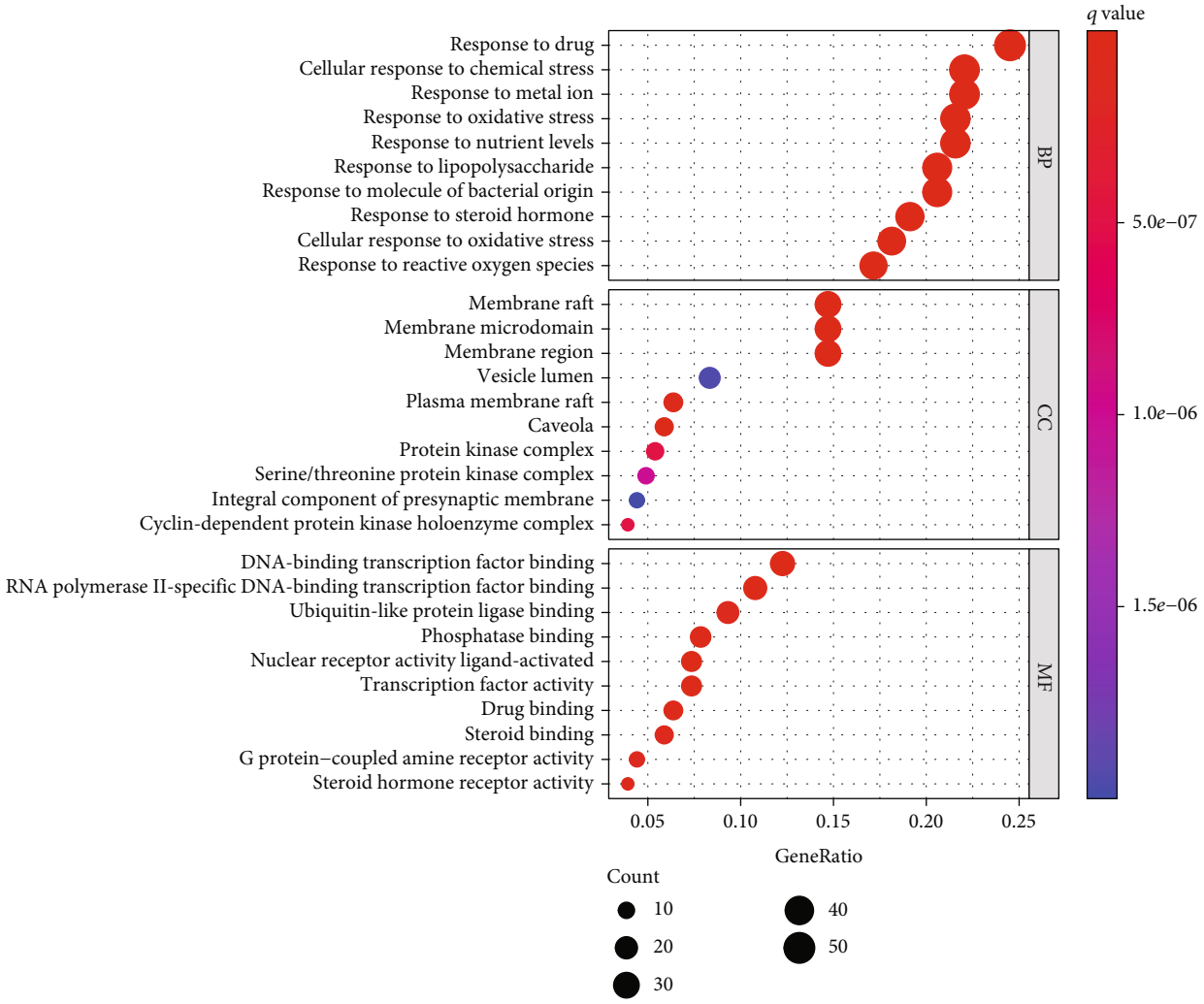

Figure 3: Top 10 GO terms of hub genes.

the potential targets of GGQL against T2DM were significantly enriched in the TNF pathways. Compared with the NFD group, the expression of TNF-α and NF-κB in the HFD group increased, while the expression of TNF-α and NF-κB in the GGQLL, GGQLH, and PIO groups decreased significantly compared with that in the HFD group (all $P < 0.01$) (Figure 8).

4. Discussion

The incidence of T2DM has been rising in recent years due to the aging of the population and changes in lifestyle [17, 18]. Currently, oral antidiabetic drugs are mainly focused on a single compound and reported to have adverse effects [19]. TCM has a rich history and has shown good results in the treatment of T2DM. Hence, TCM may be a prospective option for T2DM intervention. Due to TCM's effectiveness depending on multitarget and multicomponent, it is difficult to explore its mechanism of action. This study draws lessons from the research ideas of network pharmacology, through the analysis of various networks to identify multicomponents and multitargets involved in the treatment of T2DM by GGQL.

According to the network pharmacology analysis, we obtained 140 active compounds from GGQL that acted on 212 targets of T2DM. The active compounds were mainly flavonoids. According to the degree value, the top three active ingredients were quercetin, kaempferol, and wogonin. Quercetin is a natural polyhydroxyflavone, which can reduce the level of oxidative stress, inhibit apoptosis of INS-1 cell, and promote insulin secretion [20]. A large cross-sectional study in China showed that quercetin intake was negatively correlated with the prevalence of T2DM [21]. Kaempferol can increase the activities of AKT and hexokinase, decrease the activity of glucose-6 phosphatase in the liver, and play a hypoglycemic effect by inhibiting gluconeogenesis in the liver [22]. Wogonin can promote glucose uptake and glycolysis through the insulin receptor-1/PI3K/alkaline phosphatase pathway, inhibit gluconeogenesis in hepatocytes, and improve insulin resistance [23]. Therefore, all of these findings showed that multiple components of GGQL had a positive effect on T2DM.

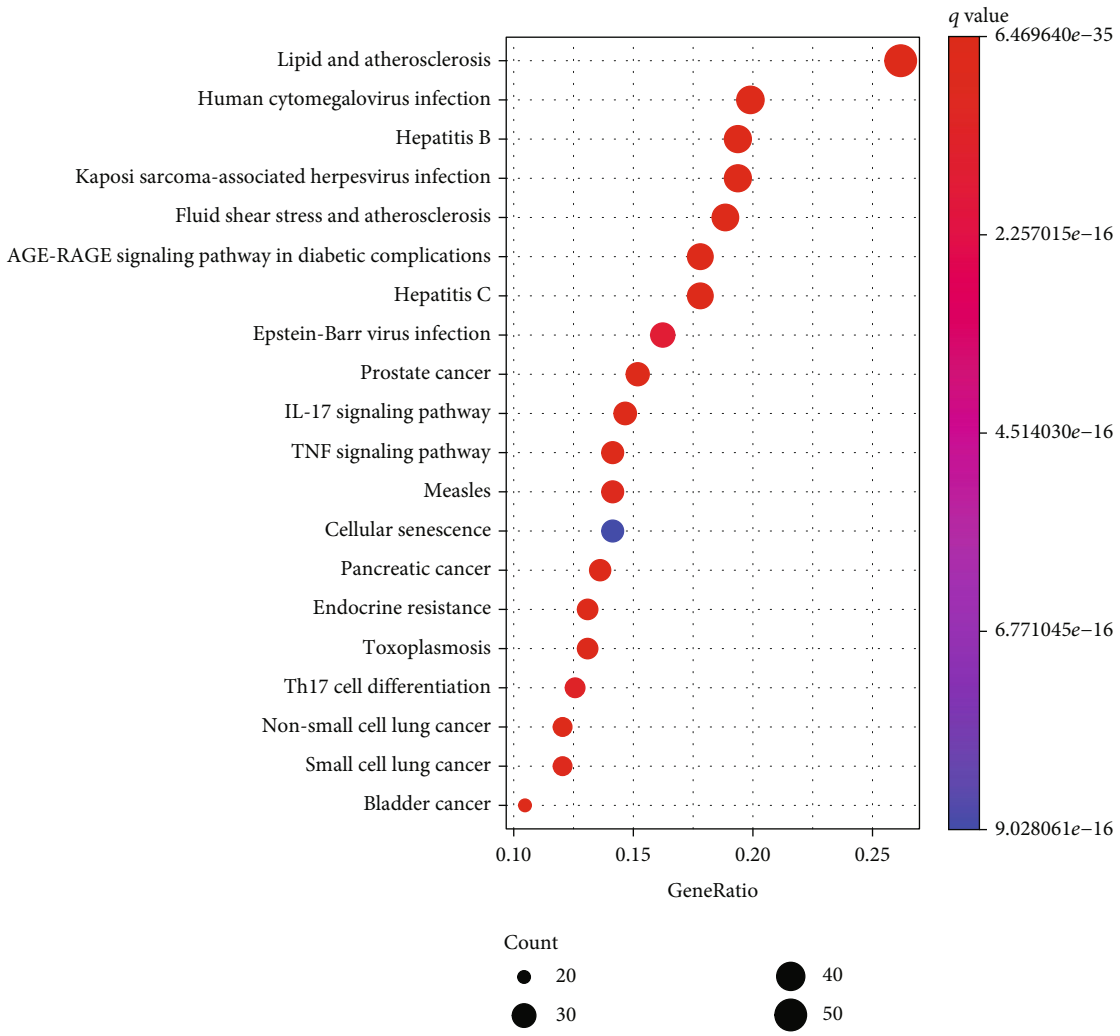

Figure 4: Top 30 KEGG pathways of hub genes.

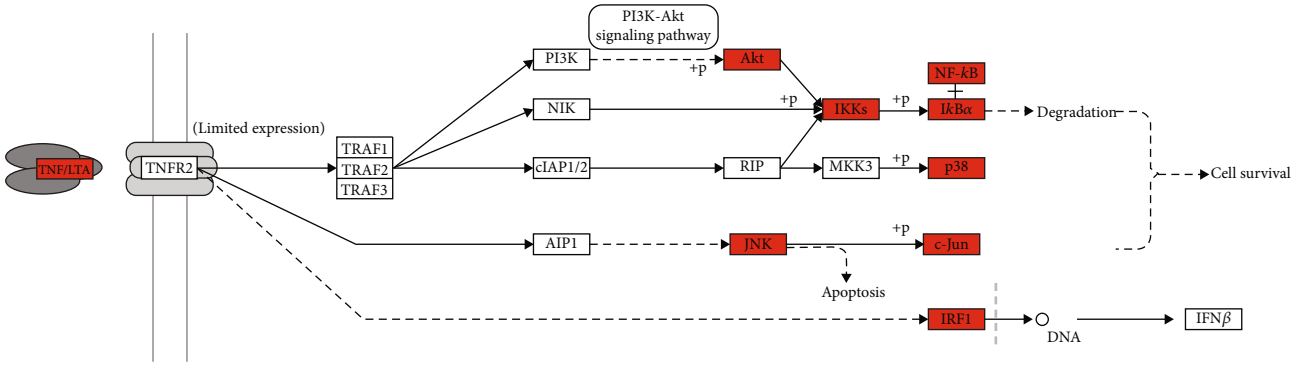

Figure 5: The key KEGG pathway: TNF signaling pathway. The red nodes represent overlapping targets between GGQL and T2DM.

18 key genes were screened by constructing PPI network and performing network topology structure with Cytoscape software, including JUN, AKT1, and STAT3. JUN is an important signal molecule connecting inflammation and insulin resistance. Studies have confirmed that high glucose-induced apoptosis can be inhibited by inhibiting the JUN signal pathway [24, 25]. Increasing the expression of AKT1 in islet cells can reduce islet cell apoptosis and increase secretory function [26, 27]. STAT3, a signal transducer and activator of transcription 3, is highly expressed in T2DM patients. Animal studies have found that inhibiting the expression of STAT3 in obese rats can prevent the

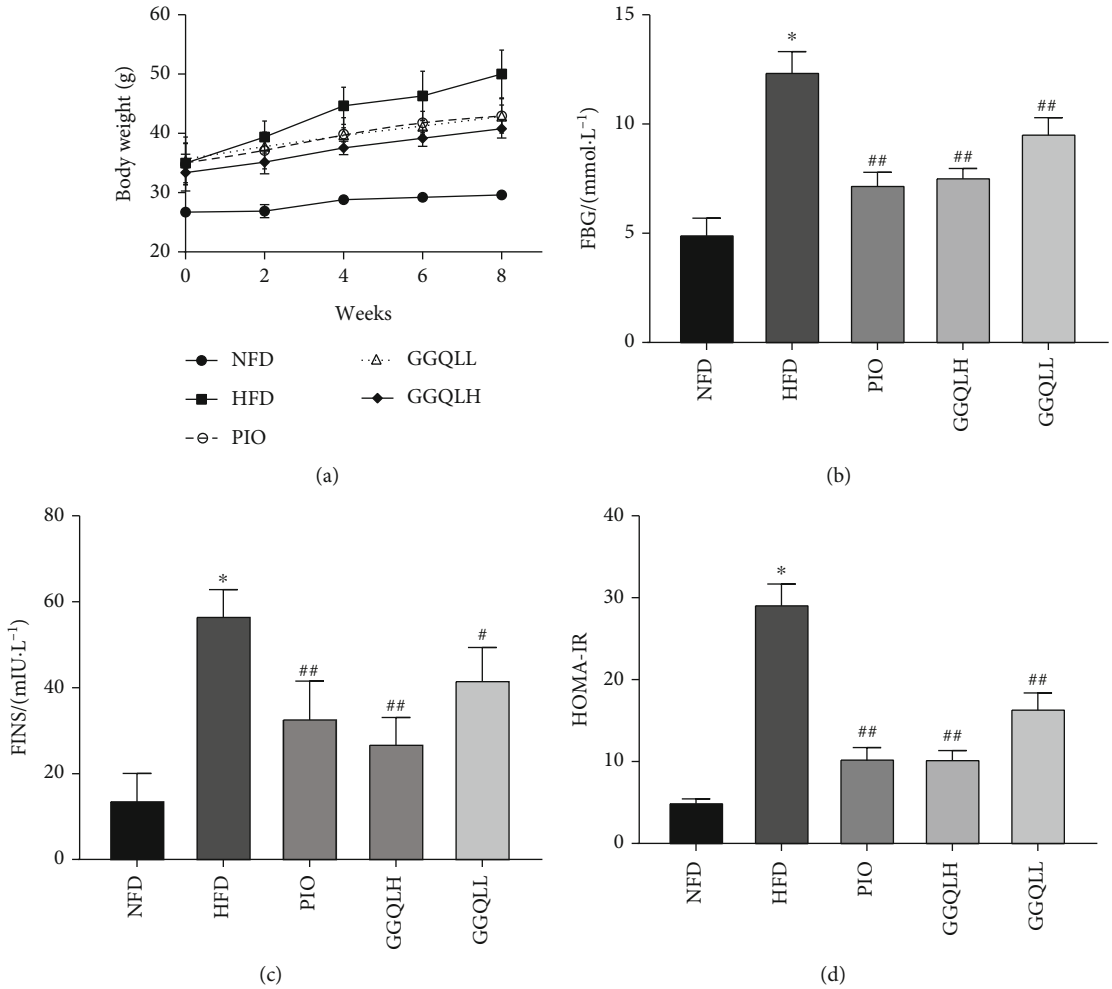

Figure 6: (a) Body weight was measured every week during the treatment period. The expression of serum (b) glucose and (c) insulin concentration. (d) HOMA-IR was calculated at the end of the experiment. $^{*}P < 0.05$; $^{\#\#}P < 0.01$. Data are expressed as the means ± SEM of at least three independent experiments.

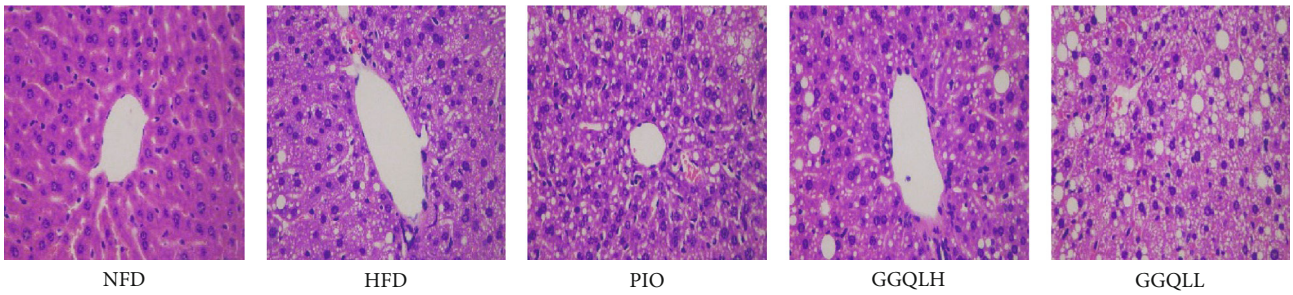

Figure 7: Effects of GGQL on hepatic pathological changes. Histological observation of the hematoxylin and eosin (H&E) sections (original magnification ×400). Macrovesicular steatosis was observed in the livers of mice.

development of lipid-induced insulin resistance and reduce the incidence of diabetes [28, 29].

In addition, the GO enrichment analysis showed that the pharmacological effects of GGQL on T2DM were related to TNF signaling. The target points in the KEGG enrichment analysis were also enriched in the TNF-α signaling pathway. In recent years, with the in-depth study of the pathogenesis of T2DM, many scholars believe that T2DM may be an immune inflammatory disease, in which TNF-α is involved in the regulation of inflammatory response and glucose and lipid metabolism [30, 31]. Skuratovskaia et al. found that TNF-α can inhibit the phosphorylation of insulin receptor substrate-1, which leads to insulin resistance in liver and adipocytes, and increases the progression of T2DM [32]. In

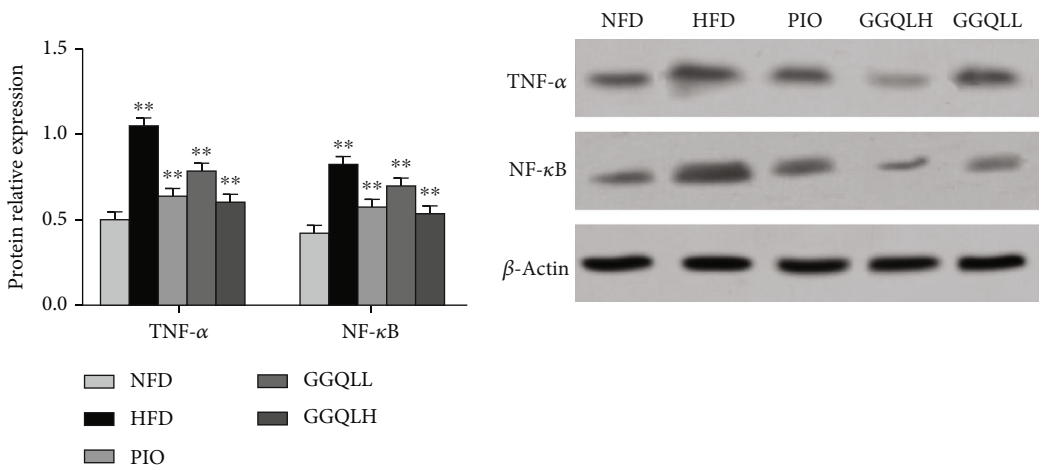

Figure 8: Western blot and densitometric analysis of the expression of TNF-α, NF-κB, and β-action in mice. $^{**}P < 0.01$ compared to the NFD group, which was considered statistically significant.

addition, a previous study has shown that TNF-α can not only induce the occurrence of diabetes but also cause damage to vascular endothelial function, initiate the process of atherosclerosis, and increase the risk of various complications of diabetes [33]. All the above studies have shown that the TNF-α signaling pathway plays an important role in T2DM. Animal experiments showed that GGQL can effectively reduce the levels of insulin, HOMA-IR, TNF-α, and IL-17 and improve the state of hyperglycemia. We also found that the protein expression levels of TNF-α and NF-κB in the liver tissues of HFD mice were significantly increased, While GGQL could restore them. Many other scholars' studies are consistent with our findings. Xu et al. found that GGQL suppressed activation of NF-κB and TNF-α to inhibit T2DM development [14]. Li et al. revealed that GGQL could reduce the TLR4 expression and NF-κB activation along with several inflammatory cytokines such as TNFα and IL-6 [34].

However, there are still several limitations in our study to be solved in the future work. One was the study only performed in vivo experiments, which lacked corresponding cellular experiments to validate the function and mechanism of GGQL on T2DM. In the future, we will conduct cellular experiments to better prove the results. Second, we only explored one pathway that we think is more likely to work. As we did not verify other possible pathways, we cannot verify whether GGQL can participate in other pathways to make a synergistic antidiabetic effect. Third, although the TNF-α signaling pathway was verified to be involved in mechanism of action, the potential upstream or downstream relationships between TNF-α still need to be further explored.

5. Conclusions

In the present study, we combined network pharmacology prediction and in vivo experiments to research the active ingredients, potential targets, and potential mechanism of GGQL against T2DM. The results suggest that GGQL ameliorates blood sugar by improving IR and inhibiting inflammation. These effects appear to be related to GGQL affecting the TNF-α signaling pathways. This work supplies a foundation for the treatment of endocrine disorder-related complex diseases with TCM and lays a certain theoretical foundation for further exploration to expand the application of GGQL. Detailed pharmacological mechanisms by which GGQL ameliorates T2DM will be investigated in our future study.

Data Availability

The data are available upon direct request to the corresponding authors.

Conflicts of Interest

The authors declare that they have no competing interests.

Authors' Contributions

Weiping Bao, Hongping Sun, and Xiang Wu contributed equally to this work.

Acknowledgments

This study was financially supported by the Medical Scientific Research Project of Jiangsu Provincial Health Commission (grant No. M2021086) and National Natural Science Foundation of China (No. 82274445) of F.YF.

References

[1] B. Yin, Y. M. Bi, G. J. Fan, and Y. Q. Xia, "Molecular mechanism of the effect of Huanglian Jiedu decoction on type 2 diabetes mellitus based on network pharmacology and molecular docking," *Journal of Diabetes Research*, vol. 2020, Article ID 5273914, 24 pages, 2020.

[2] R. Sharma and P. K. Prajapati, "Diet and lifestyle guidelines for diabetes: evidence based ayurvedic perspective," *Romanian Journal of Diabetes Nutrition and Metabolic Diseases*, vol. 21, no. 4, pp. 335–346, 2014.

[3] P. Saeedi, I. Petersohn, P. Salpea et al., "Global and regional diabetes prevalence estimates for 2019 and projections for 2030 and 2045: Results from the International Diabetes Federation Diabetes Atlas, 9th edition," *Diabetes Research and Clinical Practice*, vol. 157, p. 107843, 2019.

[4] M. Janghorbani, B. Papi, and M. Amini, "Current status of glucose, blood pressure and lipid management in type 2 diabetes clinic attendees in Isfahan, Iran," *Journal of Diabetes Investigation*, vol. 6, no. 6, pp. 716–725, 2015.

[5] J. A. Hirst, A. J. Farmer, R. Ali, N. W. Roberts, and R. J. Stevens, "Quantifying the effect of metformin treatment and dose on glycemic control," *Diabetes Care*, vol. 35, no. 2, pp. 446–454, 2012.

[6] M. Tacelli, C. Celsa, B. Magro et al., "Antidiabetic drugs in NAFLD: the accomplishment of two goals at once," *Pharmaceuticals (Basel)*, vol. 11, no. 4, p. 121, 2018.

[7] R. Sim, C. W. Chong, N. K. Loganadan et al., "Comparative effectiveness of cardiovascular, renal and safety outcomes of second-line antidiabetic drugs use in people with type 2 diabetes: a systematic review and network meta-analysis of randomised controlled trials," *Diabetic Medicine*, vol. 39, no. 3, p. e14780, 2022.

[8] R. Goodall, A. Alazawi, W. Hughes et al., "Trends in type 2 diabetes mellitus disease burden in European Union countries between 1990 and 2019," *Scientific Reports*, vol. 11, no. 1, p. 15356, 2021.

[9] Y. Jin, Z. L. Huang, L. Li et al., "Quercetin attenuates toosendanin-induced hepatotoxicity through inducing the Nrf2/GCL/GSH antioxidant signaling pathway," *Acta Pharmacologica Sinica*, vol. 40, no. 1, pp. 75–85, 2019.

[10] Z. Gao, Q. Li, X. Wu, X. Zhao, L. Zhao, and X. Tong, "New insights into the mechanisms of Chinese herbal products on diabetes: a focus on the bacteria-mucosal immunity-inflammation-diabetes axis," *Journal of Immunology Research*, vol. 2017, Article ID 1813086, 13 pages, 2017.

[11] Y. Ren, P. Xiong, C. Zhong, P. Zhang, and B. Jia, "The effect of Gegen Qinlian Decoction on clinical prognosis and islet function for type 2 diabetic mellitus: a protocol for systematic review and meta-analysis," *Medicine (Baltimore)*, vol. 100, no. 5, p. e24210, 2021.

[12] L. Ren, Y. Cheng, and F. Qin, "Herbal formula Gegen-Qinlian Decoction for type 2 diabetes mellitus: a meta-analysis of randomized controlled trials," *Evidence-based Complementary and Alternative Medicine*, vol. 2020, Article ID 3907920, 11 pages, 2020.

[13] L. He, T. Bao, Y. Yang et al., "Exploring the pathogenesis of type 2 diabetes mellitus intestinal damp-heat syndrome and the therapeutic effect of Gegen Qinlian Decoction from the perspective of exosomal miRNA," *Journal of Ethnopharmacology*, vol. 285, p. 114786, 2022.

[14] Y. Xu, J. Huang, N. Wang et al., "Network pharmacology-based analysis and experimental exploration of antidiabetic mechanisms of Gegen Qinlian Decoction," *Frontiers in Pharmacology*, vol. 12, p. 649606, 2021.

[15] M. Sui, G. F. Chen, X. D. Mao et al., "Gegen Qinlian Decoction ameliorates hepatic insulin resistance by silent information regulator1 (SIRT1)-dependent deacetylation of forkhead box O1 (FOXO1)," *Medical Science Monitor*, vol. 25, pp. 8544–8553, 2019.

[16] M. Sui, X. F. Jiang, H. P. Sun, C. Liu, and Y. Fan, "Berberine ameliorates hepatic insulin resistance by regulating microRNA-146b/SIRT1 pathway," *Diabetes Metabolic Syndrome and Obesity-Targets and Therapy*, vol. 14, pp. 2525–2537, 2021.

[17] R. Sharma, R. Bolleddu, J. K. Maji, G. Ruknuddin, and P. K. Prajapati, "In-vitro α-amylase, α-glucosidase inhibitory activities and in-vivo anti-hyperglycemic potential of different dosage forms of Guduchi (Tinospora Cordifolia Willd. Miers) prepared with Ayurvedic Bhavana process," *Frontiers in Pharmacology*, vol. 10, p. 642300, 2021.

[18] R. Sharma, N. Martins, A. Chaudhary et al., "Adjunct use of honey in diabetes mellitus: a consensus or conundrum," *Trends in Food Science & Technology*, vol. 106, pp. 254–274, 2020.

[19] R. Sharma, H. Amin, and P. K. Prajapati, "Yoga: as an adjunct therapy to trim down the Ayurvedic drug requirement in non insulin-dependent diabetes mellitus," *Ancient Science of Life*, vol. 33, no. 4, pp. 229–235, 2014.

[20] H. Jiang, Y. Yamashita, A. Nakamura, K. Croft, and H. Ashida, "Quercetin and its metabolite isorhamnetin promote glucose uptake through different signalling pathways in myotubes," *Scientific Reports*, vol. 9, no. 1, p. 2690, 2019.

[21] Q. U. Ahmed, M. N. Sarian, S. Z. Mat So'ad et al., "Methylation and acetylation enhanced the antidiabetic activity of some selected flavonoids: in vitro, molecular modelling and structure activity relationship-based study," *Biomolecules*, vol. 8, no. 4, p. 149, 2018.

[22] Z. Yao, Y. Gu, Q. Zhang et al., "Estimated daily quercetin intake and association with the prevalence of type 2 diabetes mellitus in Chinese adults," *European Journal of Nutrition*, vol. 58, no. 2, pp. 819–830, 2019.

[23] D. Gao, J. Jiao, Z. Wang et al., "The roles of cell-cell and organ-organ crosstalk in the type 2 diabetes mellitus associated inflammatory microenvironment," *Cytokine Growth Factor Reviews*, vol. S1359-6101, no. 22, p. 00024-7, 2022.

[24] H. Kaneto, Y. Nakatani, D. Kawamori et al., "Role of oxidative stress, endoplasmic reticulum stress, and c-Jun N-terminal kinase in pancreatic beta-cell dysfunction and insulin resistance," *International Journal of Biochemistry & Cell Biology*, vol. 38, no. 5-6, pp. 782–793, 2006.

[25] Y. Zhao, H. Sun, X. Li, Y. Zha, and W. Hou, "Hydroxysafflor yellow A attenuates high glucose-induced pancreatic β-cells oxidative damage via inhibiting JNK/c-jun signaling pathway," *Biochemical and Biophysical Research Communications*, vol. 505, no. 2, pp. 353–359, 2018.

[26] Z. Peng, R. Aggarwal, N. Zeng et al., "AKT1 regulates endoplasmic reticulum stress and mediates the adaptive response of pancreatic β cells," *Molecular and Cellular Biology*, vol. 40, no. 11, p. e00031, 2020.

[27] T. M. Albury-Warren, V. Pandey, L. P. Spinel, M. M. Masternak, and D. A. Altomare, "Prediabetes linked to excess glucagon in transgenic mice with pancreatic active AKT1," *Journal of Endocrinology*, vol. 228, no. 1, pp. 49–59, 2016.

[28] F. Mashili, A. V. Chibalin, A. Krook, and J. R. Zierath, "Constitutive STAT3 phosphorylation contributes to skeletal muscle insulin resistance in type 2 diabetes," *Diabetes*, vol. 62, no. 2, pp. 457–465, 2013.

[29] C. Bi, Y. Fu, and B. Li, "Brain-derived neurotrophic factor alleviates diabetes mellitus-accelerated atherosclerosis by promoting M2 polarization of macrophages through repressing the STAT3 pathway," *Cellular Signalling*, vol. 70, p. 109569, 2020.

[30] S. Gupta, A. Maratha, J. Siednienko et al., "Analysis of inflammatory cytokine and TLR expression levels in type 2 diabetes

with complications," *Scientific Reports*, vol. 7, no. 1, p. 7633, 2017.

[31] R. Fadaei, N. Bagheri, E. Heidarian et al., "Serum levels of IL-32 in patients with type 2 diabetes mellitus and its relationship with TNF-α and IL-6," *Cytokine*, vol. 125, p. 154832, 2020.

[32] D. Skuratovskaia, P. Zatolokin, M. Vulf, I. Mazunin, and L. Litvinova, "Interrelation of chemerin and TNF-α with mtDNA copy number in adipose tissues and blood cells in obese patients with and without type 2 diabetes," *BMC Medical Genomics*, vol. 12, no. S2, p. 40, 2019.

[33] B. W. van der Kolk, M. Kalafati, M. Adriaens et al., "Subcutaneous adipose tissue and systemic inflammation are associated with peripheral but not hepatic insulin resistance in humans," *Diabetes*, vol. 68, no. 12, pp. 2247–2258, 2019.

[34] R. Li, Y. Chen, M. Shi et al., "Gegen Qinlian decoction alleviates experimental colitis via suppressing TLR4/NF-κB signaling and enhancing antioxidant effect," *Phytomedicine*, vol. 23, no. 10, pp. 1012–1020, 2016.

Hindawi
Disease Markers
Volume 2022, Article ID 4231535, 7 pages
https://doi.org/10.1155/2022/4231535

Research Article

Ultrasonography Combined with Blood Biochemistry on the Early Diagnosis of Diabetic Kidney Disease

Jing Lin,[1] Guangde Liu,[1] Yuxuan Lin,[1] Chao Wei,[1] Sujun Liu,[2] and Youhua Xu[3,4,5]

[1]*Department of Ultrasound, Guangdong Provincial Hospital of Chinese Medicine-Zhuhai Hospital, Zhuhai, Guangdong, China*
[2]*Department of Nephrology, Guangdong Provincial Hospital of Chinese Medicine-Zhuhai Hospital, Zhuhai, Guangdong, China*
[3]*Faculty of Chinese Medicine, State Key Laboratory of Quality Research in Chinese Medicine, Macau University of Science and Technology, Taipa, Macao, China*
[4]*Macau University of Science and Technology Zhuhai MUST Science and Technology Research Institute, Hengqin, Zhuhai, China*
[5]*Zhuhai Hospital of Integrated Traditional Chinese and Western Medicine, Affiliated Hospital of Faculty of Chinese Medicine of Macau University of Science and Technology, Zhuhai, China*

Correspondence should be addressed to Jing Lin; fairy_linjing@126.com

Received 19 April 2022; Accepted 14 September 2022; Published 5 October 2022

Academic Editor: Yaoyao Bian

Objective. Diabetic kidney disease (DKD) has been well recognized as a microvascular complication of diabetes mellitus. Perfusion of intrarenal arteries is closely related with development of DKD. The aim of the present study was to investigate relation of ultrasonography performance of intrarenal arteries and grade of DKD. *Methods*. From May to December at 2021, a total of 54 DKD patients and 36 non-DKD cases were recruited. Ultrasonography performance of intrarenal and arteries at lower extremity was examined by high-resolution ultrasound diagnostic equipment; maximum (Vsmax) as well as minimum (Vdmin) blood velocity of arteries were recorded, and resistance index (RI) of arteries were calculated. Blood routine and biochemical parameters were determined from clinical laboratory of our hospital. *Results*. According to eGFR grading, 42.50% of the 54 DKD cases are at Grade 1, and 18.52%, 11.11%, 9.26%, and 18.52% cases were at Grade 2, 3a, 3b, and 4-5, respectively. Blood urea and creatinine were significantly positively related with progress of DKD, while level of Hb was negatively related with DKD. By ultrasonography; we found that Vsmax and Vdmin of main renal artery (MRA), segmental renal artery (SRA), and interlobular renal artery (IRA) were significantly reduced compared with healthy cases; IR of the above arteries was dramatically elevated, and changes of the above data were more obvious than that of lower extremity. Vdmin of MRA, SRA, and IRA was negatively related with grading of DKD, while RI was positively related with the grading. Converging from RI and level of Hb, we found that the level of Hb is positively related with healthy status of the kidney, while RI of the arteries is negatively with that. *Conclusions*. Resistance index (RI) of intrarenal arteries, obtained from ultrasonography combining with level of hemoglobin (Hb), is the predictor of progress of DKD.

1. Introduction

With the world population aging progress, diabetic kidney disease (DKD) has become a leading contributor to end stage of renal failure (ESRF) [1]. It is estimated that over 30% of patients with diabetes will develop into DKD within 20 years since diagnosis of diabetes [2]. Unfortunately, there is still no way to satisfactory inhibit progress of DKD to now.

Clinically, DKD is arbitrarily diagnosed with appearance and content of proteinuria. For instance, once the urine protein exceeds 300 mg/L or microalbuminuria above 30-300 mg/day, the patients will be clinically diagnosed [3, 4]. However, evidences from two decades have indicated that these two parameters are not specific for DKD [5], and usefulness of proteinuria is facing challenge recently as it lacks sensitivity and specificity in respect of early diagnosis of DKD. On the other hand, DKD has been demonstrated to be positively related with dysfunction of multiple organ systems [6], and most importantly, it will increase cardiovascular events [7]. Currently, definite diagnosis of DKD still

relies on renal biopsy and morphological findings. However, severe complication is very common during the invasive operation of renal biopsy, and most cases denied to this operation. Therefore, it is of great significance to develop a method to serve for prediction or early diagnosis of DKD.

DKD has been well recognized as a microvascular complication of diabetes mellitus. Lesion of the vascular wall and decrease of tissue perfusion is the central event during development of vascular disease as well as DKD, and they are positively related with development of DKD. Therefore, seeking a technique that reflects their early changes in cases with diabetes might help early diagnosis of DKD. In the present study, we compiled vascular perfusion of kidney and function of peripheral arteries using ultrasonic diagnosis, and further investigated relationship between grade of DKD and ultrasonic performances. Our current study may supply an noninvasive method and strategy for early diagnosis of DKD in diabetes cases.

2. Subjects and Methods

2.1. Study Population. All study population were recruited from Department of Nephrology of our hospital from May to December 2021. In general, all newly in-hospitalized DKD cases during the above period that met with the following criteria were included, and all recruited volunteers with non-DKD during this period were included. Finally, a total of 54 DKD patients (23 female and 31 male) aging from 28 to 84 years old (age = 57.72 ± 12.29) and 36 non-DKD cases (23 female and 13 male) aging from 21 to 72 years old (age = 46.78 ± 11.69) were included. All included cases have signed informed consent before study. All study plan, data collection, and ultrasonic operation were approved by Ethics Committee of Guangdong Provincial Hospital of Traditional Chinese Medicine (Approval no. BE2021-122-01).

The inclusion criteria for DKD were as follows: (1) age ≥ 18 years old; (2) DKD was diagnosed according to clinical practice guideline of Kidney Disease Outcome Quality Initiatives (K/DOQI) [8], and (3) no anatomy anomalies in the kidney or peripheral arteries and no renal tumors or renal transplantation.

The exclusion criteria were as follows: (1) malignant tumor; (2) anatomical abnormalities of urinary system; (3) accompanied with urinary or systemic infection.

2.2. Laboratory Data. All laboratory data were obtained from clinical laboratory of Guangdong Provincial Hospital of Chinese Medicine-Zhuhai Hospital. Estimated glomerular filtration rate (eGFR) was determined according to the following equation: $\text{eGFR} = 186 \times \text{Scr}^{-1.154} \times (\text{age})^{-0.203}$ [× 0.742 (if female)]. Staging of DKD is as follows: (1) Grade 1: eGFR ≥ 90; (2) Grade 2: 89 ≥ eGFR ≥ 60; (3) Grade 3a: 59 ≥ eGFR ≥ 45; (4) Grade 3b: 44 ≥ eGFR ≥ 30; (5) Grade 4: 29 ≥ eGFR ≥ 15; (6) Grade 5: eGFR < 15.

2.3. Ultrasonic Investigation of the Participants. Real-time ultrasonography at B-mode was carried out in each participant using a high-resolution ultrasound diagnostic equipment (Phillips) by well-trained and validated examiners. Maximum (Vsmax) as well as minimum (Vdmin) blood velocity of arteries of lower extremity including common femoral artery (CFA), superficial femoral artery (SFA), popliteal artery (POA), anterior tibial artery (ATA), posterior tibial artery (PTA), peroneal artery (PEA), dorsalis pedis artery (DPA), arteries within the kidney including main renal artery (MRA), segmental renal artery (SRA), and interlobular renal artery (IRA), at both sides were recorded. Resistance index (RI) of the arteries was obtained according to the following equation: RI = (Vsmax − Vdmin)/Vsmax. Mean value of the right and left side of the above values were obtained for further analysis.

Table 1: Characteristics of the subjects.

	Control (n = 36)	DKD (n = 54)	P values
Mean age (SD), y	47.42 ± 12.15	57.72 ± 12.29	<0.001
Age, n (%)			<0.001
≤40 y	10 (27.78)	5 (9.26)	
41-65 y	20 (55.56)	34 (62.96)	
>65 y	1 (2.78)	16 (29.63)	
66-70 y	0	8 (14.81)	
71-75 y	1 (2.78)	5 (9.26)	
76-80 y	0	2 (3.70)	
>80 y	0	1 (1.85)	
Women, n (%)	23 (63.89)	23 (42.59)	0.0054

2.4. Statistical Analysis. Data are expressed as mean ± SD or otherwise indicated. Data are analyzed by GraphPad Prism 9 using t-test or one-way ANOVA. Multiple linear regression of the data was obtained by GraphPad Prism 9. P values < 0.05 is considered to be statistically significant.

3. Results

3.1. Overview of the Participants. A total of 36 healthy as well as 54 DKD cases were included in this study. Within the DKD cases, 42.59% were female, and 62.96% were between 41 and 65 years old (Table 1). According to eGFR grading, 42.50% of the DKD cases are at Grade 1, and 18.52%, 11.11%, 9.26%, and 18.52% cases were at Grade 2, 3a, 3b, and 4-5, respectively (Table 2). As shown in Table 2, once the cases progress into grade 3, levels of blood urea and cr were significantly increased, while Hb was decreased.

3.2. Blood Velocity and Artery Resistance Index Was Altered in DKD Cases. To firstly evaluate haemorheological changes of renal arteries for DKD cases, maximum (Vsmax) as well as minimum (Vdmin) blood velocity of main renal artery (MRA), segmental renal artery (SRA), and interlobular renal artery (IRA) were recorded. As shown in Figure 1, the maximum and minimum blood velocity of MRA, SRA, and IRA was significantly decreased in DKD cases compared with healthy control; moreover, resistance index (IR) of the above arteries was dramatically

Table 2: Laboratory characteristic of DKD participants (mean ± SD).

	Grade 1	Grade 2	Grade 3a	Grade 3b	Grade 4-5	*P* values
N (%)	23 (42.59)	10 (18.52)	6 (11.11)	5 (9.26)	10 (18.52)	
Hb	139.74 ± 17.59	131.00 ± 23.31	127.83 ± 15.82	101.20 ± 8.84	93.90 ± 9.96	<0.001
FBG	8.51 ± 2.96	7.90 ± 1.77	9.88 ± 6.90	8.37 ± 1.59	7.31 ± 3.30	0.7881
HbA1c (%)	7.87 ± 2.42	8.97 ± 3.98	8.50 ± 3.88	8.06 ± 2.80	6.49 ± 0.84	0.4250
Blood urea (mmol/L)	4.96 ± 1.54	6.35 ± 2.70	6.46 ± 1.91	13.45 ± 3.89	19.96 ± 7.41	<0.001
Blood Cr (μmoI/L)	68.28 ± 21.05	85.28 ± 14.03	111.67 ± 20.12	154.62 ± 18.96	520.11 ± 247.32	<0.001
eGFR	113.12 ± 18.99	77.63 ± 9.20	52.71 ± 4.08	38.20 ± 3.91	11.58 ± 6.81	<0.001

Note: eGFR = $186 \times \mathrm{Scr}^{-1.154} \times (\mathrm{age})^{-0.203}$ [× 0.742 (if female)]. FBG: fasting blood glucose; Cr: creatinine; eGFR: estimated glomerular filtration rate.

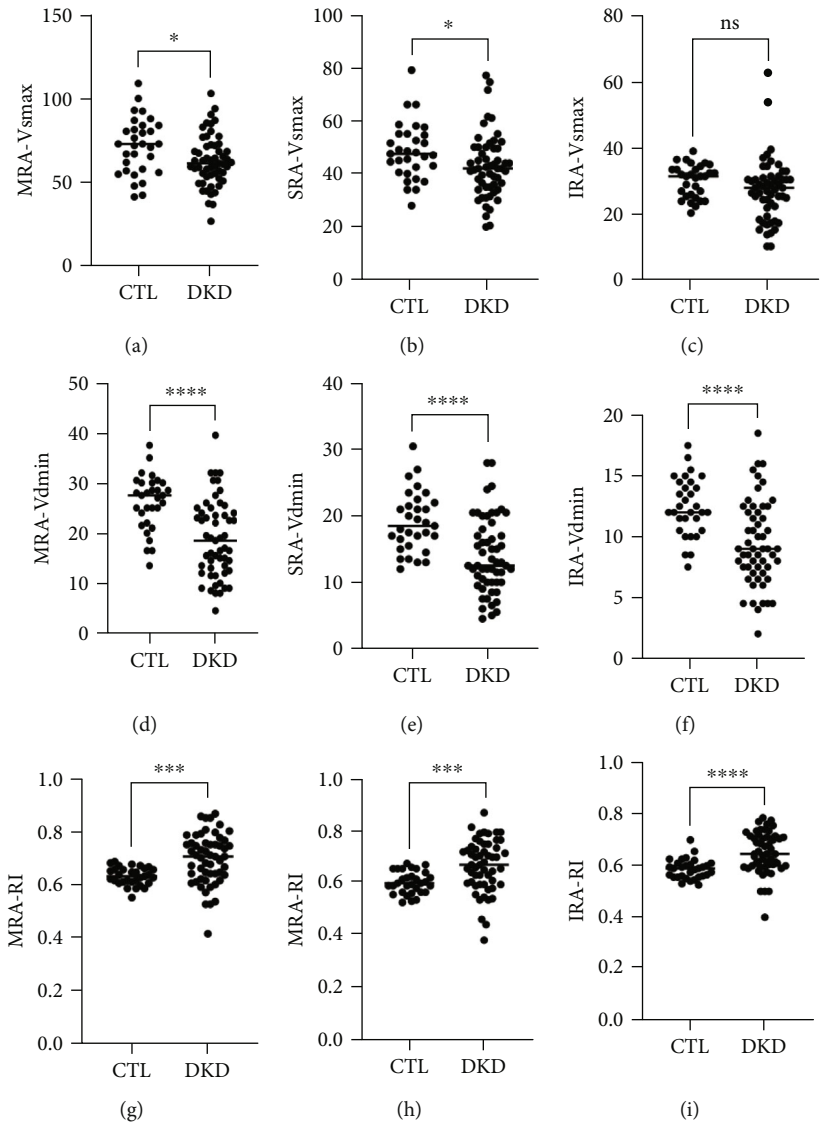

Figure 1: Ultrasonography characteristic of renal arteries in DKD cases. Main renal artery (MRA), segmental renal artery (SRA), interlobular renal artery (IRA). *p<0.05, ***p<0.001, ****p<0.0001.

elevated ($P < 0.001$ vs. ctl). These data suggested that renal perfusion was reduced in DKD.

To further determine changes of arteries in lower extremity, Vsmax in common femoral artery (CFA), superficial femoral artery (SFA), popliteal artery (POA), anterior tibial artery (ATA), posterior tibial artery (PTA), peroneal artery (PEA), and dorsalis pedis artery (DPA) was analyzed. As shown in Figure 2, Vsmax in CFA and SFA was

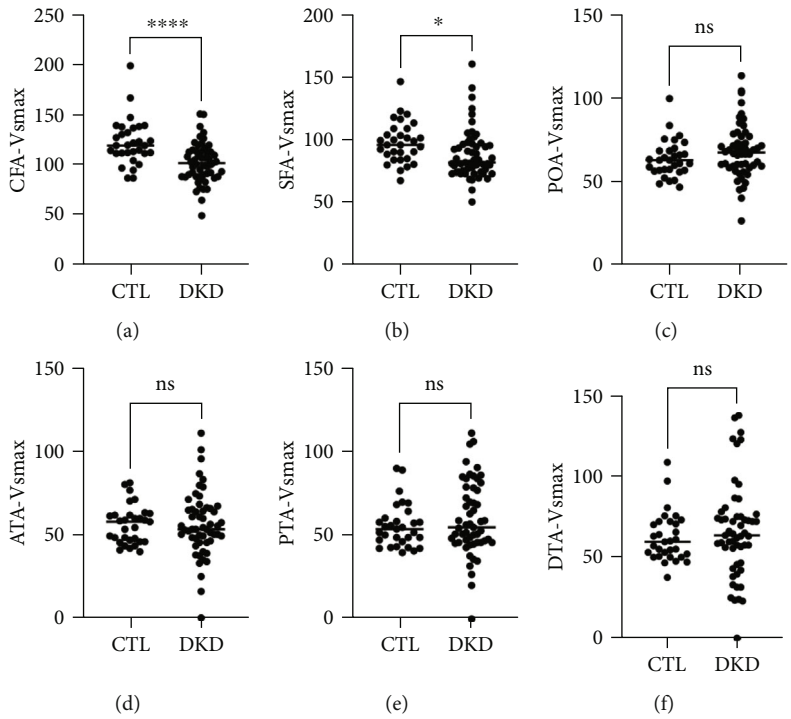

Figure 2: Ultrasonography characteristic of arteries in lower extremity of DKD cases. Common femoral artery (CFA), superficial femoral artery (SFA), popliteal artery (POA), anterior tibial artery (ATA), posterior tibial artery (PTA), peroneal artery (PEA), dorsalis pedis artery (DPA). $^{*}p<0.05$, $^{****}p<0.0001$.

significantly reduced in DKD cases ($P < 0.05$ vs. ctl), but no statistical significance was found for Vsmax in other arteries at lower extremity.

Converging with the above data, ultrasonic changes of CFA as well as arteries within the kidney were related with DKD to some extent.

3.3. Ultrasonographic Changes of CFA and Arteries within the Kidney of DKD Cases. To explore relation of ultrasonographic changes of CFA and arteries within the kidney of with grading of DKD, Vsmax, Vadmin as well as RI of the arteries were analyzed. As shown in Figure 3, Vdmin of MRA, SRA and IRA was negatively related with grading of DKD; while RI was positively related with the grading. More importantly, a more significance was found once the grading progressed into ″3″. No statistical significance was found in Vsmax or ultrasonographic changes of CFA concerning their relation with DKD grading.

3.4. Multiple Regression Analysis of the Data. Converging from the above data, we can conclude that Hb and RI are two pivotal parameters that closely related with grading of DKD. To further define correlation among the data above, multiple linear regression analysis was conducted. As shown in Figure 4, level of Hb is positively related with healthy status of the kidney, while RI of the arteries is negatively with that.

4. Discussion

With the aging progression around the world, diabetic kidney disease (DKD) has becoming one of the major reason that contributes to end stage renal disease (ESRD). Although it has been well recognized that early-diagnosis is pivotal to inhibit progression of DKD, a noninvasive, real-time, and dynamic method that reflect status of the kidney is still rare. In the present study, we supplied an equation that reflect correlation among eGFR, resistance index of arteries within the kidney, and level of Hb. Our present finding may help clinicians for early diagnosis and treatment of DKD.

It was reported that about 30-40% of cases with type 2 diabetes mellitus are likely to have kidney lesion [9]; more importantly, this lesion is believed to be irreversible [10]. In this sense, early diagnosis is pivotal. Currently, biopsy is still the gold standard for diagnosis of DKD and most other renal diseases [11]. However, most of the cases are not evaluated by biopsy due to its invasive test and possible severe side effects [12], and clinical symptoms converging with laboratory data are applied for diagnosis. In the current study, all DKD cases are clinically diagnosed, and stage of the disease was obtained according to the eGFR value.

It has been well recognized that decreased perfusion of the kidney plays a key role in the development of DKD [13]. A finding from Ma et al. indicated that the perfusion

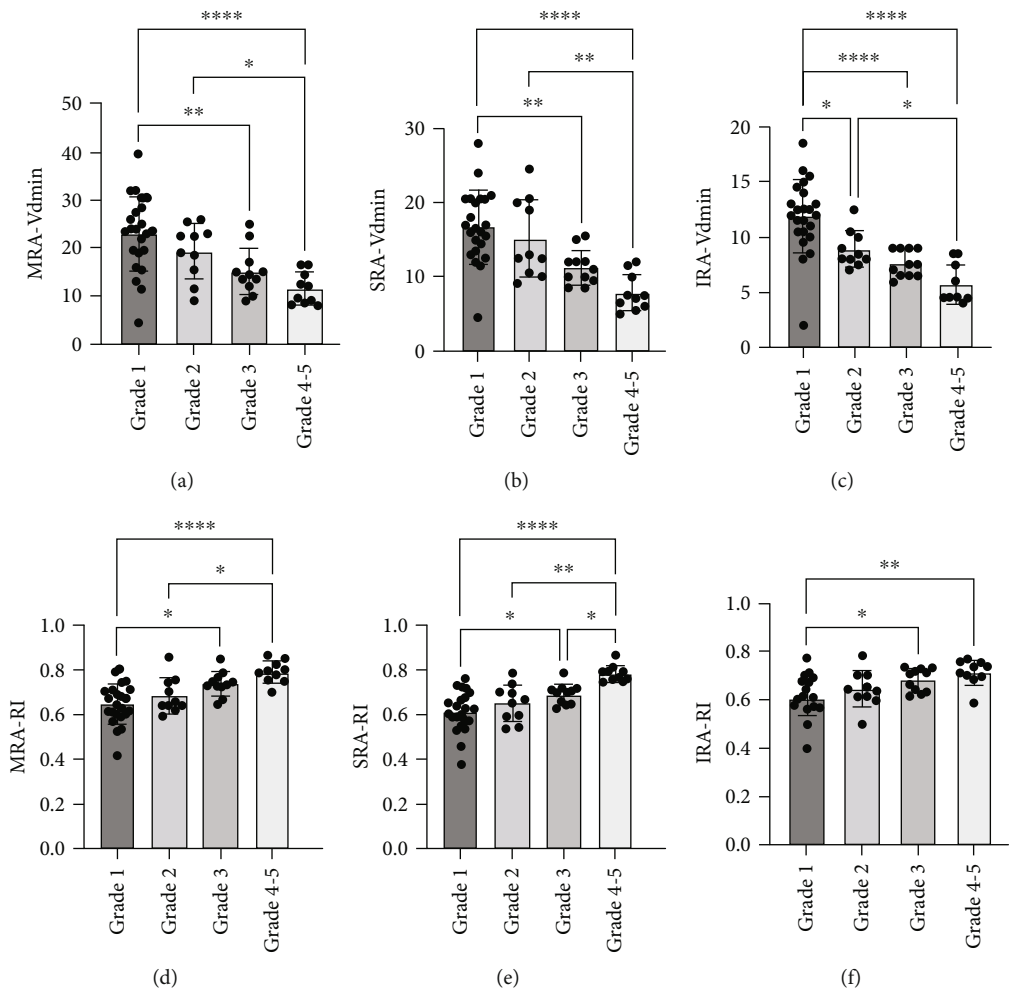

Figure 3: Ultrasonographic changes of arteries within the kidney are related with grading of DKD. Main renal artery (MRA), segmental renal artery (SRA), interlobular renal artery (IRA). *p<0.05, **p<0.01, ****p<0.0001.

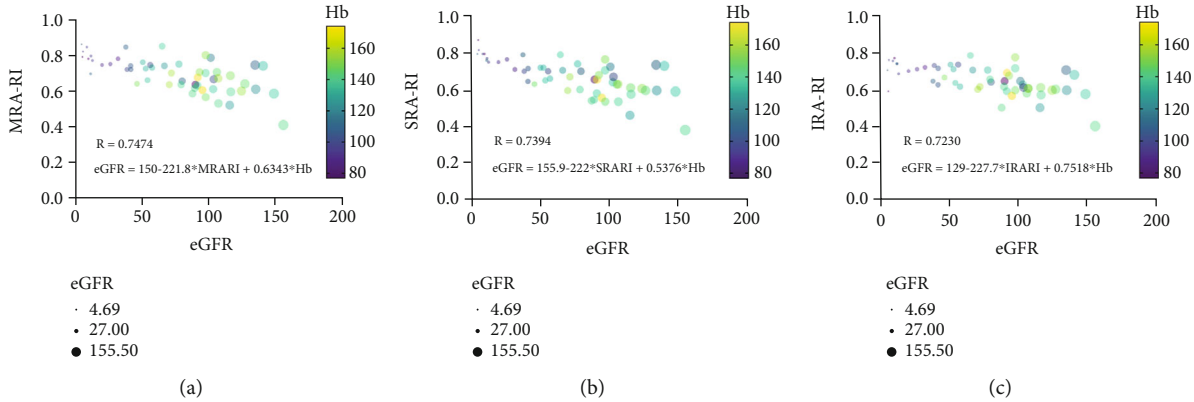

Figure 4: Multiple regression analysis of the eGFR against RI and Hb.

velocity of the microcapillary bed within the kidney in DKD cases is significantly reduced [14]. Ultrasonography is a non-invasive method that has been widely applied to evaluate morphology changes as well as hemorheology of the organism. We found that both maximum and minimum blood velocity of arteries within the kidney were significantly reduced with grading of DKD, while the resistance index of intrarenal arteries was increased. Although blood velocity

in arteries of lower extremity is also altered, there is no statistical significance among different grades of DKD.

It has been well understood that hemoglobin (Hb) production is closely related with secretion of erythropoietin (EPO). Recent findings have found reduced EPO, and anemia are independent risk factors for microvascular diseases including DKD [15–17]. In the present study, we found that Hb is negatively related with grading of DKD; this is in line with previous findings. Compelling with resistance index (IR) of intrarenal arteries, we further obtained a regression equation, and found that the level of Hb is positively related with eGFR, while RI of intrarenal arteries is negatively with that.

It should be noted that as there is still no well recognized ultrasonography that predict progress of the damage of kidney; the current finding is just an alternative for clinicians, and it cannot replace the gold standard of biopsy on diagnosis of renal damage. On the other hand, recent advances in finding biomarkers of early DKD in diabetic population by omics and molecular-biology also supplied an alternative method. For instance, long noncoding RNAs (lncRNAs) have been suggested to play a role in early development of DKD [18], and glycated peptides within the urine may predict dysfunction of proximal tubule within the kidney [19].

In summary, we show in the present that resistance index (IR) of intrarenal arteries obtained from ultrasonography combining with level of hemoglobin (Hb) are predictor of grading DKD. Our present finding supplied an alternative and noninvasive method for early diagnosis of DKD.

Data Availability

The original data can be obtained from the corresponding author upon reasonable request.

Conflicts of Interest

The authors declare that they have no potential competing conflict of interest.

Acknowledgments

This work was supported by Medical Research grant from Health Bureau of Zhuhai (File No. ZH24013310210001PWC), and Science and Technology Development Fund of Macau (File No. 0055/2019/AMJ).

References

[1] D. Del Prete, F. Anglani, M. Ceol et al., "Molecular biology of diabetic glomerulosclerosis," *Nephrology Dialysis Transplantation*, vol. 13, no. 90008, pp. 20–25, 1998.

[2] M. Marcelli, "Nutrition in diabetic nephropathy," *Giornale Italiano di Nefrologia*, vol. 23, Supplement 34, pp. s68–s70, 2006.

[3] T. T. Kouri, J. S. Viikari, K. S. Mattila, and K. M. A. Irjala, "Microalbuminuria: invalidity of simple concentration-based screening tests for early nephropathy due to urinary volumes of diabetic patients," *Diabetes Care*, vol. 14, no. 7, pp. 591–593, 1991.

[4] R. Pradeepa, R. M. Anjana, R. Unnikrishnan, A. Ganesan, V. Mohan, and M. Rema, "Risk factors for microvascular complications of diabetes among south Indian subjects with type 2 diabetes—the Chennai urban rural epidemiology study (CURES) eye study-5," *Diabetes Technology & Therapeutics*, vol. 12, no. 10, pp. 755–761, 2010.

[5] Y. Itoh, "Current topics on urinary proteins: human albumin, protein 1, beta 2-microglobulin, and type IV collagen," *Rinsho Byori*, vol. 50, no. 6, pp. 555–560, 2002.

[6] A. Flyvbjerg, "The role of the complement system in diabetic nephropathy," *Nature Reviews Nephrology*, vol. 13, no. 5, pp. 311–318, 2017.

[7] S. Yamamoto, J. Zhong, P. G. Yancey et al., "Atherosclerosis following renal injury is ameliorated by pioglitazone and losartan via macrophage phenotype," *Atherosclerosis*, vol. 242, no. 1, pp. 56–64, 2015.

[8] National Kidney Foundation, "K/DOQI clinical practice guidelines for chronic kidney disease: evaluation, classification, and stratification," *American Journal of Kidney Disease*, vol. 39, no. 2, pp. S1–266, 2002.

[9] K. J. Lipska, I. B. Hirsch, and M. C. Riddle, "Human insulin for type 2 diabetes," *JAMA*, vol. 318, no. 1, pp. 23-24, 2017.

[10] T. I. Chang, J. T. Park, J. K. Kim et al., "Renal outcomes in patients with type 2 diabetes with or without coexisting nondiabetic renal disease," *Diabetes Research and Clinical Practice*, vol. 92, no. 2, pp. 198–204, 2011.

[11] S. Imtiaz, B. Salman, K. Nasir, M. F. Drohlia, and A. Ahmad, "Clinical variables differentiating diabetic from nondiabetic kidney disease in patients with diabetes: a single-center study," *Saudi Journal of Kidney Disease and Transplantation*, vol. 28, no. 2, pp. 307–312, 2017.

[12] S. G. Sharma, A. S. Bomback, J. Radhakrishnan et al., "The modern spectrum of renal biopsy findings in patients with diabetes," *Clinical Journal of the American Society of Nephrology*, vol. 8, no. 10, pp. 1718–1724, 2013.

[13] K. J. Kelly, J. L. Burford, and J. H. Dominguez, "Postischemic inflammatory syndrome: a critical mechanism of progression in diabetic nephropathy," *American Journal of Physiology-Renal Physiology*, vol. 297, no. 4, pp. F923–F931, 2009.

[14] F. Ma, Y. Cang, B. Zhao et al., "Contrast-enhanced ultrasound with SonoVue could accurately assess the renal microvascular perfusion in diabetic kidney damage," *Nephrology Dialysis Transplantation*, vol. 27, no. 7, pp. 2891–2898, 2012.

[15] D. Collister, P. Komenda, B. Hiebert et al., "The effect of erythropoietin-stimulating agents on health-related quality of life in anemia of chronic kidney disease," *Annals of Internal Medicine*, vol. 164, no. 7, pp. 472–478, 2016.

[16] A. Traveset, E. Rubinat, E. Ortega et al., "Lower hemoglobin concentration is associated with retinal ischemia and the severity of diabetic retinopathy in type 2 diabetes," *Journal of Diabetes Research*, vol. 2016, Article ID 3674946, 8 pages, 2016.

[17] M. K. Lee, K. D. Han, J. H. Lee et al., "High hemoglobin levels are associated with decreased risk of diabetic retinopathy in Korean type 2 diabetes," *Scientific Reports*, vol. 8, no. 1, p. 5538, 2018.

[18] L. Petrica, E. Hogea, F. Gadalean et al., "Long noncoding RNAs may impact podocytes and proximal tubule function through modulating miRNAs expression in early diabetic kidney disease of type 2 diabetes mellitus patients," *International Journal of Medical Sciences*, vol. 18, no. 10, pp. 2093–2101, 2021.

[19] L. Petrica, A. Vlad, G. Gluhovschi et al., "Glycated peptides are associated with proximal tubule dysfunction in type 2 diabetes mellitus," *International Journal of Clinical and Experimental Medicine*, vol. 8, no. 2, pp. 2516–2525, 2015.

Hindawi
Disease Markers
Volume 2022, Article ID 3664931, 8 pages
https://doi.org/10.1155/2022/3664931

Research Article

Expression of Adenosine Deaminase and NLRP3 Inflammasome in Tuberculous Peritonitis and Their Relationship with Clinical Efficacy

Hongwei Su,[1] Guorong Yan,[1] Zijian Li,[1] Lin Fu,[2] and Lingdi Li[2]

[1]*The Second Department of Thoracic Surgery, Hebei Chest Hospital, Shijiazhuang 050040, Hebei, China*
[2]*Department of Orthopedics, Hebei Chest Hospital, Shijiazhuang 050040, Hebei, China*

Correspondence should be addressed to Lingdi Li; lilingdi1033@163.com

Received 22 February 2022; Accepted 11 July 2022; Published 15 September 2022

Academic Editor: Yaoyao Bian

Objective. Tuberculous peritonitis (TP) can cause multiple infections of surrounding organs and tissues, leading to organ failure and endangering life safety. In this research, the relationship between adenosine deaminase (ADA), NLRP3 inflammasome, and TP and its clinical significance will be deeply explored, so as to provide new directions and reliable reference opinions for future clinical diagnosis and treatment. *Methods*. Altogether, 59 TP patients (research group, RG) and 52 non-TP patients (control group, CG) who were admitted to our hospital from May 2014 to June 2018 were regarded as research objects. Ascites samples of RG before treatment (admission) and one month after treatment and CG before treatment were obtained, and the ADA and NLRP3 levels were tested to evaluate the clinical and prognostic significance of the two in TP. *Results*. Before treatment, ADA and NLRP3 in RG were higher than CG ($P < 0.05$), and the sensitivity and specificity of combined detection of the two in predicting TP occurrence were 89.83% and 73.08% ($P < 0.05$). In addition, ADA and NLRP3 in RG patients were positively correlated with the disappearance time of abdominal pain and ascites ($P < 0.05$) and had excellent predictive effect on the adverse reactions during treatment ($P < 0.05$). After treatment, both in RG patients decreased, which was inversely proportional to the clinical efficacy ($P < 0.05$). Prognostic follow-up manifested that ADA and NLRP3 in relapse patients were higher than those without recurrence after treatment ($P < 0.05$). *Conclusion*. The increase of ADA and NLRP3 in TP is relevant to the adverse reactions during treatment, clinical efficacy, and prognosis recurrence after treatment. It can be used as a disease marker to confirm, intervene, and evaluate TP progression promptly.

1. Introduction

Tuberculous peritonitis (TP) is a chronic and diffuse inflammation of peritoneum caused by mycobacterium tuberculosis, which is familiar in young and middle-aged women, and has a certain potential risk in any age group [1]. According to the survey, there are more than 500,000 new TP patients worldwide every year, 6-8 times higher than that in 2010, which is also relevant to the changes of people's eating habits and living environment [2]. The occurrence of TP can cause multiple infections of surrounding organs and tissues, resulting in organ failure and endangering life safety [3]. In clinical practice, conservative treatment schemes can usually achieve ideal results for early TP; but most patients have no special clinical symptoms in the early stage and may only show intermittent abdominal pain, diarrhea, etc., and they often miss the best treatment period due to lack of medical and health knowledge [4, 5]. For those with severe illness and complicated infection, surgical treatment is needed [6]. At this time, patients may not only need to remove the diseased bowel segment but also need to receive long rehabilitation and antituberculosis treatment after operation, which seriously reduces the quality of life of prognosis [7]. Thus, early detection and treatment of TP are the key to ensure patients' health. At the moment, the differential diagnosis of TP needs a series of blood routine, imaging routine, tuberculin, T-cell spot test, laparoscopy, etc., and the only diagnostic gold standard is peritoneal pathological biopsy [8].

The main reason for the poor prognosis of TP is that early TP has strong concealment, and on the other hand, the examination methods are still complicated, which cannot quickly and accurately evaluate its occurrence and development [9]. Thus, researchers are constantly trying to find a new and reliable TP evaluation method to ensure the treatment effect and prognosis of patients.

Adenosine deaminase (ADA), an enzyme involved in purine metabolism, can maintain the development of immune system [10]. Mycobacterium tuberculosis, a common pathogenic bacterium, will never get sick even if it is infected in people with sound immune system, and TP is caused by abnormal immune function of infected people [11]. This suggests that there may be a certain latent relationship between ADA and TP. For instance, Shen et al. found that ADA had a certain diagnostic potential for TP [12], which proves our conjecture. The NLRP3 responds to the stimulation of metabolic stress signals, leading to caspase-1 activation and IL-1 β production, which play an important role in a variety of diseases. Secretion of proinflammatory cytokines IL-1β and IL-18 induced by activation of NLRP3 inflammasome, as well as pyrodeath, is self-protective measures that help protect the body against exogenous microbial infection and endogenous cellular damage and maintain homeostasis. Meanwhile, NLRP3 inflammasome is also involved in the occurrence and development of diabetes, making clinical symptoms and treatment more complicated, which is one of the possible mechanisms of diabetic cardiomyopathy. Recent studies suggest that NLRP3 inflammasome may be a potential new target for the treatment of diabetes mellitus [13]. ADA and NLRP3 have been proved to have abnormal expression in TP, but their specific clinical significance is still vague.

Accordingly, this research will deeply explore the relationship and clinical significance of ADA, NLRP3, and TP, aiming at providing new directions and reliable reference opinions for future clinical diagnosis and treatment.

2. Materials and Methods

2.1. Patient Data. Altogether, 59 TP patients (research group, RG) and 52 non-TP patients (control group, CG) who were admitted to our hospital from May 2014 to June 2018 were considered as the research objects in retrospective analysis. All the subjects signed the informed consent form themselves. The protocol of this study is approved by the ethics committee of Hebei Chest Hospital (no. CL2014/44-341).

2.2. Inclusion and Exclusion Criteria. RG: inclusion criteria: age > 18 years old; TP was diagnosed by peritoneal biopsy, accompanied by abdominal pain, abdominal distension, ascites, and other clinical symptoms of TP. X-ray revealed increased abdominal density, intestinal adhesions, calcified lymph nodes, or intestinal obstruction; TP conservative treatment after admission; exclusion criteria: patients with other immune system, blood system, and tumor diseases; patients with organ dysfunction or abnormality; pregnant and lactating patients; those who cannot extract ascites after one month of treatment; prognostic follow-up losers; those who did not follow the doctor's advice during treatment. CG: cancer cells existed in ascites, and tumors were confirmed by pathological biopsy; the exclusion criteria are the same as above.

2.3. Therapeutic Methods. After admission, TP patients were treated in strict accordance with guidelines. Early patients were given oral administration, and advanced patients were given intravenous administration. Treatment plans were intensive treatment with rifampicin, isoniazid, and pyrazinamide (or ethambutol and streptomycin) for 2-3 months, and continuous treatment with rifampicin and isoniazid for 7-9 months in the consolidation period. For general exudative TP patients, it is necessary to emphasize the whole course of standardized treatment. For adhesive and caseous TP patients, it is certainly worth combining medication and appropriately extending the course of anti-tuberculosis treatment. The prognosis of TP patients was followed up for 2 years in the form of regular hospital review.

2.4. Research Samples. Ascites samples of RG before treatment (at admission) and one month after treatment and CG before treatment were obtained. Supernatant was obtained after centrifugation. ADA level was tested by automatic biochemical analyzer (kit purchased from Shanghai Yaji Biotechnology Co., Ltd.), and NLRP3 level was tested by ELISA (kit purchased from Shanghai Jihe Biotechnology Co., Ltd.).

2.5. TP Efficacy Evaluation. After 2 months of treatment, the clinical efficacy of TP patients was evaluated [14]. Cured: clinical symptoms such as abdominal distension and pain, disappearance of abdominal tenderness and rebound pain, softness of abdominal muscles, and normal body temperature; markedly effective: clinical symptoms and signs of abdominal tenderness and rebound pain were obviously improved, and most of abdominal effusion was absorbed; effective: clinical symptoms and signs were relieved, and a small amount of ascites was absorbed. Ineffective: clinical symptoms did not meet the above criteria.

3. Statistical Methods

SPSS22.0 software was used for statistical analysis. The measurement data were expressed in percentage and assessed via chi-square test. The counting data were expressed by mean $\pm$ standard deviation and evaluated through independent sample t-test and paired t-test. ROC curve was used for prediction analysis, and Pearson and Spearman correlation coefficients were applied to correlation analysis. $P < 0.05$ was regarded to be statistically remarkable.

4. Results

4.1. Comparison of Clinical Baseline Data. It was found that there was no dramatic difference in clinical baseline data such as age and gender between RG and CG ($P > 0.05$, Table 1), and both groups were comparable.

Table 1: Comparison of clinical baseline data between RG and CG $[n(\%)]/(\bar{\chi} \pm s)$.

	CG ($n = 52$)	RG ($n = 59$)	Or $t\chi^2$	P
Age (years)	43.33 ± 8.88	42.88 ± 7.46	0.290	0.772
BMI (kg/cm^2)	21.15 ± 3.71	21.68 ± 3.50	0.774	0.441
Gender			0.668	0.414
Male vs. female	14 vs. 38	12 vs. 47		
Marital status			0.308	0.579
Married vs. unmarried	42 vs. 10	50 vs. 9		
Place of residence			0.049	0.825
Urban vs. rural areas	38 vs. 14	42 vs. 17		
Smoking			0.701	0.403
Yes vs. no	18 vs. 34	25 vs. 34		
Drinking			0.122	0.727
Yes vs. no	12 vs. 40	12 vs. 47		
Family medical history			0.290	0.590
Yes vs. no	7 vs. 45	6 vs. 53		
Nationality			1.002	0.317
Han vs. ethnic minorities	50 vs. 2	54 vs. 5		

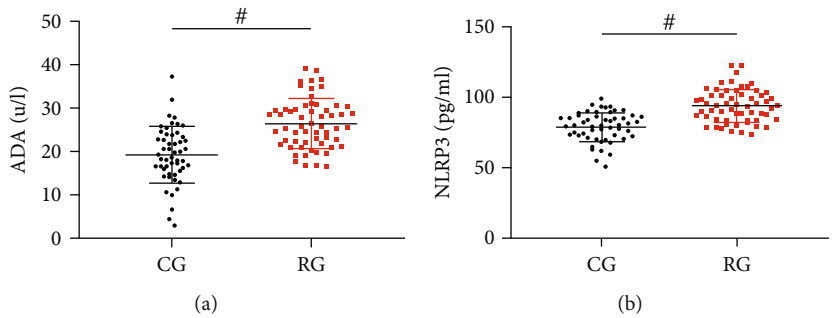

Figure 1: Comparison of ADA and NLRP3 levels. (a) ADA of ascites in RG and CG. (b) NLRP3 of ascites in RG and CG. $^{\#}P < 0.05$.

4.2. Comparison of NLRP3 and ADA Levels. ADA in RG before treatment was (26.42 ± 5.72) U/L, higher than CG ($P < 0.05$, Figure 1(a)). NLRP3 in RG before treatment was (94.05 ± 11.82) pg/mL, higher than CG ($P < 0.05$, Figure 1(b)).

4.3. Predictive Value of ADA and NLRP3 for TP. ROC curve analysis manifested that when ADA > 20.77 U/L in ascites, the sensitivity and specificity of predicting TP occurrence were 84.75% and 61.54% ($P < 0.05$, Figure 2(a)). When NLRP3 > 87.26 pg/mL, the sensitivity and specificity were 71.19% and 80.77% ($P < 0.05$, Figure 2(b)). The joint formula of ADA and NLRP3, $\text{Log}(P) = -14.679 + 0.185 \times \text{ADA} + 0.122 \times \text{NLRP3}$, was obtained by binary regression analysis. When $\text{Log}(P) > 0.38$, the sensitivity and specificity of the joint detection of ADA and NLRP3 to predict TP occurrence were 89.83% and 73.08% ($P < 0.05$, Figure 2(c)).

4.4. Relationship between ADA, NLRP3, and Disappearance Time of Abdominal Pain and Ascites. The disappearance time of abdominal pain and ascites in RG was (13.61 ± 3.62) and (35.02 ± 6.06) days, respectively. Pearson correlation coefficient analysis demonstrated that ADA and NLRP3 were positively correlated with the disappearance time of abdominal pain before treatment ($P < 0.05$, Figures 3(a) and 3(b)) and also positively correlated with the disappearance time of ascites ($P < 0.05$, Figures 3(c) and 3(d)), that is, the higher ADA and NLRP3, the longer the disappearance time of abdominal pain and ascites is.

4.5. Relationship between ADA, NLRP3, and Adverse Reactions. During the treatment, 4 patients had mild rash, 2 had abnormal liver function, 5 had vomiting, and the total adverse reaction rate was 18.64%. ADA and NLRP3 in patients with adverse reactions were higher than those without adverse reactions before treatment ($P < 0.05$, Figures 4(a) and 4(b)). ROC analysis manifested that when ADA > 24.30 U/L before treatment, the sensitivity and specificity of predicting adverse reactions in TP patients were 100.0% and 45.83% ($P < 0.05$, Figure 4(c)). When NLRP3 > 90.15 pg/mL, the sensitivity and specificity were 100.0% and 50.00% ($P < 0.05$, Figure 4(d)). Similarly, the joint formula of ADA and NLRP3, $\text{Log}(P) = -24.547 + (-0.782 \times \text{ADA}) + 0.461 \times \text{NLRP3}$, was obtained by binary regression analysis. When $\text{Log}(P) > 0.18$, the sensitivity and specificity of ADA and NLRP3 combined

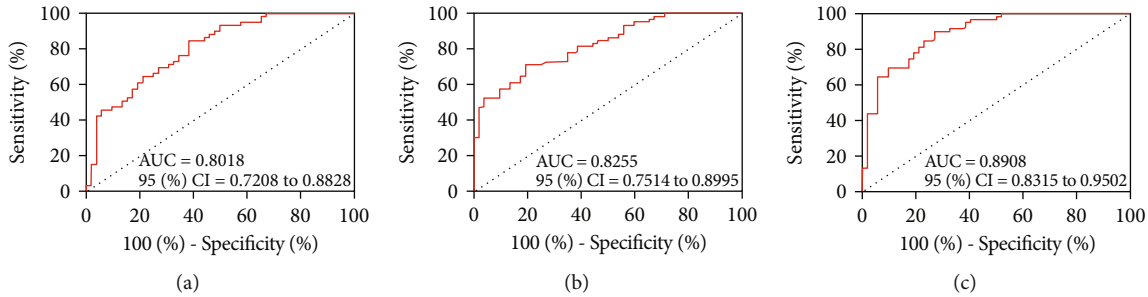

Figure 2: Predictive value of ADA and NLRP3 to TP. (a) ROC curve of ADA in ascites to predict TP occurrence. (b) ROC curve of NLRP3 in ascites to predict TP occurrence. (c) ROC curve of ADA and NLRP3 in ascites to predict TP occurrence.

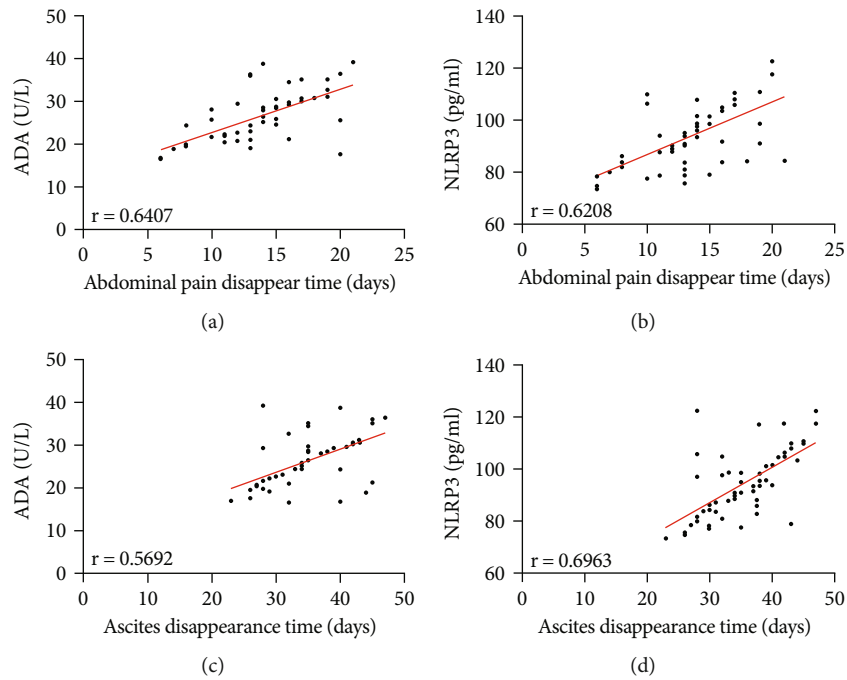

Figure 3: Relationship between ADA, NLRP3, and disappearance time of abdominal pain and ascites. (a) Correlation between ADA and disappearance time of abdominal pain before treatment. (b) Correlation between ADA and ascites before treatment. (c) Correlation between NLRP3 and disappearance time of abdominal pain before treatment. (d) Correlation between NLRP3 and ascites before treatment.

detection to predict adverse reactions were 72.73% and 83.33% ($P < 0.05$, Figure 4(e)).

4.6. Relationship between ADA, NLRP3, and Clinical Efficacy. After treatment, ADA and NLRP3 of ascites in RG were lower than those before treatment ($P < 0.05$, Figures 5(a) and 5(b)). The clinical evaluation results manifested that 15 cases were cured, 26 were markedly effective, 6 were effective, and 12 were ineffective. Subsequently, Spearman correlation coefficient analysis found that after treatment, ADA and NLRP3 in RG were negatively correlated with clinical efficacy ($P < 0.05$, Figures 5(c) and 5(d)), that is, the higher ADA and NLRP3 after treatment, the worse the efficacy is.

4.7. Relationship between ADA, NLRP3, and TP Prognosis. During the 2-year follow-up, TP recurred in 9 patients, with a total recurrence rate of 15.25%. After treatment, the ADA of relapsed patients after prognosis was higher than that of those without recurrence ($P < 0.05$, Figure 6(a)), and NLRP3 was also higher ($P < 0.05$, Figure 6(b)). Soon afterwards, ROC analysis denoted that when ADA > 23.86 U/L after treatment, the sensitivity and specificity of predicting TP recurrence were 66.675 and 80.00% ($P < 0.05$, Figure 6(c)). When NLRP3 > 78.97 pg/mL, the sensitivity and specificity were 100.0% and 42.00% ($P < 0.05$, Figure 6(d)). The joint formula of ADA and NLRP3 is $\text{Log}(P) = -7.571 + 0.112 \times \text{ADA} + 0.039 \times \text{NLRP3}$. When $\text{Log}(P) > 0.16$, the sensitivity and specificity of the joint detection of ADA and NLRP3 in predicting TP recurrence were 66.67% and 74.00% ($P < 0.05$, Figure 6(e)).

5. Discussion

This research is based on the analysis of ADA and NLRP3 that are relevant to immune function and inflammatory

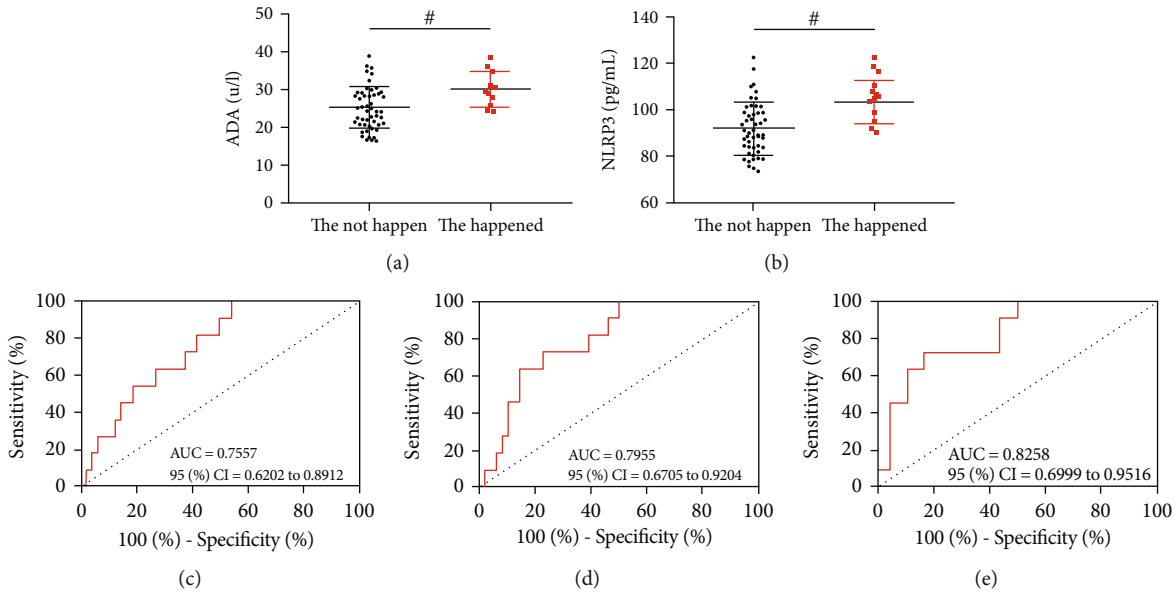

Figure 4: Relationship between ADA, NLRP3, and adverse reactions (a). Comparison of ADA of patients with and without adverse reactions before treatment. (b) Comparison of NLRP3 of patients with and without adverse reactions before treatment. (c) ROC curve of ADA predicting adverse reactions of TP patients before treatment. (d) ROC curve of NLRP3 predicting adverse reactions of TP patients before treatment. (e) ROC curve of ADA combined with NLRP3 predicting adverse reactions of TP patients before treatment. $^{\#}P < 0.05$.

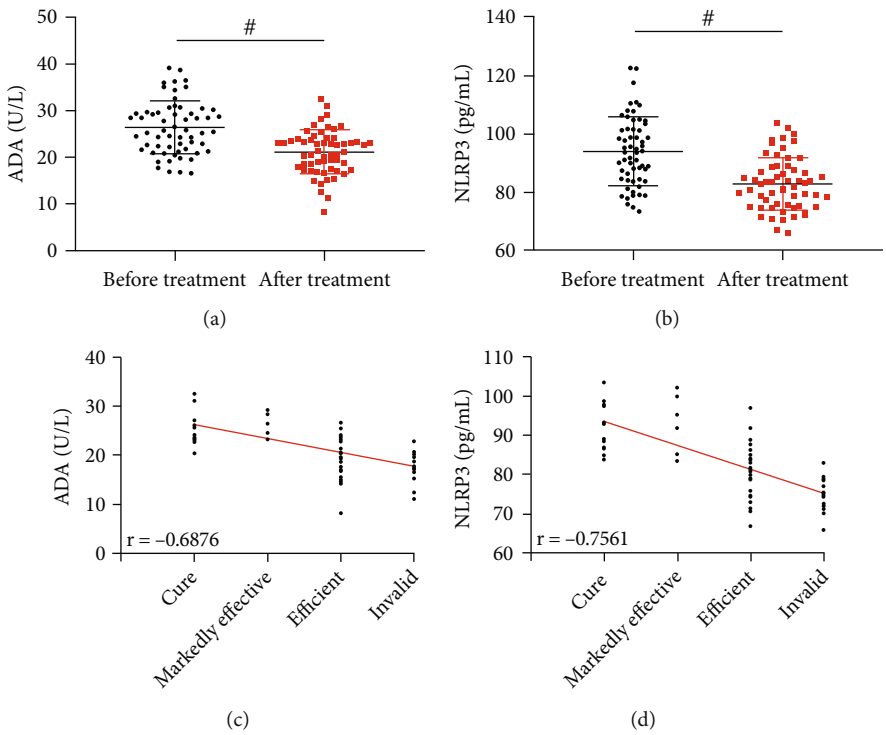

Figure 5: Relationship between ADA, NLRP3, and clinical efficacy. (a) Comparison of ADA in RG before and after treatment. (b) Comparison of NLRP3 in RG before and after treatment. (c) Correlation between ADA after treatment and clinical efficacy. (d) Correlation between NLRP3 after treatment and clinical efficacy. $^{\#}P < 0.05$.

response in human body. The purpose is to determine the exact expression and clinical significance of the two in TP. It is found that both of them have excellent evaluation effect in TP, which is quite significant for making new clinical diagnosis and treatment plans. First, the ADA and NLRP3 levels in TP patients and cancerous ascites patients were tested. It showed that ADA and NLRP3 in ascites of TP patients increased, suggesting that they might be involved

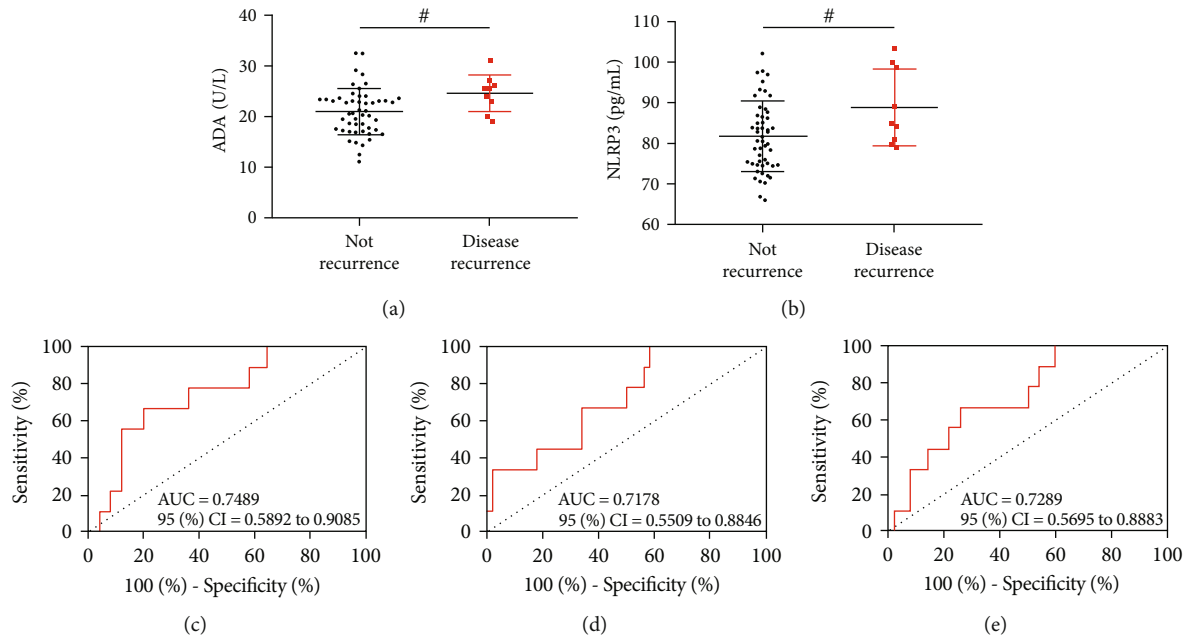

Figure 6: Relationship between ADA, NLRP3, and TP prognosis. (a) Comparison of ADA of patients with recurrence and nonrecurrence after treatment. (b) Comparison of ADA of patients with recurrence and nonrecurrence after treatment. (c) ROC curve of ADA predicting TP recurrence after treatment. (d) ROC curve of NLRP3 predicting TP recurrence after treatment. (e) ROC curve of ADA combined with NLRP3 predicting TP recurrence after treatment. $^{\#}P < 0.05$.

in disease occurrence and development. In previous studies, we also discovered that ADA and NLRP3 were elevated in liver cirrhosis and gastroenteritis, which was associated with the results of this experiment [14, 15]. It is well known that ADA, as a key enzyme of purine nucleotide metabolism in human body, can catalyze adenine nucleoside to produce inosine, generate hypoxanthine after nucleotide phosphorylase catalysis, and finally oxidized to uric acid and excreted in vitro [16, 17]. ADA is the highest in red blood cells and T lymphocytes, and its activity is directly related to the number and differentiation degree of T cells, while the immunity of tuberculosis is cellular immunity directly mediated by T lymphocytes [18, 19]. Hence, in TP, mycobacterium tuberculosis antigen stimulates the differentiation of T lymphocytes to accelerate, and the number of T lymphocytes will obviously increase, thus causing the increase of ADA. As for NLRP-3 inflammasome, research has confirmed that NLRP-3 can be activated in the case of bacterial infection, promoting the synthesis and secretion of downstream IL-1β, IL-18, and other proinflammatory mediators, and then causing extensive tissue damage [20]. Moreover, Yin et al. have verified that in severe acute peritonitis, even if the symptoms of peritonitis are alleviated, the release of proinflammatory factors can still reach several weeks, which continuously potentially affects the shape and function of peritoneum [21]. From this, both are quite essential to TP, but their specific clinical application value still needs to be further explored. Then, we analyzed the prediction effects of ADA and NLRP3 on TP by ROC curve, and the results revealed that both of them showed remarkable effects, and the sensitivity and specificity of combined detection reached 89.83% and 73.08%, respectively. Compared with the current routine clinical detection items, the detection methods of ADA and NLRP3 are more convenient and faster, which can effectively realize the early clinical screening and evaluation and improve the diagnosis rate of early TP. As the collection of ascites samples is still a difficult examination method, it is still one of the key points of follow-up research to determine whether ADA and NLRP3 in blood samples have the same excellent effect as soon as possible. What is more, this research also found that ADA and NLRP3 were directly proportional to the disappearance time of abdominal pain and ascites in TP patients, suggesting that the increased levels are directly related to the pathological manifestations of patients. This has vital reference significance for TP, which still lacks effective and rapid assessment of disease development. More than that, we confirm that ADA and NLRP3 in patients with adverse reactions during the treatment are high, and they also show excellent results in predicting adverse reactions, which further suggests that both have the potential to become clinical evaluation indicators of TP. When the patients are admitted to the hospital, the detection of ADA and NLRP3 not only can initially judge the occurrence of TP but it can evaluate its development, and timely and quickly carry out symptomatic treatment to the more serious patients to ensure the prognosis. Next, we find that after treatment, the ADA and NLRP3 levels in TP patients decrease, and their levels are directly inversely proportional to the clinical efficacy of patients, which confirms the significance of both for evaluation. In the future, we can learn about patients' rehabilitation process in time through the ADA and NLRP3 level changes

during treatment and pay attention to TP that is still at a high level after treatment, so as to effectively improve current clinical treatment effect. Not only that, in the follow-up of prognosis, we understand that the increase of levels of ADA and NLRP3 after treatment is relevant to the prognosis review of patients, and we think it is caused by the close relationship between ADA and NLRP3 and human immune function and inflammatory response, once again emphasizing the close potential relationship between them and TP.

Nevertheless, in clinical practice, there are many factors that affect the adverse reactions, clinical efficacy, and prognosis recurrence of TP patients, which may not only play a potential role in ADA and NLRP3. Therefore, we need to expand the research sample size, strictly guarantee the controllable factors of the experiment, and further analyze the results. Moreover, we will confirm the influence mechanism of ADA and NLRP3 on TP through in vitro experiments and help to further confirm the relationship between them.

6. Conclusion

The elevation of ADA and NLRP3 in TP is relevant to the adverse reactions during treatment, clinical efficacy, and prognosis recurrence. It can be used as a disease marker to confirm, intervene, and evaluate TP progression promptly.

Data Availability

The datasets used during the present study are available from the corresponding author upon reasonable request.

Conflicts of Interest

The authors declare that they have no competing interests.

Authors' Contributions

Hongwei Su and Guorong Yan contributed equally to this work.

Acknowledgments

This study was funded by the Project of Hebei Provincial Department of Health, no. 1020140509.

References

[1] U. Vaid and G. C. Kane, "Tuberculous peritonitis," *Microbiology Spectrum*, vol. 5, no. 1, 2017.

[2] K. Okamoto and S. Hatakeyama, "Tuberculous peritonitis," *The New England Journal of Medicine*, vol. 379, no. 12, article e20, 2018.

[3] G. Motoa and S. Alvarez, "Tuberculous peritonitis masquerading as carcinomatosis," *Clinical Case Reports*, vol. 8, no. 10, pp. 2078-2079, 2020.

[4] D. V. Plotkin, M. V. Sinitsyn, M. N. Reshetnikov, S. V. Kharitonov, M. S. Skopin, and I. A. Sokolina, "Tuberkuleznyĭ peritonit. Zabytaia bolezn [Tuberculous peritonitis. Forgotten disease]," *Khirurgiia (Mosk)*, no. 12, pp. 38–44, 2018.

[5] H. Kushima, R. Sakamoto, Y. Kinoshita, and H. Ishii, "Tuberculous peritonitis," *BMJ Case Reports*, vol. 14, no. 10, article e245311, 2021.

[6] B. G. Sierra, R. de la Plaza Llamas, and J. M. R. Ángel, "Tuberculous peritonitis mimicking carcinomatosis: a case report," *Gastroenterología y Hepatología*, vol. 43, no. 8, pp. 447–449, 2020.

[7] E. M. Sieloff, A. T. Ladzinski, N. Alcantara Lima, D. Vos, H. Boamah, and T. A. Melgar, "Hospitalizations for tuberculous peritonitis in the United States: results from the national inpatient sample database from 2002 to 2014," *International Journal of Mycobacteriology*, vol. 9, no. 2, pp. 167–172, 2020.

[8] B. Aslan, D. Tüney, Z. A. N. Almoabid, Y. Erçetin, and İ. E. Seven, "Tuberculous peritonitis mimicking carcinomatosis peritonei: CT findings and histopathologic correlation," *Radiology Case Reports*, vol. 14, no. 12, pp. 1491–1494, 2019.

[9] L. Yamada, M. Saito, T. Aita et al., "Tuberculous peritonitis; the effectiveness of diagnostic laparoscopy and the perioperative infectious prevention: a case report," *International Journal of Surgery Case Reports*, vol. 72, pp. 326–329, 2020.

[10] K. L. Bradford, F. A. Moretti, D. A. Carbonaro-Sarracino, H. B. Gaspar, and D. B. Kohn, "Adenosine deaminase (ADA)-deficient severe combined immune deficiency (SCID): molecular pathogenesis and clinical manifestations," *Journal of Clinical Immunology*, vol. 37, no. 7, pp. 626–637, 2017.

[11] B. Varghese, M. Enani, M. Shoukri et al., "The first Saudi Arabian national inventory study revealed the upcoming challenges of highly diverse non-tuberculous mycobacterial diseases," *PLOS Neglected Tropical Diseases*, vol. 12, no. 5, article e0006515, 2018.

[12] Y. C. Shen, T. Wang, L. Chen et al., "Diagnostic accuracy of adenosine deaminase for tuberculous peritonitis: a meta-analysis," *Archives of Medical Science*, vol. 9, no. 4, pp. 601–607, 2013.

[13] X. D. Yang, W. Li, S. Zhang et al., "PLK4 deubiquitination by Spata 2-CYLD suppresses NEK7-mediated NLRP3 inflammasome activation at the centrosome," *The EMBO Journal*, vol. 39, no. 2, article e102201, 2020.

[14] R. Zhang, Z. Xu, J. Yao et al., "Tuberculous peritonitis diagnosed using laparoscopy with assistance of a central venous catheter," *Experimental and Therapeutic Medicine*, vol. 16, no. 6, pp. 5265–5271, 2018.

[15] X. He, Y. Gao, Q. Liu, Z. Zhao, W. Deng, and H. Yang, "Diagnostic value of interferon-gamma release assays combined with multiple indicators for tuberculous peritonitis," *Gastroenterology Research and Practice*, vol. 2020, Article ID 2056168, 10 pages, 2020.

[16] Y. J. Liao, C. Y. Wu, S. W. Lee et al., "Adenosine deaminase activity in tuberculous peritonitis among patients with underlying liver cirrhosis," *World Journal of Gastroenterology*, vol. 18, no. 37, pp. 5260–5265, 2012.

[17] Y. Zhen and H. Zhang, "NLRP3 inflammasome and inflammatory bowel disease," *Frontiers in Immunology*, vol. 10, p. 276, 2019.

[18] J. M. Martinez-Vazquez, I. Ocaña, E. Ribera, R. M. Segura, and C. Pascual, "Adenosine deaminase activity in the diagnosis of tuberculous peritonitis," *Gut*, vol. 27, no. 9, pp. 1049–1053, 1986.

[19] J. Sun, H. Zhang, Z. Song et al., "The negative impact of increasing age and underlying cirrhosis on the sensitivity of adenosine deaminase in the diagnosis of tuberculous

peritonitis: a cross-sectional study in eastern China," *International Journal of Infectious Diseases*, vol. 110, pp. 204–212, 2021.

[20] H. Guo and J. P. Ting, "Inflammasome assays in vitro and in mouse models," *Current Protocols in Immunology*, vol. 131, no. 1, article e107, 2020.

[21] H. Yin, Q. Guo, X. Li et al., "Curcumin suppresses IL-1β secretion and prevents inflammation through inhibition of the NLRP3 inflammasome," *The Journal of Immunology*, vol. 200, no. 8, pp. 2835–2846, 2018.

Hindawi
Disease Markers
Volume 2022, Article ID 7285639, 7 pages
https://doi.org/10.1155/2022/7285639

Research Article

Effect of Multidisciplinary Team Continuous Nursing on Glucose and Lipid Metabolism, Pregnancy Outcome, and Neonatal Immune Function in Gestational Diabetes Mellitus

Shuping Qi[1] **and Yanmei Dong**[2]

[1]*Department of Pediatrics, The Second Children & Women's Healthcare of Jinan City, Jinan, China*
[2]*Department of Gynecology, The Second Children & Women's Healthcare of Jinan City, Jinan, China*

Correspondence should be addressed to Shuping Qi; qisongfu987086999@163.com

Received 29 January 2022; Revised 19 April 2022; Accepted 26 June 2022; Published 8 September 2022

Academic Editor: Zhaoqi Dong

Objective. To investigate the effect of multidisciplinary team (MDT) continuous nursing on glucose and lipid metabolism, pregnancy outcome, and neonatal immune function in gestational diabetes mellitus (GDM). *Methods*. A total of 90 patients with gestational diabetes mellitus (GDM) from January 2018 to December 2019 were recruited and assigned to receive routine care (routine group) or MDT continuous care (study group) according to different nursing methods. Outcome measures included glucose and lipid metabolism, pregnancy outcomes, and neonatal immune function. *Results*. There were no significant differences in glucose and lipid metabolism indices and self-rating anxiety scale (SAS) scores, before nursing. After nursing, MDT continuous care resulted in significantly lower levels of fasting blood glucose (FBG), 2 h postprandial blood glucose (2hPBG), glycosylated hemoglobin (HbAlc), triglyceride (TG), and homeostasis model insulin resistance index (HOMA-IR) versus routine care. After nursing, the SAS scores in the two groups were significantly decreased, with lower results in the study group. Patients in the study group showed better compliance than those in the routine group. MDT continuous care was associated with a significantly lower incidence of premature rupture of fetal membranes, cesarean section, premature delivery, macrosomia, and hypoglycemia versus routine nursing. There were no significant differences in immunoglobulin (Ig) A and IgM levels. Patients in the study group showed a higher IgG level and lower CD3, CD4, CD8, and CD4/CD8 levels than those in the routine group. *Conclusion*. MDT continuous nursing could effectively regulate glucose and lipid metabolism and improve pregnancy outcomes and neonatal immune function in patients with GDM.

1. Introduction

Gestational diabetes mellitus (GDM) refers to impaired glucose tolerance or diabetes that first occurs during pregnancy [1]. According to statistics, the incidence of GDM has increased by 10%-100% worldwide in the past two decades and the incidence is 1%-14% in different countries; the incidence of GDM is 1%-5% in China, which has been on a rise in recent years [2]. The risk factors mainly include advanced age, obesity, parity, ethnicity, physical inactivity, history of macrosomia, family history of type 2 diabetes, and history of GDM [3]. Many clinical studies have demonstrated that GDM is associated with adverse pregnancy outcomes, and women with GDM are at an increased risk of diabetes after pregnancy. It is predicted that 50% of GDM patients will develop diabetes in 22-28 years after pregnancy, resulting in a heavy economic and medical burden to society and family [4, 5]. Traditional treatment methods mainly rely on existing experience and knowledge and are associated with poor treatment outcomes and a high incidence of adverse pregnancy outcomes [6]. Thus, early intervention and improvement of self-management abilities of pregnant women with GDM are of great significance to reduce adverse pregnancy outcomes [7, 8]. The multidisciplinary team (MDT) model refers to a multidisciplinary team composed of clinicians, dietitians, and nurses to provide cross-

Table 1: Comparison of general data ($\bar{x} \pm s$).

Group ($n = 45$)	Age	Epilepsy	Parity	Prepregnancy BMI	Body mass
Conventional group	28.17 ± 4.03	38.52 ± 1.08	1.41 ± 0.42	24.01 ± 2.95	63.88 ± 8.25
Study group	28.54 ± 3.83	38.65 ± 1.11	1.52 ± 0.39	23.86 ± 3.14	64.12 ± 7.98
T	0.446	0.563	1.287	0.234	0.140
P	0.657	0.575	0.201	0.816	0.889

departmental nursing intervention, resolve nursing issues, and ultimately improve the quality of care [9, 10]. MDT management in China mainly focuses on patients with diabetes, coronary heart disease, and hypertension [11], and it has been reported that specialist nurse-led MDT continuous nursing intervention in out-of-hospital care of elderly diabetic patients could effectively improve the blood glucose control and reduce the incidence of readmission and adverse events [12, 13]. MDT continuous nursing involves four modules, namely, first visit, follow-up visit, one-day clinic, and postpartum. The first visit module includes GDM specialist assessment, formulation of individualized dietary prescription, pregnancy diet, exercise guidance, lifestyle guidance, and pregnancy body mass management. The follow-up visit module includes evaluation of blood glucose self-management, individualized guidance on blood glucose, nutritional assessment, assessment of body mass gain during pregnancy, fetal monitoring, and guidance on glucose-lowering drugs. The one-day clinic module includes blood glucose monitoring, individualized guidance on diet and exercise, guidance on glucose-lowering drugs, and psychological guidance. The postpartum module includes maternal and newborn body mass assessment, postpartum lifestyle guidance, review, guidance on postpartum glucose management, and breastfeeding. However, the application of MDT mode in patients with GDM is marginally explored, so this study was conducted to investigate the effects of MDT continuous care on glucose and lipid metabolism, pregnancy outcomes, and neonatal immune function in gestational diabetes.

2. Materials and Methods

2.1. General Information. A total of 90 patients with GDM from January 2018 to December 2019 were selected and assigned at a ratio of 1 : 1 to a study group or a routine group according to different nursing methods. There were no significant differences in the general data between the two groups ($P > 0.05$) (Table 1). The research was approved by the Ethics Committee of the Second Children & Women's Healthcare of Jinan City, No. JN2117.

2.2. Inclusion and Exclusion Criteria. Inclusion criteria: pregnant women who were diagnosed with GDM as per the 2010 IADPSG diagnostic criteria for gestational diabetes [14], with singleton pregnancy, with clear consciousness to perform normal communication were included.

The diagnostic criteria for hypertensive disorders during pregnancy, excessive amniotic fluid, premature rupture of membranes, postpartum hemorrhage, and fetal macrosomia [2] are as follows. Hypertensive disorders during pregnancy: pregnant women have BP ≥ 140/90 mmHg (mmHg = 0.133 kPa) for the first time during pregnancy, which returns to normal within 12 weeks after delivery, with negative results of urine protein assay. Excessive amniotic fluid: the volume of amniotic fluid in pregnancy exceeds 2000 mL. Premature rupture of fetal membranes: rupture of fetal membranes occurs before delivery. Postpartum hemorrhage: the volume of vaginal bleeding within 24 hours after vaginal delivery exceeds 500 mL or cesarean delivery exceeds 1000 mL. Fetal macrosomia: neonatal birth mass exceeds 4000 g.

Exclusion criteria: patients with underlying diseases such as hypertension and heart disease, with withdrawal of consent, and with severe mental diseases were excluded.

2.3. Nursing Methods. The routine group received routine nursing. Routine nursing included regular prenatal care after diagnosis, routine pregnancy guidance and education, assessment of fetal conditions, body mass management, self-monitoring guidance, psychological counseling during pregnancy, and dietary guidance. The fasting blood glucose (FBG), 2-hour postprandial blood glucose (2hPBG), and glycosylated hemoglobin (HbAlc) were measured at 32 and 37 weeks of pregnancy.

The study group received MDT continuous nursing: ① an MDT team composed of endocrinologists, dietitians, mother-infant specialist nurses, midwives, diabetes specialist nurses, psychological specialist nurses, and rehabilitation instructors was established. ② Nursing issues and solutions: nursing issues such as inadequate health knowledge education and poor self-management ability of patients were jointly discussed and analyzed by the MDT members to enhance the compliance and pregnancy outcomes of patients. ③ Health education [15]: the patients were given health education related to GDM to help them understand the disease and enhance treatment compliance. ④ Self-management education was also carried out to enhance patients' awareness of self-care. ⑤ Psychological intervention: psychological counseling was performed to relieve patients' negative emotions and improve treatment compliance. ⑥ Condition monitoring: the blood glucose and related indicators of patients after delivery were closely monitored, and postpartum dietary guidance was provided. Pregnant women with poor blood glucose control were given insulin injections as appropriate. The total daily nutritional intake of pregnant women (≥1500 kcal/d in early pregnancy and ≥1800 kcal/d in late pregnancy) was calculated according to the patient's prepregnancy body mass index. The daily carbohydrate intake was 50-

Table 2: Comparison of glucose and lipid metabolism parameters before and after nursing intervention between the two groups ($\bar{x} \pm s$).

Group ($n = 45$)	Time	FBG (mmol/L)	2hPBG (mmol/L)	HbAlc (%)	FINS (mmol/L)
Conventional group	Preintervention	7.81 ± 1.52	10.56 ± 2.48	6.51 ± 1.24	11.22 ± 2.85
	Postintervention	6.46 ± 1.53*	7.94 ± 2.41*	5.82 ± 1.61*	11.42 ± 2.73
Study group	Preintervention	7.91 ± 1.61	10.58 ± 2.43	6.58 ± 1.12	11.29 ± 2.38
	Postintervention	5.63 ± 1.28*	7.01 ± 1.98*	5.13 ± 1.13*	11.52 ± 3.31
T	—	0.303/2.791	0.039/1.904	0.281/2.353	0.126/0.156
P	—	0.763/0.006	0.969/0.049	0.779/0.021	0.900/0.876
Group ($n = 45$)	Time	TC (mmol/L)	TG (mmol/L)	LDL-C (mmol/L)	HOMA-IR
Conventional group	Preintervention	5.63 ± 0.88	2.81 ± 0.73	3.19 ± 0.88	1.65 ± 0.44
	Postintervention	4.83 ± 0.68	2.43 ± 0.54*	3.11 ± 0.69	1.31 ± 0.35*
Study group	Preintervention	5.71 ± 0.84	2.82 ± 0.81	3.17 ± 0.91	1.64 ± 0.45
	Postintervention	4.78 ± 0.71	2.21 ± 0.46*	3.02 ± 0.68	1.02 ± 0.23*
T	—	0.441/0.341	0.062/2.080	0.106/0.623	0.107/4.645
P	—	0.660/0.734	0.951/0.040	0.916/0.535	0.915/<0.001

Note: T value and P are the comparison results before and after nursing. $^*P < 0.05$.

60% of the total intake (≥150 g/d), the fat intake was 25%-30% of the total intake, and the protein intake was 15%-20% of the total intake. Vitamin and minerals were appropriately supplemented, and the daily intake of dietary fiber is controlled at 25-30 g.

2.4. Evaluation Criteria

2.4.1. Glucose and Lipid Metabolism Indicators. An AU5800 automatic biochemical analyzer was used to determine the levels of FBG, 2hPBG, HbAlc, fasting insulin (FINS), total cholesterol (TC), triglyceride (TG), low-density lipoprotein cholesterol (LDL-C), and homeostasis model insulin resistance index (HOMA-IR).

2.4.2. Self-Rating Anxiety Scale (SAS) Score. The SAS includes 20 items, with each item being scored as 0-4 points. A score of <50 indicates no anxiety, 50-59 indicates mild anxiety, 60-69 indicates moderate anxiety, and ≥70 indicates severe anxiety.

2.4.3. Compliance. The self-made questionnaire of our hospital was used for compliance assessment. Dietary compliance: patients adhering to the diet for 6 days or more per week were given 4 points, 3 points for 5 days, 2 points for 3-4 days, and 0 points for less than 3 days. Exercise compliance: patients who exercised 5 times or more per week were given 4 points, 3 points for 4 times, 2 points for 3 times, and 0 points for less than 3 times. Blood glucose monitoring compliance: patients who performed blood glucose monitoring 4 times or more per week were given 4 points, 3 points for 3 times, 2 points for 2 times, and 0 points for less than 2 times. A score of ≥3 points indicates good compliance and <3 points indicate poor compliance.

2.4.4. Pregnancy Outcomes. Hyperhydramnios, fetal membrane, cesarean section, neonatal distress, premature delivery, macrosomia, and hypoglycemia were recorded.

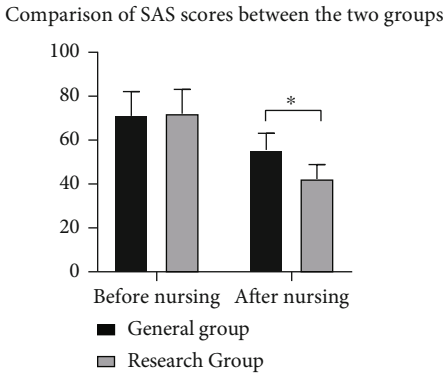

Figure 1: Comparison of SAS scores before and after nursing. $^*P < 0.05$.

2.4.5. Neonatal Immune Function. The levels of immunoglobulin G (IgG), immunoglobulin A (IgA), and immunoglobulin M (IgM) in peripheral blood of neonates were determined using immunoturbidimetry. The levels of CD3, CD4, and CD8 in T cells were determined using flow cytometry, and the CD4/CD8 values were calculated.

2.4.6. Satisfactory Glycemic Control Criteria for Pregnant Women with GDM. The pregnant women had no obvious hunger, with a fasting glucose value of 3.3-5.3 mmol/L, 2-hour postprandial glucose value of 4.4-6.7 mmol/L, and glycated hemoglobin < 5.5%. Venous blood was collected from pregnant women at 32 and 37 weeks of gestation in the outpatient laboratory to determine FBG, HbAlc, and 2hPBG levels. The values of FBG, 2hPBG, and HbAlc that were normal in two tests were considered satisfactory blood glucose control.

2.5. Statistical Analysis. SPSS 22.0 software was used for data analyses, and GraphPad Prism 8 was used to plot the graphics. Enumeration data [n (%)] and measurement data (mean ± SD) were analyzed by chi-square and t-test,

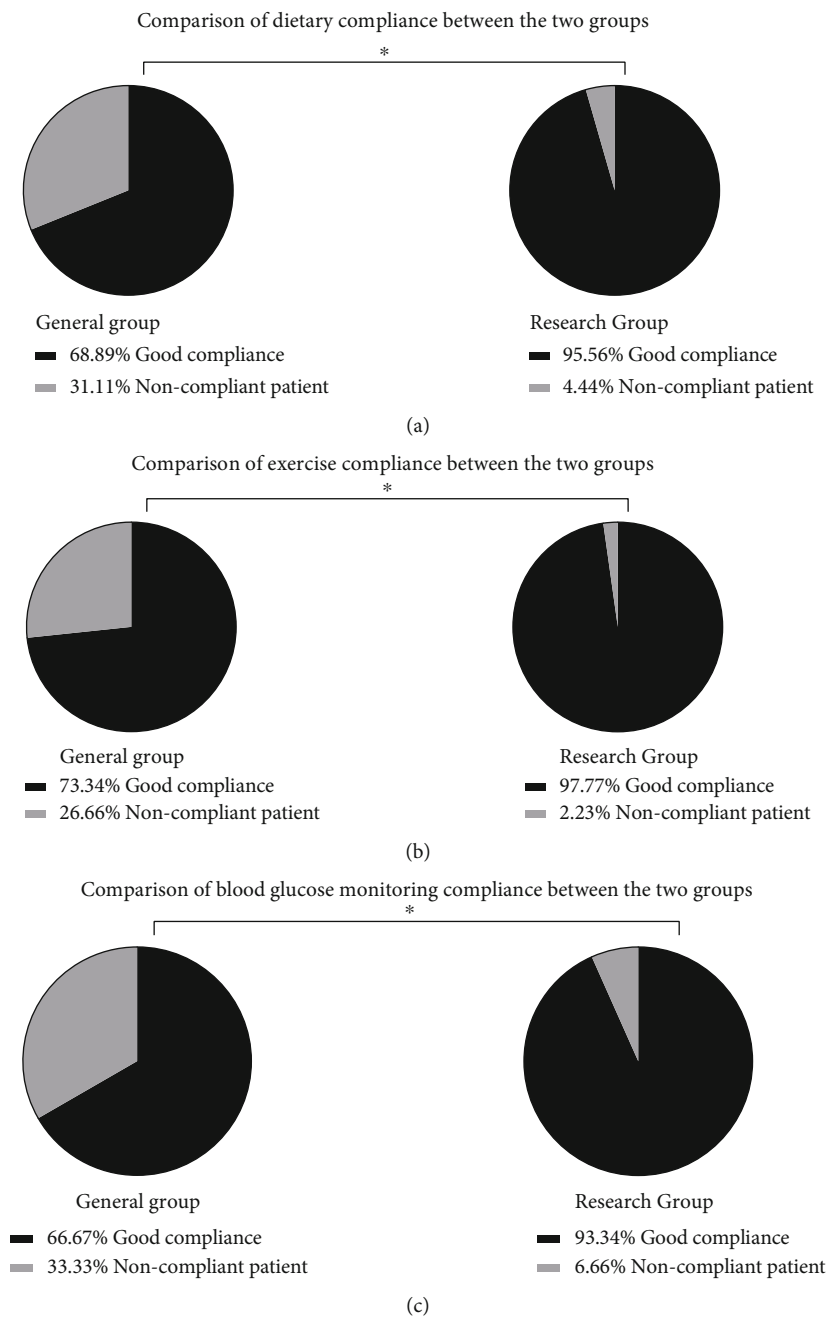

Figure 2: Comparison of patient compliance. $^{*}P < 0.05$.

Table 3: Comparison of pregnancy outcomes (%).

Group ($n = 45$)	Hyperhydramnios	Fetal membrane	Cesarean section	Fetal distress	Premature	Macrosomia	Hypoglycemia
Conventional group	4 (8.89)	9 (20.00)	25 (55.56)	3 (6.67)	7 (15.55)	6 (13.34)	6 (13.34)
Study group	1 (2.23)	2 (4.45)	13 (26.67)	0 (0.00)	1 (2.23)	1 (2.23)	1 (2.23)
X^2	1.901	5.075	6.559	3.102	4.939	3.873	3.873
P	0.167	0.024	0.010	0.078	0.026	0.049	0.049

Table 4: Comparison of peripheral blood immunoglobulin and T cell levels ($\bar{x} \pm s$).

(a)

Group ($n = 45$)	Immunoglobulins (g/L)		
	IgG	IgA	IgM
Conventional group	9.36 ± 2.01	0.31 ± 0.08	0.17 ± 0.07
Study group	10.38 ± 2.62	0.28 ± 0.09	0.16 ± 0.08
T	2.072	1.671	0.631
P	0.041	0.098	0.530

(b)

Group ($n = 45$)	T cells (%)			
	CD3*	CD4*	CD8	CD4*/CD8*
Conventional group	42.37 ± 9.29	26.98 ± 7.23	25.41 ± 6.04	1.13 ± 0.26
Study group	37.54 ± 8.21	24.17 ± 6.08	23.01 ± 5.16	0.95 ± 0.22
T	2.613	2.004	2.027	3.545
P	0.011	0.048	0.046	0.001

respectively. Differences were considered statistically significant at $P < 0.05$.

3. Results

3.1. Glycolipid Metabolism. There were no significant differences in glucose and lipid metabolism indices before nursing ($P > 0.05$). MDT continuous care resulted in significantly lower levels of FBG, 2hPBG, HbAlc, TG, and HOMA-IR versus routine care ($P < 0.05$) (Table 2).

3.2. SAS Score. There were no significant differences in SAS scores before intervention ($P > 0.05$). After nursing, the SAS scores in the two groups were significantly decreased, with lower results in the study group ($P < 0.05$) (Figure 1).

3.3. Patient Compliance. According to the results of the questionnaire survey, 31 patients in the routine group had good dietary compliance, 33 had good exercise compliance, and 30 had good blood glucose monitoring compliance; 43 patients in the study group had good dietary compliance, 44 had good exercise compliance, and 42 had good blood glucose monitoring compliance. Patients in the study group showed better compliance than those in the routine group ($P < 0.05$) (Figure 2).

3.4. Pregnancy Outcomes. There were 4 cases of conventional polyhydramnios, 9 cases of premature rupture of fetal membrane, 25 cases of cesarean section, 3 cases of fetal distress, 7 cases of premature delivery, 6 cases of macrosomia, and 6 cases of hypoglycemia in the routine group. There were 1 case of polyhydramnios, 2 cases of premature rupture of fetal membrane, 13 cases of cesarean section, 0 cases of fetal distress, 1 case of premature delivery, 1 case of macrosomia, and 1 case of hypoglycemia in the study group. MDT continuous care was associated with a significantly lower incidence of premature rupture of fetal membranes, cesarean section, premature delivery, macrosomia, and hypoglycemia versus routine nursing ($P < 0.05$) (Table 3).

3.5. Neonatal Immune Function. There were no significant differences in IgA and IgM levels ($P > 0.05$). Patients in the study group showed a higher IgG level and lower CD3, CD4, CD8, and CD4/CD8 levels than those in the routine group ($P < 0.05$) (Table 4).

4. Discussion

Gestational diabetes mellitus (GDM) is a common complication of pregnancy [16], which refers to impaired glucose tolerance or diabetes that first occurs during pregnancy, more frequently in the second and third trimesters of pregnancy. Previous clinical research has demonstrated that GDM is associated with adverse pregnancy outcomes, and women with concurrent GDM are at an increased risk of diabetes after pregnancy [17]. At present, the clinical treatment focuses on blood glucose control and complication prevention [18]. Traditional treatment mainly relies on existing experience and knowledge, and issues in the aspects of diet, psychology, and exercise are mostly handled by experience, resulting in poor treatment outcomes [19]. The MDT [9] is composed of clinicians, dietitians, and nurses to provide cross-departmental nursing intervention, resolve nursing issues, and ultimately improve the quality of care [20]. MDT is patient-centered, guided by the latest medical research results, and relies on a multidisciplinary team to develop the optimal comprehensive treatment plan for a specific disease with standardization, personalization, and continuity. This model enhances effective communication and recognition between medical and nursing care and promotes in-depth learning and exchange of knowledge and techniques of gestational diabetes among various disciplines. In addition, it ensures the integration and communication between the medical and nursing management departments,

with collaboration among the clinical group, management group, and quality control group, resulting in a significant improvement in the glycemic and body mass control of pregnant women with GDM. The results of the present study showed that MDT continuous nursing can enhance the effective communication and recognition between medical staff to improve glucose and lipid metabolism control. MDT continuous nursing carries out comprehensive and professional health education, increases the patient's understanding of the disease and the nursing, pays attention to the patient's emotional changes, relieves the patient's concerns to a certain extent, and improves the negative emotions. Tao et al. stated that the IgG level in the blood of newborns of gestational diabetes patients with poor blood glucose control was lower than that of newborns of gestational diabetes patients with good blood glucose control. Combined with the results in the present study, it indicates that MDT continuous care resulted in a superior immune function of newborns and better blood glucose control versus routine care.

5. Conclusions

MDT continuous nursing effectively regulates glucose and lipid metabolism in patients with GDM and improves pregnancy outcomes and neonatal immune function, so it is worthy of clinical promotion. The innovation of this study is the use of patient-centered MDT continuous nursing, which relies on a multidisciplinary team to develop an optimal comprehensive treatment plan that is standardized, personalized, and continuous, thereby enhancing the quality of life of patients. However, the limitation of this study lies in the absence of detailed studies on the intelligence and development of the children, which will be investigated in future studies.

Data Availability

The datasets used during the present study are available from the corresponding author upon reasonable request.

Conflicts of Interest

The authors declare that they have no conflict of interest.

References

[1] M. Lende and A. Rijhsinghani, "Gestational diabetes: overview with emphasis on medical management," *International Journal of Environmental Research and Public Health*, vol. 17, no. 24, 2020.

[2] J. Juan and H. Yang, "Prevalence, prevention, and lifestyle intervention of gestational diabetes mellitus in China," *International Journal of Environmental Research and Public Health*, vol. 17, no. 24, p. 9517, 2020.

[3] L. Rasmussen, C. W. Poulsen, U. Kampmann, S. B. Smedegaard, P. G. Ovesen, and J. Fuglsang, "Diet and healthy lifestyle in the management of gestational diabetes mellitus," *Nutrients*, vol. 12, no. 10, p. 3050, 2020.

[4] J. F. Plows, J. Stanley, P. Baker, C. Reynolds, and M. Vickers, "The pathophysiology of gestational diabetes mellitus," *International Journal of Molecular Sciences*, vol. 19, no. 11, p. 3342, 2018.

[5] D. R. Coustan, "Gestational diabetes mellitus," *Clinical Chemistry*, vol. 59, no. 9, pp. 1310–1321, 2013.

[6] K. Sushko, H. T. Menezes, P. Strachan, M. Butt, and D. Sherifali, "Self-management education among women with pre-existing diabetes in pregnancy: a scoping review," *International Journal of Nursing Studies*, vol. 117, article 103883, 2021.

[7] N. Meloncelli, A. Barnett, and S. de Jersey, "Staff resourcing, guideline implementation and models of care for gestational diabetes mellitus management," *The Australian & New Zealand Journal of Obstetrics & Gynaecology*, vol. 60, no. 1, pp. 115–122, 2020.

[8] E. Kintiraki and D. G. Goulis, "Gestational diabetes mellitus: multi-disciplinary treatment approaches," *Metabolism*, vol. 86, pp. 91–101, 2018.

[9] S. Gupta, J. A. Perry, and R. Kozar, "Transitions of care in geriatric medicine," *Clinics in Geriatric Medicine*, vol. 35, no. 1, pp. 45–52, 2019.

[10] U. S. Dankoly, D. Vissers, Z. el Farkouch et al., "Perceived barriers, benefits, facilitators, and attitudes of health professionals towards multidisciplinary team care in type 2 diabetes management: a systematic review," *Current Diabetes Reviews*, vol. 17, no. 6, article e111020187812, 2021.

[11] A. A. Shamshirsaz, K. A. Fox, H. Erfani et al., "Multidisciplinary team learning in the management of the morbidly adherent placenta: outcome improvements over time," *American Journal of Obstetrics and Gynecology*, vol. 216, no. 6, pp. 612.e1–612.e5, 2017.

[12] J. García, H. Rodríguez, and V. Casas, "The patient's opinion matters: experience in the nutritional care in an ALS multidisciplinary team," *Nutrición Hospitalaria*, vol. 31, Supplement 5, pp. 56–66, 2015.

[13] J. Musuuza, B. L. Sutherland, S. Kurter, P. Balasubramanian, C. M. Bartels, and M. B. Brennan, "A systematic review of multidisciplinary teams to reduce major amputations for patients with diabetic foot ulcers," *Journal of Vascular Surgery*, vol. 71, no. 4, pp. 1433–1446.e3, 2020.

[14] B. Pillay, A. C. Wootten, H. Crowe et al., "The impact of multidisciplinary team meetings on patient assessment, management and outcomes in oncology settings: a systematic review of the literature," *Cancer Treatment Reviews*, vol. 42, pp. 56–72, 2016.

[15] N. Meloncelli, A. Barnett, and S. de Jersey, "An implementation science approach for developing and implementing a dietitian-led model of care for gestational diabetes: a pre-post study," *BMC Pregnancy and Childbirth*, vol. 20, no. 1, p. 661, 2020.

[16] E. Chiefari, B. Arcidiacono, D. Foti, and A. Brunetti, "Gestational diabetes mellitus: an updated overview," *Journal of Endocrinological Investigation*, vol. 40, no. 9, pp. 899–909, 2017.

[17] N. Meloncelli, A. Barnett, F. Pelly, and S. de Jersey, "Diagnosis and management practices for gestational diabetes mellitus in Australia: cross-sectional survey of the multidisciplinary team," *The Australian & New Zealand Journal of Obstetrics & Gynaecology*, vol. 59, no. 2, pp. 208–214, 2019.

[18] E. C. Johns, F. C. Denison, J. E. Norman, and R. M. Reynolds, "Gestational diabetes mellitus: mechanisms, treatment, and complications," *Trends in Endocrinology and Metabolism*, vol. 29, no. 11, pp. 743–754, 2018.

[19] A. Rahmani and B. Afandi, "Improving neonatal complications with a structured multidisciplinary approach to gestational diabetes mellitus management," *Journal of Neonatal-Perinatal Medicine*, vol. 8, no. 4, pp. 359–362, 2015.

[20] K. Dittman and S. Hughes, "Increased nursing participation in multidisciplinary rounds to enhance communication, patient safety, and parent satisfaction," *Critical Care Nursing Clinics of North America*, vol. 30, no. 4, pp. 445–455.e4, 2018.

Hindawi
Disease Markers
Volume 2022, Article ID 7593750, 17 pages
https://doi.org/10.1155/2022/7593750

Research Article

A Deep Learning Model Incorporating Knowledge Representation Vectors and Its Application in Diabetes Prediction

He Xu,[1,2,3,4,5] **Qunli Zheng**,[1] **Jingshu Zhu**,[1] **Zuoling Xie**,[6] **Haitao Cheng**,[1,2,3,4,5] **Peng Li**,[1,2,3,4,5] **and Yimu Ji**[1,3,4,5]

[1]*School of Computer Science, Nanjing University of Posts and Telecommunications, Nanjing 210023, China*
[2]*Jiangsu High Technology Research Key Laboratory for Wireless Sensor Networks, Jiangsu Province, Nanjing 210023, China*
[3]*Institute of High Performance Computing and Big Data, Nanjing University of Posts and Telecommunications, Nanjing 210023, China*
[4]*Nanjing Center of HPC China, Nanjing 210023, China*
[5]*Jiangsu Research Engineering of HPC and Intelligent Processing, Nanjing University of Posts and Telecommunications, Nanjing 210023, China*
[6]*Department of Endocrinology, Zhongda Hospital Southeast University, Nanjing 210009, China*

Correspondence should be addressed to Peng Li; lipeng@njupt.edu.cn and Yimu Ji; jiym@njupt.edu.cn

Received 14 June 2022; Revised 24 July 2022; Accepted 30 July 2022; Published 12 August 2022

Academic Editor: Yaoyao Bian

The deep learning methods for various disease prediction tasks have become very effective and even surpass human experts. However, the lack of interpretability and medical expertise limits its clinical application. This paper combines knowledge representation learning and deep learning methods, and a disease prediction model is constructed. The model initially constructs the relationship graph between the physical indicator and the test value based on the normal range of human physical examination index. And the human physical examination index for testing value by knowledge representation learning model is encoded. Then, the patient physical examination data is represented as a vector and input into a deep learning model built with self-attention mechanism and convolutional neural network to implement disease prediction. The experimental results show that the model which is used in diabetes prediction yields an accuracy of 97.18% and the recall of 87.55%, which outperforms other machine learning methods (e.g., lasso, ridge, support vector machine, random forest, and XGBoost). Compared with the best performing random forest method, the recall is increased by 5.34%, respectively. Therefore, it can be concluded that the application of medical knowledge into deep learning through knowledge representation learning can be used in diabetes prediction for the purpose of early detection and assisting diagnosis.

1. Introduction

In recent years, with the development of big data and computer technology, intelligent systems based on deep learning method have been used in many fields. Deep learning as an important branch in the field of machine learning has been used in data representations with multiple levels of abstraction through multiprocessing layer models [1]. It has been widely used in the areas of speech recognition [2], image recognition [3, 4], and natural language processing [5]. With the increasing usage of medical equipment and digital recording systems, the amount of patient data is generated and the value of big data is gradually benefiting with the usage of deep learning [6]. Currently, in the medical field, deep learning is mainly used in the research of medical imaging [7, 8] and electronic health record (EHR) [9, 10]. Moreover, physician-level accuracy has been widely achieved in some complex disease diagnosis tasks, such as breast lesion detection [11], diabetes complication prediction [12], and Alzheimer's disease classification [13].

Nevertheless, deep learning-based methods have not yet been widely applied in clinical diagnosis. One of the main

factors is due to the black-box feature of deep learning algorithms. The visual or textual explanations provided by deep learning algorithms seem reasonable, but the details of the algorithm's decisions are not clearly exposed [14]. Internals of the model is difficult to grasp for patients or physicians and can contribute to trust issues. Furthermore, it is also against the ethical responsibility of clinicians to leave medical decision-making to black-box systems because it lacks interpretability [15]. In addition, the majority of deep learning models are trained on the basis of data-driven [16] methods, which require that the datasets should be high volume and quality [17]. However, medical datasets are characterized by uncertainty, heterogeneity, time dependence, sparsity, and irregularity [18–20]. These features make the medical datasets that have noisy, missing, and redundant data; thus, it is challenge to guarantee data quality. Besides, security and privacy issues in the healthcare industry restrict the access to healthcare data [21].

Consequently, owing to the black-box feature of deep learning algorithms and the complexity of medical data, it is difficult for using deep learning model to achieve perfect decision-making. However, some research [22] suggests that the knowledge-driven approach can be applied to embed external domain of medical expertise into deep learning models to improve data quality and enhance the interpretability of the models. At present, knowledge-driven approach primarily relies on the building of knowledge graphs [23], such as a knowledge-driven drug reuse approach is proposed in the literature [24], which is based on the constructed comprehensive drug knowledge graphs. Knowledge graphs, as a kind of graph-based data structure, can formally describe real-world matters and their interrelationships [25]. With its huge descriptive power of complex data and better interpretability compared with the traditional methods, it has a promising prospect in smart medical domains [26] and medical knowledge Q&A system [27]. The massive medical knowledge graphs have also been built constantly, such as IBM's Watson Health Knowledge Graph and Shanghai Shuguang Hospital's Knowledge Graph of Chinese Medicine [28]. Intelligent disease diagnosis is aimed at allowing computer machines to learn medical professional knowledge and simulate the analysis of physicians for diagnosis [29], so it is of great research significance to introduce medical professional knowledge into disease diagnosis through knowledge graphs.

However, different diseases are diagnosed differently, and the specialized knowledge has different features. It is worthwhile to consider how the medical knowledge can be widely applied to various disease diagnosis models. In addition, if the appropriate medical knowledge is selected, how to represent this knowledge and combine it rationally with deep learning models remains a challenge. In view of the above problems, this paper selects common physical measurement data as the research object, takes the normal range of medical examination indexes as the professional knowledge, and simulates the process of doctors to make the corresponding diagnosis based on the patient's medical examination data with the normal range of medical examination indicators as the reference in the actual clinical diagnosis. A disease prediction model integrating knowledge representation and deep learning is proposed and applied to diabetes prediction.

The novelty and innovation in this study are summarized as follows.

(1) According to the normal range of human physical examination indexes and adopting the knowledge representation learning method, a representation vector of human physical examination index and detection value is constructed. The representation vector can precisely describe the relationships between the physical examination indicators and the detection values, which is suitable for a variety of deep learning models and can increase the interpretability of disease prediction models

(2) A deep learning model incorporating a knowledge representation vector is proposed, which employs a constructed representation vector of medical examination indicators and detection values to obtain a relationship matrix of medical examination data. The model associates each medical examination indicator through a self-attention mechanism and utilizes convolutional neural networks for feature extraction for diabetes prediction

(3) We compared our model with other machine learning models such as support vector machines and random forests, and the results show that our model is superior to the compared machine learning models in both precision and recall, indicating that the presented model has a better diabetes prediction effect

2. Materials and Methods

2.1. Deep Learning for Disease Diagnosis. In recent years, a large amount of research work has attempted to apply deep learning to medical diagnosis to assist clinicians and improve the quality of healthcare, for example, medical image classification [30–32], lesion detection [11], and pathology slides [30, 33], as well as electronic health records [34, 35]. Although these researches have yielded valuable results, the lack of interpretability and data quality issues are still key factors limiting their clinical application.

In order to trade off the performance and interpretability of the models, a large number of researchers have researched on interpretable disease diagnosis models [14, 15, 36], focusing on interpreting deep black-box models [37]. For example, Van Molle et al. presented a method which can unravel the black box of convolutional neural networks in the dermatology domain by visualizing the learned feature maps [38]. They concluded that the features which focused on the convolutional neural network were similar to dermatologists for diagnosis. However, the method suffers from the problem that it cannot explain the causal relationship between the features detected by the model and its output, which is not universal. Because it has no specialized knowledge, it is still limited by the quality of the data.

In addition, a number of researches [22, 39–41] have attempted to incorporate domain expertise into deep learning models. Shang et al. constructed a knowledge graph for EHRs

to effectively utilize unused information hidden in EHRs [39]. And the semantic rules identified important clinical findings in EHR data. However, the quality of this knowledge graph depends on the amount of data in the EHR. Choi et al. suggested GRAM, a graph-based attention model, which is used to address the data insufficiency and interpretability issues, and supplemented the EHR with hierarchical information inherent to medical ontologies [40]. Ma et al. considered prior medical knowledge in disease risk prediction and successfully introduced a prior medical knowledge into deep learning models using posteriori regularization techniques, and it can be effectively applied to real medical datasets [41].

In the above-mentioned study, the main emphasis was on electronic health records. However, not all patients have complete records, and these records do not exist for patients who may be first-timers in a hospital. Therefore, the broad applicability of these models remains a challenge. To this end, Zou et al. [42] selected relatively easy-to-obtain physical examination data as the subject of their study and used decision trees, random forests, and neural networks to predict diabetes and validated the general applicability of the models in their experiments. However, the models based on machine learning or statistical methods have low performance.

In order to improve the generalization and performance of the model, Alade et al. proposed a feedforward network model for diagnosing diabetes in pregnant women based on expert system and applied it in web applications [43]. Azeez et al. constructed an expert system for disease diagnosis using the Mamdani reasoning method, which can be used to diagnose a variety of diseases [44]. The expert system proposed in literature [43, 44] has wide applicability and greatly improves the accuracy of disease prediction, but it still lacks the support of external professional knowledge.

Combining the advantages and disadvantages of the above studies, this paper comprehensively considers the general applicability of the model and the knowledge of medical expertise. According to the medical examination data of patients, we try to integrate medical expertise and combine with deep learning technology to build a deep learning model incorporating knowledge representation which can be used to assist the diagnosis of diabetes.

2.2. Knowledge Representation Learning. Usually, the traditional knowledge graph is represented as triples (h, r, t), where h denotes the head entity, t denotes the tail entity, and r denotes the relationship. Knowledge representation learning [45] represents the research objects (entities and relations) as dense low-dimensional real-valued vectors. Researchers have proposed several knowledge representation models. In this paper, we will introduce the TransE [46], Trans [47], and TransR [48] models which are used in our experiments. The model architecture of the three is shown in Figure 1.

The TransE model [46] uses the vector of relation $\mathbf{l}_r$ as a translation between the head entity vector $\mathbf{l}_h$ and the tail entity vector $\mathbf{l}_t$. Equation (1) shows the relationship of those three vectors.

$$\mathbf{l}_h + \mathbf{l}_r \approx \mathbf{l}_t. \tag{1}$$

Its loss function is shown in the following equation:

$$f_r(h, t) = |\mathbf{l}_h + \mathbf{l}_r - \mathbf{l}_t|_{L_1/L_2}. \tag{2}$$

That is the L_1 or L_2 distances of the vectors $\mathbf{l}_h + \mathbf{l}_r$ and $\mathbf{l}_t$.

The TransE model has relative parameters, low computational complexity, and high scalability. However, because of the simplicity of the model, the performance of the model is dramatically reduced when dealing with complex relationships. For example, in a one-to-many relationship, suppose there are two triples in the knowledge base, which includes diabetes, complications, and diabetic nephropathy and (, complications, and diabetic foot; if the TransE model is used, it will make the vectors of diabetic nephropathy and diabetic foot become the same, which is obviously inconsistent with the fact. Aiming at solving the shortcomings of TransE in handling complex relationships, the improved TransH and TransR models are proposed, respectively.

The TransH model [45] firstly processes the head entity vector $\mathbf{l}_h$ and the tail entity vector $\mathbf{l}_t$ along the normal $\mathbf{w}_r$ to the hyperplane corresponding to the relation r, denoted by $\mathbf{l}_{h_r}$ and $\mathbf{l}_{t_r}$, respectively. The relationships are shown as follows:

$$\mathbf{l}_{h_r} = \mathbf{l}_h - \mathbf{w}_r^T \mathbf{l}_h \mathbf{w}_r, \tag{3}$$

$$\mathbf{l}_{t_r} = \mathbf{l}_t - \mathbf{w}_r^T \mathbf{l}_t \mathbf{w}_r. \tag{4}$$

Its loss function is shown in the following equation:

$$f_r(h, t) = \left\|\mathbf{l}_{h_r} + \mathbf{l}_r - \mathbf{l}_{t_r}\right\|_{L_1/L_2}. \tag{5}$$

The TransR model [46] implements the projection of entity vectors onto the subspace of the relation r by defining the projection matrix $\mathbf{M}_r \in R^{(d\times k)}$, denoted $\mathbf{l}_{h_r}$ and $\mathbf{l}_{t_r}$, respectively. The relationship is shown as follows:

$$\begin{aligned} \mathbf{l}_{h_r} &= \mathbf{l}_h \mathbf{M}_r, \\ \mathbf{l}_{t_r} &= \mathbf{l}_t \mathbf{M}_r. \end{aligned} \tag{6}$$

Then, it can make $\mathbf{l}_{h_r} + \mathbf{l}_r \approx \mathbf{l}_{t_r}$, and its loss function is shown in the following equation:

$$f_r(h, t) = \left\|\mathbf{l}_{h_r} + \mathbf{l}_r - \mathbf{l}_{t_r}\right\|_{L_1/L_2}., \tag{7}$$

3. Model Architecture

In this paper, a disease prediction model fusing knowledge representation and deep learning is proposed, which is aimed at simulating the process of disease diagnosis by physicians based on the patient's physical examination data and the known normal range of physical examination indexes. The method obtains a matrix representation of patient physical examination data which is input into a deep learning model to get the result of disease prediction.

The architecture of the deep learning model incorporating the knowledge representation vector is shown in Figure 2. It is mainly divided into the following three parts:

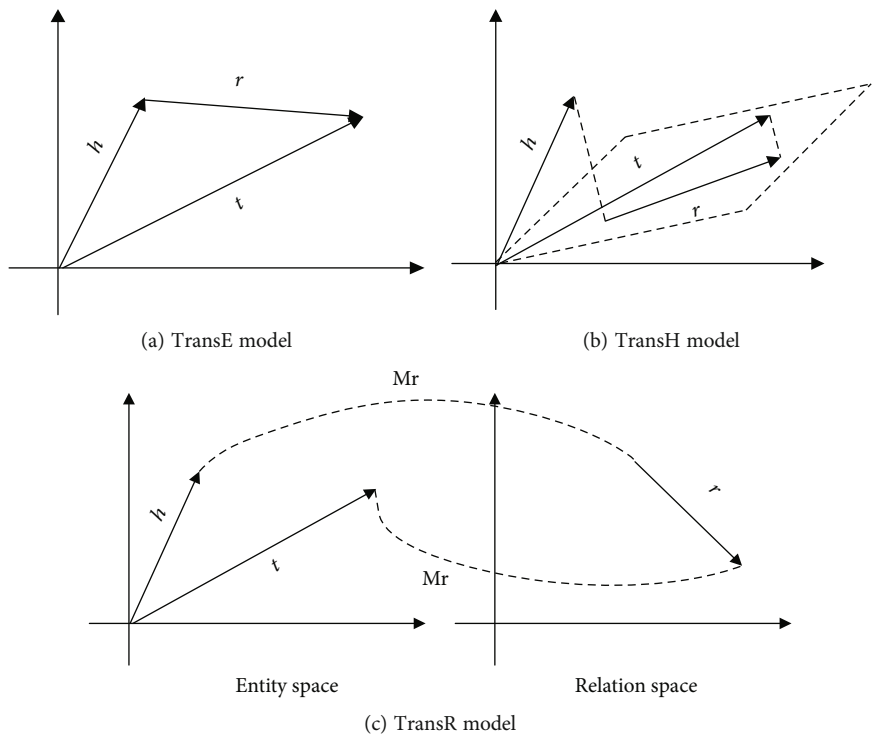

Figure 1: The models of different knowledge representation learning.

(1) According to the normal range of the test value of the physical examination indicator, the relationship between the physical examination indicator and the detection value is constructed, and then, the knowledge representation learning model is used to acquire the representation vector of the physical examination indicator and the detection value

(2) We obtain the physical examination data of patients, acquire the relationship vectors between all physical examination indicators and corresponding test values according to the representation vectors of physical examination indicators and test values in (1), and splice them into a relationship matrix

(3) The relationship matrix is input to the classifier constructed by the self-attention mechanism (self-attention) and convolutional neural network (CNN) to obtain the prediction results of diabetes

In this paper, the proposed model is referred to TH-SAC. The choice of SAC model was made by comparing various models through reading literature and experiments. This paper first tries classical machine learning methods such as logistic regression and random forest, but these methods have been widely used in disease prediction, and it is difficult to improve the prediction effect. Therefore, we began to try to use the method of deep learning. Firstly, we got the vector representation of physical examination index values through knowledge representation learning. Because a single physical examination indicator cannot fully reflect the disease status, different indicators will affect each other. Through reading literature, we know that self-attention can obtain global information, so we choose the self-attention mechanism to calculate the interaction between different indicators. However, self-attention calculations alone were used to extract features that accurately reflected disease. In this regard, CNN extraction is introduced for feature extraction on the basis of self-attention. Of course, we also had tried DNN, Bi-LSTM, and other models, as well as self-attention and CNN alone, but the effect was not good when we evaluated the accuracy, recall rate, F1 value, and so on; at last, we finally chose SAC model.

3.1. Representation Vector of Physical Examination Indicators and Detection Values. In the actual clinical diagnosis of diseases, physicians often make judgments by combining the patient's physical examination data and existing physical examination knowledge. For example, the normal range of blood glucose values in the clinical diagnosis of diabetes is 3.9-6.1 mmol/L. When the blood glucose value is greater than 7.0 mmol/L, it is considered as a possibility of diabetes mellitus [49]. As shown in Figure 2, this paper considers embedding such medical expertise in the model, namely, the normal range of physical examination indicators. Firstly, according to the normal range of physical examination indicators defined in medical science and the advice of medical experts, the values of relevant physical examination indicators are divided into seven ranges: severely low, generally low, slightly low, normal, slightly high, generally high, and seriously high. The measured value of each physical examination index corresponds to a range; that is, there is a relationship between the physical examination index and the measured value. For example, if the normal range of triglycerides is 0.45-1.81 mmol/L, the relationship between triglycerides and 0.45.mmol/L is normal.

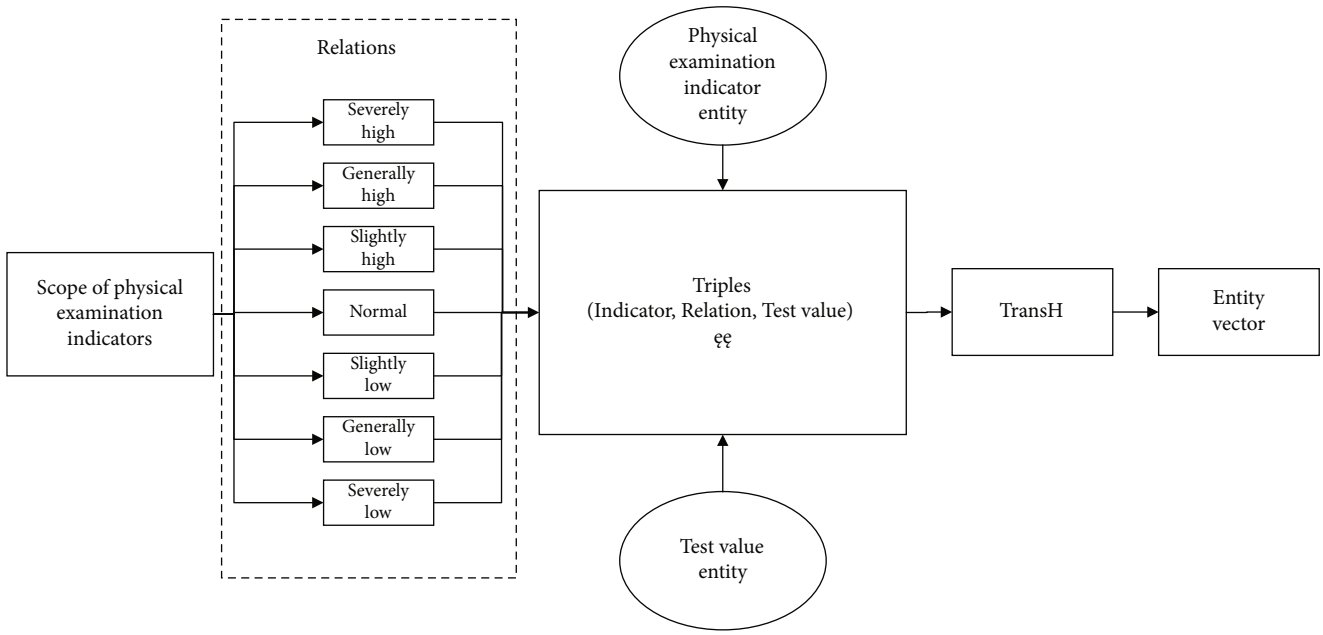

Figure 2: Physical examination indicator entity and test value entity to vector.

This relationship can be expressed in triplet form (triglyceride, normal, 0.45.mmol/L), which is the basic form of the knowledge graph. Through this method, all relevant physical examination indicators and their corresponding test values are expressed in the form of the above triplet, and then, the physical examination indicators and the corresponding test values are expressed in vector form through knowledge representation learning method.

Since it exists complex one-to-many and many-to-one relationships between the physical examination indexes and the corresponding test values, the TransH model chosen in this paper is more suitable with this kind of relational representation. Therefore, after converting the knowledge of the physical examination into the form of triples, the representation vector is obtained using the TransH model. The model uses the translation vector and the normal vector of the hyperplane to represent the relation r. The projection vectors of the entity vector and the hyperplane which is called as the relation r are calculated according to equations (3) and (4). Then, according to equation (5), the low-dimensional dense representation entity vector of the physical examination index and the test value is acquired.

3.2. Relationship Vector of Physical Examination Indicators and Detection Values. After getting the representation vector of the medical examination knowledge, in order to reflect the relationship between the medical examination indicators and their corresponding test values in the model, we use the difference between the entity vector of each medical examination indicator and its corresponding test value to represent the relationship. Based on the basic idea of knowledge representation learning model, $\mathbf{l}_h + \mathbf{l}_r \approx \mathbf{l}_t$, the relationship between the entity vector of physical examination indicator and its corresponding entity vector of detection value is represented by the difference, as shown in the following equation:

$$\mathbf{e}_r = \mathbf{e}_v - \mathbf{e}_c, \tag{8}$$

where $\mathbf{e}_v$ is the entity vector of test values, $\mathbf{e}_c$ is the entity vector of physical indicators, and $\mathbf{e}_r$ is the corresponding relationship vector between $\mathbf{e}_v$ and $\mathbf{e}_c$.

For example, the relationship between the physical vector $\mathbf{e}_{\text{fasting blood glucose}}$ of fasting blood glucose and the physical vector $\mathbf{e}_{7.1\text{mmol/L}}$ of the test value (7.1 mmol/L) is expressed as $\mathbf{e}_{7.1\text{mmol/L}} - \mathbf{e}_{\text{fasting blood glucose}}$. The relationship vectors $\mathbf{e}_r^i$ between all the physical indicators and their corresponding test values are combined to form the relationship matrix between the physical indicators and the test values of one person, as shown in the following formula:

$$\mathbf{E}^{k\times m} = \left[\mathbf{e}_r^1, \mathbf{e}_r^2, \mathbf{e}_r^3, \cdots, \mathbf{e}_r^m\right]. \tag{9}$$

Among them, k is the dimension of the entity vector, and m is the number of physical examination indicators.

3.3. SAC Classifier. The SAC classifier is key part of the TH-SAC model in Figure 3 and consists of the following layers:

(1) Input layer: the relationship matrix $\mathbf{E}^{k\times m}$ obtained by splicing the relationship vectors between all the physical examination indicators and the corresponding detection values is the input of the classifier

(2) Self-attention layer: since each medical examination index is interrelated, the relationship matrix $\mathbf{E}^{k\times m}$ is further input into the self-attention layer, so that each medical examination index can get global information, which is in line with the current medical diagnosis experience. In this paper, the number of layers adopted for the self-attentive layer is 2 in our attention mechanism. As shown in Figure 4, in the

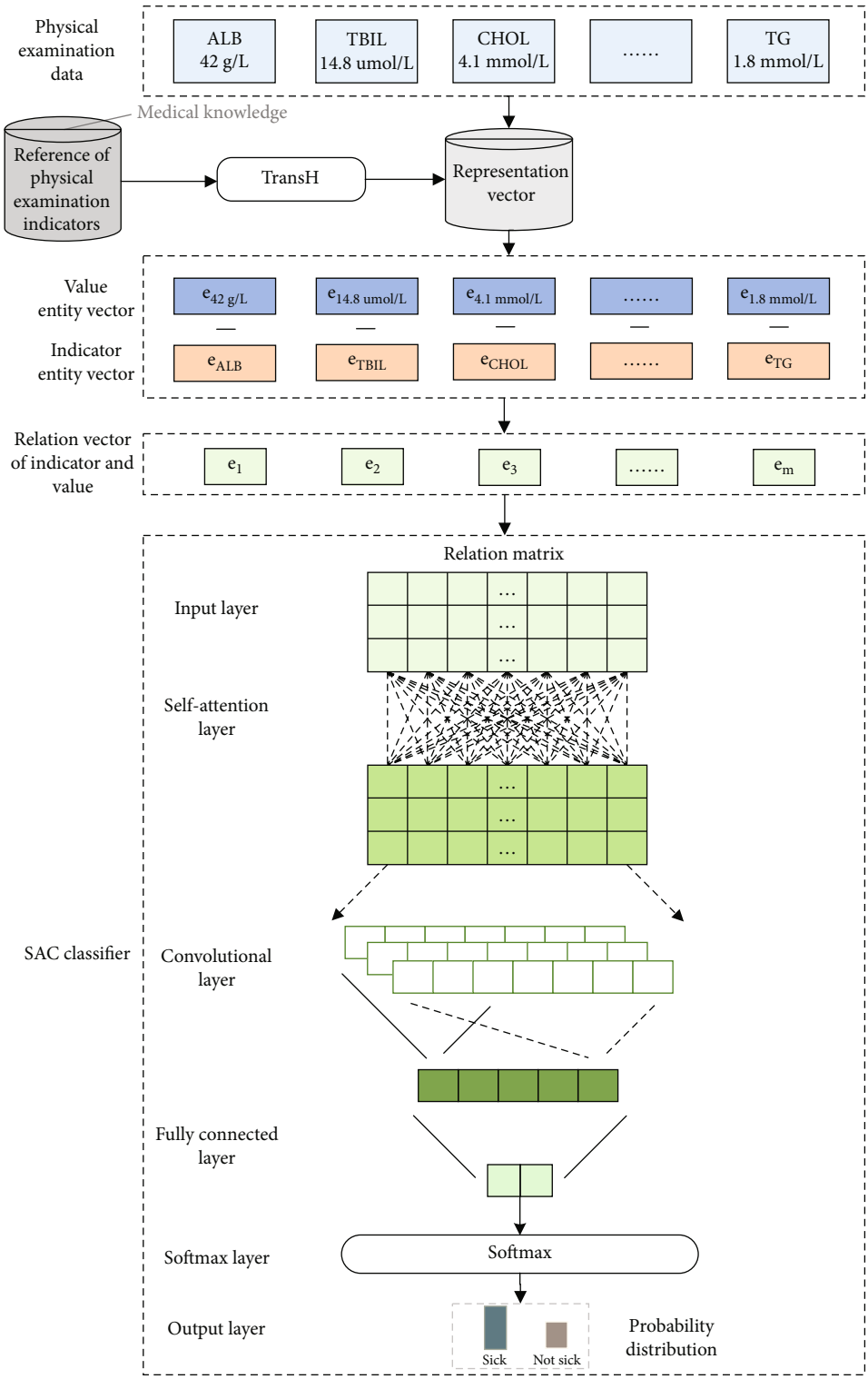

Figure 3: TH-SAC: architecture diagram of a disease prediction model integrating knowledge representation and deep learning.

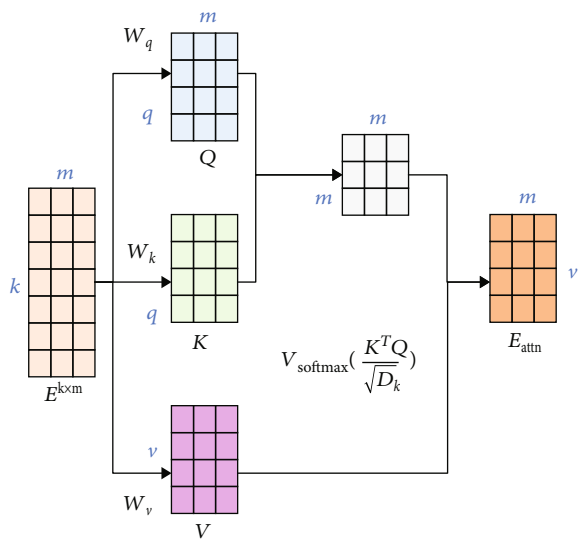

Figure 4: Self-attention mechanism

attention layer, the following three weights $\mathbf{w}_q \in \mathbf{R}^{q\times k}$, $\mathbf{w}_k \in \mathbf{R}^{q\times k}$, and $\mathbf{w}_v \in \mathbf{R}^{v\times k}$ are first defined, and each relation vector $\mathbf{e}_r^i$ is linearly mapped into three different spaces according to equations (10)–(12) to get the query vector $\mathbf{q}_i$, the key vector $\mathbf{k}_i$, and the value vector $\mathbf{v}_i$:

$$\mathbf{q}_i = \mathbf{w}_q \mathbf{e}_r^i, \tag{10}$$

$$\mathbf{k}_i = \mathbf{w}_k \mathbf{e}_r^i, \tag{11}$$

$$v_i = \boldsymbol{w}_v \mathbf{e}_r^i \tag{12}$$

For each query vector $\mathbf{q}_i$, we can calculate the output vector $\mathbf{e}_{\text{attn}}$ according to the following equation:

$$\mathbf{e}_{\text{attn}}^i = \sum_{j=1}^{m} a_{ij} \mathbf{v}_i, \tag{13}$$

where a_{ij} denotes the weight of the ith output concern to the jth input, which is calculated from the following equation:

$$\begin{aligned} a_{ij} &= \text{softmax}\left(s\left(\mathbf{k}_j, \mathbf{q}_i\right)\right), \\ s\left(\mathbf{k}_j, \mathbf{q}_i\right) &= \frac{\mathbf{k}_j^T \mathbf{q}_i}{\sqrt{D_k}}, \end{aligned} \tag{14}$$

where softmax(•) is a function normalized by columns and D_k is the dimension of $\mathbf{q}_i$.

In order to simultaneously calculate the output vector corresponding to each relation vector in the relation matrix $\mathbf{E}^{k\times m}$, the query vector $\mathbf{q}_i$, the key vector $\mathbf{k}_i$, and the value vector $\mathbf{v}_i$ can be merged into the query matrix $\mathbf{Q}$, the key matrix $\mathbf{K}$, and the value matrix $\mathbf{V}$, respectively. Then, the output matrix of the attention layer is obtained according to the following equation:

$$\mathbf{E}_{\text{attn}} = \mathbf{V}\text{softmax}\left(\frac{\mathbf{K}^T\mathbf{Q}}{\sqrt{\mathbf{D}_k}}\right). \tag{15}$$

(3) Convolutional layer: after acquiring the global information through the self-attention layer, the output matrix $\mathbf{E}_{\text{attn}}$ of the self-attention layer is input to the convolutional neural network in purpose of mining the information in the relationship matrix using deep learning model. Suppose $\mathbf{W}^f \in R^{h\times d}$, where h is the filter window size and d denotes the dimensionality of the input vector. For the local features $\mathbf{e}_{\text{attn}}^{i:i+h-1}$ of the input from row i to row $i+k-1$, the ith eigenvalue of the feature submatrix extracted by the convolutional filter is expressed as

$$c_i = f\left(\mathbf{w}^f \cdot \mathbf{e}_{\text{attn}}^{i:i+h-1} + b\right), \tag{16}$$

where $f(\cdot)$ is the nonlinear activation function relu$(\cdot)$ and b is the bias value. Thus, the local feature matrix of the output matrix $\mathbf{E}_{\text{attn}}$ obtained from the attention layer is

$$\mathbf{C} = [c_1, c_2, c_3, \cdots, c_{m-h+1}] \tag{17}$$

Subsequently, a maximum pooling operation is performed on each feature mapping, i.e.,

$$\hat{c} = \max\{\mathbf{C}\}. \tag{18}$$

Then, the final representation vector of the medical examination data is obtained as shown in the following equation:

$$\mathbf{Z}_{tj} = [\hat{c}_1, \hat{c}_2, \hat{c}_3, \cdots, \hat{c}_n]. \tag{19}$$

(4) Fully connected layer and softmax layer: the representation vector of medical examination data is transformed by the fully connected layer to obtain the score vector $\mathbf{s}$ which can be used to predict diabetes. The quantity of hidden units in the fully connected layer is 2, i.e., diabetic and nondiabetic. Finally, the score vector s is input to the softmax layer which can transform to a conditional probability distribution:

$$p_i(s) = \frac{\exp\left(s_i\right)}{\sum_{j=1}^{2} \exp\left(s_j\right)}, \quad i = 1, 2 \tag{20}$$

The whole model uses a crossentropy loss function to measure the gap between the predicted probability distribution of diabetes and the real probability distribution, and the parameters of the model are trained and updated by a back-

Table 1: The reference range of detection value of some physical examination indicators.

Medical examination indicator	Reference range
Serum alanine aminotransferase	9-50 IU/L
Serum aspartate aminotransferase	15-40 IU/L
Albumin	40.0–55.0 g/L
Total bilirubin	2.0–20.0 μmol/L
Blood urea nitrogen	3.6-9.5 mmol/L
Total cholesterol	2.86-6.10 mmol/L
Triglycerides	0.45-1.81 mmol/L
Low-density lipoprotein	0.00-3.37 mmol/L
High-density lipoprotein	1.16-1.42 mmol/L
……	……

Table 2: Entity type and quantity.

Type of entity	Example	Number of entities
Medical examination indicator	Triglycerides	16
Detection value	1.62 mmol/L	5499
Abnormally high	<HIGHEST>	1
Abnormally low	<LOWEST>	1
Unknown	<UNK>	1
Medical examination indicator	Triglycerides	16

Table 3: Relationship type and quantity.

Relationship types	Number of entities
Severely low	337
Generally low	343
Slightly low	457
Normal	1558
Slightly high	2663
Generally high	2005
Severely high	2017

Table 4: The distribution of physical examination dataset.

Disease label	Training set	Test set
Diabetes	3815	954
Nondiabetes	35924	8824
Total	39109	9778

propagation algorithm. The loss function is denoted as

$$\text{Loss} = -\frac{1}{N}\sum_{i}[y_i \cdot \log(p_i) + (1 - y_i) \cdot \log(1 - p_i)], \quad (21)$$

where N represents the number of samples and y_i represents the true label of sample i and with disease is marked as 1 and no disease is marked as 0.

Table 5: Model parameter settings.

Parameter	Value
Optimizer	Adam
Batch_size	32
Epoch	100
Dropout	0.5
Learning rate	0.0002
Entity vector dimension of physical examination data	256
Size of convolution filter window	2, 3, 4
Number of convolution filters per window size	100
Number of layers of self-attention	2

4. Experiment and Results

4.1. Experimental Data. The data that are used in the experiments are derived from the reference range of the detection values of diabetes physical examination indexes provided by Zhongda Hospital, China. The procedure of this study was approved by the Research Ethics Committee of Zhongda Hospital affiliated to Southeast University (Approval no. of Ethics Committee: 2019ZDSYLL199-P01), China. Table 1 shows the reference ranges of the test values of medical indicators. Based on this physical examination knowledge, a total of 5518 related entities, 7 types of relational entities (severely low, generally low, slightly low, normal, slightly high, generally high, and severely high), and 9410 ternary relationships are established. The types of entities and their quantities are shown in Table 2, and the types of relationships and their numbers are shown in Table 3. As it is impossible to predict the threshold value of each physical test index in practice, the entities with detection values greater than (less than) the maximum (minimum) value set in the experiment are uniformly treated as abnormally high <HIGHEST> entities (abnormally low <LOWEST> entities). In addition, all missing value items were replaced by the unknown entity <UNK>.

The physical examination data of diabetic patients provided by a large company is adopted, which contains 11 physical examination indicators, such as serum alanine aminotransferase, serum aspartate aminotransferase, and albumin, with a total number of 48887. And the training set accounts for 80%, and the test set accounts for 20%, as shown in Table 4.

4.2. Experimental Setup. The deep learning framework, PyTorch, and the knowledge representation learning framework, OpenKE, are primarily utilized in the experiments. The specific parameter settings of model are shown in Table 5. In this paper, the hyperparameter values selected in the model are optimized by grid search algorithm, and the accidental selection of the hyperparameter values is prevented by the cross-validation of fivefold.

4.3. Evaluation Indicators. In this paper, accuracy, recall and F1_score are adopted. Mean rank (MR) and Hit@10 are chosen as the evaluation metrics of the knowledge representation

model. In addition, in order to improve the credibility, the experimental results are verified by the fivefold cross-validation method.

4.3.1. Mean Rank. When evaluating the performance of the knowledge representation learning model, each triple(h, r, t) is evaluated, the head entity is removed and replaced with other entities in the knowledge base in turn, and the wrong triple entity (h, r, t) is constructed. The similarity of head and tail entities using the relation function $f_r(h, t)$ is calculated. After getting the similarity from all the triples (including the correct triples and the incorrect triples), the triples are sorted in an ascending order. The average value of all correct triple ranking positions is the MR. For better knowledge graph representation, the score of the correct triad will be smaller than the score of the incorrect triad and will be ranked more highly. Therefore, the smaller the MR value is, the better the knowledge mapping representation vector is. Specifically, MR is shown in the following equation:

$$\mathrm{MR} = \frac{1}{N_T}\sum_{i=1}^{N_T}\mathrm{rank}_i, \tag{22}$$

where N_T denotes the number of correct triples and rank_i represents the ranking of the correct triples.

4.3.2. Hit@10. The ratio of the number of correct triples contained in the top 10 of the above ranking to the total amount of correct triples is the Hit@10 value. Therefore, the larger the Hit@10 value is, the better the knowledge graph representation vector is. Specifically, as shown in the following formula,

$$\mathrm{Hit@10} = \frac{N_T^{\mathrm{rank}\le 10}}{N_T} \times 100\%, \tag{23}$$

where $N_T^{\mathrm{rank}\le 10}$ represents the number of correct triples in the top ten.

4.4. Analysis of Experimental Results

4.4.1. Comparative Analysis of Knowledge Representation Models. At first, the performance of different knowledge representation models is analyzed, and the results are illustrated in Tables 6 and 7. As shown in Table 6, from the comprehensive MR metrics and Hit@10 metrics, the TransH model performs the best effect of knowledge representation. This demonstrates that TransH can better deal with the complex relationships of "one to many" and "many to one" between physical examinations and detection values, which makes up for the deficiency of TransE. Although the TransR model takes into account these complex relationships, there are only similar relationships between the physical examination and the test value, such as high and low, and the different relationships focus on the similar properties of the entities, so the TransR model does not perform well in knowledge representation.

In addition, from Table 7, we can see that the TransH model outperforms both the TransE model and the TransR model by 0.07% and 0.15% in accuracy and 0.29% and 0.56% in recall, respectively. This further indicates that the representation of the TransH model is more rational for the triples constructed in this paper based on medical examination knowledge, which also makes the performance of prediction model better. The text continues here (Figure 3 and Table 2).

Table 6: MR and Hit@10 of different knowledge representation model.

Model	MR	Hit@10 (%)
TransE	623.0	44.9
TransH	711.6	47.9
TransR	897.8	19.0

Table 7: Accuracy and Recall Rates of Different Knowledge Representation Models.

Model	Accuracy (%)	Recall (%)	F1
TransE-SAC	97.11	87.16	0.8300
TH-SAC	97.18	87.55	0.8351
TransR-SAC	97.03	86.89	0.8295

Table 8: Accuracy and recall rates of different diabetes prediction models.

Model	Accuracy (%)	Recall (%)	F1
LR	90.29	49.9	0.1731
SVM	90.59	51.60	0.0631
NB	87.48	53.94	0.1604
RF	96.37	82.11	0.8295
XGBoost	92.42	61.64	0.3746
DNN	90.21	58.62	0.1373
TH-SA	96.05	86.15	0.7892
TH-CNN	96.26	87.03	0.8307
TH-SAC	97.18	87.55	0.8351

Table 9: Distribution of sampled physical examination dataset.

Disease label	Training set	Test set
Diabetes	35294	8824
Nondiabetes	35924	8824
Total	70588	17648

4.4.2. Comparative Analysis. For the purpose of verifying the advantages of the proposed TH-SAC model for the diabetes prediction task, some relevant diabetes prediction models are selected for experiments. The TH-SAC model is used to represent the medical examination data as vectors through knowledge representation learning, and deep learning approach is used for prediction. In this paper, the traditional machine learning methods that work well on diabetes prediction tasks and deep neural networks (DNN) are selected for comparisons,

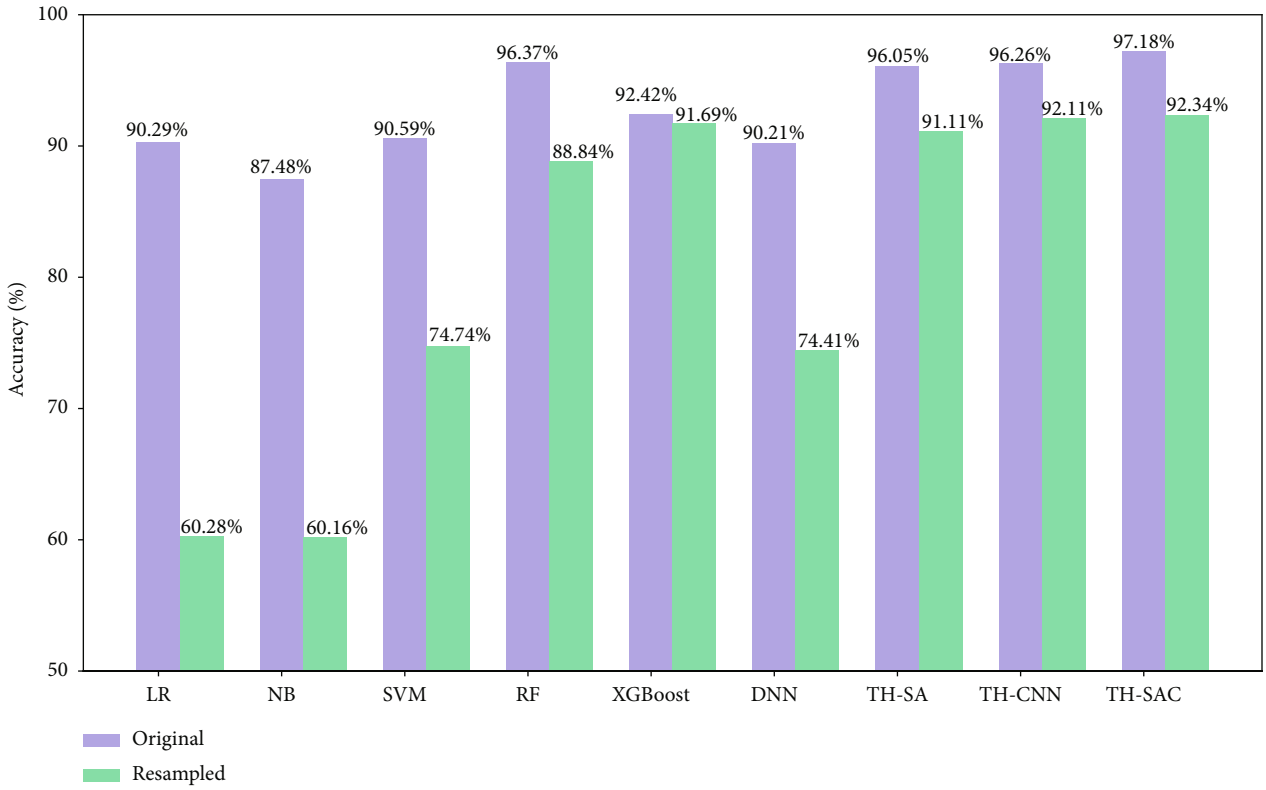

Figure 5: Comparison of accuracy of each model before and after resampling.

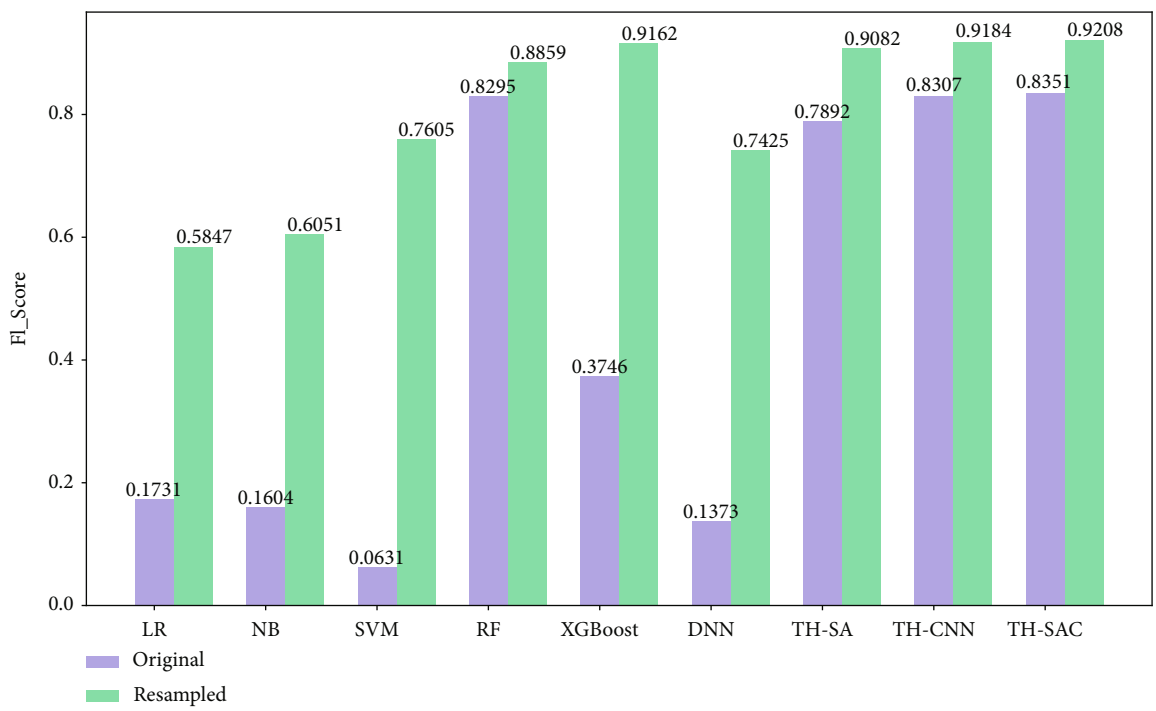

Figure 6: Comparison of F1 values for each model before and after resampling.

and the results are illustrated in Table 8. Compared with the most effective random forest methods in machine learning, it can be seen that the TH-SAC model has been improved by 0.81% and 5.34% in accuracy and recall, respectively. This is because our model is based on deep learning approach and adopts a self-attention architecture, which is better at mining effective information from complex and high-dimensional medical examination data. Compared with that of DNN

Table 10: Accuracy and recall rates of different diabetes prediction models.

Model	Accuracy (%)	Recall (%)	F1
Embedding-SAC	96.98	86.32	0.8253
TH-SAC	97.18	87.32	0.8351

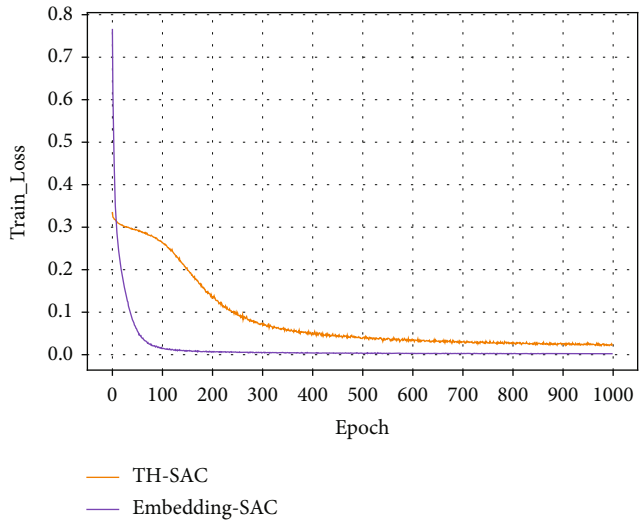

Figure 7: Training loss values of the original dataset.

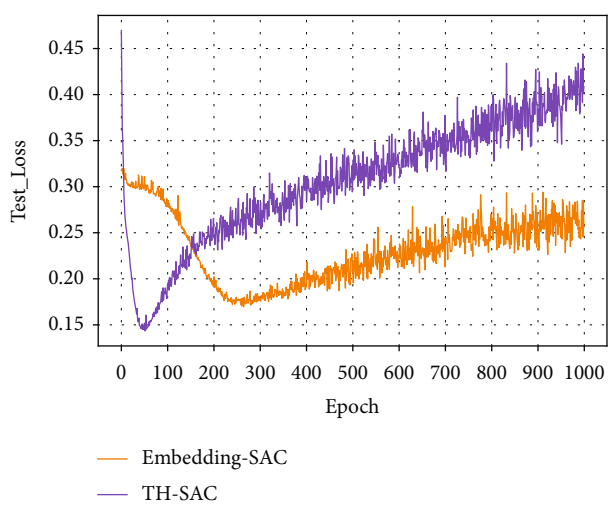

Figure 8: The test loss value of the original data set.

method, the accuracy and recall rate are improved by 6.97% and 28.83%, respectively. The results show that the method of representing medical examination data as vectors through knowledge representation learning is more superior to simply employing detection values. The embedded external knowledge not only improves the interpretability of the model but also enhances the performance of the model.

Moreover, the classifier used in the TH-SAC model is designed and implemented by integrating self-attention and convolutional neural networks (CNN). Therefore, we select the following methods for comparative experiments: self-attention and CNN are used alone, and the results are shown in Table 8. It can be seen that the SAC classifier has better performance in terms of accuracy and recall. This is because the SAC classifier is able to integrate the local features with their corresponding global dependencies, which provides more superior performance than that of only self-attention or CNN alone.

4.4.3. SMOTE Resampling Analysis. As shown in Table 4, the number of negative samples in the dataset used is much larger than the number of positive samples, and there exists the problem of unbalanced distribution. However, the degree of imbalance in the dataset can affect the accuracy of the model as well as the generalization ability [50]. In this paper, the SMOTE [51] method is adopted to address the problem of imbalanced distribution of the dataset. As shown in Table 9, the distribution of positive and negative samples in the dataset after resampling with the SMOTE method reaches a balanced state. After SMOTE resampling, the above prediction models were experimented again and compared. The experimental results are shown in Figures 5 and 6 . The accuracy of all models on the balanced dataset after resampling has decreased, and the F1 values has increased. The results indicated that more illnesses were predicted to be nonillnesses before resampling, while more nonillnesses were predicted to be illnesses after resampling. Additionally, comparing the performance of all models on the resampled datasets, the model proposed in this paper still outperforms the other models in terms of accuracy and F1 values. Moreover, it is less affected by the datasets and the accuracy of the model does not fluctuate significantly. This further proves the applicability as well as the effectiveness of the TH-SAC model.

4.4.4. Comparative Analysis of Knowledge Representation and Embedding Representation. In order to verify the effectiveness of incorporating external medical examination knowledge, this paper compares the embedding representation and knowledge representation of medical examination index entities and detection value entities. The embedding representation refers to the one-hot encoding of all entities and then multiplying them with a weight matrix. The comparison results are shown in Table 10; it can be seen that the knowledge representation significantly outperforms the random representation model in terms of prediction performance. This indicates that the entity vector constructed in this paper by the relationship between the physical examination index and the detection value plays a good role.

Figures 7–10 present the training loss values and test loss values of the two models on the original and resampled datasets. It can be seen that the loss values of the TH-SAC model in the initial training are smaller than those of the models without the introduction of knowledge, indicating that the vectors obtained by training the normal range of the medical examination indexes can provide a better representation of the relationship between the medical examination indexes and their corresponding detection values. In addition, as shown in Figures 8–10, the model with the embedded representation has the risk of overfitting.

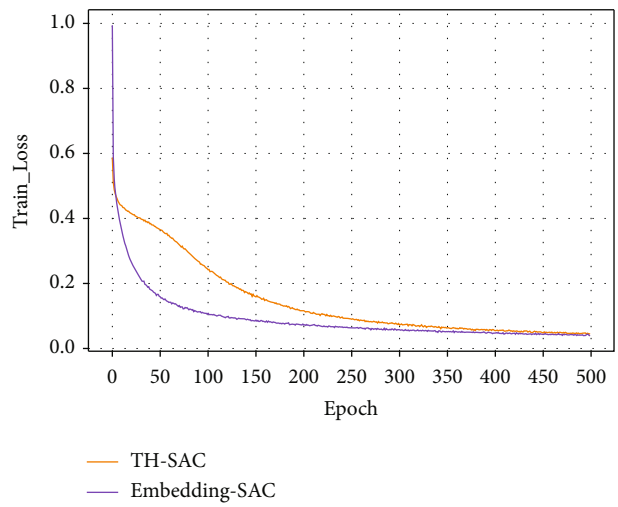

Figure 9: Training loss values for resampled dataset.

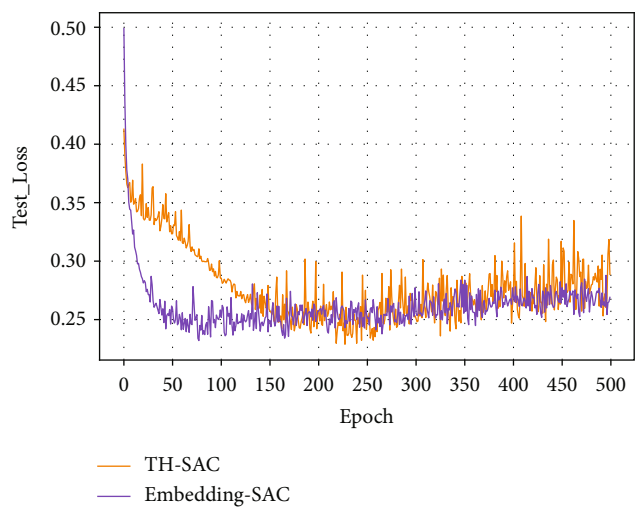

Figure 10: Test loss value for resampling dataset.

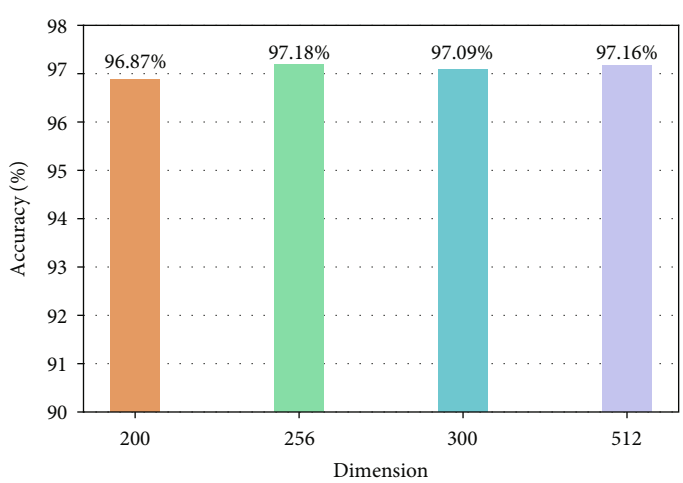

Figure 11: Accuracy of representation vectors in different dimensions.

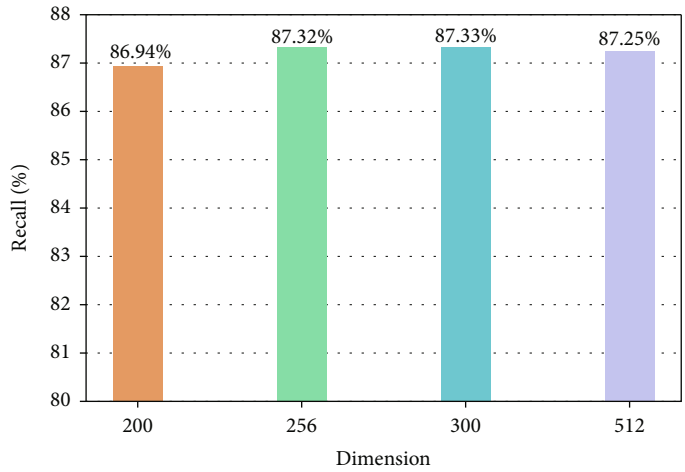

Figure 12: Recall of representation vectors in different dimensions.

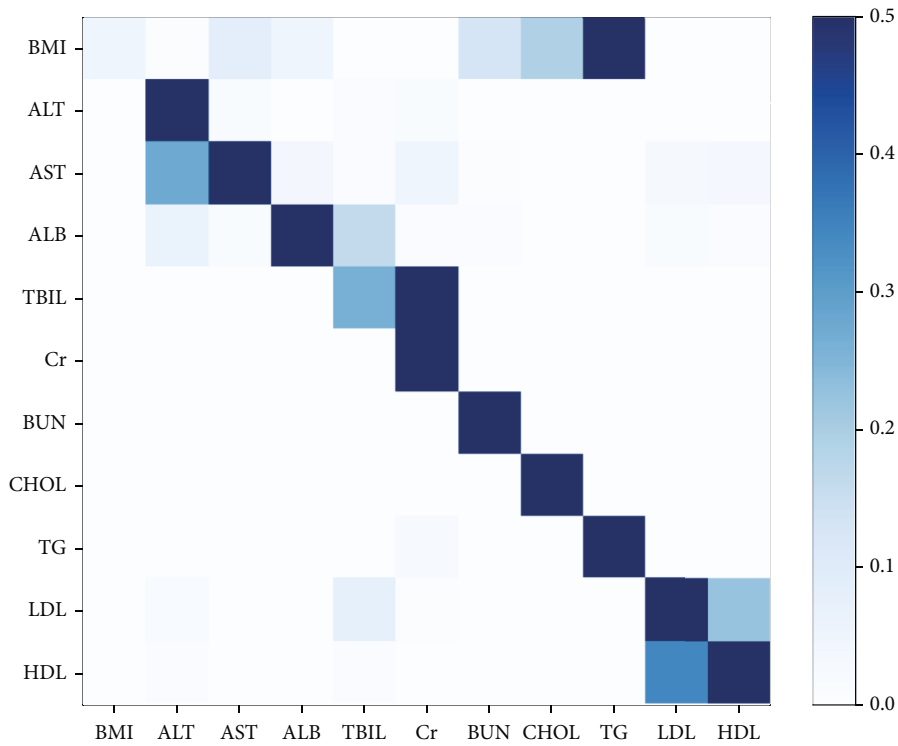

Figure 13: Visualization of the weight of the self-attentive layer.

4.4.5. Comparative Analysis of Representation Vectors with Different Dimensions. In the process of knowledge representation learning, if the vector dimension is too small or too large, there exists a risk of overfitting. In order to select the optimal dimension of the representation vector, the number of four dimensions of 200, 256, 300, and 512 is selected in our experiments, and the results are shown in Figures 11 and 12.

From Figures 11 to 12, it can be seen that the accuracy and recall are lower in the lower 200-dimensional representation vector because the information contained is not comprehensive. However, the higher the dimension is, the more complex the model parameters are, and the longer the training time is. Therefore, considering the accuracy, recall, and complexity of the model parameters, we selected the dimension number of the representation vector which is 256 in this paper.

4.4.6. Self-Attention Mechanism Weight Visualization. As shown in Figure 13 and Table 11, the weights of the self-attention layer in our model are visualized. It can be seen that there is a strong correlation between low-density lipoprotein (LDL) and high-density lipoprotein (HDL) and BMI with total cholesterol and triglycerides, which is consistent with the medical expertise. It also indicated that the model proposed in this paper has the interpretability.

Table 11: The numerical values of the weight of the self-attentive layer.

	BMI	ALT	AST	ALB	TBIL	Cr	BUN	CHOL	TG	LDL	HDL
BMI	0.044682	0.0063637	0.082328	0.043529	0.0024994	0.0017869	0.12636	0.18994	0.50183	0.00024223	0.00043629
ALT	4.254*e*-05	0.95567	0.013733	0.0014261	0.012931	0.014677	8.8271*e*-05	0.0003062	6.7363*e*-06	0.00067861	0.00044125
AST	0.0024338	0.27391	0.57118	0.036222	0.0088331	0.045473	0.0044836	0.00071565	1.6739*e*-05	0.025368	0.031365
ALB	0.001296	0.06182	0.17392	0.70461	0.16075	0.013515	0.0104	0.0032933	0.00039018	0.014664	0.011861
TBIL	1.9193*e*-08	2.5626*e*-07	4.1367*e*-08	2.6728*e*-07	0.25978	0.74022	2.3709*e*-07	8.6627*e*-07	4.7918*e*-06	5.7109*e*-07	1.6839*e*-07
Cr	8.3536*e*-16	9.8131*e*-14	5.6186*e*-16	9.2363*e*-14	2.0324*e*-12	1.0	9.2502*e*-14	8.219*e*-14	4.5131*e*-13	3.925*e*-14	4.0831*e*-14
BUN	2.4488*e*-05	3.7696*e*-05	3.0095*e*-05	0.000663	6.1397*e*-05	2.97775*e*-05	0.99901	3.3287*e*-06	3.4574*e*-06	5.81*e*-05	8.1024*e*-05
CHOL	4.7872*e*-07	2.9578*e*-08	2.7738*e*-08	7.6755*e*-07	8.7449*e*-08	1.0327*e*-09	1.8206*e*-07	0.99996	1.4392*e*-07	4.8578*e*-06	3.181*e*-05
TG	3.7574*e*-07	7.568*e*-09	5.1691*e*-10	1.1795*e*-06	2.7954*e*-06	0.023429	2.0787*e*-05	0.00045578	0.97609	4.4345*e*-08	1.37772*e*-07
LDL	0.0024032	0.018078	0.001621	0.0015858	0.077337	0.0070292	0.00026765	0.00030051	9.7969*e*-05	0.66945	0.22183
HDL	0.0038618	0.0082498	0.0018781	0.0011091	0.011362	0.00010898	0.00043675	0.00049594	8.7666*e*-05	0.34158	0.63083

5. Conclusions

Deep learning generally has problems in the medical field, such as insufficient data, low quality, and lack of interpretability of models. In this paper, a disease prediction model combining knowledge representation and deep learning is proposed and applied in the field of diabetes. According to the relationship between physical examination index and test value, the vector representation of physical examination knowledge entity is constructed through the TransH model, and then, the relationship matrix of patient physical examination data is obtained. Then feature extraction was carried out through the constructed self-attention mechanism and convolutional neural network, and a deep learning model for disease prediction was designed and implemented. In the experiment, the accuracy rate and recall rate of the model in this paper were 97.18% and 87.55%, respectively, which were better than those of the traditional machine learning method and the deep learning method without introducing knowledge representation. Therefore, the medical knowledge introduced in this paper improves the validity and efficiency of the model to a certain extent.

However, there are still some limitations to our approach. In this paper, the range of physical examination index values is divided according to the experience of medical experts, except the normal range. Moreover, the accuracy of prediction depends to some extent on the accuracy of range division, so whether the range division is optimal remains to be further studied. In addition, the knowledge of physical examination used in this paper is incomplete and does not take into account the relationship between the normal range of physical examination indicators and age and sex. And the patient's related symptoms and the actual clinical diagnosis are different. In the next step, we will try to introduce the above relationship to improve the disease prediction model and build a computer-aided diagnosis system.

Data Availability

The data presented in this study are available from the corresponding authors on reasonable request.

Conflicts of Interest

The authors declare that they have no conflicts of interest.

Acknowledgments

This work was supported in part by the Scientific and Technological Support Project of Jiangsu Province under Grant BE2019740, Natural Science Foundation of Jiangsu Province (Higher Education Institutions) (BK20170900, 19KJB520046, and 20KJA520001), Six Talent Peaks Project in Jiangsu Province (RJFW-111), and in part by the Postgraduate Research and Practice Innovation Program of Jiangsu Province under Grant SJCX21_0283, SJCX22_0267, and SJCX22_0275.

References

[1] Y. Lecun, Y. Bengio, and G. Hinton, "Deep learning," *Nature*, vol. 521, no. 7553, pp. 436–444, 2015.

[2] M. Malik, M. K. Malik, K. Mehmood, and I. Makhdoom, "Automatic speech recognition: a survey," *Multimedia Tools and Applications*, vol. 80, no. 6, pp. 9411–9457, 2021.

[3] K. He, X. Zhang, S. Ren, and J. Sun, "Deep residual learning for image recognition," in *Proceedings of the IEEE Conference on Computer Vision and Pattern Recognition*, vol. 1, pp. 770–778, Las Vegas, Nevada, 2016.

[4] A. Krizhevsky, I. Sutskever, and G. E. Hinton, "ImageNet classification with deep convolutional neural networks," *Communications of the ACM*, vol. 60, no. 6, pp. 84–90, 2017.

[5] D. W. Otter, J. R. Medina, and J. K. Kalita, "A survey of the usages of deep learning for natural language processing," *IEEE Transactions on Neural Networks and Learning Systems*, vol. 32, no. 2, pp. 604–624, 2021.

[6] A. Esteva, A. Robicquet, B. Ramsundar et al., "A guide to deep learning in healthcare," *Nature Medicine*, vol. 25, no. 1, pp. 24–29, 2019.

[7] G. Litjens, T. Kooi, B. E. Bejnordi et al., "A survey on deep learning in medical image analysis," *Medical Image Analysis*, vol. 42, pp. 60–88, 2017.

[8] A. S. Panayides, A. Amini, N. D. Filipovic et al., "AI in medical imaging informatics: current challenges and future directions," *IEEE Journal of Biomedical and Health Informatics*, vol. 24, no. 7, pp. 1837–1857, 2020.

[9] B. Shickel, P. J. Tighe, A. Bihorac, and P. Rashidi, "Deep EHR: a survey of recent advances in deep learning techniques for electronic health record (EHR) Analysis," *IEEE Journal of Biomedical and Health Informatics*, vol. 22, no. 5, pp. 1589–1604, 2018.

[10] A. Rajkomar, E. Oren, K. Chen et al., "Scalable and accurate deep learning with electronic health records," *NPJ Digital Medicine*, vol. 1, no. 1, pp. 1–10, 2018.

[11] M. H. Yap, G. Pons, J. Marti et al., "Automated breast ultrasound lesions detection using convolutional neural networks," *IEEE Journal of Biomedical and Health Informatics*, vol. 22, no. 4, pp. 1218–1226, 2018.

[12] S. Ravizza, T. Huschto, A. Adamov et al., "Predicting the early risk of chronic kidney disease in patients with diabetes using real-world data," *Nature Medicine*, vol. 25, no. 1, pp. 57–59, 2019.

[13] T. Jo, K. Nho, and A. J. Saykin, "Deep learning in Alzheimer's disease: diagnostic classification and prognostic prediction using neuroimaging data," *Frontiers in Aging Neuroscience*, vol. 11, p. 220, 2019.

[14] E. Tjoa and C. Guan, "A survey on explainable artificial intelligence (XAI): toward medical XAI," *IEEE Transactions on Neural Networks and Learning Systems*, vol. 32, no. 11, pp. 4793–4813, 2021.

[15] S. Tonekaboni, S. Joshi, M. D. McCradden, and A. Goldenberg, "What clinicians want: contextualizing explainable machine learning for clinical end use," *Machine Learning for Healthcare Conference, PMLR*, pp. 359–380, 2019.

[16] D. P. Solomatine and A. Ostfeld, "Data-driven modelling: some past experiences and new approaches," *Journal of Hydroinformatics*, vol. 10, no. 1, pp. 3–22, 2008.

[17] G. Hu, X. Peng, Y. Yang, T. M. Hospedales, and J. Verbeek, "Frankenstein: learning deep face representations using small data," *IEEE Transactions on Image Processing*, vol. 27, no. 1, pp. 293–303, 2018.

[18] J. Luo, M. Wu, D. Gopukumar, and Y. Zhao, "Big data application in biomedical research and health care: a literature

review," *Biomedical Informatics Insights*, vol. 8, p. BII.S31559, 2016.

[19] J. Andreu-Perez, C. C. Poon, R. D. Merrifield, S. T. C. Wong, and G. Z. Yang, "Big data for health," *IEEE Journal of Biomedical and Health Informatics*, vol. 19, no. 4, pp. 1193–1208, 2015.

[20] R. Miotto, F. Wang, S. Wang, X. Jiang, and J. T. Dudley, "Deep learning for healthcare: review, opportunities and challenges," *Briefings in Bioinformatics*, vol. 19, no. 6, pp. 1236–1246, 2018.

[21] H. K. Patil and R. Seshadri, "Big Data Security and Privacy Issues in Healthcare," in *2014 IEEE international congress on big data*, pp. 762–765, Anchorage, AK, USA, 2014.

[22] I. C. Kaadoud, L. Fahed, and P. Lenca, "Explainable AI: a narrative review at the crossroad of knowledge discovery, knowledge representation and representation learning," in *Twelfth International Workshop Modelling and Reasoning in Context (MRC)@ IJCAI 2021*, Montreal (virtual), Canada, 2021.

[23] A. Hogan, E. Blomqvist, M. Cochez et al., "Knowledge graphs," *Synthesis Lectures on Data, Semantics, and Knowledge*, vol. 12, no. 2, pp. 1–257, 2022.

[24] Y. Zhu, C. Che, B. Jin, N. Zhang, C. Su, and F. Wang, "Knowledge-driven drug repurposing using a comprehensive drug knowledge graph," *Health Informatics Journal*, vol. 26, no. 4, pp. 2737–2750, 2020.

[25] M. Nickel, K. Murphy, V. Tresp, and E. Gabrilovich, "A review of relational machine learning for knowledge graphs," *Proceedings of the IEEE*, vol. 104, no. 1, pp. 11–33, 2016.

[26] M. Alawad, S. Gao, M. C. Shekar et al., "Integration of domain knowledge using medical knowledge graph deep learning for cancer phenotyping," 2021, https://arxiv.org/abs/2101.01337.

[27] Z. Jiang, C. Chi, and Y. Zhan, "Research on medical question answering system based on knowledge graph," *IEEE Access*, vol. 9, pp. 21094–21101, 2021.

[28] K. Q. Yuan, Y. Deng, D. Y. Chen, B. Zhang, K. Lei, and Y. Shen, "Construction techniques and research development of medical knowledge graph," *Application Research of Computers*, vol. 35, no. 7, pp. 1929–1936, 2018.

[29] E. J. Topol, "High-performance medicine: the convergence of human and artificial intelligence," *Nature Medicine*, vol. 25, no. 1, pp. 44–56, 2019.

[30] R. Feng, X. Liu, J. Chen, D. Z. Chen, H. Gao, and J. Wu, "A deep learning approach for colonoscopy pathology WSI analysis: accurate segmentation and classification," *IEEE Journal of Biomedical and Health Informatics*, vol. 25, no. 10, pp. 3700–3708, 2021.

[31] N. Strodthoff, P. Wagner, T. Schaeffter, and W. Samek, "Deep learning for ECG analysis: benchmarks and insights from PTB-XL," *IEEE Journal of Biomedical and Health Informatics*, vol. 25, no. 5, pp. 1519–1528, 2021.

[32] A. Y. Hannun, P. Rajpurkar, M. Haghpanahi et al., "Cardiologist-level arrhythmia detection and classification in ambulatory electrocardiograms using a deep neural network," *Nature Medicine*, vol. 25, no. 1, pp. 65–69, 2019.

[33] A. Sinha and J. Dolz, "Multi-scale self-guided attention for medical image segmentation," *IEEE Journal of Biomedical and Health Informatics*, vol. 25, no. 1, pp. 121–130, 2021.

[34] O. Jacobson and H. Dalianis, "Applying deep learning on electronic health records in Swedish to predict healthcare-associated infections," in *Proceedings of the 15th Workshop on Biomedical Natural Language Processing*, pp. 191–195, Berlin, Germany, 2016.

[35] Z. C. Lipton, D. C. Kale, C. Elkan, and R. Wetzel, "Learning to diagnose with LSTM recurrent neural networks," 2015, https://arxiv.org/abs/1511.03677.

[36] A. J. London, "Artificial intelligence and black-box medical decisions: accuracy versus explainability," *Hastings Center Report*, vol. 49, no. 1, pp. 15–21, 2019.

[37] D. Castelvecchi, "Can we open the black box of AI?," *Nature News*, vol. 538, no. 7623, pp. 20–23, 2016.

[38] P. V. Molle, M. D. Strooper, T. Verbelen, B. Vankeirsbilck, P. Simoens, and B. Dhoedt, "Visualizing convolutional neural networks to improve decision support for skin lesion classification," in *Understanding and Interpreting Machine Learning in Medical Image Computing Applications*, pp. 115–123, Springer, 2018.

[39] Y. Shang, Y. Tian, M. Zhou et al., "EHR-oriented knowledge graph system: toward efficient utilization of non-used information buried in routine clinical practice," *IEEE Journal of Biomedical and Health Informatics*, vol. 25, no. 7, pp. 2463–2475, 2021.

[40] E. Choi, M. T. Bahadori, L. Song, W. F. Stewart, and J. Sun, "GRAM: Graph-based attention model for healthcare representation learning," in *Proceedings of the 23rd ACM SIGKDD International Conference on Knowledge Discovery and Data Mining*, pp. 787–795, Halifax, NS, Canada, 2017.

[41] F. Ma, J. Gao, Q. Suo, Q. You, J. Zhou, and A. Zhang, "Risk prediction on electronic health records with prior medical knowledge," in *Proceedings of the 24th ACM SIGKDD International Conference on Knowledge Discovery & Data Mining*, pp. 1910–1919, London, United Kingdom, 2018.

[42] Q. Zou, K. Qu, Y. Luo, D. Yin, Y. Ju, and H. Tang, "Predicting diabetes mellitus with machine learning techniques," *Frontiers in Genetics*, vol. 9, p. 515, 2018.

[43] O. M. Alade, O. Y. Sowunmi, S. Misra, R. Maskeliūnas, and R. Damaševičius, "A neural network based expert system for the diagnosis of diabetes mellitus," in *International Conference on Information Technology Science*, pp. 14–22, Springer, Cham, 2018.

[44] N. A. Azeez, T. Towolawi, C. V. Vyver et al., "A fuzzy expert system for diagnosing and analyzing human diseases," in *International Conference on Innovations in Bio-Inspired Computing and Applications*, pp. 474–484, Springer, Cham, 2019.

[45] Y. Lin, X. Han, R. Xie, Z. Liu, and M. Sun, "Knowledge representation learning: A Quantitative Review," 2018, https://arxiv.org/abs/1812.10901.

[46] A. Bordes, N. Usunier, A. Garcia-Duran, J. Weston, and O. Yakhnenko, "Translating embeddings for modeling multi-relational data," in *Proceedings of the 26th International Conference on Neural Information Processing Systems*, vol. 2, Lake Tahoe, NV, 2013.

[47] Z. Wang, J. Zhang, J. Feng, and Z. Chen, "Knowledge graph embedding by translating on hyperplanes," in *Proceedings of the AAAI Conference on Artificial Intelligence*, vol. 28, Québec City, Québec, Canada, 2014no. 1.

[48] Y. Lin, Z. Liu, M. Sun, Y. Liu, and X. Zhu, "Learning entity and relation embeddings for knowledge graph completion," in *Twenty-ninth AAAI Conference on Artificial Intelligence*, vol. 29, Austin, Texas, USA, 2015no. 1.

[49] H. D. McIntyre, P. Catalano, C. Zhang, G. Desoye, E. R. Mathiesen, and P. Damm, "Gestational diabetes mellitus," *Nature Reviews Disease Primers*, vol. 5, no. 1, pp. 1–19, 2019.

[50] F. Thabtah, S. Hammoud, F. Kamalov, and A. Gonsalves, "Data imbalance in classification: experimental evaluation," *Information Sciences*, vol. 513, pp. 429–441, 2020.

[51] N. V. Chawla, K. W. Bowyer, L. O. Hall, and W. P. Kegelmeyer, "SMOTE: synthetic minority over-sampling technique," *Journal of Artificial Intelligence Research*, vol. 16, pp. 321–357, 2002.

Hindawi
Disease Markers
Volume 2022, Article ID 3150380, 10 pages
https://doi.org/10.1155/2022/3150380

Research Article

Hepatic Steatosis Index and the Risk of Type 2 Diabetes Mellitus in China: Insights from a General Population-Based Cohort Study

Xintian Cai,[1] Jing Gao,[2] Shasha Liu,[1] Mengru Wang,[1] Junli Hu,[1] Jing Hong,[1] Qing Zhu,[1] Guzailinuer Tuerxun,[1] Yujie Dang,[1] and Nanfang Li[1]

[1]*Hypertension Center of People's Hospital of Xinjiang Uygur Autonomous Region, Xinjiang Hypertension Institute, National Health Committee Key Laboratory of Hypertension Clinical Research, Key Laboratory of Xinjiang Uygur Autonomous Region, Xinjiang Clinical Medical Research Center for Hypertension Diseases, Urumqi, Xinjiang, China*
[2]*Research and Education Center of Xinjiang Uygur Autonomous Region People's Hospital, Urumqi, Xinjiang, China*

Correspondence should be addressed to Nanfang Li; lnanfang2016@sina.com

Received 23 February 2022; Accepted 27 July 2022; Published 3 August 2022

Academic Editor: Ghulam Ashraf

Purpose. In the Chinese population, we looked at the relationship between the hepatic steatosis index (HSI) and the risk of type 2 diabetes mellitus (T2DM). *Methods*. To evaluate the association between HSI and the risk of T2DM, Cox regression models were employed. Hazard ratios (HR) and 95 percent confidence intervals (CI) were computed. A stratified analysis with interaction testing was also carried out. Additionally, we evaluated the incremental predictive value of the HSI over the established risk factors using the C-statistic, the IDI, and the NRI. *Results*. During a median follow-up period of 2.97 years, 433 (1.97%) participants developed new-onset T2DM. The smoothing curve fit plot showed a positive correlation between HSI and the risk of T2DM. After adjusting for all noncollinear variables, the risk of T2DM increased by 62% for every 1 standard deviation (SD) increase in HSI. Subgroup analysis indicated that higher HSI levels were associated with a higher risk of T2DM in those aged < 40 years. The addition of HSI enhanced the reclassification and discrimination of established risk factors, with an IDI of 0.027 and an NRI of 0.348 (both $P < 0.001$). *Conclusion*. Our findings suggest that an elevated HSI is substantially associated with a greater risk of T2DM in the Chinese population. HSI has the potential to be an available and supplementary monitoring method for the management of T2DM risk stratification in the Chinese population.

1. Introduction

The burden of diabetes is rapidly increasing due to China's economic growth, urbanization, and aging population [1–3]. The most recent publications in China show that the country's overall prevalence of diabetes has increased to 12.8% [2]. By 2045, an estimated 693 million people in China will have diabetes [1]. Type 2 diabetes mellitus (T2DM) represents nearly ninety percent of all diabetes cases and can damage many organs and physiological systems, leading to a variety of conditions that can affect an individual's quality of life and even premature death [4–6]. It is therefore critical to identify people in the general population who are at risk for T2DM so that appropriate interventions, such as dietary advice and exercise encouragement, can be implemented at an early stage [7, 8].

Currently, the most common cause of liver disease worldwide is nonalcoholic fatty liver disease (NAFLD) [9, 10]. The development of NAFLD is strongly related to adverse lifestyle choices, insulin resistance, metabolic syndrome, and visceral obesity [11–13]. NAFLD is a robust independent risk factor for T2DM, according to an increasing body of research [14, 15]. Liver biopsy is the gold standard for NAFLD diagnosis and NAFLD severity assessment [16]. Nevertheless, for economic, practical, and safety reasons, it is not feasible to perform this operation on each patient with suspected NAFLD. To diagnose NAFLD early and to reduce the cost of screening,

common clinical laboratory indicators have been widely applied to construct NAFLD-related risk scoring systems [3, 17–22]. Among these, the hepatic steatosis index (HSI) has been widely used in healthcare. Specifically, HSI is a validated risk classification scheme based on the alanine aminotransferase (ALT)/aspartate transaminase (AST) ratio, gender, and routine measurements of body mass index (BMI) [17]. HSI has been reported to be a good indicator to identify the presence or absence of hepatic steatosis [23]. Moreover, a significant correlation between HSI and fatty liver grade measured by ultrasonography has been demonstrated, a finding that suggests that HSI may reflect not only the presence but also the severity of NAFLD [23, 24]. Furthermore, similar to NAFLD, HSI is closely associated with insulin resistance and metabolic syndrome, suggesting that it may be utilized to predict the risk of T2DM in the general population [18, 25–27]. The research by Sviklāne et al. showed that HSI may be a surrogate indicator of liver fat content and metabolic syndrome in patients with type 1 diabetes mellitus [19]. Data from Wang et al. indicated that HSI is independently associated with carotid atherosclerosis in T2DM and is possibly a simple and valuable marker to evaluate the progress of macrovascular complications of diabetes mellitus [17]. More importantly, the study by Song et al. confirmed that higher HSI in early gestation was independently associated with a higher risk of gestational diabetes mellitus [28]. This cohort study presented that HSI in the first trimester may be used to predict the risk of gestational diabetes mellitus in Chinese pregnant women.

To our knowledge, no research has investigated the possible association between HSI and the risk of T2DM. Therefore, we designed the present study to investigate the association between HSI and the risk of T2DM in a Chinese population.

2. Material and Methods

2.1. Data Source. The data come from the Dryad digital repository (10.5061/dryad.ft8750v). The site allows others to gain access to the raw data for free. In the source text, the owners state that they have relinquished the relevant proprietary rights to this dataset [29]. Therefore, the database is available for secondary analysis without infringement of the owners' copyright.

2.2. Study Population. This study is a post hoc analysis of a cohort study conducted by the Rich Health Care Group in China; the design of which was described in detail in previous studies [29]. Briefly, the study recruited 685277 adult subjects (aged ≥ 20 years) who participated in health screenings between 2011 and 2016. The detailed selection process of participants is depicted in Figure 1. Subjects meeting the following criteria were excluded from this study: (1) no available weight and height ($n = 103946$); (2) presence of extreme BMI ($n = 152$); (3) no fasting plasma glucose ($n = 31370$); (4) visit interval less < two years ($n = 324233$); (5) diagnosed with diabetes at baseline ($n = 7112$); (6) diabetes status not determined at follow-up ($n = 6630$); (7) no available gender information ($n = 1$); (8) no available smoking and alcohol consumption status ($n = 151603$); (9) no available ALT and AST values ($n = 38025$). A total of 22,025 subjects were eventually enrolled.

2.3. Ethical Approval. The original clinical dataset was provided by Chen et al. [29]. No reapplication was required for this study as the study ethics had been approved in a previous study [29]. The data was anonymized and therefore did not require informed consent.

2.4. Data Collection. All subjects were requested to complete a standardized questionnaire containing age, family history of diabetes, gender, and smoking/alcohol consumption status. Height and weight, as well as blood pressure, were measured according to standard guidelines. Fasting venous blood samples were collected at each visit after a minimum fast of 10 h. Serum triglyceride (TG), low-density lipoprotein cholesterol (LDL-C), total cholesterol (TC), high-density lipoprotein cholesterol (HDL-C), blood urea nitrogen (BUN), ALT, serum creatinine (Scr), AST, and fasting plasma glucose (FPG) were measured by an automated analyzer (Beckman 5800). HSI was calculated as follows: $\text{HSI} = 8 \times (\text{ALT/AST ratio}) + \text{BMI}$ (+2, if female) [23].

2.5. Ascertainment of Incident T2DM. A diagnosis of T2DM was defined as FPG > 7.00 mmol/L and/or self-reported T2DM during follow-up. Patients were censored at the date of diagnosis of T2DM or at the last visit, whichever came first.

2.6. Missing Data Treatment. Missing data is an unavoidable feature of observational studies, with missing data accounting for 4.68% of all covariates in this dataset (Supplementary Table 1). To minimize bias due to missing covariates, the missing data in this study were filled using multiple interpolations, and five imputations were established. As a sensitivity analysis, this study also compared whether the imputation data differed significantly from the raw data (Supplementary Table 2). The outcomes revealed that the imputation data was not significantly different from the raw data. Therefore, the primary results of all the analyses in this paper are based on the raw data.

2.7. Statistical Analysis. Cox regression models were performed to estimate the relationship between HSI and the risk of T2DM, and hazard ratios (HR) and 95% confidence intervals (CI) were calculated. The collinearity among covariates was assessed by calculating VIF of covariates before building the model (Supplementary Table 3) [30]. Kaplan-Meier survival curves were then employed to show the risk of T2DM for each HSI quintile, and compliance with the proportional risk assumptions used to build the Cox model was ascertained by looking at the Kaplan-Meier curves corresponding to the HSI quintile. Following the above premise, we implemented a model adjustment strategy concerning the statement of STROBE [31]. To validate the robustness of results derived from the primary analyses, sensitivity analyses were conducted. Furthermore, we performed a stratified analysis with interaction tests. Detailed statistical methods are described in Supplementary Methods.

Statistical analyses were performed using R software, version 4.0.1.

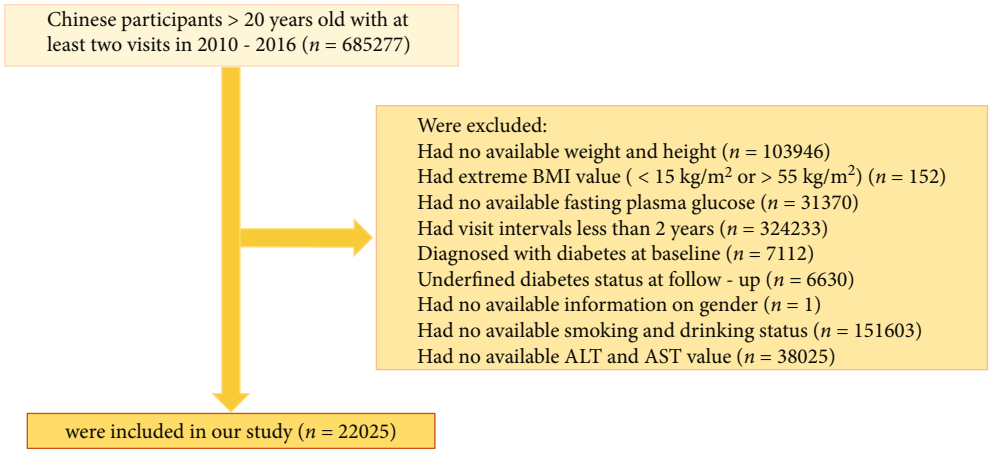

Figure 1: Participant flow diagram.

3. Results

3.1. Characteristics of Study Participants. Of the 685277 participants enrolled in the former research, 22025 met the current inclusion criteria (Figure 1). The mean age at baseline was 41.54 ± 12.35 years, with slightly more male participants than female participants (66.07% vs. 33.93%). Baseline characteristics by HSI quintiles are summarized in Table 1.

3.2. Participant Follow-Up Results. During a median follow-up period of 2.97 years (IQR, 2.17–3.88), 433 (1.97%) participants had new-onset T2DM. The cumulative prevalence of T2DM was 0.30% (13/4400) in the Q1 group, 0.75% (33/4397) in the Q2 group, 1.45% (64/4416) in the Q3 group, 2.91% (128/4405) in the Q4 group, and 4.42% (195/4407) in the Q5 group. Figure 2 demonstrates the results of Kaplan-Meier analysis based on HSI quintiles, with a progressive increase in the cumulative prevalence of T2DM with increasing HSI (log-rank test $P < 0.001$).

3.3. The Relationship of HSI with the Risk of T2DM. The smoothing curve fit plots revealed a positive correlation between HSI and the risk of T2DM (Figure 3 and Supplement Figure 1). Overall, there was a significant positive association between HSI and the risk of new-onset T2DM in the multivariate regression model (Table 2). In model IV, the risk of T2DM increased by 62% for every 1 SD increase in HSI (HR: 1.62, 95% CI: 1.41–1.89). When HSI was assessed as quintiles, compared to those in quintile 1, the adjusted HRs (95% CI) for new-onset T2DM in quintile 2, quintile 3, quintile 4, and quintile 5 were 1.66 (0.85-3.22), 1.82 (0.98-3.46), 3.19 (1.64-5.92), and 3.48 (1.85-7.16; P for trend, <0.001), respectively. The kernel outcomes of the complete data analysis were in agreement with the original data (Supplementary Table 4). Further, to validate the robustness of the primary analysis outcomes, investigators performed sensitivity analyses after excluding current smokers and drinkers, respectively, and these results demonstrated equivalent independent correlations (Supplementary Tables 5 and 6).

3.4. Independent Association of HSI with the Risk of T2DM in Different Subgroups. The results of subgroup analysis indicated that age played an interactive role between HSI and the risk of T2DM (P for interaction, 0.005). Higher HSI levels were related to a higher risk of T2DM (HR: 2.17, 95% CI: 1.76-2.67) in those aged < 40 years. Other variables did not substantially modify the association between HSI levels and risk of T2DM (Figure 4).

3.5. The Discriminative Power of HSI for T2DM. We evaluated the discriminative power of HSI for T2DM at different time points (Figure 5). The AUCs were 0.711 at 3 years and 0.717 at 4 years, which indicated helpful discrimination for T2DM.

3.6. The Incremental Impact of HSI on the Predictive Value for New-Onset T2DM. We further assessed the predictive ability of HSI beyond established risk factors for new-onset T2DM (Table 3). First, the Hosmer-Lemeshow test revealed that the model calibration was adequate with the addition of HSI to established risk factors ($P > 0.05$). Second, Table 3 demonstrated that the addition of HSI significantly improved the reclassification and discrimination of established risk factors with an IDI of 0.027 and an NRI of 0.348 (both $P < 0.001$). Furthermore, the C-statistics of established risk factors [0.791 (0.769-0.812)] changed after the addition of the HSI [0.846 (0.829-0.863), $P < 0.001$].

4. Discussion

T2DM is a substantial public health and economic problem worldwide and is common in the general population [32–34]. Thus, it is crucial that individuals at high risk for T2DM are identified, which may contribute to avoiding an unprecedented increase in the incidence of the disease [8, 35]. Furthermore, the results of the subgroup analysis demonstrated that a stronger association between HSI and the risk of T2DM was observed in participants aged < 40 years. This study provides the first evidence of an independent association between HSI and new-onset T2DM, and the

Table 1: Baseline characteristics of the overall participants stratified by HSI quintiles.

HSI	Q1 (18.87-27.23)	Q2 (27.24-29.79)	Q3 (29.80-32.42)	Q4 (32.43-35.97)	Q5 (35.98-66.44)	P value
No. of participants	4400	4397	4416	4405	4407	
Age (years)	37.89 ± 12.14	41.27 ± 12.51	43.12 ± 12.52	44.20 ± 12.67	41.20 ± 10.89	<0.001
Gender, *n* (%)						<0.001
Male	2280 (51.82%)	2429 (55.24%)	2842 (64.36%)	3263 (74.07%)	3738 (84.82%)	
Female	2120 (48.18%)	1968 (44.76%)	1574 (35.64%)	1142 (25.93%)	669 (15.18%)	
Height (cm)	166.16 ± 8.08	166.25 ± 8.25	167.08 ± 8.27	168.19 ± 8.22	170.05 ± 7.89	<0.001
Weight (kg)	54.19 ± 7.17	60.38 ± 7.82	65.56 ± 8.19	71.07 ± 8.45	79.53 ± 10.39	<0.001
BMI (kg/m^2)	19.56 ± 1.53	21.77 ± 1.53	23.42 ± 1.67	25.08 ± 1.87	27.46 ± 2.69	<0.001
SBP (mmHg)	113.05 ± 14.16	115.83 ± 14.99	118.54 ± 14.96	122.08 ± 15.17	125.54 ± 14.80	<0.001
DBP (mmHg)	70.59 ± 9.31	72.15 ± 9.70	74.00 ± 10.02	76.45 ± 10.08	79.21 ± 10.26	<0.001
FPG (mmol/L)	4.81 ± 0.61	4.89 ± 0.61	4.98 ± 0.64	5.05 ± 0.64	5.12 ± 0.65	<0.001
TC (mmol/L)	4.41 ± 0.83	4.61 ± 0.85	4.74 ± 0.88	4.87 ± 0.89	5.00 ± 0.91	<0.001
TG (mmol/L)	0.89 ± 0.52	1.10 ± 0.73	1.36 ± 1.01	1.71 ± 1.27	2.04 ± 1.31	<0.001
HDL-C (mmol/L)	1.46 ± 0.29	1.42 ± 0.29	1.36 ± 0.34	1.30 ± 0.28	1.23 ± 0.28	<0.001
LDL-C (mmol/L)	2.51 ± 0.62	2.65 ± 0.66	2.74 ± 0.68	2.82 ± 0.69	2.91 ± 0.71	<0.001
ALT (IU/L)	12.00 (10.00-15.10)	15.00 (12.00-19.30)	19.00 (15.00-24.42)	25.00 (19.00-32.30)	40.20 (29.40-59.00)	<0.001
AST (IU/L)	21.00 (18.30-24.80)	21.20 (18.20-25.10)	22.40 (19.00-27.00)	24.00 (20.30-29.00)	28.00 (22.80-36.00)	<0.001
HSI	25.28 ± 1.47	28.53 ± 0.73	31.07 ± 0.76	34.04 ± 1.01	39.87 ± 3.50	<0.001
BUN (mmol/L)	4.48 ± 1.17	4.59 ± 1.18	4.70 ± 1.17	4.86 ± 1.18	4.85 ± 1.14	<0.001
Scr (mmol/L)	69.81 ± 15.04	70.75 ± 15.59	72.96 ± 15.16	75.21 ± 14.94	76.92 ± 13.90	<0.001
Smoking status, *n* (%)						<0.001
Current smoker	584 (13.27%)	639 (14.53%)	770 (17.44%)	952 (21.61%)	1242 (28.18%)	
Ever smoker	129 (2.93%)	156 (3.55%)	188 (4.26%)	240 (5.45%)	282 (6.40%)	
Never smoker	3687 (83.80%)	3602 (81.92%)	3458 (78.31%)	3213 (72.94%)	2883 (65.42%)	
Drinking status, *n* (%)						<0.001
Current drinker	101 (2.30%)	89 (2.02%)	103 (2.33%)	147 (3.34%)	140 (3.18%)	
Ever drinker	519 (11.80%)	608 (13.83%)	784 (17.75%)	900 (20.43%)	1026 (23.28%)	
Never drinker	3780 (85.91%)	3700 (84.15%)	3529 (79.91%)	3358 (76.23%)	3241 (73.54%)	
Family history of diabetes, *n* (%)						<0.001
No	4246 (96.50%)	4174 (94.93%)	4134 (93.61%)	4138 (93.94%)	4096 (92.94%)	
Yes	154 (3.50%)	223 (5.07%)	282 (6.39%)	267 (6.06%)	311 (7.06%)	

The variables are presented as mean ± SD or median (quartile 1-quartile 3) or *n* (%).

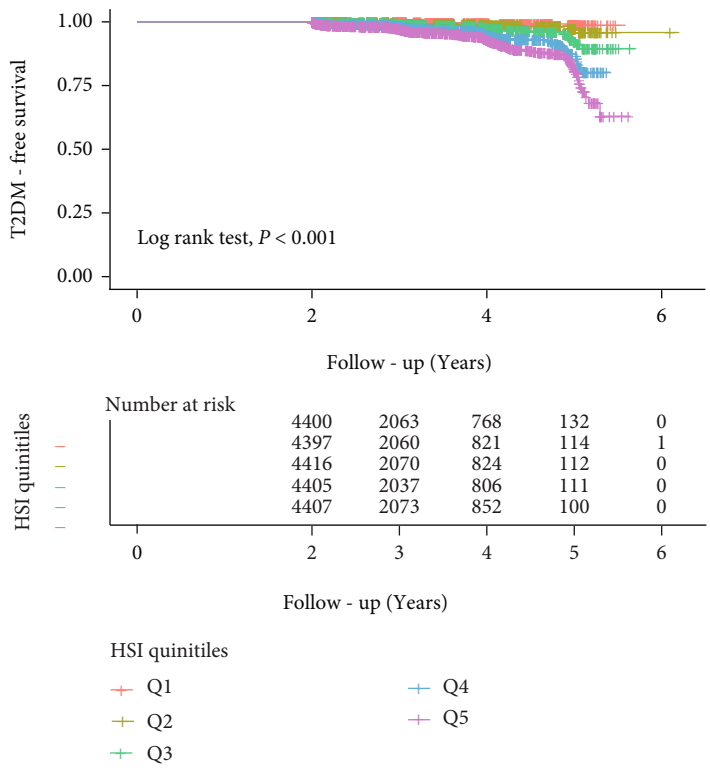

Figure 2: Kaplan-Meier analysis of incident T2DM according to the HSI quintiles. The vertical axis is the diabetes-free survival rate, and the horizontal axis is the follow-up time (years).

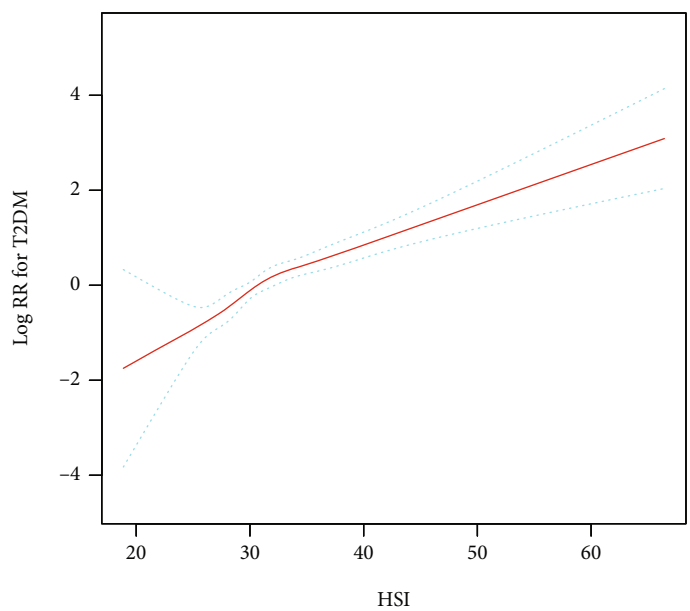

Figure 3: The association between HSI and the risk of T2DM. *The spline was adjusted for all noncollinear variables.

addition of HSI to the baseline model significantly enhanced the performance of predicting the risk of T2DM.

Substantial research has confirmed that hepatic fat accumulation is an independent risk factor for the risk of T2DM [15, 36]. In a longitudinal study of 129 Swedish adults with biopsy-proven NAFLD and elevated serum transaminase levels, the prevalence of T2DM and impaired glucose tolerance increased from 8.5% at baseline to 80% at the end of 14 years [37]. Similarly, in a Korean retrospective cohort study, a total of 13218 participants without T2DM at

Table 2: Association between HSI and risk of T2DM in different models.

	Crude model HR (95% CI)	Model I HR (95% CI)	Model II HR (95% CI)	Model III HR (95% CI)	Model IV HR (95% CI)
Continuous					
HSI (per SD increase)	1.86 (1.73, 2.00)	2.09 (1.93, 2.27)	1.63 (1.42, 1.87)	1.62 (1.40, 1.87)	1.62 (1.41, 1.89)
Categorical					
HSI (quintile)					
*Q*1	Ref	Ref	Ref	Ref	Ref
*Q*2	2.54 (1.34, 4.83)	2.04 (1.08, 3.88)	1.68 (0.88, 3.23)	1.63 (0.85, 3.13)	1.66 (0.85, 3.22)
*Q*3	4.90 (2.70, 8.90)	3.47 (1.91, 6.29)	1.84 (0.98, 3.44)	1.75 (0.93, 3.29)	1.82 (0.98, 3.46)
*Q*4	9.98 (5.64, 17.66)	6.78 (3.83, 12.00)	3.01 (1.60, 5.66)	2.99 (1.58, 5.64)	3.19 (1.64, 5.92)
*Q*5	15.24 (8.69, 26.72)	13.05 (7.44, 22.90)	3.46 (1.75, 6.83)	3.24 (1.62, 6.47)	3.48 (1.85, 7.16)
P for trend	< 0.001	< 0.001	< 0.001	< 0.001	< 0.001

Crude model adjusted for none. Model I adjusted for gender and age. Model II adjusted for age, SBP, DBP, FPG, TG, and BMI. Model III adjusted for age, gender, BMI, SBP, DBP, FPG, TG, LDL-C, AST, BUN, smoking status, drinking status, and family history of diabetes. Model IV adjusted for age, gender, BMI, SBP, DBP, FPG, TG, HDL-C, LDL-C, AST, BUN, Scr, smoking status, drinking status, and family history of diabetes. Abbreviations: Ref: reference; CI: confidence interval; HR: hazard ratios.

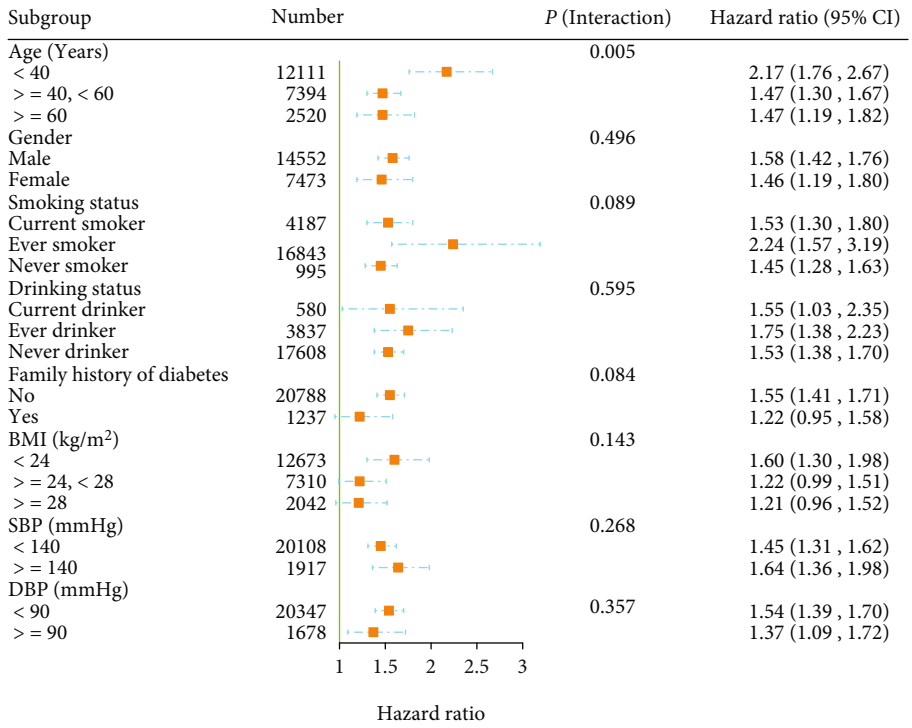

Figure 4: Subgroup analysis of associations between HSI (per 1 SD increment) and risk of T2DM. *Adjusted for all noncollinear variables, if not be stratified.

baseline were enrolled and followed for 5 years [38]. In this study, those patients with NAFLD who progressed to a more severe stage had a significantly increased risk of new-onset T2DM compared to subjects with NAFLD in remission over the same period (OR: 2.49, 95% CI: 1.49-4.14) [38]. In addition, the results of a prospective cohort study conducted in Spain demonstrated that hepatic steatosis was strongly associated with the risk of new-onset T2DM during follow-up. And this association was independent of possible confounding factors such as lifestyle, family history of diabetes, education level, lipid levels, hypertension, and transaminase levels [39]. Likewise, similar conclusions were reached in an open-label, cluster-randomized trial (DiRECT) [40]. In a 5-year observational cohort study, Busquets-Cortés et al. [41] included a total of 16,648 adults with prediabetes. This study further demonstrated that regular physical activity and a healthy diet can help reverse prediabetes by improving the degree of hepatic steatosis.

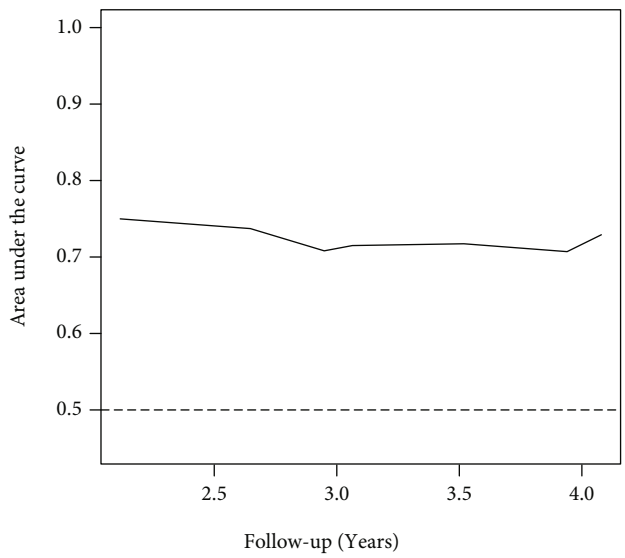

Figure 5: Time-dependent receiver operating characteristic curve.

Table 3: Discrimination of predictive model for risk of T2DM using *C*-statistics, NRI, and IDI.

	C-statistic	*P* value	NRI (95% CI)	*P* value	IDI (95% CI)	*P* value
Established risk factors	0.791 (0.769-0.812)	Ref.		Ref.		Ref.
Established risk factors+HSI	0.846 (0.829-0.863)	<0.001	0.348 (0.284-0.410)	<0.001	0.027 (0.018-0.038)	<0.001

Established risk factors included age, gender, family history of diabetes, smoking status, and drinking status. Abbreviations: Ref: reference; IDI: integrated discrimination improvement; NRI: net reclassification improvement.

The HSI, recently developed by Lee et al., can be used as a simple tool to screen for hepatic steatosis [23]. Liver biopsy has long been considered the "gold standard" for the diagnosis of hepatic steatosis [42]. However, due to its invasive nature and resulting complications, it has not been widely used in clinical practice. Radiological diagnosis using ultrasonography, computed tomography, and magnetic resonance imaging has been demonstrated to accurately assess the extent of hepatic steatosis [43–45]. However, there are limitations to this noninvasive examination, including the high cost of evaluation and the specialized equipment required. Therefore, the great advantages of HSI are its simplicity, accuracy, and accessibility. A survey by Wang et al. revealed that HSI was significantly and positively correlated with hepatic insulin resistance and abnormal lipid metabolism [17]. Additionally, HSI was positively correlated with fasting blood insulin and C-peptide, TG, TC, and LDL-C levels, but negatively correlated with HDL-C. This was similar to the findings of Kitade et al. [25]. In addition, Kitade et al. revealed a positive correlation between HSI and insulin resistance and β-cell function in a nondiabetic population [25]. Tripolino et al. and Sviklāne et al. both found a strong correlation between HSI and risk indicators of lipid metabolism [19, 46]. The results of all these studies indicate that HSI is strongly associated with insulin resistance and lipid metabolism disorders and that HSI has better predictive value as a predictor of T2DM. Therefore, this study used a large sample size and longitudinal design to confirm a causal relationship between HSI and T2DM in Chinese adults, independent of traditional risk factors. The reasons for this strange finding are unclear, but it may be essential to note the following two points. First, with rapid economic development, young people will inevitably reduce their need for physical activity and are more prone to various metabolic diseases [47, 48]. Second, in modern society, young people have developed increasingly unhealthy lifestyle habits, leading to the premature development of multiple metabolic diseases [49, 50].

The exact mechanism of the association between HSI and the risk of T2DM remains unclear. However, there are several possible explanations. Insulin resistance is linked to hepatic steatosis [51, 52]. In animal models of hepatic steatosis, the ability of insulin to inhibit hepatic gluconeogenesis is diminished even when muscle insulin resistance is not significantly altered [53]. Hepatic steatosis or hepatic fat infiltration may induce hepatic insulin resistance through activation of JNK1 and PKC-epsilon, which may interfere with tyrosine phosphorylation of IRS-1 and IRS-2. This further contributes to the impaired ability of insulin to activate glycogen synthesis and inhibit gluconeogenesis [54]. In addition, another possible mechanism may involve inflammatory effects in the liver that impair insulin signaling, resulting in the inability to inhibit glucose production and the eventual development of hyperglycemia [55, 56].

The greatest advantage of the study is that it is from a multicenter, large-scale cohort study in China. Therefore, there was a sufficient sample size available for analysis to confirm the robustness and reliability of the outcomes. Secondly, the independent relationship between HSI and T2DM was confirmed after adjustment for a series of conventional risk factors. Further, *C*-statistic, IDI, and NRI analyses validated the incremental predictive value of HSI over and above the established risk factors. Finally, a variety of sensitivity analyses were

conducted in the current research to improve the rigor of the findings. With these reliable statistical analyses, it can be concluded that the conclusions of this study are more reliable, and the results can be applicable to most Chinese populations.

The strengths of this study are evident, but several limitations should also be considered when making cautious interpretations. First, the 2-hour oral glucose tolerance test was not used in this study to diagnose T2DM, so this may have resulted in missing cases of new-onset T2DM. Second, patient follow-up was relatively short, and the primary effect of shorter follow-up was a lower rate of endpoint events. Finally, the findings of this study are currently applicable mainly to the Chinese population. Therefore, the applicability of the study results to other populations or ethnicities needs to be further investigated.

5. Conclusions

In general, our findings demonstrate that an elevated HSI is significantly associated with a greater risk of T2DM. HSI may be an accessible and supplementary monitoring method in the management of T2DM risk stratification in the Chinese population.

Data Availability

Raw dataset is stored in Dryad (10.5061/dryad.ft8750v).

Conflicts of Interest

The authors stated that none of them had competing interests.

Authors' Contributions

Xintian Cai, Jing Gao, and Shasha Liu have contributed equally to this production.

Acknowledgments

The research was granted by the Chinese Academy of Medical Sciences (2020-RW330-002).

Supplementary Materials

Table 1: the description of missing data. Table 2: sensitivity comparative analysis between preimputation and postimputation. Table 3: collinearity diagnostics steps. Table 4: results of multivariate Cox regression among original data and postimputation data. Table 5: HRs and 95% CI for risk of type 2 diabetes mellitus excluding current smoker. Table 6: HRs and 95% CI for risk of type 2 diabetes mellitus excluding current drinker. Figure 1: the association between HSI and the risk of T2DM in postimputation data. *(Supplementary Materials)*

References

[1] N. H. Cho, J. E. Shaw, S. Karuranga et al., "IDF diabetes atlas: global estimates of diabetes prevalence for 2017 and projections for 2045," *Diabetes Research and Clinical Practice*, vol. 138, pp. 271–281, 2018.

[2] Y. Li, D. Teng, X. Shi et al., "Prevalence of diabetes recorded in mainland China using 2018 diagnostic criteria from the American Diabetes Association: national cross sectional study," *BMJ*, vol. 369, article m997, 2020.

[3] J. Xu, X. Shi, and Y. Pan, "The association of aspartate aminotransferase/alanine aminotransferase ratio with diabetic nephropathy in patients with type 2 diabetes," *Diabetes, Metabolic Syndrome and Obesity: Targets and Therapy*, vol. 14, pp. 3831–3837, 2021.

[4] N. Holman, B. Young, and R. Gadsby, "Current prevalence of type 1 and type 2 diabetes in adults and children in the UK," *Diabetic Medicine: A Journal of the British Diabetic Association*, vol. 32, no. 9, pp. 1119-1120, 2015.

[5] X. Cai, Q. Zhu, T. Wu et al., "Development and validation of a novel model for predicting the 5-year risk of type 2 diabetes in patients with hypertension: a retrospective cohort study," *BioMed Research International*, vol. 2020, Article ID 9108216, 12 pages, 2020.

[6] G. Xie, Y. Zhong, S. Yang, and Y. Zou, "Remnant cholesterol is an independent predictor of new-onset diabetes: a single-center cohort study," *Diabetes, Metabolic Syndrome and Obesity: Targets and Therapy*, vol. 14, pp. 4735–4745, 2021.

[7] D. Umpierre, P. A. Ribeiro, C. K. Kramer et al., "Physical activity advice only or structured exercise training and association with HbA1cLevels in type 2 Diabetes," *JAMA*, vol. 305, no. 17, pp. 1790–1799, 2011.

[8] F. Magkos, M. F. Hjorth, and A. Astrup, "Diet and exercise in the prevention and treatment of type 2 diabetes mellitus," *Nature Reviews. Endocrinology*, vol. 16, no. 10, pp. 545–555, 2020.

[9] Z. M. Younossi, A. B. Koenig, D. Abdelatif, Y. Fazel, L. Henry, and M. Wymer, "Global epidemiology of nonalcoholic fatty liver disease-meta-analytic assessment of prevalence, incidence, and outcomes," *Hepatology: Official Journal of the American Association for the Study of Liver Diseases*, vol. 64, no. 1, pp. 73–84, 2016.

[10] X. Cai, X. Aierken, A. Ahmat et al., "A nomogram model based on noninvasive bioindicators to predict 3-year risk of nonalcoholic fatty liver in nonobese mainland Chinese: a prospective cohort study," *BioMed Research International*, vol. 2020, Article ID 8852198, 12 pages, 2020.

[11] S. L. Friedman, B. A. Neuschwander-Tetri, M. Rinella, and A. J. Sanyal, "Mechanisms of NAFLD development and therapeutic strategies," *Nature Medicine*, vol. 24, no. 7, pp. 908–922, 2018.

[12] M. Eslam, L. Valenti, and S. Romeo, "Genetics and epigenetics of NAFLD and NASH: clinical impact," *Journal of Hepatology*, vol. 68, no. 2, pp. 268–279, 2018.

[13] L. Ji, X. Cai, Y. Bai, and T. Li, "Application of a novel prediction model for predicting 2-year risk of non-alcoholic fatty liver disease in the non-obese population with normal blood lipid levels: a large prospective cohort study from China," *International Journal of General Medicine*, vol. 14, pp. 2909–2922, 2021.

[14] H. Tilg, A. R. Moschen, and M. Roden, "NAFLD and diabetes mellitus," *Nature Reviews. Gastroenterology & Hepatology*, vol. 14, no. 1, pp. 32–42, 2017.

[15] G. Targher, K. E. Corey, C. D. Byrne, and M. Roden, "The complex link between NAFLD and type 2 diabetes mellitus – mechanisms and treatments," *Nature Reviews. Gastroenterology & Hepatology*, vol. 18, no. 9, pp. 599–612, 2021.

[16] A. Wieckowska and A. E. Feldstein, "Diagnosis of nonalcoholic fatty liver disease: invasive versus noninvasive," *Seminars in Liver Disease*, vol. 28, no. 4, pp. 386–395, 2008.

[17] C. Wang, Z. Cai, X. Deng et al., "Association of hepatic steatosis index and fatty liver index with carotid atherosclerosis in type 2 diabetes," *International Journal of Medical Sciences*, vol. 18, no. 14, pp. 3280–3289, 2021.

[18] J. Chung, H. S. Park, Y. J. Kim, M. H. Yu, S. Park, and S. I. Jung, "Association of hepatic steatosis index with nonalcoholic fatty liver disease diagnosed by non-enhanced CT in a screening population," *Diagnostics (Basel, Switzerland)*, vol. 11, no. 12, article 2168, 2021.

[19] L. Sviklāne, E. Olmane, Z. Dzērve, K. Kupčs, V. Pīrāgs, and J. Sokolovska, "Fatty liver index and hepatic steatosis index for prediction of non-alcoholic fatty liver disease in type 1 diabetes," *Journal of Gastroenterology and Hepatology*, vol. 33, no. 1, pp. 270–276, 2018.

[20] A. R. Khang, H. W. Lee, D. Yi, Y. H. Kang, and S. M. Son, "The fatty liver index, a simple and useful predictor of metabolic syndrome: analysis of the Korea National Health and Nutrition Examination Survey 2010-2011," *Diabetes, Metabolic Syndrome and Obesity: Targets and Therapy*, vol. 12, pp. 181–190, 2019.

[21] A. Jawahar, B. Gonzalez, N. Balasubramanian, W. Adams, and A. Goldberg, "Comparison of correlations between lipid profile and different computed tomography fatty liver criteria in the setting of incidentally noted fatty liver on computed tomography examinations," *European Journal of Gastroenterology & Hepatology*, vol. 29, no. 12, pp. 1389–1396, 2017.

[22] Y. H. Lee, H. Bang, Y. M. Park et al., "Non-laboratory-based self-assessment screening score for non-alcoholic fatty liver disease: development, validation and comparison with other scores," *PloS One*, vol. 9, no. 9, article e107584, 2014.

[23] J. H. Lee, D. Kim, H. J. Kim et al., "Hepatic steatosis index: a simple screening tool reflecting nonalcoholic fatty liver disease," *Digestive and liver disease: official journal of the Italian Society of Gastroenterology and the Italian Association for the Study of the Liver*, vol. 42, no. 7, pp. 503–508, 2010.

[24] P. J. Meffert, S. E. Baumeister, M. M. Lerch, J. Mayerle, W. Kratzer, and H. Völzke, "Development, external validation, and comparative assessment of a new diagnostic score for hepatic steatosis," *The American Journal of Gastroenterology*, vol. 109, no. 9, pp. 1404–1414, 2014.

[25] H. Kitade, G. Chen, Y. Ni, and T. Ota, "Nonalcoholic fatty liver disease and insulin resistance: new insights and potential new treatments," *Nutrients*, vol. 9, no. 4, p. 387, 2017.

[26] A. F. Cicero, S. D'Addato, A. Reggi, G. M. Reggiani, and C. Borghi, "Hepatic steatosis index and lipid accumulation product as middle-term predictors of incident metabolic syndrome in a large population sample: data from the Brisighella Heart Study," *Internal and Emergency Medicine*, vol. 8, no. 3, pp. 265–267, 2013.

[27] X. Cai, J. Gao, J. Hu et al., "Dose-response associations of metabolic score for insulin resistance index with nonalcoholic fatty liver disease among a nonobese Chinese population: retrospective evidence from a population-based cohort study," *Disease Markers*, vol. 2022, Article ID 4930355, 10 pages, 2022.

[28] S. Song, Y. Duo, Y. Zhang et al., "The predictive ability of hepatic steatosis index for gestational diabetes mellitus and large for gestational age infant compared with other noninvasive indices among Chinese pregnancies: a preliminary double-center cohort study," *Diabetes, Metabolic Syndrome and Obesity: Targets and Therapy*, vol. 14, pp. 4791–4800, 2021.

[29] Y. Chen, X. P. Zhang, J. Yuan et al., "Association of body mass index and age with incident diabetes in Chinese adults: a population-based cohort study," *BMJ Open*, vol. 8, no. 9, article e021768, 2018.

[30] X. T. Cai, Q. Zhu, S. S. Liu et al., "Associations between the metabolic score for insulin resistance index and the risk of type 2 diabetes mellitus among non-obese adults: insights from a population-based cohort study," *International Journal of General Medicine*, vol. 14, pp. 7729–7740, 2021.

[31] J. P. Vandenbroucke, E. von Elm, D. G. Altman et al., "Strengthening the Reporting of Observational Studies in Epidemiology (STROBE): explanation and elaboration," *PLoS Medicine*, vol. 4, no. 10, article e297, 2007.

[32] P. Zimmet, Z. Shi, A. El-Osta, and L. Ji, "Epidemic T2DM, early development and epigenetics: implications of the Chinese famine," *Nature Reviews. Endocrinology*, vol. 14, no. 12, pp. 738–746, 2018.

[33] M. Wei, L. Dong, F. Wang et al., "The prevalence and control of type 2 diabetes mellitus in residents of a rural town, Shandong Province, China," *Diabetes, Metabolic Syndrome and Obesity: Targets and Therapy*, vol. 14, pp. 4505–4512, 2021.

[34] X. Chen, M. Duan, R. Hou et al., "Prevalence of abdominal obesity in Chinese middle-aged and older adults with a normal body mass index and its association with type 2 diabetes mellitus: a nationally representative cohort study from 2011 to 2018," *Diabetes, Metabolic Syndrome and Obesity: Targets and Therapy*, vol. 14, pp. 4829–4841, 2021.

[35] M. D. Campbell, T. Sathish, P. Z. Zimmet et al., "Benefit of lifestyle-based T2DM prevention is influenced by prediabetes phenotype," *Nature Reviews. Endocrinology*, vol. 16, no. 7, pp. 395–400, 2020.

[36] E. E. Canfora, R. Meex, K. Venema, and E. E. Blaak, "Gut microbial metabolites in obesity, NAFLD and T2DM," *Nature Reviews. Endocrinology*, vol. 15, no. 5, pp. 261–273, 2019.

[37] M. Ekstedt, L. E. Franzén, U. L. Mathiesen et al., "Long-term follow-up of patients with NAFLD and elevated liver enzymes," *Hepatology: official journal of the American Association for the Study of Liver Diseases*, vol. 44, no. 4, pp. 865–873, 2006.

[38] K. C. Sung, S. H. Wild, and C. D. Byrne, "Resolution of fatty liver and risk of incident diabetes," *The Journal of Clinical Endocrinology and Metabolism*, vol. 98, no. 9, pp. 3637–3643, 2013.

[39] J. Franch-Nadal, L. Caballeria, M. Mata-Cases et al., "Fatty liver index is a predictor of incident diabetes in patients with prediabetes: the PREDAPS study," *PloS One*, vol. 13, no. 6, article e0198327, 2018.

[40] M. E. Lean, W. S. Leslie, A. C. Barnes et al., "Primary care-led weight management for remission of type 2 diabetes (DiRECT): an open-label, cluster-randomised trial," *The Lancet*, vol. 391, no. 10120, pp. 541–551, 2018.

[41] C. Busquets-Cortés, M. Bennasar-Veny, Á. A. López-González, S. Fresneda, M. Abbate, and A. M. Yáñez, "Utility of fatty liver index to predict reversion to normoglycemia in people with prediabetes," *PloS One*, vol. 16, no. 4, article e0249221, 2021.

[42] J. Neuberger, J. Patel, H. Caldwell et al., "Guidelines on the use of liver biopsy in clinical practice from the British Society of Gastroenterology, the Royal College of Radiologists and the

Royal College of Pathology," *Gut*, vol. 69, no. 8, pp. 1382–1403, 2020.

[43] L. Miele, M. A. Zocco, F. Pizzolante et al., "Use of imaging techniques for non-invasive assessment in the diagnosis and staging of non-alcoholic fatty liver disease," *Metabolism: Clinical and Experimental*, vol. 112, article 154355, 2020.

[44] E. A. Selvaraj, F. E. Mózes, A. Jayaswal et al., "Diagnostic accuracy of elastography and magnetic resonance imaging in patients with NAFLD: a systematic review and meta-analysis," *Journal of Hepatology*, vol. 75, no. 4, pp. 770–785, 2021.

[45] G. Besutti, L. Valenti, G. Ligabue et al., "Accuracy of imaging methods for steatohepatitis diagnosis in non-alcoholic fatty liver disease patients: a systematic review," *Liver International: Official Journal of the International Association for the Study of the Liver*, vol. 39, no. 8, pp. 1521–1534, 2019.

[46] C. Tripolino, C. Irace, A. Cutruzzolà et al., "Hepatic steatosis index is associated with type 1 diabetes complications," *Diabetes, Metabolic Syndrome and Obesity: Targets and Therapy*, vol. 12, pp. 2405–2410, 2019.

[47] B. M. Gabriel and J. R. Zierath, "Circadian rhythms and exercise – re-setting the clock in metabolic disease," *Nature Reviews. Endocrinology*, vol. 15, no. 4, pp. 197–206, 2019.

[48] D. Hansen, J. Niebauer, V. Cornelissen et al., "Exercise prescription in patients with different combinations of cardiovascular disease risk factors: a consensus statement from the EXPERT working group," *Sports Medicine (Auckland, N.Z.)*, vol. 48, no. 8, pp. 1781–1797, 2018.

[49] K. M. Lin, J. Y. Chiou, H. W. Kuo, J. Y. Tan, S. H. Ko, and M. C. Lee, "Associations between unhealthy lifestyle behaviors and metabolic syndrome by gender in young adults," *Biological Research for Nursing*, vol. 21, no. 2, pp. 173–181, 2019.

[50] H. Freisling, V. Viallon, H. Lennon et al., "Lifestyle factors and risk of multimorbidity of cancer and cardiometabolic diseases: a multinational cohort study," *BMC Medicine*, vol. 18, no. 1, p. 5, 2020.

[51] M. J. Watt, P. M. Miotto, W. De Nardo, and M. K. Montgomery, "The liver as an endocrine organ-linking NAFLD and insulin resistance," *Endocrine Reviews*, vol. 40, no. 5, pp. 1367–1393, 2019.

[52] V. T. Samuel and G. I. Shulman, "Nonalcoholic fatty liver disease as a nexus of metabolic and hepatic diseases," *Cell Metabolism*, vol. 27, no. 1, pp. 22–41, 2018.

[53] L. Zhao, Z. Cang, H. Sun, X. Nie, N. Wang, and Y. Lu, "Berberine improves glucogenesis and lipid metabolism in nonalcoholic fatty liver disease," *BMC Endocrine Disorders*, vol. 17, no. 1, p. 13, 2017.

[54] R. J. Perry, V. T. Samuel, K. F. Petersen, and G. I. Shulman, "The role of hepatic lipids in hepatic insulin resistance and type 2 diabetes," *Nature*, vol. 510, no. 7503, pp. 84–91, 2014.

[55] D. Yadav, E. Choi, S. V. Ahn et al., "Incremental predictive value of serum AST-to-ALT ratio for incident metabolic syndrome: the ARIRANG study," *PloS One*, vol. 11, no. 8, article e0161304, 2016.

[56] H. Niu and Y. Zhou, "Nonlinear relationship between AST-to-ALT ratio and the incidence of type 2 diabetes mellitus: a follow-up study," *International Journal of General Medicine*, vol. 14, pp. 8373–8382, 2021.

Hindawi
Disease Markers
Volume 2022, Article ID 7979500, 6 pages
https://doi.org/10.1155/2022/7979500

Research Article

Expression of miR-155 in Serum Exosomes in Children with Epilepsy and Its Diagnostic Value

Ya Liu,[1] Gang Yu,[2] Yan-Yan Ding,[2] and Yong-Xia Zhang[3]

[1]*Pediatric Department of Liaocheng Second People's Hospital, Liaocheng, Shandong Province, China*
[2]*Maternity & Child Care Center of Dezhou, Dezhou, Shandong Province, China*
[3]*Department of Paediatric Rehabilitation, Linyi People's Hospital, Linyi, Shandong Province, China*

Correspondence should be addressed to Yong-Xia Zhang; zhangyongxia1234@yeah.net

Received 30 December 2021; Accepted 22 February 2022; Published 26 July 2022

Academic Editor: Hongsheng Zhang

Objective. This study was designed to analyze the expression of miR-155 in serum exosomes in children with epilepsy and to explore its diagnostic value. *Methods*. From March 2020 to March 2021, 43 hospitalized children with epilepsy admitted to the Department of Neurology of the hospital were included, and another 43 gender- and age-matched healthy children were randomly selected as the healthy control group during the same period. Then fasting serum samples of the two groups were collected to extract the exosomes. The morphology of the exosomes was evaluated under a transmission electron microscope, and the expression of specific protein markers on the surface was detected by Western Blot. In addition, the relative expression of miR-155 in serum exosomes in children with epilepsy with different courses of the disease and different degrees of abnormal electroencephalography (EEG) was compared, and the area under the receiver operating characteristic (ROC) curve (ROC-AUC) was used to evaluate the diagnostic value of miR-155. *Results*. A higher relative expression level of miR-155 in serum exosomes was obtained in the epilepsy group, as compared to the healthy control group ($P<0.05$), and the relative expression of miR-155 in serum exosomes in children with epilepsy was correlated with the course of the disease and the degree of abnormal EEG (both $P<0.05$). In addition, the expression of miR-155 in serum exosomes showed high diagnostic efficiency for epilepsy (AUC = 0.813, $P<0.05$). *Conclusion*. The expression of miR-155 in serum exosomes in children with epilepsy is up-regulated, and its level is related to the course of the disease and the degree of abnormal EEG, so miR-155 in serum exosomes may be used as a biomarker for the diagnosis and assessment of the severity of epilepsy.

1. Introdution

Micro ribonucleic acid (miRNA) is a non-coding RNA with a length of about 22 nt, which can bind to complementary sites on messenger RNA to reduce its stability, down-regulate translation, and regulate gene expression. In recent years, studies have found a variety of miRNAs differentially expressed in the serum of patients with epilepsy, which provides new research directions for the diagnosis and treatment of epilepsy [1]. Related animal experiments also revealed different expression levels of miRNA in the brain tissue and serum of rats in different stages of epilepsy [2]. Epilepsy is one of the main causes of children's disability that triggers dysfunction in children and compromises their quality of life [3]. Early diagnosis of epilepsy mainly relies on medical history, electroencephalography (EEG), magnetic resonance imaging, biochemical examination, etc., which are of great significance for prognosis improvement and prevention of status epilepticus. Nonetheless, the effect of conventional EEG in capturing epileptic discharge waves is rather poor [4], and studies have shown that the brain magnetic resonance imaging results of most patients with epilepsy are negative [5]. Therefore, for non-invasive biochemical examination, it is of essential clinical significance to seek new high-sensitivity biomarkers for the early diagnosis of epilepsy. Exosomes are small vesicles containing complex RNA and proteins. In recent years, it has been reported that exosome miRNA is involved in the occurrence and development of a variety of central nervous system diseases including epilepsy [6]. Accordingly, it is speculated that

Table 1: Comparison of general data.

Group	No.	Age ($\bar{x}$±s, years old)	BMI ($\bar{x}$±s, kg/m^2)	Gender (male, n/%)
Epilepsy group	43	8.56 ± 2.14	18.11 ± 2.13	26/60.47
Healthy control group	43	8.45 ± 2.18	18.15 ± 2.15	28/65.12
t/χ^2 value		0.236	0.087	10.234
P value		0.814	0.931	0.786

analysis of exosomes can help identify subtle changes in the physiological and pathological processes of patients with epilepsy. MiR-155 is a versatile RNA. One study has pointed out that the expression of miR-155 exerts a certain effect on seizures and progression [7]. Therefore, this study analyzed the expression of miR-155 in serum exosomes in children with epilepsy and explored its diagnostic value, aiming to provide more references for the diagnosis and treatment of epilepsy.

2. Materials and Methods

2.1. Ethical Statement. The study was reviewed and approved by the Linyi People's Hospital ethics committee, was carried out in accordance with The Code of Ethics of the World Medical Association (Declaration of Helsinki) for experiments involving humans. Children and their legal guardians signed informed consent forms.

2.2. Clinical Data. A total of 43 children with epilepsy admitted to the neurology department of the hospital from March 2020 to March 2021 were included into the epilepsy group. Inclusion criteria [8, 9]: (1) Patients at 0-14 years old; (2) Patients diagnosed as pediatric epilepsy [10]; (3) Patients who had not taken immunosuppressants, hormonal drugs, or other drugs that affect the results of this study in the past 3 months; (4) Children and their legal guardians signed informed consent forms. Exclusion criteria [8, 9]: (1) Patients with secondary epilepsy caused by head injury, etc.; (2) Patients with a history of brain injury or craniocerebral surgery; (3) Patients complicated with infectious diseases, endocrine system diseases, or malignant tumors. Among the 43 cases of children with epilepsy, there were 26 male and 17 female cases, aged 1-13 years old, with an average age of (8.56 ± 2.14) years. In terms of disease course, there were 11 cases with the course shorter than 1 year, 15 cases with the course between 1 to 3 years, 10 cases with the course between 3 to 5 years, and 7 cases with the course longer than 5 years. In terms of the abnormal degree of EEG, there were 13 mild cases, 22 moderate cases, and 8 severe cases. Another 43 gender- and age-matched healthy children were randomly selected as the healthy control group during the same period. Among them, there were 28 males and 15 females, aged 1-14 years old, with an average age of (8.45 ± 2.18) years.

2.3. Methods

2.3.1. Main Reagents and Instruments. Serum/plasma exosome extraction and RNA isolation kit (Cat. No.: YB-024-A, Shanghai Yubo Biotechnology Co., Ltd.), membrane sealing fluid (article number: YT8900, Beijing Yita Biotechnology Co., Ltd.), rabbit monoclonal to anti-human CD63 antibody and rabbit monoclonal to anti-human CD9 antibody (article numbers: ab134045 and ab92726, Abcam, USA), ECL chemiluminescence detection kit (rabbit IgG) (article number: ASW2020, Shanghai Jizhi Biochemical Technology Co., Ltd.), serum/plasma miRNA extraction and isolation kit (article number: DP503, Beijing Tiangen Biochemical Technology Co., Ltd.), reverse transcription kit (article number: BTN60906, Beijing Biolab Technology Co., Ltd.), transmission electron microscope (model number: JEM-2100, JEOL Ltd.), and microspectrophotometer (model number: Nanodrop2000, Thermo Fisher Scientific). Real-time fluorescent quantitative PCR instrument (Thermo Fisher, USA; model: Applied Biosystems).

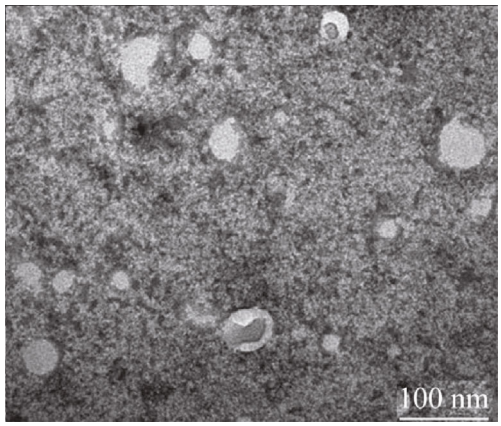

Figure 1: Morphology of serum exosomes in children with epilepsy under transmission electron microscope.

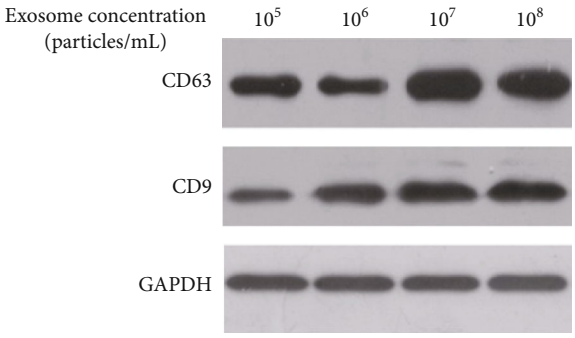

Figure 2: The expression of specific protein markers on the surface of serum exosomes in children with epilepsy.

2.3.2. Serum Specimen Collection. Before medication, 5 mL fasting venous blood was collected from each subject, placed

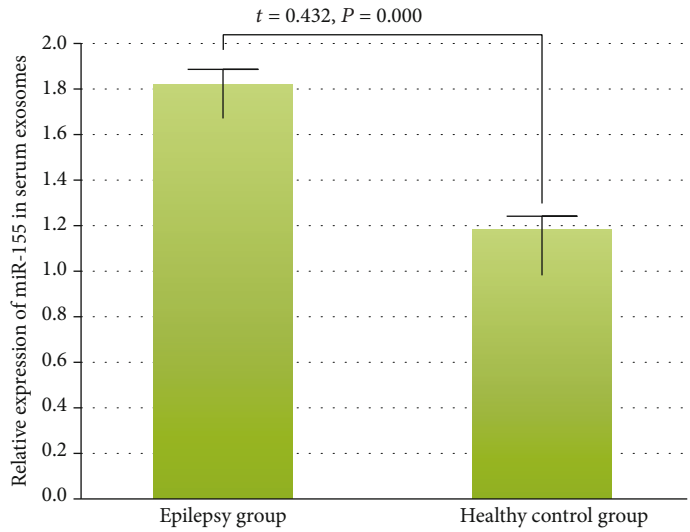

Figure 3: Comparison of the relative expression of miR-155 in serum exosomes.

at room temperature, and centrifuged at 3000 r/min for 10 min. The supernatant was then transferred into an EP tube and stored in a refrigerator at -80°C for later use.

2.3.3. Serum Exosome Extraction and Morphological Observation. The serum sample was thawed in a water bath at 25°C, and centrifuged at 3000 r/min for 15 minutes at 4°C to remove cells or cell debris. Then the supernatant was collected, filtered with a filter membrane (0.22 μm), and placed in a new eppendorf (EP) tube, followed by addition of exosome extraction reagent, well mixing, and store at 4°C for 30 min. It was then centrifuged at 1500 r/min for 30 minutes at 4°C to aspirate the supernatant. Subsequently, it was centrifuged again at 1500 r/min for 5 min at 4°C to remove the residual liquid. Then, the diluent was added and mixed evenly with a pipette to completely dissolve the precipitate. The resuspended exosomes were transferred to the spin column and placed in the collection tube, followed by centrifugation at 2000 r/min for 5 minutes at 4°C. After discarding of the spin column, the serum exosomes were obtained. Afterwards, 15 μL of the exosomal solution was added on a 100-mesh sample-loading copper mesh, and placed at room temperature for 1 minute. Phosphotungstic acid was added dropwise and placed at room temperature for 5 minutes. The filter paper was used to absorb excess liquid from the edge, and the exosomes were evaluated and photographed under a transmission electron microscope.

2.3.4. Western Blot Analysis for Detection of the Expression of Specific Protein Markers on the Surface of Exosome. The Bicinchoninic Acid (BCA) method was used to quantify the protein in the exosome solution: The measurement wavelength of the microplate reader was set as 570 nm to determine the optical density (OD) value, and then a standard curve was drawn to calculate the protein concentration of each sample. The protein sample was subjected to sodium dodecyl sulfate-polyacrylamide gel electrophoresis (SDS-PAGE), transferred to a polyvinylidene fluorid (PVDF) membrane by the wet method, and immersed in the membrane blocking solution. After incubation for 1 hour at room temperature, the primary antibody diluent was added and incubated overnight at 4°C (using Glyceraldehyde-3-phosphate dehydrogenase (GAPDH) as internal control). Then the liquid was discarded and the membrane was rinsed 3 times with Tris-buffered-saline with Tween (TBST) solution, 10 minutes each time. After that, the secondary antibody diluent was added and incubated at room temperature for 2 hours in the dark, and then the membrane was rinsed 3 times with TBST solution, 10 minutes each time. Finally, the electrochemiluminescence (ECL) method was used for color development, the gel imaging system for observation and photographing of the target protein bands, and the Image J software for quantitative analysis.

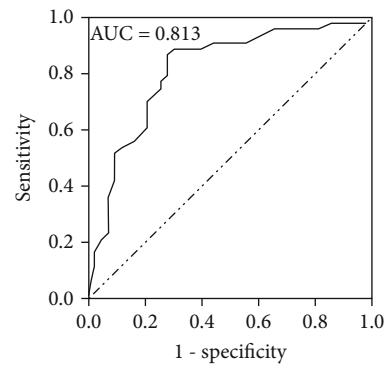

Figure 4: ROC curve analysis of miR-155 in serum exosomes in the diagnosis of epilepsy.

2.3.5. Real Time Fluorescent Quantitative Polymerase Chain Reaction (qRT-PCR) for Measurement of the Expression Level of miR-155 in Serum Exosomes. miRNA was extracted from serum exosomes in strict accordance with the miRNA extraction kit instructions, and its concentration was determined by a micro-spectrophotometer. The cDNA was obtained according to the instructions of the reverse transcription kit, diluted by 10 times, and then added into a

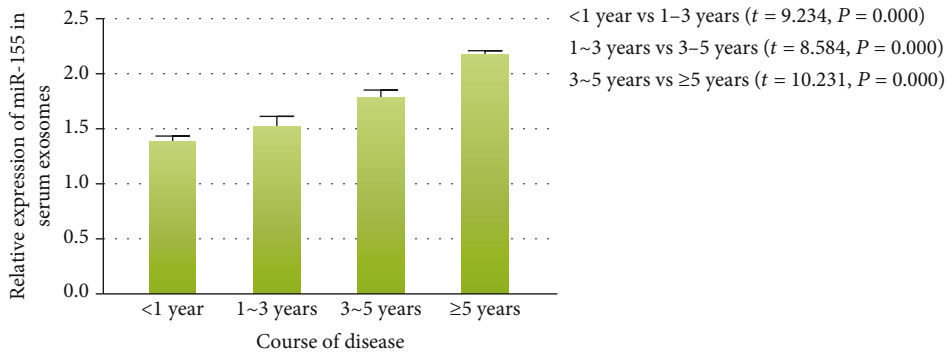

Figure 5: Comparison of miR-155 expression in serum exosomes in children with epilepsy in different courses of the disease.

dedicated PCR tube. The PCR reaction system consisted of 10 μL 2 × real-time PCR Master Mix, 0.4 μL Gene specific primer set, 0.2 μL Gene specific probe, 0.2 μL Taq DNA polymerase, 2.0 μL RT product, and 7.2 μL ddH2O, and the reaction conditions were as follows: pre-denaturation at 95°C for 3 min, denaturation for 12 s at 95°C, and annealing and extending for 40 s at 62°C, with U6 as the internal reference gene. Each sample was determined repeatedly three times. The fluorescence signal was then collected to measure the cycle threshold (Ct). The relative expression of the target gene was expressed by the 2-△△Ct method [11].

2.4. Statistical Analysis. SPSS20.0 software was used for data analysis. The measurement data in normal distribution were represented by (x±s), and compared between groups using the independent sample t-test. The count data were expressed by frequency or composition ratio; as the total number of cases in this study was ≥40 and the minimum theoretical frequency was >5, the chi-square non-correction method was used for statistical analysis. The correlation was analyzed by Spearman rank correlation analysis. In addition, the area under the receiver operating characteristic curve (ROC) (ROC-AUC) was used to evaluate the diagnostic value. $P < 0.05$ was considered statistically significant.

3. Results

3.1. Comparison of General Data. There were no significant differences in gender, age, and body mass index (BMI) between the two groups (P<0.05). See Table 1.

3.2. Identification of Serum Exosomes. It was found that the size of the serum exosomes obtained by centrifugation was mainly within a range of 50-100 nm under a transmission electron microscope, in line with the normal size range of exosomes of 30-200 nm, and they were round, quasi-circular or cup-shaped, uniform in size and with a complete lipid envelope, as shown in Figure 1. Western Blot analysis showed that the surface of the extracted 43 cases of serum exosomes all expressed CD63 and CD9, and as the concentration of exosomes increased, the relative expression of the above two protein markers was also up-regulated, as shown in Figure 2.

Table 2: Correlation between miR-155 in serum exosomes and course of disease and abnormality of EEG.

	r value	p value
Courses of disease	0.876	0.002
Abnormality of EEG	0.911	0.001

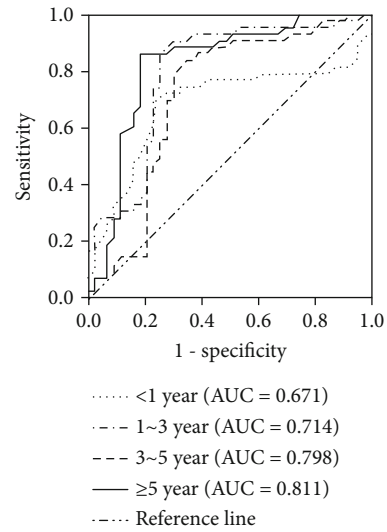

Figure 6: ROC curve analysis of miR-155 in serum exosomes in the diagnosis of epilepsy in different courses of the disease.

3.3. Comparison of the Relative Expression of miR-155 in Serum Exosomes. The epilepsy group showed a higher expression level of miR-155 in serum exosomes than the healthy control group (P<0.05). See Figure 3.

3.4. ROC Curve Analysis of miR-155 in Serum Exosomes in the Diagnosis of Epilepsy. The specificity and sensitivity of miR-155 in serum exosomes in diagnosing epilepsy were 78.24% and 84.11%, respectively, and the AUC was 0.813. See Figure 4.

3.5. Comparison of miR-155 Expression in Serum Exosomes in Children with Epilepsy in Different Courses of the Disease. As the course of epilepsy prolonged, the expression level of miR-155 in serum exosomes in children with

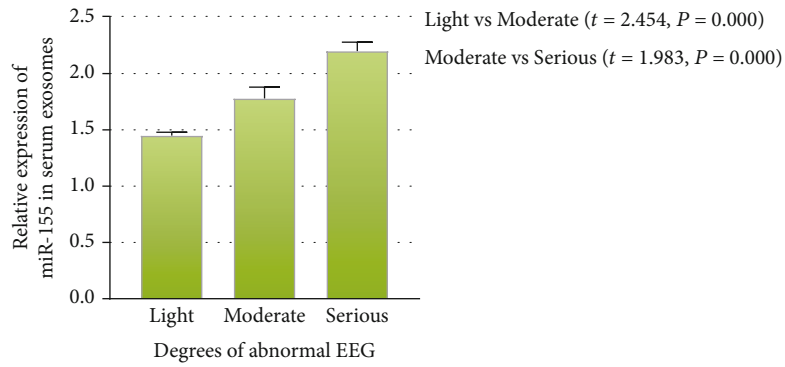

Figure 7: Comparison of miR-155 expression in serum exosomes in children with epilepsy with different degrees of abnormal EEG.

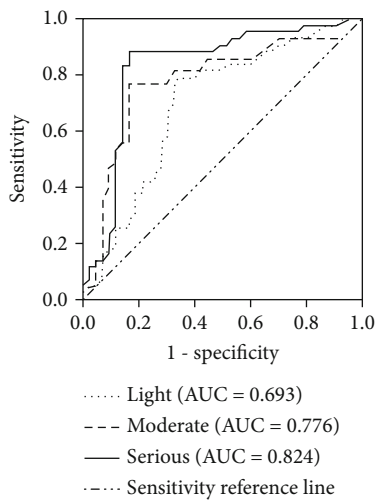

Figure 8: ROC curve analysis of miR-155 in serum exosomes in the diagnosis of epilepsy with different degrees of abnormal EEG.

epilepsy gradually increased ($P < 0.05$), so it was positively correlated with the course of the disease ($r = 0.876$, $P = 0.002$). See Figure 5 and Table 2.

3.6. ROC Curve Analysis of miR-155 in Serum Exosomes in the Diagnosis of Epilepsy in Different Courses of Disease. The AUC of miR-155 in serum exosomes diagnosed as epilepsy with a course of less than 1 year, 1 to 3 years, 3 to 5 years, and ≥ 5 years were 0.671, 0.714, 0.798, and 0.811, respectively. See Figure 6.

3.7. Comparison of miR-155 Expression in Serum Exosomes in Children with Epilepsy with Different Degrees of Abnormal EEG. Results showed that the more severe the abnormality of EEG in children with epilepsy, the higher the expression of miR-155 in their serum exosomes ($P < 0.05$), so the expression level of miR-155 in serum exosomes was positively correlated with the abnormality of EEG ($r = 0.911$, $P = 0.001$). See Figure 7 and Table 2.

3.8. ROC Curve Analysis of miR-155 in Serum Exosomes in the Diagnosis of Epilepsy with Different Degrees of Abnormal EEG. The AUC of miR-155 in serum exosomes to diagnose mild, moderate, and severe degrees of abnormal EEG were 0.693, 0.776, and 0.824, respectively. See Figure 8.

4. Discussion

Research data has shown that the prevalence rate of epilepsy in children is about 15 times higher than that of adults [12]. The pathological changes of epileptic seizures are highly complicated, and most of the changes are considered to be related to the abnormal activity and discharge of brain cells, glial cell proliferation, and neuronal cell death [3]. Electroencephalogram is currently the most widely used and relatively sensitive auxiliary diagnostic method [13], but its application effects are undermined by the potential failure of short-range EEG in recording epileptiform waves [14] and the huge time and economic costs of continuous video EEG monitoring [15]. On the contrary, the blood biochemical test is characterized by high specificity and simple operation compared with EEG. MiRNAs are small RNA molecules that are widely found in cells and can regulate gene expression. One recent study has found that miRNAs can extensively regulate cortical development, inflammatory response, neuron and glial cell function, apoptosis, etc., and thus play an important role in the occurrence and development of epilepsy as a key regulator [16]. MiR-155 widely exists in eukaryotes, which can inhibit the expression or translation of target genes at the post-transcriptional level and participate in a variety of physiological and pathological processes. One study has concluded that miR-155 can regulate the expression of AP-1 in astrocytes and promote its transcription, thus playing a key role in pentylenetetrazole-induced epilepsy [17]. Exosomes naturally exist in body fluids such as blood and saliva. It has been confirmed that exosomes containing miRNAs related to cell sources can pass through biological barriers to transfer functional nucleic acid molecules between cells, thereby exerting various biological functions. Nevertheless, the miRNA in the blood has poor stability and can be decomposed by ribonuclease, while the miRNA in exosomes is highly stable. It has been pointed out that exosome biomarkers have high sensitivity and specificity in the diagnosis of many diseases [18]. Thus, it is speculated that miRNA in serum exosome is expected to be a non-invasive molecular marker of epilepsy in children.

After identification, it was found that the size of exosomes in the serum of children with epilepsy extracted in this study was mainly within the range of 50-100 nm, which

was in line with the normal size range of exosomes [19], and the specific protein markers were expressed on the surface, which indicates that this study has successfully isolated exosomes from serum samples. In this study, the expression of miR-155 in children with epilepsy was found to be up-regulated, indicating that the high expression of miR-155 in serum exosomes is related to the occurrence of epilepsy and that it may be considered as an early diagnostic marker and therapeutic target, whereas the molecular mechanism of its action still requires further analysis. According to comparison results of the expression of miR-155 in serum exosomes in children with epilepsy in different courses of the disease, with the prolongation of the disease course, the expression level of miR-155 gradually elevated, indicating that the changes of miR-155 expression are related to the progression of epilepsy in children, which is of great significance for the prognosis evaluation of children. Furthermore, the more severe the abnormality of EEG in children, the higher the expression level of miR-155 in their serum exosomes, which suggests that the detection of miR-155 in serum exosomes could be a supplement to the diagnosis of epilepsy and improve the early diagnostic effect.

In summary, the expression of miR-155 in serum exosomes in children with epilepsy significantly elevated, and its level was related to the course of the disease and the degree of abnormal EEG, so it could be used as a new marker for the diagnosis and assessment of the severity of epilepsy. Yet, this study presents a limitation that mechanism of miR-155 in epilepsy has not been explored, and further analysis is scheduled in the future.

Data Availability

The datasets used during the present study are available from the corresponding author upon reasonable request.

Conflicts of Interest

The authors declare that they have no conflict of interest.

References

[1] Y. Fenghua, "Research progress on the correlation between microRNA and epilepsy," *Chinese Journal of Practical Pediatrics*, vol. 32, no. 4, pp. 314–318, 2017.

[2] Y. Ma, "The challenge of microRNA as a biomarker of epilepsy," *Current Neuropharmacology*, vol. 16, no. 1, pp. 37–42, 2017.

[3] W. S. Huang and L. Zhu, "MiR-134 expression and changes in inflammatory cytokines of rats with epileptic seizures," *European Review for Medical and Pharmacological Sciences*, vol. 22, no. 11, pp. 3479–3484, 2018.

[4] L. Grau-López, M. Jiménez, J. Ciurans et al., "Clinical predictors of adverse events during continuous video-EEG monitoring in an epilepsy unit," *Epileptic Disorders*, vol. 22, no. 4, pp. 449–454, 2020.

[5] B. Ridley, A. Marchi, J. Wirsich et al., "Brain sodium MRI in human epilepsy: Disturbances of ionic homeostasis reflect the organization of pathological regions," *NeuroImage*, vol. 157, no. 8, pp. 173–183, 2017.

[6] Y. Yu, K. Hou, T. Ji et al., "The role of exosomal microRNAs in central nervous system diseases," *Molecular and Cellular Biochemistry*, vol. 476, no. 5, pp. 2111–2124, 2021.

[7] G. H. Gong, F. M. An, Y. Wang, M. Bian, D. Wang, and C. X. Wei, "Comprehensive circular RNA profiling reveals the regulatory role of the CircRNA-0067835/miR-155 pathway in temporal lobe epilepsy," *Cellular Physiology and Biochemistry*, vol. 51, no. 3, pp. 1399–1409, 2018.

[8] Z. Zhu, S. Wang, Q. Cao, and G. Li, "CircUBQLN1 promotes proliferation but inhibits apoptosis and oxidative stress of hippocampal neurons in epilepsy via the miR-155-mediated SOX7 upregulation," *Journal of Molecular Neuroscience*, vol. 71, no. 9, pp. 1933–1943, 2021.

[9] L. G. Huang, J. Zou, and Q. C. Lu, "Silencing rno-miR-155-5p in rat temporal lobe epilepsy model reduces pathophysiological features and cell apoptosis by activating Sestrin-3," *Brain Research*, vol. 1689, no. 2, pp. 109–122, 2018.

[10] D. Jing and W. Xin, "Interpretation of guidelines for diagnosis and treatment of epilepsy," *Journal of Clinical Internal Medicine*, vol. 33, no. 2, pp. 142–144, 2016.

[11] K. J. Livak and T. D. Schmittgen, "Analysis of Relative Gene Expression Data Using Real-Time Quantitative PCR and the $2-\Delta\Delta CT$ Method," *Methods*, vol. 25, no. 4, pp. 402–408, 2001.

[12] A. Lekoubou, K. G. Bishu, and B. Ovbiagele, "The direct cost of epilepsy in children: evidence from the medical expenditure panel survey, 2003-2014," *Epilepsy & Behavior*, vol. 83, no. 6, pp. 103–107, 2018.

[13] Y. Xiafeng, C. Dezhe, Z. Xianbo et al., "Application of electroencephalogram within 48 hours of admission in the prognosis of patients with supratentorial large-area cerebral infarction and prediction of epilepsy after infarction," *Shandong Medicine*, vol. 57, no. 15, pp. 77–79, 2017.

[14] W. Junling and Y. Xiaofeng, "Research progress of simultaneous recording of EEG and functional magnetic resonance imaging in the diagnosis and treatment of epilepsy," *Journal of Clinical Neurology*, vol. 33, no. 4, pp. 74–77, 2020.

[15] Z. Wei, "The application value of video EEG in the diagnosis of epilepsy," *Bethune Medical Journal*, vol. 15, no. 5, pp. 655–655, 2017.

[16] H. Wen Fang, X. J. Zhiping, L. Zhang, and Y. Zhou, "Study on the molecular mechanism of miRNA regulation of SCN2A in epilepsy," *International Journal of Psychiatry*, vol. 45, no. 4, pp. 121–124, 2018.

[17] W. Gao, Y. Bi, L. Ding, W. Zhu, and M. Ye, "SSa ameliorates the Glu uptaking capacity of astrocytes in epilepsy via AP-1/miR-155/GLAST," *Biochemical and Biophysical Research Communications*, vol. 493, no. 3, pp. 1329–1335, 2017.

[18] L. Yi, S. Bingbing, X. Xiaosong, T. Xiaopeng, Z. Hongwen, and C. Zhiwen, "Research progress of exosomal miRNA and disease diagnosis and treatment," *Journal of International Pathology and Clinical Medicine*, vol. 38, no. 9, pp. 2003–2017, 2018.

[19] M. Tucci, A. Passarelli, F. Mannavola et al., "Serum exosomes as predictors of clinical response to ipilimumab in metastatic melanoma," *Oncoimmunology*, vol. 7, no. 2, article e1387706, 2018.

Hindawi
Disease Markers
Volume 2022, Article ID 7383745, 7 pages
https://doi.org/10.1155/2022/7383745

Research Article

A Randomized Study on the Effect of Metformin Combined with Intensive-Exercise Diet Therapy on Glucose and Lipid Metabolism and Islet Function in Patients with Renal Cell Carcinoma and Diabetes

Yang Liu,[1,2] Ling-Ling Meng,[3] Jian-Wei Li,[2] Yin-Shan Jin,[1] and Rui-Hua An[1]

[1]*Department of Urology, The First Affiliated Hospital of Harbin Medical University, No.23 You Zheng Street, Harbin 150001, Heilongjiang, China*
[2]*The Second Department of Urology, Cangzhou Central Hospital of Hebei Province, Cangzhou, Hebei, China*
[3]*The Third Department of Endocrinology, Cangzhou Central Hospital of Hebei Province, Cangzhou, Hebei, China*

Correspondence should be addressed to Rui-Hua An; anfyrw622@163.com

Received 3 March 2022; Revised 21 April 2022; Accepted 25 April 2022; Published 15 July 2022

Academic Editor: Zhaoqi Dong

Objective. To evaluate the effect of metformin combined with intensive-exercise diet therapy on glucose and lipid metabolism and islet function in diabetes patients with localized renal cell carcinoma after laparoscopic resection. *Methods*. A total of 120 renal cancer patients with diabetes mellitus treated in the oncology department of our hospital from January 2018 to December 2020 were recruited and assigned via random number table method at a ratio of 1 : 1 to receive either metformin (control group) or metformin plus intensive exercise diet therapy (study group) after laparoscopic nephrectomy. Outcome measures included glucose and lipid metabolism, pancreatic islet function, lifestyle, clinical efficacy, and adverse reactions. *Results*. After the intervention, the fasting blood glucose (FBG), 2 h postprandial blood glucose (PBG), glycosylated hemoglobin (HbA1c), triglyceride (TG), total cholesterol (TC), and low-density lipoprotein cholesterol (LDL-C) of the two groups of patients decreased significantly, and the study group had significantly lower results. After treatment, the two groups had elevated levels of high-density lipoprotein cholesterol (HDL-C), fasting serum insulin (FINS), and homeostasis model assessment of β-cell function (HOMA-β), and higher results were obtained in the study group ($P < 0.05$). After the intervention, the study group showed higher results of health promoting lifestyle profile-II (HPLP-II) and a 12-month progression-free survival rate than the control group. There were no significant differences in the incidence of adverse reactions between the two groups. *Conclusion*. Metformin combined with intensive-exercise diet therapy significantly improves the glucose and lipid metabolism and islet function of renal cancer patients with diabetes and effectively enhances the 12-month progression-free survival. Further trials are, however, required prior to clinical application.

1. Introduction

Both malignant tumors and diabetes show a rising incidence in recent years, which poses a threat to the life safety of people. Research has reported a higher incidence of tumor progression in diabetic patients than in the nondiabetic population due to their impaired immune function [1]. Hyperglycemia provides energy for the tumor cells and promotes tumor growth [2]. Additionally, glucose and lipid metabolism disorders, anti-apoptosis of insulin, and mitosis enhancement in diabetic patients further induce the development of tumors [3]. A prior study reported that patients with fasting blood glucose levels higher than 7.8 mmol/l have a 25% higher chance of dying from tumors than those with a fasting blood glucose level lower than 5.6 mmol/l [4]. The renal cancer ranks the third in urinary system tumors, and

its incidence has shown a rising tend [5]. A previous study revealed that the incidence and mortality of diabetes patients with renal cancer increased by 47% and 43% [6] versus those without diabetes. Diabetic complications such as hypertension and end-stage renal disease are associated with a high risk of renal cancer [7]. Therefore, the exploration of appropriate glucose control drugs for patients with renal cell carcinoma complicated with diabetes mellitus is of great significance.

Metformin is a widely used oral hypoglycemic agent and a first-line drug for type 2 diabetes. It activates AMP-activated protein kinase (AMPK) by activating liver kinase B1 (LKB1) to reduce blood glucose and blood insulin levels [8]. Research has demonstrated that metformin has an impact on the tumor suppressor gene liver kinase B1 (LBK1) to upregulate the expression of AMPK signal pathway and achieve the antitumor effect [9]. It has also been reported that metformin has obtained promising results in treating malignant tumors such as lung cancer, breast cancer, and kidney cancer [10]. A variety of traditional Chinese medicines have been proved effective in tumor treatment, such as Melissa officinalis L. and anthraquinone derivatives emodin [11–13]. An epidemiological study suggested that excessive intake of food, overnutrition, and lack of exercise are risk factors for impaired glucose tolerance and diabetes [14]. The importance of these approaches has been recognized with the development of therapeutic approaches and nursing concepts. The control of blood sugar and amelioration of the quality of life can be realized by the exercise diet therapy, yet its application in patients with renal carcinoma complicated with diabetes mellitus has been marginally explored. Accordingly, this study adopted metformin combined with exercise and diet therapy for patients with renal cancer and diabetes and gained desirable outcomes. The results are reported as follows.

2. Data and Methods

2.1. General Information. Totally, 120 cases of renal cell carcinoma with diabetes treated in the oncology department of our hospital from January 2018 to December 2020 were recruited and randomized into a control group ($n = 60$) and a study group ($n = 60$) using the random number table method. This study was reviewed and approved by the ethics committee of the First Affiliated Hospital of Harbin Medical University (approved no. LC 2018-11/233). The experiment was carried out in accordance with the Declaration of Helsinki, and all patients and their families provided undersigned informed consent forms.

2.2. Inclusion and Exclusion Criteria

2.2.1. Inclusion Criteria. Patients aged 18~75 years, who were diagnosed with renal cancer by postoperative pathology after laparoscopic nephrectomy, who met the diagnostic criteria for type 2 diabetes, with a tumor stage $T_1N_0M_0$ or $T_2N_0M_0$, and with unilateral renal carcinoma with good contralateral renal function were included.

2.2.2. Exclusion Criteria. Patients with a history of abdominal surgery; with serious dysfunction of the heart, liver, lung, and other organs; with complicated with hypertension or endocrine diseases; with sports contraindication, being unable to exercise as planned; and with mental and neurological dysfunctions that prevent cooperation with dietary interventions were excluded.

2.3. Intervention Methods. All patients were given conventional treatment after laparoscopic nephrectomy, and different blood glucose control schemes were adopted as follows.

2.3.1. Control Group. The control group received oral administration of 0.5 g metformin (Zhengda Tianqing Pharmaceutical Group Co., Ltd., approval no. H20031104) for blood glucose control after meals, twice daily. The dosage was adjusted according to blood sugar and urine sugar, with the maximum daily dose within 2 g. Patients received exercise diet instruction, such as total calories control, diet instruction, a daylong stream of mini meals, and daily exercises. A similar metformin regimen was introduced to the patients in the study group.

2.3.2. Study Group. The study group also received intensive exercise diet therapy: (1) diet intervention. The patients were instructed to follow an individualized diet plan based on their conditions, with carbohydrates accounting for 50% to 60% of total calories, protein about 10% to 20%, and fat about 20% to 30%. The diet was customized according to the patient's situation. (2) Exercise intervention: exercise stress electrocardiogram test combined with plasma lactate determination was used to determine the personalized target heart rate of moderate-intensity aerobic exercise. Patients were instructed by well-trained and experienced doctors to perform the exercise. A heart rate monitor was used to analyze the exercise heart rate and determine the exercise intensity to maintain the target heart rate. Patients were instructed to perform exercise 30 to 45 minutes each time, 6 times a week. Telephone follow-ups were conducted once every 2 weeks, and patients were reviewed once a month for diet and exercise instruction and intervention plan adjustment according to the patient's condition.

2.4. Outcome Measures

2.4.1. Glucose and Lipid Metabolism and Islet Function. Before the intervention and at 6 months of intervention, fasting venous blood was collected to determine the patient's glucose and lipid metabolism indices, including fasting blood-glucose (FBG) and glycosylated hemoglobin (HbA1c), 2 h postprandial blood glucose (PBG), triglyceride (TG), total cholesterol (TC), high-density lipoprotein cholesterol (HDL-C), and low density lipoprotein cholesterol (LDL-C). Before the intervention and 6 months after the intervention, fasting serum insulin (FINS) was determined by high-performance liquid chromatography, and the homeostasis model assessment of β-cell function (HOMA-β) index was calculated by the following formula: [HOMA $- \beta = 20$ FINS /(FPG $- 3.5$)].

Table 1: Comparison of the general data.

	Control group ($n = 60$)	Study group ($n = 60$)	t/χ^2	P
Age ($\bar{x} \pm s$, year-old)	59.28 ± 8.46	61.50 ± 11.25	1.220	0.225
Gender (male/female)	38/22	34/26	0.556	0.456
BMI ($\bar{x} \pm s$, kg/m^2)	28.59 ± 5.16	27.13 ± 4.92	1.576	0.118
Staging and grading			0.926	0.336
$T_1N_0M_0$	42	37		
$T_2N_0M_0$	18	23		
Tumor diameter	3.26 ± 1.06	3.11 ± 0.82	0.815	0.417
Tumor location			0.906	0.341
Left	36	41		
Right	24	19		

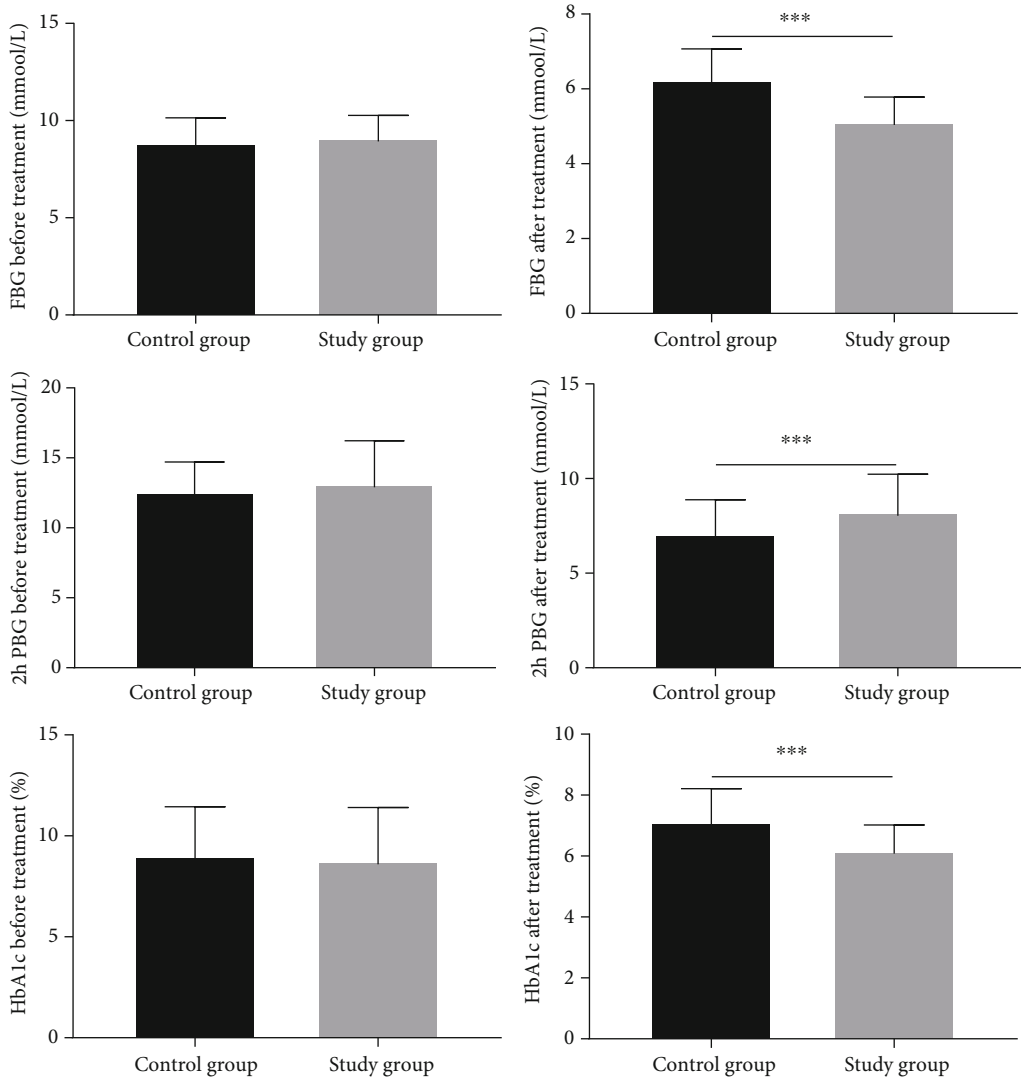

Figure 1: Comparison of the glucose metabolism levels. Note: *** indicated $P < 0.001$ compared between the two groups.

2.4.2. The Quality of Life. The health-promoting lifestyle profile-II (HPLP-II) [15] was used to assess the quality of life before and after treatment, including health education, self-realization, interpersonal support, and nutrition enhancement. There are 48 items in 6 domains of regular exercise and stress management. Each item is divided into 1 to 4 points, which represent never, occasionally, often, and always. The higher the score, the better the quality of life.

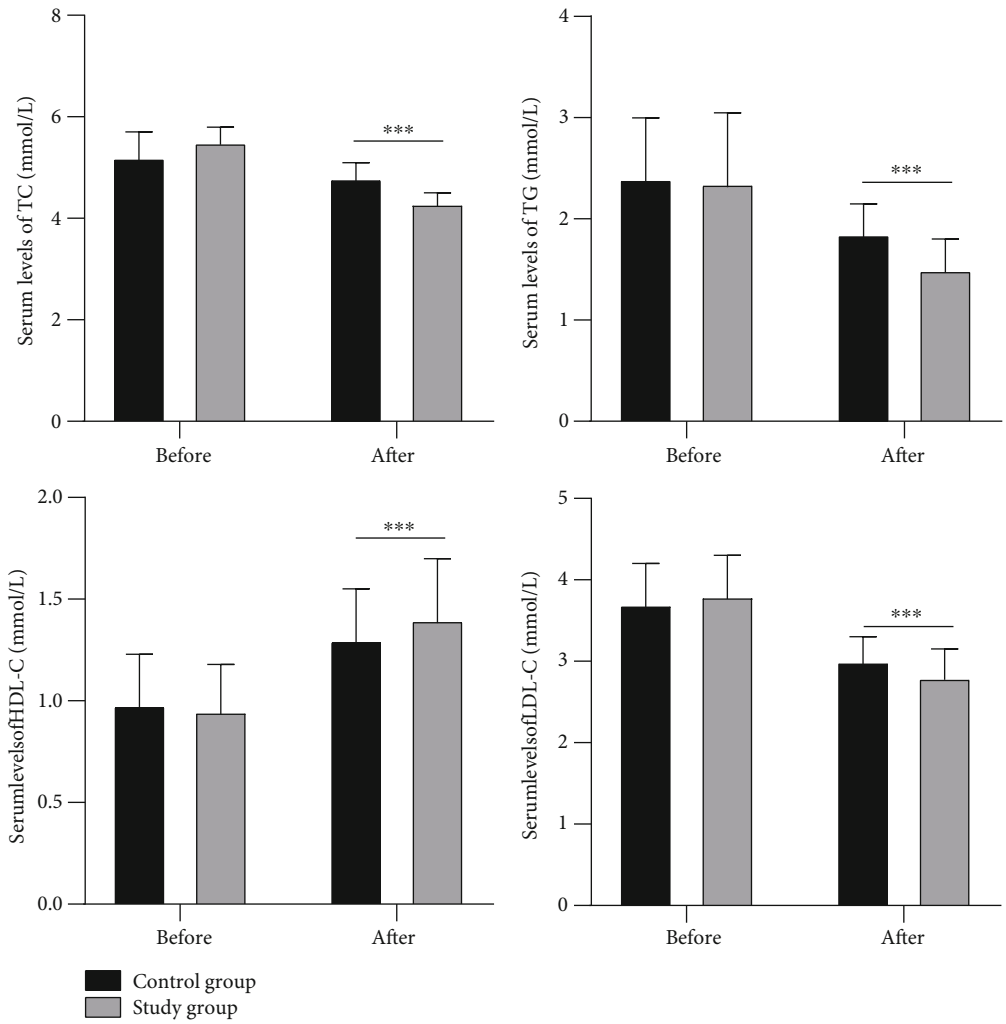

Figure 2: Comparison of the serum levels of TC, TG, HDL-C, and LDL-C. Note: *** indicated $P < 0.001$ compared between the two groups.

2.4.3. Long-Term Efficacy. All patients were followed up for 12 months after surgery, and the progression-free survival rate and overall survival rate of the patients were recorded.

2.4.4. Adverse Reactions. The postoperative adverse reactions were recorded as per the Common Adverse Reaction Event Evaluation Criteria (CTCAE) [16].

Grade 1: mild and no symptoms that require no treatment. Grade 2: moderate symptoms that require minor, local, or noninvasive treatment, with restriction in daily activities. Grade 3: severe but not immediately life-threatening symptoms or disability that require hospitalization or prolonged hospital stay with restricted daily activities. Grade 4: life-threatening symptoms that require urgent treatment. Level 5: death due to adverse events.

2.5. Statistical Analysis. SPSS 23.0 was used for data analyses, and GraphPad Prism 8.0 was used to plot the graphics in the text. In this study, measurement data are expressed as mean ± standard deviation ($\bar{x} \pm s$), paired t-test was used for intra-group comparison between different timepoints, and two-independent sample t-test was used for intergroup comparison. Enumeration data are expressed by rate and analyzed using the chi-square test. $\alpha = 0.05$ was assumed as statistical significance.

3. Results

3.1. Comparison of General Data. As shown in Table 1, the basic data of the two groups of patients, such as age, gender, BMI, tumor stage, and tumor diameter and location, were comparable (all $P > 0.05$).

3.2. Comparison of Glucose Metabolism Indicators. As shown in Figure 1, there were no significant differences in FBG, 2 h PBG, and HbA1c between the two groups of patients before the treatment (all $P > 0.05$). After the treatment, the above indices of the two groups of patients were significantly decreased, and the study group had significantly lower results (all $P < 0.05$).

3.3. Comparison of Blood Lipid Indexes. As shown in Figure 2, before the treatment, there were no significant differences in serum TC, TG, HDL-C, and LDL-C levels between the two groups of patients (all $P > 0.05$). After the treatment, TC, TG, and LDL-C of the two groups of patients

Table 2: Comparison of the pancreas islet function ($\bar{x} \pm s$).

	FINS (mU/l)			HOMA-β		
	Before	After	Δ	Before	After	Δ
Control group ($n = 60$)	8.12 ± 2.15	11.26 ± 2.86	1.24 ± 0.53	3.94 ± 1.05	5.79 ± 1.25	1.60 ± 0.63
Study group ($n = 60$)	8.06 ± 2.51	9.22 ± 1.47	0.56 ± 0.27	4.12 ± 1.18	4.72 ± 1.18	0.51 ± 0.25
t	0.141	4.917	8.855	-0.887	4.846	12.46
P	0.888	<0.001	<0.001	0.377	<0.001	<0.001

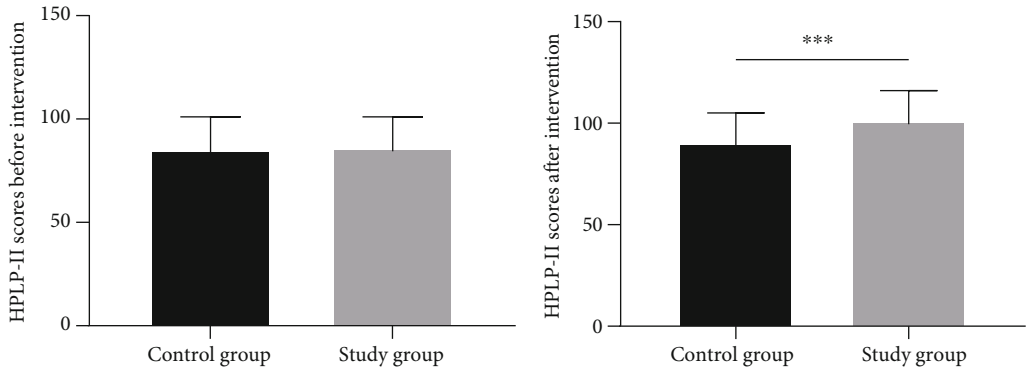

Figure 3: Comparison of the HPLP-II scores. Note: *** indicated $P < 0.001$ compared between the two groups.

decreased significantly, and the study group had lower results. The level of HDL-C was significantly increased, and the study group showed significantly higher results than the control group (all $P < 0.05$).

3.4. Comparison of Islet Function. As shown in Table 2, before the treatment, there were no statistically significant differences in FINS and HOMA-β between the two groups of patients (all $P > 0.05$). After the treatment, the above indicators of the two groups of patients were elevated, in which the study group had significantly higher results than the control group (all $P < 0.05$).

3.5. Comparison of Lifestyles. As shown in Figure 3, there were no significant differences in HPLP-II scores between the two groups of patients before the treatment ($P > 0.05$). After the treatment, the study group had higher levels of HPLP-II than the control group ($P < 0.05$).

3.6. Comparison of the Long-Term Efficacy. As shown in Table 3, 6 months after treatment, there were no significant differences in the progression-free survival rate and overall survival rate of the two groups of patients (all $P > 0.05$). 12 months after treatment, the progression-free survival rate of the study group was significantly higher than that of the control group ($P < 0.05$). The two groups presented similar overall survival rate ($P > 0.05$).

3.7. Comparison of Adverse Reactions between the Two Groups of Patients. As shown in Table 4, there were no significant differences in the incidence of all grades of adverse reactions and ≥3 grades of adverse reactions between the two groups of patients (all $P > 0.05$).

Table 3: Comparison of the long-term clinical outcome.

	6 months after intervention		12 months after intervention	
	PFS	OS	PFS	OS
Control group ($n = 60$)	51	56	40	51
Study group ($n = 60$)	53	58	51	55
χ^2	0.289	0.175	5.502	1.294
P	0.591	0.675	0.019	0.255

Table 4: Comparison of all grade AEs grade ≥ 3 AEs.

	All grades	Grade ≥ 3
Control group ($n = 60$)	22	12
Study group ($n = 60$)	16	9
χ^2	1.386	0.520
P	0.239	0.471

4. Discussion

In recent years, the incidence of kidney cancer has been increasing year by year. Despite the rapid development of early detection in recent years, the survival of renal cancer patients remains unsatisfactory [17]. Research has shown that diabetes is a risk factor for the poor prognosis of kidney cancer, which necessitates timely treatment and regular monitoring of the blood glucose level of patients with kidney cancer [18]. Diabetes is a chronic metabolic disease with abnormally elevated blood sugar levels as the main manifestation, among which noninsulin-dependent diabetes (type 2 diabetes) accounts for more than 90%. The main mechanism is insulin resistance. The body's ability to absorb and utilize

glucose decreases, leading to elevated blood sugar levels. Disorders of glucose metabolism may trigger various pulmonary dysfunctions and involve multiple organs and tissues such as cardiovascular system, cerebrovascular system, eyes, liver, and kidney, which seriously compromises the quality of life of patients [19]. Research has shown that hyperinsulinemia and elevated insulin-like growth factor-1 in patients with type 2 diabetes are closely related to malignant tumors. About 8-18% of new malignant tumors cases are comorbid with diabetes [20]. Surgery is the treatment of choice for localized renal cancer, with a 5-year disease-free survival rate of about 90% and a recurrence and metastasis rate of 20-30% [21].

Metformin effectively lowers the blood sugar and lipids of patients and is considered the optimal choice for the treatment of type 2 diabetes. It has been found that metformin could lower the risk of prostate cancer, breast cancer, liver cancer, and other tumors in diabetic patients [22]. Lifestyle changes, high-sugar, high-fat diet intake, and long-term nutritional imbalance are the main causes of impaired glucose tolerance and insulin resistance [23]. Therefore, in addition to drug treatment, exercise diet intervention contributes to the control of blood sugar levels. In the present study, the glucose and lipid metabolism and insulin function of the two groups of patients were significantly improved after the treatment. For patients with kidney cancer and diabetes, the role of dietary exercise intervention is essential in blood sugar control and disease recovery. In the present study, metformin combined with intensive-exercise diet therapy was adopted for the first time and obtained good clinical effect. However, this study still has the following shortcomings. First, the effect of intensive-exercise diet therapy in this study is easily affected by cognitive ability and compliance, which complicates the evaluation of the implementation of dietary exercise programs. Secondly, intensified exercise diet intervention requires community family care support, along with high medical costs, which may prevent its extensive application. In the future, the new treatment concepts need to be popularized, and multicenter, large-scale studies need to be conducted to obtain more reliable data for clinical references.

5. Conclusion

The use of metformin combined with intensive-exercise diet therapy significantly improves the glucose and lipid metabolism and islet function of renal cancer patients with diabetes and effectively increases the 12-month progression-free survival rate. Further trails are, however, required prior to clinical application.

Data Availability

The datasets used during the present study are available from the corresponding author upon reasonable request.

Conflicts of Interest

The authors declare that they have no conflict of interest.

References

[1] G. Shlomai, B. Neel, D. LeRoith, and E. J. Gallagher, "Type 2 diabetes mellitus and cancer: the role of pharmacotherapy," *Journal of Clinical Oncology*, vol. 34, no. 35, pp. 4261–4269, 2016.

[2] S. C. Chang and W. V. Yang, "Hyperglycemia, tumorigenesis, and chronic inflammation," *Critical Reviews in Oncology/Hematology*, vol. 108, pp. 146–153, 2016.

[3] J. M. K. de Filette, J. J. Pen, L. Decoster et al., "Immune checkpoint inhibitors and type 1 diabetes mellitus: a case report and systematic review," *European Journal of Endocrinology*, vol. 181, no. 3, pp. 363–374, 2019.

[4] J. Luo, Y. J. Chen, and L. J. Chang, "Fasting blood glucose level and prognosis in non-small cell lung cancer (NSCLC) patients," *Lung Cancer*, vol. 76, no. 2, pp. 242–247, 2012.

[5] X. D. Song, Y. N. Tian, H. Li, B. Liu, A. L. Zhang, and Y. Hong, "Research progress on advanced renal cell carcinoma," *The Journal of International Medical Research*, vol. 48, no. 6, 2020.

[6] J. Wojciechowska, W. Krajewski, M. Bolanowski, T. Kręcicki, and T. Zatoński, "Diabetes and cancer: a review of current knowledge," *Experimental and Clinical Endocrinology & Diabetes*, vol. 124, no. 5, pp. 263–275, 2016.

[7] S. I. Hallan and B. E. Vikse, "Relationship between chronic kidney disease prevalence and end-stage renal disease risk," *Current Opinion in Nephrology and Hypertension*, vol. 17, no. 3, pp. 286–291, 2008.

[8] Z. Lv and Y. Guo, "Metformin and its benefits for various diseases," *Frontiers in Endocrinology*, vol. 11, p. 191, 2020.

[9] C. F. Chiang, T. T. Chao, Y. F. Su et al., "Metformin-treated cancer cells modulate macrophage polarization through AMPK-NF-κB signaling," *Oncotarget*, vol. 8, no. 13, pp. 20706–20718, 2017.

[10] M. Podhorecka, B. Ibanez, and A. Dmoszyńska, "Metformin - its potential anti-cancer and anti-aging effects," *Advances in Hygiene & Experimental Medicine/Postepy Higieny i Medycyny Doswiadczalnej*, vol. 71, pp. 170–175, 2017.

[11] N. Nayebi, A. Esteghamati, A. Meysamie et al., "The effects of a Melissa officinalis L. based product on metabolic parameters in patients with type 2 diabetes mellitus: a randomized double-blinded controlled clinical trial," *Journal of Complementary and Integrative Medicine*, vol. 16, no. 3, 2019.

[12] M. Martorell, N. Castro, M. Victoriano et al., "An update of anthraquinone derivatives emodin, diacerein, and catenarin in diabetes," *Evidence-based Complementary and Alternative Medicine*, vol. 2021, Article ID 3313419, 13 pages, 2021.

[13] M. Seyed Hashemi, N. Namiranian, H. Tavahen et al., "Efficacy of pomegranate seed powder on glucose and lipid metabolism in patients with type 2 diabetes: a prospective randomized double-blind placebo-controlled clinical trial," *Complementary Medicine Research*, vol. 28, no. 3, pp. 226–233, 2021.

[14] H. Ghavami, M. Radfar, S. Soheily, S. A. Shamsi, and H. R. Khalkhali, "Effect of lifestyle interventions on diabetic peripheral neuropathy in patients with type 2 diabetes, result of a randomized clinical trial," *A□rı*, vol. 30, no. 4, pp. 165–170, 2018.

[15] P. Sousa, P. Gaspar, D. C. Vaz, S. Gonzaga, and M. A. Dixe, "Measuring health-promoting behaviors: cross-cultural validation of the health-promoting lifestyle profile-II," *International Journal of Nursing Knowledge*, vol. 26, no. 2, pp. 54–61, 2015.

[16] A. Trotti, A. D. Colevas, A. Setser et al., "CTCAE v3.0: development of a comprehensive grading system for the adverse effects of cancer treatment," *Seminars in Radiation Oncology*, vol. 13, no. 3, pp. 176–181, 2003.

[17] U. Capitanio, K. Bensalah, A. Bex et al., "Epidemiology of renal cell carcinoma," *European Urology*, vol. 75, no. 1, pp. 74–84, 2019.

[18] S. W. Lai, C. L. Lin, and K. F. Liao, "Association between diabetes mellitus and kidney cancer," *Postgraduate Medical Journal*, vol. 96, no. 1132, pp. 104-105, 2020.

[19] K. Kaul, J. M. Tarr, S. I. Ahmad, E. M. Kohner, and R. Chibber, "Introduction to diabetes mellitus," *Advances in Experimental Medicine and Biology*, vol. 771, pp. 1–11, 2012.

[20] H. Takahashi, T. Takayama, K. Hosono et al., "Correlation of the plasma level of insulin-like growth factor-1 with the number of aberrant crypt foci in male individuals," *Molecular Medicine Reports*, vol. 2, no. 3, pp. 339–343, 2009.

[21] B. Ljungberg, K. Bensalah, S. Canfield et al., "EAU guidelines on renal cell carcinoma: 2014 update," *European Urology*, vol. 67, no. 5, pp. 913–924, 2015.

[22] Y. Fujita and N. Inagaki, "Metformin: new preparations and nonglycemic benefits," *Current Diabetes Reports*, vol. 17, no. 1, p. 5, 2017.

[23] M. Z. Allende-Vigo, "Diabetes mellitus prevention," *American Journal of Therapeutics*, vol. 22, no. 1, pp. 68–72, 2015.

Hindawi
Disease Markers
Volume 2022, Article ID 1417104, 7 pages
https://doi.org/10.1155/2022/1417104

Research Article

Application of Endoscopic Ultrasound Combined with Multislice Spiral CT in Diagnosis and Treatment of Patients with Gastrointestinal Eminence Lesions

Jie Xiong,[1] **Jie Jiang**,[2] **Ying Chen**,[1] **Ye Chen**,[1] **Chenyi Xie**,[3] **and Shuchang Xu**[1]

[1]*Department of Gastroenterology and Hepatology, Tongji Hospital, Tongji University School of Medicine, Shanghai 200065, China*
[2]*National Center for Liver Cancer, Second Military Medical University, Shanghai 200438, China*
[3]*Center of Minimally Invasive Treatment for Tumor, Department of Medical Ultrasound, Shanghai Tenth People's Hospital, Tongji University School of Medicine, Shanghai 200072, China*

Correspondence should be addressed to Chenyi Xie; xie_chenyi@126.com and Shuchang Xu; xschang@163.com

Received 24 February 2022; Revised 21 April 2022; Accepted 17 May 2022; Published 29 June 2022

Academic Editor: Zhaoqi Dong

Objective. To evaluate the application of endoscopic ultrasound (EUS) combined with multislice spiral CT (MSCT) in the diagnosis and treatment of patients with gastric eminence lesions. *Methods*. A total of 160 patients with gastric eminence lesions enrolled in our hospital from June 2018 to June 2021 were included and received EUS and MSCT. The results of the two examinations and the postoperative pathological results were compared. *Results*. The common pathological types of gastric eminence lesions include polyps and stromal tumors, with the most common sites of lesions in the gastric antrum, followed by the fundus of the stomach and the gastric body. Gastric eminence lesions mostly originate from the mucosal layer and muscularis mucosa, accounting for 83.13% of the total. With pathological results as the gold standard, the detection rate of MSCT was 90.63%, and that of EUS was 78.13%. With the joint diagnosis as a reference, the receiver operating curve (ROC) revealed a higher diagnostic efficiency of MSCT and EUS. *Conclusion*. The accuracy of MSCT in the diagnosis of gastric eminence lesions is significantly higher than that of EUS, both of which can offer useful guidance for the choice of endoscopic treatment methods. The combination of MSCT and EUS examination before endoscopic gastroscopy may provide a better treatment efficacy on gastric protruding lesions with high safety.

1. Introduction

Gastric eminence lesions are mostly caused by the compression of extramural organs or lesions and the large folds of the gastric mucosa [1–3]. Gastric eminence lesions are caused by the degeneration and necrosis of the vagus nerve and sympathetic nerve, resulting in abnormal secretion of various intestinal hormones and changes in the intestinal environment [4]. Currently, the diagnostic efficiency of the property and origin of the lesion by electronic gastroscopy is poor, so endoscopy and multislice spiral CT (MSCT) are frequently used in clinical practice for preoperative diagnosis to provide a guidance for subsequent treatment [5–8]. Endoscopic ultrasound (EUS), with ultrasound and endoscopy, can clearly show the digestive tract wall, adjacent organs, and tissues, which helps clarify the cause of the lesion by preliminarily determining the property of the lesion according to its echo characteristics [9–12]. MSCT can clearly show the depth, location, and size of tumor infiltration and can effectively determine the presence of lymph node metastasis in the lung, mediastinum, and distal organ tissues. EUS allows direct visualization of mucosal lesions in the gastrointestinal tract, while real-time scanning can be performed using endoscopic ultrasound, thus further improving diagnostic accuracy. To further enhance the treatment efficacy of gastric

eminence lesions this study explored the application value of EUS combined with MSCT in the diagnosis of patients with gastric eminence lesions to provide a clinical reference of endoscopic treatment.

2. Research Design

2.1. Patient Screening and Grouping. A total of 160 patients with gastric eminence lesions enrolled in Tongji Hospital, Tongji University School of Medicine, from June 2018 to June 2021 were included for retrospective analysis. This study has been approved by the ethics committee of Tongji Hospital, Tongji University School of Medicine, No. 197TJ29-1.

2.2. Inclusion Criteria. Patients who were diagnosed with gastric eminence lesions after receiving electronic gastroscopy in our hospital and received endoscopic treatment after further determination of the range and property of the lesions by EUS and MSCT, with complete clinical data, and who were fully informed of the purpose and process of the study and provided written informed consent were included.

2.3. Exclusion Criteria. Patients with progressive gastric cancer; with external pressure lesions; with other serious organic diseases, coagulation dysfunction, or malignant tumors; and with cognitive impairment, communication impairment, or physical impairment were excluded.

2.4. Methods. EUS examination: the examination was carried out using an ultrasound host (model: Fuji SU-8000) + EUS (model: Fuji EG-530UT), equipped with 12, 15, and 20 MHz ultrasound probes. Small superficial lesions were inspected with the 12 MHz ultrasound microprobe. The water filling method and the water bag technique were used, and the frequency and scanning method of the ultrasound probe was switched according to the size and location of the lesion [13–16].

MSCT examination: the patients fasted for 8 hours, drank 600-1000 ml of water 20 minutes before the examination, and received 20 mg of amidoamine (Fujian Sanai Pharmaceutical Co., Ltd., Approval No. H35020158) through intramuscular injection. With the patients in a supine position according to the conditions of the gastric lesions, a plain CT scan was performed, ranging from the right side of the diaphragm to the duodenum, with a voltage of 120 KV, a current of 250-300 mA, a thickness of 5 mm, a pitch of 1.25, and reconstruction thickness of 0.625 mm [17–20]. Then, contrast CT was performed after the injection of the iopromide (Schering Pharmaceutical Co., Ltd., Approval No. H10970166) using a high-pressure syringe, with an injection speed of 3.5 ml/s. Arterial phase was scanned 30 s after injection covering the esophagus, abdomen, and whole stomach, and venous phase was scanned 60 s after the injection to observe the tissue damage adjacent to the lesion and the liver and distant metastasis.

The imaging examination results of all patients were diagnosed by two radiologists and sonographers.

Endoscopic treatment was performed for some eminence lesions, including high-frequency electrocoagulation resection, mucosal resection, mucosal dissection-tumorectomy, mucosal dissection-tumor excision plus titanium clip closure, and puncture sclerotherapy; some submucosal tumors were surgically removed, and pathological examination was performed. Mucosal dissection-tumor tumorectomy uses a double-port therapeutic endoscope. A snare is placed through one port to cover the mucosal tissue on the tumor surface, and high-frequency electrical resection of the surface mucosa is performed, or a needle knife is used to cut the mucosal tissue on the surface of the tumor to expose the submucosal tumor; then, a biopsy forceps is used through another hole to clamp the tumor and lift it up, and a snare is used to cover the tumor at the bottom of the tumor, to perform high-frequency electrical resection.

2.5. Postoperative Follow-Up. The patients received reexamination by gastroscopy at 3, 6, and 12 months after surgery to obtain the patient recovery data. Biopsy was performed again to determine the occurrence of local recurrence if necessary.

2.6. Statistical Analyses. The data obtained in this study were analyzed using SPSS20.0 software, and GraphPad Prism 7 (GraphPad Software, San Diego, USA) was used to plot the graphics. The counting data are expressed as $n(\%)$ and analyzed using the chi-square test. The measurement data are expressed as mean ± SD and analyzed using the t-test. The specificity and sensitivity of receiver operating curve (ROC) and the area under the curve (AUC) were calculated. Differences were considered statistically significant at $P < 0.05$. Sensitivity = number of true positives/(number of true positives + number of false negatives) ∗ 100%; specificity = number of true negatives/(number of true negatives + number of false positives) ∗ 100%. The sensitivity and specificity of this study are for the detection of gastric eminence lesions, with no subdivision of the disease.

3. Results

3.1. The Distribution of Gastric Eminence Lesions. The distribution of the lesions of 160 patients was analyzed. The diameter of gastric eminence lesions was about 1.47 ± 0.95 cm. The common pathological types of gastric eminence lesions include polyps and stromal tumors, with the most common sites of lesions in the gastric antrum, followed by the fundus of the stomach and the gastric body. The pathological types of the gastric antrum were mostly polyps, of the fundus lesions were mostly stromal tumors, of the gastric body lesions were mainly polyps on the greater curvature side, and of the gastric angle were chiefly malignant (Table 1).

3.2. Histological Characteristics of Gastric Eminence Lesions. Gastric eminence lesions mostly originate from the mucosal layer and muscularis mucosa, accounting for 83.13% of the total (Table 2).

3.3. Diagnosis Results of Pathology, EUS, and MSCT. With pathological results as the gold standard, the detection rate

Table 1: The distribution of different pathological types of gastric eminence lesions.

	Polyp	Stromal tumor	Malignant lesions	Lipoma	Adenoma	Papilloma	Hemangioma	Cyst	Schwannoma	Lymphangiomyoma	Total
Cardia	11	0	0	0	0	2	0	0	0	0	15
Fundus of stomach	4	35	0	0	0	0	0	1	0	0	40
Greater curvature of the stomach	5	3	3	0	0	0	0	0	1	0	12
Lesser curvature of the stomach	2	3	0	0	0	0	1	0	0	0	6
Gastric anterior wall	3	2	0	0	1	0	0	0	0	1	7
Gastric posterior wall	3	2	0	1	0	0	0	0	0	0	6
Gastric angle	0	0	3	0	0	0	0	0	0	0	3
Greater curvature of gastric antrum	14	0	6	1	1	0	0	0	0	0	22
Lesser curvature of gastric antrum	13	0	0	0	0	0	0	0	0	0	13
Anterior wall of gastric antrum	13	1	1	2	0	0	0	0	0	0	17
Posterior wall of gastric antrum	11	0	4	0	2	0	0	0	0	0	17
Pylorus	2	0	0	0	0	0	0	0	0	0	2
Total	81	48	17	4	4	2	1	1	1	1	160

Table 2: Origin level of different pathological types of gastric eminence lesions.

Type of lesion	Mucosal layer	Muscularis mucosa	Submucosa	Muscularis propria	Unclear origin	Total
Polyp	77	1	1	1	2	81
Stromal tumor	0	42	4	2	0	48
Malignant lesions	0	9	7	1	0	17
Lipoma	0	0	4	0	0	4
Adenoma	0	3	1	0	0	4
Papilloma	0	1	1	0	0	2
Hemangioma	0	0	0	0	0	1
Cyst	0	0	1	0	0	1
Schwannoma	0	0	1	0	0	1
Lymphangiomyoma	0	0	0	1	0	1
Total	77	56	20	5	2	160

of MSCT was 90.63%, and that of EUS was 78.13% ($X^2 = 9.4815$, $P = 0.005$). The preoperative MSCT examination did not provide a clear diagnosis result for 15 patients, with gastric antrum being the most common lesion (40%) and muscularis mucosa being the most common level of lesion causes (46.67%). The preoperative EUS examination did not provide a clear diagnosis result for 35 patients, with gastric antrum being the most common lesion (40%), muscularis mucosa being the most common level of lesion causes (45.71%), and stromal tumor (25.71%) being the most frequent type of lesions (Tables 3–5).

3.4. ROC Curve Evaluates the Diagnostic Efficacy of EUS and MSCT. With the joint diagnosis as a reference, the ROC curve was formulated to compare the diagnostic efficiency: combined detection > MSCT > EUS ($P < 0.05$). The AUC of MSCT was 0.855 (0.850, 0.900), with a sensitivity of 0.806 and specificity of 0.807; the AUC of EUS was 0.871 (0.860, 0.963), with a sensitivity of 0.845 and specificity of 0.811; and the AUC of the combined assay was 0.900 (0.955, 0.999), with a sensitivity of 0.916 and specificity 0.914 (Figure 1).

3.5. Treatment Results. Among the 160 patients, 83 patients (77 cases with polyps, 4 cases with stromal tumors, 1 case with malignant lesions, and 1 case with papilloma) underwent high-frequency electrocoagulation resection, and 6 patients (2 cases with polyps, 1 case with stromal tumors, 1 case with adenoma, 1 case with papilloma, and 1 case with cysts) underwent high-frequency electrocoagulation resection, with good healing of the wound 6 months after treatment and no local recurrence after 6-24 months of follow-up. Of 69 patients (2 cases with polyps, 42 cases with stromal tumors, 15 cases with malignant lesions, 4 cases with lipoma, 3 cases with adenoma, 1 case with hemangioma, 1 case with schwannoma, and 1 case with lymphangioma) who received mucosal dissection-tumorectomy, 3 cases experienced intraoperative bleeding, and 2 cases had delayed postoperative bleeding, for which hemostasis was performed successfully. Due to the large tumor body and the risk of perforation, 2 patients (1 case with stromal tumors and 1 case with malignant lesions) were transferred to surgical treatment, in which the tumors were further determined as gastric fundus stromal tumors, with a propensity for malignancy. The 2 patients were lost at postoperative follow-up (see Table 6 for details).

4. Discussion

In the diagnosis of gastric eminence lesions, EUS presents the shape and size of the lesion through endoscopy and clearly shows the structure of the stomach wall, from the mucosal layer to the muscularis mucosa, the submucosal layer, the muscularis propria, and the serosal layer, with hyperecho, hypoecho, hyperecho, hypoecho, and hyperecho signals, respectively. It yields high accuracy in determining the size of the lesion and the origin and range of the lesion tissue [21–24].

Table 3: Diagnosis results of pathology, EUS, and MSCT.

Type of lesion	Pathological results	MSCT	EUS	MSCT and EUS
Polyp	81	72	70	81
Stromal tumor	48	44	36	48
Malignant lesions	17	14	10	17
Lipoma	4	5	4	4
Adenoma	4	5	2	4
Papilloma	2	2	1	2
Hemangioma	1	1	1	1
Cyst	1	2	1	1
Schwannoma	1	0	0	0
Lymphangiomyoma	1	0	0	0
Total	160	145	125	158

With pathological results as the gold standard, the detection rate of EUS was 78.13%. 35 patients had unclear EUS results, with gastric antrum being the most common lesion (40%), muscularis mucosa being the most common level of lesion causes (45.71%), and stromal tumor (25.71%) being the most frequent type of lesion, indicating a high rate of missed diagnosis of the stromal tumors, which is consistent with the research results by Ikoma et al. [25]. MSCT can realize multidirectional and multiangle observation of the lesion by using technologies such as MPR, which clearly presents the tumor size, location, shape, growth pattern, boundary, enhancement characteristics, ulcer, and calcification degree and shows the relationship between the disease and surrounding organs and lymph node metastasis, especially for stromal tumors. In the present study, the detection rate of MSCT was 90.63%, which was significantly higher than that of 78.13% for EUS.

The common pathological types of gastric eminence lesions tumor include polyps and stromal tumors, with the most common sites of lesions in the gastric antrum, followed by the fundus of the stomach and the gastric body. Gastric eminence lesions mostly originate from the mucosal layer and muscularis mucosa, accounting for 83.13% of the total. With the joint diagnosis as a reference, the ROC curve revealed a higher diagnostic efficiency of MSCT versus EUS. Clinically, misdiagnosis is frequently seen in stromal tumors as hypoechoic and well-defined masses in EUS. Stromal tumors mostly occur in the fundus of the stomach, which originate in the muscle layer. The signs of MSCT for mesenchymal tumors are intracavernous growth with clear borders and uniform enhancement on enhancement scans when the tumor is small in size and irregular in shape with blurred borders and inhomogeneous enhancement on enhancement scans when the tumor is large in size. In terms of misdiagnosis in the present study, EUS mostly involved stromal tumors, while MSCT had a high diagnostic yield for stromal tumors, suggesting that MSCT plays a certain auxiliary role in distinguishing stromal tumors. The ROC revealed that in the diagnosis of gastric eminence lesions, the performance of a single ultrasound image is undesirable, while the

Table 4: The pathological condition of undiagnosed patients by MSCT.

Origin level	n	Lesion site	Type of lesion
Muscularis mucosa	7	Antrum (3 cases) Fundus of stomach (3 cases) Stomach body (1 case)	3 cases of polyps 3 cases of stromal tumor 1 case of stromal tumor
Submucosa	4	Antrum (3 cases) Stomach body (1 case)	3 cases of polyps 1 case of gastric mucosa-associated lymphoma
Muscularis propria	3	Stomach body (2 cases) Antrum (1 case)	2 cases of lymphangiomas 1 case of polyps
Unclear origin	1	Antrum (1 case)	1 case of polyps

Table 5: The pathological condition of undiagnosed patients by EUS.

Origin level	n	Lesion site	Type of lesion
Muscularis mucosa	16	Fundus of stomach (8 cases) Antrum (8cases)	8 cases of stromal tumors 8 cases of malignant lesions
Submucosa	12	Antrum (7 cases) Fundus of stomach (4 cases) Stomach body (1 case)	7 cases of lipoma 4 cases of stromal tumors 1 case of schwannoma
Muscularis propria	5	Stomach body (4 cases)	2 cases of polyp, 1 case of stromal tumors, 2 cases of lymphangioma
Unclear origin	2	Cardia	2 cases of polyps

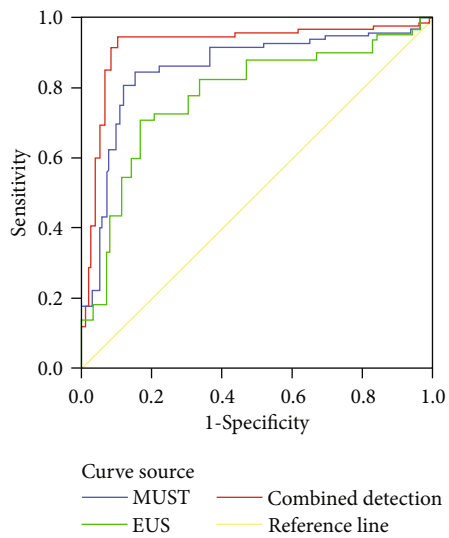

Figure 1: ROC curve.

Table 6: Treatment methods for different pathological types of lesions.

Lesion	n	Endoscopic minimally invasive treatment	
		High-frequency electrocoagulation resection	Mucosal dissection-tumorectomy
Polyp	81	79	2
Stromal tumor	48	5	43
Malignant lesions	17	1	16
Lipoma	4	0	4
Adenoma	4	1	3
Papilloma	2	2	0
Hemangioma	1	0	1
Cyst	1	1	0
Schwannoma	1	0	1
Lymphangioma	1	0	1
Total	160	89	71

combination of EUS and MSCT is more effective. Furthermore, the combination of clinical manifestations and pathological characteristics of the patients can prominently enhance the accuracy of the diagnosis of lesions.

Among the 160 patients, 83 underwent high-frequency electrosurgery, and 6 underwent nylon thread ligation, with good healing of the wound 6 months after treatment and no local recurrence after 6-24 months of follow-up. Of 69 patients who received mucosal dissection-tumorectomy, 3 cases experienced intraoperative bleeding and 2 cases had delayed postoperative bleeding, for which hemostasis was performed successfully; 2 cases were transferred to surgical treatment. In this study, no cases of perforation were found, which may be attributed to the operation skills or the small sample size of this study, suggesting that mucosal dissection-tumorectomy is safe in the treatment of gastric eminence lesions and can enhance the treatment effect. The microultrasound of ultrasound endoscopy cannot penetrate the intrinsic muscle layer of the tumor and

identify the level of lesion, and some patients have peritoneal fibrosis and inflammatory reaction, which may further thicken the esophageal wall and adversely affect the accuracy of staging diagnosis. MSCT is a cross-sectional scan, which cannot effectively distinguish esophageal cancer from the normal esophageal wall and is less effective in identifying soft tissues.

Chinese medicine has accumulated a wealth of experience in the treatment of gastric eminence lesions, which can effectively relieve symptoms and enhance clinical efficacy. Gastric eminence lesions can be treated with catgut embedding acupuncture. The catgut used is an allogeneic protein, and when the allogeneic protein is buried in the acupuncture point, the body's rejection reaction to the allogeneic protein continues to stimulate the acupuncture point, thereby achieving the purpose of treating diseases, with the advantages of economic applicability, simple operation, short duration, and high efficiency.

5. Conclusion

The accuracy of MSCT in the diagnosis of gastric eminence lesions is significantly higher than that of EUS, both of which can offer useful guidance for the choice of endoscopic treatment methods. The combination of MSCT and EUS examination before endoscopic gastroscopy may provide a better treatment efficacy on gastric protruding lesions with high safety. The limitation of this study is that less follow-up study was performed in postoperative patients; therefore, this study only serves as a guide for diagnosis, and further research in the treatment is required in future studies.

Data Availability

The datasets used and/or analyzed during the current study are available from the corresponding author on reasonable request.

Conflicts of Interest

The authors declare that they have no conflicts of interest.

Authors' Contributions

Jie Xiong and Jie Jiang contributed equally to this work.

Acknowledgments

This project was supported by Clinical Research Project of Tongji Hospital of Tongji University (Grant No. ITJ(QN)2101).

References

[1] O. Goto, H. Kambe, K. Niimi et al., "Discrepancy in diagnosis of gastric submucosal tumor among esophagogastroduodenoscopy, CT, and endoscopic ultrasonography: a retrospective analysis of 93 consecutive cases," *Abdominal Imaging*, vol. 37, no. 6, pp. 1074–1078, 2012.

[2] R. S. Okten, S. Kacar, F. Kucukay, N. Sasmaz, and T. Cumhur, "Gastric subepithelial masses: evaluation of multidetector CT (multiplanar reconstruction and virtual gastroscopy) versus endoscopic ultrasonography," *Abdominal Imaging*, vol. 37, no. 4, pp. 519–530, 2012.

[3] S. W. Hwang, D. H. Lee, S. H. Lee et al., "Preoperative staging of gastric cancer by endoscopic ultrasonography and multidetector-row computed tomography," *Journal of Gastroenterology and Hepatology*, vol. 25, no. 3, pp. 512–518, 2010.

[4] L. Jianfeng, "Changes of gastrointestinal dynamics in diabetic gastrointestinal lesions," *Foreign Medicine: Endocrinology*, vol. 15, no. 4, p. 4, 1995.

[5] G. Tao, L. Xing-Hua, Y. Ai-Ming et al., "Enhanced magnifying endoscopy for differential diagnosis of superficial gastric lesions identified with white-light endoscopy," *Gastric cancer: official journal of the International Gastric Cancer Association and the Japanese Gastric Cancer Association*, vol. 17, no. 1, pp. 122–129, 2014.

[6] Q. Chen, H. H. Cheng, S. Deng et al., "Diagnosis of superficial gastric lesions together with six gastric lymphoma cases via probe-based confocal laser endomicroscopy: a retrospective observational study," *Gastroenterology Research and Practice*, vol. 2018, Article ID 5073182, 8 pages, 2018.

[7] I. Hirata, Y. Nakagawa, M. Ohkubo, N. Yahagi, and K. Yao, "Usefulness of magnifying narrow-band imaging endoscopy for the diagnosis of gastric and colorectal lesions," *Digestion*, vol. 85, no. 2, pp. 74–79, 2012.

[8] M. M. Zhang, N. Zhong, X. Gu et al., "In vivo real-time diagnosis of endoscopic ultrasound-guided needle-based confocal laser endomicroscopy in gastric subepithelial lesions," *Journal of Gastroenterology and Hepatology*, vol. 35, no. 3, pp. 446–452, 2020.

[9] S. Maki, K. Yao, T. Nagahama et al., "Magnifying endoscopy with narrow-band imaging is useful in the differential diagnosis between low-grade adenoma and early cancer of superficial elevated gastric lesions," *Gastric Cancer: official journal of the International Gastric Cancer Association and the Japanese Gastric Cancer Association*, vol. 16, no. 2, pp. 140–146, 2013.

[10] H. Omura, N. Yoshida, T. Hayashi et al., "Interobserver agreement in detection of "white globe appearance" and the ability of educational lectures to improve the diagnosis of gastric lesions," *Gastric Cancer: official journal of the International Gastric Cancer Association and the Japanese Gastric Cancer Association*, vol. 20, no. 4, pp. 620–628, 2017.

[11] H. Nakanishi, H. Doyama, H. Ishikawa et al., "Evaluation of an e-learning system for diagnosis of gastric lesions using magnifying narrow-band imaging: a multicenter randomized controlled study," *Endoscopy: Journal for Clinical Use Biopsy and Technique*, vol. 49, no. 10, pp. 957–967, 2017.

[12] D. Dias-Silva, P. Pimentel-Nunes, J. Magalhães et al., "The learning curve for narrow-band imaging in the diagnosis of precancerous gastric lesions by using web-based video," *Gastrointestinal Endoscopy*, vol. 79, no. 6, pp. 910–920, 2014.

[13] S. Shah, C. Nakata, S. Itzkowitz, and A. D. Polydorides, "Prevalence of precursor lesions at diagnosis of gastric cancer in a multi-ethnic cohort at an academic center in NYC," *The American Journal of Gastroenterology*, vol. 111, Suppl.1, pp. S486–S487, 2016.

[14] E. Raddaoui, M. A. Almadi, A. M. Aljebreen, and F. Alsaif, "Cytologic diagnosis of gastric submucosal lesions by endoscopic ultrasound-guided fine-needle aspiration: a single

center experience in Saudi Arabia," *Indian Journal of Pathology and Microbiology*, vol. 58, no. 4, p. 448, 2015.

[15] J. Arend, D. Kuester, A. Roessner, H. Lippert, and F. Meyer, "Gastric high-risk gist and retroperitoneal liposarcoma – a challenging combination of two mesenchymal tumor lesions with regard to diagnosis and treatment. Polish," *Journal of Surgery*, vol. 85, no. 5, pp. 284–288, 2013.

[16] X. Liu, X. Ren, X. Ma, X. Sun, Y. Wu, and Z. Li, "Analysis of clinical features and endoscopic ultrasonography in the diagnosis of gastric submucosal tumors," *Journal of Medical Imaging and Health Informatics*, vol. 10, no. 7, pp. 1570–1574, 2020.

[17] S. F. Wang, Y. S. Yang, L. X. Wei et al., "Diagnosis of gastric intraepithelial neoplasia by narrow-band imaging and confocal laser endomicroscopy," *World Journal of Gastroenterology*, vol. 18, no. 34, pp. 4771–4780, 2012.

[18] S. A. Tuzcu, Z. Pekkolay, F. Kılınç, and A. K. Tuzcu, "^{68}Ga-DOTATATE PET/CT can be an alternative imaging method in insulinoma patients," *Journal of Nuclear Medicine Technology*, vol. 45, no. 3, pp. 198–200, 2017.

[19] P. R. Pfau and A. Chak, "Endoscopic ultrasonography," *Endoscopy: Journal for Clinical Use Biopsy and Technique*, vol. 34, no. 1, pp. 21–28, 2002.

[20] S. W. Seo, S. J. Hong, J. P. Han et al., "Accuracy of a scoring system for the differential diagnosis of common gastric subepithelial tumors based on endoscopic ultrasonography," *Journal of Digestive Diseases*, vol. 14, no. 12, pp. 647–653, 2013.

[21] L. Sang, Z. Zhou, and C. Wu, "Diagnosis of pulmonary embolism by treatment based on analysis of multi-slice spiral CT pulmonary artery images," *Journal of Medical Imaging and Health Informatics*, vol. 9, no. 5, pp. 867–872, 2019.

[22] M. Wang, C. Wei, Z. Shi, and J. Zhu, "Study on the diagnosis of small hepatocellular carcinoma caused by hepatitis B cirrhosis via multi-slice spiral CT and MRI," *Oncology Letters*, vol. 15, no. 1, pp. 503–508, 2017.

[23] J. Liu, H. Fan, and G. P. Qiu, "Vascular permeability determined using multi-slice spiral CT perfusion can predict response to chemoradiotherapy in patients with advanced cervical squamous cell carcinoma," *International Journal of Clinical Pharmacology and Therapeutics*, vol. 55, no. 7, pp. 619–626, 2017.

[24] I. Komaei, G. Currò, F. Mento et al., "Gastric histopathologic findings in south Italian morbidly obese patients undergoing laparoscopic sleeve gastrectomy: is histopathologic examination of all resected gastric specimens necessary?," *Obesity Surgery*, vol. 30, no. 4, pp. 1339–1346, 2020.

[25] N. Ikoma, J. H. Lee, M. S. Bhutani et al., "Preoperative accuracy of gastric cancer staging in patient selection for preoperative therapy: race may affect accuracy of endoscopic ultrasonography," *Gastrointestinal Oncology*, vol. 8, no. 6, pp. 1009–1017, 2017.

Hindawi
Disease Markers
Volume 2022, Article ID 7251450, 12 pages
https://doi.org/10.1155/2022/7251450

Research Article

Pharmacological Mechanism of Ganlu Powder in the Treatment of NASH Based on Network Pharmacology and Molecular Docking

Rui Gao,[1] Xiaobo Zhang,[1] Zhen Zhou,[2] Jiayi Sun,[3] Xuehua Tang,[4] Jialiang Li,[1] Xin Zhou,[1] and Tao Shen[1]

[1]*School of Basic Medicine, Chengdu University of Traditional Chinese Medicine, Chengdu, China*
[2]*Menzies Institute for Medical Research, University of Tasmania, Hobart, Tasmania, Australia*
[3]*Innovative Institute of Chinese Medicine and Pharmacy, Chengdu University of Traditional Chinese Medicine, Chengdu, China*
[4]*Academic Department, Chengdu Hemoyunyin Medical Laboratory Co., Ltd, China*

Correspondence should be addressed to Xin Zhou; zhouxin@cdutcm.edu.cn and Tao Shen; shentaotcm@aliyun.com

Received 28 January 2022; Revised 18 April 2022; Accepted 19 April 2022; Published 29 June 2022

Academic Editor: Zhaoqi Dong

Nonalcoholic steatohepatitis (NASH), a progression of nonalcoholic fatty liver disease (NAFLD), is a clinical syndrome characterized by liver steatosis, inflammation, and hepatocellular damage. Ganlu powder (GLP) is a classic traditional Chinese medicine prescription that has shown favorable treatment effects on NASH. However, the underlying therapeutic mechanisms are still poorly understood. This study is aimed at exploring the potential mechanism of GLP in the treatment of NASH via network pharmacology and molecular docking. PubMed and CNKI databases were used to identify the components of GLP. Swiss and STITCH databases were employed to obtain corresponding drug targets. NASH targets were adopted from the Therapeutic Target Database (TTD), DisGeNET, DrugBank, GeneCards, and MalaCards databases. Cytoscape software was utilized to construct "drug-ingredient-target-disease" networks and the protein-protein interaction (PPI) network of GLP in NASH. AKT1 was identified as the key target. The GO functional enrichment analysis revealed that GLP might treat NASH by modulating the inflammatory response and regulating phosphatidylinositol 3-kinase signaling. The KEGG analysis showed that GLP might treat NASH by regulating the tumor necrosis factor (TNF) signal pathway by affecting the role of AKT1. According to the network pharmacology results, a virtual docking of active compounds with AKT1 was carried out, and the results indicated that the 7 components, berberine, epiberberine, jatrorrhizine, coptisine, palmatine, evodiamine, and rutecarpine, can bind stably with AKT1 and have higher binding energy than AKT1 inhibitors. The overall study findings suggest that GLP may treat NASH by regulating AKT1.

1. Introduction

Nonalcoholic fatty liver disease (NAFLD) is one of the most common chronic liver diseases in the world [1]. It is a chronic metabolic disease caused by genetic and environmental factors and a hepatic presentation of metabolic syndrome. According to statistics, NAFLD is affecting approximately 20%-30% of the world population, which has become an increasingly serious public health problem [2, 3]. Nonalcoholic steatohepatitis (NASH), a severe form of NAFLD, is characterized by hepatic steatosis, inflammation, and hepatocyte injury. NASH can progress to cirrhosis and liver cancer and lead to poor clinical consequences [4, 5]. It was estimated that around 20% of NAFLD patients developed NASH in 10-15 years [6], and this rate is expected to rise to 27% in 2030, with NASH-associated all-cause mortality rising to up to 40% [7, 8]. Changes in lifestyle, such as regular exercise and developing healthy dietary habits, are primary strategies for managing NASH [9]. Notwithstanding this, it is often challenging for NASH patients to maintain a healthy lifestyle as it is often difficult for them to change their established living habits

and the health benefits from lifestyle modifications often take a long time to emerge [10]. More importantly, lifestyle changes are frequently insufficient to improve patients' conditions, and pharmacological treatment is therefore needed.

Currently, there are no drugs approved for the treatment of NASH by the U.S. Food and Drug Administration (FDA). NASH is not unifactorial but a common multifactorial condition; thus, the effect of treatment for a single target is suboptimal [11]. Traditional Chinese medicine (TCM), which has been used in China for more than 2000 years, possesses the advantages of multicomponent, multitarget, and multipathway and thus has a great potential for improving hepatic steatosis and reducing inflammation [12, 13]. Ganlu powder (GLP), also known as Ganlu san or Coptis-Evodia herb couple, was a classic TCM formula initially recorded in *Sheng ji zong lu* and composed of two herbs, namely *Coptidis Rhizoma* and *Evodiae Fructus*, which have been mainly used for the treatment of gastrointestinal diseases including diarrhea, dysentery, and other inflammatory diseases. Pharmacological studies showed that GLP can lower blood lipids, improve inflammation, and regulate cholesterol metabolism. Zhang et al. [14] found that GLP is also effective for treating NASH. It can effectively improve the symptoms of NAFLD patients, reduce liver inflammation, improve liver steatosis, regulate glucose and lipid metabolism, and lower body weight and waist circumference of obese individuals, without raising apparent adverse reactions.

As with many other TCMs, the underlying mechanisms of GLP in treating NASH remain poorly understood. The nature of TCM makes it difficult for traditional methods to fully understand how these herbs with multiple active ingredients exert their synergistic biological effects through multiple targets and pathways in human beings [15, 16]. Network pharmacology is an emerging discipline proposed by professor Hopkins in 2007 [17]. This approach breaks the previous concept of a single ingredient/single target/disease and can thus be used as a useful tool in the studies of the "multicomponent, multitarget, and multibiological regulation function synergy" model of Chinese herbs [18, 19]. In this study, we studied the potential targets of GLP for NASH using network pharmacology and used the maximum degree value to identify the core targets in the gene network that indicate the role of the nodes in network pharmacology. DAVID database was used for enrichment analysis to determine the Gene Ontology and KEGG pathways that involved GLP. The results of network pharmacology were validated by virtual molecular docking, a computational chemistry technique based on the known ligand and receptor structure, used to simulate the binding interactions of bioactive components with core targets [20]. These analyses were able to provide valuable insight in understanding the molecular mechanisms of GLP in the treatment of NASH.

2. Materials and Methods

2.1. Bioactive Compounds and Target Fishing. Two databases, PubMed (https://pubmed.ncbi.nlm.nih.gov/) and CNKI (https://www.cnki.net/), were utilized for bioactive compounds screening. The chemical structure of the components was drawn by ChemDraw 15.0. Swiss ADME was used to predict the drug-like properties and gastrointestinal absorption of the obtained ingredients of GLP, and the ingredients that did not meet the criteria were excluded. In order to comprehensively obtain the targets of bioactive components of GLP, the collected ingredients were imported into STITCH and Swiss Target Prediction for target prediction. During STITCH retrieval, the species was set to "homo sapiens"; during the Swiss Target Prediction retrieval, the SMILES number of the corresponding components was uploaded for target fishing. Finally, the targets downloaded from the two databases were merged and deduplicated, after which the targets of GLP were obtained.

Table 1: The ADME properties of 7 components of GLP.

Compound	GI absorption	Drug likeness				
		Lipinski	Ghose	Veber	Egan	Muegge
Berberine	High	Yes	Yes	Yes	Yes	Yes
Epiberberine	High	Yes	Yes	Yes	Yes	Yes
Jatrorrhizine	High	Yes	Yes	Yes	Yes	Yes
Coptisine	High	Yes	Yes	Yes	Yes	Yes
Palmatine	High	Yes	Yes	Yes	Yes	Yes
Evodiamine	High	Yes	Yes	Yes	Yes	Yes
Rutecarpine	High	Yes	Yes	Yes	Yes	Yes

Abbreviations: ADME: absorption, distribution, metabolism, and excretion (ADME); GI: gastrointestinal; GLP: Ganlu powder.

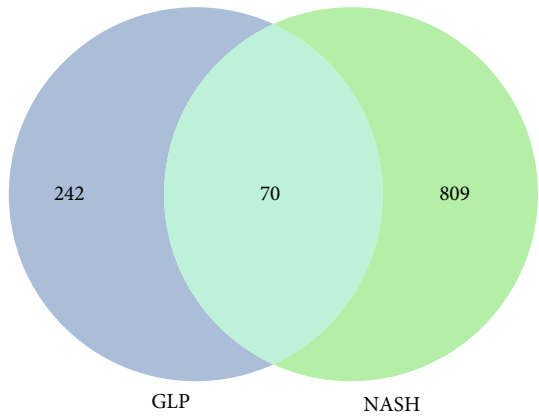

Figure 1: The 70 overlapped genes between NASH and GLP.

2.2. NASH Targets Acquisition. Five databases including Therapeutic Target Database, DisGeNET, DrugBank, GeneCards, and MalaCards were used for NASH targets screening; "nonalcoholic steatohepatitis" was used as the keyword for retrieval [21]. The obtained data from different databases were combined for analysis.

2.3. Drug-Compounds-Target-Disease Network Construction. The obtained targets of 7 compounds of GLP and NASH-related targets were merged together and delineated with the Venn diagram plotted by an online tool (http://www.bioinformatics.com.cn/plot_basic_proportional_2_or_3_venn_diagram_028). The intersection of GLP and NASH-related

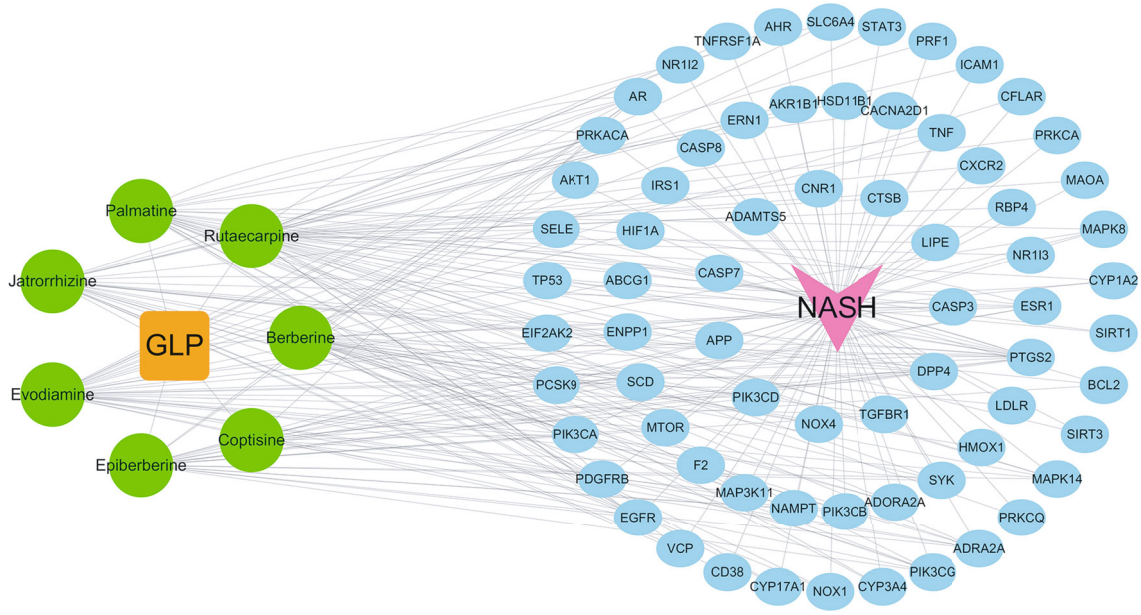

Figure 2: Drug-ingredient-target-disease network of GLP. The orange node represents drug, the green nodes represent ingredients, the blue nodes represent targets, and the red node represents disease (NASH).

targets was derived. The "drug-component-target-disease" interaction was established through Cytoscape3.7.1. In the network, nodes represent the compounds of GLP and the targets of NASH, edges represent the relationship between each node, and the number of edges is defined as "degree."

2.4. Protein-Protein Interaction (PPI) Network Construction. The STITCH database is a platform for exploring known and predicted interactions between compounds and proteins [22]. Seventy common targets of the drug and the disease were introduced into the STRING database, the organism was set as "homo sapiens," and the confidence level was set to "high confidence (confidence score > 0.7)." The PPI interaction network was downloaded, and the degree of the nodes was analyzed using the R language (version 3.6.3). The topological properties of the network were calculated with the Cytoscape Network Analyzer plugin in Cytoscape 3.7.2.

2.5. GO and KEGG Enrichment Analyses. Gene Ontology (GO) is a widely used bioinformatic method for annotating genes, typically including biological processes (BP), molecular function (CC), and molecular functions (MF). KEGG is an important technique for analyses of functions between different genes. To better interpret the functions of those overlapped targets, GO and KEGG enrichment analyses were conducted using the Database for Annotation, Visualization, and Integrated Discovery (DAVID), and the top 20 terms with p value < 0.01 were plotted by bar graphs or bubble map [23].

2.6. Molecular Docking. Based on the results of network pharmacology, the three-dimensional (3D) structure of the core target was downloaded from the Protein Data Bank (PDB) database (http://www.rcsb.org/). Meanwhile, we searched the inhibitors of core targets from DrugBank and PubMed. The protein structure was processed using PyMOL (version 1.7.2.1) to remove excess ligands, including removing water molecules and excess Mg^{2+}, Cu^{2+}, and $SO4^{2-}$. ChemDraw was then used to optimize small ligand molecules and save the files in a mol2 format. The standardized proteins and ligands were imported into AutoDockTools (version 1.5.6) and converted into a PDBQT format. Using the AutoDock Vina software (version 1.1.2), we ran a program for molecular docking using docking parameters; the complex conformation with the minimum binding energy and highest binding affinity for each molecule was selected for further analysis [24]. Generally, the binding energy < 0 kcal/mol indicates that the ligand can bind to the receptor protein, while the binding energy ≤ −5.0 kcal/mol reveals that the ligand and the protein have a good binding ability [25]. Finally, the docking result was visualized by PyMOL and Discovery Studio.

3. Results

3.1. Bioactive Ingredients and Corresponding Targets. By searching PubMed and CNKI, we obtained the ingredients of the two herbs of GLP. After the screening of absorption, distribution, metabolism, and excretion (ADME) properties, we retained 7 main ingredients (5 in *Coptidis Rhizoma* and 2 in *Evodiae Fructus*) including berberine, palmatine, jatrorrhizine, coptisine, epiberberine, evodiamine, and rutecarpine. The ADME properties of each component are shown in Table 1. Although the literature reports that there are some other components in Coptis and Evodia, they were not considered in this analysis due to their relatively low content. Afterwards, we obtained 32 targets from STITCH, 637 targets from SwissTargetPrediction, and 312 targets were retained after merging and deduplication.

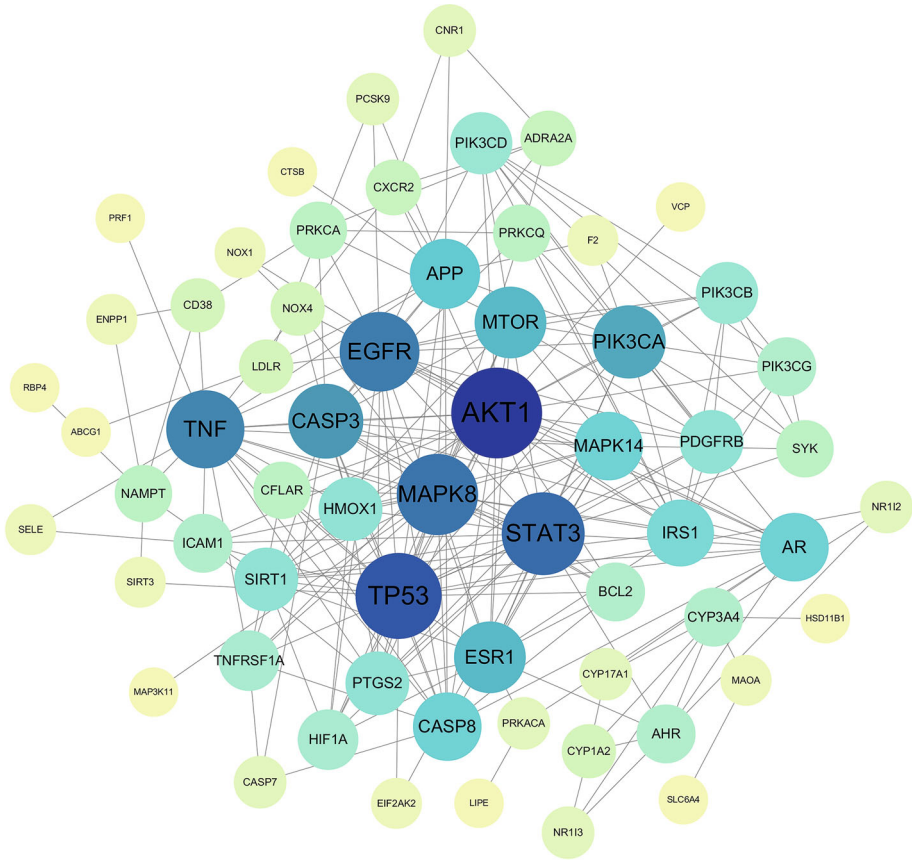

Figure 3: The protein-protein interaction (PPI) network.

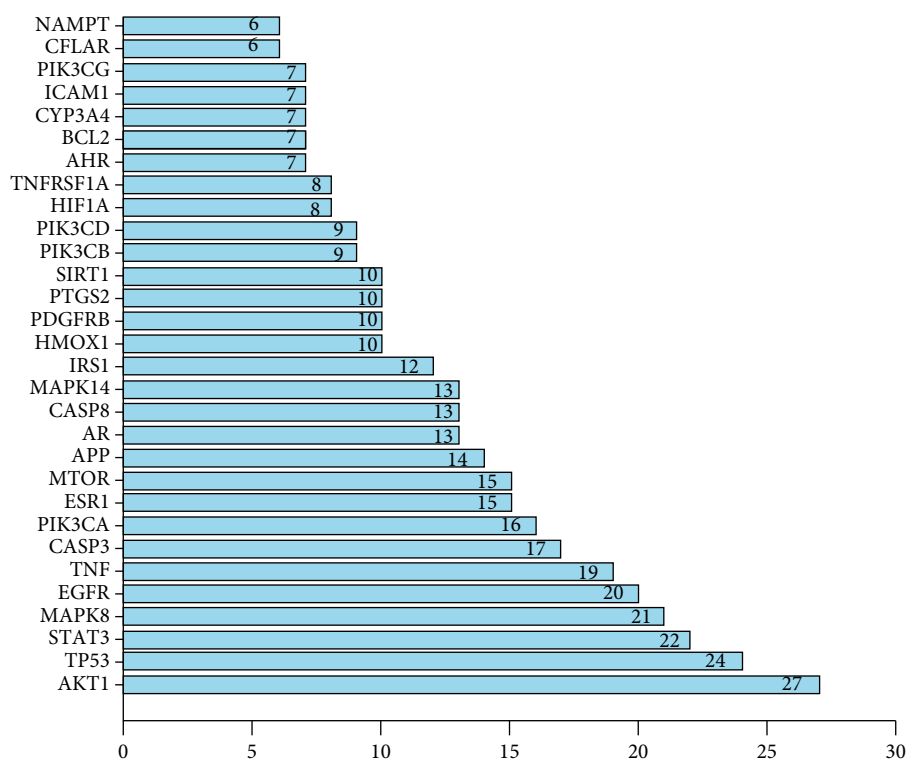

Figure 4: Ranking chart of the degree value of the PPI network. The x-axis represents the number of neighboring proteins of the target protein. The y-axis represents the target proteins.

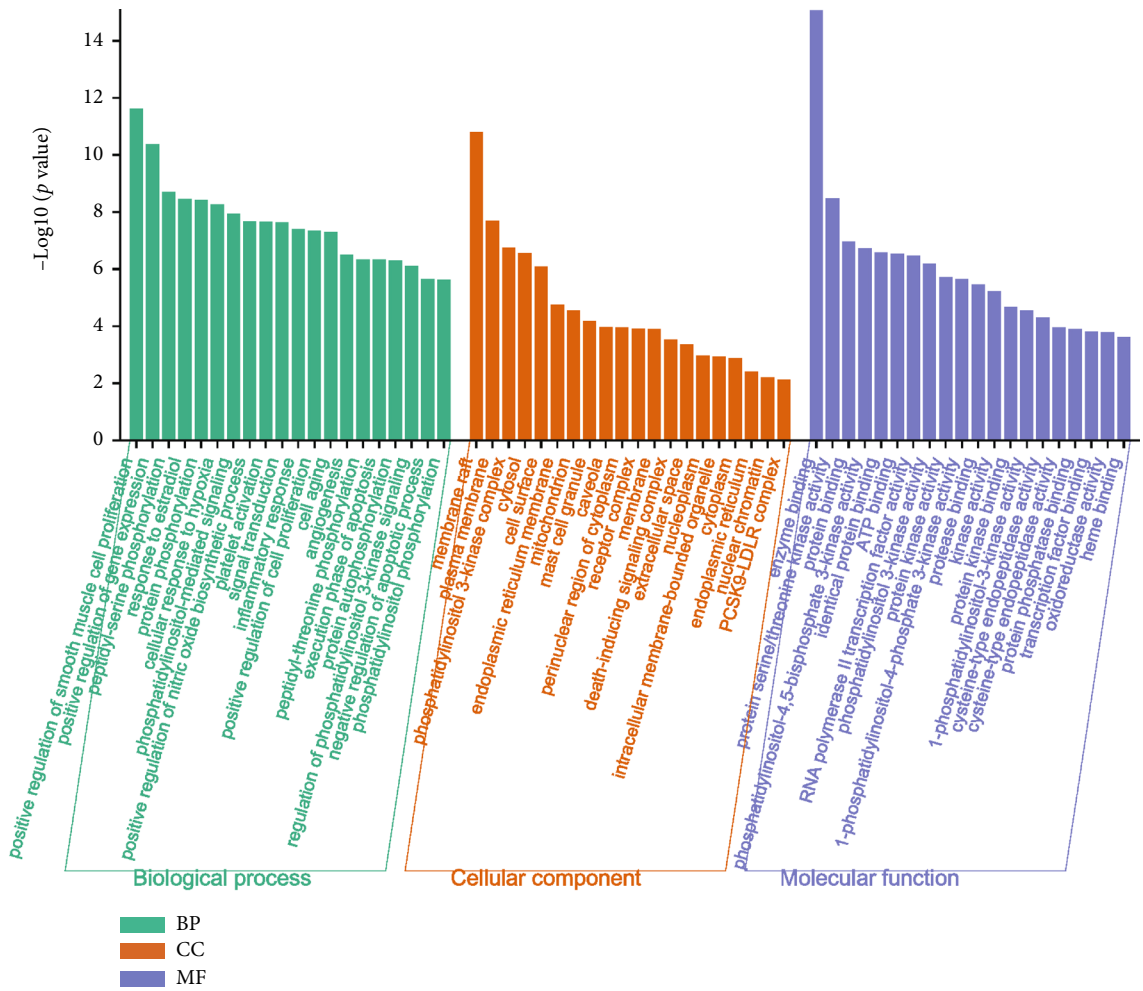

Figure 5: The Gene Ontology (GO) analysis of the 70 overlapping gene symbols associated with NASH. The x-axis represents the categories in the GO of the target genes, while the y-axis represents the p value (-log10) in the GO of the target genes.

3.2. NASH Targets Screening. "Nonalcoholic steatohepatitis" was set as a search term and subjected to these five databases: TTD, DisGeNET, DrugBank, GeneCards, and MalaCards, from which 0, 434, 0, 652, and 48 targets were obtained, respectively. 879 NASH-related targets were identified after mergence and duplicate removal.

3.3. GLP-Compounds-Targets-NASH Network. After obtaining the GPL targets and the NASH targets, the Venn diagram was generated by mapping the intersection (Figure 1). The "GLP-compounds-targets-NASH" network was built with Cytoscape. In the complex network (Figure 2), the relationship between the identified active components and 35 targets is characterized by a total of 48 nodes and 44 edges.

3.4. PPI Network Analysis. Importing the 70 junction targets of GLP and NASH into the STRING database, we constructed a PPI network with 62 nodes and 235 edges (Figure 3). In the figure, the top 8 targets are AKT1, TP53, STAT3, MAPK8, EGFR, TNF, CASP3, and PIK3CA, among which AKT1 has the highest degree (Figure 4), indicating that it may be a key target of GLP in the treatment of NASH.

3.5. GO and KEGG Enrichment Analyses. The DAVID web was used to perform GO and KEGG enrichment analyses of 70 intersected targets, the top 20 items with p-values < 0.01 were visualized. In the BP category (Figure 5), the intersected genes were significantly enriched to protein phosphorylation, signal transduction, inflammatory response, protein autophosphorylation, regulation of phosphatidylinositol 3-kinase signaling, etc. The KEGG enrichment analysis revealed that the 70 intersected genes were highly related to NAFLD, HIF-1 signaling pathway, and insulin resistance, especially the TNF signaling pathway (Figures 6 and 7). Interestingly, AKT1 was involved in various processes.

3.6. Molecular Docking Evaluation. To further confirm whether the bioactive compounds of GLP can directly interact with the core target, the binding energy and dominant mode between the compounds with the key target were evaluated through molecular docking. The results show that all 7

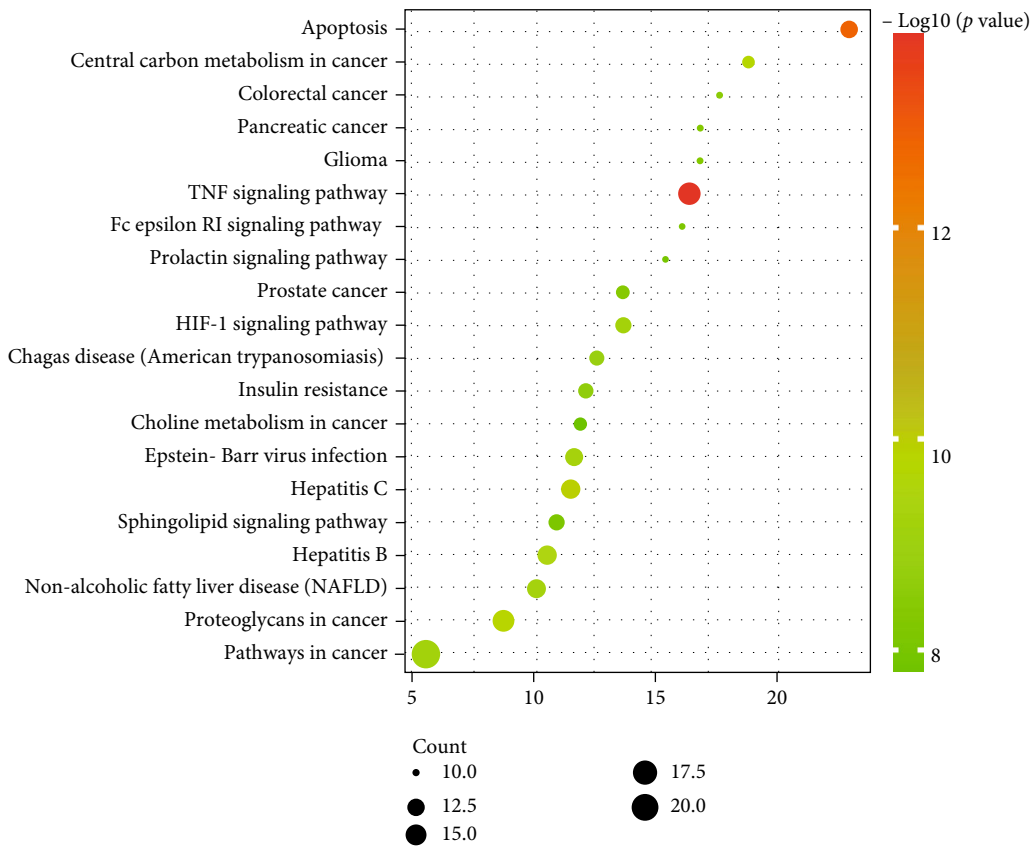

Figure 6: The KEGG pathway enrichment result of the 70 overlapping genes. The x-axis represents the fold enrichment of each pathway, the y-axis represents the main pathways (p value < 0.01), the size of the bubble indicates target counts in each pathway, and the color of the bubble indicates the p value.

components of GLP could be docked to AKT1 (PDB id: 3OCB), and they are located in the active pocket of the inhibitor resveratrol, which fits well in the docking position (Figure 8). The drug molecule and the protein receptor form various intermolecular forces, such as hydrogen bonds, C-H bonds, π-Alkyl, and other interaction forces (Figure 9). In addition, the 7 components have higher binding energy than the AKT1 inhibitor, resveratrol (Table 2).

4. Discussion

NASH is a metabolic stress liver injury strongly correlated with insulin resistance and genetic susceptibility, which can progress to liver cirrhosis and hepatocellular carcinoma. In addition, patients with NASH are at an increased risk of cardiovascular disease (CVD). The benefit of maintaining a healthy lifestyle is self-evident. The vast majority of patients, however, have difficulties in adhering to these healthy living habits, and the effect of behavioral changes on body weight and blood glucose management is often suboptimal. Due to the multiple and complex pathogenesis of NASH, there are no approved drugs for treatment. With the advancement of clinical medical research, the advantages of Chinese herbal medicine in the treatment of NASH have attracted substantial attention. As a historically old formula of TCM, the therapeutic effects of GLP on NASH attract our attention. In this study, 7 main active ingredients and 312 potential therapeutic targets of GLP, together with 879 NASH potential targets and 70 common targets, were screened using network analysis. As the complex network described, AKT1 is considered the core target of GLP in NASH treatment.

AKT1 is a member of the AKT kinase family, which regulates glycolipid metabolism, proliferation, and cell survival through a series of downstream substrates. Usually, the activation of AKT requires two key phosphorylation processes. Phosphoinositide-dependent protein kinase 1 (PDK1) initially phosphorylates AKT on threonine 308 (T308), an active phosphorylation site of AKT, leading to the activation process; mTORC2 then phosphorylates AKT on serine 473 to fully activate AKT [26].

In lipid metabolism, activated AKT induces the activation of mTOR, which subsequently recruits CRTC2 as a complex to promote SREBP-1 activity and adipogenesis. Yu et al. [27] found that transplanting the AKT plasmid into the mice through the tail intravenous injection can accelerate liver steatosis and inflammatory damage. AKT regulates fat synthesis factor SREPB-1 through the PI3K-AKT-mTOR signaling pathway, which increases the fatty acid synthesis and lipid content of liver cells and accelerates the NAFLD progression. In NASH animal models, it was also found that the PI3K-AKT signal was activated, leading to an aggravated

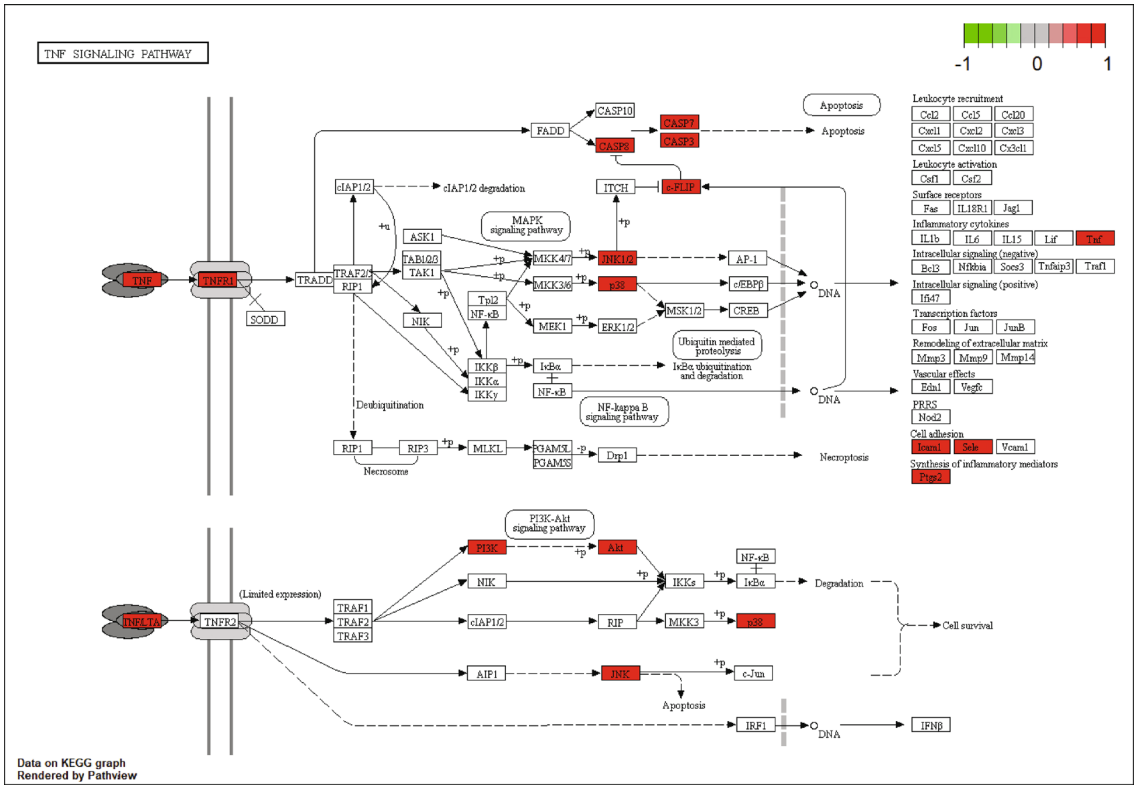

Figure 7: The KEGG pathway map of GLP treats NASH. The red nodes within the predicted signaling pathway represent the targets relevant with the corresponding pathway.

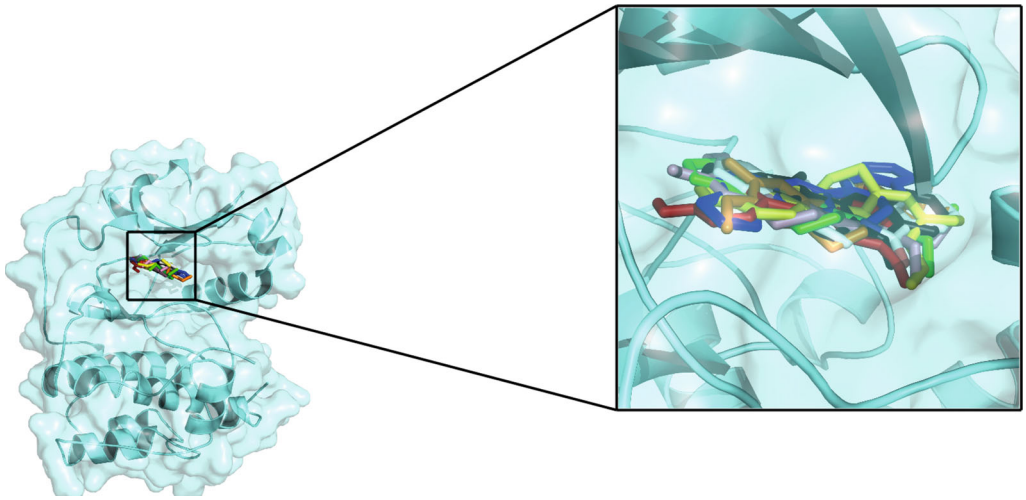

Figure 8: 3D docking conformation of 7 ingredients and resveratrol with AKT1. In the figure, the red stick represents resveratrol, the green stick represents berberine, the yellow stick represents epiberberine, the pink stick represents jatrorrhizine, the blue stick represents coptisine, the orange-yellow stick represents palmatine, the white stick represents evodiamine, and the black stick represents rutecarpine.

liver damage. Inhibiting this pathway can markedly attenuate hepatocyte injury, inhibit hepatic stellate cell activation, and delay hepatic fibrosis progression [28, 29]. Nong and Chen [30] found that the Tiaogan Quzhi formula could improve the liver steatosis, inflammatory infiltration, and cell necrosis of NAFLD rats through the PI3K/AKT-mTOR signaling pathway. Similarly, Fan et al. found that another TCM formula, Tangganjian decoction, improves the hepatic glucose and lipid metabolism in rats with type 2 diabetes mellitus (T2DM) and NAFLD via activating the IRS/PI3K/AKT signaling pathway [31]. In general, AKT1 plays a crucial role in glucose and lipid metabolism and thus is a

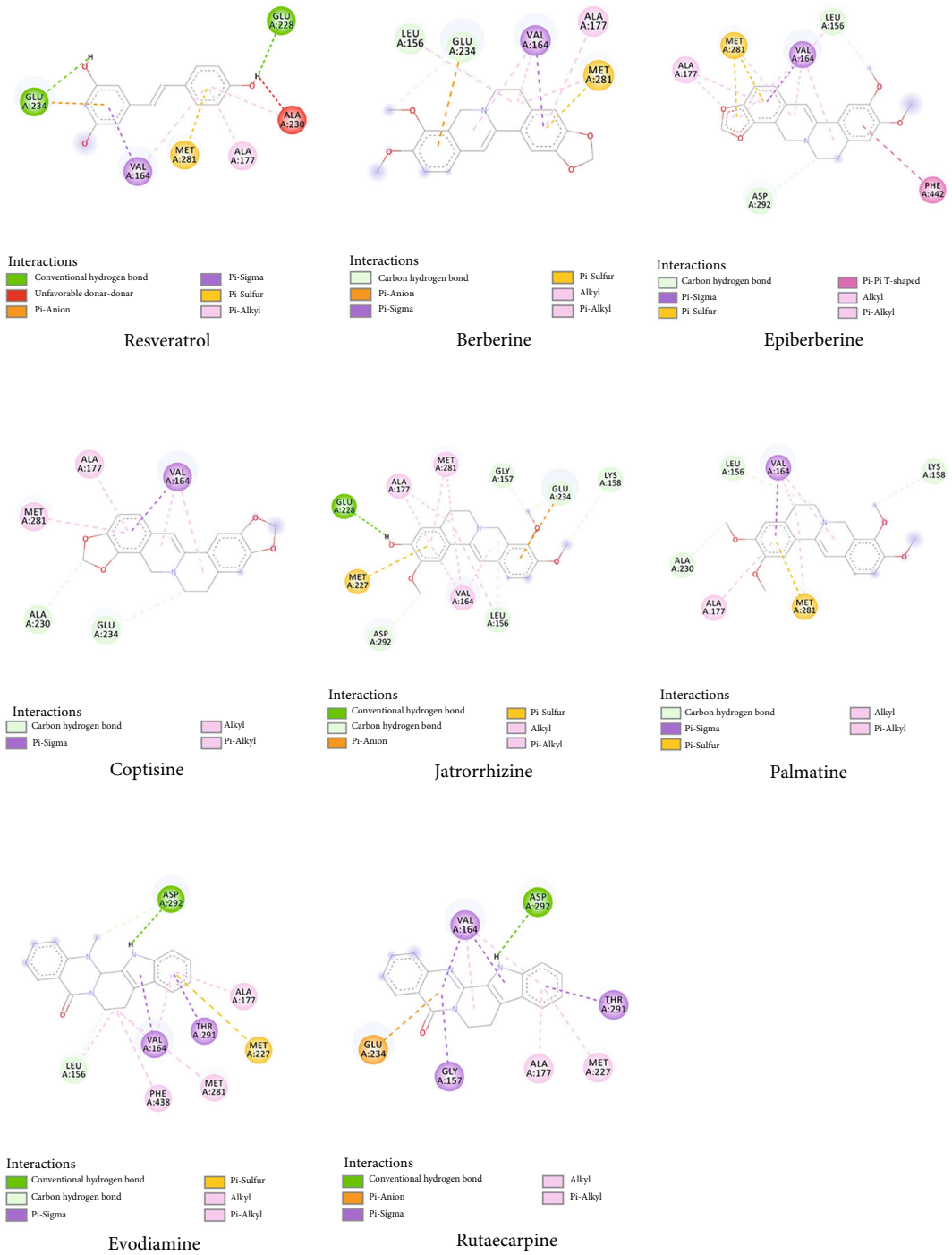

Figure 9: 2D docking conformation of 7 ingredients and resveratrol with AKT1.

promising therapeutic target for metabolic diseases. The PPI result in our study revealed that GLP is effective in improving and treating NASH, possibly due to its regulation of AKT1.

According to the GO enrichment analysis result, the common targets of GLP and NASH were enriched to inflammatory response and regulation of phosphatidylinositol 3-kinase signaling, and AKT1 was also involved in these biological processes. Accumulating evidence has revealed that NASH is a metabolic inflammatory disease induced by lipid-oversupplied steatosis, and chronic inflammation is the main driver of NASH and one of the clinical features used to distinguish NASH from NAFLD [4, 32, 33]. In animal models of NASH, NF-κB mRNA expressions in liver tissues were significantly increased. Other clinical studies also found that the NF-κB activity was increased in NASH patients. AKT regulates NF-κB signal transduction through phosphorylation of IKKα, which leads to the degradation

Table 2: Molecular docking of 7 bioactive ingredients and the inhibitor with AKT1.

Compound	Structure	Receptor	Binding energy (kcal/mol)
Berberine	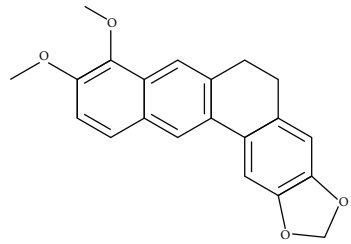	AKT1	-9.30
Epiberberine	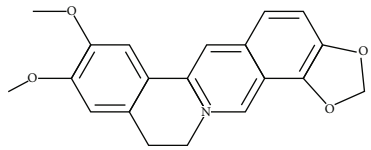	AKT1	-10.40
Jatrorrhizine	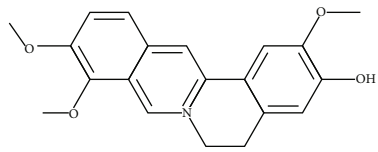	AKT1	-8.80
Coptisine	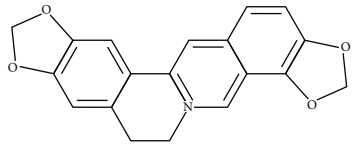	AKT1	-10.20
Palmatine	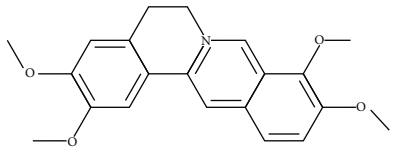	AKT1	-8.70
Evodiamine	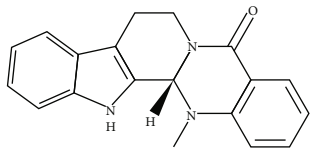	AKT1	-11.00
Rutecarpine	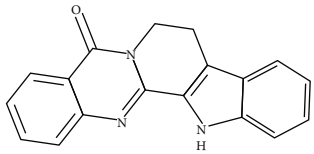	AKT1	-10.40
Resveratrol	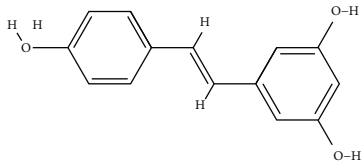	AKT1	-8.50

of IκB [34]. This process releases NF-κB from the cytoplasm into the nucleus to further regulate the expression of downstream target genes and finally mediate multiple pathological processes such as liver inflammation and apoptosis. The evidence indicates that GLP may reduce liver damage by regulating the release of downstream inflammatory factors through AKT1.

KEGG enrichment results showed that the TNF signaling pathway was the most important signaling pathway, which involved the core target AKT1. TNF has two types: tumor necrosis factor-alpha (TNF-α) and tumor necrosis factor-beta (TNF-β). TNF-α, mainly secreted by activated macrophages, can promote the expression of proinflammatory factors and participate in systemic inflammation.

Insulin resistance is involved in the development and progression of NASH. In NASH progression, TNF-α induces the activation of JNK, leading to the Ser site on the IRS protein in the phosphorylated insulin signaling pathway and consequently resulting in insulin resistance [35]. Our results showed that GLP could regulate the TNF signaling pathway through AKT1; thus, it might reduce insulin resistance in patients with NASH.

The protein-small molecular docking analysis showed that all 7 components of GLP were successfully docked to AKT1, located in the active pocket of resveratrol and fitting well in the active pocket. Meanwhile, the 7 components have better binding energy than the AKT1 inhibitor, resveratrol. The drug molecules and the protein receptors form multiple intermolecular forces, including hydrogen bonding, C-H bonding, π-alkyl hydrogen bonding, and other interactions. The docking score revealed that berberine, epiberberine, coptisine, evodiamine, and rutecarpine had higher interaction energy with AKT1 than resveratrol. This suggests that they were the most important active components contributing to the therapeutic effects of the GLP on NASH. It has been reported that berberine can induce autophagy by inhibiting mTOR, AKT, and MAPK (ERK, JNK, and p38) pathways [36]. Additionally, berberine induces autophagic death in acute lymphoblastic leukemia (ALL) cells by inactivating AKT/mTORC1 signaling [37]. Epiberberine is an alkaloid with low toxicity and exerts various activities including anti-adipogenesis via AKT and ERK pathways [38]. In an in vitro experiment, epiberberine inhibits the phosphorylation of AKT, which then downregulates the major transcription factors of adipogenesis during adipocyte differentiation [39]. Coptisine can inhibit LPS-stimulated inflammation by blocking nuclear factor-kappa B, MAPK, and PI3K/AKT activation in macrophages, demonstrating its anti-inflammation properties. Evodiamine and rutecarpine, two alkaloids isolated from the unripe fruit of Evodia Fructus, were identified as two major active substances of Evodiae Fructus. Evodiamine inhibits cell proliferation by inducing cellular apoptosis via suppressing the PI3K/AKT pathway [40]. Moreover, evodiamine can significantly reduce the production of proinflammatory cytokines and inhibit the activation of inflammation-related pathways such as AKT, NF-κB p65, ERK1/2, p38, and JNK [41]. Nie et al. [42] found that Rutecarpine ameliorates hyperlipidemia and hyperglycemia in fat-fed, streptozotocin-treated rats via regulating the IRS-1/PI3K/AKT signaling pathway. Although Nie et al.'s study did not report whether this bioactive compound directly inhibits AKT1, our docking result supports the possible protein-small molecule interaction.

5. Conclusion

In summary, this study tackles the molecular mechanism of GLP in the treatment of NASH based on bioinformatics and system pharmacology. Our findings indicate that multiple compounds in GLP may play a role in the treatment of NASH through the synergy of targets and signaling pathways. The active ingredients of GLP can act on the key gene target AKT1 and exert pharmacological effects through the TNF signaling pathway. Due to the limitations of biological calculation methods, future research with in vitro and in vivo experiments is needed to verify our findings.

Data Availability

The datasets used and/or analyzed during the current study are available from the corresponding author upon reasonable request.

Conflicts of Interest

The authors declare that they have no conflicts of interest.

Authors' Contributions

Rui Gao and Xiaobo Zhang contributed equally to this work.

Acknowledgments

This study was supported by grants from the National Natural Science Foundation of China (Grant No. 81973743), Sichuan Science and Technology Innovation Seedling Project (Grant No. 20MZGC0241), and Key R&D program of Sichuan Provincial Department of Science and Technology in 2022 (Grant No. 22ZDYF0905). We are grateful to Han Yu for research suggestions in this study. The authors are thankful to Chengdu University of Traditional Chinese Medicine for help in conducting this study.

References

[1] F. Baratta, D. Pastori, L. Polimeni et al., "Does lysosomial acid lipase reduction play a role in adult non-alcoholic fatty liver disease?," *International Journal of Molecular Sciences*, vol. 16, no. 12, pp. 28014–28021, 2015.

[2] B. J. Perumpail, M. A. Khan, E. R. Yoo, G. Cholankeril, D. Kim, and A. Ahmed, "Clinical epidemiology and disease burden of nonalcoholic fatty liver disease," *World Journal of Gastroenterology*, vol. 23, no. 47, pp. 8263–8276, 2017.

[3] Z. Younossi, Q. M. Anstee, M. Marietti et al., "Global burden of NAFLD and NASH: trends, predictions, risk factors and prevention," *Nature Reviews. Gastroenterology & Hepatology*, vol. 15, no. 1, pp. 11–20, 2018.

[4] V. Manne, P. Handa, and K. V. Kowdley, "Pathophysiology of nonalcoholic fatty liver disease/nonalcoholic steatohepatitis," *Clinics in Liver Disease*, vol. 22, no. 1, pp. 23–37, 2018.

[5] M. Povsic, O. Y. Wong, R. Perry, and J. Bottomley, "A structured literature review of the epidemiology and disease burden of non-alcoholic steatohepatitis (NASH)," *Advances in Therapy*, vol. 36, no. 7, pp. 1574–1594, 2019.

[6] C. P. Day, "Non-alcoholic steatohepatitis (NASH): where are we now and where are we going?," *Gut*, vol. 50, no. 5, pp. 585–588, 2002.

[7] M. M. Chen, J. J. Cai, Y. Yu, Z. G. She, and H. Li, "Current and emerging approaches for nonalcoholic steatohepatitis treatment," *Gene Expression*, vol. 19, no. 3, pp. 175–185, 2019.

[8] C. Peng, A. G. Stewart, O. L. Woodman, R. H. Ritchie, and C. X. Qin, "Non-alcoholic steatohepatitis: a review of its mechanism, models and medical treatments," *Frontiers in Pharmacology*, vol. 11, article 603926, 2020.

[9] V. Ratziu, Z. Goodman, and A. Sanyal, "Current efforts and trends in the treatment of NASH," *Journal of Hepatology*, vol. 62, no. 1, pp. S65–S75, 2015.

[10] D. Black, S. Brockbank, S. Cruwys, K. Goldenstein, P. Hein, and B. Humphries, "The future R&D landscape in non-alcoholic steatohepatitis (NASH)," *Drug Discovery Today*, vol. 24, no. 2, pp. 560–566, 2019.

[11] Y. Mizunoe, M. Kobayashi, R. Tagawa, Y. Nakagawa, H. Shimano, and Y. Higami, "Association between lysosomal dysfunction and obesity-related pathology: a key knowledge to prevent metabolic syndrome," *International Journal of Molecular Sciences*, vol. 20, no. 15, p. 3688, 2019.

[12] Y. Xu, W. Guo, C. Zhang et al., "Herbal medicine in the treatment of non-alcoholic fatty liver diseases-efficacy, action mechanism, and clinical application," *Frontiers in Pharmacology*, vol. 11, p. 601, 2020.

[13] R. Jadeja, R. V. Devkar, and S. Nammi, "Herbal medicines for the treatment of nonalcoholic steatohepatitis: current scenario and future prospects," *Evidence-Based Complementary and Alternative Medicine : ECAM*, vol. 2014, article 648308, p. 18, 2014.

[14] Y. Zhang, J.-X. Luo, Y.-G. Li, H.-F. Fu, F. Yang, and X.-Y. Hu, "An open-label exploratory clinical trial evaluating the effects of GLS (Coptidis Rhizoma-Evodiae Fructus 2 : 1) on fibroblast growth factor 21 in patients with nonalcoholic fatty liver disease," *Evidence-Based Complementary and Alternative Medicine : ECAM*, vol. 2022, Article ID 4583645, 11 pages, 2022.

[15] B. Liang, X. X. Zhang, and N. Gu, "Virtual screening and network pharmacology-based synergistic mechanism identification of multiple components contained in Guanxin V against coronary artery disease," *BMC Complementary Medicine and Therapies*, vol. 20, no. 1, p. 345, 2020.

[16] Y. Tang, Y. Zhang, L. Li, Z. Xie, C. Wen, and L. Huang, "Kunxian capsule for rheumatoid arthritis: inhibition of inflammatory network and reducing adverse reactions through drug matching," *Frontiers in Pharmacology*, vol. 11, p. 485, 2020.

[17] A. L. Hopkins, "Network pharmacology," *Nature Biotechnology*, vol. 25, no. 10, pp. 1110-1111, 2007.

[18] X. Zhang, T. Shen, X. Zhou et al., "Network pharmacology based virtual screening of active constituents of Prunella vulgaris L. and the molecular mechanism against breast cancer," *Scientific Reports*, vol. 10, no. 1, article 15730, 2020.

[19] B. Zhang, Z. Hao, W. Zhou et al., "Formononetin protects against ox-LDL-induced endothelial dysfunction by activating PPAR-γ signaling based on network pharmacology and experimental validation," *Bioengineered*, vol. 12, no. 1, pp. 4887–4898, 2021.

[20] X. Li, H. W. Yang, Y. Jiang, J. Y. Oh, Y. J. Jeon, and B. Ryu, "Ishophloroglucin A isolated from Ishige okamurae suppresses melanogenesis induced by α-MSH: In Vitro and In Vivo," *Marine Drugs*, vol. 18, no. 9, p. 470, 2020.

[21] L. Qin, H. Chen, X. Ding et al., "Utilizing network pharmacology to explore potential mechanisms of YiSui NongJian formula in treating myelodysplastic syndrome," *Bioengineered*, vol. 12, no. 1, pp. 2238–2252, 2021.

[22] H. Zhan, Y. Bai, Y. Lv, X. Zhang, L. Zhang, and S. Deng, "Pharmacological mechanism of mylabris in the treatment of leukemia based on bioinformatics and systematic pharmacology," *Bioengineered*, vol. 12, no. 1, pp. 3229–3239, 2021.

[23] X. B. Qin, W. J. Zhang, L. Zou, P. J. Huang, and B. J. Sun, "Identification potential biomarkers in pulmonary tuberculosis and latent infection based on bioinformatics analysis," *BMC Infectious Diseases*, vol. 16, no. 1, p. 500, 2016.

[24] H. Qiu, X. Zhang, H. Yu, R. Gao, J. Shi, and T. Shen, "Identification of potential targets of triptolide in regulating the tumor microenvironment of stomach adenocarcinoma patients using bioinformatics," *Bioengineered*, vol. 12, no. 1, pp. 4304–4319, 2021.

[25] X. Zhang, R. Gao, Z. Zhou et al., "A network pharmacology based approach for predicting active ingredients and potential mechanism of Lianhuaqingwen capsule in treating COVID-19," *International Journal of Medical Sciences*, vol. 18, no. 8, pp. 1866–1876, 2021.

[26] P. Liu, W. Gan, Y. R. Chin et al., "PtdIns(3,4,5)P3-dependent activation of the mTORC2 kinase complex," *Cancer Discovery*, vol. 5, no. 11, pp. 1194–1209, 2015.

[27] Y. Zhaoyang, H. Yang, and L. Wei, "Establishment of AKT gene-mediated non-alcoholic fatty liver models in mice," *Acta Medicinae Universitatis Science of Technologiae Huazhong*, vol. 45, pp. 170–175, 2016.

[28] B. Liu, X. Deng, Q. Jiang et al., "Scoparone improves hepatic inflammation and autophagy in mice with nonalcoholic steatohepatitis by regulating the ROS/P38/Nrf2 axis and PI3K/AKT/mTOR pathway in macrophages," *Biomedicine & Pharmacotherapy = Biomedecine & Pharmacotherapie*, vol. 125, article 109895, 2020.

[29] C. X. Cai, H. Buddha, S. Castelino-Prabhu et al., "Activation of insulin-PI3K/Akt-p70S6K pathway in hepatic stellate cells contributes to fibrosis in nonalcoholic steatohepatitis," *Digestive Diseases and Sciences*, vol. 62, no. 4, pp. 968–978, 2017.

[30] C. Nong and W. Chen, "Experiment study on intervention effect of Tiaogan Quzhi prescription on non-alcoholic fatty disease by PI3K/AKT-mToR signal pathway," *Chinese Journal of Traditional Medical Science and Technology*, vol. 20, 2013.

[31] Y. Fan, J. Li, A. Hu et al., "Tangganjian decoction ameliorates type 2 diabetes mellitus and nonalcoholic fatty liver disease in rats by activating the IRS/PI3K/AKT signaling pathway," *Biomedicine & Pharmacotherapy = Biomedecine & Pharmacotherapie*, vol. 106, pp. 733–737, 2018.

[32] Y. H. Han, K. O. Shin, J. Y. Kim et al., "A maresin 1/RORα/12-lipoxygenase autoregulatory circuit prevents inflammation and progression of nonalcoholic steatohepatitis," *The Journal of Clinical Investigation*, vol. 129, no. 4, pp. 1684–1698, 2019.

[33] T. Ren, J. Zhu, L. Zhu, and M. Cheng, "The combination of blueberry juice and probiotics ameliorate non-alcoholic steatohepatitis (NASH) by affecting SREBP-1c/PNPLA-3 pathway via PPAR-α," *Nutrients*, vol. 9, no. 3, p. 198, 2017.

[34] Z. Tianyu and G. Liying, "Identifying the molecular targets and mechanisms of xuebijing injection for the treatment of COVID-19 via network parmacology and molecular docking," *Bioengineered*, vol. 12, no. 1, pp. 2274–2287, 2021.

[35] S. Softic, D. E. Cohen, and C. R. Kahn, "Role of dietary fructose and hepatic de novo lipogenesis in fatty liver disease," *Digestive Diseases and Sciences*, vol. 61, no. 5, pp. 1282–1293, 2016.

[36] Q. Zhang, X. Wang, S. Cao et al., "Berberine represses human gastric cancer cell growth in vitro and in vivo by inducing cytostatic autophagy via inhibition of MAPK/mTOR/p70S6K and Akt signaling pathways," *Biomedicine & Pharmacotherapy = Biomedecine & Pharmacotherapie*, vol. 128, article 110245, 2020.

[37] J. Liu, P. Liu, T. Xu et al., "Berberine induces autophagic cell death in acute lymphoblastic leukemia by inactivating AKT/

mTORC1 signaling," *Drug Design, Development and Therapy*, vol. 14, pp. 1813–1823, 2020.

[38] L. Liu, J. Li, and Y. He, "Multifunctional epiberberine mediates multi-therapeutic effects," *Fitoterapia*, vol. 147, article 104771, 2020.

[39] J. S. Choi, J. H. Kim, M. Y. Ali et al., "Anti-adipogenic effect of epiberberine is mediated by regulation of the Raf/MEK1/2/ERK1/2 and AMPKα/Akt pathways," *Archives of Pharmacal Research*, vol. 38, no. 12, pp. 2153–2162, 2015.

[40] R. Wang, D. Deng, N. Shao et al., "Evodiamine activates cellular apoptosis through suppressing PI3K/AKT and activating MAPK in glioma," *Oncotargets and Therapy*, vol. 11, pp. 1183–1192, 2018.

[41] Y. Yang, X. Ran, H. Wang et al., "Evodiamine relieve LPS-induced mastitis by inhibiting AKT/NF-κB p65 and MAPK signaling pathways," *Inflammation*, vol. 45, no. 1, pp. 129–142, 2022.

[42] X. Q. Nie, H. H. Chen, J. Y. Zhang et al., "Rutaecarpine ameliorates hyperlipidemia and hyperglycemia in fat-fed, streptozotocin-treated rats via regulating the IRS-1/PI3K/Akt and AMPK/ACC2 signaling pathways," *Acta Pharmacologica Sinica*, vol. 37, no. 4, pp. 483–496, 2016.

Hindawi
Disease Markers
Volume 2022, Article ID 4428484, 5 pages
https://doi.org/10.1155/2022/4428484

Research Article

Prognostic Value of Serum Interleukin-6, NF-κB plus MCP-1 Assay in Patients with Diabetic Nephropathy

Zhongwu An,[1] Jibao Qin,[1] Weibo Bo,[1] Haiying Li,[1] Ling Jiang,[1] Xin Li,[1] and Jie Jiang[2]

[1]*The Clinical Laboratory of Lianyungang Oriental Hospital, The Affiliated Lianyungang Oriental Hospital of Xuzhou Medical University, Lianyungang, China*
[2]*The Department of Pharmacy of Lianyungang Oriental Hospital, The Affiliated Lianyungang Oriental Hospital of Xuzhou Medical University, China*

Correspondence should be addressed to Jie Jiang; zhiyezemei513@126.com

Received 10 January 2022; Revised 23 February 2022; Accepted 24 February 2022; Published 17 June 2022

Academic Editor: Yaoyao Bian

Objective. To assess the prognostic value of serum interleukin-6 (IL-6), nuclear factor-κB (NF-κB), and monocyte chemoattractant protein 1(MCP-1) assay in patients with diabetic nephropathy. *Methods*. From May 2019 to March 2020, 104 patients with diabetic nephropathy treated in our institution assessed for eligibility were recruited and assigned at a ratio of 1 : 1 to either the observation group ([urinary albumin excretion rate (UAER)] of 30 mg-300 mg/24 h) or the research group ([UAER] >300 mg/24 h). IL-6, MCP-1, renal function indices, and NF-κB levels were determined, and their correlation with DN was analyzed. Logistic regression was used to analyze the influencing factors of end-stage renal disease in patients with diabetic nephropathy. The receiver operating characteristic (ROC) curve was drawn, and the area under the curve (AUC) was calculated to analyze the predictive value of combined detection of IL-6, MCP-1, and NF-κB in the prognosis of patients with diabetic nephropathy. *Results*. The eligible patients with UAER of 30 mg-300 mg/24 h were associated with significantly higher levels of IL-6, MCP-1, NF-κB, blood urea nitrogen (BUN), and serum creatinine (Scr) versus those with UAER >300 mg/24 h ($P < 0.05$). During the follow-up, a total of 38 patients progressed to end-stage renal diseases. Eligible patients with end-stage renal diseases showed significantly higher serum IL-6, MCP-1, and NF-κB levels versus those without end-stage renal diseases ($P < 0.05$). Serum IL-6, MCP-1, and NF-κB are independent risk factors for the occurrence of end-stage renal disease in patients with diabetic nephropathy. The AUCs of IL-6, MCP-1, and NF-κB for predicting the prognosis of patients with diabetic nephropathy were 0.562, 0.634, and 0.647, respectively, and the AUC of the three combined detection for predicting the prognosis of patients with diabetic nephropathy was 0.889. *Conclusion*. Serum IL-6, NF-κB, and MCP-1 levels are closely related to renal injury and poor prognosis in patients with diabetic nephropathy, and the combined assay is valuable for assessing patients' condition and prognosis.

1. Introduction

Diabetic nephropathy, a kidney disease associated with diabetes mellitus is one of the microvascular complications in diabetic patients and has become the second cause of terminal-stage renal disease worldwide, second only to glomerulonephritis, with a predisposition to combined macrovascular events. Diabetic nephropathy is associated with genetic background and risk factors and may lead to proteinuria, edema, hypertension, and even kidney failure, posing a great threat to the life safety of patients. Epidemiological studies have confirmed the prevalence of diabetic nephropathy up to about 273-482/10,000 people. The clinical development of diabetic nephropathy contributes to an increased incidence of mortality and end-stage renal failure in patients. Interleukin 6 (IL-6) is a cytokine produced by immune cells that facilitates the regulation and promotion of the immune response and stimulates the production of acutely relevant reactants, which shows a trend of increase in the blood in response to inflammation or tissue damage [1–4]. Nuclear factor-κB (NF-κB) is a key class of nuclear transcription factors that are usually present in the cytoplasm of almost all cell types in homo- or heterodimeric inactive

form. It is involved in the activation of immune cells, development of T and B lymphocytes, stress response, cellular regulation, and many other cellular activities. Multiple factors activate and translocate NF-κB from the cytoplasm to the nucleus, where it binds to the KB site of NF-κB-responsive genes and regulates the transcription of NF-κB-responsive genes [5–7]. Monocyte chemotactic protein 1 (MCP-1) belongs to a small cytokine of the CC chemokine family, which has been identified as an important proinflammatory cytokine secreted by monocytes, macrophages, fibroblasts, vascular endothelial cells, B cells, and smooth muscle cells during an inflammatory response. Moreover, MCP-1 has specific chemotactic activation on monocytes/macrophages [8–10]. Accordingly, the present study investigated the prognostic value of the combined assay of IL-6, NF-κB, and MCP-1 in diabetic nephropathy to provide a reference for future clinical practice.

2. Materials and Methods

2.1. Baseline Data. From May 2019 to March 2020, 104 patients with diabetic nephropathy treated in our institution assessed for eligibility were recruited and assigned at a ratio of 1 : 1 to either the observation group ([Urinary albumin excretion rate] UAER of 30 mg-300 mg/24 h) or the research group (UAER >300 mg/24 h). The clinical baseline features of the observation group (aged 50-77 years, mean age of [62.31 ± 12.10] years, 29 males and 23 females, a mean body mass index (BMI) of [22.68 ± 3.12] kg/m^2, and mean diabetes duration of (5.21 ± 1.38) years) were comparable with those of the research group (aged 51-77 years, mean age of [62.41 ± 12.02] years, 28 males and 24 females, a mean BMI of [22.49 ± 3.07] kg/m^2, and a mean diabetes duration of (5.33 ± 1.45) years) ($P > 0.05$). The observation group had a significantly lower FPG (4.37 ± 1.21 vs. 5.68 ± 1.32) mmol/L and a significantly higher glycated hemoglobin (5.14 ± 1.13 vs. 4.67 ± 1.15) % than the research group. (Table 1). Patients provided written informed consent, and this study was approved by the medical ethics committee (Ethics No. 20190456).

2.2. Inclusion and Exclusion Criteria. Inclusion criteria were as follows: ① Diabetic patients were diagnosed as per the diagnostic criteria established by the World Health Organization Professional Committee on Diabetes in 1999: (a) fasting blood glucose ≥7.0 mmol/L; (b) random blood glucose ≥11.1 mmol/L; (c) OGTr 2 h blood glucose value ≥11.1 mmol/L; any one of the above three points can be diagnosed; ②Patients were diagnosed with nephropathy based on the clinical renal function assessment; ③ aged 19-79 years; and ④ Patients received no relevant treatment before enrollment.

Exclusion criteria were as follows: ① Patients with renal tumor; ② with severe psychiatric disease; ③ with hypertensive nephropathy, primary renal disease; ④ with cerebrovascular disease; ⑤ with hematologic disease; and ⑥ diabetic patients with renal insufficiency and without proteinuria.

2.3. Assay Method. Before treatment, 5 mL of fasting peripheral venous blood was collected from patients and stored in a 4°C refrigerator. IL-6, MCP-1, and NF-κB monoclonal antibodies were added, respectively, followed by 5 min rinsing with PBS solution. 5 mL of the sheep anti-human primary antibody was then added at a ratio of 1 : 500, left overnight at 4°C, and washed 3 times with PBS buffer for 5 min each time followed by the addition of 2 mL of mouse-derived secondary antibody (1 : 1000), placed at room temperature for 2 h, and washed with PBS solution for 5 min. Color development was carried out by adding horseradish peroxidase, and a termination solution was added for the termination of the reaction. The optical density (OD) value was measured at 450 nm. IL-6, MCP-1, and NF-κB kits were purchased from Wuhan Fien Biotechnology Co., Ltd (Item No. EH0201), Wuhan Fien Biotechnology Co., Ltd (Item No. EH0222), Shanghai Hengfei Biotechnology Co. (Item No. CSB-E12107h-1). The assay instrument was a SpectraMax iD5 enzyme marker from Molecular Devices, USA.

2.4. Assay of Blood Urea Nitrogen (BUN) and Blood Creatinine (Scr). After randomization, 5 mL of peripheral venous blood was collected from patients in fasting state before treatment and stored in a refrigerator at 4°C. The supernatant was separated by centrifugation at 1000 r/min for 5 min with a radius of 10 cm. The BUN and Scr levels were determined using a fully automated biochemical method, the kits were purchased from Nanjing Biyuntian Bioassay Company, and the microcentrifuge HITETIC was purchased from Shanghai Precision Instruments Co.

2.5. Statistical Analysis. SPSS22.0 was used for data analyses, and GraphPad Prism 8 was used for image rendering. The measurement data are expressed as ($-x \pm s$) and processed by the independent samples t-test. The count data are expressed as the number of cases (rate) and analyzed using the chi-square test. Logistic regression was used to analyze the influencing factors of end-stage renal disease in patients with diabetic nephropathy. The receiver operating characteristic (ROC) curve was drawn, and the area under the curve (AUC) was calculated to analyze the predictive value of combined detection of IL-6, MCP-1, and NF-κB in the prognosis of patients with diabetic nephropathy. Differences were considered statistically significant at $P < 0.05$.

3. Results

3.1. IL-6, MCP-1, and NF-κB. The levels of IL-6, MCP-1, and NF-κB in the observation group were (6.23 ± 2.77) ng/L, (20.17 ± 5.32) μg/L, and (24.78 ± 6.87) μg/L, respectively, and the levels of IL-6, MCP-1, and NF-κB in the research group were (10.88 ± 4.27) ng/L, (28.12 ± 6.02) μg/L, and (52.29 ± 9.24) μg/L, respectively. The levels of IL-6, MCP-1, and NF-κB in the research group were higher than those in the observation group ($P < 0.05$). (Table1).

3.2. Renal Function Indices. The BUN level was (8.82 ± 2.11) and Scr level was (85.15 ± 17.94) in the observation group, and the BUN level was (12.06 ± 2.90) and Scr level was (107.13 ± 23.82) in the research group. The research group had statistically higher BUN and Scr levels than the observation group ($P < 0.05$). (Figure 1).

Table 1: Comparison of baseline features [n (%)].

	Observation group ($n = 52$)	Research group ($n = 52$)	t or $x2$	P
Mean age	62.31 ± 12.10	62.41 ± 12.02	-0.042	0.967
Gender			0.039	0.844
Male	29	28		
Female	23	24		
BMI (kg/m^2)	22.68 ± 3.12	22.49 ± 3.07	0.313	0.755
Diabetes duration (yr.)	5.21 ± 1.38	5.33 ± 1.45	0.432	0.666
FPG (mmol/L)	4.37 ± 1.21	5.68 ± 1.32	5.275	≤0.001
Glycated hemoglobin (%)	5.14 ± 1.13	4.67 ± 1.15	2.102	0.038
IL-6 (ng/L)	6.23 ± 2.77	10.88 ± 4.27	6.588	≤0.001
MCP-1 (μg/L)	20.17 ± 5.32	28.12 ± 6.02	7.136	≤0.001
NF-κB (μg/L)	24.78 ± 6.87	52.29 ± 9.24	17.229	≤0.001

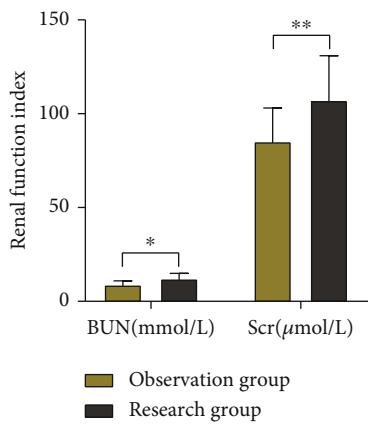

Figure 1: Comparison of renal function indices($-x \pm s$).

Table 2: Logistic regression analysis of factors affecting the occurrence of end-stage renal disease in patients with diabetic nephropathy.

	β	SE	HR	95% CI	P
IL-6	1.053	0.231	1.934	1.328-1.997	0.011
MCP-1	1.257	0.345	1.836	1.382-1.935	0.024
NF-κB	1.536	0.483	2.346	1.586-2.697	0.017

3.3. Serum IL-6, NF-κB, and MCP-1 Levels and Prognosis in Patients with Diabetic Nephropathy. During the follow-up, a total of 38 patients progressed to end-stage renal diseases. Eligible patients with end-stage renal diseases showed significantly higher serum IL-6, MCP-1, and NF-κB levels versus those without end-stage renal diseases ($P < 0.05$).

3.4. Logistic Regression Analysis of Factors Affecting the Occurrence of End-Stage Renal Disease in Patients with Diabetic Nephropathy. Gender, age, BMI, course of disease, FPG, glycosylated hemoglobin, BUN, Scr, IL-6, MCP-1, and NF-κB were used as single factors, and the occurrence of end-stage renal disease was the end point. Multivariate analysis showed that serum IL-6, MCP-1, and NF-κB were independent risk factors for the development of end-stage renal disease in patients with diabetic nephropathy (Table 2).

3.5. Predictive Value of Combined Detection of IL-6, MCP-1, and NF-κB in the Prognosis of Patients with Diabetic Nephropathy. The AUCs of IL-6, MCP-1, and NF-κB for predicting the prognosis of patients with diabetic nephropathy were 0.562, 0.634, and 0.647, respectively, and the AUC of the three combined detection for predicting the prognosis of patients with diabetic nephropathy was 0.889 (Table 3).

4. Discussion

Diabetic nephropathy is one of the microvascular complications in diabetic patients and has become the second cause of end-stage renal disease worldwide, second only to glomerulonephritis, and is prone to macrovascular events. The proportion of diabetic patients with renal failure is increasing year by year, and the risk of end-stage renal failure increases with age. Diabetic nephropathy assessments provide an effective reference for clinical immunotherapy and hormone therapy, which promotes early clinical intervention and thus lays the foundation for the improvement of renal function in the long run. Urine protein or 24-hour urine protein quantification is the traditional index for DN disease assessment, which can effectively indicate the degree of renal impairment and glomerular filtration membrane damage. However, urine protein quantification is affected by dietary habits and metabolic consumption of patients, which is, therefore, considered deficient for early prediction. Serum markers such as IL-6 and MCP-1 are significantly altered in the early stages of kidney injury, and the detection of relevant molecular markers in peripheral blood provides a novel auxiliary reference for the clinical management of diabetic nephropathy. To date, some studies have explored the expression of MCP-1 in diabetic nephropathy patients and concluded that MCP-1 can influence the level of end-stage renal function in diabetic nephropathy patients; however, the specific exploration of IL-6 and MCP-1 in

Table 3: Predictive value of combined detection of IL-6, MCP-1 and NF-κB on the prognosis of patients with diabetic nephropathy.

	Sensitivity/%	Specificity/%	SE	*P*	AUC	95% CI
IL-6	63.82	76.38	0.034	≤0.001	0.562	0.458-0.679
MCP-1	64.28	77.75	0.042	≤0.001	0.634	0.573-0.712
NF-κB	65.37	78.11	0.017	≤0.001	0.647	0.591-0.754
IL-6 + MCP-1 + NF-κB	89.67	84.58	0.006	≤0.001	0.889	0.738-0.998

diabetic nephropathy patients with varying UAER levels is marginally explored [11–13].

IL-6 and MCP-1 affect the activation of inflammatory signaling pathways and promote the disruption of the charge barrier and physiological barrier of the renal filtration membrane, leading to leakage of urinary protein. The rise of MCP-1 in monocytes or macrophages can exacerbate the release of oxidoreductase, which leads to apoptosis of the filtration membrane foot cells and an increase of the filtration membrane pore size. Dong et al. concluded that in patients with diabetic nephropathy, serum IL-6 expression increases with the elevation of diabetic complications, especially in patients with lower limb microangiopathy or renal microangiopathy. The expression of IL-6 and MCP-1 increased more significantly in patients with diabetic nephropathy with more severe urinary protein and overall disease exacerbation. The leakage of urinary protein exacerbates the deterioration of the nutritional status of the body and induces damage to the renal tubules or collecting ducts, which leads to increased elevation of IL-6 and MCP-1. Basic clinical trials have shown that activation of the NF-κB inflammatory signaling pathway is an important pathological mechanism in the development of diabetic nephropathy, and it maintains the stability of the renal internal environment and mediates pathogen-specific responses. At rest, NF-κB exists as a p50/p65 dimer in the cytoplasm, and homo- and/or heterodimers formed by the two subunits bind to its inhibitory protein IκB to form an inactive trimer. NF-κB originating from inflammatory response activation stimulates the induction of IL-6 and MCP-1 secretion, which in turn activates IκB kinase complexes (IKKs). IKKs phosphorylate the serine of the IκB subunit regulatory site of the trimeric p50/p65/IκB, resulting in ubiquitination modification of the IκB subunit, the degradation by proteases, and subsequent release of p50/p65 and nuclear translocation to the κB site on the corresponding target gene to regulate gene transcription [14–17]. IL-6 and MCP-1 can activate a large number of inflammatory cells, and the resulting inflammatory cascade amplification is associated with distant organ damages, which positively regulates the activation of NF-κB and aggravates the damage to the intracellular and basement membranes, thereby eliciting proteinuria. IL-6 is mostly activated and released by the overexpression of NF-κB, leading to the accumulation of neutrophils, basophils, and T cells in the kidney, which induces glomerular production of interstitial proteins to promote glomerular fibrosis, thereby contributing to the pathological damage of the kidney. In the present study, the significantly higher IL-6, MCP-1, and NF-κB levels in the research group than in the observation group suggest the involvement of IL-6, MCP-1, and NF-κB in the progression of diabetic nephropathy, which was consistent with the results of the previous research [18–21]. The levels of creatinine (Scr) and urea nitrogen (BUN) in the research group were significantly higher than those in the observation group; the more severe the patients' diabetic nephropathy, the higher their serum levels of Scr and BUN, which were mainly related to the patients' renal impairment due to long-term dysglycemia. Moreover, the research results of the present study demonstrated that during the follow-up, a total of 38 patients progressed to end-stage renal disease. Eligible patients with end-stage renal diseases showed significantly higher serum IL-6, MCP-1, and NF-κB levels versus those without end-stage renal diseases, and multivariate analysis showed that serum IL-6, MCP-1, and NF-κB were independent risk factors for the development of end-stage renal disease in patients with diabetic nephropathy. The AUCs of IL-6, MCP-1, and NF-κB for predicting the prognosis of patients with diabetic nephropathy were 0.562, 0.634, and 0.647, respectively, and the AUC of the three combined detection for predicting the prognosis of patients with diabetic nephropathy was 0.889. This further confirmed a close correlation between serum IL-6, MCP-1, and NF-κB levels and the prognosis of patients with diabetic nephropathy, which is of clinical value for the prognostic assessment of the disease.

To sum up, serum IL-6, NF-κB, and MCP-1 levels are closely related to renal injury and poor prognosis in patients with diabetic nephropathy, and the combined assay is valuable for assessing patients' condition and prognosis.

Data Availability

The datasets used during the present study are available from the corresponding author upon reasonable request.

Conflicts of Interest

The authors declare that they have no conflict of interest.

Authors' Contributions

Zhongwu An and Jie Jiang contributed equally to this work.

References

[1] J. Cui, X. Zhang, C. Guo, and L. Zhang, "The association of interieukin-6 polymorphism (rs1800795) with microvascular complications in Type 2 diabetes mellitus," *Bioscience Reports*, vol. 40, no. 10, 2020.

[2] Z. Lou, Q. Li, C. Wang, and Y. Li, "The effects of microRNA-126 reduced inflammation and apoptosis of diabetic nephropathy through PI3K/AKT signalling pathway by VEGF," *Archives of Physiology and Biochemistry*, pp. 1–10, 2020.

[3] X. Q. Min and Y. Xie, "LncRNA CASC2 alleviates the progression of diabetic nephropathy by regulating the miR-144/SOCS2 signalling Axis," *Kidney & Blood Pressure Research*, vol. 45, no. 6, pp. 837–849, 2020.

[4] R. Pang and D. Gu, "Triptolide improves renal injury in diabetic nephropathy rats through TGF-β1/Smads signal pathway," *Endocrine, Metabolic & Immune Disorders Drug Targets*, vol. 21, no. 10, pp. 1905–1911, 2021.

[5] H. J. Sun, S. P. Xiong, X. Cao et al., "Polysulfide-mediated sulfhydration of SIRT1 prevents diabetic nephropathy by suppressing phosphorylation and acetylation of p65 NF-κB and STAT3," *Redox Biology*, vol. 38, p. 101813, 2021.

[6] P. M. Tang, Y. Y. Zhang, J. S. C. Hung et al., "DPP4/CD32b/NF-κB circuit: a novel druggable target for inhibiting CRP-driven diabetic nephropathy," *Molecular Therapy*, vol. 29, no. 1, pp. 365–375, 2021.

[7] J. Xu, Y. Wang, Z. Wang, L. Guo, and X. Li, "Fucoidan mitigated diabetic nephropathy through the downregulation of PKC and modulation of NF-κB signaling pathway: in vitro and in vivo investigations," *Phytotherapy Research*, vol. 35, no. 4, pp. 2133–2144, 2021.

[8] Q. Du, Y. X. Fu, A. M. Shu et al., "Loganin alleviates macrophage infiltration and activation by inhibiting the MCP-1/CCR2 axis in diabetic nephropathy," *Life Sciences*, vol. 272, p. 118808, 2021.

[9] X. Fang, J. Hu, and H. Zhou, "Knock-down of long non-coding RNA ANRIL suppresses mouse mesangial cell proliferation, fibrosis, inflammation via regulating Wnt/β-catenin and MEK/ERK pathways in diabetic nephropathy," *Experimental and Clinical Endocrinology & Diabetes*, vol. 130, no. 1, pp. 30–36, 2022.

[10] M. Li, Q. Guo, H. Cai, H. Wang, Z. Ma, and X. Zhang, "miR-218 regulates diabetic nephropathy via targeting IKK-β and modulating NK-κB-mediated inflammation," *Journal of Cellular Physiology*, vol. 235, no. 4, pp. 3362–3371, 2020.

[11] B. Sanchez Alamo, A. Shabaka, M. V. Cachofeiro Ramos, and G. M. Fernandez Juarez, "FC 085SERUM interleukin-6 levels predict renal disease progression in diabetic kidney disease," *Clinical Nephrology*, vol. 36, Supplement_1, 2021.

[12] E. Xiang, B. Han, Q. Zhang et al., "Human umbilical cord-derived mesenchymal stem cells prevent the progression of early diabetic nephropathy through inhibiting inflammation and fibrosis," *Stem Cell Research & Therapy*, vol. 11, no. 1, p. 336, 2020.

[13] N. Zhang, Q. Zheng, Y. Wang et al., "Renoprotective effect of the recombinant anti-IL-6R fusion proteins by inhibiting JAK2/STAT3 signaling pathway in diabetic nephropathy," *Frontiers in Pharmacology*, vol. 12, p. 681424, 2021.

[14] W. H. Dong, Q. Q. Chu, S. Q. Liu, D. T. Deng, and Q. Xu, "Isobavachalcone ameliorates diabetic nephropathy in rats by inhibiting the NF-κB pathway," *Journal of Food Biochemistry*, vol. 44, no. 9, article e13405, 2020.

[15] W. Huang, Y. Man, C. Gao et al., "Short-chain fatty acids ameliorate diabetic nephropathy via GPR43-mediated inhibition of oxidative stress and NF-κB signaling," *Oxidative Medicine and Cellular Longevity*, vol. 2020, Article ID 4074832, 21 pages, 2020.

[16] F. Li, Y. Chen, Y. Li, M. Huang, and W. Zhao, "Geniposide alleviates diabetic nephropathy of mice through AMPK/SIRT1/NF-κB pathway," *European Journal of Pharmacology*, vol. 886, p. 173449, 2020.

[17] M. Y. Qi, Y. H. He, Y. Cheng et al., "Icariin ameliorates streptozocin-induced diabetic nephropathy through suppressing the TLR4/NF-κB signal pathway," *Food & Function*, vol. 12, no. 3, pp. 1241–1251, 2021.

[18] C. Liu, S. Zhao, C. Zhu et al., "Ergosterol ameliorates renal inflammatory responses in mice model of diabetic nephropathy," *Biomedicine & Pharmacotherapy*, vol. 128, p. 110252, 2020.

[19] P. Raina, R. Sikka, H. Gupta et al., "Association of eNOS and MCP-1 genetic variants with type 2 diabetes and diabetic nephropathy susceptibility: a case-control and meta-analysis study," *Biochemical Genetics*, vol. 59, no. 4, pp. 966–996, 2021.

[20] K. Siddiqui, S. S. Joy, T. P. George, M. Mujammami, and A. A. Alfadda, "Potential role and excretion level of urinary transferrin, KIM-1, RBP, MCP-1 and NGAL markers in diabetic nephropathy," *Diabetes Metab Syndr Obes*, vol. Volume 13, pp. 5103–5111, 2020.

[21] H. Wang, X. Huang, P. Xu et al., "Apolipoprotein C3 aggravates diabetic nephropathy in type 1 diabetes by activating the renal TLR2/NF-κB pathway," *Metabolism*, vol. 119, p. 154740, 2021.

Hindawi
Disease Markers
Volume 2022, Article ID 6704347, 6 pages
https://doi.org/10.1155/2022/6704347

Research Article

Effect of Standardized Nutritional Intervention in Patients with Nasopharyngeal Carcinoma Receiving Radiotherapy Complicated with Diabetes Mellitus

Yuhong Ge

Department of Head and Neck Comprehensive Radiation Therapy, Affiliated Tumor Hospital of Xinjiang Medical University, Urumqi, China

Correspondence should be addressed to Yuhong Ge; yuhedi172996@163.com

Received 30 January 2022; Revised 22 March 2022; Accepted 25 April 2022; Published 15 June 2022

Academic Editor: Zhaoqi Dong

Objective. To evaluate the effect of standardized nutritional intervention in patients with nasopharyngeal carcinoma receiving radiotherapy complicated with diabetes mellitus and the impact on quality of life. *Methods*. From January 2019 to December 2020, 100 diabetic patients with nasopharyngeal carcinoma receiving radiotherapy were assessed for eligibility and recruited. They were concurrently and randomly assigned (1 : 1) to receive either conventional nursing (control group) or standardized nutritional intervention (observation group). The outcomes include clinical efficacy and quality of life. *Results*. Standardized nutritional intervention was associated with significantly lower levels of fasting blood glucose (FBG), 2 h postprandial blood glucose (2hPBG), and glycated hemoglobin (HbA1c) versus conventional nursing ($P < 0.001$). The patients given standardized nutritional intervention showed significantly higher hemoglobin (Hb), prealbumin (PA), and albumin (ALB) levels versus those given conventional nursing at 4 weeks after the start of radiotherapy and at the end of radiotherapy ($P < 0.001$). The two groups showed similar Morisky scores before intervention ($P > 0.05$). After intervention, the observation group outperformed the control group in terms of treatment compliance ($P < 0.05$). Standardized nutritional intervention provided patients with a significantly better quality of life versus conventional nursing ($P < 0.05$). Standardized nutritional intervention was associated with a significantly lower incidence of adverse events and higher nursing satisfaction versus conventional nursing ($P < 0.05$). *Conclusion*. Standardized nutritional intervention for patients with nasopharyngeal carcinoma given radiotherapy complicated with diabetes mellitus can efficiently restore the normal nutritional status of patients, reduce the complications of radiotherapy, and improve the quality of life of patients, so it is worthy of wide clinical application.

1. Introduction

Nasopharyngeal carcinoma is a highly prevalent malignant tumor, with a predominant incidence of head and neck malignant tumors and a high mortality rate [1]. It is a common malignant tumor in the south of China, with the age of onset mostly between 30 and 60 years [2]. The prevalence of nasopharyngeal cancer in China is about 39.84 per ten thousand, with an incidence of about 14.68 per ten thousand and a mortality of about 8.73 per ten thousand [3]. Its clinical symptoms mostly include nasal congestion, bloody nasal discharge, congestion in the ear, hearing loss, diplopia, and headache [4]. Given its moderate sensitivity to radiation therapy, radiotherapy is the current treatment of choice for nasopharyngeal carcinoma. Diabetes mellitus is a group of metabolic diseases characterized by hyperglycemia, and the long-term presence of hyperglycemia leads to chronic damage and dysfunction of various organs and tissues, such as the eyes, kidneys, heart, blood vessels, and nerves [4]. With the continuous improvement of the living standard, the dietary structure and lifestyle of people have undergone significant changes, resulting in a marked increase in the prevalence of diabetes [5]. An epidemiological survey conducted by Mainous et al. found the prevalence of uropathy

in American adults aged 40-49, 50-59, and 60-69 years to be 4.5%, 11.4%, and 15.1%, respectively [6], and it has been shown that 9% of cancer patients had diabetes mellitus at the time of cancer diagnosis, suggesting a close association between long-term diabetes mellitus and tumorigenesis [7, 8]. With the continuous application of new technologies such as intensity-modulated radiation therapy (IMRT) in clinical practice, the survival of nasopharyngeal cancer has markedly improved [9]. However, radiotherapy may cause collateral damage to normal tissue cells, and complications of radiotherapy including radioactive oral mucositis, radioactive esophagitis, radioactive skin damage, and restricted mouth opening seriously compromise the patients' nutritional status and quality of life. Standardized nutritional intervention is a new management approach that provides patients with nutrients and energy to perform the metabolic and immunomodulatory functions of nutrients [10, 11]. Moreover, it helps the patients master reasonable dietary habits and lifestyles and prevent related complications, thereby enhancing their quality of life. This study was conducted to develop nutritional plans for diabetic patients undergoing radiotherapy for nasopharyngeal carcinoma through standardized nutritional intervention. The results are as follows.

2. Materials and Methods

2.1. Baseline Data. From January 2019 to December 2020, 100 diabetic patients with nasopharyngeal carcinoma receiving radiotherapy were assessed for eligibility and recruited. They were concurrently and randomly assigned to control group ($n = 50$) or observation group ($n = 50$). The baseline characteristics of the observation group (31 males, 19 females, aged 35-71 years, mean age of [45.02 ± 3.68] years, course of disease of [3-11] years, and mean course of disease of [7.02 ± 3.64] years) were comparable with those of the control group (35 males, 15 females, aged 36 - 70 years, mean age of [45.45 ± 3.34] years, course of disease of [3-11] years, and mean course of disease of [7.56 ± 3.17] years) ($P > 0.05$) (Table 1). The studies involving human participants were reviewed and approved by Affiliated Tumor Hospital of Xinjiang Medical University. The patients provided their written informed consent to participate in this study.

2.2. Inclusion and Exclusion Criteria. Inclusion criteria: ① patients with pathologically confirmed primary nasopharyngeal carcinoma; ② with diabetes mellitus diagnosed before radiotherapy as per the 1999 WHO diagnostic criteria for diabetes mellitus; and ③ with normal consciousness to conduct normal communication.

Exclusion criteria: ① patients with other primary tumors; ② with withdrawal of consent; and ③ with severe psychiatric disorders.

2.3. Nursing Methods. Patients in the control group were given conventional nursing, including therapeutic care, disease health education, dietary guidance, and medication care.

Patients in the observation group received standardized nutritional intervention. A nutrition management team consisting of nutrition specialist nurses, doctors, and dietitians was established. The patients were regularly educated about nutrition knowledge of nasopharyngeal carcinoma and diabetes, the detriments of the disease, the necessity of blood glucose control, and the importance of individualized nutritional interventions. Nutritional dietary guidance was provided through online channels to address radiotherapy nutrition-related issues [12] and collect follow-up data. The patients were encouraged to perform patient self-management, and the nutrition nurses instructed the patients to accurately record their weight and the amount and type of food for their daily consumption. The intervention was continued for one month. And they all were followed-up for six months.

2.4. Evaluation Criteria. ① Glucose levels: the blood glucose values after dietary care were compared between the two groups, and the patients' fasting blood glucose (FBG), 2 h postprandial blood glucose (2hPBG), and glycated hemoglobin (HbA1c) levels after the intervention were determined for analyses. 5 ml of fasting venous blood in the morning before and after the intervention of the two groups of women was collected, centrifuged (Avanti JXN-30/26, Beckman Company) at 3000 r/min for 10 min, and then, an automatic biochemical analyzer (Nanjing Baden Medical Co., Ltd.) was used to measure maternal FBG and 2 h postprandial blood glucose (2 h PBG). High-performance liquid chromatography (HPLC) was used to detect the HbA1c levels of the two groups before and after the intervention, and the normal value was 4-6%.

② Nutritional status: serum nutritional indices, including hemoglobin (Hb), prealbumin (PA), and albumin (ALB) levels, were determined and compared between the two groups of patients before the intervention, at 4 weeks after the start of radiotherapy, and at the end of radiotherapy.

③ Compliance: the Morisky compliance scale [13, 14] was used to evaluate the patients' compliance with treatment before and after the nursing intervention in four aspects: medication compliance, body mass control, diet control, and appropriate exercise, with a total score of 50 points. The higher the score, the better the compliance.

④ Quality of life: the quality of life of patients in both groups before and after radiotherapy was evaluated by the FACT-H&N scale [15]. The FACT-H&N consists of 11 head and neck entries (HN1 to 11). GP1 to GP7, GE1 to GE6, HN2, HN3, HN6, HN8, and HN9 are reverse entries, and the rest are positive entries. Scores for positive entries = (0 + answer option number); score for reverse entries = (4 − answer option number). Higher scores represent better life quality.

⑤ Adverse events: complications such as radioactive skin damage, radioactive mucositis, oral ulcers, difficulty in opening mouth, otitis media, and dry mouth were monitored and recorded in both groups.

⑥ Satisfaction: the nursing satisfaction questionnaire (including the attitude of medical staff, the efficiency of

Table 1: Comparison of baseline data ($\bar{x} \pm s$).

Groups	n	Male	Female	Age	Mean age	Course of disease	Mean course of disease
Observation group	50	31	19	35-71	45.02 ± 3.68	3-11	7.02 ± 3.64
Control group	50	35	15	36-70	45.45 ± 3.34	3-11	7.56 ± 3.17
t	—	—	—	—	0.612	—	0.791
P	—	—	—	—	0.542	—	0.431

Table 2: Comparison of blood glucose levels after intervention ($\bar{x} \pm s$).

n	n	FBG (mmol/L)	2Hpbg (mmol/L)	HbA1c (%)
Observation group	50	6.58 ± 0.64	8.95 ± 0.35	8.06 ± 2.35
Control group	50	7.01 ± 0.62	9.86 ± 0.65	11.98 ± 2.36
t	—	3.412	8.716	8.323
P	—	0.001	<0.001	<0.001

Note: FBG: fasting blood glucose; 2hPBG: two-hour postprandial blood glucose; HbA1c: glycated hemoglobin.

Table 3: Comparison of nutritional status related blood indices ($\bar{x} \pm s$).

Groups	n	Timepoint	Hb (g/L)	PA (mg/L)	ALB (g/L)
		Before intervention	132.65 ± 11.16	271.17 ± 23.43	44.02 ± 3.98
Observation group	50	At 4 weeks of intervention	131.17 ± 10.77	268.07 ± 22.32	42.78 ± 4.12
		At the end of intervention	130.55 ± 10.86	267.25 ± 19.78	41.17 ± 3.76
		Before intervention	131.84 ± 12.04	270.61 ± 21.19	43.75 ± 4.23
Control group	50	At 4 weeks of intervention	123.76 ± 11.25	234.95 ± 16.44	37.83 ± 4.33
		At the end of intervention	106.73 ± 9.88	210.07 ± 14.56	34.82 ± 1.77
		Before intervention	0.349	0.125	0.329
t	—	At 4 weeks of intervention	3.364	8.448	5.856
		At the end of intervention	11.472	16.462	10.805
		Before intervention	0.728	0.901	0.743
P	—	At 4 weeks of intervention	0.001	<0.001	<0.001
		At the end of intervention	<0.001	<0.001	<0.001

Note: t-values and P values are for the same period comparison between the two groups. Hb: hemoglobin; PA: prealbumin; ALB: albumin.

medical staff, and explanation of diseases by medical staff) developed by our hospital was used, containing a total of four items (highly satisfied, satisfied, less satisfied, and dissatisfied).

2.5. Statistical Analysis. The SPSS22.0 software was used for data analyses, and GraphPad Prism 8 was used for image rendering. The count data were expressed as [n (%)] and processed using the chi-square test. The measurement data were expressed as ($\bar{x} \pm s$) and analyzed using the t-test. Differences were considered statistically significant at $P < 0.05$.

3. Results

3.1. Blood Glucose Levels. Standardized nutritional intervention was associated with significantly lower levels of FBG, 2hPBG, and HbA1c (6.58 ± 0.64, 8.95 ± 0.35, 8.06 ± 2.35) versus conventional nursing (7.01 ± 0.62, 9.86 ± 0.65, 11.98 ± 2.36) ($P < 0.001$) (Table 2).

3.2. Nutritional Status. Before radiotherapy, the Hb, PA, and ALB levels of the two groups were similar ($P > 0.05$). The patients given standardized nutritional intervention showed significantly higher Hb, PA, and ALB levels (131.17 ± 10.77, 268.07 ± 22.32, 42.78 ± 4.12/130.55 ± 10.86, 267.25 ± 19.78, 41.17 ± 3.76) versus those given conventional nursing at 4 weeks after the start of radiotherapy and at the end of radiotherapy ($P < 0.001$) (Table 3).

3.3. Compliance. The two groups showed similar Morisky scores before intervention ($P > 0.05$). After intervention, the observation group (39.21 ± 2.13, 41.67 ± 2.25, 41.99 ± 1.84, 43.07 ± 3.68) outperformed the control group (28.15 ± 3.68, 30.01 ± 2.54, 31.65 ± 2.17, and 34.26 ± 3.98) in terms of control body mass, medication compliance, appropriate exercise, and diet control ($P < 0.05$) (Figure 1).

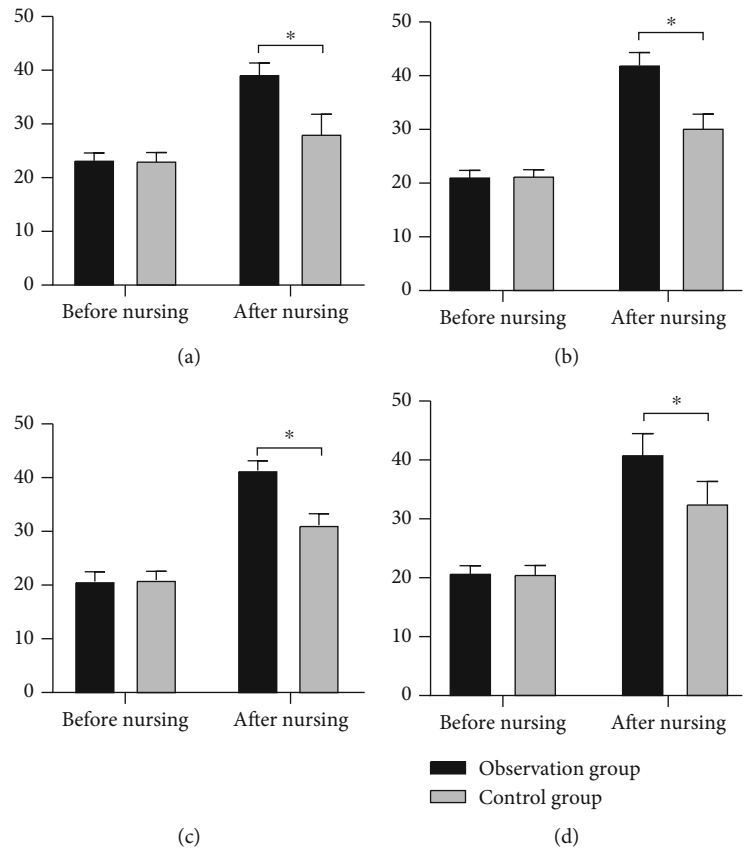

Figure 1: Comparison of Morisky scores. Note: * indicates the differences between the two groups were statistically significant; (a) is the comparison of control body mass; (b) is the comparison of medication compliance; (c) is the comparison of appropriate exercise; (d) is the comparison of control diet.

Table 4: Comparison of FACT-H&N scores ($\bar{x} \pm s$).

Groups	n	Before intervention	After intervention
Observation group	50	105.87 ± 5.65	91.27 ± 7.68*
Control group	50	106.09 ± 5.73	79.88 ± 5.37*
t	—	0.193	8.594
P	—	0.847	<0.001

Note: * is a statistically significant difference between pre- and postintervention in the same group, $P < 0.05$.

3.4. Quality of Life. Standardized nutritional intervention (91.27 ± 7.68) provided patients with a significantly better quality of life versus conventional nursing (79.88 ± 5.37) ($P < 0.05$) (Table 4).

3.5. Adverse Events. Standardized nutritional intervention (2 [4.00%] cases of radioactive skin injury, 2 cases [4.00%] of radioactive mucositis, 3 [6.00%] cases of oral ulcers, 1 case [2.00%] of difficulty in opening the mouth, and 2 cases [4.00%] of dry mouth) was associated with a significantly lower incidence of adverse events versus the conventional nursing (8 cases [16.00%] of radioactive skin injury, 9 [18.00%] cases of radioactive mucositis, 12 [24.00%] cases of oral ulcer, 7 [14.00%] cases of difficulty in opening mouth, 4 [8.00%] cases of otitis media, and 9 [18.00%] cases of dry mouth) ($P < 0.05$) (Table 5).

3.6. Nursing Satisfaction. Standardized nutritional intervention (94.00%, including 32 [64.00%] cases of highly satisfied, 15 [30.00%] cases of satisfied, 2 [4.00%] cases of less satisfied, and 1 [2.00%] case of dissatisfied) resulted in a significantly higher nursing satisfaction versus conventional nursing (64.00%, including 16 [32.00%] cases of highly satisfied, 18 [36.00%] cases of satisfied, 13 [26.00%] cases of less satisfied, and 5 [10.00%] cases of dissatisfied) ($P < 0.05$) (Figure 2).

Table 5: Comparison of incidence of adverse events (%).

Groups	n	Radioactive skin injury	Radioactive mucositis	Oral ulcers	Difficulty in opening mouth	Otitis media	Dry mouth
Observation group	50	2 (4.00)	2 (4.00)	3 (6.00)	1(2.00)	0 (0.00)	2 (4.00)
Control group	50	8 (16.00)	9 (18.00)	12 (24.00)	7 (14.00)	4 (8.00)	9 (18.00)
t	—	4.000	5.005	6.353	4.891	4.167	5.005
P	—	0.046	0.025	0.012	0.027	0.041	0.025

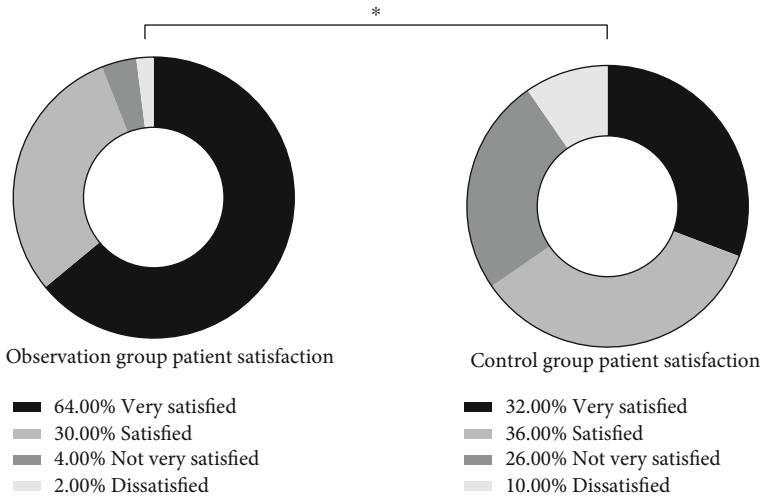

Figure 2: Comparison of SF-36 scores. Note: * indicates the differences between the two groups were statistically significant.

4. Discussion

In recent years, the prevalence of diabetes mellitus has increased year by year as the living standard of the population improves with the development of the economy. Epidemiological surveys have revealed that 9% of cancer patients have diabetes mellitus at the time of cancer diagnosis, suggesting a strong association between long-term diabetes mellitus and carcinoma [8, 16]. Nasopharyngeal carcinoma is a common malignancy in clinical practice with a high lethality rate [17]. The optimal clinical treatment modality is radiotherapy [18]. However, radiotherapy may result in serious complications such as radiation oral mucositis, pain, and restricted mouth opening that impair feeding and result in insufficient nutritional intake, water, and electrolyte imbalance [19, 20]. Normative nutritional intervention is a new management model that supplies nutrients and energy to patients.

The results in the present study showed significantly lower levels of FBG, 2hPBG, and HbA1c in patients receiving standardized nutritional intervention versus conventional nursing, suggesting that personalized dietary care of patients through standardized nutritional intervention effectively ameliorates the patients' blood glucose levels and improves the efficiency of disease control [21]. All these might be attributed to the fact that the diet formulated by standardized nutritional intervention is scientific and reliable, which contributes greatly to the control of blood sugar especially targeting patients undergoing radiotherapy for nasopharyngeal carcinoma. Also, the patients were regularly educated about nutrition knowledge of nasopharyngeal carcinoma and diabetes, the detriments of the disease, further reinforcing their consciousness towards nasopharyngeal carcinoma, and diabetes-related nutrition. Previous research has indicated a better nutritional status of patients receiving standardized nutritional intervention versus conventional nursing [22], which was consistent with the results of the present study. Moreover, standardized nutritional intervention herein was associated with higher Morisky scores and quality of life and a lower incidence of adverse events versus conventional nursing. Standardized nutritional intervention for patients undergoing synchronous radiotherapy for nasopharyngeal carcinoma can effectively improve patient compliance with promising diet control, blood glucose control, and exercise management. Possibly, the standardized nutritional intervention encouraged to perform patient self-management, and patients thus build a habit of monitoring and managing themselves, which serves as a contributor to prominent outcomes.

Here, the observation group showed significantly higher nursing satisfaction versus the control group. Radiotherapy for nasopharyngeal carcinoma complicated with diabetes

mellitus features a long course and various adverse events, which seriously compromises the physical and mental health and quality of life of patients. The standardized nutritional intervention provides patients with regular nutritional education, regular follow-up, and the design of reasonable diet plans according to patients' specific conditions, which boosts treatment quality versus conventional nursing interventions. Consistently, the findings of the present study were similar to the previous ones [12, 21].

In conclusion, standardized nutritional intervention for patients with nasopharyngeal carcinoma combined with diabetes mellitus during radiotherapy can efficiently maintain the normal nutritional status of patients, reduce the complications of radiotherapy, and improve the quality of life of patients, so it is worthy of wide clinical application.

Data Availability

The datasets used during the present study are available from the corresponding author upon reasonable request.

Conflicts of Interest

The authors declare that they have no conflict of interest.

References

[1] G. Guo, M. Fu, S. Wei, and R. Chen, "Impact of diabetes mellitus on the risk and survival of nasopharyngeal carcinoma: a meta-analysis," *Oncotargets and Therapy*, vol. 11, pp. 1193–1201, 2018.

[2] C. Yuan, V. W. Wu, S. P. Yip, D. L. Kwong, and M. Ying, "Ultrasound evaluation of carotid atherosclerosis in post-radiotherapy nasopharyngeal carcinoma patients, type 2 diabetics, and healthy controls," *Ultraschall in der Medizin-European Journal of Ultrasound*, vol. 38, no. 2, pp. 190–197, 2017.

[3] P. Y. OuYang, Z. Su, J. Tang et al., "Diabetes, prediabetes and the survival of nasopharyngeal carcinoma: a study of 5,860 patients," *PLoS One*, vol. 9, no. 10, article e111073, 2014.

[4] H. Peng, L. Chen, Y. Zhang et al., "Prognostic value of diabetes in patients with nasopharyngeal carcinoma treated with intensity-modulated radiation therapy," *Scientific Reports*, vol. 6, no. 1, article 22200, 2016.

[5] X. S. Peng, G. F. Xie, W. Z. Qiu, Y. H. Tian, W. J. Zhang, and K. J. Cao, "Type 2 diabetic mellitus is a risk factor for nasopharyngeal carcinoma: a 1:2 matched case-control study," *PLoS One*, vol. 11, no. 10, article e0165131, 2016.

[6] A. Avagimyan, L. Sukiasyan, K. Sahakyan, T. Gevorgyan, and A. Aznauryan, "The molecular mechanism of diabetes mellitus-related impairment of cardiovascular homeostasis (review)," *Georgian Medical News*, vol. 315, pp. 99–103, 2021.

[7] P. J. Goodwin, "Diabetes and cancer: unraveling the complexity," *Journal of the National Cancer Institute*, vol. 113, no. 4, pp. 347-348, 2021.

[8] P. Ramos-Garcia, M. . M. Roca-Rodriguez, M. Aguilar-Diosdado, and M. A. Gonzalez-Moles, "Diabetes mellitus and oral cancer/oral potentially malignant disorders: a systematic review and meta-analysis," *Oral Diseases*, vol. 27, no. 3, pp. 404–421, 2021.

[9] W. K. J. Lam and J. Y. K. Chan, "Recent advances in the management of nasopharyngeal carcinoma," *F1000Research*, vol. 7, article 1, 2018.

[10] J. Ji, D. D. Jiang, Z. Xu, Y. Q. Yang, K. Y. Qian, and M. X. Zhang, "Continuous quality improvement of nutrition management during radiotherapy in patients with nasopharyngeal carcinoma," *Nursing Open*, vol. 8, no. 6, pp. 3261–3270, 2021.

[11] W. Xiao, C. W. H. Chan, J. Xiao et al., "Managing the nutrition impact symptom cluster in patients with nasopharyngeal carcinoma using an educational intervention program: a pilot study," *European Journal of Oncology Nursing*, vol. 53, article 101980, 2021.

[12] W. Xiao, C. W. Chan, J. Xiao, C. L. Wong, and K. M. Chow, "Development of a nurse-led educational intervention program in managing the nutrition impact symptom cluster in patients with nasopharyngeal carcinoma following the Medical Research Council framework," *Asia-Pacific Journal of Oncology Nursing*, vol. 8, no. 6, pp. 653–661, 2021.

[13] W. Y. Lam and P. Fresco, "Medication adherence measures: an overview," *BioMed Research International*, vol. 2015, Article ID 217047, 12 pages, 2015.

[14] T. M. Nguyen, A. La Caze, and N. Cottrell, "What are validated self-report adherence scales really measuring?: a systematic review," *British Journal of Clinical Pharmacology*, vol. 77, no. 3, pp. 427–445, 2014.

[15] L. M. Chen, Q. L. Yang, Y. Y. Duan et al., "Multidimensional fatigue in patients with nasopharyngeal carcinoma receiving concurrent chemoradiotherapy: incidence, severity, and risk factors," *Support Care Cancer*, vol. 29, no. 9, pp. 5009–5019, 2021.

[16] T. Tan, Y. Shen, X. Zhou, B. Zhou, and M. Cheng, "Correlation of quality of life with self-care efficacy and social support in patients with nasopharyngeal carcinoma after radiotherapy," *Zhong Nan Da Xue Xue Bao. Yi Xue Ban*, vol. 44, no. 6, pp. 672–678, 2019.

[17] A. W. Lee, W. T. Ng, J. J. Pan et al., "International guideline on dose prioritization and acceptance criteria in radiation therapy planning for nasopharyngeal carcinoma," *International Journal of Radiation Oncology • Biology • Physics*, vol. 105, no. 3, pp. 567–580, 2019.

[18] S. Haberer-Guillerm, E. Touboul, and F. Huguet, "Intensity modulated radiation therapy in nasopharyngeal carcinoma," *European Annals of Otorhinolaryngology, Head and Neck Diseases*, vol. 132, no. 3, pp. 147–151, 2015.

[19] X. S. Sun, X. Y. Li, Q. Y. Chen, L. Q. Tang, and H. Q. Mai, "Future of radiotherapy in nasopharyngeal carcinoma," *The British Journal of Radiology*, vol. 92, no. 1102, p. 20190209, 2019.

[20] Y. J. Chen, S. C. Chen, C. P. Wang et al., "Trismus, xerostomia and nutrition status in nasopharyngeal carcinoma survivors treated with radiation," *European Journal of Cancer Care*, vol. 25, no. 3, pp. 440–448, 2016.

[21] C. Li and J. Duan, "Effect of high-quality nursing intervention on psychological emotion, life quality and nursing satisfaction of patients with nasopharyngeal carcinoma undergoing radiotherapy," *American Journal of Translational Research*, vol. 13, no. 5, pp. 4928–4938, 2021.

[22] W. Xiao, C. W. H. Chan, Y. Fan et al., "Symptom clusters in patients with nasopharyngeal carcinoma during radiotherapy," *European Journal of Oncology Nursing*, vol. 28, pp. 7–13, 2017.

Hindawi
Disease Markers
Volume 2022, Article ID 6053410, 5 pages
https://doi.org/10.1155/2022/6053410

Research Article

Combination of Calcitriol and Zoledronic Acid on PINP and β-CTX in Postoperative Patients with Diabetic Osteoporosis: A Randomized Controlled Trial

Qingchang Hu,[1] Qi Wang,[2] Fan Liu,[3] Lishuai Yao,[2] Lei Zhang,[2] and Guangdong Chen[4]

[1]*Department of Emergency Medicine, Cangzhou Central Hospital, Cangzhou, China*
[2]*People's Hospital of Qingxian, Qingxian, China*
[3]*Anesthesia Operating Room, Cangzhou Central Hospital, Cangzhou, China*
[4]*Department of Orthopaedics, Cangzhou Central Hospital, Cangzhou, China*

Correspondence should be addressed to Guangdong Chen; guantun120@126.com

Received 29 December 2021; Revised 29 January 2022; Accepted 9 February 2022; Published 3 June 2022

Academic Editor: Zhaoqi Dong

Objective. To explore the effect of calcitriol combined with zoledronic acid in posterior cruciate ligament tibial avulsion fractures of the knee joint in patients with diabetic osteoporosis. *Methods*. Between January 2020 and January 2022, 60 patients with diabetic osteoporosis treated in our hospital were included. All patients underwent knee joint posterior cruciate ligament tibial avulsion fractures, and they were randomized (1 : 1) into the observation group (calcitriol combined with zoledronic acid) and control group (calcitriol). The two groups were compared with respect to the improvement of bone mineral density and bone metabolism indexes, the pain degree (VAS) and knee joint function (Lysholm), and the incidence of refracture. *Results*. Both groups showed an increasing bone mineral density after treatment, and significant increase was observed in the observation group vs. control group (all $p < 0.05$). After treatment, VAS scores decreased in the two groups, and Lysholm scores increased compared to the corresponding values before treatment (all $p < 0.05$), with more notable changes in the observation group versus control group (all $p < 0.05$). The observation group had fewer cases of refractures than the control group (2 cases vs. 8 cases) ($p < 0.05$). *Conclusion*. Calcitriol combined with zoledronic acid used in patients with diabetic osteoporosis after the posterior cruciate ligament tibial attachment avulsion fracture of the knee joint yields a promising result in enhancing bone mineral density and bone metabolism indicators, relieving pain, improving knee joint function, and reducing the risk of refracture.

1. Introduction

Diabetes is a chronic metabolic disease with high incidence rate and disability rate. Long-term hyperglycemia stimulation may cause disorder of calcium and phosphorus metabolism in bone tissue, resulting in bone remodeling and bone microstructure damage and further undermining bone quality. The bulk of evidences recognize diabetic disease as an independent risk factor for osteoporosis. Diabetic osteoporosis, a serious complication of diabetes, is a systemic bone metabolism disease characterized by hyperglycemia, hyperinsulinemia, osteopenia, reduced bone turnover rate, and increased bone fragility [1–3]. Diabetic patients with osteoporosis are more prone to fracture in lumbar spine due to the cancellous bones, with the major presentations of varying degrees of activity limitation and severe pain. They are susceptible to knee joint dysfunction in case of external force, of which, the avulsed tibial end of the cruciate ligament is frequently seen. Clinically, the mainstay is arthroscopic surgery, which helps maintain stable knee joint function and improve the quality of life of patients [4]. However, there is a higher risk of refracture after surgery due to the patient's own osteoporosis together with the reduction of bone mass and activity. In this regard, standardized adjuvant treatment after surgery should be urgently addressed. Calcitriol is a basic drug for the treatment of osteoporosis, which is beneficial to the absorption of calcium in the intestine and intake of calcium [5]. Zoledronic acid, a special type

of bisphosphonate, inhibits the function of osteoclasts, reduces bone resorption, and enhances the quality of vertebral bone [6]. Nevertheless, the combination of the two has yet been investigated. Accordingly, this study was designed to explore the combination of calcitriol and zoledronic acid in osteoporosis surgery by analyzing 60 cases of diabetic osteoporosis patients with knee joint posterior cruciate ligament tibial avulsion fractures.

2. Study Design and Participants

2.1. Participants. Totally 60 cases of diabetic osteoporosis patients undergoing surgery for avulsion fractures of the posterior cruciate ligament of the knee in our hospital from January 2020 to January 2022 were selected and randomized at a ration 1 : 1 via random envelopes into the observation group (male : female = 16 : 14; aged 43-78 years old (62.59 ± 7.32) years; body mass index (54.32 ± 5.03) kg (44~75 kg); glycosylated hemoglobin: (6.49 ± 2.22) %, (6.51 ± 2.10) %; the cause of fracture: 15 cases of sports injury, 7 cases of traffic accidents, 6 cases of accidental falls, and 2 cases of others) and the control group (male : female = 17 : 13; aged 40-77 (62.31 ± 7.57) years old; body mass index (54.28 ± 5.10) kg (43~78 kg); the cause of fracture: 14 cases of sports injuries, 7 cases of traffic accidents, 7 cases of accidental falls, and 2 cases of others). The baseline information were well balanced in the two groups ($p > 0.05$).

2.2. Inclusion and Exclusion Criteria. Inclusion criteria were as follows: (1) the patients were diagnosed with osteoporosis by X-ray diagnosis and imaging examination [5], and all underwent tibial avulsion fractures of the posterior cruciate ligament of the knee joint; (2) met the diagnostic criteria of WHO diabetes in 1999, (3) patients and their family members were informed of the purpose and significance of the study before the study, signed the consent form on the premise of understanding the purpose of the study, and the medical ethics committee authorized the study before the commencement of the study, (4) with normal communication ability, and (5) with complete clinical data. Exclusion criteria were as follows: (1) with damaged vital organs; (2) with mental disorders or unconsciousness; (3) cancer patients; (4) with other types of fractures; (5) poor coordination or unable to follow the rules of the study; (6) allergies or intolerance to the study drugs; (7) with immune system diseases or abnormal blood tests; and (8) with thyroid disease, osteoarthritis, or rheumatoid arthritis, which can cause osteoporosis.

2.3. Methods. All patients were treated with routine control of blood glucose. Fasting blood glucose was measured once a week to ensure good blood glucose control. The control group was as follows: patients were treated with calcitriol capsules (CHIN TENG Pharmaceutical Industrial Co., Ltd., approval number HC20171016, specification: 0.25 μg × 10 s) after operation, at a dose of 0.25 μg each time, 1 time/d. The observation group was as follows: on the basis of the control group, zoledronic acid injection (Novartis Pharma Stein AG, approval number H20123153, specification: 100 mL: 5 mg (Yigu)) dissolved with 100 mL normal saline was administered via intravenous infusion, at a speed of 15 minutes or more, and the treatment was performed once in a year.

2.4. Observation Index. After a year of treatment, the improvement of the patient's bone mineral density and bone metabolism index before and after treatment was detected; the pain degree and the improvement of knee joint function were evaluated; whether the patient has refracture after operation was observed. (1) The bone density test mainly includes the greater trochanter and the neck of the femur, using the South Korean Auster dual-energy X-ray bone densitometer EXA-3000 (Shanghai Sanwei Medical Equipment Co., Ltd.). (2) 3 mL fasting in the morning peripheral venous blood was collected and centrifuged at 3000 r/min, and then the samples were processed for a total of 10 minutes to isolate the serum. Serum PINP indicators and β-CTX were detected by chemiluminescence immunoassay, and the kit was purchased from Shanghai Qiming Biotechnology Co., Ltd. (3) The VAS scale was used to evaluate the degree of pain in patients. The scale was marked on a 10 cm moving scale, and the left and right ends represent, respectively, no pain (0 point) and severe pain (10 points), mild pain (1 to 3 points): slight pain but does not affect sleep and life and can be tolerated; moderate pain (4 to 6 points): obvious pain and need to use analgesics to help sleep; and severe pain (7 to 10 points): severe pain and intolerable, seriously affects sleep, and even results in passive posture and neurological disorders [6]. (4) Lysholm scale was used to evaluate knee joint function, including claudication, support, instability, and swelling and other 8 items. The total score is 100 points. A score of <70 indicates that the knee joint function is affected. A higher score indicates better knee joint functions [7]. (5) One year after treatment, all patients underwent X-ray examination to assess the rate of re-fracture. All the above indicators were collected by researcher blind to the grouping.

2.5. Statistical Analysis. Statistical analysis was done by using SPSS22.0 software package. The counting data and measurement data were expressed as (%) and ($x \pm s$), respectively, and processed using X^2 and t-test, respectively. A p value of <0.05 indicates that the difference is statistically significant.

3. Results

3.1. Comparison of the Bone Mineral Density. Both groups showed an increased bone mineral density after treatment, and the increase value in the observation group was more notable ($p < 0.05$). Before treatment, no distinctive difference was observed in bone mineral density between the two groups ($p > 0.05$), see Table 1.

3.2. Comparison of Bone Metabolism Indexes. The β-CTX and PINP indexes of patients in the two groups were not statistically different before treatment ($p > 0.05$). After treatment, the indexes in two groups were lower than the

Table 1: Comparison of bone mineral density between the two groups ($\bar{x} \pm s$, mg/cm^3).

Groups	n	Greater trochanter		Femoral neck	
		Before treatment	After treatment	Before treatment	After treatment
Observation group	30	0.63 ± 0.02	0.86 ± 0.13*	0.65 ± 0.06	0.89 ± 0.14*
Control group	30	0.62 ± 0.03	0.75 ± 0.14*	0.63 ± 0.05	0.73 ± 0.16*
t	/	1.519	3.154	1.403	4.122
p	/	0.134	0.003	0.166	<0.001

Note: compared with the same group before treatment, $^*p < 0.05$.

Table 2: Comparison of bone metabolism indexes between the two groups ($\bar{x} \pm s$).

Groups	n	β-CTX (ng/mL)		PINP (ng/mL)	
		Before treatment	After treatment	Before treatment	After treatment
Observation group	30	0.47 ± 0.03	0.20 ± 0.02*	38.26 ± 3.04	15.05 ± 2.15*
Control group	30	0.45 ± 0.09	0.27 ± 0.04*	38.37 ± 3.18	19.54 ± 2.36*
t	/	1.155	8.573	0.137	7.703
p	/	0.253	<0.001	0.892	<0.001

Note: compared with the same group before treatment, $^*p < 0.05$.

Table 3: Comparison of VAS scores and Lysholm scores between the two groups ($\bar{x} \pm s$, point).

Groups	n	VAS		Lysholm	
		Before treatment	After treatment	Before treatment	After treatment
Observation group	30	6.32 ± 1.04	1.84 ± 0.14*	48.94 ± 4.43	78.42 ± 6.57*
Control group	30	6.29 ± 1.01	2.96 ± 0.23*	49.32 ± 4.52	68.34 ± 5.77*
t	/	0.113	22.783	0.329	6.314
p	/	0.910	<0.001	0.743	<0.001

Note: compared with the same group before treatment, $^*p < 0.05$.

Table 4: Comparison of the incidence of refracture between the two groups (%).

Groups	n	Number of refractures	Ratio
Observation group	30	2	6.7
Control group	30	8	26.7
X^2	/	4.320	
p	/	0.038	

corresponding values before treatment, with significant reduction in the observation group ($p < 0.05$), as shown in Table 2.

3.3. Comparison of VAS Scores and Lysholm Scores. After treatment, significant decrease was observed in VAS scores in both groups, whereas significant increase was observed in Lysholm scores when compared to those before treatment (all $p < 0.05$), and the changes was more greater in the observation group versus control group (all $p < 0.05$), see Table 3.

3.4. Comparison of the Incidence of Refracture. The observation group had fewer number of refractures than the control group (2 cases vs. 8 cases) ($p < 0.05$, Table 4).

4. Discussion

As people ages, the metabolic function decreases; also, less amount of exercise and changes in dietary structure results in bone density decline. All these easily lead to diabetic osteoporosis. Diabetic osteoporosis, with insidious clinical manifestations in the early stage, can be painful and easy to fracture as the disease progresses. Among them, posterior cruciate ligament tibial attachment avulsion fracture is a very common type, which not only negatively affects knee joint function but also accelerates the degeneration of the knee joint [8]. To our best understanding, early surgery benefits fracture reduction and prognosis of patients. In recent years, studies have found that patients with posterior cruciate ligament tibial attachment avulsion fractures accounts for 70% to 80%, which is presumably related to postoperative fractures and loosening of the prosthesis. Knowingly, osteoporosis patients suffer reduced bone mass after surgery and stress changes. Therefore, despite the improved motor function, the diabetic osteoporosis has not been fundamentally resolved. Therefore, postoperative treatments need to be supplemented to improve patient prognosis and prevent refracture.

Normally, diabetic osteoporosis patients suffer pain after surgery and require immobilization, during which bone loss is likely to occur, and thus bone density enhancement should be accordingly emphasized to accelerate the recovery of

patients' mobility. Calcitriol, a metabolite, is a commonly used drug for the treatment of osteoporosis and mainly metabolized by the liver and kidneys. Its product 1-25 dihydroxyvitamin D3 can promote the absorption of calcium and regulate the balance of Ca2+, which is conducive to fracture synthesis, promotes the increase of bone density and bone mass by stimulating the activity of osteoblasts, and plays a role in alleviating osteoporosis [9]. However, the single use of calcitriol yields limited effectiveness, and adverse reactions such as hypercalcemia and malnutrition are prone to occur. In this study, the observation group was treated with zoledronic acid plus alcitriol, and the results were promising. As a bisphosphonate drug, after being absorbed by osteoclasts, zoledronic acid inhibits the activity and synthesis of osteoclasts, accelerates their apoptosis, reduces the number of osteoclasts, and significantly improves bone resorption. Additionally, after the drug is combined with hydroxyapatite crystals, it can effectively block the adsorption of osteoclasts to the bone surface, inhibit its biological activity on the bone surface, reduce bone resorption, and promote the improvement of bone density [10]. Remarkably, the results of this study found that the two groups of patients had increased greater trochanter and femoral neck bone density after treatment, suggesting that both methods are effective in improving bone density. Interestingly, the increase in the observation group is greater, indicating that the combination of zoledronic acid generates more excellent results.

Previous study pointed out that most patients with diabetic osteoporosis have abnormal bone metabolism. As important markers of bone formation in the human body, β-CTX and PINP are highly expressed in patients with osteoporosis, and it has been used in the evaluation of osteoporosis [11–13]. In this study, the observation group outperformed the control group in the improvement of bone metabolism indicators, confirming the effect of zoledronic acid in improving the level of bone metabolism. Zoledronic acid can directly acts on the surface of bones, ensuing hydroxyphosphoric lime crystals to deposit on the bone, which is conducive to the formation of new bone, healing of fractures, and pain relief and prevention of refractures. According to our study results, superior performance was observed with respect to VAS score and Lysholm score in the observation group, with lower incidence of refracture, indicating a good safety profile. However, the present study conclusions might be moderated to null due to the limited experimental duration and smaller sample size. Therefore, further studies with larger sample size and longer follow-up are required to verify and replicate our results.

Taken together, the combination of calcitriol and zoledronic acid is an alternative for patients with diabetic osteoporosis knee joint posterior cruciate ligament tibial anchor avulsion fractures, with respect to the improvement of bone density and bone metabolism, pain relief, and knee joint function enhancement and reduction of refracture risk.

Data Availability

The datasets used during the present study are available from the corresponding author upon reasonable request.

Conflicts of Interest

The authors declare that they have no conflict of interest.

Authors' Contributions

Qingchang Hu and Qi Wang contributed equally to this work.

Acknowledgments

This research was supported by the "Intermediate and long-term clinical efficacy observation of new type of fixed support bone plate fixation and reconstruction and arthroscopic anchor fixation for repair of posterior cruciate ligament tibial avulsion fractures of the knee joint."

References

[1] C. E. Murray and C. M. Coleman, "Impact of diabetes mellitus on bone health," *International Journal of Molecular Sciences*, vol. 20, no. 19, p. 4873, 2019.

[2] S. Mohsin, S. Kaimala, J. J. Sunny, E. Adeghate, and E. M. Brown, "Type 2 diabetes mellitus increases the risk to hip fracture in postmenopausal osteoporosis by deteriorating the trabecular bone microarchitecture and bone mass," *Journal Diabetes Research*, vol. 2019, article 3876957, 2019.

[3] R. Ma, R. Zhu, L. Wang et al., "Diabetic osteoporosis: a review of its traditional Chinese medicinal use and clinical and preclinical research," *Evidence-based Complementary and Alternative Medicine*, vol. 2016, Article ID 3218313, 13 pages, 2016.

[4] C. Weibing, D. Yong, Y. Chunmei et al., "The clinical effect of anchoring internal fixation in the treatment of posterior cruciate ligament tibial avulsion fractures," *Chinese and Foreign Medicine*, vol. 38, no. 28, 2019.

[5] K. Uenishi, M. Tokiwa, S. Kato, and M. Shiraki, "Stimulation of intestinal calcium absorption by orally administrated vitamin D3 compounds: a prospective open-label randomized trial in osteoporosis," *Osteoporosis International*, vol. 29, no. 3, pp. 723–732, 2018.

[6] Q. Wei and L. Xingye, "Two-year follow-up of bone mineral density and bone metabolism markers in elderly patients with osteoporotic intertrochanteric fractures after hip replacement with zoledronic acid intervention," *Chinese Tissue Engineering Research*, vol. 25, no. 33, pp. 5265–5272, 2021.

[7] Osteoporosis and Bone Mineral Disease Branch of Chinese Medical Association, "Guidelines for the diagnosis and treatment of primary osteoporosis (2017)," *Chinese Journal of Practical Internal Medicine*, vol. 38, no. 2, pp. 127–150, 2018.

[8] H. Chuan, Y. Qin, C. Qihui et al., "The effect of zoledronic acid on VAS score and bone mineral density after PKP surgery for severe osteoporotic lumbar fractures," *Journal of Cervical and Lumbar Pain*, vol. 39, no. 6, pp. 712–714, 2018.

[9] W. Zhao Zongquan T. Z. Yihong et al., "Epidemiological investigation of senile osteoporosis and research on preventive measures," *Chinese Journal of Osteoporosis*, vol. 25, no. 7, pp. 994–997, 2019.

[10] L. Yuhang, Z. Yongming, and W. Jianhua, "The effect of zoledronate sodium combined with calcitriol in the treatment of primary osteoporosis," *Chinese Electronic Journal of Geriatric Orthopedics and Rehabilitation*, vol. 5, no. 4, pp. 206–210, 2019.

[11] Y. Weike, J. Ruiping, W. Mingjing et al., "The effect of anti-osteoporosis treatment on the clinical efficacy of knee osteoarthritis patients after total knee arthroplasty," *Journal of Xinxiang Medical College*, vol. 37, no. 12, pp. 1147–1151, 2020.

[12] J. Xie, S. Li, L. Xiao et al., "Zoledronic acid ameliorates the effects of secondary osteoporosis in rheumatoid arthritis patients," *Journal of Orthopaedic Surgery and Research*, vol. 14, no. 1, p. 421, 2019.

[13] L. Chunyang, Z. Hongtao, and Z. Kang, "Correlation analysis of serum PINP, β-CTX levels and recurrence of vertebral collapse after osteoporotic vertebral compression fracture," *Chinese Journal of Bone and Joint Injury*, vol. 35, no. 9, pp. 951–953, 2020.

Hindawi
Disease Markers
Volume 2022, Article ID 8326767, 5 pages
https://doi.org/10.1155/2022/8326767

Research Article

Effects of Metformin on Renal Function, Cardiac Function, and Inflammatory Response in Diabetic Nephropathy and Its Protective Mechanism

Zhiping Zhang,[1] Hongyu Dong,[2] Jiaqi Chen,[1] Min Yin,[1] and Feng Liu[1]

[1]*Department of Nephrology, China-Japan Union Hospital of Jilin University, Changchun, China*
[2]*Department of Rheumatology and Immunology, Shijingshan Teaching Hospital of Capital Medical University, Beijing Shijingshan Hospital, Beijing 100043, China*

Correspondence should be addressed to Hongyu Dong; hoyud@163.cm and Feng Liu; f_liu@jlu.edu.cn

Received 27 January 2022; Revised 13 May 2022; Accepted 20 May 2022; Published 3 June 2022

Academic Editor: Liu Jinhui

Objective. To investigate the effect of metformin on renal function, cardiac function, and inflammatory response in diabetic nephropathy and its protective mechanism. *Methods*. A total of 88 patients with diabetic nephropathy who were admitted to our hospital from April 2019 to October 2020 were recruited and grouped according to different treatment methods, namely, the experimental group ($n = 44$) and the control group ($n = 44$). The patients in the experimental group were treated with metformin, and the patients in the control group were treated with liraglutide injection (nonmetformin). Left ventricular end-diastolic diameter (LVEDD), left ventricular ejection fraction (LVEF), left ventricular end-systolic diameter (LVESD), and inflammatory response (hs-CRP, TNF-α, IL-6) were compared. *Results*. Compared with corresponding values before treatment, BUN, Scr, hs-CRP, TNF-α, IL-6, LVEDD, and LVESD were decreased after treatment, whereas LVEF was increased (all $P < 0.05$), with significant change in the experimental group (all $P < 0.001$). *Conclusion*. Metformin can effectively improve the level of renal function and cardiac function in patients with diabetic nephropathy and help patients control and reduce the body's inflammatory response, and its therapeutic efficacy is superior to that of liraglutide injection.

1. Introduction

Type 2 diabetes is one of the endocrine diseases characterized by elevated blood sugar, which is ascribed to impaired biological effects of the human body or defective insulin secretion. Recent years witness a rising incidence of type 2 diabetes, with the improvement of people's living standards. Delayed and ineffective treatment gives rise to complications of the heart, kidneys, and other organs, among which diabetic nephropathy is of higher occurrence and is associated with renal failure. Consequently, early intervention is required to curb the development of the disease [1, 2]. Diabetic hyperglycemia may either directly induce nephropathy or indirectly induce nephropathy by altering hemodynamics and also induce protein kinase C (PKC) activity, increase glycation end products, and promote the generation of triacylglycerol. In addition, hyperglycemia can also lead to changes in hemodynamics, causing glomerular filtration, shear stress, and microalbuminuria. These changes stimulate resident kidney cells to produce more TGF-β1, which in turn downregulates glucose transporter 1 and increases intracellular glucose transport and D-glucose uptake. TGF-β1 causes excessive accumulation of interstitial proteins (collagens I, II, III, and IV; fibronectin; and laminin) in the glomerulus, resulting in mesangial expansion and thickness of glomerular basement membrane and thereby changing the structure of the nephron. At present, the incidence of nephropathy in type 2 diabetic patients in China is as high as 30-50%. It is worth noting that there remains no cure to delay the progression of diabetic nephropathy. Additionally, a US study revealed a higher prevalence of diabetic nephropathy despite the effective control of cardiovascular complications, imposing substantial health care and

economic burden. Liraglutide is a long-acting glucagon-like peptide 1 (GLP-1) analog to lower blood sugar and inhibit glucagon secretion by promoting insulin release. Metformin is one of the commonly used drugs for the treatment of diabetes, and its main mechanism of action is to improve insulin sensitivity by inhibiting intestinal absorption of glucose, increase glucose utilization, and then lower blood sugar levels, with good safety profile [3, 4]. However, there are few related studies on its impact on renal function, cardiac function, and inflammatory response and its protective mechanism [5–7]. Accordingly, the principal aim of the present study was to explore the effects of metformin on renal function, cardiac function, and inflammatory response in diabetic nephropathy and its protective mechanism.

2. Materials and Methods

2.1. Baseline Data. A total of 88 patients with diabetic nephropathy who were treated in our hospital from April 2019 to October 2020 were assigned into groups according to different treatment methods, namely, the experimental group ($n = 44$) and the control group ($n = 44$). The study protocol was approved by the Ethics Committee of China-Japan Union Hospital of Jilin University (approval no. 60301-198), and all the subjects signed the informed consent and voluntarily participated in the clinical trial. In the experimental group, there were 24 males and 20 females; aged between 60 and 80 years; the disease duration was between 5 and 14 years. In the control group, there were 23 males and 21 females; the age ranged from 60 to 79 years, and the disease duration was between 5 and 14 years. The baseline data were similar in the two groups (Table 1).

2.2. Inclusion and Exclusion Criteria. The participants were eligible if they met the following criteria: (1) met the diagnostic criteria for diabetic nephropathy; (2) had complete medical data; (3) had normal cognition and good coordination; (4) aged 18-70 years; (5) used stable dose of metformin for more than 3 months; (6) HbA1c 7.0%-10.0%, no significant change in body weight at least 12 weeks before screening; (7) showing left ventricular ejection fraction (LVEF) > 50% by echocardiography; and (8) agreed to continue to maintain the previous diet and exercise habits throughout the study process, not using antihypertensive drugs such as statin lipid-lowering drugs and angiotensin-converting enzyme inhibitor (ACEI)/angiotensin II receptor antagonists during treatment (ARB). Patients were assessed as ineligible if they (1) had mental disorder; (2) had heart, liver, and renal failure; (3) received other clinical trials recently; (4) withdrew from the study; (5) had chronic complications of diabetes with notable clinical significance, such as proliferative retinopathy; (6) have had or are currently suffering from ischemic cardiovascular and cerebrovascular disease or peripheral vascular disease; (7) had systolic blood pressure > 160 mm within the last 12 weeks before screening Hg (1 mm Hg = 0.133 kPa) and/or diastolic blood pressure>100 mm Hg; (8) had a history of pancreatic or thyroid disease; and (9) had type 2 diabetes mellitus complicated with pregnancy.

2.3. Methods. Both groups of patients received medication for 4 months, with strict diet and exercise management during the period. The patients in the experimental group were treated with metformin (approval no. H20023370, specification: 0.5 g/tablet), 1 tablet/time, 3 times/d. The patients in the control group were subcutaneously injected with liraglutide injection (produced by Novo Nordisk, Denmark, approval no. J20160037, specification: 3 ml: 18 mg), 0.6 g/time, 1 time/d.

2.4. Outcomes

2.4.1. Renal Function Indicators. Blood urea nitrogen (BUN) and serum creatinine (Scr) were detected in the two groups of patients. The venous blood was collected and centrifuged at a speed of 1000 r/min and a radius of 10 cm for 5 min, and then, the supernatant was secured. The urea nitrogen (BUN) and serum creatinine (Scr) values were detected by an automatic biochemical method. The detection kit and the supporting kit were purchased from Nanjing Biyuntian Biological Testing Company, and the microcentrifuge HITETIC was purchased from Shanghai Precision Instrument Co., Ltd.

2.4.2. Cardiac Function Indicators. The color Doppler ultrasound diagnostic instrument purchased from Beijing Beiden Medical Co., Ltd. was used to detect the cardiac function indicators of patients, including left ventricular end-diastolic diameter (LVEDD), left ventricular end-systolic diameter (LVESD), left ventricular end-diastolic diameter (LVESD), left ventricular end-diastolic diameter (LVESD), and ventricular ejection fraction (LVEF).

2.4.3. Inflammatory Response Indicators. 3 mL of venous blood was collected from patients before and after treatment, and high-sensitivity C-reactive protein (hs-CRP), tumor necrosis factor-α (TNF-α), and interleukin-6 (IL-6) monoclonal antibodies were added. Monoclonal antibody was mixed and washed with PBS for 5 min. According to the ratio of 1 : 500, 5 mL of human-sheep-labeled primary antibody was added and left overnight at 4°C; then, it was washed 3 times with PBS buffer, 5 min each time, and 2 mL of mouse-derived secondary antibody (1 : 1000) was added; finally, it was left at room temperature for 2 hours and washed with PBS buffer for 5 minutes. The chromogenic substrate horseradish peroxidase was added to make the colorless chromogenic reagent blue, and the stop buffer was added to make it yellow. OD values were measured at 450 nm.

2.5. Statistical Analysis. All data analyses were performed with SPSS22.0. The measurement data are expressed as $x \pm s$, and two independent sample t-tests were used for comparison between groups, and a paired t-test was used for comparison within groups; the count data are expressed as the number of cases (rate) and analyzed by a chi-square test. Statistical significance was set at $P < 0.05$.

3. Results

3.1. Renal Function. There was no significant difference in BUN and Scr between the two groups before treatment ($P > 0.05$). After treatment, BUN and Scr were lower than the

Table 1: Patients' characteristic profile ($x \pm s$).

Index	Experimental group ($n = 44$)	Control group ($n = 44$)	t	P
Average age (years)	66.42 ± 3.72	66.10 ± 3.69	1.441	0.531
Average disease duration (years)	7.85 ± 2.11	7.62 ± 2.01	2.475	0.634
Urine albumin/creatinine ratio (ACR, mg/g)	280.47 ± 33.54	281.21 ± 32.69	5.245	0.548
Fasting blood glucose (mmol/L)	7.75 ± 2.40	7.76 ± 2.38	3.564	0.685
HbA1c (%)	8.54 ± 2.06	8.48 ± 2.11	2.475	0.365
Triglycerides (TG, mmol/L)	2.49 ± 0.72	2.47 ± 0.68	1.454	0.254
Total cholesterol (TC, mmol/L)	4.75 ± 1.03	4.72 ± 1.10	3.457	0.541
Low-density lipoprotein cholesterol (LDL-C, mmol/L)	3.42 ± 0.91	3.38 ± 0.89	5.456	0.477
High-density lipoprotein cholesterol (HDL-C, mmol/L)	1.12 ± 0.21	1.14 ± 0.19	1.045	0.698
Serum uric acid (mmol/L)	360.52 ± 91.89	360.61 ± 92.87	3.745	0.371
AST (U/L)	28.58 ± 11.64	28.21 ± 10.94	2.475	0.654
ALT (U/L)	26.45 ± 11.14	26.78 ± 12.36	2.315	0.638
Glomerular filtration rate (GFR [$ml^{-1}\,min^{-11}\,(1.73\,m^2)^{-11}$])	78.13 ± 26.11	77.87 ± 25.96	1.457	0.638

corresponding values before treatment ($P < 0.05$); the decrease was greater in the experimental group as compared with the control group [BUN (8.63 ± 2.07) and Scr (72.42 ± 16.78) vs. BUN (12.26 ± 2.93) and Scr (89.51 ± 23.26)] ($P < 0.001$); see Table 2.

3.2. Cardiac Function. There was no significant difference in LVEDD, LVEF, and LVESD between the two groups before treatment ($P > 0.05$). After treatment, in the experimental group, LVEDD was53.27 ± 1.02, LVEF was53.51 ± 1.24, and LVESD was51.15 ± 0.65, and in the control group, LVEDD was56.02 ± 1.39, LVEF was49.06 ± 1.37, and LVESD was54.13 ± 1.13. Overall, LVEDD and LVESD were decreased, and LVEF was increased in both groups ($P < 0.05$) after treatment, with greater change in the experimental group ($P < 0.001$); see Table 3.

3.3. Comparison of Inflammatory Responses. There was no significant difference in hs-CRP, TNF-α, and IL-6 between the two groups before treatment ($P > 0.05$); after treatment, in the experimental group, hs-CRP was9.08 ± 1.12, TNF-α was14.51 ± 1.24, and IL-6 was11.15 ± 1.45; in the control group, hs-CRP was11.14 ± 1.19, TNF-α was19.06 ± 1.37, and IL-6 was16.84 ± 1.22. Overall, hs-CRP, TNF-α, and IL-6 were lower than the corresponding values before treatment ($P < 0.05$), with lower results in the experimental group ($P < 0.001$), as shown in Table 4.

4. Discussion

The main clinical manifestations of diabetic patients include polyphagia, polydipsia, polyuria, and weight loss. Delayed treatment might lead to metabolic disorders such as abnormal amount of carbohydrates, electrolytes, proteins, and fats, impairing organs such as the kidneys and resulting in diabetic nephropathy that can cause renal failure. As a result, early intervention is an urgent to prevent the development of the disease [8, 9]. In severe cases, diabetic nephropathy can even cause death and serves as the main contributor to death in patients with diabetes [10–12]. Metformin has been confirmed to be an effective alternative in early diabetic nephropathy [13, 14]. To our knowledge, the nephroprotective effect of metformin is closely related to its inhibition of Adenosine Monophosphate-Activated Protein Kinase (AMPK)/mammalian target of rapamycin (mTOR) signaling pathway. DeFronzo et al. [15] believed that metformin, as a first-line oral hypoglycemic drug, not only acts as a hypoglycemic agent but also acts as an AMPK activator, intervening in the pathological development process of the abovementioned diabetic nephropathy by activating the AMPK signaling pathway, thereby exerting a renal protective effect and delaying the diabetic nephropathy development; Klotho is an antiaging gene, and its expressed klotho protein is produced in the distal convoluted tubules of the kidney. With the progression of kidney disease, the expression of klotho protein in patients with diabetic nephropathy decreases, and the decrease of klotho can activate the mTOR signaling pathway and aggravate kidney damage. In this study, we compared the renal function indexes of the patients in the experimental group before and after treatment. The results showed that after treatment, BUN and Scr were lower than the corresponding values before treatment; the decrease was greater in the experimental group as compared with the control group. These findings suggest that metformin is effective in the improvement of renal function. The possible explanation is that metformin regulates the mTOR pathway by upregulating klotho and protects renal tubular cells, thereby delaying renal progression in patients with diabetic nephropathy. Diabetic nephropathy is a chronic low-grade inflammatory disease, and diabetic nephropathy and inflammatory response were closely correlated. CRP, one of the acute response phase proteins, can reflect the level of inflammation in the body and the progress of cerebrovascular disease; TNF-α and IL-6 are proinflammatory factors, both of which can promote the chemotaxis and adhesion of inflammatory factors, and adversely affect patients. Notably, we found that the inflammatory response (hs-CRP, TNF-α,

Table 2: Comparison of renal function indexes of patients ($x \pm s$).

Groups	n	BUN (mmol/L)		Scr (μmol/L)	
		Before treatment	After treatment	Before treatment	After treatment
Study group	44	16.33 ± 3.18	8.63 ± 2.07*	92.24 ± 18.08	72.42 ± 16.78*
Control group	44	16.28 ± 3.15	12.26 ± 2.93*	92.31 ± 17.99	89.51 ± 23.26*
t	—	0.074	-6.712	-0.018	-3.953
P	—	0.941	<0.001	0.986	<0.001

Note: compared with before treatment within the same group, $^*P < 0.05$.

Table 3: Comparison of cardiac function indexes of patients ($x \pm s$).

Groups	n	LVEDD (mm)		LVEF (%)		LVESD (mm)	
		Before treatment	After treatment	Before treatment	After treatment	Before treatment	After treatment
Study group	44	59.46 ± 3.08	53.27 ± 1.02*	47.44 ± 4.08	53.51 ± 1.24*	58.50 ± 2.09	51.15 ± 0.65*
Control group	44	59.39 ± 3.05	56.02 ± 1.39*	47.51 ± 3.99	49.06 ± 1.37*	58.49 ± 2.05	54.13 ± 1.13*
t	—	0.107	-10.58	-0.081	15.974	0.023	-15.163
P	—	0.915	<0.001	0.936	<0.001	0.982	<0.001

Note: compared with before treatment within the same group, $^*P < 0.05$.

Table 4: Comparison of inflammatory responses in patients ($x \pm s$).

Groups	n	hs-CRP (mg/L)		TNF-α (ng/L)		IL-6 (pg/mL)	
		Before treatment	After treatment	Before treatment	After treatment	Before treatment	After treatment
Study group	44	15.07 ± 0.72	9.08 ± 1.12*	27.44 ± 1.41	14.51 ± 1.24*	25.87 ± 2.14	11.15 ± 1.45*
Control group	44	15.05 ± 0.74	11.14 ± 1.19*	27.51 ± 1.39	19.06 ± 1.37*	25.93 ± 2.17	16.84 ± 1.22*
t	—	0.128	-8.362	-0.235	-16.333	-0.131	-19.918
P	—	0.898	<0.001	0.815	<0.001	0.896	<0.001

Note: compared with before treatment within the same group, $^*P < 0.05$.

and IL-6) of the patients in the experimental group was declined after treatment, indicating that metformin can effectively reduce the inflammatory response of the patients. It might be attributed to the fact that metformin can enhance insulin resistance, regulate blood lipids and blood pressure, and effectively reduce the chemotaxis and adhesion of inflammatory factors [15–18]. Similarly, several studies concluded that metformin dose-dependently upregulated catalase (CAT), NADPH quinone oxidoreductase (NQO1) and glutathione S-transferase (GSTα) mRNA expression in renal tissue, decreased Heme oxygenase 1 (HO-1), TNF-α, IL-6 mRNA expression, and transforming growth factor in blood β1 (TGF-β1) levels, indicating that metformin exerts renal protection by reducing the levels of renal oxidative stress, inflammation, and fibrosis [17, 18]. Liu et al. [13] also found that metformin reduced GRP78, eIF2α, and C/EBP homologous protein (CHOP) by activating AMPK and attenuated high glucose-induced oxidative stress in human proximal tubular epithelial cells. Mariano and Biancone [14] found that metformin activates AMPK, reduces the production of RAGE and ROS, and further reduces the expression of its downstream signal TGF-β1, thereby inhibiting tubular fibrosis. Since a number of studies have been conducted on the drug mechanism of metformin and are relatively complete, this study innovatively increased the discussion of cardiac function indicators on this basis. Relevant studies have shown that dimethicone has a good protective effect on the cardiovascular system, and the 2016 *European Heart Failure Guidelines* recommended dimethicone as the first-line drug for patients with diabetes and heart failure. Promisingly, we observed in the present study that the cardiac function indexes of the patients in the experimental group were significantly improved after treatment, suggesting that metformin could effectively improve the cardiac function of the patients such as LVEDD, left LVEF, and LVESD. Presumably, metformin reduces endothelial cell oxidative stress by improving insulin resistance, blood sugar, blood lipids, and other cardiovascular-related risk factors, thereby protecting vascular endothelial cell function and further reduce the occurrence of cardiovascular disease. Additionally, it can promote myocardial glucose uptake and further improve the insulin sensitivity, thereby reducing myocardial cell damage and boosting cardiac function [19–21].

In conclusion, metformin is a reliable drug to improve the renal function and cardiac function of patients with diabetic nephropathy and helps patients control and minimize inflammatory response, which is superior to liraglutide injection.

Data Availability

The datasets used during the present study are available from the corresponding author upon reasonable request.

Conflicts of Interest

The authors declare that they have no conflict of interest.

References

[1] E. Xiang, B. Han, Q. Zhang et al., "Human umbilical cord-derived mesenchymal stem cells prevent the progression of early diabetic nephropathy through inhibiting inflammation and fibrosis," *Stem Cell Research & Therapy*, vol. 11, no. 1, p. 336, 2020.

[2] X. X. Zhang, J. Kong, and K. Yun, "Prevalence of diabetic nephropathy among patients with type 2 diabetes mellitus in China: a meta-analysis of observational studies," *Journal Diabetes Research*, vol. 2020, p. 2315607, 2020.

[3] A. Deshmukh and P. Manjalkar, "Synergistic effect of micronutrients and metformin in alleviating diabetic nephropathy and cardiovascular dysfunctioning in diabetic rat," *Journal of Diabetes and Metabolic Disorders*, vol. 20, no. 1, pp. 533–541, 2021.

[4] X. Jiang, X. L. Ruan, Y. X. Xue, S. Yang, M. Shi, and L. N. Wang, "Metformin reduces the senescence of renal tubular epithelial cells in diabetic nephropathy via the MBNL1/miR-130a-3p/STAT3 pathway," *Oxidative Medicine and Cellular Longevity*, vol. 2020, Article ID 8708236, 2020.

[5] L. Agius, B. E. Ford, and S. S. Chachra, "The metformin mechanism on gluconeogenesis and AMPK activation: the metabolite perspective," *International Journal of Molecular Sciences*, vol. 21, no. 9, p. 3240, 2020.

[6] N. Apostolova, F. Iannantuoni, A. Gruevska, J. Muntane, M. Rocha, and V. M. Victor, "Mechanisms of action of metformin in type 2 diabetes: effects on mitochondria and leukocyte-endothelium interactions," *Redox Biology*, vol. 34, article 101517, 2020.

[7] K. Chen, Y. Li, Z. Guo, Y. Zeng, W. Zhang, and H. Wang, "Metformin: current clinical applications in nondiabetic patients with cancer," *Aging (Albany NY)*, vol. 12, no. 4, pp. 3993–4009, 2020.

[8] W. J. Huang, W. J. Liu, Y. H. Xiao et al., "Tripterygium and its extracts for diabetic nephropathy: efficacy and pharmacological mechanisms," *Biomedicine & Pharmacotherapy*, vol. 121, article 109599, 2020.

[9] N. U. Khan, J. Lin, X. Liu et al., "Insights into predicting diabetic nephropathy using urinary biomarkers," *Biochim Biophys Acta Proteins Proteom*, vol. 1868, no. 10, article 140475, 2020.

[10] S. Li, L. Zheng, J. Zhang, X. Liu, and Z. Wu, "Inhibition of ferroptosis by up-regulating Nrf2 delayed the progression of diabetic nephropathy," *Free Radical Biology & Medicine*, vol. 162, pp. 435–449, 2021.

[11] S. Rayego-Mateos, J. L. Morgado-Pascual, L. Opazo-Ríos et al., "Pathogenic pathways and therapeutic approaches targeting inflammation in diabetic nephropathy," *International Journal of Molecular Sciences*, vol. 21, no. 11, p. 3798, 2020.

[12] N. M. Selby and M. W. Taal, "An updated overview of diabetic nephropathy: diagnosis, prognosis, treatment goals and latest guidelines," *Diabetes, Obesity & Metabolism*, vol. 22, Suppl 1, pp. 3–15, 2020.

[13] X. Liu, D. Liu, Y. Shuai et al., "Effects of HuoxueJiangtang decoction alone or in combination with metformin on renal function and renal cortical mRNA expression in diabetic nephropathy rats," *Pharmaceutical Biology*, vol. 58, no. 1, pp. 1123–1130, 2020.

[14] F. Mariano and L. Biancone, "Metformin, chronic nephropathy and lactic acidosis: a multi-faceted issue for the nephrologist," *Journal of Nephrology*, vol. 34, no. 4, pp. 1127–1135, 2021.

[15] R. DeFronzo, G. A. Fleming, K. Chen, and T. A. Bicsak, "Metformin-associated lactic acidosis: current perspectives on causes and risk," *Metabolism*, vol. 65, no. 2, pp. 20–29, 2016.

[16] M. Kodali, S. Attaluri, L. N. Madhu et al., "Metformin treatment in late middle age improves cognitive function with alleviation of microglial activation and enhancement of autophagy in the hippocampus," *Aging Cell*, vol. 20, no. 2, article e13277, 2021.

[17] C. W. Ng, A. A. Jiang, E. M. S. Toh et al., "Metformin and colorectal cancer: a systematic review, meta-analysis and meta-regression," *International Journal of Colorectal Disease*, vol. 35, no. 8, pp. 1501–1512, 2020.

[18] I. Pernicova and M. Korbonits, "Metformin—mode of action and clinical implications for diabetes and cancer," *Nature Reviews. Endocrinology*, vol. 10, no. 3, pp. 143–156, 2014.

[19] X. Meng, J. Ma, A. N. Kang, S. Y. Kang, H. W. Jung, and Y. K. Park, "A novel approach based on metabolomics coupled with intestinal flora analysis and network pharmacology to explain the mechanisms of action of bekhogainsam decoction in the improvement of symptoms of streptozotocin-induced diabetic nephropathy in mice," *Frontiers in Pharmacology*, vol. 11, p. 633, 2020.

[20] D. K. Mostafa, M. M. Khedr, M. K. Barakat, A. A. Abdellatif, and A. M. Elsharkawy, "Autophagy blockade mechanistically links proton pump inhibitors to worsened diabetic nephropathy and aborts the renoprotection of metformin/enalapril," *Life Sciences*, vol. 265, article 118818, 2021.

[21] H. Ren, Y. Shao, C. Wu, X. Ma, C. Lv, and Q. Wang, "Metformin alleviates oxidative stress and enhances autophagy in diabetic kidney disease via AMPK/SIRT1-FoxO1 pathway," *Molecular and Cellular Endocrinology*, vol. 500, article 110628, 2020.

Hindawi
Disease Markers
Volume 2022, Article ID 6900660, 7 pages
https://doi.org/10.1155/2022/6900660

Research Article

Role of EPO and TCF7L2 Gene Polymorphism Contribution to the Occurrence of Diabetic Retinopathy

Chao Liu,[1] Ga-Li Bai,[1] Ping Liu,[2] and Lin Wang[2]

[1]*Department of Ophthalmology, The Fourth Affiliated Hospital of Harbin Medical University, Harbin, 150001 Heilongjiang Province, China*
[2]*Department of Ophthalmology, The First Affiliated Hospital of Harbin Medical University, Harbin, 150001 Heilongjiang Province, China*

Correspondence should be addressed to Ping Liu; pingliu53@126.com and Lin Wang; wang_lin365@sina.cn

Received 30 December 2021; Revised 18 February 2022; Accepted 6 April 2022; Published 29 May 2022

Academic Editor: Yaoyao Bian

Objective: For studying the association of EPO (rs551238), EPO (rs1617640), and TCF7L2 (rs7903146) gene with diabetic retinopathy in Northern Chinese population. *Methods*: We conducted a case-control study, which enrolled 680 subjects and performed SNP genotyping and calculated allele frequencies. *Results*: When comparison was performed between DR patients and normal persons, the EPO (rs551238) AA genotype has a significant risk association with DR, and AC genotype has a significant protective association with DR. The EPO (rs551238) A allele has a significant risk association with DR, and C allele has a significant protective association with DR. When comparison was performed between DR patients and DM patients, the EPO (rs551238) CC genotype has a significant protective association with DR; the EPO (rs551238) A allele has a significant risk association with DR; and C allele has a significant protective association with DR. When comparison was performed between DR patients and normal persons, the EPO (rs1617640) GT genotype has a significant protective association with DR, and TT genotype has a significant risk association with DR. The EPO (rs1617640) G allele has a significant protective association with DR, and T allele has a significant risk association with DR. In addition, we found that TT genotype does not exist in rs7903146 of TCF7L2 in Chinese population so that the data could not be used. *Conclusions*: EPO (rs551238, rs1617640) genotype is a susceptible gene for DR in Chinese type 2 diabetic patients, especially the high-risk PDR.

1. Introduction

It is well known that the main complication of diabetes mellitus is diabetic retinopathy. The main reasons for loss of vision are complications of proliferative diabetic retinopathy (PDR) and diabetic maculopathy resulted by vitreous hemorrhage, tractional retinal detachment, and neovascular glaucoma. It is reported that compared to 2010, the number of patients with diabetes will increase 69% in developing countries and 20% in industrialized countries by 2030 [1].

Although most patients can not notice early retinal changes, over time, potentially vision-threatening retinal changes develop in patients with diabetes [2]. Diabetic retinopathy is the main microvascular complication of diabetes retinopathy, and 3%-4% of European are affected [3, 4]. In industrialized nations, diabetes mellitus is the main cause of blindness in working-age population [3]. There is about one-third of patients that have characteristics of diabetic retinopathy once diabetes mellitus is surely diagnosed.

It is reported that, in patients with type 1 diabetes, proliferative diabetic retinopathy is an independent marker of long-term nephropathy [5]. The incidence rate of DR is 25.2% in Chinese DM patients, and the ratio is 12.4% in patients who were primary diagnosed as type 2 DM. With the trend of younger diabetic patients in recent years, diabetic nephropathy and other complications have been effectively controlled. DR is the most common blind disease that affects the quality of life of diabetic patients. How to prevent and treat DR has always been a concern of people [3].

It is reported that EPO has the relationship with ischemic retinal disease such as PDR (7.8). The concentration of EPO in tissues is regulated by hypoxia, and it is a

multifunctional glucoprotein [6, 7]. The function of EPO is stimulating the formation of red blood cells and increasing their differentiation of erythrocyte precursors [8]. It is said that hypoxia is the main stimulus factor which regulates the role of erythrocyte [9, 10]. The EPO and its receptors are produced by a para-endocrine system in retina. It is suggested that EPO prevents neurons from apoptosis resulted by ischemic damage [10]. EPO also plays a role of stimulating the differentiation and migration of endothelial cells [11]. The EPO concentration in patients suffered from PDR was significantly higher than those normal persons [12]. There is a paper [12] reported that EPO is able to stimulate retinal angiogenesis in PDR, and EPO is activated locally in the retina.

Transcription factor 7-like2 (TCF7L2) belongs to T-cell-specific high-mobility group. It is reported that single-nucleotide polymorphism(SNP) in human TCF7L2 genes has a close relationship with occurrences of type 2 diabetes after extensive genome studies in numerous ethnic populations [13–15]. TCF7L2 single nucleotide polymorphisms lead to decreased β-cell function, including impaired insulin secretion and processing, and increased insulin resistance [16, 17]. However, the mechanism of TCF7L2 gene function and how its genetic polymorphism influence the susceptibility of type 2 diabetes has not been elucidated. There are several reports suggested that the expression of TCF7L2 is up-regulated in diabetic subjects [18].

In this study, we aimed to analyze the association of EPO (rs551238), EPO (rs1617640), and TCF7L2 (rs7903146) gene with DR in Northern Chinese population.

2. Methods

We strictly complied with the Declaration of Helsinki when performing the study, and all participants signed the informed consent forms. The research was approved by the Ethics Committee of the Eye Hospital of the First Clinical Hospital Affiliated Harbin Medical University, Harbin, China (No. HMU7703). The subjects were 320 Han Chinese patients with DR, 235 normal healthy controls, and 125 Han Chinese patients with DM (without DR). All selected subjects were patients who attended the Eye Hospital of the First Clinical Hospital Affiliated Harbin Medical University, Harbin, China, from April 2014 to January 2015.

All tested subjects are all Hei Longjiang Han Chinese people, and there are no blood relationship among the tested subjects. We strictly conform to American DM diagnosed standard and ensure the ages of all tested subjects are above or equal to 30 years old; courses of the DM are above or equal to 5 years. We detailed record the patients materials and medical history which contained age, gender, body length, body weight, condition of cigarette smoking and alcohol drinking, and course of the disease. We also measured the systolic pressure and diastolic pressure of patients.

All enrolled study cases all performed strict ophthalmology examination contained vision, slit lamp examination of anterior segment, and intraocular pressure. Fundus examination was performed by two skilled physicians using an ophthalmoscope after pupil dilation with Mydrin. If there was not pathology found in eyeground (microaneurysm, retinal hemorrhage, cotton-wool spot, formation of retinal neovascularization, vitreous hemorrhage), these patients will belong to DR group. Fundus fluorescein angiography (FFA) was performed in all patients diagnosed with DR. The eyeground condition of patients was considered at different stages in relation to DR classification criteria by two skillful doctors.

We also chose unrelated healthy subjects who were selected from the Health Examination Department of our hospital as ARC healthy controls. All patients and healthy controls were sex-, age-, and ethnically matched.

DR, diabetes, cataract, glaucoma, fundus oculi disease, hypertension, tumor and other related ocular diseases were not observed in the healthy control group. We performed full ophthalmic examination including visual acuity examination, slit lamp biomicroscope examination, lens examination, and fundus examination in all DR, DM patients, and healthy control subjects. Blood sampling and DNA extraction were also carried out.

Venous blood (2 ml) was collected in EDTA tubes from all DR, DM patients, and healthy controls. Genomic DNA was extracted from the collected blood using an Omega DNA blood extraction kit (Omega, USA) according to the manufacturer's instructions. All blood samples were stored in 1.5-ml Eppendorf tubes and then centrifuged at -20°C.

During SNP genotyping, based on earlier studies which suggested that EPO and TCF7L2 polymorphisms were related to DR and other age-related diseases, we chose EPO (rs551238), EPO (rs1617640), and TCF7L2 (rs7903146) as candidate SNPs. Amplification of the target DNA in EPO and TCF7L2 is analyzed by LDR assay using the primers as shown in Table 1. The EPO and TCF7L2 reactions were performed in a 15 μl reaction mixture containing 1 μl genomic DNA, 0.3 μl Taq enzymes (Fermentas Corporation, EP 0460), 0.15 μl primer mixture, 0.3 μl dNTPs (Fermentas Corporation, R0192), 1.5 μl $MgCl_2$, and 1.5 μl 10 × buffer for amplification of DNA. The conditions were as follows: initial denaturation at 94°C for 3 min followed by 35 cycles of denaturation at 94°C for 15 s, annealing at 62°C for 15 s, extension at 72°C for 30 s, and a final extension at 72°C for 3 min.

The ligation detection reaction (LDR) was performed in a 10 μl reaction mixture containing 3 μl PCR reaction product, 1 μl 10 × Taq DNA ligase buffer, 0.125 μl Taq DNA ligase (40 μ/μl, NEB Corporation M02081), and 0.01 μl probe (10p per strip). This was followed by 30 cycles at 94°C for 30 s and 60°C for 3 min. 1 μl extension products was obtained, and 8 μl loading sample was added. After denaturation at 95°C for 3 min, the mixture was immediately placed in an ice bath, and then, a sequencer (ABI 3730XL) was used. The probe sequences of the EPO and TCF7L2 genes are shown in Table 2.

Statistical analysis: In this study, the Chi-square test was used to assess the Hardy-Weinberg equilibrium. We directly counted the number of genotypes and alleles. SPSS (version 17.0, SPSS Inc., Chicago, IL, USA) was used to compare allele and genotype frequencies among DR, DM patients, and healthy controls. The comparison of genotypes and

Table 1: Primers used for LDR analysis of the EPO and TCF7L genes.

Rs number	Primers	Amplification bands
rs551238	CCAGGGTTGGCAGCTGTTACC TCTCACACAGCCTGTCTGACC	227 bp
rs1617640	AGCTAGGCTGCATTGCTGAGT CACCCATTTGACAGATGAGGA	219 bp
rs7903146	TGCCTCAAAACCTAGCACAGCT GTAGCAGTGAAGTGCCCAAGC	229 bp

the frequencies of alleles was analyzed by χ^2 test. Meanwhile, OR value and 95% confidence area (95% CI) were calculated. P value <0.05 was considered statistically significant.

3. Results

The results showed that the EPO and TCF7L2 genetic variants were in Hardy-Weinberg equilibrium both in DR patients and in the healthy controls. The PCR reaction products of EPO (rs551238), EPO (rs1617640), TCF7L2 (rs7903146) in ethidium bromide were stained with 1% agarose gel. The result is shown in Figure 1.

The primers used for LDR analysis of the EPO and TCF7L genes and probe sequences of the EPO and TCF7L genes are, respectively, shown in Table 1 and Table 2.

When comparison was performed between DR patients and normal persons, the EPO (rs551238) AA genotype has significant risk association with DR susceptibility with OR of 1.960 (1.374-2.795) ($P = 0$); AC genotype has a significant protective association with DR susceptibility with OR of 0.517 (0.360-0.742) ($P = 0.001$). The EPO (rs551238) A allele has a significant risk association with DR susceptibility with OR of 1.690 (1.248-2.288) ($P = 0.001$); C allele has a significant protective association with DR susceptibility with OR of 0.592 (0.437-0.801) ($P = 0.001$). The Bonferroni correction was performed ($P = 0.001 < 0.05$). The results are shown in Table 3.

When comparison was performed between DR patients and DM patients, the EPO (rs551238) CC genotype has a significant protective association with DR susceptibility with OR of 0.375 (0.138-1.022) ($P = 0.047$). The EPO (rs551238) A allele has a significant risk association with DR susceptibility with OR of 1.524 (1.052-2.206) ($P = 0.025$). C allele has a significant protective association with DR susceptibility with OR of 0.656 (0.453-0.950) ($P = 0.025$). The Bonferroni correction was performed ($P = 0.032 < 0.05$). The results are shown in Table 4.

When comparison was performed between DR patients and normal persons, the EPO (rs1617640) GT genotype has a significant protective association with DR susceptibility with OR of 0.649 (0.451-0.933) ($P = 0.019$); TT genotype has a significant risk association with DR susceptibility with OR of 1.594 (1.116-2.278) ($P = 0.010$). The EPO (rs1617640) G allele has a significant protective association with DR susceptibility with OR of 0.678 (0.498-0.923) ($P = 0.013$); T allele has a significant risk association with DR susceptibility with OR of 1.476 (1.084-2.010) ($P = 0.013$). The Bonferroni correction was performed ($P = 0.013 < 0.05$). The results are shown in Table 3.

When comparison was performed between DR patients and DM patients, there were no obvious differences in the EPO (rs1617640). The results are shown in Table 4.

In our study, we found TT genotype did not exist in rs7903146 of TCF7L2 in Chinese population so the data could not be used.

There was no obvious significance between normal persons and DM patients, and the table are shown in Table 5.

4. Discussion

We performed a case-control study of the three polymorphisms associated with DR in Heilongjiang Han Chinese populations. Our results showed that the SNP, EPO1 (rs551238), and EPO2 (rs1617640) were significantly associated with susceptibility to DR.

In response to anemia and hypoxia (26), EPO, which is a glycoprotein hormone, plays an important role in increasing the production of red blood cells, and EPO is produced in adult kidney and fetal liver.

Watanabe et al. suggested that EPO is an ischemia-induced angiogenic factor in both patient and animal models with PDR [12]. It is reported by Garcia-Ramirez et al. [19] that compared with nondiabetic controls, EPO is overexpressed in the retina of DM patients. Tong et al. [20] reported that rs1617640 in the expression of EPO play an important role in the occurrence of DM. However, about the relationship of rs551238, rs1617640, and DR, the related materials are still not sufficient. In our study, we dedicated to study the relationship among rs551238 and rs1617640 and the occurrence of DM and call into question the validity of association between rs551238, rs1617640, and DR.

The role of transcription factor 7-like 2(TCF7L2) is regulating fundamental processes such as growth of vascular and mediating pathological neovascularization in DM. In addition, TCF7L2 has an important role in the Wnt-signaling pathway [21]. There also is a study indicated that TCF7L2 gene has close relationship with macrovascular and microvascular complications [22]. There were many studies indicated that rs7903146 in TCF7L2 has a close relationship with type 2 DM [13, 23]. However, the mechanism of type 2 DM still remains unclear, and the association between TCF7L2 and DR has been conflicting [13, 22]. Here, we studied the role of TCF7L2 (rs7903146) in DR using a genetic association research.

The product of TCF7L2 is a transcription factor which has the function of activating genes downstream in Wnt signaling pathway of type 2 DR [24–27]. About how the TCF7L2 influence the susceptibility of DR needed to be elucidated. The results of our study show that the P ($P = 0$)

Table 2: Probe sequences of the EPO and TCF7L genes.

Rs number	Probe sequences
rs551238	CACCTTATTGACCAGCGTAGGCAGA-FAM-
rs1617640	GAGTGAGATTCCCAGAGCAGGAGACTTT-FAM-
rs7903146	TATATAATTTAATTGCCGTATGAGGCACTTT-FAM-

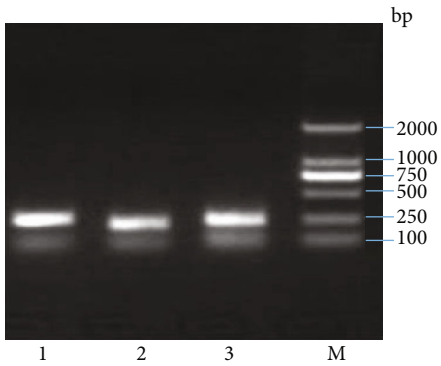

Figure 1: Ethidium bromide stained 1% agarose gel of products from PCR reactions using rs551238 primers, rs1617640 primers, and rs7903146 primers. Lanes 1 to 3: products from reactions with primers for rs551238, rs1617640, and rs7903146. Lane 4: molecular size standards.

value of the AA genotype of EPO1 (rs551238) was significantly increased, while the $P\,(P = 0)$ value of AC genotype of EPO1 (rs551238) was significantly decreased compared with controls. Our study also show that the $p\,(p = 0.001)$ value of the "A" allele of EPO1 (rs551238) was significantly increased, while the $p\,(p = 0.001)$ value of "C" allele of EPO1 (rs551238) was significantly decreased compared with controls. When comparison was performed between DR and DM patients, there were no obvious differences in genotype of AA, AC, and CC. The results still suggested that the $P\,(P = 0.025)$ value of the "A" allele of EPO1 (rs551238) was significantly increased, while the $p\,(p = 0.025)$ value of "C" allele of EPO1 (rs551238) was significantly decreased when comparison was performed between DR patients and DM patients.

The results of our study showed that the $p\,(p = 0.019)$ value of GT genotype of EPO2 (rs1617640) was significantly decreased compared with control. Our study also show that the $p\,(p = 0.010)$ value of TT genotype of EPO2 (rs1617640) was significantly increased compared with controls. Our study also show that the $p\,(p = 0.013)$ value of the "G" allele of EPO2 (rs1617640) was significantly decreased, while the $p\,(p = 0.013)$ value of "T" allele of EPO2 (rs1617640) was significantly increased. When comparison was performed between DR patients and DM patients, there are no obvious differences in genotype of :GG GT TT" and allele of "G" and "T."

When we studied the differences in rs7903146 among DR patients, DR patients, and normal persons, we found that "TT" genotype did not existed in Heilongjiang Chinese people. So the data studied TCF7L2 (rs7903146) was not balanced, and the data cannot elucidate the role of TCF7L2 (rs7903146) in occurrence of DR.

When comparison was performed between DM patients and normal persons, there are no obvious differences which suggested that EPO1 (rs551238), EPO2 (rs1617640), and TCF7L2 (rs7903146) did not play role in occurrence of DM, and the three SNPs are not signs of DM.

From our study, we found that allele "A" was the risk factor and allele "C" was the protective factor when compared between DR patients and normals, diabetics and normals in EPO1 (rs551238).

Our data showed that "G" allele plays a protective role, while "T" allele plays a risk role in occurrence of DR. However, when comparison was performed in DR and DM patients, there were no obvious differences existed in genotypes and alleles. We can see when a patient affected from DM, the "T" allele is not a risk factor for distinguishing DR and DM, but the "T" allele is really a significant sign for distinguishing DR patients and normal people. So we can concluded that if "T" allele is the main allele in a DM patient, we could not predict that he or she will suffer from DR, but at the least, the "T" allele is a risk signal for the DM patient, because it is a significant risk factor when comparison was performed between DR patients and normal people.

From our data, it can be seen that the TT genotype does not exist in the Han people of Heilongjiang, China, so the data is unbalanced. We can accurately determine which genotypes and alleles play a risk factor in the occurrence of DR, or we need a large number of samples to determine the role of TCF7L2 (rs7903146) in DR development.

To decrease the influencing factors in our research, we adopted measures verifying the study findings. We selected patients with DR and if complicated by other systemic or ophthalmology complications, we will exclude these patients. We adopted LDR assay to determine the genotype.

Similar to other gene polymorphism research, our study had some limitations. Firstly, the biological function of SNP, EPO1 (rs551238), EPO2 (rs1617640), and TCF7L2 (rs7903146) requires further investigation. Secondly, the size of the patient group in our study was relatively small, and the number of patient-control sample will influence the susceptibility of gene detection. In addition, we only recruited patients from the Han Chinese people, and other ethnic groups should be recruited in our future study. The results required in our study should perform a larger sample size which included other ethnic groups. Thirdly, a stratification analysis on the relationship between different ages of DR and the four gene polymorphisms should have been performed. Moreover, we calculated the odds ratio of different genotypes and alleles of the studied SNPs. The reference

Table 3: Frequences of genotypes and alleles of EPO and TCF7L genes polymorphisms in diabetes retinopathy patients and normal controls.

SNP	*Genotype DR (%)* Allele	*Normal controls (%)* ($n = 320$)		*p value*	*OR (95% CI)* ($n = 235$)
	AA	(71.88%) 230	(56.60%) 133	≤0.001	1.960 (1.374-2.795)
	AC	(25.63%) 82	(40.00%) 94	≤0.001	0.517 (0.360-0.742)
rs551238 (EPO1)	CC	(2.50%) 8	(3.40%) 8	0.529	0.728 (0.269-1.967)
	A	(97.50%) 312	(96.60%) 227	0.001	1.690 (1.248-2.288)
	C	(28.13.3%) 90	(47.66%) 112	0.001	0.592 (0.437-0.801)
	GG	(1.88%) 6	(2.98%) 7	0.396	0.622 (0.206-1.877)
	GT	(26.89%) 86	(36.17%) 85	0.019	0.649 (0.451-0.933)
rs1617640 (EPO2)	TT	(71.25%) 228	(60.85%) 143	0.01	1.594 (1.116-2.278)
	G	(28.75.3%) 92	(39.15%) 92	0.013	0.678 (0.498-0.923)
	T	(98.13%) 314	(97.02%) 228	0.013	1.476 (1.084-2.010)
	CC	(87.19%) 279	(94.89%) 223	0.002	0.366 (0.188-0.713)
	CT	(12.81%) 41	(5.11%) 12	0.002	2.731 (1.402-5.320)
rs7903146 (TCF7L2)	TT	(0.00) 0	(0.00) 0		
	C	(100.00%) 320	(100.00%) 235	0.003	0.383 (0.199-0.737)
	T	(12.81%) 41	(5.11%) 12	0.003	2.612 (1.357-5.028)

OR: odds ratio.

Table 4: Frequences of genotypes and alleles of EPO and TCF7L genes polymorphisms in diabetes retinopathy patients and diabetes mellitus patients.

SNP	*Genotype* Allele	*DR (%)* ($n = 320$)	*DM (%)*	*p value*	*OR (95% CI)* ($n = 125$)
	AA	(71.88%) 230	(63.20%) 79	0.074	1.488 (0.961-2.305)
	AC	(25.62%) 82	(30.40%) 38	0.308	0.789 (0.500-1.245)
rs551238 (EPO1)	CC	(2.50%) 8	(6.40%) 8	0.047	0.375 (0.138-1.022)
	A	(97.50%) 312	(78.4%) 196	0.025	1.524 (1.052-2.206)
	C	(29.13%) 90	(36.80%) 46	0.025	0.656 (0.453-0.950)
	GG	(1.88%) 6	(3.20%) 4	0.397	0.578 (0.160-2.084)
	GT	(26.88%) 86	(29.60%) 37	0.563	0.874 (0.554-1.380)
rs1617640 (EPO 2)	TT	(71.25%) 228	(67.20%) 84	0.402	1.210 (0.775-1.888)
	G	(28.75%) 92	(32.80%) 41	0.326	0.824 (0.559-1.214)
	T	(98.13%) 314	(96.80%) 121	0.326	1.214 (0.824-1.789)
	CC	(87.19%) 279	(96.00%) 120	0.006	0.284 (0.109-0.735)
	CT	(12.81%) 41	(4.00%) 5	0.006	3.527 (1.360-9.145)
rs7903146 (TCF7L2)	TT	(0) 0	(0) 0		
	C	(100.00%) 320	(100.00%) 120	0.008	0.298 (0.116-0.763)
	T	(12.81%) 41	(4.00%) 5	0.008	3.354 (1.310-8.588)

OR: odds ratio.

genotype or allele for each SNP for calculating the odds ratio should be analyzed in future investigations.

Overall, our study identify "A" allele of EPO1 (rs551238) as a risk factor and "T" allele of EPO2 (rs1617640) as a risk signal in occurrence of DR. In future studies, the biological functions of EPO1 (rs551238) and EPO2 (rs1617640), contributing to the occurrence of DR, should be evaluated. To our knowledge, the present study is the first report of an association among EPO1 (rs551238), EPO2 (rs1617640), and DR in a Han Chinese population. Meanwhile, it has been reported that EPO is associated with DR by regulating caspase-3 expression and oxidative stress [28]. EPO regulates the inner blood-retinal barrier in DR through repressing microglia phagocytosis by Src/Akt signaling [29]. The potential mechanism between the genotype of EPO with the risk of DR should be confirmed in future investigations.

Table 5: Frequences of genotypes and alleles of EPO and TCF7L genes polymorphisms in normal controls and diabetes mellitus patients.

SNP	*Genotype* Allele	*Normal controls (%)* ($n = 235$)	*DM (%)*	*p value*	*OR (95% CI)* ($n = 125$)
	AA	(56.60%) 133	(63.20%) 79	0.225	0.759 (0.486-1.186)
	AC	(40.00%) 94	(30.40%) 38	0.072	1.526 (0.962-2.422)
rs551238 (EPO1)	CC	(3.4%) 8	(6.40%) 8	0.189	0.515 (0.189-1.408)
	A	(95.60%) 227	(93.60%) 117	0.583	0.902 (0.623-1.304)
	C	(47.66.4%) 112	(36.80%) 46	0.583	1.109 (0.767-1.604)
	GG	(2.98%) 7	(3.20%) 4	0.908	0.929 (0.627-3.235)
	GT	(36.17%) 85	(29.60%) 37	0.148	1.409 (0.885-2.244)
rs1617640 (EPO 2)	TT	(60.85%) 143	(67.20%) 84	0.235	0.759 (0.481-1.197)
	G	(39.15%) 92	(32.80%) 41	0.328	1.216 (0.822-1.798)
	T	(97.02%) 228	(96.80%) 121	0.328	0.823 (0.556-1.217)
	CC	(94.89%) 223	(96.00%) 120	0.638	0.774 (0.266-2.250)
	CT	(5.11%) 12	(4.00%) 5	0.638	1.291 (0.444-3.725)
rs7903146 (TCF7L2)	TT	(0) 0	(0) 0		
	C	(100.00%) 235	(100.00%) 125	0.642	0.779 (0.271-2.236)
	T	(5.11%) 12	(4.00%) 5	0.642	1.284 (0.447-3.686)

Moreover, the investigations of the regulatory mechanisms underlying TCF7L2 are still limited, and the mechanism between the genotype of TCF7L2 with the risk of DR should be explored in the future.

Taken together, our finding demonstrated the independent contribution of EPO gene polymorphism to DR susceptibility in the Heilongjiang Han Chinese population. We hope that our study will establish background data for further investigation into the mechanism of EPO genes and the development of DR.

Data Availability

The datasets used during the present study are available from the corresponding author upon reasonable request.

Conflicts of Interest

The authors declare that they have no conflicts of interest.

Acknowledgments

This work was supported by grants from the National Natural Science Foundation of China (Grant No. 81700818), the Heilongjiang Postdoctoral Research Initiation Fund (Grant No. LBH-Q15105), and the Research and Innovation Fund of the First Hospital of Harbin Medical University (Grant No. 2017B016).

References

[1] J. E. Shaw, R. A. Sicree, and P. Z. Zimmet, "Global estimates of the prevalence of diabetes for 2010 and 2030," *Diabetes Research and Clinical Practice*, vol. 87, no. 1, pp. 4–14, 2010.

[2] E. Stefansson, T. Bek, M. Porta, N. Larsen, J. K. Kristinsson, and E. Agardh, "Screening and prevention of diabetic blindness," *Acta Ophthalmologica Scandinavica*, vol. 78, no. 4, pp. 374–385, 2000.

[3] E. Prokofyeva and E. Zrenner, "Epidemiology of major eye diseases leading to blindness in Europe: a literature review," *Ophthalmic Research*, vol. 47, no. 4, pp. 171–188, 2012.

[4] H. P. Hammes, "Optimal treatment of diabetic retinopathy," *Therapeutic Advances in Endocrinology and Metabolism*, vol. 4, no. 2, pp. 61–71, 2013.

[5] C. Karlberg, C. Falk, A. Green, A. K. Sjolie, and J. Grauslund, "Proliferative retinopathy predicts nephropathy: a 25-year follow-up study of type 1 diabetic patients," *Acta Diabetologica*, vol. 49, no. 4, pp. 263–268, 2012.

[6] S. Masuda, M. Nagao, K. Takahata et al., "Functional erythropoietin receptor of the cells with neural characteristics. Comparison with receptor properties of erythroid cells," *The Journal of Biological Chemistry*, vol. 268, no. 15, pp. 11208–11216, 1993.

[7] E. Morishita, S. Masuda, M. Nagao, Y. Yasuda, and R. Sasaki, "Erythropoietin receptor is expressed in rat hippocampal and cerebral cortical neurons, and erythropoietin prevents in vitro glutamate-induced neuronal death," *Neuroscience*, vol. 76, no. 1, pp. 105–116, 1997.

[8] W. Jelkmann, "Erythropoietin: structure, control of production, and function," *Physiological Reviews*, vol. 72, no. 2, pp. 449–489, 1992.

[9] K. Ruscher, D. Freyer, M. Karsch et al., "Erythropoietin is a paracrine mediator of ischemic tolerance in the brain: evidence from an in vitro model," *The Journal of Neuroscience*, vol. 22, no. 23, pp. 10291–10301, 2002.

[10] S. Masuda, M. Okano, K. Yamagishi, M. Nagao, M. Ueda, and R. Sasaki, "A novel site of erythropoietin production. Oxygen-dependent production in cultured rat astrocytes," *The Journal of Biological Chemistry*, vol. 269, no. 30, pp. 19488–19493, 1994.

[11] A. Anagnostou, Z. Liu, M. Steiner et al., "Erythropoietin receptor mRNA expression in human endothelial cells," *Proceedings*

of the National Academy of Sciences of the United States of America, vol. 91, no. 9, pp. 3974–3978, 1994.

[12] D. Watanabe, K. Suzuma, S. Matsui et al., "Erythropoietin as a retinal angiogenic factor in proliferative diabetic retinopathy," *The New England Journal of Medicine*, vol. 353, no. 8, pp. 782–792, 2005.

[13] S. F. Grant, G. Thorleifsson, I. Reynisdottir et al., "Variant of transcription factor 7-like 2 (TCF7L2) gene confers risk of type 2 diabetes," *Nature Genetics*, vol. 38, no. 3, pp. 320–323, 2006.

[14] J. C. Florez, K. A. Jablonski, N. Bayley et al., "TCF7L2 polymorphisms and progression to diabetes in the diabetes prevention program," *The New England Journal of Medicine*, vol. 355, no. 3, pp. 241–250, 2006.

[15] L. J. Scott, K. L. Mohlke, L. L. Bonnycastle et al., "A genome-wide association study of type 2 diabetes in Finns detects multiple susceptibility variants," *Science*, vol. 316, no. 5829, pp. 1341–1345, 2007.

[16] S. Bonetti, M. Trombetta, G. Malerba et al., "Variants and haplotypes of TCF7L2 are associated with beta-cell function in patients with newly diagnosed type 2 diabetes: the Verona newly diagnosed type 2 diabetes study (VNDS) 1," *The Journal of Clinical Endocrinology and Metabolism*, vol. 96, no. 2, pp. E389–E393, 2011.

[17] R. J. Strawbridge, J. Dupuis, I. Prokopenko et al., "Genome-wide association identifies nine common variants associated with fasting proinsulin levels and provides new insights into the pathophysiology of type 2 diabetes," *Diabetes*, vol. 60, no. 10, pp. 2624–2634, 2011.

[18] V. Lyssenko, R. Lupi, P. Marchetti et al., "Mechanisms by which common variants in the TCF7L2 gene increase risk of type 2 diabetes," *The Journal of Clinical Investigation*, vol. 117, no. 8, pp. 2155–2163, 2007.

[19] M. Garcia-Ramirez, C. Hernandez, and R. Simo, "Expression of erythropoietin and its receptor in the human retina: a comparative study of diabetic and nondiabetic subjects," *Diabetes Care*, vol. 31, no. 6, pp. 1189–1194, 2008.

[20] Z. Tong, Z. Yang, S. Patel et al., "Promoter polymorphism of the erythropoietin gene in severe diabetic eye and kidney complications," *Proceedings of the National Academy of Sciences of the United States of America*, vol. 105, no. 19, pp. 6998–7003, 2008.

[21] J. Chen, A. Stahl, N. M. Krah et al., "Wnt signaling mediates pathological vascular growth in proliferative retinopathy," *Circulation*, vol. 124, no. 17, pp. 1871–1881, 2011.

[22] C. Ciccacci, D. Di Fusco, L. Cacciotti et al., "TCF7L2 gene polymorphisms and type 2 diabetes: association with diabetic retinopathy and cardiovascular autonomic neuropathy," *Acta Diabetologica*, vol. 50, no. 5, pp. 789–799, 2013.

[23] Y. Tong, Y. Lin, Y. Zhang et al., "Association between TCF7L2 gene polymorphisms and susceptibility to type 2 diabetes mellitus: a large human genome epidemiology (HuGE) review and meta-analysis," *BMC Medical Genetics*, vol. 10, no. 1, p. 15, 2009.

[24] A. Helgason, S. Palsson, G. Thorleifsson et al., "Refining the impact of TCF7L2 gene variants on type 2 diabetes and adaptive evolution," *Nature Genetics*, vol. 39, no. 2, pp. 218–225, 2007.

[25] S. Papadopoulou and H. Edlund, "Attenuated Wnt signaling perturbs pancreatic growth but not pancreatic function," *Diabetes*, vol. 54, no. 10, pp. 2844–2851, 2005.

[26] C. Prunier, B. A. Hocevar, and P. H. Howe, "Wnt signaling: physiology and pathology," *Growth Factors*, vol. 22, no. 3, pp. 141–150, 2004.

[27] F. Yi, P. L. Brubaker, and T. Jin, "TCF-4 mediates cell type-specific regulation of proglucagon gene expression by β-catenin and glycogen synthase Kinase-3β^*," *The Journal of Biological Chemistry*, vol. 280, no. 2, pp. 1457–1464, 2005.

[28] M. Tian, S. Liu, L. Liu et al., "Correlations of the severity of diabetic retinopathy with EPO, Caspase-3 expression and oxidative stress," *European Review for Medical and Pharmacological Sciences*, vol. 23, no. 22, pp. 9707–9713, 2019.

[29] H. Xie, C. Zhang, D. Liu et al., "Erythropoietin protects the inner blood-retinal barrier by inhibiting microglia phagocytosis via Src/Akt/cofilin signalling in experimental diabetic retinopathy," *Diabetologia*, vol. 64, no. 1, pp. 211–225, 2021.

Hindawi
Disease Markers
Volume 2022, Article ID 6721695, 6 pages
https://doi.org/10.1155/2022/6721695

Research Article

Effect of Compound Lactic Acid Bacteria Capsules on the Small Intestinal Bacterial Overgrowth in Patients with Depression and Diabetes: A Blinded Randomized Controlled Clinical Trial

Fang Wei,[1] Lei Zhou,[2] Qingqing Wang,[1] Guoqi Zheng,[1] and Shanshan Su[1]

[1]*Digestive Department, Cangzhou Central Hospital, Cangzhou, China*
[2]*Department of General Surgery, Cangxian Hospital, Cangzhou, China*

Correspondence should be addressed to Shanshan Su; sushanshan1002@hotmail.com

Received 12 January 2022; Accepted 7 April 2022; Published 29 May 2022

Academic Editor: Zhaoqi Dong

Objective. The objective is to explore the clinical effect of compound lactic acid bacteria capsules on the small intestinal bacterial overgrowth (SIBO) in patients with depression and diabetes. *Methods*. From January 2020 to January 2021, 60 SIBO patients with depression and diabetes in our hospital were selected and randomized into observation group (compound lactic acid bacteria capsules combined with escitalopram) and control group (Escitalopram) according to the odd and even numbers, 30 cases in each group. The two groups were compared in terms of SAS, SDS, levels of inflammatory factors, immune function, fasting plasma glucose (FPG), treatment effect, and the incidence of adverse reactions. *Results*. Both self-rating anxiety scale (SAS) and self-rating depression scale (SDS) scores in both groups showed a decline after treatment ($P < 0.05$), and the reduction was more significant in the observation group ($t = 10.047$, 17.862, all $P \leq 0.001$). Both IL-2 and TNF-α in both groups showed a decline after treatment ($P < 0.05$), and the reduction was more greater in the observation group in relative to the control group ($P < 0.05$). CD3+ and CD+4 in both groups showed an increase after treatment ($P < 0.05$), and the increase was more greater in the observation group as compared to the control group ($P < 0.05$). After treatment, the FPG levels of patients in both groups showed a decline ($P < 0.05$), and the reduction of FPG levels was more significant in the observation group than that in the control group ($t = 3.948$, $P \leq 0.001$). The control group experienced a remarkably higher incidence of adverse reactions. *Conclusion*. The compound lactic acid bacteria capsule is a boon for SIBO patients with depression and diabetes. It can mitigate depression symptoms, improve immune function, reduce the level of inflammatory factors, and lower the FPG levels, along with fewer adverse reactions and robust effects.

1. Introduction

Depression, a common mental disorder, is characterized by symptoms such as affective, cognitive, psychomotor, or autonomic disorders, which poses threats on work, study, and interpersonal relationships. The predisposing factors of depression are complex and diverse such as biochemistry, neuroendocrine and genetics, and psychosocial factors. The main manifestations are different degrees of depression and decreased interest and even self-injury and suicidal behavior in severe cases [1]. Diabetes is a common chronic disease, and depression is twice as common in individuals with diabetes as in the general population [2]. The comorbidity of depression and diabetes is associated with poor outcomes and may share biological origins [3]. In recent years, studies have found that depression is associated with small intestinal bacterial overgrowth (SIBO). Long-term depression will cause gastrointestinal reactions such as anorexia, abdominal distension, and loss of appetite and further develop into SIBO [4]. The improvement of the quality of life and relief of symptoms for SIBO patients with depression and diabetes is the priority in clinical setting. Escitalopram was previously the mainstay for the treatment of depression, which is beneficial to improve the symptoms of depression. And alternative medicine (CAM) is often used in order to alleviate these problems [5–9]. The compound

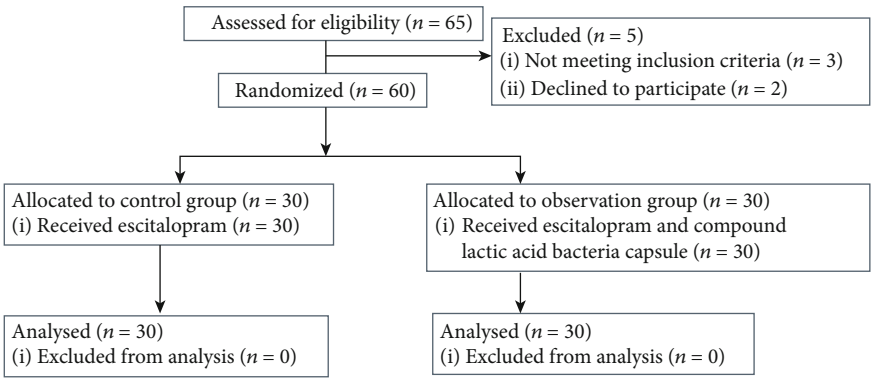

Figure 1: Study flowchart.

Table 1: Comparison of SAS and SDS scores between the two groups (point, $\bar{x} \pm s$).

Groups	n	SAS		t	P	SDS		t	P
		Before treatment	After treatment			Before treatment	After treatment		
Observation group	30	63.14 ± 4.73	36.12 ± 2.94	26.593	≤0.001	64.26 ± 4.64	39.75 ± 2.15	26.271	≤0.001
Control group	30	63.24 ± 4.59	43.16 ± 2.46	21.097	≤0.001	64.37 ± 4.58	50.14 ± 2.36	15.122	≤0.001
t	/	0.083	10.047			0.101	17.862		
p	/	0.934	≤0.001			0.920	≤0.001		

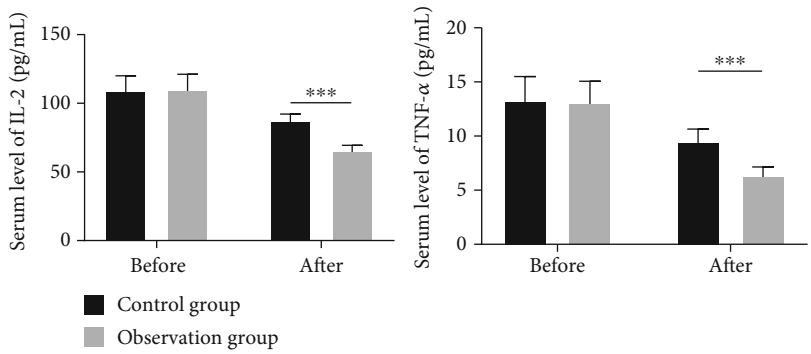

Figure 2: Comparison of the levels of inflammatory factors between the two groups (pg/ml, $\bar{x} \pm s$). Note: ∗∗∗represents the comparison between the two groups after treatment.

lactic acid bacteria capsule is a drug for the treatment of intestinal flora disorders. This study sets to explore the effect of compound lactic acid bacteria capsules on the SIBO by enrolling 60 patients with depression and diabetes in our hospital from January 2020 to January 2021.

2. Materials and Methods

2.1. General Information. A total of 60 cases of SIBO patients with depression and diabetes admitted to our hospital from January 2020 to January 2021 were selected. Random envelopes were issued from serial 1 to 60 and placed in the envelopes. The grouping was based on the number of odd or even numbers of the cards each person held, with 30 cases each.

2.2. Inclusion and Exclusion Criteria. Inclusion criteria are as follows: (1) The patient was diagnosed as SIBO with depression after clinical examination and breath test [10, 11], and the diagnosis of diabetes was in accordance with the guidance of 1999 WHO criteria; (2) informed the patients and their family of the purpose and significance of the study, obtained the patient's signed informed consent form, and obtained the approval from ethics committee; (3) can communicate normally and cooperate to complete the study; and (4) the clinical data is complete. Exclusion criteria are as follows: (1) damage to vital organs; (2) patients with other types of mental illness; (3) cancer patients; (4) patients with long-term drinking history; (5) poor compliance or failure to persist until the end of the study; (6) those who had an allergic reaction to the study drug; (7) those who had immune system diseases or coagulation abnormalities; (8) pregnant

Table 2: Comparison of immune function indexes between the two groups ($\bar{x} \pm s$).

Groups	n	CD_3^+ (%)	CD^+_4 (%)	CD_8^+ (%)	CD_4^+/CD_8^+
Observation group ($n = 30$)	Before treatment	57.94 ± 6.22	29.32 ± 3.41	26.69 ± 2.53	1.05 ± 0.15
	After treatment	68.23 ± 7.72	41.48 ± 4.03	27.20 ± 2.37	1.57 ± 0.26
	t	5.685	12.627	0.805	9.386
	P	≤0.001	≤0.001	0.424	≤0.001
Control group ($n = 30$)	Before treatment	57.03 ± 6.95	29.50 ± 3.63	26.32 ± 2.49	1.06 ± 0.16
	After treatment	62.49 ± 5.56	35.28 ± 3.61	26.45 ± 2.20	1.34 ± 0.10
	t	3.357	6.1921	0.214	8.707
	p	0.001	≤0.001	0.831	≤0.001
	$t1$	0.534	0.209	0.570	0.255
	P	0.595	0.836	0.571	0.800
	$t2$	3.305	6.284	1.270	4.296
	P	0.002	≤0.001	0.209	≤0.001

Note: t1 represents the comparison between the two groups before treatment, and t2 represents the comparison between the two groups after treatment.

Table 3: Comparison of fasting plasma glucose (FPG) between the two groups (mmol/L, $\bar{x} \pm s$).

Groups	n	Before treatment	After treatment	t	P
Observation group	30	10.3 ± 1.5	8.4 ± 1.0	5.736	≤0.001
Control group	30	10.8 ± 1.8	9.8 ± 1.6	2.270	0.027
t	/	-1.092	-3.948		
P	/	0.279	≤0.001		

women; and (9) those who had systemic infectious diseases. The study was reviewed and approved by Cangzhou Central Hospital Ethics Committee (approval no. 2019-273-12).

2.3. Method. The control group was given escitalopram orally (Jilin Province West Point Pharmaceutical Technology Development Co., Ltd.; National Medicine Standard H20140106; specification: 10 mg∗7 tablets), 10 mg/time, once a day. The observation group was given compound lactic acid bacteria capsule (Jiangsu Meitong Pharmaceutical Co., Ltd.; National Medicine Standard H19980184; specification: 0.33 g × 10 capsules/box) on the basis of the control group, 3 times/d at a dose of 0.66 g/time. The treatment period of both groups was 1 week. (Compound lactic acid bacteria capsules are not chemical preparations, but live bacteria preparations. Packed in film enteric-coated capsules, it is not affected by gastric acid and directly reaches the intestines for reproduction to exert its pharmacological effects. And they are not absorbed by the intestinal tract, and 1 week is therefore deemed a treatment cycle.) All participants, statistician, and investigators were blinded to the allocation of the patients and the type of medicines.

2.4. Observation Indicators. The anxiety and depression, inflammatory factor levels, and immune function before and after treatment, treatment effectiveness, and adverse reactions were compared. (1) The SAS scale was used to evaluate the anxiety, which includes 20 items, and scored using a 4-likert scale; the higher the score, the more severe the anxiety; the SDS scale was used to assess the depression, which includes 20 items, and scored using a 4-likert scale; the higher the score, the more severe the depression [12]. (2) 5 mL fasting peripheral venous blood in the morning was collected, centrifuged at 3000 r/min for a total of 10 minutes, and the serum was separated. Serum IL-2 and TNF-α were detected by ELISA, and the kit was provided by Shanghai Bohu Biotechnology Co., Ltd. (3) Immune function indexes CD3+, CD+4, CD8+, and CD4+/CD8+ were detected by flow cytometer BD FACSCalibur cell counter (Shanghai Musen Biotechnology Co., Ltd.). (4) fasting plasma glucose (FPG) was measured by a Hitachi LST008 analyzer (Hitachi High-Technologies). (5) Efficacy criteria are as follows: If the SAS and SDS reduced by≥75%, and the clinical indicators returned to normal, it is considered markedly effective. If the SAS and SDS reduced by 50%~75%, and the inflammatory index and immune function have been improved but did not return to normal, it is considered effective. If the patient's symptoms changed little before and after treatment or worsened, it is considered ineffective. The total effective rate = markedly effective rate + effective rate [13].

2.5. Statistical Methods. Statistical analysis was done by SPSS22.0 software package. The counting data and measurement data were expressed as $n(\%)$ and ($x \pm s$), respectively, which were analyzed by X^2 and t test. A P value of <0.05 indicates that the difference is statistically significant.

3. Results

3.1. Participants Profiles. In the observation group, male: female = 16 : 14, aged 23-62 (43.59 ± 4.32) years old, and the body mass index was (23.37 ± 1.31) kg/m^2; in the control group, male: female was 17 : 13, aged 22-64 (43.31 ± 4.57) years old, and the body mass index was (23.33 ± 1.24) kg/m^2. The baseline information of the two groups were similar ($P > 0.05$) (Figure 1).

Table 4: Comparison of efficacy between the two groups (%).

Groups	*n*	Markedly effective	Effective	Ineffective	Total effectiveness (%)
Observation group	30	22 (73.3)	6 (20.0)	2 (6.7)	28 (93.3)
Control group	30	16 (53.3)	5 (16.7)	9 (30.0)	21 (70.0)
X^2	/	/	/	/	5.455
p	/	/	/	/	0.020

Table 5: Comparison of adverse reactions between the two groups (%).

Groups	*n*	Constipate	Nausea	Dizziness	Dry mouth	Adverse reaction rate (%)
Observation group	30	1 (3.3)	0 (0.0)	1 (3.3)	0 (0.0)	2 (6.7)
Control group	30	2 (6.7)	2 (6.7)	1 (3.3)	3 (10.0)	8 (26.7)
X^2	/	/	/	/	/	4.320
P	/	/	/	/	/	0.038

3.2. Comparison of SAS and SDS Scores. Both SAS and SDS scores in both groups showed a decline after treatment ($P < 0.05$), and the reduction was greater in the observation group ($P < 0.05$) (see Table 1).

3.3. Comparing the Levels of Inflammatory Factors. IL-2 and TNF-α in both groups showed a decline after treatment, whereas CD3+ and CD4+ showed an increase ($P < 0.05$), and the changes were greater in the observation group in relative to the control group ($P < 0.05$) (Figure 2).

3.4. Comparison of Immune Function Indexes. CD3+, CD+4, and CD4+/CD8+ in both groups showed an increase after treatment ($P < 0.05$), and the increase was greater in the observation group compared to the control group ($P < 0.05$) (see Table 2).

3.5. Comparison of the FPG Levels. After treatment, the FPG levels of patients in both groups show a decline ($P < 0.05$), and the reduction of FPG levels is greater in the observation group than that in the control group ($P < 0.05$), as shown in Table 3.

3.6. Comparison of the Efficacy. The observation group garners a notably higher efficacy than the control group, as shown in Table 4.

3.7. Comparison of Adverse Reactions. The control group experiences a remarkably higher incidence of adverse reactions, as shown in Table 5.

4. Discussion

In addition to persistent negative mood, patients with depression often experience gastrointestinal discomforts such as abdominal distension, acid reflux, and anorexia. They show no organic disease after examination and diagnosis in the department of gastroenterology and neurology. Nevertheless, the outcome remains undesirable after symptomatic treatment. In recent years, some scholars have found that there is a certain correlation between depression patients and the balance of intestinal microecology. When the intestinal microecology is out of balance, it will lead to aggravation of anxiety and depression symptoms, which counteracts on the gastrointestinal tract, causing microbiota imbalance [14], among which SIBO is the most common type. Consequently, it is particularly important to find a reliable and safe treatment for SIBO combined with depression.

Escitalopram is a common drug for clinical treatment of depression. As a 5-HT reuptake inhibitor, it has a certain selectivity and can effectively inhibit the presynaptic membrane of the central nervous system, which also can suppress 5-HT transporter. It is mainly used clinically for the treatment of depression, anxiety, somatization disorders, and psychotic anxiety. Despite the fewer side effects of the drug, the overall tolerance is favorable. Yet, the drug remains unsatisfactory for SIBO combined with depression. This study combined with compound lactic acid bacteria capsules on this basis and achieved excellent results. As a compound preparation, the compound lactic acid bacteria capsule is an important probiotic in the human intestine. Its main ingredients are *Lactobacillus* and *Streptococcus lactis*, which act on the body to multiply in the intestinal tract, increase the production of lactic acid, and inhibit the reproduction of spoilage bacteria. Through the regulation of the flora, the fermentation of spoilage bacteria can be avoided, and the occurrence of flatulence in the intestine is prevented [15]. Additionally, the drug can also speed up the body's digestion and exert a certain antidiarrheal role. The combination of the two drugs plays a role in antidepression and regulation of intestinal flora and mitigates patients' related symptoms. Remarkably, the present study showed that the observation group was superior to the control group in terms of SAS and SDS and the inflammatory factor, reflecting the robust effect of the treatment program on the patients' depressive symptoms and inflammatory response. Studies have found that the main function of T lymphocytes is immunosuppression; the long-term depression will inhibit immune function to a certain extent and increase the susceptibility of mental

illness and inflammation, further undermining the neuroendocrine system as the disease progresses [16]. Notably, the immune function indicators of the patients in this study improved after treatment, and the observation group witnessed more prominent progress than the control group, suggesting the value of compound lactic acid bacteria in improving the immune function of patients. Animal studies revealed that diabetic mice treated with *Lactobacillus* showed significantly decreased FPG levels [17]. In consistent with the above study, we found that patients in the observation group had significant lower FPG levels than those in the control group. In addition, *Lactobacillus* treatment was demonstrated to regulate the expression genes that are related to glucose and lipid metabolism [18]. In terms of the effectiveness and safety of the treatment in this study, the observation group outperformed the control group, suggesting the feasibility of the treatment plan. However, on one hand, due to the limitation of research time and existing conditions, and the small sample size, the large-scale research is needed; on the other hand, the observation indicators are relatively fewer; the follow-up and various outcome measures are necessary in the future to provide more clinic references. The small sample size should be stated as a major limitation of this study. Yet, this study was a pilot clinical study, and we planned to investigate our hypothesis in a minimum sample size. Moreover, the exact cause of the adverse reactions was not investigated. Hence, it is suggested that future trials should be planned with larger sample size.

5. Conclusion

To conclude, the compound lactic acid bacteria capsule is a boon for SIBO patients with depression and diabetes. It can mitigate depression symptoms, improve immune function, and reduce the level of inflammatory factors and FPG, with fewer adverse reactions and robust effects.

Data Availability

The datasets used during the present study are available from the corresponding author upon reasonable request.

Conflicts of Interest

The authors declare that they have no conflicts of interest.

Authors' Contributions

Fang Wei and Lei Zhou are co-first author.

Acknowledgments

This study was supported by the Hebei Province Medical Science Research Project Program, No. 20210924.

References

[1] M. Haofei, L. Xuanjun, L. Sihui, H. Yilei, and J. Yanbin, "Research progress on genes related to cognitive impairment in depression," *Chinese Journal of Nervous and Mental Diseases*, vol. 45, no. 10, pp. 628–631, 2019.

[2] R. J. Anderson, K. E. Freedland, R. E. Clouse, and P. J. Lustman, "The prevalence of comorbid depression in adults with diabetes," *Diabetes Care*, vol. 24, no. 6, pp. 1069–1078, 2001.

[3] C. D. Moulton, J. C. Pickup, and K. Ismail, "The link between depression and diabetes: the search for shared mechanisms," *The Lancet Diabetes and Endocrinology*, vol. 3, no. 6, pp. 461–471, 2015.

[4] L. Yinghui and Y. Yonggui, "Research progress on the correlation between depression and intestinal flora," *Journal of Southeast University (Medical Edition)*, vol. 40, no. 2, pp. 250–255, 2021.

[5] N. Nayebi, A. Esteghamati, A. Meysamie et al., "The effects of a Melissa officinalis L. based product on metabolic parameters in patients with type 2 diabetes mellitus: a randomized double-blinded controlled clinical trial," *Journal of Complementary and Integrative Medicine*, vol. 16, no. 3, 2019.

[6] X. Xu, M. Zhang, X. Wu, C. Zheng, and G. Huang, "The effect of electroacupuncture treatment with different intensities for functional diarrhea: a randomized controlled trial," *Evidence-based Complementary and Alternative Medicine*, vol. 4, Article ID 2564979, 8 pages, 2022.

[7] M. S. Hashemi, M. H. Hashempur, M. H. Lotfi et al., "The efficacy of asafoetida (Ferula assa-foetida oleo-gum resin) versus chlorhexidine gluconate mouthwash on dental plaque and gingivitis: a randomized double-blind controlled trial," *European Journal of Integrative Medicine*, vol. 29, article 100929, 2019.

[8] M. Maghbool, T. Khosravi, S. Vojdani et al., "The effects of eugenol nanoemulsion on pain caused by arteriovenous fistula cannulation in hemodialysis patients: a randomized double-blinded controlled cross-over trial," *Complementary Therapies in Medicine*, vol. 52, 2020.

[9] W. Y. Tang, J. T. Liang, J. Wu et al., "Efficacy and safety of Dahuang Zhechong pill in silicosis: a randomized controlled trial," *Evidence-based Complementary and Alternative Medicine*, vol. 18, Article ID 4354054, 9 pages, 2021.

[10] L. Jin, L. Lingjiang, and X. Xiufeng, "Interpretation of Chinese guidelines for the prevention and treatment of depressive disorders (second edition): evaluation and diagnosis," *Chinese Journal of Psychiatry*, vol. 50, no. 3, pp. 169–171, 2017.

[11] Gastrointestinal Functional Diseases Collaboration Group, Chinese Medical Association Gastroenterology Branch Gastrointestinal Dynamics Group, and Chinese Medical Association Gastroenterology Branch, "Expert consensus on irritable bowel syndrome in China (2015, Shanghai)," *Chinese Journal of Digestion*, vol. 36, no. 5, pp. 299–312, 2016.

[12] S. Jiuying, X. Yao, Z. Yunian, S. Zhiyong, C. Yingchun, and Z. Zhiqing, "The effect of comprehensive systemic nursing on anxiety, depression experience and quality of life in elderly patients with depression," *International Journal of Psychiatry*, vol. 44, no. 5, pp. 894–896, 2017.

[13] C. Xiubing, W. Yuehui, Z. Jian, and Z. Youbao, "Comparison of the efficacy of venlafaxine and deanxit in the treatment of functional gastrointestinal diseases with anxiety disorders," *Anhui Medicine*, vol. 24, no. 1, pp. 174–178, 2020.

[14] Z. Tao, L. Huting, and Z. Xiao, "Progress in the study of neurobiological mechanisms of gastrointestinal diseases with comorbid depression," *Acta Physiologica Sinica*, vol. 70, no. 1, pp. 71–78, 2018.

[15] P. Meiyun, L. Haiyan, and L. Yihui, "The effect of compound lactic acid bacteria capsules on intestinal bacterial overgrowth and blood ammonia in patients with liver cirrhosis," *Chinese and Foreign Medical Research*, vol. 15, no. 35, pp. 1-2, 2014.

[16] T. Chaozhi and L. Haige, "The role of lymphocyte subsets in the pathogenesis of depression," *Chinese Journal of Immunology*, vol. 36, no. 6, pp. 767–770, 2020.

[17] P. S. Hsieh, H. H. Ho, S. H. Hsieh et al., "*Lactobacillus salivarius* AP-32 and *Lactobacillus reuteri* GL-104 decrease glycemic levels and attenuate diabetes-mediated liver and kidney injury in db/db mice," *BMJ Open Diabetes Research & Care*, vol. 8, no. 1, article e001028, 2020.

[18] F. Yan, N. Li, J. Shi et al., "Lactobacillus acidophilus alleviates type 2 diabetes by regulating hepatic glucose, lipid metabolism and gut microbiota in mice," *Food & Function*, vol. 10, no. 9, pp. 5804–5815, 2019.

Hindawi
Disease Markers
Volume 2022, Article ID 8779061, 6 pages
https://doi.org/10.1155/2022/8779061

Research Article

Correlation Analysis of Blood Glucose Level with Inflammatory Response and Immune Indicators in Patients with Sepsis

Qi Wei,[1] Jinglin Zhao,[1] Hao Wang,[1] Cuicui Liu,[2] Caihong Hu,[3] Chao Zhao,[2] Qingchun Dai,[1] Zhi Hui,[1] and Rui Wang[1]

[1]*Department of Critical-Care Medicine, Cangzhou Central Hospital, Cangzhou, China*
[2]*Department of Pharmacology, Cangzhou Medical College, Cangzhou, China*
[3]*Department of Imaging, Cangzhou Medical College, Cangzhou, China*

Correspondence should be addressed to Rui Wang; ruhuangzhi14196@163.com

Received 20 December 2021; Revised 28 February 2022; Accepted 29 March 2022; Published 26 May 2022

Academic Editor: Zhaoqi Dong

Objective. To analyze the correlation of blood glucose level with inflammatory response and immune indicators in patients with sepsis. *Methods*. Between February 2019 and February 2021, 30 sepsis patients and 30 sepsis patients complicated with diabetes mellitus admitted to our hospital were recruited and assigned to either the experimental group (sepsis patients) or the observation group (sepsis patients with diabetes mellitus). Another 30 healthy subjects in the same period were included as the control group. The levels of IL-6, TNF-α, IL-1β, CD4+, and CD8+ in the three groups of patients were compared to analyze the correlation of blood glucose levels with inflammatory response and immune indicators in patients with sepsis. The difference of counting data was analyzed using the chi-square test, and the difference of measurement data was analyzed using the t-test. *Results*. The control group showed the lowest levels of IL-6 at 14.32 ± 4.98 pg/ml, followed by 18.33 ± 3.27 pg/ml in the experimental group and then 22.64 ± 5.16 pg/ml in the observation group ($P < 0.05$). The levels of other inflammatory factors including TNF-α and IL-1β were the lowest in the control group, followed by the experimental group, and then the observation group ($P < 0.05$). The lowest immune function indicator CD4+ and CD8+ levels were found in the observation group, followed by the experimental group, and then the control group ($P < 0.05$). The blood glucose level of patients with sepsis was positively correlated with the levels of IL-6, TNF-α, and IL-1β and was negatively correlated with the levels of CD4+/CD8+. The higher the blood glucose, the lower the number of immune cells. *Conclusion*. The blood glucose level of patients with sepsis is positively correlated with inflammatory response and negatively with immune indicators. An increased blood sugar level is associated with aggravated inflammatory responses and a decreased number of immune cells, which provides a reference for the disease severity assessment and treatment of patients with sepsis.

1. Introduction

Sepsis is an infectious disease caused by multiple inflammatory factors that cooperate in the pathology of immune dysfunction and is the leading cause of death in intensive care unit (ICU) patients [1–3]. As a syndrome characterized by uncontrollable inflammation, sepsis involves a massive and persistent inflammatory response and a prolonged state of immunosuppression, leading to an increased risk of secondary nosocomial infections [4, 5]. Factors such as inflammatory response, immune response, and infection are risk factors for the development of sepsis, and the disease may be exacerbated by dysregulation of inflammatory factor levels in patients [3, 6]. Relevant studies have shown that the risk of sepsis infection in diabetic patients is 2.5-6.0 times higher than in nondiabetic patients. Moreover, patients with sepsis are predisposed to insulin resistance due to glycemic changes [5, 7]. Previous research has also demonstrated that the higher the blood glucose level in sepsis patients, the more severe the patient's condition [8]. The present study was conducted to explore the correlation between blood glucose levels and inflammation and immune indicators in patients with sepsis.

Table 1: Comparison of clinical data of patients in the three groups [n (%)].

Items	Control group ($n = 30$)	Experimental group ($n = 30$)	Observation group ($n = 30$)	χ^2/t	P
Gender					
Male	14 (46.67)	13 (43.33)	11 (36.67)	0.6171	0.432
Female	16 (53.33)	17 (56.67)	19 (63.33)		
Average age (year)	45.62 ± 7.58	48.27 ± 8.13	46.33 ± 7.42	0.367	0.715
Systolic blood pressure/(kPa)	16.34 ± 4.28	17.10 ± 4.35	16.55 ± 4.29	0.19	0.85
Diastolic blood pressure/(kPa)	11.17 ± 2.64	10.89 ± 2.83	11.46 ± 2.70	0.421	0.676
APACHEII scores	21.60 ± 6.57	24.55 ± 7.41	24.48 ± 6.63	1.69	0.096

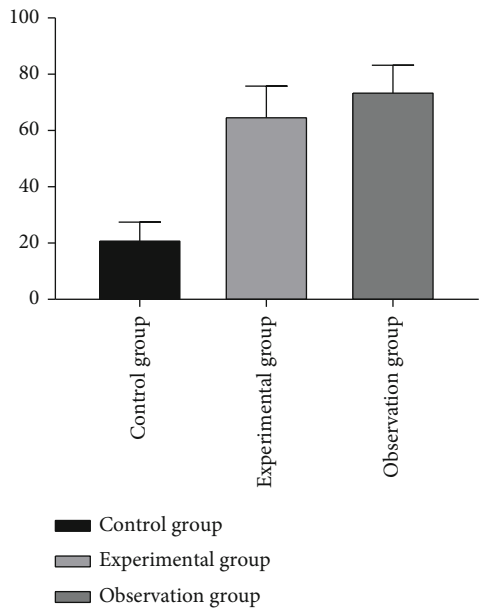

Figure 1: Comparison of IL-6 levels of inflammatory factors in the three groups ($\bar{x} \pm s$). Note: the abscissa represents the control group, experimental group, and observation group; the ordinate represents the level of IL-6 (pg/ml); the level of IL-6 in the control group was 14.32 ± 4.98 pg/ml; the level of IL-6 in the experimental group was 18.33 ± 3.27 pg/ml; the level of IL-6 in the observation group was 22.64 ± 5.16 pg/ml; ∗ indicates that there is a significant difference in IL-6 levels between the control group and the experimental group ($t = 3.687, P < 0.001$); ∗∗ indicates that there is a significant difference in IL-6 levels between the control group and the observation group ($t = 6.355, P < 0.001$); ∗∗∗ indicates that there is a significant difference in IL-6 levels between the experimental group and the observation group ($t = 3.864, P < 0.001$).

2. Materials and Methods

2.1. General Information. From February 2019 to February 2021, 30 sepsis patients and 30 sepsis patients complicated with diabetes mellitus admitted to our hospital were recruited and assigned to either the experimental group (sepsis patients) or the observation group (sepsis patients with diabetes mellitus). Another 30 healthy subjects in the same period were included in the control group. After enrollment, blood pressure was measured with an electronic manometer. The II acute physiology and chronic health evaluation were performed.

2.2. Inclusion Criteria and Exclusion Criteria. The following are the inclusion criteria: patients who met the diagnostic criteria for sepsis, those with sepsis and diabetes who met the 2018 version of the diagnostic criteria for diabetes issued by the American Diabetes Association (ADA), and those who provided written informed consent after being fully informed of the purpose and process of the study. This study was ratified by the hospital ethics committee.

The following are the exclusion criteria: patients with tumors, those who were pregnant or lactating women, those with autoimmune diseases, those with severe mental illnesses, and those with medications that might affect the blood glucose levels, such as glucocorticoids.

2.3. Method. After admission, 4 ml of venous blood was collected from all subjects. 2 ml of blood sample was naturally clotted at room temperature for 30 min, followed by centrifugation at 1000 g for 10 min to obtain the serum. The serum was then stored at -20°C for assays. A multiplex microsphere flow-through immunofluorescence luminescence was used to determine the levels of interleukin-6 (IL-6), tumor necrosis factor-α (TNF-α), and interleukin-1β (IL-1β). The remaining 2 ml of blood samples was anticoagulated with EDTA-K2 at room temperature, vortexed and mixed for 3 seconds, and used for the determination of the CD4+ and CD8+ levels with flow cytometry.

12 cytokine assay kits were purchased from Qingdao Risskell Biotechnology Co., Ltd., China; CD3+, CD4+, and CD8+ fluorescent monoclonal antibody kits were purchased from Beijing Tong Sheng Times Biotechnology Co.

2.4. Observational Indicators. The levels of IL-6, TNF-α, IL-1β, CD4+, and CD8+ in the three groups of patients were compared to analyze the correlation of blood glucose levels with inflammatory response and immune indicators in patients with sepsis.

2.5. Statistical Analyses. SPSS20.0 was used for data analyses, and GraphPad Prism 7 (GraphPad Software, San Diego, USA) was used to plot the graphics.The counting data are expressed as [n(%)]and analyzed using the chi-square test, and the measurement data are expressed as $\bar{x} \pm s$ and

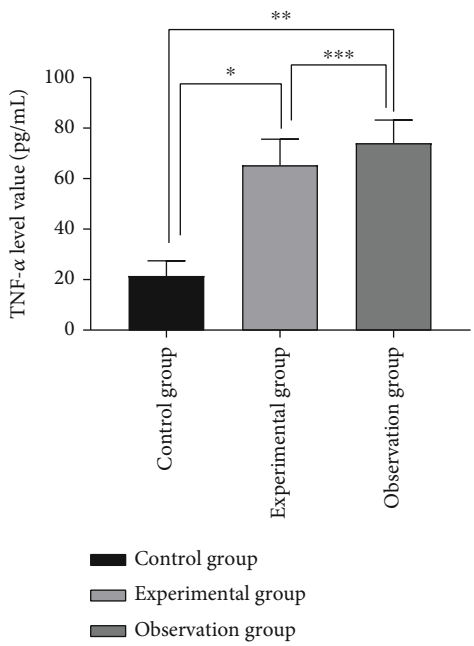

Figure 2: Comparison of TNF-α levels of inflammatory factors in the three groups ($\bar{x} \pm s$). Note: the abscissa represents the control group, experimental group, and observation group; the ordinate represents the level of TNF-α (pg/ml); the level of TNF-α in the control group was 21.42 ± 6.03 pg/ml; the level of TNF-α in the experimental group was 65.27 ± 10.32 pg/ml; the level of TNF-α in the observation group was 74.05 ± 9.14 pg/ml; $*$ indicates that there is a significant difference in the TNF-α level between the control group and the experimental group ($t = 19.765$, $P < 0.001$); $**$ indicates that there is a significant difference in the TNF-α level between the control group and the observation group ($t = 26.326$, $P < 0.001$); $***$ indicates that there is a significant difference in the TNF-α level between the experimental group and the observation group ($t = 3.488$, $P < 0.001$);

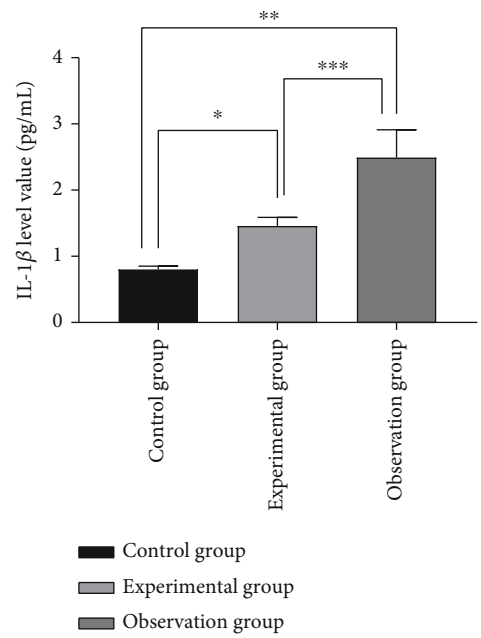

Figure 3: Comparison of IL-1β levels of inflammatory factors in the three groups ($\bar{x} \pm s$). Note: the abscissa represents the control group, experimental group, and observation group; the ordinate represents the level of IL-1β (pg/ml); the level of IL-1β of the control group was 0.80 ± 0.05 pg/ml; the level of IL-1β of the experimental group was 1.46 ± 0.13 pg/ml; the level of IL-1β in the observation group was 2.49 ± 0.42 pg/ml; $*$ indicates that there is a significant difference in IL-1β levels between the control group and the experimental group ($t = 25.954$, $P < 0.001$); $**$ indicates that there is a significant difference in IL-1β levels between the control group and the observation group ($t = 21.885$, $P < 0.001$); $***$ indicates that there is a significant difference in IL-1β levels between the experimental group and the observation group ($t = 12.832$, $P < 0.001$);

analyzed using the t-test. Statistically significant result was defined as $P < 0.05$.

3. Results

3.1. Baseline Patient Profile. There were no significant differences in the baseline characteristics between the three groups of participants ($P > 0.05$). See Table 1.

3.2. Comparison of IL-6 Levels of Inflammatory Factors in the Three Groups. The levels of inflammatory factors including IL-6 were the lowest in the control group, followed by the experimental group, and then the observation group ($P < 0.05$). See Figure 1.

3.3. Comparison of TNF-α Levels of Inflammatory Factors in the Three Groups. The level of TNF-α in the control group was significantly lower than that of the other two groups ($P < 0.05$), and the observation group showed a higher level of TNF-α than the experimental group ($P < 0.05$). See Figure 2 for details.

3.4. Comparison of IL-1β Levels of Inflammatory Factors in the Three Groups. The levels of inflammatory factors including IL-1β were the lowest in the control group, followed by the experimental group, and then the observation group ($P < 0.05$). See Figure 3.

3.5. Immune function indicators. Sepsis patients with diabetes mellitus in the observation group were associated with the lowest CD4+ and CD8+ levels in the control group, followed by the sepsis patients in the experimental group, and then the healthy participants in the control group ($P < 0.05$). See Table 2.

3.6. Correlation Analysis of Blood Glucose Levels and IL-6, TNF-α, and IL-1β Levels in Patients with Sepsis. The blood glucose level of patients with sepsis was positively correlated with the levels of IL-6, TNF-α, and IL-1β. The higher the blood glucose level, the higher the level of IL-6, TNF-α, and IL-1β. See Figure 4.

3.7. Correlation Analysis of Blood Glucose Levels and CD4+ and CD8+ Levels in Patients with Sepsis. The blood glucose level of patients with sepsis was negatively correlated with the levels of CD4+/CD8+. The higher the blood glucose, the lower the number of immune cells. See Figure 5.

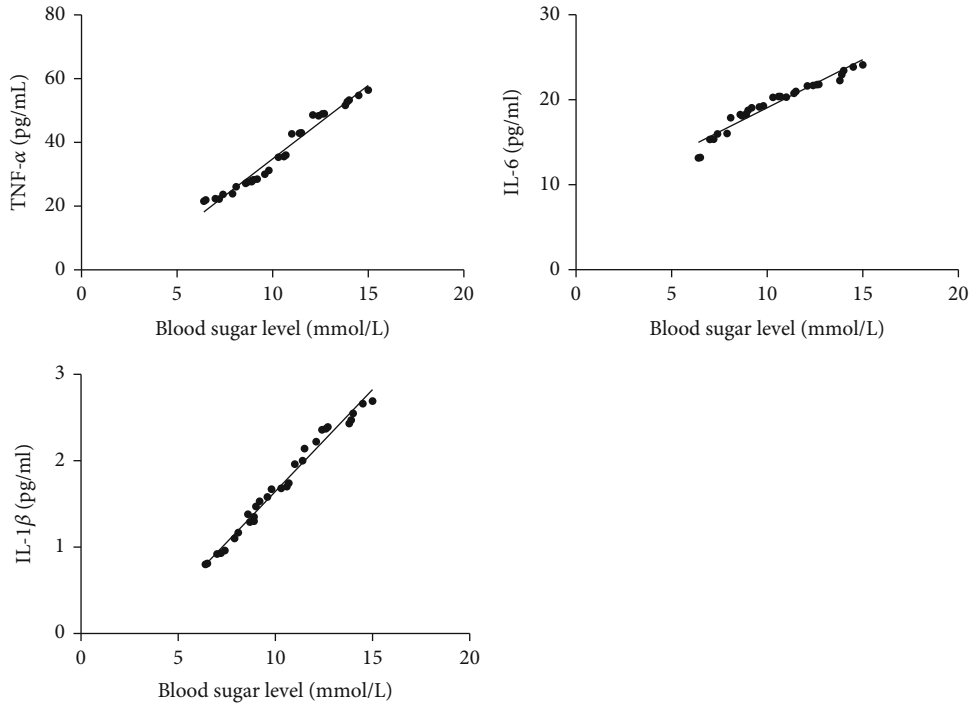

Figure 4: Correlation analysis of blood glucose levels and IL-6, TNF-α, and IL-1β levels in patients with sepsis. Note: the abscissa indicates the blood glucose level; the ordinate indicates the level of IL-6, TNF-α, and IL-1β.

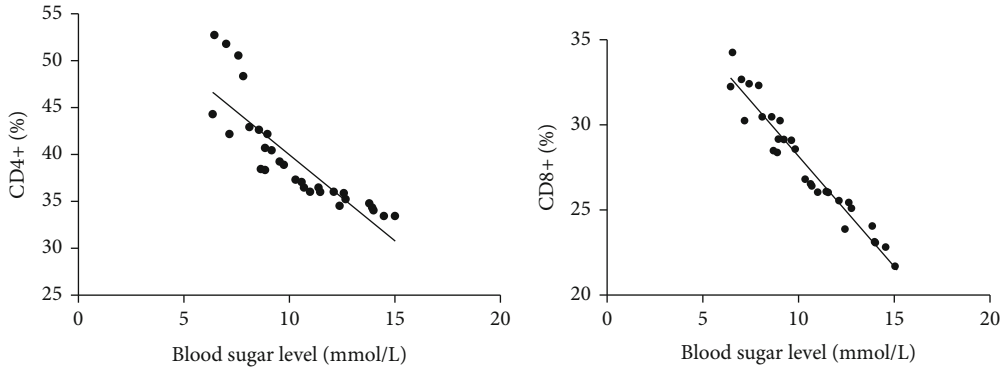

Figure 5: Correlation analysis of blood glucose levels and CD4+ and CD8+ levels in patients with sepsis. Note: the abscissa represents the blood glucose level; the ordinate represents the level of CD4+ and CD8+.

4. Discussion

Sepsis is a critical illness in intensive care medicine and is associated with protein, sugar, and lipid metabolism disorder and intensive inflammatory responses [9, 10]. Inflammation is a defensive measure of the body in the face of traumatic injury. Mitochondrial damage-related pattern molecules are released when the body is subject to strong stimuli such as severe trauma, burns, and major surgical operations, which initiate inflammatory responses through activation of neutrophils and mitogen-activated protein kinase signaling pathways [11–13]. IL-6 is a broad pleiotropic cytokine that plays a key role in host defense by regulating immunity and inflammatory responses [14]. TNF-α and IL-1β are proinflammatory factors that stimulate T cells to secrete large amounts of inflammatory mediators, which compromise the immune function and exacerbate the systemic inflammatory response [15–17]. CD4+ is an important immune cell that is primarily involved in infection control in the body. CD8+ is generated during the differentiation of lymphocyte surface antigens and can identify different stages of lymphocyte development. Studies have demonstrated that CD8+ belongs to an important subgroup of T lymphocytes and exerts cell proliferation and expansion effects after differentiation to directly participate in the body's immune regulation [18–20]. It has been found that there is an interplay between the blood glucose level of patients with sepsis and the development of the disease. Specifically, high blood sugar levels may aggravate inflammatory responses and impair the body's resistance, thereby accelerating disease development [21].

Table 2: Comparison of immune function indicators in the three groups ($\bar{x} \pm s$).

Groups	n	CD4+ (%)	CD8+ (%)
Observation group	30	34.61 ± 10.25	22.28 ± 10.21
Experimental group	30	49.36 ± 9.34*	29.94 ± 11.18*#
Control group	30	58.54 ± 10.27*#	35.46 ± 9.67*#

* indicates compared with the control group, $P < 0.05$; # indicates compared with the experimental group, $P < 0.05$.

The levels of inflammatory factors including IL-6, TNF-α and IL-1β, were the lowest in the control group, followed by the experimental group, and then the observation group ($P < 0.05$), which is consistent with the research results by Kim et al. [22], indicating a severe systemic inflammatory response in patients with sepsis complicated with diabetes. In addition, a previous study showed that the serum IL-6 level was significantly positively correlated with blood glucose level upon intensive care unit (ICU) admission ($n = 153$; $r = 0.24$, $P = 0.01$) [23]. In the present study, the lowest immune function indicators CD4+ and CD8+ levels were found in the observation group, followed by the experimental group, and then the control group ($P < 0.05$), suggesting that patients with sepsis are associated with abnormal expression levels of T lymphocytes, which underscores the role of the assay of CD4+ and CD8+ levels for early diagnosis and treatment of sepsis. Moreover, the blood glucose level of patients with sepsis was positively correlated with the levels of IL-6, TNF-α and IL-1β and was negatively correlated with the levels of CD4+/CD8+; the higher the blood glucose, the lower the number of immune cells, which is in line with the results of the report by Nakamura et al. [24], indicating that the high blood glucose levels are associated with more severe immunity dysfunction in the patients with sepsis. As blood sugar levels increase, IL-6, TNF-α and IL-1β levels present a trend of increase, whereas the level of CD4+/CD8+ shows a downward trend. In conclusion, the blood glucose level of patients with sepsis is positively correlated with inflammatory response and negatively with immune indicators. An increased blood sugar level is associated with aggravated inflammatory responses and a decreased number of immune cells, which provides a reference for the disease severity assessment and treatment of patients with sepsis.

Data Availability

The datasets used during the present study are available from the corresponding author upon reasonable request.

Conflicts of Interest

The authors declare that there is no conflict of interest.

Acknowledgments

This study was supported by the Cangzhou City Key R&D Plan Guidance Project (Project Number 204106107).

References

[1] A. Kumar, P. Sagar, B. Kashyap, S. V. Madhu, and N. Jain, "Bacteriological prof ILe of se Psis and its correlation with Procalcitonin in patients with diabetes mellitus," *International Journal of Diabetes in Developing Countries*, vol. 39, no. 1, pp. 144–147, 2019.

[2] M.-S. Hsieh, S.-Y. Hu, C.-K. How et al., "Hospital outcomes and cumulative burden from complications in type 2 diabetic sepsis patients: a cohort study using administrative and hospital-based databases," *TheraPeutic Advances in Endocrinology and Metabolism*, vol. 10, no. 1, 2019.

[3] H. Li, D. Wang, W. Wei, L. Ouyang, and N. Lou, "The predictive value of coefficient of PCT × BG for anastomotic leak in esophageal carcinoma patients with ARDS after esophagectomy," *Journal of Intensive Care Medicine*, vol. 34, no. 7, pp. 572–577, 2019.

[4] J. Chen, H. Xia, L. Zhang, H. Zhang, D. Wang, and X. Tao, "Protective effects of melatonin on sePsis-induced liver injury and dysregulation of gluconeogenesis in rats through activating SIRT1/STAT3 pathway," *Biomedicine & Pharmacotherapy*, vol. 117, no. 117, article 109150, 2019.

[5] K. Stoudt and S. Chawla, "Don't sugar coat it: glycemic control in the intensive care unit," *Journal of Intensive Care Medicine*, vol. 34, no. 11-12, pp. 889–896, 2019.

[6] P. Ying, C. Yang, X. Wu, Q. Cai, and W. Xin, "Effect of hydrocortisone on the 28-day mortality of patients with septic acute kidney injury," *Renal Failure*, vol. 41, no. 1, pp. 794–799, 2019.

[7] A. Musa, B. G. Ilah, A. M. Sakajiki, A. O. Adeniji, and I. Yusuf, "Prevalence and outcome of hy poglycemia in children attending emergency pediatric unit of a specialist hospital in Nigeria," *Sahel Medical Journal*, vol. 22, no. 2, pp. 77–81, 2019.

[8] W. Wang, W. Chen, Y. Liu et al., "Blood glucose levels and mortality in patients with sepsis: dose–response analysis of observational studies," *Journal of Intensive Care Medicine*, vol. 36, no. 2, pp. 182–190, 2021.

[9] J. He, G. Zheng, X. Qian et al., "Effect of high-dose intravenous vitamin C on point-of-care blood glucose level in septic patients: a retrospective, single-center, observational case series," *Current Medical Research and Opinion*, vol. 37, no. 4, pp. 555–565, 2021.

[10] C. T. Huang, J. H. Lue, T. H. Cheng, and Y. J. Tsai, "Glycemic control with insulin attenuates sepsis-associated encephalopathy by inhibiting glial activation via the suppression of the nuclear factor kappa B and mitogen-activated protein kinase signaling pathways in septic rats," *Brain Research*, vol. 1738, article 146822, 2020.

[11] J. Kealy, C. Murray, E. W. Griffin et al., "Acute inflammation alters brain energy metabolism in mice and humans: role in suppressed spontaneous activity, impaired cognition, and delirium," *The Journal of Neuroscience: The Official Journal of the Society for Neuroscience*, vol. 40, no. 29, pp. 5681–5696, 2020.

[12] Y. Wang, Z. Xu, D. Yue, Z. Zeng, W. Yuan, and K. Xu, "Linkage of lnc RNA CRNDE sponging mir-181a-5p with aggravated inflammation underlying sepsis," *Innate Immunity*, vol. 26, no. 2, pp. 152–161, 2020.

[13] H. Xiong, H. Wang, and Q. Yu, "Circular RNA circ 0003420 mediates inflammation in sepsis-induced liver damage by downregulating neuronal PAS domain protein 4," *Immunopharmacology and Immunotoxicology*, vol. 43, no. 3, pp. 271–282, 2021.

[14] J. P. Sikora, J. Sobczak, D. Zawadzki, P. Przewratil, A. Wysocka, and M. Burzyńska, "Respiratory burst and tnf-α receptor expression of neutrophils after sepsis and severe injury-induced inflammation in children," *International Journal of Environmental Research and Public Health*, vol. 18, no. 4, p. 2187, 2021.

[15] C. Lehmann, M. Aali, J. Zhou, and B. Holbein, "Comparison of treatment effects of different iron chelators in experimental models of sepsis," *Life*, vol. 11, no. 1, p. 57, 2021.

[16] C. H. Huang, S. C. Wang, I. C. Chen et al., "Protective effect of piplartine against lps-induced sepsis through attenuating the MAPKs/NF-κB signaling pathway and NLRP3 inflammasome activation," *Pharmaceuticals*, vol. 14, no. 6, p. 588, 2021.

[17] B. Ruggerone, D. Scavone, R. Troìa, M. Giunti, F. Dondi, and S. Paltrinieri, "ComParison of protein carbonyl (PCO), paraoxonase-1 (PON1) and C-reactive protein (CRP) as diagnostic and prognostic markers of septic inflammation in dogs," *Veterinary Sciences*, vol. 8, no. 6, p. 93, 2021.

[18] H. Alsaegh, H. Eweis, F. Kamal, and A. Alrafiah, "Celecoxib decrease seizures SuscePtibILity in a rat model of inflammation by inhibiting HMGB1 translocation," *Pharmaceuticals*, vol. 14, no. 4, p. 380, 2021.

[19] Q. Li, Y. Tan, S. Chen et al., "Irisin alleviates LPS-induced liver injury and inflammation through inhibition of NLRP3 inflammasome and NF-κB signaling," *Journal of Receptors and Signal Transduction*, vol. 41, no. 3, pp. 294–303, 2021.

[20] R. Zazula, M. Moravec, F. Pehal, T. Nejtek, M. Protuš, and M. Müller, "Myristic acid serum levels and their significance for diagnosis of systemic inflammatory response, sepsis, and bacteraemia," *Journal of Personalized Medicine*, vol. 11, no. 4, p. 306, 2021.

[21] K. C. Moon, C.-W. Park, J. S. Park, and J. K. Jun, "Fetal growth restriction and subsequent low grade fetal inflammatory response are associated with early-onset neonatal sepsis in the context of early preterm sterile intrauterine environment," *Journal of Clinical Medicine*, vol. 10, no. 9, p. 2018, 2021.

[22] E. J. Kim, J. B. Seo, J. S. Yu et al., "Anti-inflammatory effects of a polyphenol, catechin-7,4′-O-digallate, from Woodfordia uniflora by regulating NF-κB signaling pathway in mouse macrophages," *Pharmaceutics*, vol. 13, no. 3, p. 408, 2021.

[23] M. Nakamura, S. Oda, T. Sadahiro et al., "Correlation between high blood IL-6 level, hyperglycemia, and glucose control in septic patients," *Critical Care*, vol. 16, no. 2, p. R58, 2012.

[24] U. Gergs, T. Gerigk, J. Wittschier et al., "Influence of serotonin 5-HT4 receptors on responses to cardiac stressors in transgenic mouse models," *Biomedicine*, vol. 9, no. 5, p. 569, 2021.

Hindawi
Disease Markers
Volume 2022, Article ID 2334335, 6 pages
https://doi.org/10.1155/2022/2334335

Research Article

Effects of Different Delivery Modes on Pelvic Floor Function in Parturients 6–8 Weeks after Delivery Using Transperineal Four-Dimensional Ultrasound

Chao Wang,[1,2] Qirong Wang,[3] Xuemei Zhao,[4] Xia Wang,[2] Wenji Zhou,[2] and Liqing Kang[5]

[1]*Graduate School, Tianjin Medical University, Tianjin City 300070, China*
[2]*The No. 2 Department of Ultrasound, Binzhou No. 2 People's Hospital, Binzhou, Shandong Province 256800, China*
[3]*Maternal and Child Health Planning Service Center of Zhanhua, Binzhou, Shandong Province 256800, China*
[4]*Department of Pelvic Floor Disease Rehabilitation and Treatment, Binzhou No. 2 People's Hospital, Binzhou, Shandong Province 256800, China*
[5]*Department of Medical Imaging, Cangzhou Central Hospital, Cangzhou Teaching Hospital of Tianjin Medical University, Cangzhou, Hebei Province 061001, China*

Correspondence should be addressed to Liqing Kang; 13333367921@163.com

Received 11 January 2022; Revised 17 February 2022; Accepted 26 February 2022; Published 18 May 2022

Academic Editor: Yaoyao Bian

Objective. To evaluate the effects of different delivery modes on pelvic floor function in parturients 6–8 weeks after delivery using transperineal four-dimensional ultrasound. *Methods*. Pelvic floor function 6–8 weeks after delivery in 40 vaginal delivery parturients between November 2018 and December 2020 was assessed by four-dimensional ultrasound, with 40 selective cesarean section delivery parturients as a control group. The imaging results of the two groups were compared. *Results*. The levels of clinical indexes such as UVJ-M, A_r, A_v, θ, D_r, D_v, and ARJ-VDv in the selective cesarean section group were significantly lower than those in the vaginal delivery group 6–8 weeks after delivery ($P < 0.05$). However, no significant difference in CV-VD was observed under Valsalva action and at rest between the two groups ($P > 0.05$). No significant difference in ARJ-VD was found at rest between the two groups ($P > 0.05$). The incidence of pelvic organ prolapse in the selective cesarean section group (40.0%) was significantly lower than that in the vaginal delivery group (62.5%) ($P < 0.05$). No significant difference in the parameters of pelvic diaphragm hiatus at rest was observed between the two groups ($P > 0.05$). The parameters of pelvic diaphragm hiatus under maximum Valsalva action in the vaginal delivery group were significantly higher than those in the selective cesarean section group ($P < 0.05$). Whether the patient was complicated with diabetes had no significant effect on the functional injury of pelvic floor muscle ($P > 0.05$). *Conclusion*. The pelvic floor function 6–8 weeks after delivery was significantly more affected in vaginal delivery than in selective cesarean section. Selective cesarean section had certain but limited protective effect on maternal pelvic floor tissue.

1. Introduction

With the rapid development of social economy and the continuous improvement of people's living standards, people's health consciousness has been further enhanced, and women of childbearing age pay more and more attention to pregnancy and pelvic floor function [1]. Pelvic floor dysfunction may be caused by pregnancy and childbirth, chronic constipation, and chronic cough, and intense physical exercise may also increase the risk of the disease. The occurrence of pelvic floor dysfunction is also related to age, perimenopausal period, heredity, drugs, lifestyle, and other factors. More than 45% of women were reported to have pelvic floor dysfunction in varying degrees [2, 3]. The progression of female pregnancy will slowly enlarge the uterus and change its position [4]. Especially for women in the third trimester, when the position of the uterus is close to the vertical state, thus, the supporting tissue of the

Table 1: Demographic characteristics in the two groups ($\bar{x} \pm s$).

Items	Vaginal delivery group ($n = 40$)	Selective cesarean section group ($n = 40$)	t	P
Age (years)	24.25 ± 1.77	23.62 ± 1.51	1.7	0.093
Height (cm)	163.25 ± 5.82	162.23 ± 5.81	0.789	0.433
Predelivery weight (kg)	62.11 ± 2.71	61.92 ± 2.86	0.309	0.758
Neonatal weight (kg)	3.16 ± 0.83	3.05 ± 0.68	0.648	0.51

pelvic floor will be under relatively greater pressure [5, 6]. Early detection of pelvic function problems in women is important to the improvement of the therapeutic effect. Transperineal four-dimensional pelvic floor ultrasound has the advantages of easy operation, high accuracy, and less injury; it has also become an important way to detect the function of women's pelvic floor in clinic [7].

The traditional diagnosis is based on anatomical diagnosis of clinical symptoms and mainly uses the POP-Q evaluation method. The main examination methods of pelvic floor dysfunction include anorectal manometry, pelvic floor electromyography, perianal, perineal, and intracavitary ultrasound, and defecography. The treatment of pelvic floor dysfunction can be divided into nonoperative treatment and surgical treatment. Nonoperative treatment is the first-line treatment of pelvic organ prolapse (POP). For all patients with organ prolapse, nonoperative treatment should be conducted first. At the same time, it is also suitable for patients who retain reproductive function or cannot tolerate surgical treatment. Surgical treatment can relieve symptoms, increase the strength, endurance, and support of pelvic floor muscles, and prevent the aggravation of prolapse. Patients can also try traditional Chinese medicine and acupuncture. The main purpose of surgical treatment is to relieve symptoms and restore normal anatomical position and organ function. This study is aimed at investigating the effects of different delivery modes on the pelvic floor function of parturients 6–8 weeks after delivery by transperineal four-dimensional pelvic floor ultrasound.

2. Materials and Methods

2.1. General Information. Eighty parturients who were visited 6–8 weeks after obstetrical delivery in Binzhou No. 2 People's Hospital between November 2018 and December 2020 were divided into the selective cesarean section group ($n = 40$) and vaginal delivery group ($n = 40$) according to the mode of delivery. This study was approved by the Ethics Committee of Binzhou No. 2 People's Hospital, and the informed consents were signed by all patients.

The inclusion criteria were as follows: (1) all parturients were first-born and singleton, (2) no POP occurred before pregnancy, (3) no pelvic floor injury occurred before delivery, (4) no history of chronic cough, (5) no history of constipation, and (6) all parturients participated in the study voluntarily.

The exclusion criteria were as follows: (1) fetal malformations in antenatal examination, (2) complications during pregnancy, (3) pelvic floor injury before delivery, (4) severe medical or surgical diseases, (5) severe mental illness, and (6) parturients cannot participate in the whole study.

2.2. Research Methods. A GE-E10 US system was selected as the testing instrument, and the RIC5-9-D endocavity transducer was installed on the instrument. First, let the pregnant woman urinate thoroughly and then check the bladder, keep the bladder in a proper filling state, and ensure that the urine volume was controlled within 50 ml. After the parturient was kept in a supine position, and the lithotomy position was taken, the coupling agent was applied on the vaginal probe, which was covered with a layer of condom, and was placed in the vagina. The uterus, bilateral appendages, and bilateral ovaries were strictly examined. Next, the probe was placed at the position below the external orifice of the urethra, and then the vaginal vestibule position of the two groups of parturients were examined by ultrasound. The indexes of θ, D_r, D_v, A_r, A_v, CV-VD, UVJ-M, and ARJ-VD of the two groups were examined under Valsava action and at rest.

2.3. Research Index. The ultrasonographic results of two groups with different delivery methods were compared, including the posterior angle of vesicourethral angle (A_r, A_v), the vertical distance of bladder neck to the inferior edge of pubic symphysis (D_r, D_v), the angle of urethral tilt (θ), urethrovesical junction mobility (UVJ-M), the vertical distance of external cervical orifice to the inferior edge of pubic symphysis (CV-VD), the vertical distance between the anorectal junction and the inferior margin of pubic symphysis (ARJ-VD), and pelvic diaphragmatic hiatus parameters. The probability of POP between the two groups was recorded and compared. To ensure the consistency of the inspection results and the accuracy of the data, all tests and data entry were conducted by the same team, and members may not be changed without special reasons in the course of the study.

2.4. Statistical Method. The study used the statistical software SPSS25.0 to process the data. Counting data were expressed as (%), and χ^2 test was used to compare the differences of parameters between the two groups. Measurement data were expressed as ($\bar{x} \pm s$), and t-test was used to compare the differences of parameters between the two groups. Statistical significance was set at $P < 0.05$.

3. Results

3.1. Demographic Characteristics in the Two Groups. Table 1 summarizes the clinical features of the parturients. All the

Table 2: Pelvic floor characteristics detected by transperineal ultrasound in the two groups ($\bar{x} \pm s$).

Items	Vaginal delivery group ($n = 40$)	Selective cesarean section group ($n = 40$)	t	P
A_r (°)	97.69 ± 10.25	92.26 ± 7.52	2.7014	0.009
A_v (°)	145.26 ± 24.72	126.25 ± 22.31	3.6106	0.001
D_r (cm)	24.25 ± 4.26	27.26 ± 3.87	3.3077	0.001
D_v (cm)	9.42 ± 1.25	11.26 ± 4.28	2.6099	0.011
θ (°)	46.26 ± 25.26	27.15 ± 21.68	3.6308	0.000
UVJ-M (cm)	22.26 ± 8.28	15.62 ± 7.24	3.8181	0.000
CV-VDr (cm)	26.62 ± 4.26	27.15 ± 6.11	0.4500	0.652
CV-VDv (cm)	14.25 ± 10.06	16.14 ± 10.38	0.8269	0.512
ARJ-VDr (cm)	12.15 ± 3.25	13.26 ± 3.82	1.3997	0.169
ARJ-VDv (cm)	2.13 ± 1.28	3.87 ± 4.28	2.4634	0.000

Abbreviations: A_r and A_v: the posterior angle of vesicourethral angle at rest and Valsalva action, respectively; D_r and D_v: the vertical distance of bladder neck to the inferior edge of pubic symphysis at rest and Valsalva action, respectively; θ: the angle of urethral tilt; UVJ-M: urethrovesical junction mobility; CV-VDr and CV-VDv: the vertical distance of external cervical orifice to the inferior edge of pubic symphysis at rest and Valsalva action, respectively; ARJ-VDr and ARJ-VDv: the vertical distance between the anorectal junction and the inferior margin of pubic symphysis at rest and Valsalva action, respectively.

differences of demographic characteristics between the two groups were not statistically significant ($P > 0.05$).

3.2. Characteristics of Pelvic Floor Detected by Transperineal Ultrasound in the Two Groups. The results of perineal ultrasound examination in Table 2 show that the clinical indexes such as UVJ-M, A_r, A_v, D_r, D_s, θ, and ARJ-VDv in the selective cesarean section group were significantly lower than those in the vaginal delivery group 6–8 weeks after delivery ($P < 0.05$). However, no significant difference in CV-VD was observed between the two groups under Valsalva action and at rest ($P > 0.05$). No significant difference in ARJ-VD in the resting period was found between the two groups with different delivery methods ($P > 0.05$).

3.3. Comparison of the Incidence of POP between the Two Groups. The data in Table 3 show that the incidence of POP in the selective cesarean section was 40.0%, which was significantly lower than that of the 62.5% in the vaginal delivery group ($P < 0.05$).

3.4. Comparison of Parameters of Pelvic Diaphragmatic Hiatus between the Two Groups at Rest. The data in Table 4 show that the parameters of the pelvic diaphragm hiatus in the resting state between the vaginal group and the selective cesarean section group were statistically insignificant ($P > 0.05$).

3.5. Comparison of Parameters of Pelvic Diaphragmatic Hiatus under Maximum Valsalva Action between the Two Groups. The data in Table 5 show that the parameters of the pelvic diaphragm hiatus under the maximum Valsalva action in the vaginal group were significantly higher than those in the selective cesarean section group ($P < 0.05$).

3.6. Comparison of Parameters of Pelvic Diaphragmatic Hiatus in Patients with and without Diabetes at Rest and Maximum Valsalva. In this study, 31 pregnant women with diabetes and 49 cases without diabetes were considered. No significant difference was found in left and right diameter, anterior and posterior diameter, and the area of pelvic diaphragmatic hiatus between patients with and without diabetes at rest and under maximum Valsalva action ($P > 0.05$), see Table 6.

4. Discussion

The rectum, urethra, fascia, muscles, vagina, and other tissues are located in the pelvic floor tissues. Thus, they can produce a certain load-bearing effect on various tissues and organs in the pelvic cavity. Accordingly, they can effective ensure their anatomical positions. After pregnancy and childbirth, pelvic floor damage may take place in pregnant women, which may causes pelvic organ prolapse, stress urinary incontinence, postpartum urinary incontinence, and other symptoms [8, 9].

4.1. Observation and Exploration of Pelvic Floor Anatomy and Function by Transperineal Ultrasound. With the widespread application of ultrasound, CT, and MRI, the anatomical structure of the pelvic floor tissue can be clearly demonstrated [10]. Among them, the ultrasound has the advantages of low cost, no radioactivity, simplicity, high acceptance by patients, and strong reproducibility and is the first choice for the evaluation of pelvic floor dysfunction [11–13]. The pelvic organs, such as the bladder, urethra, pubic bone, bladder neck, and vagina, can be clearly visualized by four-dimensional perineal ultrasound. Under the resting and Valsalva movement state, the pelvic floor function can be evaluated by the mobility parameters of the pelvic organs such as bladder neck, cervix, rectal ampullary, and the angle parameters of urethral tilt angle and urethral rotation angle [14, 15].

4.2. Effect of Pregnancy on Pelvic Floor Function. During pregnancy, the uterus will gradually expand and change from the original horizontal position to the longitudinal position in the pelvic and abdominal cavity [16, 17]. Especially for women in the third trimester of pregnancy, the

Table 3: Incidence of POP in the two groups.

Items	Vaginal delivery group ($n = 40$)	Selective cesarean section group ($n = 40$)	χ^2	P
Normal	15	24	—	
Abnormal	25	16	—	
Incidence of abnormal	62.50%	40.00%	4.0525	0.044

Table 4: Parameters of pelvic diaphragmatic hiatus in two groups of patients at rest ($\bar{x} \pm s$).

Items	Vaginal delivery group ($n = 40$)	Selective cesarean section group ($n = 40$)	t	P
Left and right diameter (cm)	3.59 ± 0.68	3.61 ± 0.72	0.1277	0.911
Anterior and posterior diameter (cm)	4.63 ± 0.87	4.61 ± 0.86	0.1034	0.897
Area (cm^2)	16.66 ± 4.56	16.56 ± 4.35	0.5135	0.925

Table 5: Pelvic diaphragmatic hiatus under maximum Valsalva action in two groups ($\bar{x} \pm s$).

Items	Vaginal delivery group ($n = 40$)	Selective cesarean section group ($n = 40$)	t	P
Left and right diameter (cm)	6.28 ± 0.39	4.48 ± 0.44	19.36	0.000
Anterior and posterior diameter (cm)	7.13 ± 0.57	5.76 ± 0.48	11.64	0.000
Area (cm^2)	34.76 ± 2.96	20.81 ± 2.18	24.01	0.000

Table 6: Comparison of parameters of pelvic diaphragmatic hiatus in patients with and without diabetes at rest and under maximum Valsalva ($\bar{x} \pm s$).

Items	Left and right diameter (cm)		Anterior and posterior diameter (cm)		Area (cm^2)	
	Resting	Valsalva	Resting	Valsalva	Resting	Valsalva
Complicated with diabetes mellitus ($n = 31$)	3.69 ± 0.65	5.4 ± 0.97	4.70 ± 0.78	5.66 ± 0.83	17.35 ± 4.37	28.56 ± 7.14
Without diabetes ($n = 49$)	3.53 ± 0.72	5.37 ± 1.02	4.57 ± 0.90	5.31 ± 0.87	16.14 ± 4.44	27.44 ± 7.73
t	1.001	0.142	0.635	1.818	1.192	0.65
P	0.32	0.887	0.527	0.073	0.237	0.518

position of the uterus is close to a vertical state, and the pelvic floor supporting tissues will be relatively stressed. With the slowly grow up of uterus, the spine position of pregnant women will bend forward, and the pelvic cavity will be subjected to pressure from the front and lower parts. The dissolution rate of pelvic floor ligament collagen in pregnant women in the third trimester of pregnancy also continues to increase. The ligaments will gradually become loose; although the cervical ring is affected by the combined force of the posterior and inferior, it faces downward as a whole and plays a role in the genital hiatus [18, 19]. When the delivery is completed, the parturient's uterus will no longer continue to receive the force from the front and lower parts, her hormone levels will slowly return to normal, and so will the support force received from the pelvic floor. The cervical ring will also return to its original state [20]. Relevant studies have shown that many physiological changes that occur during pregnancy will be effectively improved within 6–8 weeks in the postpartum period. If the pelvic floor structure and function fails to be repaired in time after delivery, a series of pelvic floor dysfunction diseases may happen, such as genital prolapse, fecal incontinence, and urinary incontinence [21]. Routine pelvic floor function examination should be performed 42 days after delivery, and pelvic floor rehabilitation treatment can be conducted after 42 days of postpartum lochia. The best time for pelvic floor muscle rehabilitation is within 3 months after delivery in order to avoid urinary incontinence, uterine prolapse, and other pelvic floor dysfunction in the future. In addition, pelvic floor rehabilitation treatment can be conducted at any time for menopausal women and elderly patients with pelvic floor dysfunction, such as sneezing leakage, laughter leakage, and chronic pelvic pain. The sooner the treatment start, the better the outcome is.

4.3. Structure of the Pelvic Floor Shortly after Delivery Is Affected by Different Modes of Delivery. Hormone secretion in female will change significantly during pregnancy. Thus, the collagen of the pelvic floor ligament will gradually become loosen and dissolved. This condition will reduce the tension of the pelvic floor muscles. In the third trimester of pregnancy, the pelvic floor structure will be compressed

by the weight of the uterus, which will affect the pelvic floor structure and function [22, 23]. During the vaginal delivery of the parturient, the vagina will be stretched, which will lead to lacerations of nerves, pelvic floor muscle fibers, birth canal stretch, and perineal lacerations [24]. This study showed that the incidence of POP in the cesarean section group was significantly lower than that in the vaginal delivery group ($P < 0.05$). The different ways that women choose to give birth have different effects on their postpartum pelvic floor structure and function. Compared with cesarean section, vaginal delivery will cause more recent damage to the pelvic floor structure. No matter what kind of delivery was chosen, the mother needs to receive biological treatment or rehabilitation training in time after childbirth to promote the increase in pelvic floor muscle tension and effectively avoid the appearance of pelvic floor dysfunction diseases. In this study, the differences in the parameters of pelvic diaphragm hiatus in patients at rest between the two groups were not statistically insignificant ($P > 0.05$), and the parameters of the pelvic diaphragm hiatus under the maximum Valsalva action in the vaginal group were significantly higher than those in the selective cesarean section group ($P < 0.05$). The pelvic diaphragm hiatus was the weakest area of female pelvic tissue. The uneven force of the female pelvic diaphragm hiatus or the bottom of the pelvic cavity during delivery, especially vaginal delivery, may increase the risk of female pelvic diaphragm hiatus damage, which leads to long-term pelvic floor tissue prolapse and other complications.

4.4. Protective Effect of Selective Cesarean Section on Pelvic Floor Function. The results of this study show that the indicators of A_v, A_r, and UVJ-M in the cesarean section were significantly smaller than those in the vaginal delivery group ($P < 0.05$), indicating that the structure damage and the impairment of pelvic floor function of the vaginal delivery group were more severe than that of the selective cesarean section. Vaginal delivery may damage pelvic floor muscles and fascia tissue, weaken the pelvic organ supporting structure, and change the mobility of pelvic floor and bladder neck position. These changes are important causes of stress urinary incontinence. Cesarean section can effectively prevent the pelvic floor tissue from tearing or dilating, which avoids damage to the urinary tract and effectively protects the early pelvic floor function of the parturient. However, this conclusion has yet to be verified by a large amount of data in the future, and further exploration is needed.

Some studies have shown that the severity of pelvic floor functional disorders is positively correlated with the course of diabetes; that is, the symptoms of pelvic floor functional disorders are more serious when the history of diabetes is longer. Focusing on pelvic floor functional disorders with diabetic symptoms, reducing the severity of pelvic floor dysfunction, and actively controlling the level of blood glucose are important to improve the prognosis of patients and their quality of life. However, in this study, whether diabetes has significant effect on pelvic floor muscle function damage is unclear. This inadequacy may be due to that the included pregnant women have less menstruation, the course of disease is still short, and their blood glucose levels are well controlled. We will include more cases and draw more profound conclusions in future studies.

In summary, the transperineal four-dimensional pelvic floor ultrasonography was performed on women with different delivery methods. Comparing various parameters shows that the pelvic floor function of women with vaginal delivery is significantly more affected than that with cesarean section. Selective cesarean section has a certain protective effect on the pelvic floor tissue of the lying-in woman, but the protective effect is limited.

Data Availability

The analyzed data sets generated during the study are available from the corresponding author on reasonable request.

Conflicts of Interest

The authors declare that they have no conflicts of interest.

References

[1] M. Mabrouk, D. Raimondo, S. del Forno et al., "Pelvic floor muscle assessment on three- and four-dimensional transperineal ultrasound in women with ovarian endometriosis with or without retroperitoneal infiltration: a step towards complete functional assessment," *Ultrasound in Obstetrics & Gynecology*, vol. 52, no. 2, pp. 265–268, 2018.

[2] M. O. Nyhus, K. A. Salvesen, and I. Volloyhaug, "Association between pelvic floor muscle trauma and contraction in parous women from a general population," *Ultrasound in Obstetrics & Gynecology*, vol. 53, no. 2, pp. 262–268, 2019.

[3] K. Jundt, I. Scheer, B. Schiessl, K. Karl, K. Friese, and U. M. Peschers, "Incontinence, bladder neck mobility, and sphincter ruptures in primiparous women," *European Journal of Medical Research*, vol. 15, no. 6, pp. 246–252, 2010.

[4] G. A. van Veelen, K. J. Schweitzer, and C. H. van der Vaart, "Reliability of pelvic floor measurements on three- and four-dimensional ultrasound during and after first pregnancy: implications for training," *Ultrasound in Obstetrics & Gynecology*, vol. 42, no. 5, pp. 590–595, 2013.

[5] D. Baud, J. Sichitiu, V. Lombardi et al., "Comparison of pelvic floor dysfunction 6 years after uncomplicated vaginal versus elective cesarean deliveries: a cross-sectional study," *Scientific Reports*, vol. 10, no. 1, article 21509, 2020.

[6] G. A. van Veelen, K. J. Schweitzer, and C. H. van der Vaart, "Ultrasound imaging of the pelvic floor: changes in anatomy during and after first pregnancy," *Ultrasound in Obstetrics & Gynecology*, vol. 44, no. 4, pp. 476–480, 2014.

[7] W. C. Huang, J. M. Yang, and H. F. Chen, "Four-dimensional Introital ultrasound in assessing perioperative pelvic floor muscle functions of women with cystoceles," *Ultraschall in der Medizin-European Journal of Ultrasound*, vol. 42, no. 4, pp. e31–e41, 2021.

[8] S. Thibault-Gagnon, S. Yusuf, S. Langer et al., "Do women notice the impact of childbirth-related levator trauma on pelvic floor and sexual function? Results of an observational ultrasound study," *International Urogynecology Journal*, vol. 25, no. 10, pp. 1389–1398, 2014.

[9] M. Majida, I. H. Brækken, K. Bø, and M. E. Engh, "Levator hiatus dimensions and pelvic floor function in women with and without major defects of the pubovisceral muscle," *International Urogynecology Journal*, vol. 23, no. 6, pp. 707–714, 2012.

[10] M. Majida, I. H. Braekken, W. Umek, K. Bø, J. Šaltytė Benth, and M. Ellstrøm Engh, "Interobserver repeatability of three- and four-dimensional transperineal ultrasound assessment of pelvic floor muscle anatomy and function," *Ultrasound in Obstetrics & Gynecology*, vol. 33, no. 5, pp. 567–573, 2009.

[11] A. G. Cheng, E. C. Oxford, J. Sauk et al., "Impact of mode of delivery on outcomes in patients with perianal Crohn's disease," *Inflammatory Bowel Diseases*, vol. 20, no. 8, pp. 1391–1398, 2014.

[12] H. Li, R. F. Wu, F. Qi et al., "Postpartum pelvic floor function performance after two different modes of delivery," *Genetics and Molecular Research*, vol. 14, no. 2, pp. 2994–3001, 2015.

[13] R. R. Guzman, K. A. Salvesen, and I. Volloyhaug, "Anal sphincter defects and fecal incontinence 15-24 years after first delivery: a cross-sectional study," *Ultrasound in Obstetrics & Gynecology*, vol. 51, no. 5, pp. 677–683, 2018.

[14] L. P. Chamié, D. M. Ribeiro, A. H. Caiado, G. Warmbrand, and P. C. Serafini, "Translabial US and dynamic MR imaging of the pelvic floor: normal anatomy and dysfunction," *Radiographics*, vol. 38, no. 1, pp. 287–308, 2018.

[15] P. Driusso, A. Beleza, D. M. Mira et al., "Are there differences in short-term pelvic floor muscle function after cesarean section or vaginal delivery in primiparous women? A systematic review with meta-analysis," *International Urogynecology Journal*, vol. 31, no. 8, pp. 1497–1506, 2020.

[16] Y. Zhao, L. Zou, M. Xiao, W. Tang, H. Y. Niu, and F. Y. Qiao, "Effect of different delivery modes on the short-term strength of the pelvic floor muscle in Chinese primipara," *BMC Pregnancy and Childbirth*, vol. 18, no. 1, p. 275, 2018.

[17] F. Siafarikas, J. Staer-Jensen, G. Hilde, K. Bø, and M. Ellström Engh, "The levator ani muscle during pregnancy and major levator ani muscle defects diagnosed postpartum: a three- and four-dimensional transperineal ultrasound study," *BJOG*, vol. 122, no. 8, pp. 1083–1091, 2015.

[18] I. H. Brækken, M. Majida, M. Ellstrøm-Engh, H. P. Dietz, W. Umek, and K. Bø, "Test-retest and intra-observer repeatability of two-, three- and four-dimensional perineal ultrasound of pelvic floor muscle anatomy and function," *International Urogynecology Journal and Pelvic Floor Dysfunction*, vol. 19, no. 2, pp. 227–235, 2008.

[19] Y. J. Mao, Z. J. Zheng, J. H. Xu, J. Xu, and X. L. Zhang, "Pelvic floor biometry in asymptomatic primiparous women compared with nulliparous women: a single-center study in Southern China," *The Journal of International Medical Research*, vol. 48, no. 4, 2020.

[20] A. Grouin, C. Brochard, L. Siproudhis et al., "Perianal Crohn's disease results in fewer pregnancies but is not exacerbated by vaginal delivery," *Digestive and Liver Disease*, vol. 47, no. 12, pp. 1021–1026, 2015.

[21] J. Cassadó, M. Simó, N. Rodríguez et al., "Prevalence of levator ani avulsion in a multicenter study (PAMELA study)," *Archives of Gynecology and Obstetrics*, vol. 302, no. 1, pp. 273–280, 2020.

[22] N. Martinho, S. Botelho, A. Nagib et al., "Four-dimensional translabial ultrasound concordance with digital palpation and surface electromyography during dynamic pelvic floor muscles assessment: a cross-sectional study," *Neurourology and Urodynamics*, vol. 39, no. 1, pp. 403–411, 2020.

[23] K. van Delft, R. Thakar, and A. H. Sultan, "Pelvic floor muscle contractility: digital assessment vs transperineal ultrasound," *Ultrasound in Obstetrics & Gynecology*, vol. 45, no. 2, pp. 217–222, 2015.

[24] D. Raimondo, A. Youssef, M. Mabrouk et al., "Pelvic floor muscle dysfunction on 3D/4D transperineal ultrasound in patients with deep infiltrating endometriosis: a pilot study," *Ultrasound in Obstetrics & Gynecology*, vol. 50, no. 4, pp. 527–532, 2017.

Hindawi
Disease Markers
Volume 2022, Article ID 6103086, 10 pages
https://doi.org/10.1155/2022/6103086

Research Article

circ_000166/miR-296 Aggravates the Process of Diabetic Renal Fibrosis by Regulating the SGLT2 Signaling Pathway in Renal Tubular Epithelial Cells

Sheng Chen

Department of Nephrology, Ningbo Medical Center Lihuili Hospital, Ningbo, Zhejiang 315000, China

Correspondence should be addressed to Sheng Chen; css220104@163.com

Received 5 January 2022; Revised 8 February 2022; Accepted 12 February 2022; Published 16 May 2022

Academic Editor: Yaoyao Bian

Diabetic renal fibrosis is a common cause of end-stage renal disease, and the circRNA-miRNA-mRNA network may play an important role in the progression of diabetic nephropathy- (DN-) induced renal fibrosis. In this study, the role of circ_000166/miR-296/SGLT2 in the process of DN-related renal fibrosis was studied by constructing an animal model of DN renal fibrosis via lentiviral transfection, plasmid transfection, and dual-luciferase reporting techniques. Compared with that of normal controls, the expression of circ_000166 in the kidney tissues of DN renal fibrosis mice substantially increased. Silencing circ_000166 could minimize kidney damage and decrease urine protein levels, thereby inhibiting the progression of renal fibrosis. Moreover, circ_000166 could act as the ceRNA of miR-296 and competitively bind to miR-296, leading to an increase in the expression of the SGLT2 gene regulated by miR-296. Through mutual verification via in vivo and in vitro experiments, miR-296 was overexpressed and SGLT2 was silenced. Results showed that DN renal fibrosis and cell apoptosis were considerably reduced. We postulate that circ_000166/miR-296/SGLT2 may become a new target in the progression of DN renal fibrosis, and the regulation of this pathway may be a promising strategy for clinical treatment of DN renal fibrosis.

1. Introduction

Diabetic nephropathy (DN) is one of the most common microvascular complications among patients with diabetes and an important cause of disability and death [1, 2]. It is characterized by excessive accumulation of the extracellular matrix (ECM), thickening of the glomerulus and tubular basement membrane, and increase in the mesangial matrix, features that eventually develop into glomerular sclerosis and tubular interstitial fibrosis [3, 4].

Noncoding RNA (ncRNA) includes microRNA (miRNA), long ncRNA (lncRNA), and circular RNA (circRNA). Numerous studies reported that ncRNA plays a key role in various human diseases [5–7]. The present study investigated the interaction between miRNA and circRNA. miRNA can induce gene silencing by binding to the $3'$-untranslated region of target mRNA, thereby inducing translational inhibition. The biological effects of circRNA are mainly mediated by miRNA [8, 9]. circRNA is a new type of ncRNA characterized by a covalent closed loop [10]. circRNA can be used as one of the competing endogenous RNAs (ceRNA) that can competitively bind to miRNA, thereby blocking the translation or inducing the degradation of the target mRNA [11]. When miRNA is competitively bound by circRNA, the level of mRNA transcription regulated by miRNA will increase [1]. A recent study demonstrated that circRNA_000166 can promote the proliferation, migration, and invasion of colon cancer cells by upregulating the expression of ELK1 in miK-330-5p sponge [12].

Diabetic renal fibrosis is caused by the unbalanced metabolism of ECM molecules that may eventually lead to renal failure. Previous studies reported that circ-AKT3 inhibits ECM accumulation in mesangial cells of DN by regulating miR-296-3p/E-cadherin signals [13]. miRNA imbalance is closely related to the occurrence of diabetic renal fibrosis. Moreover, circRNA can act as a real sponge of miRNA to regulate the expression of the target gene. Thus, the circRNA-miRNA-mRNA network may play a very important role in the process of renal fibrosis caused by DN [14].

Sodium-glucose cotransporter 2 (SGLT2) is a protein mainly expressed in the apical membrane of the proximal tubule of the kidneys, and 90% of the glucose filtered by the glomerulus can be reabsorbed by this protein [15, 16]. Increased glucose uptake by cultured proximal renal tubular cells through SGLT2 can cause proapoptotic effects [17]. Apoptosis of renal tubular epithelial cells and atrophy of renal tubules eventually lead to tubular interstitial fibrosis [18].

This study investigated the role of the circ_000166/miR-296/SGLT2 network in the process of diabetic renal fibrosis. Elucidating the circ_000166/miR-296/SGLT2 regulatory network will help us to better understand the molecular mechanisms of diabetic renal fibrosis and recognize how they may serve as new biomarkers of DN and potential therapeutic targets.

2. Materials and Methods

2.1. Animals and Exposures. All animal experiments of this study were approved by the experimental animal ethics committee of Affiliated Hospital of Weifang Medical University. Male C57BL/6J mice (Beijing HFK Biotechnology Co., Ltd.) (8 weeks old, 25 ± 1 g in weight) were raised in a special-grade sterile animal room at 23 ± 1°C in a 12-hour day-night cycle. All mice had free access to food and water. Fourteen C57BL/6J mice were selected as normal controls and fed with a standard diet (8% fat). The other groups of mice were fed with a high-fat diet feed (40% fat) for 8 weeks. Afterward, the mice in the DN model group were intraperitoneally injected with 50 mg/kg streptozotocin (STZ, Sigma Chemicals, St. Louis, MO) dissolved in 100 mM citrate buffer (pH 4.5) for five consecutive days. The mice were then anesthetized with pentobarbital sodium and then killed using a carbon dioxide treatment device. The mice in the control group received an equal volume of citrate buffer. The mice with fasting blood glucose > 12 mmol/L were designated as the T1DM model mice (blood was drawn from the tail vein to measure plasma glucose via standard laboratory methods). The DN standard was 24 h UMA level ≥ 30 mg. Renal fibrosis was assessed via renal histopathology.

2.2. Cell Cultures and Exposure. Renal tubular epithelial cells (HK-2, American Type Culture Collection, Rockville, Maryland, USA) were cultured in DMEM/F12 medium containing 10% FBS (Gibco) at 37°C. The HK-2 cells were inoculated in a 12-well plate and cultured in a constant-temperature incubator at 37°C for 16–24 h. When the cell confluence reached 30%, the medium was replaced, and HiTransG P infection solution and the corresponding amount of virus (20 μL/well) were added. After 16 h, the medium was changed into a regular medium and the culture was continued. The groups consisted of the mimic-NC group, miR-296 mimic group, inhibitor-NC group, and miR-296 inhibitor group. The expression of miR-296 and SGLT2 in each group was detected 72 h after infection. HK-2 cells were seeded into a 12-well plate. When the cells reached 70% confluence, si-NC, si-circ_000166, vector-NC, and vector-circ_00016 (GenePharma Co Ltd., Shanghai, China) were transfected into the HK-2 cells. Lipofectamine 2000 (11668027, American Thermoelectric) and siRNA were premixed in Opti-MEM (31985062, American Thermoelectric) and then transfected into the cells following the manufacturer's instructions. At 24 h after transfection, the expression of miR-296 and SGLT2 in each group of cells was detected.

2.3. In Vitro Cell Model. When the cells were fused to 80%, the medium was replaced with serum-free DMEM low-glucose medium. The serum-free medium was discarded after 24 h of synchronization. The cells were divided into a normal group (D-glucose concentration in medium: 5.5 mmol/L) and a high-glucose group (D-glucose concentration in high-glucose medium: 25 mmol/L). Each group was provided with three holes. The cells were cultured for 48 h in an incubator at 37°C. Afterward, the cells were collected for subsequent tests.

2.4. Lentiviral Transfection. Lentivirus carrying the si-NC and si-circ_000166 target genes, as well as sh-NC and sh-SGLT2 lentivirus expression vectors (synthesized by Jiangsu Genechem Technology Co., Ltd.), was constructed. The animals were transfected by disinfecting the abdomen and then anesthetizing the mice in each group via intraperitoneal injection of 40 mg/kg sodium pentobarbital. Subsequently, the abdominal cavity was opened from the midline of the abdomen to expose both kidneys. A 29-gauge syringe was used to slowly inject 150–200 μL of a solution of the lentiviral vector (titer 1×10^6 CFU/mL) carrying the corresponding target gene into the kidney parenchyma. The incision was closed, and the mice were returned to the cage to breed. The mice were sacrificed on the 28th day, and their kidneys were removed for later use. The lentivirus was transfected by adding 2 mL of fresh medium containing 6 μg/mL polybrene to HK-2 cells and adding an appropriate amount of virus suspension. The cells were incubated at 37°C. After 24 h, `the virus-containing medium was replaced with fresh medium. After 72 h of continuous cultivation, the expression of fibrosis-related factors in each group was detected.

2.5. Dual-Luciferase Assay. The luciferase reporter gene test was performed using the dual-luciferase reporter assay system (Promega, USA) following the manufacturer's protocols. HK-2 cells (1.5×10^4/well) were inoculated into a 96-well plate. After 12 h, the cells were transiently cotransfected with the pRL-TK plasmid (Promega) containing the Renilla luciferase gene for internal standardization and various constructs containing pMIR-circ_000166 and pMIR-circ_000166-mut. At 36 h after transfection, the cells were lysed, and luciferase activity was measured. Finally, 100 μL of the protein extract was analyzed using a luminometer. All experiments were conducted at least three times.

2.6. qRT-PCR. HK-2 cells were lysed with the TRIzol reagent (9108, TaKaRa, Biotech, Japan), and total RNA was extracted therefrom in accordance with the manufacturer's instructions. The total RNA was reverse-transcribed (AT301-03, TransGen Biotech, Beijing, China), and the samples were normalized. The expression levels of circ_000166,

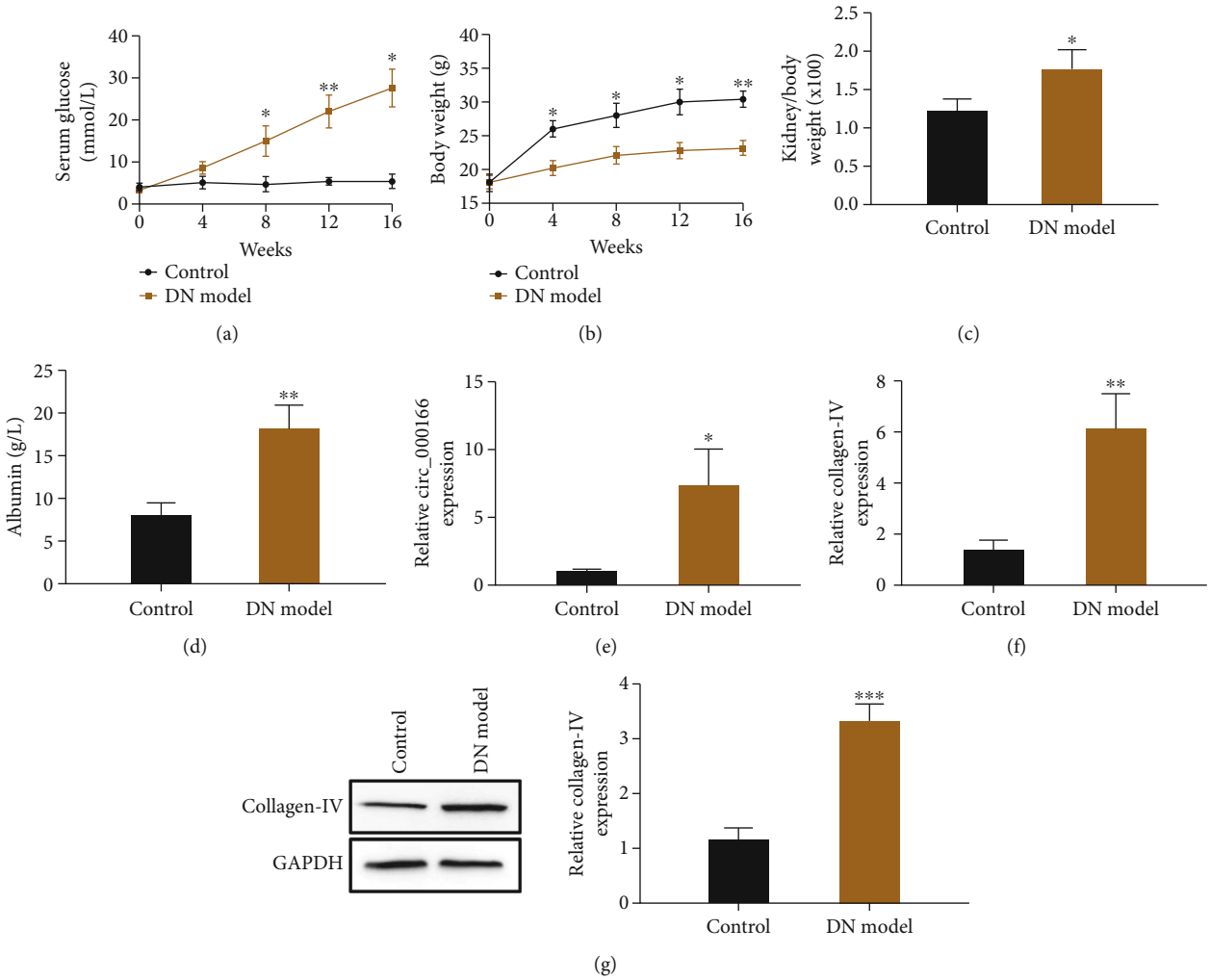

Figure 1: The expression of circ_000166 in the kidney tissue of diabetic renal fibrosis model mice is increased. At 0, 4, 8, 12, and 16 weeks, (a) blood sugar level, (b) weight, (c) the ratio of kidney-to-body weight, and (d) urine protein levels of the normal control group and T1DM group mice were measured. (e) The expression levels of circ_000166 in the kidney tissues of the two groups of mice were detected by qRT-PCR, and (f, g) the expression levels of collagen IV in the kidney tissues of the two groups of mice were detected by qRT-PCR and western blot. The data are expressed as mean ± standard (control group ($n = 7$), DN group ($n = 7$)). $^{*}p < 0.05$, $^{**}p < 0.01$, and $^{***}p < 0.001$.

collagen IV, TGF-β1, ACE, AT1, VEGF, miR-296, SGLT2, GAPDH, and U6 were detected using the TransStart Top Green qPCR SuperMix kit (AQ131-04, TransGen Biotech, Beijing, China). circ_000166, hsa_circ_000166, and miR-296 were standardized with U6, whereas the others were standardized with GAPDH. Expression analysis was calculated via the comparative Ct method. The primers used were as follows: GAPDH: forward: CCACATCGCTCAGACA CCAT, reverse: CCAGGCGCCCAATACG; U6: forward: CGCTTCGGCAGCACATATAC, reverse: TTCACGAAT TTGCGTGTCAT; circRNA_000166: forward: CCATAT TGAATCACAGTGCGT, reverse: ACAGCGCAGTAAGG TGCTCG; miR-296: forward: TGCCTAATTCAGAGGG TTGG, reverse: CTCCACTCCTGGCACACAG; TGF-β1: forward: GAGGCGGTGCTCGCTTTGTA, reverse: CGTT GTTGCGGTCCACCATTA; ACE: forward: ACGAGCACG ACATCAACTTCCTCA, reverse: AGTAGTTCATCATG GCCGAGGCT; AT1: forward: AGGATGACTGTCCCAA AGCTGGAA, reverse: ACGTTTCGGTGGATGATAGCT GGT; VEGF: forward: AGCACAGCAGATGTGAATGC, reverse: AATGCTTTCTCCGCTCTGAA; collagen IV: forward: AATCCCAGGAGGACGAGGTGT, reverse: GGAT TACCCACTTGCCCCCAG; and SGLT2: forward: CTCC GGAGCTGTATTCATCCA, reverse: AGCCCTCCTGT CACCGTGTA.

2.7. Flow Cytometry. The cells were collected and then centrifuged. Each group of cells were then turned into pellets and divided into groups. Afterward, 500 μL of binding buffer was added to suspend the cells, and then, 5 μL of Annexin V-EGFP was added. The solution was then mixed well. Subsequently, 5 μL of propidium iodide was added and mixed well. The mixture was allowed to react at room temperature in the dark for 5–15 min. Cell apoptosis was detected via flow cytometry at excitation wavelength of 488 nm and emission wavelength of 530 nm.

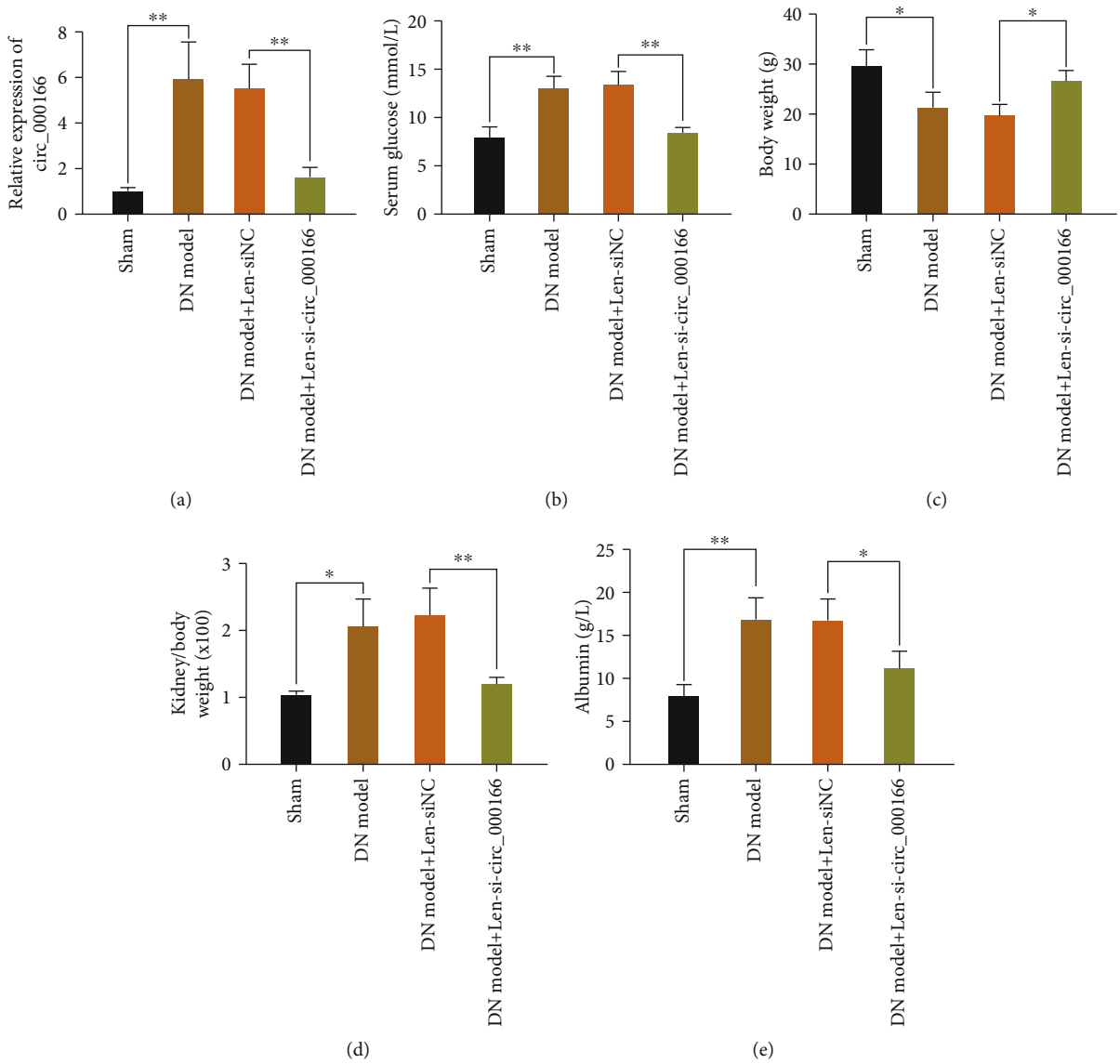

Figure 2: The expression of circ_000166 decreased in the kidney of DN mice. (a) Detect the expression level of circ_000166 in the kidney tissue of each group of mice by qRT-PCR. Compare (b) the blood glucose level, (c) weight, (d) kidney-to-body weight ratio, and (e) urine protein levels of mice between the two groups. All values are expressed as mean ± standard. $^{*}p < 0.05$, $^{**}p < 0.01$, and $^{***}p < 0.001$.

2.8. Western Blotting. A cell lysate (Beyotime, China) containing RIPA and PMSF (100 : 1) was used to extract tissue proteins. The tissue protein extract was analyzed via sodium dodecyl sulfate polyacrylamide gel electrophoresis (SDS-PAGE), transferred onto a PVDF membrane, and then analyzed via western blotting. The antibodies incubated for western blotting were collagen IV (ab6586, Abcam), TGF-β1 (ab215715, Abcam), ACE (SC-2908, Santa Cruz, CA), AT1 (SC-2225, Santa Cruz, CA), VEGF (SC-152, Santa Cruz, CA), and GAPDH (AB-P-R001, Abcam). The extract was incubated with the horseradish peroxidase-conjugated anti-rabbit secondary antibody (1 : 5000, ZB-2301, ZSGB-Bio, Beijing, China), and then, its protein bands were determined using an ECL blot detection reagent (WBKLS0500, Millipore Corporation).

2.9. Statistical Analysis. Statistical analysis was performed using SPSS 19.0 software. All values are expressed as mean ± standard deviation (SD) of three biological replicates or samples. Data were analyzed via one-way ANOVA or LSD test. $p < 0.05$ was considered statistically significant.

3. Results

3.1. circ_000166 Is Upregulated in Kidney Tissues of DN Mice. We performed intraperitoneal injection of STZ to establish a T1DM mouse model. At 0, 4, 8, 12, and 16 weeks, blood glucose levels and weight changes in each group were recorded. The ratio of the kidney-to-body weight and urine protein levels of mice were compared. Compared with those

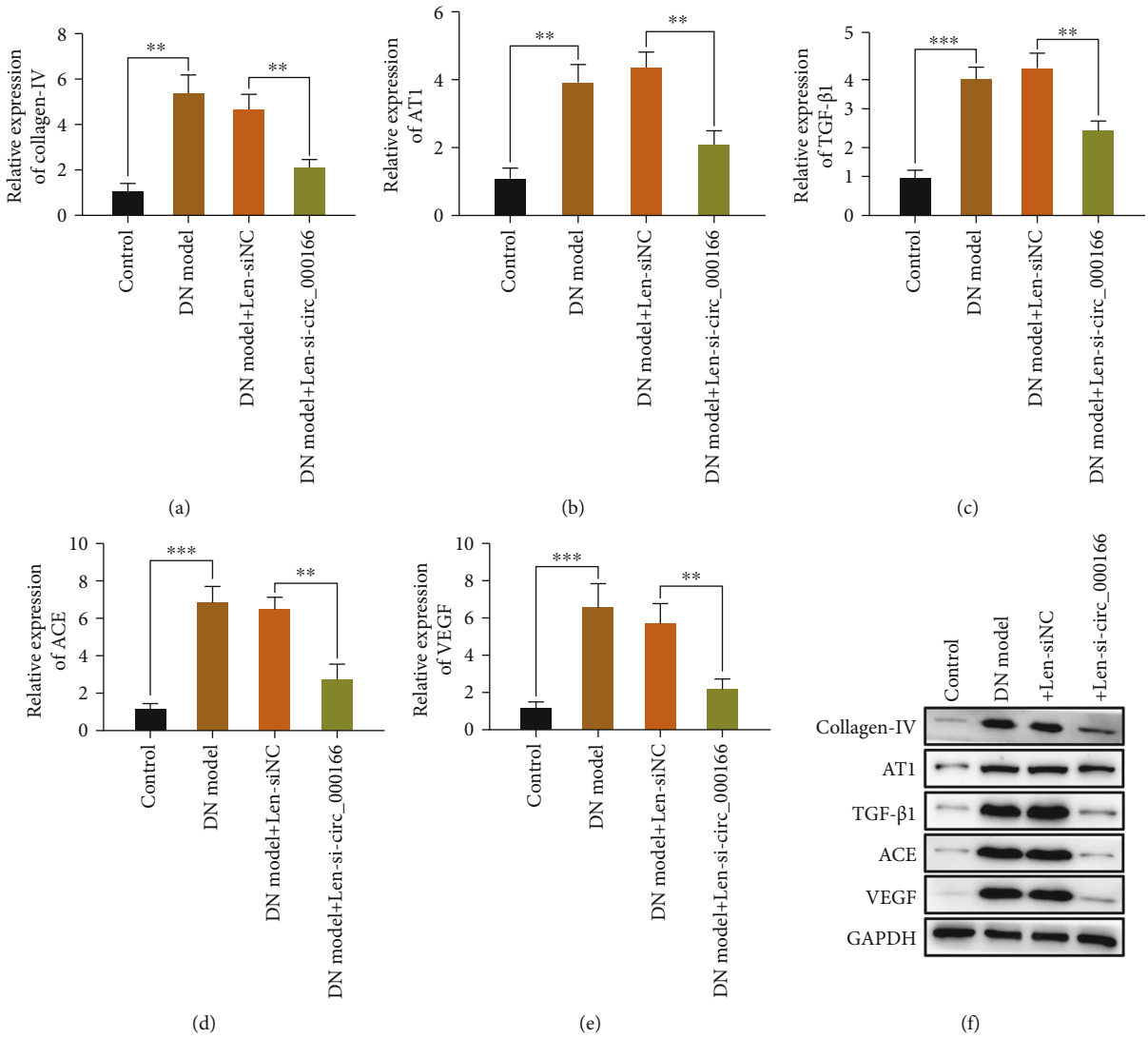

Figure 3: Si-hsa_circ_000166 can inhibit the progression of diabetic renal fibrosis. We used qRT-PCR to detect the expression levels of (a) collagen IV, (b) TGF-β1, (c) ACE, (d) AT1, and (e) VEGF in the kidney tissues of mice in each group. (f) The expression levels of the above factors were quantitatively analyzed by western blot. The data are average ± standard ($n = 10$ per group). $^{*}p < 0.05$, $^{**}p < 0.01$, and $^{***}p < 0.001$.

of the NC mice, the blood glucose level (Figure 1(a)), the ratio of the kidney-to-body weight (Figure 1(c)), and the urine protein level (Figure 1(d)) of the T1DM mice significantly increased, and their weight significantly decreased (Figure 1(b)). We further supplemented the renal pathology results of the DN model. The epithelial and stromal structures of renal tubules were disordered in mice after DN modeling compared with those of the control group (Figure S1). We performed qRT-PCR to detect the expression levels of circ_000166 (Figure 1(e)) and collagen IV (Figure 1(f)) in the two groups of mice. Compared with that of the normal control group, the expression of circ_000166 and collagen IV of the T1DM mouse group increased. We conducted western blot to verify the expression of collagen IV in the kidney tissues of the two groups of mice (Figure 1(g)). The results were consistent with those detected by qRT-PCR, indicating that the diabetic renal fibrosis mouse model was successfully modeled.

3.2. Knockdown circ_000166 by Lentivirus Can Inhibit the Occurrence and Development of DN. We transfected si-hsa_circ_000166 by injection of lentivirus in the DN model mice. We performed qRT-PCR to detect the expression level of hsa_circ_000166 (Figure 2(a)). We then detected blood glucose levels (Figure 2(b)), body weight changes (Figure 2(c)), kidney-to-body weight ratios (Figure 2(d)), and urine protein levels (Figure 2(e)) of the NC, DN, DN+Len-siNC, and DN+Len-si-hsa_circ_000166 groups, respectively. Compared with those in the NC group, the blood glucose levels, kidney-to-body weight ratios, and urine protein levels in the DN and DN+Len-siNC groups increased. In the DN+Len-si-hsa_circ_000166 group, the blood glucose levels, kidney-to-body weight ratios, and urine proteins were

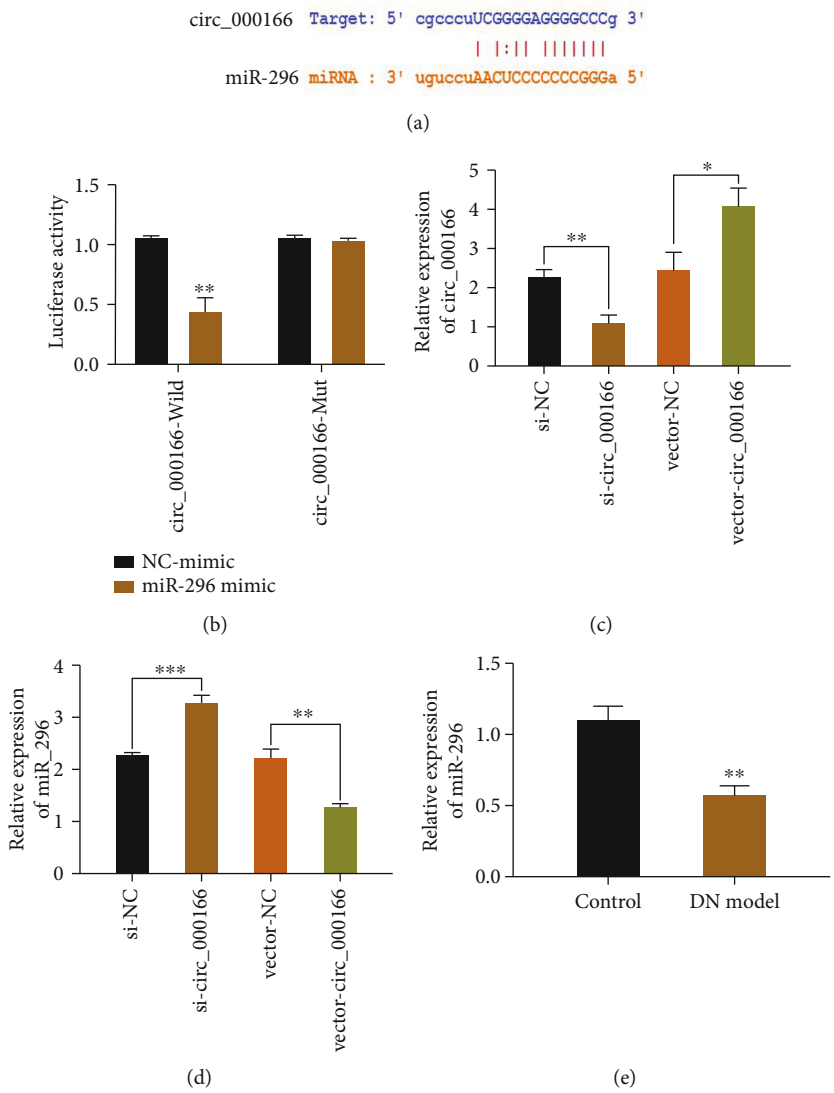

Figure 4: circ_000166 can serve as the ceRNA of miR-296. (a) Sequence of circ_000166 and miR-296 in mouse. (b) The dual-luciferase report detects luciferase activity in mouse kidneys. (c–e) We used qRT-PCR to detect the expression of circ_000166 and miR-296 in each group of mouse kidneys. The data are average ± standard. $^{*}p < 0.05$, $^{**}p < 0.01$, and $^{***}p < 0.001$.

significantly lower than those in the DN and DN+Len-siNC groups, but they increased compared with those in the NC group. However, the opposite trend was observed in weight changes. These results demonstrated that silencing circ_000166 can inhibit DN occurrence and development.

3.3. Lentivirus Knockdown circ_000166 Can Inhibit the Process of Diabetic Renal Fibrosis. We detected the expression levels of renal fibrosis-related factors, namely, collagen IV, TGF-β1, ACE, AT1, and VEGF, via qRT-PCR and western blot (Figures 3(a)–3(f)). Compared with those in the NC group, the expression levels of these factors in the kidneys of mice in the DN and DN+Len-siNC groups increased. Moreover, the expression levels of these factors in the kidneys of mice in the DN+Len-si-hsa_circ_000166 group were significantly lower than those in the DN and DN+Len-siNC groups. These results showed that silencing circ_000166 can inhibit the occurrence and development of diabetic renal fibrosis.

3.4. circ_000166 Can Act as a ceRNA for miR-296. circ_000166 is the target of miR-296, but the circ_000166 mutants are not the target of miR-296 (Figure 4(a)). By constructing a luciferase reporter vector, luciferase and circ_000166 genes were connected and then transfected into cells for detection. Results showed that the miR-296 mimic significantly reduced the relative luciferase activity of circ_000166-Wild but had no significant effect on circ_000166-Mut (Figure 4(b)). The expression level of circ_000166 in different cells was measured via qRT-PCR. After si-circ_000166 treatments, the expression level of circ_000166 significantly decreased, whereas that of miR-296 significantly increased. After treatment with vector-circ_000166, the expression of circ_000166 significantly increased (Figure 4(c)),

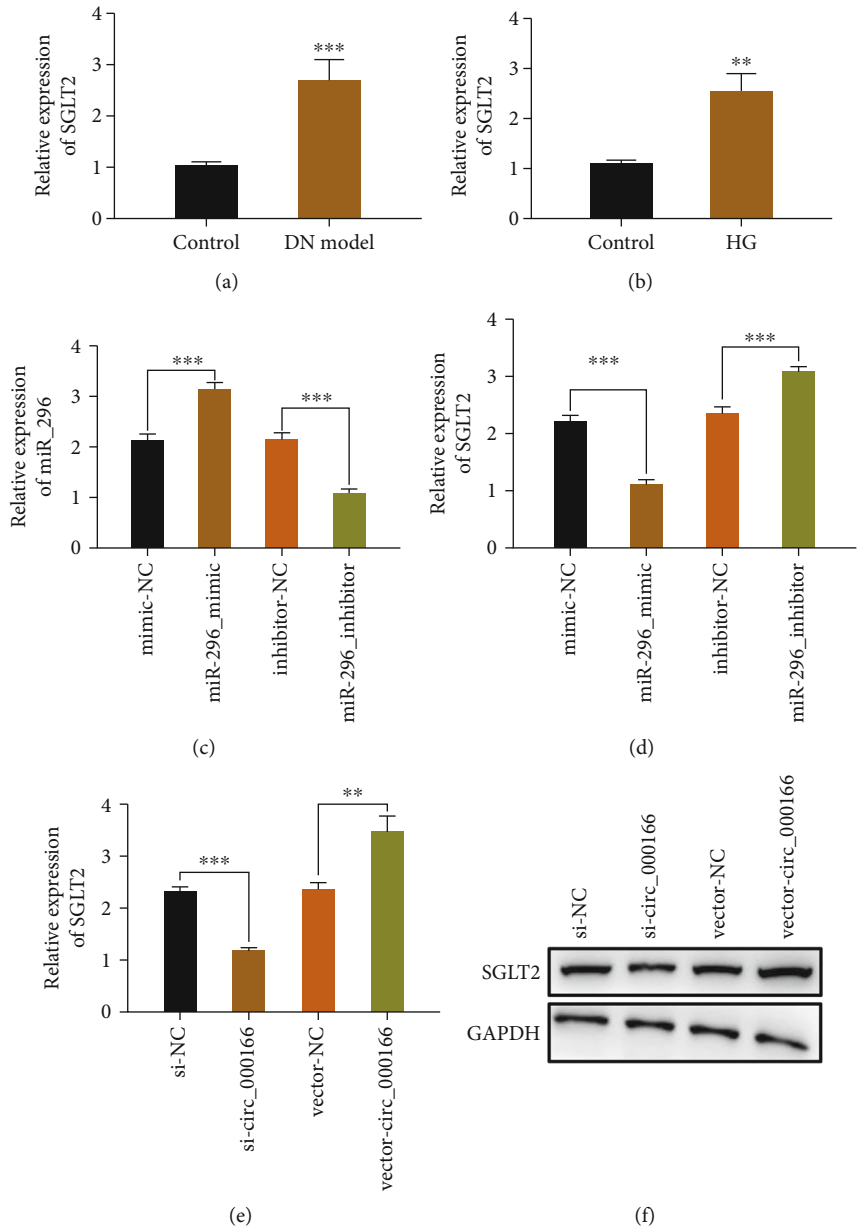

Figure 5: SGLT2 as a target gene regulated by miR-296. (a, b) We used qRT-PCR to detect the expression of SGLT2 in the kidney tissue and the cells of each group. High-glucose group (high-glucose medium containing D-glucose: 25 mmol/L). (c, d QRT-PCR was used to detect the effect of the miR-296 mimic and miR-296 inhibitor on the expression of SGLT2. (e, f) QRT-PCR and western blotting were used to detect the effect of inhibiting circ_000166 on the expression of SGLT2. The data are expressed as mean ± standard. $^{*}p < 0.05$, $^{**}p < 0.01$, and $^{***}p < 0.001$.

whereas that of miR-296 significantly decreased (Figure 4(d)). The expression level of miR-296 in the T1DM group was significantly lower than that in the normal control group (Figure 4(e)). These results fully demonstrated that circ_000166 can serve as the ceRNA of miR-296.

3.5. SGLT2 as a Target Gene Regulated by miR-296. Compared with that in the normal control group, the mRNA expression of SGLT2 in the DN and HG groups increased (Figures 5(a) and 5(b)). The miR-296 mimic could increase miR-296 expression and reduce SGLT2 expression, whereas the miR-296 inhibitor could inhibit miR-296 expression and promote SGLT2 expression (Figures 5(c) and 5(d)). Inhibition of circ_000166 could decrease the expression of SGLT2, and vector_circ_000166 could increase the expression of SGLT2 (Figures 5(e) and 5(f)). These results indicated that SGLT2 may be a target gene regulated by miR-296.

3.6. Overexpression of miR-296 and Knockdown of SGLT2 Can Reverse the Promotion of Diabetic Renal Fibrosis Regulated by hsa_circ_000166. circ_000166 was added to the cultured DN cell model. Afterward, the miR-296 mimic and sh-SGLT2 were added to the DN cell model. Subsequently, the expression levels of SGLT2, collagen IV, TGF-

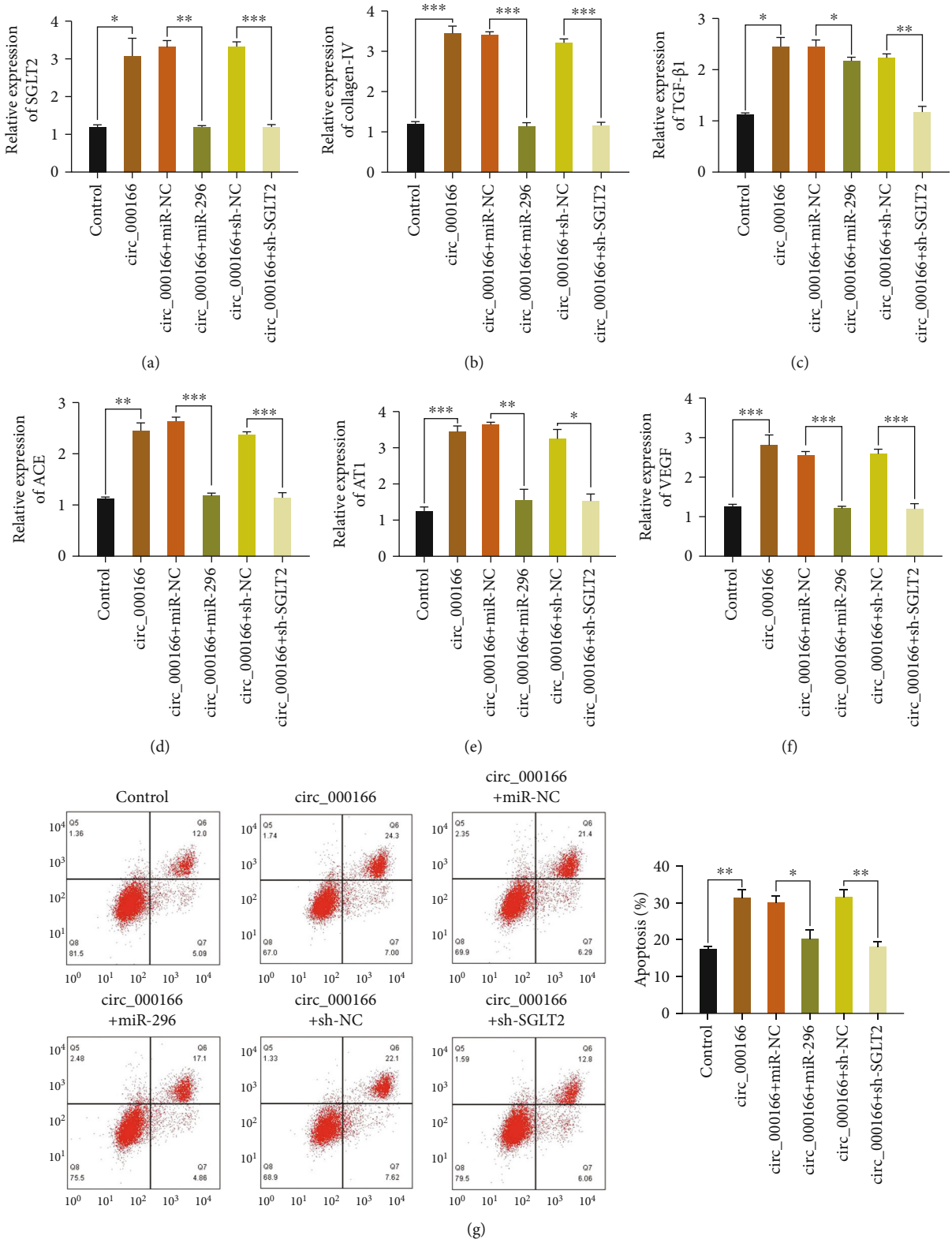

Figure 6: Overexpression of miR-296 and knockdown of SGLT2 reverse the promotion of hsa_circ_000166 on diabetic renal fibrosis. We used qRT-PCR to detect the expression levels of (a) SGLT2, (b) collagen IV, (c) TGF-β1, (d) ACE, (e) AT1, and (f) VEGF in each group of cells. Flow cytometry was used to detect apoptosis in each group (g).

β1, ACE, AT1, and VEGF in each group of cells were detected via qRT-PCR. circ_000166 could increase the mRNA expression levels of these factors in each group of cells. Overexpression of miR-296 and knockdown of SGLT2 could reverse the effects of hsa_circ_000166 on these factors (Figures 6(a)–6(f)). Cell apoptosis in each group was detected via flow cytometry. circ_000166 could increase apoptosis in each group. Overexpression of miR-296 and knockdown of SGLT2 could reverse the proapoptotic effect of hsa_circ_000166 (Figure 6(g)). In sum, both the overexpression of miR-296 and the silencing of SGLT2 reversed the progression of diabetic renal fibrosis regulated by circ_00016.

4. Discussion

Diabetic renal fibrosis is one of the most common causes of end-stage renal disease [19]. Many studies reported STZ-induced renal fibrosis in C57BL/6 mice [20, 21]. Our group also successfully constructed an animal model of diabetic renal fibrosis through STZ induction. Profibrotic activity is closely related to renal dysfunction [22]. Thus, promoting the renal fibrosis target of DN and preventing it are important.

Recent studies comprehensively explored the role of ncRNA in the process of gene expression. The circRNA-miRNA-mRNA network is closely related to the occurrence and development of numerous diseases, such as osteoporosis [23], cancer [24], and viral infections [25]. circRNA can act as a bridge between nc-RNA and c-mRNA. circRNA is produced by the reverse splicing mechanism during posttranscriptional processing and is expressed in large amounts in eukaryotic cells. circRNA can function by regulating RNA transcription and protein production, as well as by acting as a sponge for microRNA (miRNA).

Liu et al. [26] claimed that miRNA-296 promotes the healing of diabetic wounds by targeting SGLT2. Zhang et al. [27] reported that miRNA-296 can downregulate the expression of SGLT2 in lung cancer. Therefore, we suppose that miRNA-296 can regulate SGLT2 gene expression. SGLT2 plays a key role in the process of diabetic renal fibrosis. At present, SGLT2 inhibitors have become a new drug for the treatment of diabetes [28, 29]. SGLT2 inhibitors have been proven to have good metabolic characteristics [30] and can substantially reduce atherosclerosis events, hospitalization due to heart failure and cardiovascular diseases, total mortality, and the progress of chronic kidney diseases [31, 32]. However, the effects of circ_000166 on miRNA-296-SGLT2 remain unclear.

In this study, the circRNA-miRNA-mRNA network was used as an entry point to explore the role of circ_000166/miR-296/SGLT2 in the progression of diabetic renal fibrosis. Compared with those in normal controls, the expression levels of circ_000166 in the kidney tissues of mice with diabetic renal fibrosis significantly increased. Silencing circ_000166 could minimize kidney damage and decrease urine protein levels, thereby inhibiting the progression of renal fibrosis. Results of dual-luciferase report tests showed that circ_000166 and miR-296 were internally regulated. circ_000166 could act as the ceRNA of miR-296 and competitively bind to miR-296, resulting in increased expression of the SGLT2 gene regulated by miR-296. These results were verified via in vivo and in vitro experiments. The lentivirus and plasmid vector transfection technology was used to overexpress miR-296 and silence SGLT2. Results showed that DN renal fibrosis and apoptosis were significantly reduced. circ_000166/miR-296/SGLT2 may become a new target in the progression of diabetic renal fibrosis, which is important to delay the progression of this disease and prevent end-stage renal disease.

We focused on the circ_000166/miR-296/SGLT2 regulatory network as the research object. We found that the interaction of this network can reduce the expression of diabetic renal fibrosis-related factors. Hence, it may become an effective target for intervention in the treatment of diabetic renal fibrosis.

Data Availability

The analyzed data sets generated during the study are available from the corresponding author on reasonable request.

Conflicts of Interest

The author declares that he has no conflicts of interest.

Supplementary Materials

Figure S1: histological image stained with hematoxylin and eosin (H&E) of kidney tissue. Results showed the structural derangements of tubular epithelia and interstitium in the DN model. *(Supplementary Materials)*

References

[1] X. Ge, L. Xi, Q. Wang et al., "Circular RNA Circ_0000064 promotes the proliferation and fibrosis of mesangial cells via miR-143 in diabetic nephropathy," *Gene*, vol. 758, 2020.

[2] C. Huang, L. Cheng, X. Feng, X. Li, and L. Wang, "Dencichine ameliorates renal injury by improving oxidative stress, apoptosis and fibrosis in diabetic rats," *Life Sciences*, vol. 258, 2020.

[3] S. M. Mauer, M. W. Steffes, E. N. Ellis, D. E. Sutherland, D. M. Brown, and F. C. Goetz, "Structural-functional relationships in diabetic nephropathy," *The Journal of Clinical Investigation*, vol. 74, no. 4, pp. 1143–1155, 1984.

[4] Y. S. Kanwar, J. Wada, L. Sun et al., "Diabetic nephropathy: mechanisms of renal disease progression," *Experimental Biology and Medicine*, vol. 233, no. 1, pp. 4–11, 2008.

[5] A. Schwarzer, S. Emmrich, F. Schmidt et al., "The non-coding RNA landscape of human hematopoiesis and leukemia," *Nature Communications*, vol. 8, no. 1, p. 218, 2017.

[6] Y. Chi, D. Wang, J. Wang, W. Yu, and J. Yang, "Long Non-Coding RNA in the Pathogenesis of Cancers," *Cells*, vol. 8, no. 9, 2019.

[7] B. Chen and S. Huang, "Circular RNA: an emerging non-coding RNA as a regulator and biomarker in cancer," *Cancer Letters*, vol. 418, pp. 41–50, 2018.

[8] H. Zhu, F. Du, and C. Cao, "Restoration of circPSMC3 sensitizes gefitinib-resistant esophageal squamous cell carcinoma

cells to gefitinib by regulating miR-10a-5p/PTEN axis," *Cell Biology International*, vol. 45, no. 1, pp. 107–116, 2021.

[9] D. Fanale, S. Taverna, A. Russo, and V. Bazan, "Circular RNA in exosomes," *Advances in Experimental Medicine and Biology*, vol. 1087, pp. 109–117, 2018.

[10] B. Wei and L. Yu, "Circular RNA PRKCI and microRNA-545 relate to sepsis risk, disease severity and 28-day mortality," *Scandinavian Journal of Clinical and Laboratory Investigation*, vol. 80, no. 8, pp. 659–666, 2020.

[11] W. Zhang and S. Zhang, "Downregulation of circRNA_0000285 suppresses cervical cancer development by regulating miR197-3p-ELK1 axis," *Cancer Management and Research*, vol. Volume 12, pp. 8663–8674, 2020.

[12] G. Zhao and G. J. Dai, "Hsa_circRNA_000166 promotes cell proliferation, migration and invasion by regulating miR-330-5p/ELK1 in colon cancer," *Oncotargets and Therapy*, vol. - Volume 13, pp. 5529–5539, 2020.

[13] B. Tang, W. Li, T. T. Ji et al., "Circ-AKT3 inhibits the accumulation of extracellular matrix of mesangial cells in diabetic nephropathy via modulating miR-296-3p/E-cadherin signals," *Journal of Cellular and Molecular Medicine*, vol. 24, no. 15, pp. 8779–8788, 2020.

[14] T. S. Loganathan, S. A. Sulaiman, N. A. Abdul Murad et al., "Interactions among non-coding RNAs in diabetic nephropathy," *Frontiers in Pharmacology*, vol. 11, p. 191, 2020.

[15] I. Sabolić, I. Vrhovac, D. B. Eror et al., "Expression of Na^+-D-glucose cotransporter SGLT2 in rodents is kidney-specific and exhibits sex and species differences," *American Journal of Physiology. Cell Physiology*, vol. 302, no. 8, pp. C1174–C1188, 2012.

[16] R. Santer and J. Calado, "Familial renal glucosuria and SGLT2: from a Mendelian trait to a therapeutic target," *Clinical Journal of the American Society of Nephrology*, vol. 5, no. 1, pp. 133–141, 2010.

[17] S. Maeda, T. Matsui, M. Takeuchi, and S. Yamagishi, "Sodium-glucose cotransporter 2-mediated oxidative stress augments advanced glycation end products-induced tubular cell apoptosis," *Diabetes/Metabolism Research and Reviews*, vol. 29, no. 5, pp. 406–412, 2013.

[18] M. Kato, S. Putta, M. Wang et al., "TGF-β activates Akt kinase through a microRNA-dependent amplifying circuit targeting PTEN," *Nature Cell Biology*, vol. 11, no. 7, pp. 881–889, 2009.

[19] G. Liang, L. Song, Z. Chen et al., "Fibroblast growth factor 1 ameliorates diabetic nephropathy by an anti-inflammatory mechanism," *Kidney International*, vol. 93, no. 1, pp. 95–109, 2018.

[20] Y. Wang, Q. Fang, Y. Jin et al., "Blockade of myeloid differentiation 2 attenuates diabetic nephropathy by reducing activation of the renin-angiotensin system in mouse kidneys," *British Journal of Pharmacology*, vol. 176, no. 14, pp. 2642–2657, 2019.

[21] S. Yang, L. Zhao, Y. Han et al., "Probucol ameliorates renal injury in diabetic nephropathy by inhibiting the expression of the redox enzyme p66Shc," *Redox Biology*, vol. 13, pp. 482–497, 2017.

[22] T. T. Ma and X. M. Meng, "TGF-β/Smad and renal fibrosis," *Advances in Experimental Medicine and Biology*, vol. 1165, pp. 347–364, 2019.

[23] W. Shen, B. Sun, C. Zhou, W. Ming, S. Zhang, and X. Wu, "CircFOXP1/FOXP1 promotes osteogenic differentiation in adipose-derived mesenchymal stem cells and bone regeneration in osteoporosis via miR-33a-5p," *Journal of Cellular and Molecular Medicine*, vol. 24, no. 21, pp. 12513–12524, 2020.

[24] A. Wu, Y. Li, M. Kong et al., "Upregulated hsa_circ_0005785 facilitates cell growth and metastasis of hepatocellular carcinoma through the miR-578/APRIL axis," *Frontiers in Oncology*, vol. 10, p. 1388, 2020.

[25] J. S. Nahand, S. Jamshidi, M. R. Hamblin et al., "Circular RNAs: new epigenetic signatures in viral infections," *Frontiers in Microbiology*, vol. 11, p. 1853, 2020.

[26] X. Liu, Y. Wang, X. Zhang et al., "MicroRNA-296-5p promotes healing of diabetic wound by targeting sodium-glucose transporter 2 (SGLT2)," *Diabetes/Metabolism Research and Reviews*, vol. 35, no. 2, article e3104, 2019.

[27] X. Zhang, X. Zhang, X. Liu et al., "MicroRNA-296, a suppressor non-coding RNA, downregulates SGLT2 expression in lung cancer," *International Journal of Oncology*, vol. 54, no. 1, pp. 199–208, 2019.

[28] S. Verma and J. J. V. McMurray, "SGLT2 inhibitors and mechanisms of cardiovascular benefit: a state-of-the-art review," *Diabetologia*, vol. 61, no. 10, pp. 2108–2117, 2018.

[29] M. S. Kelly, J. Lewis, A. M. Huntsberry, L. Dea, and I. Portillo, "Efficacy and renal outcomes of SGLT2 inhibitors in patients with type 2 diabetes and chronic kidney disease," *Postgraduate Medicine*, vol. 131, no. 1, pp. 31–42, 2019.

[30] S. Filippas-Ntekouan, T. D. Filippatos, and M. S. Elisaf, "SGLT2 inhibitors: are they safe?," *Postgraduate Medicine*, vol. 130, no. 1, pp. 72–82, 2018.

[31] T. A. Zelniker and E. Braunwald, "Mechanisms of cardiorenal effects of sodium-glucose cotransporter 2 inhibitors," *Journal of the American College of Cardiology*, vol. 75, no. 4, pp. 422–434, 2020.

[32] V. Tsimihodimos, T. D. Filippatos, and M. S. Elisaf, "SGLT2 inhibitors and the kidney: effects and mechanisms," *Diabetes and Metabolic Syndrome: Clinical Research and Reviews*, vol. 12, no. 6, pp. 1117–1123, 2018.

Hindawi
Disease Markers
Volume 2022, Article ID 6318721, 8 pages
https://doi.org/10.1155/2022/6318721

Research Article

Muscle Energy Technique plus Neurac Method in Stroke Patients with Hemiplegia Complicated by Diabetes Mellitus and Assessment of Quality of Life

Jingyan Wang, Shuang Wang, Hongmei Wu, Shuxin Dong, and Baojun Zhang

Department of Rehabilitation Medicine, First Affiliated Hospital of Jiamusi University, Jiamusi, China

Correspondence should be addressed to Baojun Zhang; ganbing_0452@163.com

Received 10 January 2022; Accepted 21 March 2022; Published 9 May 2022

Academic Editor: Zhaoqi Dong

Objective. To analyze the role of muscle energy technique (MET) plus Neurac method in stroke patients with hemiplegia complicated by diabetes mellitus and the impact on quality of life. *Methods*. From January 2021 to December 2021, 100 stroke patients with hemiplegia complicated by diabetes mellitus treated in our institution and assessed for eligibility were recruited and randomly assigned (1 : 3) via the random sampling method to either the conventional rehabilitation group or the experimental group. The patients in the experimental group were randomized (1 : 1 : 1) into either the MET group (receives MET), the Neurac group (receives Neurac), or the joint group (receives MET plus Neurac). The primary endpoint is the clinical efficacy, and the second endpoint is the quality of life. *Results*. The eligible patients had similar pretreatment Barthel index scores, Visual Analogue Scale (VAS) scores, Berg balance scale (BBS) scores, Tinetti scores, Fugl-Meyer scores, and quality of life (QoL) scores ($P > 0.05$). The treatment herein achieved significant improvements in Barthel index scores, VAS scores (2.71 ± 0.28), BBS scores, Tinetti scores, Fugl-Meyer scores, and QoL scores (99.67 ± 10.62), and MET plus Neurac method obtained the best results versus both the conventional rehabilitation and monotherapy of either MET or Neurac ($P < 0.05$). *Conclusion*. Neurac method plus MET improves the independent mobility of stroke patients with hemiplegia and diabetes, relieves pain, enhances balance and stability, mitigates limb dysfunction, and boosts patients' quality of life, so it is worthy of clinical application.

1. Introduction

Stroke is a group of acute diseases that include ischemic stroke and hemorrhagic stroke due to sudden rupture of blood vessels in the brain or failure of blood flow to the brain after vascular obstruction [1, 2]. Currently, functional impairment resulting in poor self-care abilities is associated with 70%-80% of stroke patients, such as limitation of motor function, sensory deficits, cognitive impairment, and speech and swallowing disorders, among which limited motor function severely compromises the daily life of hemiplegic patients [3, 4]. Moreover, the presence of knee hyperextension, knee hyperflexion, and inversion of the foot may lead to a failure of normal weight-bearing in the lower extremities in the support phase, which increases the patient's risk of falling. The close association of diabetes mellitus and cerebrovascular events constitutes an independent risk factor for stroke, and the comorbidity with diabetes mellitus may further aggravate the disease and cause a poor prognosis [5, 6]. Thus, an urgent need exists to explore effective rehabilitation treatment methods to improve the motor function and the quality of life of stroke patients with hemiplegia and diabetes mellitus. MET is a technique for musculoskeletal system disorders by applying isometric contraction, relaxation, and reciprocal inhibition to the targeted muscles. It relaxes tense muscles, activates relaxed muscles, and restores muscle length, tone, and stability to enhance the function of the musculoskeletal system and alleviate pain [7, 8]. In MET, patients are required to use their muscles to proactively and consciously fight against

the resistance imposed by the therapist by using specific muscles to perform contraction, relaxation, and cross-inhibition to adjust muscle length and tone, increase muscle strength and stability, and restore the normal biomechanics of the joint, thereby achieving good therapeutic results [9–11]. The Neurac method is derived from sling exercise, where the patient receives rehabilitation using a sling system with the aid of the physical therapist, which allows reconstruction of normal movement patterns through high levels of neuromuscular stimulation. This approach has been applied in the treatment of long-term skeletal muscle disorders that cause pain or loss of function [12]. At present, the efficiency of the two treatment methods is marginally explored in treating patients with stroke hemiplegia and diabetes mellitus. Accordingly, this study was conducted to assess their efficacy in stroke patients with hemiplegia complicated by diabetes mellitus and the impact on quality of life, to further provide new ideas and directions in clinical practice.

2. Materials and Methods

2.1. Baseline Data. From January 2021 to December 2021, 100 stroke patients with hemiplegia complicated by diabetes mellitus treated in our institution and assessed for eligibility were recruited. They were concurrently randomly assigned via the random sampling method to either the conventional rehabilitation group ($n = 25$) or the experimental group ($n = 75$). The patients in the experimental group were randomized (1 : 1 : 1) into either the MET group (receives MET, $n = 25$), the Neurac group (receives Neurac, $n = 25$), or the joint group (receives MET plus Neurac, $n = 25$). All eligible patients showed comparable baseline characteristics (conventional rehabilitation group: 15 males and 10 females, aged 48-69 years, mean age of 57.45 ± 4.96 years, course of disease of 25-55 days, mean course of disease of 30.12 ± 4.27 days, 12 cases of cerebral infarction, and 13 cases of cerebral hemorrhage; MET group: 16 males and 9 females, aged 45-70 years, mean age of 58.30 ± 4.73 years, course of disease of 23-57 days, mean course of disease of 31.44 ± 4.38 days, 11 cases of cerebral infarction, and 14 cases of cerebral hemorrhage; Neurac group: 14 males and 11 females, aged 43-68 years, mean age of 56.98 ± 4.64 years, course of disease of 23-58 days, mean course of disease of 31.37 ± 4.50 days, 10 cases of cerebral infarction, and 15 cases of cerebral hemorrhage; and joint group: 17 males and 8 females, aged 43-70 years, mean age of 58.19 ± 4.55 years, course of disease of 22-56 days, mean course of disease of 30.72 ± 4.59 days, 16 cases of cerebral infarction, and 9 cases of cerebral hemorrhage ($P > 0.05$)). This protocol was approved by the ethics committee of the First Affiliated Hospital of Jiamusi University (JMUH39771).

2.2. Inclusion and Exclusion Criteria. Inclusion criteria are as follows: ① patients met the diagnostic criteria established for stroke in Chinese medicine and Western medicine (fasting blood sugar > 7.0 or two hours postprandial blood sugar > 11.1 mm/L) [13] and were confirmed by imaging CT or MRI for the first stroke with a duration of ≤3 months; ② aged between 18 and 79 years old, with normal heart rate, blood pressure, body temperature, and pulse; and ③ the enrolled patients had Glasgow Coma Scale scores of no less than 15 points, muscle strength of grade 2 or higher, and were able to cooperate actively. Patients and their families voluntarily participated in this experimental study and signed the informed consent form.

Exclusion criteria are as follows: ① patients with severe aphasia and cognitive dysfunction; ② with a previous history of psychiatric disorders; and ③ with severe infections, heart failure, tumors, asthma, and other serious complications or hepatic dysfunction or renal dysfunction.

2.3. Methods. The conventional rehabilitation group adopted conventional rehabilitation training. Patients received conventional diabetes treatment, regular blood glucose monitoring, medication as prescribed by the doctor, and dietary guidance. The rehabilitation training included active and passive activities of the hemiplegic side of the limb, turning and movement training, early healthy limb position placement, muscle strength training, balance training, occupational therapy, walking training, traditional rehabilitation therapy, and physiotherapy, 40 min/time, 1 time/d, 5d/week, for a total of 4 weeks.

Patients in the MET group were given MET on top of conventional treatment. (1) Respiratory training (to help ease the overexcited sympathetic nerves): in a supine position, the patient was instructed to bend the hips and knees and place the feet on the Bobath ball and breathe with a relaxed abdomen. The therapist placed both hands on the patient's abdomen and instructed the patient to do a slow "yawn-like" exhalation, and the therapist slowly pressed both hands onto the abdomen to promote diaphragmatic uplift. Patients held their breath for 5-10 s at the end of exhalation, 10 sets/time. (2) Tension-reducing isometric contraction-relaxation technique for pectoralis major and pectoralis minor: the patient lied in a supine position with the head turned to the opposite side of the training side and the shoulder joint abducted at 90° hanging out of the bed. The therapist pressed the patient's pectoralis major with one hand and held the patient's elbow with the other, rotated the shoulder externally and pressed down to a point where the patient could feel resistance without pain and instructed the patient to use 20% of maximum contraction against the resistance and relax after holding for 5-10 s. The therapist then continued to stretch to the next new resistance point and repeated 3-5 times. The middle and lower part of the muscle strength enhancement training was used for the rhomboid muscles and trapezius. The patient was seated with the shoulder abducted at 90° on the table. The therapist instructed the patient to contract the scapula inwards and placed the hand on the medial side of the scapula to apply resistance outward, 20 pieces/set, 3-5 sets/time. Shoulder joint hold-relaxation technique: with the patient in a seated position, the therapist assisted the patient to flex the shoulder joint forward to the point where the patient could feel the resistance without pain and instructed the patient to remain still. The therapist appropriately applied resistance at the distal end of the upper extremity according to the actual condition. The resistance should be reduced immediately in the case of

Table 1: Comparison of Barthel index scores.

Groups	Before treatment	2 weeks of treatment	4 weeks of treatment
Conventional rehabilitation group	35.59 ± 4.16	40.37 ± 5.44	56.91 ± 7.33
MET group	33.91 ± 5.10	52.41 ± 6.56*#	62.43 ± 8.10*#
Neurac group	34.72 ± 4.96	53.72 ± 6.83*#	63.59 ± 8.26*#
Joint group	35.46 ± 4.24	60.59 ± 8.17*	80.28 ± 9.47*

∗ indicates $P < 0.05$ versus conventional rehabilitation group within the same time period; # indicates $P < 0.05$ versus the joint group.

Table 2: Comparison of VAS scores.

Groups	Before treatment	2 weeks of treatment	4 weeks of treatment
Conventional rehabilitation group	8.36 ± 0.75	6.28 ± 1.05	5.37 ± 0.69
MET group	8.29 ± 0.81	5.46 ± 0.78*#	4.41 ± 0.42*#
Neurac group	8.59 ± 0.94	5.40 ± 0.728*#	4.39 ± 0.50*#
Joint group	8.74 ± 1.02	4.12 ± 0.528*	2.71 ± 0.28*

∗ indicates $P < 0.05$ versus conventional rehabilitation group within the same time period; # indicates $P < 0.05$ versus the joint group.

compensatory movements such as shrugging. The patient maintained for 5-10 s and then slowly relaxed, after which the therapist stretched the shoulder to a next resistance point for training and repeated 3-5 times. (3) Treatment of the elbow joint: biceps isometric contraction-relaxation training: with the patient in a supine position and the forearm rotated back in a neutral shoulder position, the therapist slowly stretched the patient's elbow to a point of resistance without pain and instructed the patient to use 20% of the maximum contraction force against it to achieve an isometric contraction, hold for 5-10 s, and then relax, after which the stretch was continued to the next new point of resistance and repeated 3-5 times. Triceps centrifugal MET training: the therapist assisted the patient to straighten the elbow joint to the maximum angle, held the patient's wrist joint, and applied resistance in the direction of elbow flexion, and the patient kept passively flexing the elbow joint to the maximum under confrontation, 20 pieces/set, 3-5 sets/time. (4) Wrist training: the therapist dorsally stretched the patient's wrist to a point of resistance without pain and instructed the patient to use 20% of the maximum contraction force against it to achieve isometric contraction, hold for 5-10 s, and then relax, and the therapist then dorsally stretched the wrist to the next new point of resistance and repeated 3-5 times. Centrifugal training of wrist extensors: the therapist instructed the patient to dorsally extend the wrist joint to the maximum angle, immobilized the wrist joint in the palmar flexion direction, and applied a constant resistance, and the patient maintained passive palmar flexion under confrontation to the maximum, 20 pieces/set, 3-5 sets/time.

The Neurac group used the Neurac method for training. (1) Supine pelvic lifting: using an elastic cord attached to a wide sling placed at the pelvis, the knee joint was kept straight by pressing down on the rigid knee sling so that the body would not rotate and flex laterally, which can increase lower limb muscle strength and impedance through repetitive training. The adjustment of the length of the elastic cord helps to reduce the weight-bearing to accommodate the patient's physical condition [14]. (2) Lateral recumbent hip abduction: the therapist instructed the patient to lift the healthy leg, extend the hip, and use straightening of the affected leg and downward pressure on the rigid narrow sling to lift the body so that the seventh thoracic vertebra and the inner ankle of the affected limb could be on the same level. The patient was only required to maintain a normal physiological curvature without side-bending and rotation. (3) Lateral recumbent hip inversion: with the patient's head resting on a pillow or arm and the other arm placed at the forehead, a nonelastic cord was placed near the knee joint of the upper leg at a height such that the lower edge of the knee joint of the upper leg was slightly above shoulder level, and the elastic cord was placed at the pelvis with the central point of each sling suspended. The spinal curvature should be kept within a normal range during training. The lower leg was lifted off the bed and pressed down to raise the pelvis, and the body was to be kept straight with normal spinal curvature and the lower hip in a posterior extension position without lateral flexion or rotation of the body [15]. (4) Neutral lumbar spine position in a supine position: the length of the rigid cord was adjusted to allow hip flexion > 30°, and the treatment bed was lowered to bring the pelvis off the bed. Adjustment of the elastic cord at the pelvis enables the therapist to adjust the curvature of the lumbar spine using less force. For patients with upper extremity dysfunction, the patient was instructed to kneel and then straighten the arms until the shoulder joint was flexed at 90° and then performed a push-up. This is followed by supine shoulder abduction: the hand strap was placed on both elbows above shoulder height, with the split sling applied to the head and the wide sling applied under the upper back, and the pelvis was to offload the weight. The patient then extended the knees and

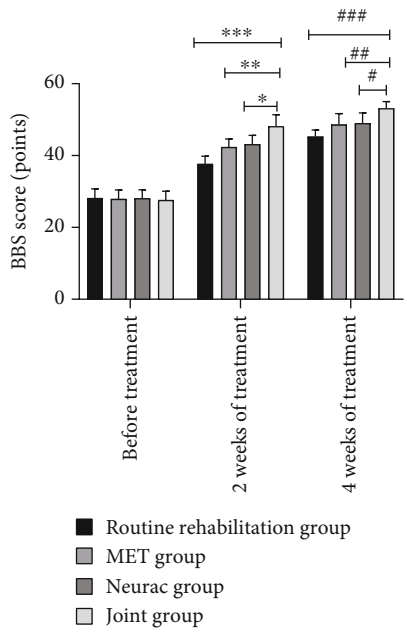

Figure 1: Comparison of BBS scores. Note: The abscissa indicates pretreatment, 2 weeks of treatment, and 4 weeks of treatment; the ordinate indicates BBS score, points. The BBS scores of the conventional rehabilitation group before treatment, 2 weeks of treatment, and 4 weeks of treatment were 28.17 ± 2.55, 37.69 ± 2.12, and 45.30 ± 1.83, respectively. The BBS scores before treatment, at 2 weeks of treatment, and at 4 weeks of treatment in the MET group were 27.94 ± 2.48, 42.37 ± 2.26, and 48.65 ± 3.01, respectively. The BBS scores before treatment, at 2 weeks of treatment, and at 4 weeks of treatment in the Neurac group were 28.11 ± 2.35, 43.18 ± 2.42, and 49.04 ± 2.81, respectively. The BBS scores before, 2 weeks, and 4 weeks of treatment in the joint group were 27.61 ± 2.47, 48.16 ± 3.20, and 53.17 ± 1.87, respectively. ∗ and # indicate significant differences in the BBS scores between the conventional rehabilitation group and the joint group after 2 weeks of treatment and 4 weeks of treatment ($t = 13.638$, 15.039, $P < 0.001$). ∗∗ and ## indicate significant differences in the BBS scores between the MET group and the joint group after 2 weeks of treatment and 4 weeks of treatment ($t = 7.390$, 6.377, $P < 0.001$). ∗∗∗ and ### indicate significant differences in the BBS scores between the Neurac group and the joint group after 2 weeks of treatment and 4 weeks of treatment ($t = 6.206$, 6.118, $P < 0.001$).

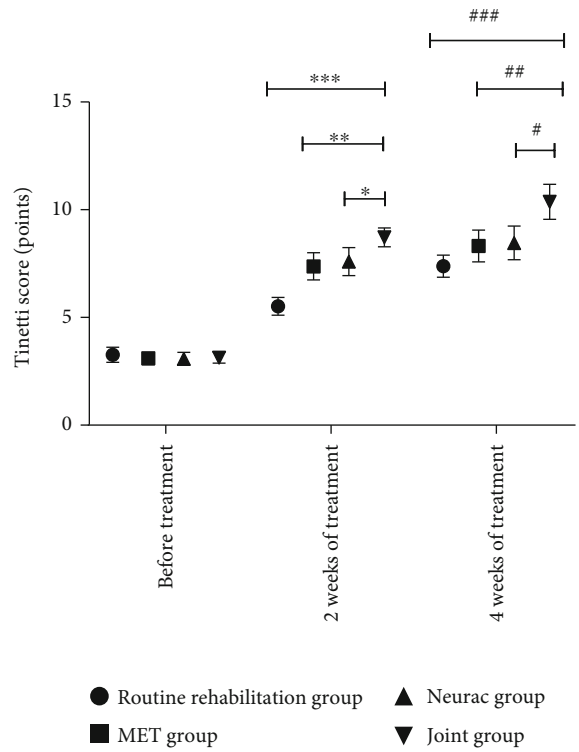

Figure 2: Comparison of Tinetti scores. Note: The abscissa indicates pretreatment, 2 weeks of treatment, and 4 weeks of treatment; the ordinate indicates Tinetti score, points. The Tinetti scores of the conventional rehabilitation group before, 2 weeks, and 4 weeks of treatment were 3.27 ± 0.35, 5.52 ± 0.41, and 7.38 ± 0.51, respectively. The Tinetti scores before treatment, at 2 weeks of treatment, and at 4 weeks of treatment in the MET group were 3.10 ± 0.29, 7.37 ± 0.63, and 8.32 ± 0.74, respectively. The Tinetti scores before treatment, at 2 weeks of treatment, and at 4 weeks of treatment in the Neurac group were 3.08 ± 0.30, 7.59 ± 0.65, and 8.46 ± 0.78, respectively. The Tinetti scores before, at 2 weeks, and at 4 weeks of treatment in the combined group were 3.13 ± 0.25, 8.72 ± 0.44, and 10.37 ± 0.81, respectively. ∗ and # indicate significant difference in the Tinetti scores between the conventional rehabilitation group and the joint group after 2 weeks of treatment and 4 weeks of treatment ($t = 26.604$, 15.619, $P < 0.001$). ∗∗ and ## indicate significant differences in the Tinetti scores between the MET group and the joint group after 2 weeks of treatment and 4 weeks of treatment ($t = 8.784$, 9.343, $P < 0.001$). ∗∗∗ and ### indicate significant differences in Tinetti scores between the Neurac group and the joint group after 2 weeks and 4 weeks of treatment ($t = 7.198$, 8.493, $P < 0.001$).

hips, lifted the body off the treatment table, and abducted the straightened arm 180°.

The patients in the joint group were treated with MET plus Neurac method, and the specific treatment methods were the same as those in the MET and Neurac groups. All four groups of patients underwent 4 weeks of training and were followed up by telephone 1 month after treatment.

2.4. Outcomes. (1) The Barthel (BI) index scale was used to assess patients' quality of daily living before, 2 weeks after, and 4 weeks after treatment, including items such as dressing, body transfer, walking, and bowel and urinary control. The total score of each item was 100 points. 100 points mean independent daily living; 61-99 points are mild impairment of daily life and occasionally require assistance; 41-60 points are moderate dependence and mostly require assistance; ≦40 points mean severe dependence and require full-time care. (2) Visual Analogue Scale (VAS): pain was divided into 0-10 levels on this sliding scale, with 0 points indicating no pain and 10 points indicating unbearable pain. A personal check was made on a piece of paper marked with 10 intervals with 0 for no pain and 10 for maximum pain. This test tool has a test-retest reliability. (3) Berg balance scale (BBS): the BBS was used to assess the balance function of hemiplegic patients: the sum of the scores was 56 points,

Table 3: Comparison of Fugl-Meyer scores.

Groups	Before treatment	2 weeks of treatment	4 weeks of treatment
Conventional rehabilitation	14.69 ± 3.12	18.01 ± 4.25	20.54 ± 4.33
MET group	15.28 ± 3.04	20.75 ± 3.67*#	23.44 ± 4.19*#
Neurac group	14.74 ± 2.98	20.66 ± 2.58*#	24.02 ± 3.95*#
Joint group	15.21 ± 2.71	23.34 ± 2.16*	29.16 ± 3.08*

∗ indicates $P < 0.05$ versus conventional rehabilitation group within the same time period; # indicates $P < 0.05$ versus the joint group.

Table 4: Comparison of QoL scores.

Groups	Before treatment	2 weeks of treatment	4 weeks of treatment
Conventional rehabilitation group	41.27 ± 5.13	56.71 ± 7.28	75.42 ± 8.26
MET group	42.54 ± 5.29	65.83 ± 8.10*#	86.19 ± 10.22*#
Neurac group	41.38 ± 5.07	67.34 ± 8.50*#	87.37 ± 10.15*#
Joint group	43.15 ± 5.12	74.60 ± 9.25*	99.67 ± 10.62*

∗ indicates $P < 0.05$ versus conventional rehabilitation group within the same time period; # indicates $P < 0.05$ versus the joint group.

and the higher the scores, the better the balance ability of the stroke patients. A sum of all scores less than 40 points indicates a risk of falling. Fourteen items are assessed to determine the patients' ability to maintain balance through sitting, standing, and postural changes, and about 20 minutes is taken. If the items cannot be performed at minimum, 0 points are given, and for completely independent, the maximum of 4 points is noted. (4) Tinetti gait assessment: gait assessment items include the starting step, lifting height, step length, gait symmetry, stride continuity, walking path, trunk stability, and step width. The full score is 12 points, where the walking path and trunk stability are scored on three levels of 0, 1, and 2 points, and the other items are scored on two levels of 0 points and 1 point. (5) The Fugl-Meyer scale was applied to assess the motor function of the lower extremities, and the main items include neuroreflex activity, common flexor movement, common extensor movement, joint common movement, detachment movement, and coordination/speed, with a full score of 34 points: (I) unsupported sitting: 0 points: unable to maintain the sitting position; 1 point: able to sit, but less than 5 minutes; and 2 points: able to sit for more than 5 minutes; (II) unaffected wing spread response: 0 points: no shoulder abduction or elbow joint extension, 1 point: weakened response, and 2 points: the response is normal; (III) wing-spreading response on the affected side: the score is the same as that of item (II); (IV) standing under support: 0 points: unable to stand, 1 point: can stand under the maximum support of others, and 2 points: able to stand for 1 minute with a little support from others; (V) standing without support: 0 points: unable to stand, 1 point: unable to stand for more than 1 minute, and 2 points: able to balance standing for more than 1 minute; (VI) standing on the healthy side: 0 points: unable to maintain 12 seconds, 1 point: able to balance standing for 49 seconds, and 2 points: able to balance standing for more than 10 seconds; (VII) standing on the affected side: the score is the same as item (VI). (6) The WHO/Q0L-26 World Health Organization Quality of Life Measurements Short Form (WHOQOL-BREF) was used to assess patients' quality of life, which includes 5 domains (physical, psychological, social, environmental, and integrated) and 26 items with a total score of 130 points. The higher the score, the better the quality of life. All questions are rated on a 5-point Likert scale, and the item is scored between 1 and 5. Raw scores in each domain were changed to a 4–20 score based on the guideline. All domain scores were linearly changed such that they varied from 0 to 100 with "100" demonstrating the highest possible QoL.

2.5. Statistical Analysis. SPSS 20.0 was used for data analyses, and GraphPad Prism 7 (GraphPad Software, San Diego, USA) was used to visualize the data into corresponding images. The count data were expressed as n (%) and processed using the χ^2 test, and the measurement data were expressed as ($\bar{x} \pm s$) and processed using the t-test. Differences were considered statistically significant at $P < 0.05$.

3. Results

3.1. Barthel Index Scores. The pretreatment Barthel index scores were similar among all eligible patients ($P > 0.05$). All treatment methods adopted in the present study showed significant enhancement in the Barthel index scores, with the best results observed in the joint group ($P < 0.05$) (Table 1).

3.2. Comparison of VAS Scores. No significant differences were obtained in VAS scores among the four groups of patients ($P > 0.05$). After treatment, all patients obtained markedly decreased VAS scores, and those receiving the combined therapy had the lowest scores versus those of other groups ($P < 0.05$) (Table 2).

3.3. BBS Scores. The pretreatment BBS scores were similar in all eligible patients ($P > 0.05$). After treatment, a remarkable increase in the BBS scores in all four groups was observed, with the best results achieved by the joint group ($P < 0.05$) (Figure 1).

3.4. Tinetti Scores. Before treatment, the four groups presented similar Tinetti scores ($P > 0.05$). After treatment, the joint group showed significantly higher Tinetti scores versus the other treatment methods ($P < 0.05$) (Figure 2).

3.5. Fugl-Meyer Scores. Before treatment, no significant differences were obtained in the Fugl-Meyer scores among the four groups ($P > 0.05$). After treatment, the Fugl-Meyer scores of the four groups were increased significantly, with the highest results obtained in the joint group ($P < 0.05$) (Table 3).

3.6. QoL Scores. The pretreatment QoL scores were similar among the four groups of patients ($P > 0.05$). After treatment, MET plus Neurac achieved more significant improvements in the quality of life versus the other groups ($P < 0.05$) (Table 4).

4. Discussion

The loss of control of higher centers over lower centers after the onset of stroke leads to sensory, motor, speech, swallowing, and cognitive dysfunction, and the disease has a high prevalence, which seriously jeopardizes patients' health and life safety [16]. Most patients are prone to hemiparesis, aphasia, and decreased limb function, where hemiparesis occurs due to loss and decrease in coordination between various muscle groups after stroke, leading to impaired motor and static balance and trunk control [17, 18]. Comorbid diabetes mellitus in stroke patients aggravates brain tissue damage and increases the disability rate. Research has shown [19] that hyperglycemia causes decreased erythrocyte activity in the body and damage to vascular endothelial tissue, promotes the development of atherosclerosis and thrombosis, and aggravates the degree of cerebral infarction and injury. Moreover, hypoglycemia compromises the neurological and cardiovascular systems of stroke patients, resulting in cognitive dysfunction [20]. Therefore, effective rehabilitation training plays an important role in the recovery of limb functions and improving the quality of life. Conventional rehabilitation training applied in stroke patients with hemiplegia combined with diabetes can improve the limb motor function of patients but fails to achieve the desired effectiveness [21]. MET promotes blood supply to muscle fibers through activation of target muscles, which contributes to the reconstruction and strengthening of tissue fibers, stretching contracted muscle fibers, enhancing muscle strength, increasing the range of motion of joints, and promoting the uniform distribution of external forces to the individual muscles of the restored stable muscle groups. In addition, the active contraction and diastole of the muscles allow the soft tissues around the joints to form spirals or inspirals, which accelerates the movement of the body's deep cells and body fluids, facilitating the elimination of stagnant material and speeding up the rate of tissue reoxidation and removal of metabolites [22]. The Neurac method is a neuromuscular functional training technique used to treat long-term skeletal muscle disorders and is derived from sling therapy, where the patient is gradually rehabilitated through a sling system and the assistance of a physical therapist. It is used to reestablish normal movement patterns through high levels of neuromuscular stimulation.

In the present study, all eligible patients obtained significantly elevated Barthel index scores, and MET plus Neurac presented the best results versus other treatment methods, indicating that patients had significant improvement in limb function through rehabilitation training and were able to perform certain activities of daily living independently and that the combination of MET and Neurac potentiates the treatment effectiveness. The increased VAS scores after treatment and the highest scores observed in the joint group suggested that the combined treatment better alleviated the pain during rehabilitation training. A study by Wolf et al. [23] used the MET in rehabilitation training for patients after anterior cruciate ligament reconstruction, and the scoring of knee pain found that the inclusion of the MET in rehabilitation training reduced pain and facilitated the functional rehabilitation of patients. The significantly higher elevation of BBS scores and Tinetti scores of the joint group after treatment indicates that the combination treatment can improve the patient's balance, increase the stability of walking, and reduce the risk of falling. MET enhances the balance of the muscle groups around the joint by lengthening the tense and shortened muscle groups and strengthening the relaxed and elongated muscle groups, to restore the normal biomechanics of the joint. The Neurac method assists patients' active movement with the aid of sling movement system, using open chain and closed chain movements for training, which can more effectively improve the coordinated contraction of muscle groups, enhance the weak links of trunk stabilizing muscle groups and power muscle groups, strengthen patients' control of the trunk, and reinforce the balance control and stability state. Here, the combination of MET and Neurac method obtained significantly higher Fugl-Meyer versus conventional rehabilitation and monotherapy of either MET or Neurac, which was similar to the findings of SAMUEL [24] et al., suggesting that MET combined with the Neurac method could improve the dysfunction of patients' lower limbs, activate nerves and muscles, and restore muscle strength, allowing patients to reestablish normal movement patterns. In addition, the superior quality of life of patients receiving joint treatment in the present indicates better quality of life benefits of joint treatment.

To sum up, Neurac method plus MET improves the independent mobility of stroke patients with hemiplegia and diabetes, relieves pain, enhances balance and stability, mitigates limb dysfunction, and boosts patients' quality of life, so it is worthy of clinical application.

Data Availability

The datasets used during the present study are available from the corresponding author upon reasonable request.

Conflicts of Interest

The authors declare that they have no conflicts of interest.

Authors' Contributions

Jingyan Wang and Shuang Wang contributed equally to this work.

Acknowledgments

This study was supported by the Scientific Research Project of Heilongjiang Provincial Health Commission (No. 2020-333).

References

[1] S. Fabi, J. S. Dover, E. Tanzi, L. E. Bowes, F. Tsai Fu, and A. Odusan, "A 12-week, prospective, non-comparative, non-randomized study of magnetic muscle stimulation for improvement of body satisfaction with the abdomen and buttocks," *Lasers in Surgery and Medicine*, vol. 53, no. 1, pp. 79–88, 2021.

[2] F. G. Bouwman, M. M. E. Van Ginneken, J.-P. Noben et al., "Differential expression of equine muscle biopsy proteins during normal training and intensified training in young standardbred horses using proteomics technology," *Comparative biochemistry and physiology, part D Genomics & proteomics*, vol. 5, no. 1, pp. 55–64, 2010.

[3] L. Tzelves, P. Mourmouris, and A. Skolarikos, "Does bipolar energy provide any advantage over monopolar surgery in transurethral resection of non-muscle invasive bladder tumors? A systematic review and meta-analysis," *World Journal of Urology*, vol. 39, no. 4, pp. 1093–1105, 2021.

[4] I. Jacob Carolyn and P. Katya, "Safety and efficacy of a novel high-intensity focused electromagnetic technology device for noninvasive abdominal body shaping," *Journal of Cosmetic Dermatology*, vol. 17, no. 5, pp. 783–787, 2018.

[5] S.-Y. Kim and J.-S. Oh, "Scapula muscle exercises using the Neurac technique for a patient after radical dissection surgery: a case report," *Physiotherapy Theory and Practice*, vol. 36, no. 12, pp. 1485–1492, 2020.

[6] A.-J. Gwon, S.-Y. Kim, and D.-W. Oh, "Effects of integrating Neurac vibration into a side-lying bridge exercise on a sling in patients with chronic low back pain: a randomized controlled study," *Physiotherapy Theory and Practice*, vol. 36, no. 8, pp. 907–915, 2020.

[7] N. Tanaka, S. Matsushita, Y. Sonoda et al., "Effect of stride management assist gait training for poststroke hemiplegia: a single center, open-label, randomized controlled trial," *Journal of stroke and cerebrovascular diseases: The official journal of National Stroke Association*, vol. 28, no. 2, pp. 477–486, 2019.

[8] Z. Wu, J. Xu, C. Yue, Y. Li, and Y. Liang, "Collaborative care model based telerehabilitation exercise training program for acute stroke patients in China: a randomized controlled trial," *Journal of stroke and cerebrovascular diseases: The official Journal of National Stroke Association*, vol. 29, no. 12, p. 105328, 2020.

[9] C. Phongamwong, P. Rowe, K. Chase, A. Kerr, and L. Millar, "Treadmill training augmented with real-time visualisation feedback and function electrical stimulation for gait rehabilitation after stroke: a feasibility study," *BMC Biomedical Engineering*, vol. 1, no. 1, 2019.

[10] A. Rochette, A. Dugas, and A.-S. Morissette-Gravel, "Inclusion of relatives in stroke rehabilitation: perception of quality of services they received in the context of early supported discharged (ESD), in- and out-patient services," *Topics in Stroke Rehabilitation*, vol. 28, no. 2, pp. 142–152, 2021.

[11] Y. Kim, K. Lee, H. J. Hwang, and N. J. Paik, "Clinical application of virtual reality for upper limb motor rehabilitation in stroke: review of technologies and clinical evidence," *Journal of Clinical Medicine*, vol. 9, no. 10, p. 3369, 2020.

[12] M. Tani, Y. Ono, M. Matsubara et al., "Action observation facilitates motor cortical activity in patients with stroke and hemiplegia," *Neuroscience Research: The Official Journal of the Japan Neuroscience Society*, vol. 133, pp. 7–14, 2018.

[13] S. H. Lee, J.-Y. Lee, and M.-Y. Kim, "Virtual reality rehabilitation with functional electrical stimulation improves upper extremity function in patients with chronic stroke: a pilot randomized controlled study," *Archives of Physical Medicine and Rehabilitation*, vol. 99, no. 8, pp. 1447–1453.e1, 2018.

[14] Q. Q. Sun, D. D. Xie, J. Tao et al., "Acupuncture regulation promotes functional recovery in patients with post-stroke hemiplegia: study protocol for a multicenter randomized parallel controlled tria," *Asia Pacific Journal of Clinical Trials: Nervous System Diseases*, vol. 2, no. 3, pp. 108–116, 2017.

[15] G. W. Kim, Y. H. Won, J. H. Seo, and M. H. Ko, "Effects of newly developed compact robot-aided upper extremity training systems (neuro-X?) in patients with stroke: a pilot study," *Journal of Rehabilitation Medicine*, vol. 50, no. 7, pp. 607–612, 2018.

[16] J. S. Noh, J. H. Lim, T. W. Choi, S. G. Jang, and S. B. Pyun, "Effects and safety of combined rTMS and action observation for recovery of function in the upper extremities in stroke patients: a randomized controlled trial," *Restorative Neurology and Neuroscience*, vol. 37, no. 3, pp. 219–230, 2019.

[17] S. B. Moon, Y. H. Ji, H. Y. Jang et al., "Gait analysis of hemiplegic patients in ambulatory rehabilitation training using a wearable lower-limb robot: a pilot study," *International Journal of Precision Engineering and Manufacturing*, vol. 18, no. 12, pp. 1773–1781, 2017.

[18] X.-M. Yu, X.-M. Jin, Y. Lu et al., "Effects of body weight support-Tai Chi footwork training on balance control and walking function in stroke survivors with hemiplegia: a pilot randomized controlled trial," *Evidence-based Complementary and Alternative Medicine*, vol. 2020, 9 pages, 2020.

[19] W. Zhao, P. Zhang, M. Qi, and Y. Song, "Research on combined rehabilitation method and its mechanism of traditional Chinese medicine Daoyin technique with biofeedback technique," *Journal of Biomedical Science and Engineering*, vol. 12, no. 12, pp. 514–521, 2019.

[20] H. Wang, C. Yang, W. Yang, M. Deng, Z. Ma, and Q. Wei, "A rehabilitation gait for the balance of human and lower extremity exoskeleton system based on the transfer of gravity center," *Industrial Robot*, vol. 46, no. 5, pp. 608–621, 2019.

[21] Q. Zhan, L. Tang, Y. Wang et al., "Feasibility and effectiveness of a newly modified protocol-guided selective dorsal rhizotomy via single-level approach to treat spastic hemiplegia in pediatric cases with cerebral palsy," *Child's nervous system: ChNS: official journal of the International Society for Pediatric Neurosurgery*, vol. 35, no. 11, pp. 2171–2178, 2019.

[22] S. G. Rozevink, C. K. van der Sluis, and J. M. Hijmans, "HoMEcare aRm rehabiLItatioN (MERLIN): preliminary evidence of long term effects of telerehabilitation using an unactuated training device on upper limb function after stroke," *Journal of Neuro Engineering and Rehabilitation*, vol. 18, no. 1, 2021.

[23] T. J. Wolf, M. Doherty, A. Boone et al., "Cognitive oriented strategy training augmented rehabilitation (COSTAR) for ischemic stroke: a pilot exploratory randomized controlled study," *Disability and Rehabilitation*, vol. 43, no. 2, pp. 201–210, 2021.

[24] S. Ow, A. Mg, Y. Geng et al., "Decoding movement intent patterns based on spatiotemporal and adaptive filtering method towards active motor training in stroke rehabilitation systems," *Neural Computing & Applications*, vol. 33, no. 10, pp. 4793–4806, 2021.

Hindawi
Disease Markers
Volume 2022, Article ID 5013622, 12 pages
https://doi.org/10.1155/2022/5013622

Research Article

Liraglutide Alleviates Diabetic Atherosclerosis through Regulating Calcification of Vascular Smooth Muscle Cells

Li-Li Shi,[1] Ming Hao,[2] Zhou-Yun Jin,[1] Gui-Fang Peng,[1] Ying-Ying Tang,[3] and Hong-Yu Kuang[2]

[1]*Department of Cadre Ward, The First Affiliated Hospital of Harbin Medical University, Harbin 150081, China*
[2]*Department of Endocrinology, The First Affiliated Hospital of Harbin Medical University, Harbin 150081, China*
[3]*Department of Endocrinology, The Heilongjiang Provincial Hospital, Harbin 150001, China*

Correspondence should be addressed to Ying-Ying Tang; tangneiyou3@126.com
and Hong-Yu Kuang; kuangzechen958@163.com

Received 17 December 2021; Revised 15 February 2022; Accepted 22 February 2022; Published 25 April 2022

Academic Editor: Yaoyao Bian

Background. Diabetes mellitus (DM) is a group of metabolic diseases characterized by hyperglycemia, which can induce the development of atherosclerosis (AS). Calcification of vascular smooth muscle cells (VSMCs) exerts an important role in the process of AS. In this study, the effects of liraglutide (LIRA) on VSMC under high-glucose condition and its mechanism were explored. *Method*. After VSMC was treated by high glucose with or without LIRA *in vitro*, the alkaline phosphatase (ALP) activity was measured by the detection kit, osteogenic marker protein expression was detected by Western blotting, and calcification was determined by alizarin red staining. Subsequently, the DM rat model was established and the ALP activity, calcification, and osteogenic marker proteins were determined *in vivo*. Immunohistochemical (IHC) staining and hematoxylin-eosin staining were performed on the thoracic aorta of DM rats. *Result*. The positive rate of SMα-actin expression in the DM + AS group was significantly lower than that in control rats, but LIRA administration increased the positive rate in the model. The expression of Cbfα-1 and OPN in the DM + AS group was significantly higher than that in the control group, while it was decreased after treatment of LIRA. The ALP activity and calcium content were increased in DM + AS rats, and the treatment of LIRA decreased the phenotypes in the rats, so as to delay the progression of AS in DM rats. Meanwhile, LIRA inhibited the ALP activity, upregulated SM-α expression, and downregulated expression of OPN and Cbfα-1 in VSMC under high-glucose (HG) conditions. Mechanically, HG-enhanced ALP activity, AKT, and ERK phosphorylation were inhibited by LIRA, PI3K antagonist LY294002, or ERK1/2 antagonist PD98059, in which cotreatment of LIRA with LY294002 and PD98059 could further enhance the effect of LIRA on VSMC, and GLP-1R antagonists reversed the phenotypes in the model. LIRA blocked the osteogenic transformation of VSMC through PI3K and ERK1/2 signaling pathways, which can be reversed by GLP-1R antagonists. *Conclusion*. LIRA inhibited the abnormalities in VSMC calcification mediated by the GLP-1R, which was related to PI3K/Akt and ERK1/2 MAPK pathways. Therefore, the prospect and significance of LIRA in the treatment of DM complicated with AS were clarified.

1. Introduction

Diabetes mellitus (DM) has become a rising epidemic that seriously threatens human health and life. The harm of diabetes to human health mainly comes from the concurrent damage of many organs, especially cardiovascular diseases, such as atherosclerosis (AS) [1]. It has been demonstrated that hyperglycemia can lead to AS through a variety of mechanisms, including the functional regulation of vascular smooth muscle cells (VSMC). Notably, hyperglycemia not only promotes the proliferation and migration of VSMC [2] but also induces osteogenic changes of VSMC, which is one of the main causes of vascular calcification [3]. More importantly, it is well known that vascular calcification is an important pathological process and manifestation of AS [4]. Although traditional hypoglycemic drugs such as

biguanides, sulfonylureas, and insulin are capable of alleviating AS [5], they do not provide any guidance. Moreover, long-term application of sulfonylureas and insulin could induce obesity and further increase the risk of cardiovascular disease [6]. Although the mechanistic study has shown that several signaling pathways are involved in the regulation of VSMC calcification in DM combined with AS, such as phosphatidylinositol-4-diphosphate 3-kinase (PI3K)/protein kinase B (AKT) and the ERK1/2 MAPK signaling pathway [7, 8], no targeted therapy has been developed till now. Therefore, inhibiting migration, proliferation, and especially calcification of VSMC could be a promising strategy for the treatment of DM complicated with AS.

Glucagon-like peptide-1 (GLP-1) is an important regulator of glucose metabolism [9]. The GLP-1 receptor (GLP-1R) was expressed on the surface of aortic smooth muscle cells in both humans and rats. Accumulating evidence showed that GLP-1 could stimulate insulin secretion in a glucose-dependent manner, reduce gastric emptying, inhibit food intake, and increase natriuresis [10]. Therefore, after some biomedical modifications for achieving enhanced therapeutic efficiency and sustained effects, GLP-1R agonists have been widely used in the clinical treatment of type 2 diabetes mellitus (T2DM) as well as clinical evaluation of obesity [11]. Moreover, liraglutide (LIRA), which is a synthetic analogue of GLP-1, has also been commonly used in the treatment of DM and obesity [12]. On the other hand, besides the application of GLP-1/GLP-1R in treating DM, recent studies revealed the significant cardio- and neuroprotective effects of GLP-1 [13]. It has been reported that LIRA reduces AS in T2DM rats by targeting ER-associated macrophage-derived macrovesicle production [14]. LIRA represses AS by regulating inflammatory pathways in Apo $E^{-/-}$ mice [15]. LIRA inhibits AS by modulating proinflammatory mediators and immune cell phenotypes in apolipoprotein E-deficient mice [16]. However, till now, the mechanism of the cardioprotective effects of GLP-1R agonists or GLP-1 analogue such as LIRA is rarely reported and remains largely unknown. In this respect, we noticed that the alleviation of osteoblast differentiation and calcification of human VSMC was reported in the previous study [17]. Therefore, in this study, we aimed to further demonstrate the effects of osteoblast differentiation and calcification of VSMC in high-glucose condition, clarifying the function and mechanism of LIRA as well as GLP-1 in DM combined with AS.

Herein, the effects of the GLP-1 analogue LIRA on VSMC or vascular calcification in high-glucose condition and the involvement of related signaling pathways were investigated *in vitro* and *in vivo*. Therefore, the prospect and significance of LIRA in the treatment of DM complicated with AS were further clarified.

2. Materials and Methods

2.1. Construction of the DM Animal Model. All procedures involving animal experimental protocols were approved by the Institutional Animal Care and Use Committees (IACUC) of the first affiliated Hospital of Harbin Medical University and follow the ARRIVE guidelines. Clean Sprague-Dawley (SD) rats (Beijing HFK Bioscience, China, 7 weeks, weight ± 200 g) were randomly divided into groups of control, LIRA, DM + AS, and DM + AS + LIRA ($n = 30$ per group). Among them, the control and LIRA were fed with normal diet and DM + AS and DM + AS + LIRA were fed with high-fat diet. The high-fat feed is composed of 10% lard, 5% egg yolk powder, 5% whole milk powder, 0.1% bile salt, 1% cholesterol, 5%sucrose, and 73.9% basic feed. After feeding for one month, DM + AS and DM + AS + LIRA were injected intraperitoneally with STZ (35 mg/kg, dissolved in precooled 0.01 M, pH = 4.4 sodium citrate buffer) to induce DM, while control and LIRA were injected with citric acid buffer. The blood glucose of the rats was measured on the 7th and 14th days. The model was established when the blood glucose was ≥16.9 mmol/L; otherwise, 20 mg/kg STZ was replenished again until the model was successfully established. In order to prevent fatal hypoglycemia, rats were given 20% glucose orally for one day after being injected with STZ. After successful establishment of the model, the rats of LIRA and DM + AS + LIRA were continued to be given LIRA (Selleck, USA, NN2211, 200 μg/kg, 2 times/day) until the end of the experiment. In the experiment, the mental state, water intake, food intake, and urine volume of rats were observed and blood glucose was monitored regularly. At 0, 2, and 4 months after the establishment of the model, some rats were killed and the medial edge of the thoracic aorta was taken for further correlation detection.

2.2. Immunohistochemical (IHC) Staining. After the tissue samples were deparaffinized, repaired, and blocked with citric acid antigen, they were incubated with antibody SMα-actin (Abcam, USA, ab7817, 1 : 200) overnight at 4°C. Afterwards, horseradish peroxidase- (HRP-) conjugated secondary antibody IgG (Abcam, USA, ab150077, goat anti-rabbit, 1 : 400) was added to continue incubation for 1 h at 37°C. As soon as the sections develop, they were immersed in deionized water and stained with DAB (Solarbio, China, DA1010) followed by hematoxylin for visualization. All tissues were pictured with microscopic and viewed with ImageScope and CaseViewer.

2.3. Hematoxylin-Eosin Staining. Tissue samples were embedded in paraffin and stained with hematoxylin and eosin in turn. Subsequently, the tissue sample was dehydrated with ethanol and xylene and sealed with neutral gum. The staining effect was observed and photographed under a 400x microscope.

2.4. Collection of VSMC. SD rats aged 5–8 weeks were anesthetized on the sterile operating table, and the whole thoracic aorta was quickly isolated. Subsequently, the blood vessels were cut into tissue blocks of 1–2 mm size and soaked in T25 bottles (containing 2 mL fetal bovine serum) 30 min. The tissue blocks were placed at the bottom of the DMEM (ThermoFisher, USA) culture flask (containing 15% FBS) and cultured at 37°C in a 5% CO_2 incubator for 12 h. After a week, a large number of cells distributed around the tissue

mass can be subcultured. The calcifying medium contained 10 mM β-glycerophosphate (β-GP, Beyotime, ST637) and 50 μg/mL ascorbate (Merck, USA, 134-03-2). The obtained VSMC was intervened differently, including control (5.5 mM glucose), high glucose (HG, 25 mM glucose), LIRA (100 nM), HG + LIRA (20 mM), HG + LY294002 (PI3K antagonist, 50 μM, MCE, USA, HY-10108), HG + LY294002 + LIRA, HG + PD98059 (ERK antagonist, 50 μM, MCE, USA, HY-12028), HG + PD98059 + LIRA, and HG + Exe (9-39) (GLP-1 receptor antagonist, 200 nM, MCE, USA, HY-P0264) + LIRA.

2.5. Detection of Alkaline Phosphatase (ALP) Vitality. The 100 μL substrate buffer (ALP kit, Sigma, USA, MAK447) and 20 μL samples (5 μg/μL) were added to the 96-well plate and fully shaken, incubated at 37°C for 15 min. After the termination solution of 80 μL reaction was added and oscillated for 1 min, the absorbance at 520 nm was measured by an enzyme-labeling instrument. The ALP activity is defined as 1 unit of 1 mg phenol produced by the interaction of 15 min with a matrix at 37°C per gram of protein.

2.6. Western Blotting. RIPA lysate was used to prepare tissue homogenate to extract protein and NP-40 lysate to obtain cell protein. The protein concentration was measured using the BCA protein kit (TaKaRa, Otsu, Japan, T9300A). Protein was degenerated in sodium dodecyl sulfate (SDS) buffer, followed by separating on SDS-polyacrylamide electrophoresis (PAGE) gel using electrophoresis. After that, they were transferred onto polyvinylidene difluoride (PVDF, Millipore, USA, IPVH00010) membrane and incubated with primary antibody actin (Abcam, USA, ab8226, 1 : 400), BAX (Abcam, USA, ab32503, 1 : 200), Bcl-2 (Abcam, USA, ab182858, 1 : 200), caspase-3 (Abcam, USA, ab32351, 1 : 1000), Cbfα-1 (Abcam, USA, ab113203,1 : 200), OPN (Abcam, USA, ab228748, 1 : 200), SM-α (Abcam, USA, ab7817, 1 : 500), Akt (Abcam, USA, ab8805, 1 : 200), p-Akt (Abcam, USA, ab38449, 1 : 100), ERK1/2 (Abcam, USA, ab184699,1 : 1000), p-ERK1/2 (Abcam, USA, ab278538,1 : 1000), and β-actin (Abcam, USA, ab8226, 1 : 1000) overnight at 4°C. Next, they were incubated with horseradish peroxidase- (HRP-) conjugated secondary antibodies IgG (Abcam, USA, ab150077, goat anti-rabbit, 1 : 5000) at room temperature for 45 min. After the membrane was washed in TBST, the blot was visualized by the enhanced chemiluminescence ECL kit (Thermo Fisher Scientific, NY, USA).

2.7. Cell Calcification Detection. The fourth generation of VSMC was collected with a density of 1×10^5 cells/mL. After the cells reached 80% fusion, they were cultured without serum for 24 h. After being cultured with different media for 14 days, the cells in each group were stained with alizarin red. The cells were incubated for 30 min at room temperature, washed twice with PBS, and photographed under a microscope.

2.8. Analysis of the Cellular Calcium Content. According to the method provided in the literature [18], we used the calcium colorimetric analysis kit (Abcam, USA, ab102505, 1 : 1000) to analyze the cellular calcium content. Then, the operation was carried out according to the protocol of the kit and the OD value was determined at the wavelength of 610 nm.

2.9. Statistical Analysis. All the experiments were repeated three times, and all the data were shown as mean ± standard deviation. All data were processed using SPSS version 17.0 (Chicago, USA). $P < 0.05$ was considered to be statistically significant.

3. Results

3.1. LIRA Inhibits the Osteogenic Transformation of VSMC in the Thoracic Aorta of DM Rats. The DM rat models were established, and the thoracic aorta of DM rats in 0, 2, and 4 months were used to determine the condition of AS. The osteoblast-like alteration of VSMC was determined by the detection of SMα-actin, Cbfα-1, and OPN. The results of IHC staining (Figure 1(a)) showed that the positive rate of SMα-actin expression in the DM + AS group was significantly lower than that in the control group at 2 months and 4 months but the positive rate increased significantly after LIRA administration. Subcutaneous injection of LIRA alone had no effect on the expression of SMα-actin in rats. In addition, these results were further detected by immunoblotting (Figure 1(b)). Additionally, the expression of OPN and Cbfα-1 in the DM + AS group increased compared with 2 months. The expression of Cbfα-1 and OPN in the DM + AS group was significantly higher than that in the control group at 2 months and 4 months, while was decreased after treatment with LIRA. Similarly, subcutaneous injection of LIRA in DM rats alone had no effect on the expression of Cbfα-1 and OPN (Figures 1(c) and 1(d)).

3.2. LIRA Slows Down the Progression of as in DM Rats by Inhibiting Vascular Calcification. HE staining showed that there was no significant difference in HE staining of the thoracic aorta among the four groups at 0 months. At 2 months, the DM + AS group showed a thickened arterial wall, endothelial cells were slightly protuberant and irregular, and the arrangement of middle fusiform smooth muscle cells was disordered and thickened obviously. Moreover, in the DM + AS + LIRA group, there was no obvious protuberance of intimal cells and no obvious thickening of the media layer and smooth muscle cells are arranged relatively neatly and slightly thickened. At 4 months, the demarcation of each layer of the arterial wall in the DM + AS group was unclear, endothelial cells fell off, intima thickened, cells arranged irregularly, intima thickened obviously, elastic fibers arranged disorderly, light stained foam cells could be seen in the sub intima, and intima protruded to form plaques. At the same time, in the DM + AS+LIRA group, the boundaries of each layer of the arterial wall were relatively clear, intima media thickening was significantly reduced, the arrangement of cells was relatively regular, foam cells were rare, and there was no obvious plaque formation. The results were similar to those *in vitro* that there was no significant

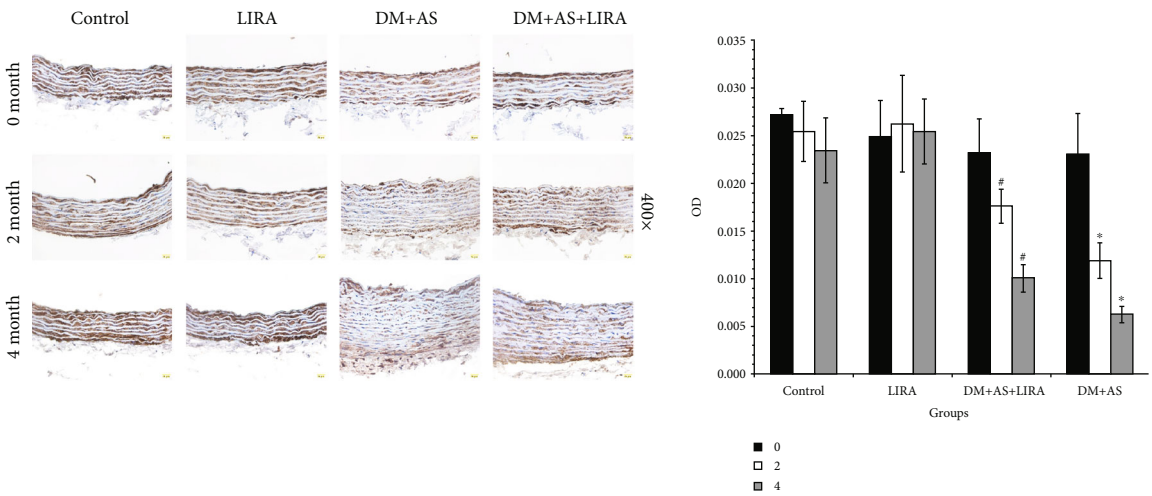

(a)

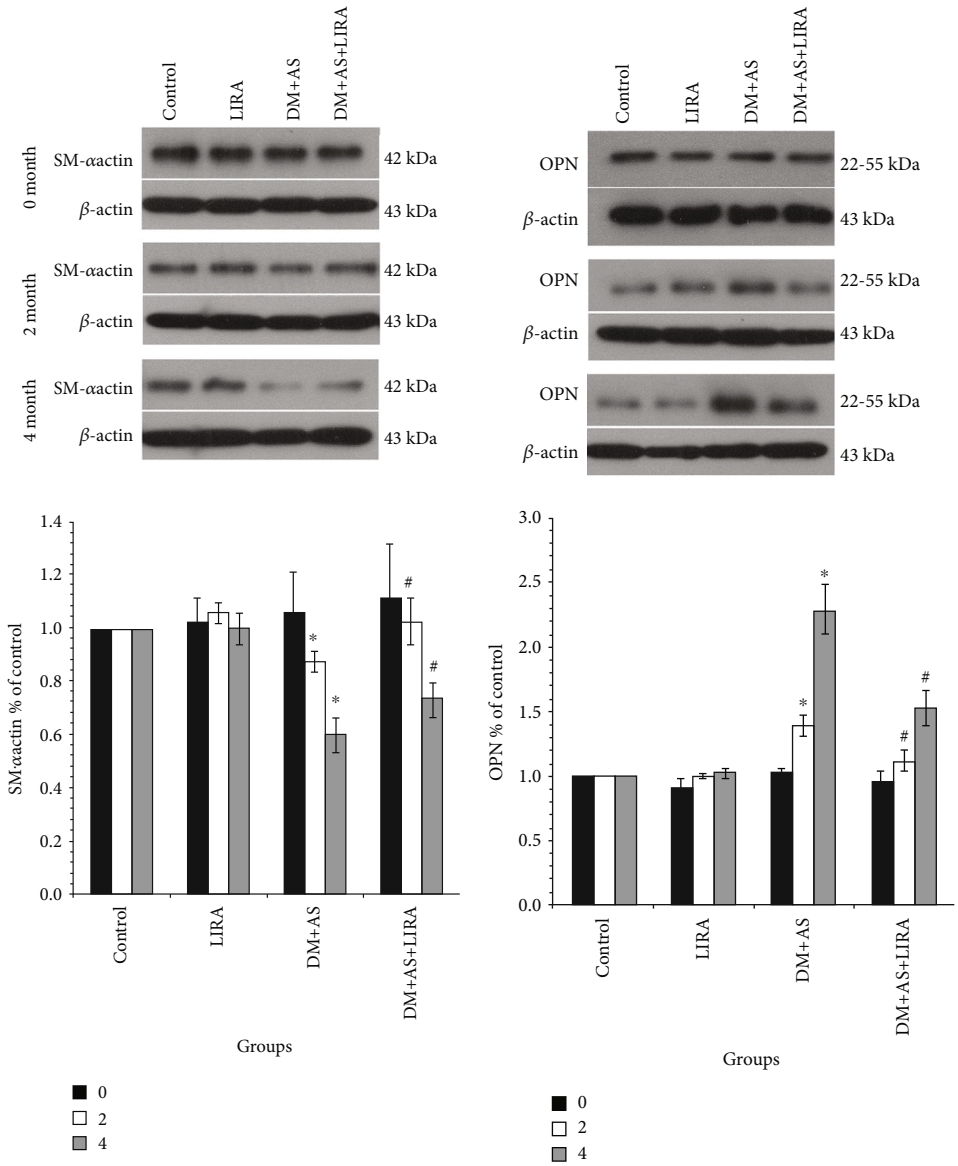

(b) (c)

Figure 1: Continued.

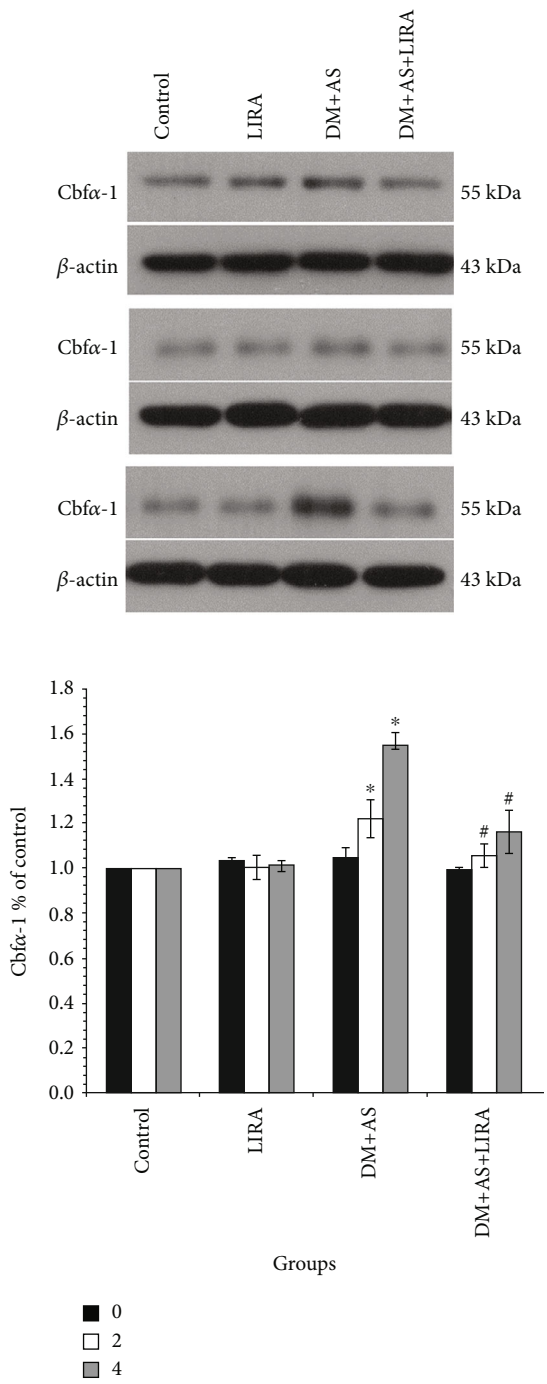

(d)

Figure 1: LIRA inhibits the osteogenic transformation of VSMC in the thoracic aorta of DM rats. (a) IHC showed the expression of SMα-actin in the rat thoracic aorta (400x). In group DM + AS, 0 months vs. 2 months ($P < 0.01$) and 2 months vs. 4 months ($P < 0.01$). In months 2 and months 4, DM + AS vs. control ($P < 0.01$) and DM + AS + LIRA vs. DM + AS ($P < 0.01$); in group DM + AS, 0 months vs. 2 months ($P < 0.01$) and 2 months vs. 4 months ($P < 0.01$). Protein expression of (b) SMα-actin, (c) OPN, and (d) Cbfα-1. Data were from three independent experiments expressed as mean ± standard deviation. In month 2 and month 4, DM + AS vs. control ($P < 0.01$) and DM + AS + LIRA vs. DM + AS ($P < 0.01$). In group DM + AS, 0 months vs. 2 months ($P < 0.01$) and 2 months vs. 4 months ($P < 0.01$). $^{*}P < 0.01$ vs. control; $^{\#}P < 0.01$ vs. DM + AS.

change in the thoracic aorta in the LIRA group and control group (Figure 2(a)).

Then, we detected the effect of LIRA on ALP activity, calcification, and osteogenic marker protein *in vivo*. The ALP activity and calcium content of the thoracic aorta in rats could reflect the degree of vascular calcification to some extent. Our results showed that the ALP activity and calcium content of DM + AS rats increased significantly from 0 to 4

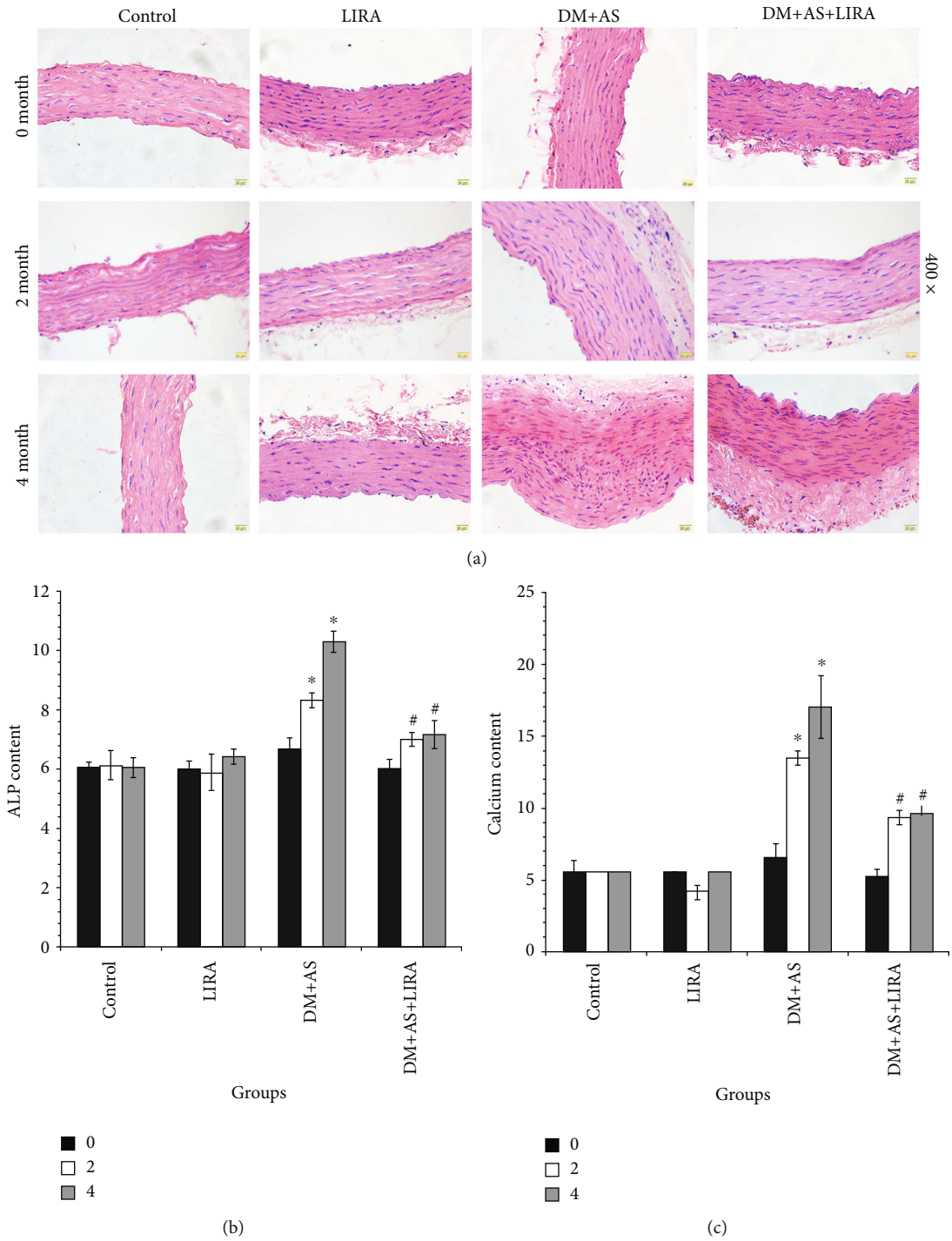

Figure 2: LIRA slows down the progression of AS in DM rats by inhibiting vascular calcification. (a) HE staining of the thoracic aorta showed the effect of LIRA on the progression of AS in DM rats (400x). (b) ALP activity detection in vitro. (c) Calcium content detection. Data were from three independent experiments expressed as mean ± standard deviation. $^{*}P < 0.01$ vs. control; $^{\#}P < 0.01$ vs. DM + AS. In group DM + AS, 0 months vs. 2 months ($P < 0.01$) and 2 months vs. 4 months ($P < 0.01$).

month, which indicated that the degree of AS and calcification became stronger with the extension of time. The activity of ALP in the thoracic aorta of rats was detected at 0, 2, and 4 months, showing that the ALP activity in the DM + AS group was the highest. After being treated with LIRA, the ALP activity decreased significantly (Figure 2(b)). Furthermore, the calcium content (Figure 2(c)) was the highest in the DM + AS group and significantly decreased in the DM + AS + LIRA group compared with control. That is to say, LIRA can delay the progression of AS in DM rats by inhibiting the calcification of the thoracic aorta.

3.3. LIRA Inhibits the ALP Activity of VSMC through the PI3K/AKT and ERK1/2 MAPK Signaling Pathways. Next,

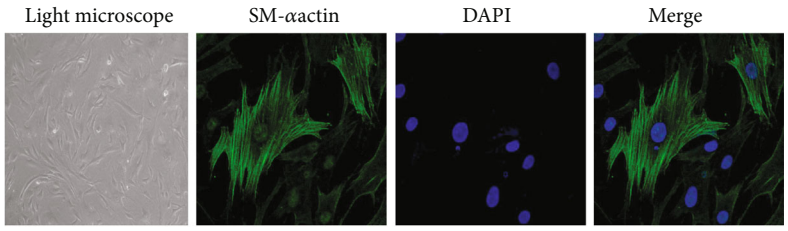

(a)

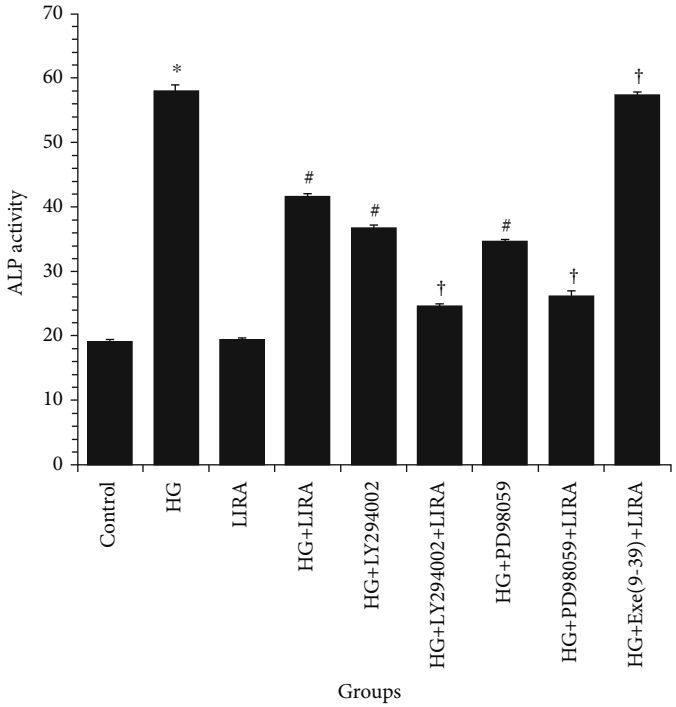

(b)

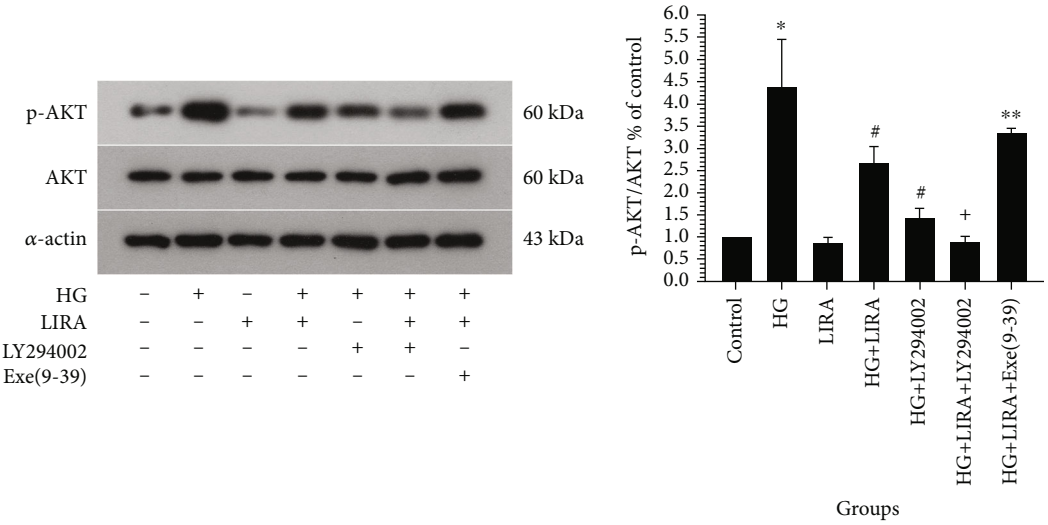

(c)

Figure 3: Continued.

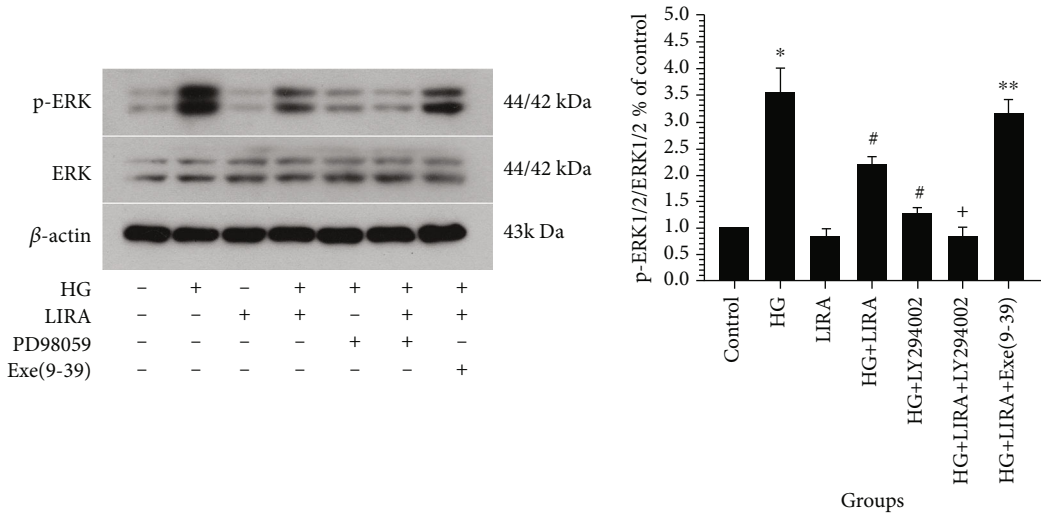

(d)

Figure 3: LIRA inhibits the ALP activity of VSMC through the PI3K/AKT and ERK1/2 MAPK signaling pathways. (a) Cell identification by the cell morphology under light microscope (100x) and SMα-actin immunofluorescence (400x). (b) ALP activity detection. Data from three independent experiments are expressed as mean ± standard deviation; $^{*}P < 0.01$ vs. control; $^{\#}P < 0.01$ vs. HG; $^{\dagger}P < 0.01$ vs. HG + LIRA. (c) Protein expression of phosphorylated Akt in VSMC. (d) Protein expression of phosphorylated ERK1/2 in VSMC. Data from three independent experiments are expressed as mean ± standard deviation; $^{*}P < 0.01$ vs. control; $^{\#}P < 0.01$ vs. HG; $^{**}P < 0.05$, $^{\dagger}P < 0.01$ vs. HG + LIRA.

we extracted vascular smooth muscle cells from the thoracic aorta of SD rats to establish an *in vitro* model. Through the cell morphology under the light microscope and the immunofluorescence detection of SM-α actin, we confirmed that VSMC was successfully extracted and the purity met the experimental requirements (Figure 3(a)). As illustrated in Figure 3(b), the ALP activity is an indicator of cell calcification. On the one hand, high glucose can promote the increase of ALP. The ALP activity was reduced after administration of LIRA on a high-glucose basis. In addition, the ALP activity was decreased after VSMC were treated with PI3K antagonist LY294002 or ERK1/2 antagonist PD98059. Furthermore, the VSMC were pretreated with HG + Exe (9-39) + LIRA which contributed to the increase in the ALP level in VSMC (Figure 3(b)). The results of phosphorylated AKT (p-AKT, Figure 3(c)) and p-ERK1/2 (Figure 3(d)) protein expression in each group were shown, which revealed that high glucose could significantly increase the expression of p-AKT and p-ERK1/2 in VSMC. These results showed that LIRA can reduce the ALP activity of VSMC induced by high glucose through PI3K and ERK1/2 signaling pathways and this effect was GLP-1 receptor dependent.

3.4. LIRA Inhibits the Osteogenic Transformation and Calcification of VSMC under High-Glucose Condition. Firstly, the protein expression of self-labeled protein SMα-actin and bone marker OPN and Cbfα-1 in VSMC under different environments was detected. The expression of SMα-actin in VSMC (Figure 4(a)) was the lowest in the HG group, while the expression of SMα-actin increased after LIRA intervention. On the basis of HG and LIRA, the expression of SMα-actin was further increased when VSMC were treated with ERK1/2 antagonist PD98059, while the expression of SMα-actin was decreased in cells treated with GLP-1 receptor antagonist Exe-9-39. On the other hand, expression of OPN (Figure 4(b)) was the highest in the HG group but decreased significantly after intervention by LIRA. Treatment with PI3K antagonist LY294002 or ERK antagonist PD98059 could reduce the expression of OPN. On the basis of HG and LIRA, the expression of OPN could be increased through treatment with GLP-1 receptor antagonist Exe-9-39. At the same time, the expression of Cbfα-1 (Figure 4(c)) in the HG group was significantly increased but decreased after administration of LIRA compared with that in the control group. The VSMC were treated with antagonists PD98059, which could reduce the expression of Cbfα-1. On the basis of HG and LIRA, VSMC treated with PD98059 further decreased the expression of Cbfα-1. On the contrary, VSMC treated with GLP-1 receptor antagonist Exe-9-39 increased its expression. Interestingly, there was no significant difference in the expression of OPN, Cbfα-1, and SMα-actin in VSMC between the LIRA group and the control group. That is, LIRA attenuated SMα-actin expression and enhanced the expression of OPN and Cbfα-1 partly through the inhibition of PI3K/ERK signaling pathway under high-glucose condition.

Then, we determine the calcification of VSMC using alizarin red staining (Figure 4(d)). Compared with the control group, the alizarin red staining was stronger in the HG group and there were some calcified nodules but the staining level decreased after the intervention of LIRA. Meanwhile, LIRA alone had no effect on the alizarin red staining level of VSMC. Our results showed that high glucose could promote the cartilage-like or osteoblast-like transformation of VSMC and eventually lead to calcification, which could be reversed by LIRA.

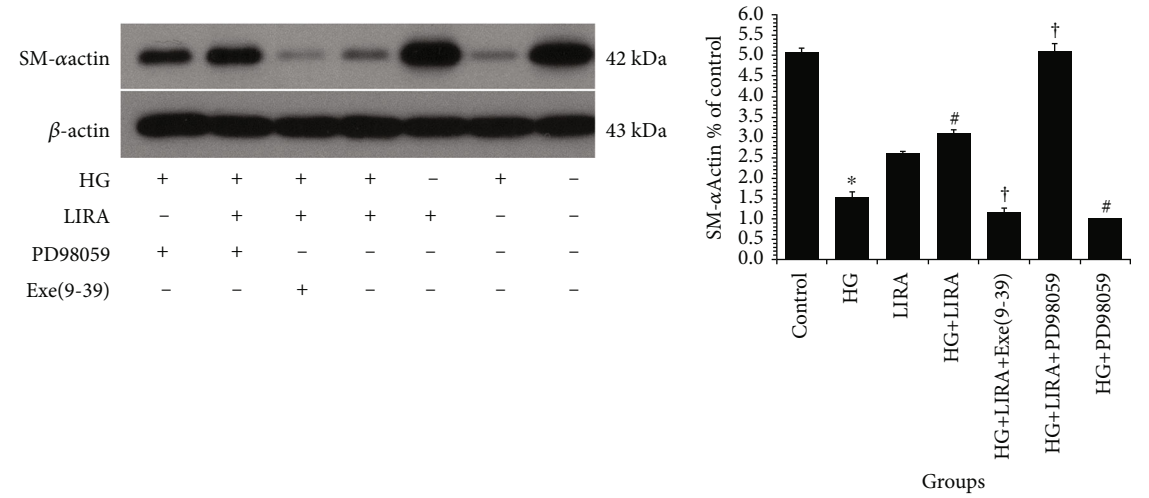

(a)

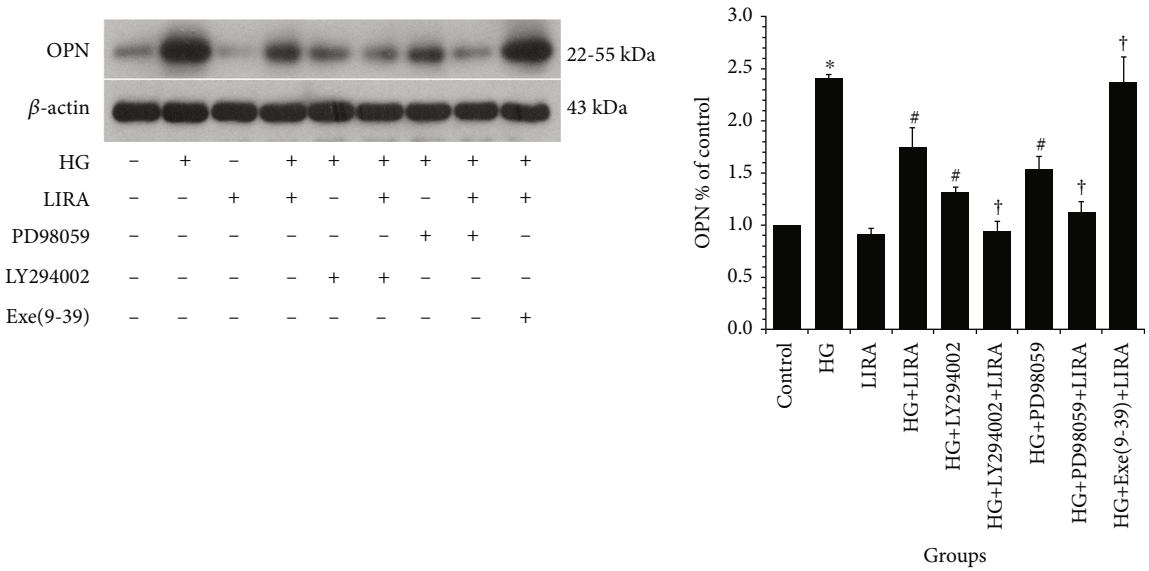

(b)

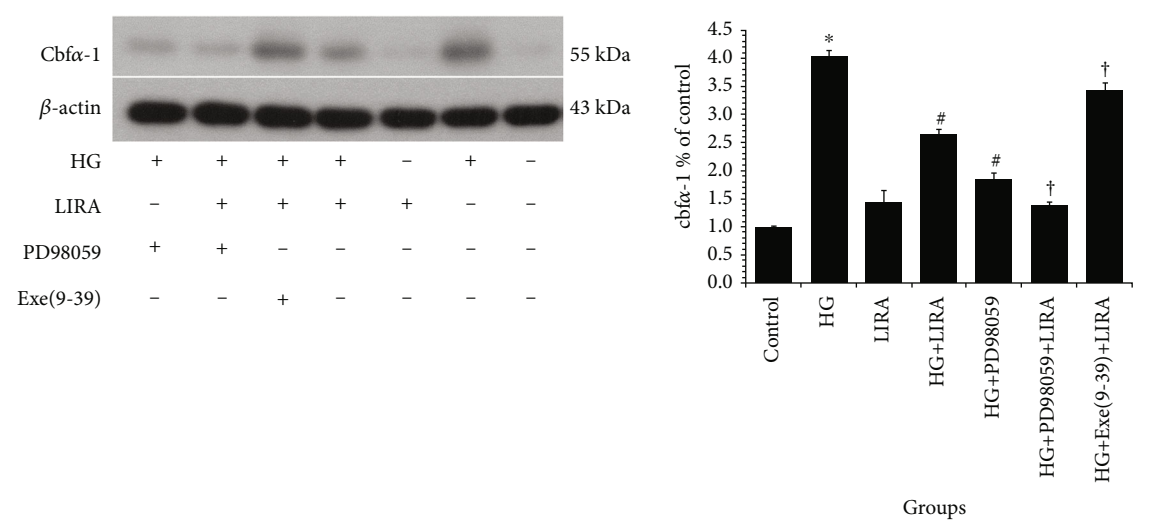

(c)

Figure 4: Continued.

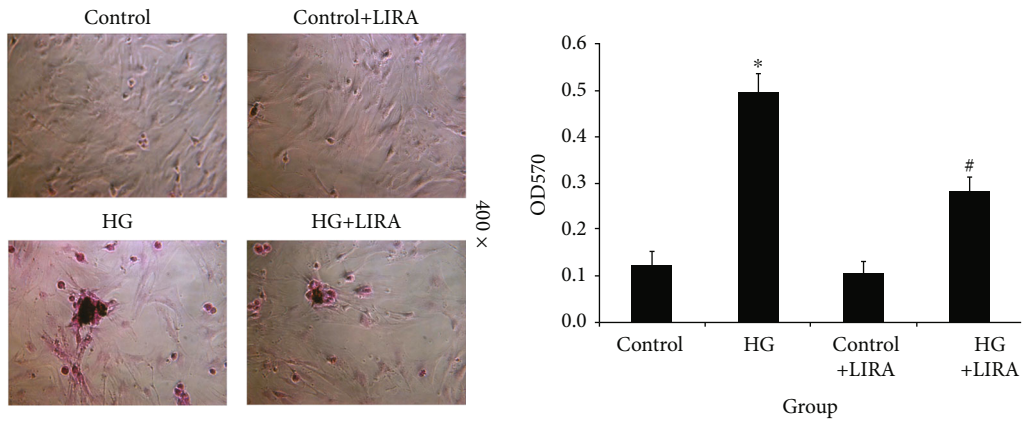

(d)

Figure 4: LIRA inhibits the osteogenic transformation and calcification of VSMC under high-glucose condition. Protein expression of (a) SMα-actin, (b) OPN, and (c) Cbfα-1. Data from three independent experiments are expressed as mean ± standard deviation. $^{*}P < 0.01$ vs. control; $^{\#}P < 0.01$ vs. HG; $^{\dagger}P < 0.01$ vs. HG + LIRA. (d) Calcification of VSMC tested by alizarin red staining (400x). Data from three independent experiments are expressed as mean ± standard deviation; $^{*}P < 0.01$ vs. control; $^{\#}P < 0.01$ vs. HG; $^{**}P < 0.05$, $^{\dagger}P < 0.01$ vs. HG + LIRA.

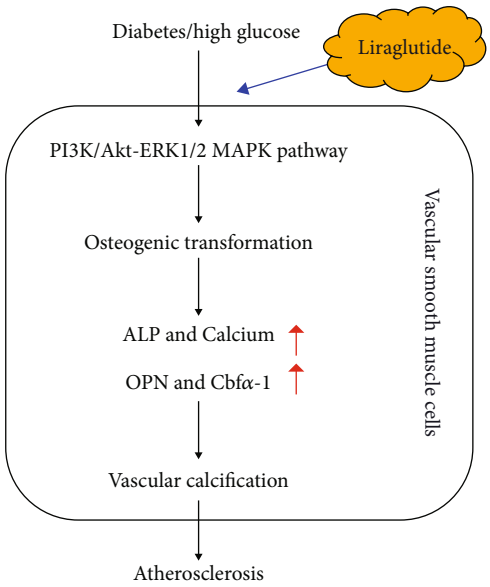

Figure 5: Schematic diagram of the mechanism of protective effect of liraglutide on diabetic atherosclerosis-induced vascular calcification.

Collectively, LIRA has the function of inhibiting the transition of VSMC to osteoblast or chondrocyte and the vascular calcification under high-glucose condition, partly via regulating the PI3K/ERK signaling pathway.

4. Discussion

Atherosclerosis (AS) is the most common cardiovascular complication of DM. Vascular remodeling is an important component of the development of AS, which is closely related to the pathological changes of VSMC, including proliferation, migration, and apoptosis [3]. Studies indicated that vascular calcification, which was proved to be partially triggered by osteochondrogenic transdifferentiation of VSMC, also played an important role in the development of AS [17]. Therefore, the investigation of the mechanism underlying the calcification of VSMC and the exploration of the inhibitor of VSMC calcification have been considered as a promising strategy for the treatment of AS. Recently, reports demonstrated the critical role of osteogenic transformation of VSMC in atherosclerotic calcification and the glucose metabolism involved in arterial calcification [19]. In our study, both the *in vitro* and *in vivo* experiments showed that the high-glucose environment could induce osteogenic transformation and calcification of VSMC, thus promoting vascular calcification.

GLP-1 and its analogues (such as LIRA) can regulate blood glucose through a variety of signaling pathways, which has been used in the treatment of DM [20]. At present, more and more studies focus on the cardioprotective effect of GLP-1, including the regulation of cardiovascular risk factors and the impact of cardiac function [21]. In this study, we aim to elucidate the potential regulatory effects of LIRA on DM complicated with AS from the aspects of VSMC phenotype regulation.

Actually, the influence of LIRA on functions or phenotypes of VSMC, especially in DM complicated with AS, is relatively rarely investigated. A previous study demonstrated that LIRA attenuated high-glucose-induced abnormal cell migration, proliferation, and apoptosis of VSMC by activating the GLP-1 receptor and inhibiting ERK1/2 and PI3K/Akt signaling pathways [22]. It has been reported that LIRA was delayed AS in ApoE-deficient mice by enhancing AMP-activated protein kinase and cell cycle regulation and inhibiting the proliferation of VSMC [23]. Furthermore, LIRA-inhibited AGEs induced coronary smooth muscle cell phenotypic transition through inhibiting the NF-κB signaling pathway [24]. Otherwise, LIRA can prevent osteoblastic differentiation of VSMC, resulting in the slowing of arterial calcification (Hu, 2016 #26). There was also evidence that LIRA

attenuates osteogenic differentiation and calcification of VSMC through GLP-1R and subsequently activation of the PI3K/Akt/mTOR/S6K1 signaling pathway [25]. Herein, the results of our study revealed that, although LIRA intervention alone possesses relatively weak regulatory effects on VSMC calcification, it could significantly attenuate the high-glucose-induced calcification of VSMC, exerting cardioprotective ability. As expected, this phenomenon is GLP-1R dependent and could be partially eliminated by the treatment of GLP-1R antagonists. Therefore, LIRA could be an option for the treatment of DM combined with AS.

On the other hand, the involvement of PI3K/Akt and ERK1/2 signaling pathways in the regulation of VSMC phenotypes especially calcification has been previously elucidated. For example, Ponnusamy et al. indicated that FTI-277 (farnesyl transferase inhibitor) could suppress VSMC calcification through regulating the PI3K/Akt signaling pathway [7]. Recently, it was reported that microRNA-155 is able to attenuate vascular calcification through regulating Akt signaling and inducing apoptosis of VSMC (Li, 2021, #28). Yang et al. proved the participation of the ERK1/2 pathway in the promotion of VSMC calcification by *Porphyromonas gingivalis*-derived outer membrane vesicles (Yang et al., 2016, #29). Herein, we also recognize the PI3K/Akt and ERK1/2 pathway as downstream of LIRA in the regulation of VSMC calcification. LIRA significantly inhibited the high-glucose-induced activation of Akt and ERK1/2 pathways in VSMC. Administration of antagonists of PI3K/Akt or ERK1/2 signaling pathways could partially abolish the protective effects of LIRA on VSMC calcification. There are some literatures about the influence of LIRA on diabetic AS. It has been reported that LIRA reduces AS in T2DM rats by targeting ER-associated macrophage-derived macrovesicle production [14]. LIRA represses AS by regulating inflammatory pathways in $ApoE^{-/-}$ mice [15]. In this study, we identified that LIRA attenuated diabetic AS by regulating calcification of vascular smooth muscle cells via targeting PI3K/Akt and ERK1/2 signaling. Our finding provides new insights into the mechanism by which LIRA regulates diabetic AS by regulating a novel downstream PI3K/Akt and ERK1/2 signaling, presenting the new phenotypes affected by LIRA in diabetic AS. Meanwhile, there were some limitations in the current study. For example, the PI3K/Akt and ERK1/2 signaling may just be two of the downstream pathways of LIRA-mediated diabetic AS and other potential mechanisms should be explored in the model in future studies. In addition, the validation of the LIRA/PI3K/Akt axis and LIRA/ERK1/2 axis should be performed in the rat model in future investigations.

5. Conclusion

In this study, we confirmed that the structural and functional changes of VSMC induced by high glucose exert an important role in the process of DM combined with AS *in vivo* and *in vitro*. LIRA, an analogue of GLP-1, can improve the calcification of VSMC induced by high glucose, thus showing the potential of LIRA in treating DM combined with AS. Mechanistically, the intervention of LIRA on the calcification of VSMC in DM combined with AS was mediated by GLP-1R and was closely related to the inhibition of PI3K/AKT and ERK1/2 signaling pathways (Figure 5).

Abbreviations

DM: Diabetes mellitus
AS: Atherosclerosis
VSMCs: Vascular smooth muscle cells
LIRA: Liraglutide
ALP: Alkaline phosphatase
IHC: Immunohistochemical
HG: High glucose
PI3K: Phosphatidylinositol-4-diphosphate 3-kinase
AKT: Protein kinase B
GLP-1: Glucagon-like peptide-1
GLP-1R: GLP-1 receptor
T2DM: Type 2 diabetes mellitus.

Data Availability

The datasets used during the present study are available from the corresponding author upon reasonable request.

Conflicts of Interest

The authors declare that they have no competing interests.

Authors' Contributions

Li-Li Shi and Ming Hao contributed equally to the work.

Acknowledgments

This research was supported by the National Natural Science Foundation of China (no. 81900760), the Natural Science Foundation of Heilongjiang Province (no. LH2019H084), and the Heilongjiang Postdoctoral Research Starting Fund (no. LBH-Q19120).

References

[1] D. Glovaci, W. Fan, and N. D. Wong, "Epidemiology of diabetes mellitus and cardiovascular disease," *Current Cardiology Reports*, vol. 21, no. 4, p. 21, 2019.

[2] A. K. Srivastava, "Hyperglycemia-induced protein kinase signaling pathways in vascular smooth muscle cells: implications in the pathogenesis of vascular dysfunction in diabetes," *Advances in Experimental Medicine and Biology*, vol. 498, pp. 311–318, 2001.

[3] K. Yahagi, F. D. Kolodgie, C. Lutter et al., "Pathology of human coronary and carotid artery atherosclerosis and vascular calcification in diabetes mellitus," *Arteriosclerosis, Thrombosis, and Vascular Biology*, vol. 37, no. 2, pp. 191–204, 2017.

[4] A. L. Durham, M. Y. Speer, M. Scatena, C. M. Giachelli, and C. M. Shanahan, "Role of smooth muscle cells in vascular calcification: implications in atherosclerosis and arterial stiffness," *Cardiovascular Research*, vol. 114, no. 4, pp. 590–600, 2018.

[5] L. Wu and J. E. Gunton, "The Changing Landscape of Pharmacotherapy for Diabetes Mellitus: A Review of Cardiovascular Outcomes," *International Journal of Molecular Sciences*, vol. 20, no. 23, p. 5853, 2019.

[6] W. H. H. Sheu, S. P. Chan, B. J. Matawaran et al., "Use of SGLT-2 inhibitors in patients with type 2 diabetes mellitus and abdominal obesity: an Asian perspective and expert recommendations," *Diabetes and Metabolism Journal*, vol. 44, no. 1, pp. 11–32, 2020.

[7] A. Ponnusamy, S. Sinha, G. D. Hyde et al., "FTI-277 inhibits smooth muscle cell calcification by up-regulating PI3K/Akt signaling and inhibiting apoptosis," *PLoS One*, vol. 13, no. 4, article e0196232, 2018.

[8] W. W. Yang, B. Guo, W. Y. Jia, and Y. Jia, "Porphyromonas gingivalis-derived outer membrane vesicles promote calcification of vascular smooth muscle cells through ERK1/2-RUNX2," *FEBS Open Bio*, vol. 6, no. 12, pp. 1310–1319, 2016.

[9] C. H. Byon, A. Javed, Q. Dai et al., "Oxidative stress induces vascular calcification through modulation of the osteogenic transcription factor Runx2 by AKT signaling," *The Journal of Biological Chemistry*, vol. 283, no. 22, pp. 15319–15327, 2008.

[10] T. Pan, X. Shi, H. Chen et al., "Geniposide suppresses interleukin-1β-induced inflammation and apoptosis in rat chondrocytes via the PI3K/Akt/NF-κB signaling pathway," *Inflammation*, vol. 41, no. 2, pp. 390–399, 2018.

[11] D. J. Drucker, "Mechanisms of action and therapeutic application of glucagon-like peptide-1," *Cell Metabolism*, vol. 27, no. 4, pp. 740–756, 2018.

[12] E. Brown, D. J. Cuthbertson, and J. P. Wilding, "Newer GLP-1 receptor agonists and obesity-diabetes," *Peptides*, vol. 100, pp. 61–67, 2018.

[13] D. Sharma, S. Verma, S. Vaidya, K. Kalia, and V. Tiwari, "Recent updates on GLP-1 agonists: current advancements & challenges," *Biomedicine & Pharmacotherapy*, vol. 108, pp. 952–962, 2018.

[14] J. Li, X. Liu, Q. Fang, M. Ding, and C. Li, "Liraglutide attenuates atherosclerosis via inhibiting ER-induced macrophage derived microvesicles production in T2DM rats," *Diabetology and Metabolic Syndrome*, vol. 9, no. 1, p. 94, 2017.

[15] G. Rakipovski, B. Rolin, J. Nohr et al., "The GLP-1 analogs liraglutide and semaglutide reduce atherosclerosis in ApoE$^{-/-}$ and LDLr$^{-/-}$ mice by a mechanism that includes inflammatory pathways," *JACC: Basic to Translational Science*, vol. 3, no. 6, pp. 844–857, 2018.

[16] R. Bruen, S. Curley, S. Kajani et al., "Liraglutide attenuates preestablished atherosclerosis in apolipoprotein E-deficient mice via regulation of immune cell phenotypes and proinflammatory mediators," *The Journal of Pharmacology and Experimental Therapeutics*, vol. 370, no. 3, pp. 447–458, 2019.

[17] H. T. Ding, C. G. Wang, T. L. Zhang, and K. Wang, "Fibronectin enhances in vitro vascular calcification by promoting osteoblastic differentiation of vascular smooth muscle cells via ERK pathway," *Journal of Cellular Biochemistry*, vol. 99, no. 5, pp. 1343–1352, 2006.

[18] J. T. Tupper and F. Zorgniotti, "Calcium content and distribution as a function of growth and transformation in the mouse 3T3 cell," *The Journal of Cell Biology*, vol. 75, no. 1, pp. 12–22, 1977.

[19] N. A. Rashdan, A. M. Sim, L. Cui et al., "Osteocalcin regulates arterial calcification via altered Wnt signaling and glucose metabolism," *Journal of Bone and Mineral Research*, vol. 35, no. 2, pp. 357–367, 2020.

[20] W. V. Tamborlane, M. Barrientos-Perez, U. Fainberg et al., "Liraglutide in children and adolescents with type 2 diabetes," *The New England Journal of Medicine*, vol. 381, no. 7, pp. 637–646, 2019.

[21] M. Almutairi, R. Al Batran, and J. R. Ussher, "Glucagon-like peptide-1 receptor action in the vasculature," *Peptides*, vol. 111, pp. 26–32, 2019.

[22] G. Guan, J. Zhang, S. Liu, W. Huang, Y. Gong, and X. Gu, "Glucagon-like peptide-1 attenuates endoplasmic reticulum stress-induced apoptosis in H9c2 cardiomyocytes during hypoxia/reoxygenation through the GLP-1R/PI3K/Akt pathways," *Naunyn-Schmiedeberg's Archives of Pharmacology*, vol. 392, no. 6, pp. 715–722, 2019.

[23] T. Jojima, K. Uchida, K. Akimoto et al., "Liraglutide, a GLP-1 receptor agonist, inhibits vascular smooth muscle cell proliferation by enhancing AMP-activated protein kinase and cell cycle regulation, and delays atherosclerosis in *ApoE* deficient mice," *Atherosclerosis*, vol. 261, pp. 44–51, 2017.

[24] B. Di, H. W. Li, W. Li, and B. Hua, "Liraglutide inhibited AGEs induced coronary smooth muscle cell phenotypic transition through inhibiting the NF-κB signal pathway," *Peptides*, vol. 112, pp. 125–132, 2019.

[25] J. K. Zhan, Y. J. Wang, Y. Wang et al., "The protective effect of GLP-1 analogue in arterial calcification through attenuating osteoblastic differentiation of human VSMCs," *International Journal of Cardiology*, vol. 189, pp. 188–193, 2015.

Hindawi
Disease Markers
Volume 2022, Article ID 2159660, 5 pages
https://doi.org/10.1155/2022/2159660

Research Article

The Efficacy of Double-Heart Nursing in Combination with Seaweed Polysaccharide for Patients with Coronary Heart Disease Complicated with Diabetes: A Pilot, Randomized Clinical Trial

Yulei Hu,[1] Yan Wang,[2] Fengwei An,[3] and Nini Dai[4]

[1]*Department of Cardiology, Jiaozhou Central Hospital of Qingdao, Jiaozhou, China*
[2]*Department of Rheumatology, The Fifth People's Hospital of Qingdao, Qingdao, China*
[3]*Outpatient Department, The Fifth People's Hospital of Qingdao, Qingdao, China*
[4]*Department of Pediatrics, Qingdao Hospital of Traditional Chinese Medicine (Qingdao Hiser Hospital), Qingdao, China*

Correspondence should be addressed to Nini Dai; daidiji93224@163.com

Received 12 January 2022; Revised 11 February 2022; Accepted 14 February 2022; Published 4 April 2022

Academic Editor: Yaoyao Bian

Objective. To study and explore the effect of double-heart nursing combined with seaweed polysaccharide on improving the self-efficacy and quality of life of patients with coronary heart disease and diabetes. *Methods*. Eligible 214 patients with coronary heart disease and diabetes who were diagnosed and treated in our hospital between year 2017 and 2020 were randomized at a ratio of 1 : 1 to either control group (seaweed polysaccharide) or observation group (double-heart nursing combined with seaweed polysaccharide). The self-efficacy and quality of life of the two groups of patients after treatment were compared. *Results*. The observation group reported a lower blood glucose level after treatment vs. the control group [$(6.28 \pm 4.49/8.24 \pm 2.01)$ vs. $(7.74 \pm 4.18/11.41 \pm 3.12)$] ($p < 0.05$); a lower incidence of lesions in the observation group versus the control group after treatment ($p < 0.05$); and significantly lower SAS and SDS scores of the observation group vs. the control group was observed [$(41.27 \pm 4.08/43.81 \pm 2.93)$ vs. $(62.74 \pm 3.48/61.58 \pm 3.85)$] ($p < 0.05$). Regarding the self-efficacy, the observation group was superior to the control group after treatment ($p < 0.05$). The treatment with double-heart nursing combined with seaweed polysaccharide was associated with the improvement of the quality of life with respect to social function, psychological function, and material life (each $p < 0.05$). The observation obtained a significantly higher satisfaction rate in comparison with the control group [107 (98.13%) vs.95 (88.80%)] ($p < 0.05$). *Conclusion*. Seaweed polysaccharide and double-heart nursing might be practical in improving the self-efficacy and quality of life of patients with coronary heart disease and diabetes mellitus, compared with conventional clinical treatment alone.

1. Introduction

Coronary heart disease is a common and frequently-occurring disease [1], and it is usually associated with depression and anxiety and other negative emotions, which is not well manageable and controllable [2, 3]. Diabetes is a frequently seen endocrine disease [4] and predisposes to declined immunity. Complications such as diabetic retinopathy, vascular disease, and neuropathy may occur if blood sugar is not favorably controlled. Also, diabetes is a major contributing factor for coronary heart disease. The diabetes combined with coronary heart disease reports more difficulty to control and the dangerousness vs. coronary heart disease alone [5]. In recent years, the morbidity and mortality of coronary heart disease have witnessed a rising trend. As a chronic disease, although the radical cure for coronary heart disease remains unknown, a number of risk factors such as external stimuli have been identified, leading to alternative nursing taken into consideration. Double-heart nursing, a mode adapting to cardiovascular diseases, pays attention to the patient's psychological health, respects the patient's subjective feeling while treating the physical illness, which has been widely applied clinically and achieved remarkable results [6]. Seaweed polysaccharide, a multicomponent

Table 1: Comparison of general data between the two groups ($\bar{x} \pm s$).

Groups	n	Gender	Age (year)	Course of disease (year)	Blood sugar level
Control group	107	49/58	55.01 ± 8.73/54.33 ± 7.95	5.62 ± 4.03	11.65 ± 3.34
Observation group	107	55/52	56.14 ± 6.88/55.72 ± 8.17	5.18 ± 4.67	11.48 ± 3.72
t	—	—	1.052/1.261	0.738	0.352
p	—	—	0.294/0.209	0.461	0.725

mixture [7], has an immunoregulatory role in the physiological function of the human body.

Some studies reported its use as an additive ingredient in food for diabetics. Seaweed polysaccharide has many biological activities, and one of its component of low molecular weight fucoidan sulfate (LMSF) is an inherent intercellular water-soluble polysaccharide in brown algae, mainly composed of fucose and organic sulfate, contains galactose, xylose, and a small amount of uronic acid. The experiments conducted by the Qingdao Ocean University demonstrated that LMSF can directly scavenge peroxyanion free radicals and hydroxyl free radicals *in vitro* and also significantly enhance the SOD binding capacity in serum and tissues *in vivo*. Accordingly, it can serve as a potential drug in lowering blood lipids and preventing atherosclerosis [8, 9]. The present study was designed to explore the treatment effectiveness of double-heart nursing in combination with seaweed polysaccharide on coronary heart disease complicated with diabetes.

2. Study Design

2.1. Participants. Eligible 214 patients with coronary heart disease and diabetes who were diagnosed and treated in our hospital between year 2017 and 2020 were randomized at a ratio of 1 : 1 to either control group or observation group. In the control group, there were 49 males and 58 females, with an age of 42-81 years and 40-72 years, respectively; in the observation group, there were 55 males and 52 females with an age of 45-76 years and 41-79 years, respectively. It should be noted that there were no significant differences between the two groups regarding the baseline values in the different domains ($p > 0.05$) (See Table 1).

2.2. Inclusion and Exclusion Criteria. Inclusion criteria are as follows: in compliance with diagnostic criteria for diabetes and coronary heart disease, patients were informed of the study and voluntarily signed the consent form; this study has been approved by the ethics committee of our hospital.

Exclusion criteria are as follows: allergies to the drugs used in the study; patients with congenital heart disease or psychiatric diseases; and patients who did not complete the treatment due to transfer midway or other reasons.

2.3. Interventions. The patients in the control group were given routine symptomatic nursing, including blood glucose measurement, basic nursing, vital signs monitoring, and medication following doctor's orders.

Table 2: Comparison of blood glucose levels in the two groups after treatment ($\bar{x} \pm s$, point).

Groups	n	FBG	2hBG
Control group	107	7.74 ± 4.18	11.41 ± 3.12
Observation group	107	6.28 ± 4.49	8.24 ± 2.01
t	—	2.462	8.835
p	—	0.015	<0.001

The patients in the observation group were given double-heart nursing combined with seaweed polysaccharide for treatment. Upon admission, routine examination and diagnosis were performed, and then, seaweed polysaccharide was orally administrated.

Double-heart nursing: first of all, emotional counseling nursing should be implemented for patients. Nurses should strengthen active communication with patients, carry out peer education, encourage patients, and guide patients to carry out psychological adjustment. In addition, nurses should inform the family members of patients of the value of social support nursing in detail and guide the family members to accompany and care for patients as much as possible, so as to reduce their psychological burden. Secondly, nurses give health knowledge guidance to patients, inform patients of the pathogenic factors and treatment methods of the disease, and put forward reasonable prognostic suggestions and assist patients in making diet and exercise plans and explain the use methods and precautions of drugs. Nurses help patients strengthen self-management and improve their self-management ability, so as to form good eating habits, medication habits, and exercise habits and fundamentally enhance patients' treatment compliance.

2.4. Outcomes. 200 ml of blood was drawn intravenously in the fasting state and two hours after meals, and the changes of blood glucose were compared between the two groups.

The adverse lesions including hyperlipidemia, microvascular disease, and eye disease were compared, which diagnoses through laboratory examination and fundus examination.

The self-rating anxiety scale (SAS) and the self-rating depression scale (SDS) were applied to assess and compare the psychological state of the two groups of patients; the score of 55 or below represents normal, the score of 56-65 represents mild anxiety or depression, the score of 66-75 represents moderate anxiety or depression, and the score

Table 3: Incidence of adverse lesions in the two groups after treatment (%).

Groups	n	Hyperlipidemia	Microvascular disease	Eye disease	Total
Control group	107	19	11	8	38 (35.51)
Observation group	107	11	7	5	23 (21.50)
X^2	—	—	—	—	5.519
p	—	—	—	—	0.023

of 76 or above represents severe anxiety or depression; and lower scores indicate better psychological state.

The purpose-built disease management ability questionnaire was employed to assess self-efficacy of the two groups, with 10-15 suggesting the average disease management ability and 15-20 suggesting the good disease management ability; the higher the score, the better the patient's self-efficacy and disease management ability.

WHO Quality of Life-Abbreviated Version was simplified according to WHO QOL-100 and consists of 26 items in four fields: physical health, psychological function, social relations, and material environment. It mainly evaluates the individual's quality of life. The higher the score, the better the quality of life. Cronbach's of each dimension is α. The coefficients are >0.70.

The satisfaction questionnaire developed by our hospital (including medical staff attitude, medical staff efficiency, and medical staff disease explanation) was used to assess the satisfaction and rated as very satisfied, satisfied, not very satisfied, and dissatisfied.

The above indicators were collected at admission and discharge.

2.5. Statistical Analysis. GraphPad Prism 8 software and SPSS 22.0 software were employed for graphics plotting and data analysis. Enumeration data [n (%)] and measurement data ($x \pm s$) were verified via $\chi 2$ tests and t-tests, respectively. The level of significance was set at $p \leq 0.05$.

3. Results

3.1. Blood Sugar Levels. The observation group reported a lower blood glucose level after treatment vs. the control group [(6.28 ± 4.49/8.24 ± 2.01) vs. (7.74 ± 4.18/11.41 ± 3.12)] ($p < 0.05$), indicating that double-heart nursing combined with seaweed polysaccharide plays a favorable sugar-lowering function in coronary heart disease and diabetes mellitus, as shown in Table 2.

3.2. Incidence of Lesions. The chi-square test revealed a lower incidence of lesions in the observation group versus the control group after treatment, suggesting that double-heart nursing combined with seaweed polysaccharide in the treatment of coronary heart disease complicated with diabetes leads to a high safety profile ($p < 0.05$, Table 3).

3.3. Mental State. Significantly lower SAS and SDS scores of the observation group vs. the control group were observed [(41.27 ± 4.08/43.81 ± 2.93) vs. (62.74 ± 3.48/61.58 ± 3.85)] ($p < 0.05$, Figure 1). It implies that treatment with double-heart nursing combined with seaweed polysaccharide results in a good mental health after treatment.

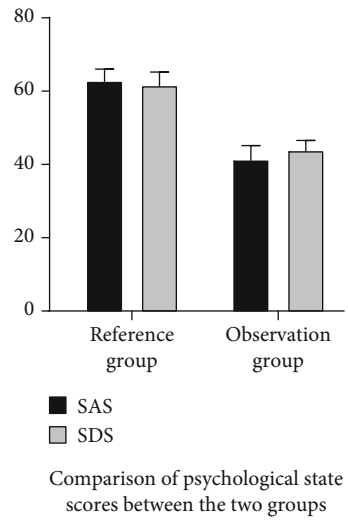

Figure 1: Comparison of psychological state scores between the two groups.

3.4. Self-Efficacy. Regarding the self-efficacy, the observation group was superior to the control group after treatment ($p < 0.05$, Table 4).

3.5. Quality of Life. The t-test results showed that treatment with double-heart nursing combined with seaweed polysaccharide was associated with the improvement of the quality of life with respect to social function, psychological function, and material life (each $p < 0.05$, Table 5).

3.6. Patient Satisfaction. The results showed that 39 (36.45%) patients in the control group were very satisfied, 56 (52.35%) satisfied, 10 (9.35%) not very satisfied, and 2 (1.85%) dissatisfied; in the observation group, 46 (42.99%) were very satisfied, 59 (55.14%) satisfied, 2 (1.87%) not very satisfied, and 0 (0.00%) dissatisfied. The observation obtained a significantly higher satisfaction rate in comparison with the control group [107 (98.13%) vs. 95 (88.80%)] ($p < 0.05$).

Table 4: Comparison of disease management ability between the two groups after treatment ($\bar{x} \pm s$, point).

Groups	n	Symptom perception	Disease management	Emotional management	Medication
Control group	107	12.74 ± 3.01	13.71 ± 2.65	12.05 ± 1.58	15.12 ± 2.14
Observation group	107	18.21 ± 1.35	17.87 ± 2.32	17.85 ± 2.65	18.59 ± 1.57
t	—	17.152	12.218	19.446	13.524
p	—	<0.001	<0.001	<0.001	<0.001

Table 5: Comparison of quality of life between the two groups after treatment ($\bar{x} \pm s$, point).

Groups	n	Body function	Social function	Mental function	Material life
Control group	107	68.95 ± 2.98	65.85 ± 4.15	64.12 ± 3.58	67.88 ± 2.74
Observation group	107	81.24 ± 3.84	84.15 ± 4.09	83.28 ± 4.65	84.65 ± 3.27
t	—	26.115	32.488	33.772	40.661
p	—	<0.001	<0.001	<0.001	<0.001

4. Discussion

Nowadays, the morbidity and mortality of coronary heart disease continue to rise [10]. However, there remains no radical treatment due to its long course, chronic property and ease to recur, and complications of depression and anxiety [11]. Diabetes is a trigger of coronary heart disease [12], and coronary heart disease combined with diabetes is considered more dangerous and risky than ordinary coronary heart disease [13, 14]. Additionally, issues such as poor compliance and insufficient disease knowledge also exist in some patients [15], thereby necessitating an effective alternative. Dual-heart nursing concentrates on patient's psychological and mental health and subjective feelings and is considered a scientific therapy [16, 17]. Seaweed polysaccharide is a multicomponent mixture and has proven to have a good effect on the treatment of diabetes[18] [19, 20]. According to our results, the observation group outperformed the control group in terms of blood glucose level and the incidence of lesion, probably because sargassum confusum oligosaccharides (SCOs) in seaweed polysaccharides could significantly lower fasting blood glucose levels, protect the structure of liver cells, and increase the abundance of Bacillus and Clostridium XIVa, reduce the abundance of Bacteroides, Allobaculum, and Clostridium IV and play an antidiabetic role through the JNK-IRS1/PI3K signaling pathway [19, 20]. Moreover, our results showed that SAS and SDS scores in the observation group were lower than those of the control group, and the healthy mentality is presumably attributed to that the double-heart nursing was given from the humanistic care while the seaweed polysaccharide was administered. Also, the present study reported a better self-efficacy in the observation group versus the control group. Assumedly, the medical staffs' explanation about the disease knowledge, communication with the patient's family in dual-heart nursing, allows the patient to recognize their symptoms and to manage their emotions, thereby benefiting medication compliance. More importantly, we observed a better quality of life in the observation group, which might be contributed to the administration of seaweed polysaccharide stimulated differentiation and maturation and reproduction of various immune active cells (such as macrophages, T lymphocytes, and B lymphocytes), so that the patient's immune system can be restored and strengthened and further their body function. Double-heart nursing requires the patient to be followed up by the nursing staff after discharge and pays attention to the patient's physical changes and adjusts, which contributes a lot to maintaining good living habits, social function, psychological function, and material life. Notably, treatment with seaweed polysaccharide and double-heart nursing yielded a higher satisfaction in the present study. Consistently, the research conducted by the Yantai Laiyang Central Hospital obtained similar conclusions.

As previously noted, seaweed polysaccharide and double-heart nursing might be practical in improving the self-efficacy and quality of life of patients with coronary heart disease and diabetes mellitus, compared with conventional clinical treatment alone, and it is worthy of wide application and promotion.

Data Availability

The datasets used during the present study are available from the corresponding author upon reasonable request.

Conflicts of Interest

The authors declare that they have no conflicts of interest.

References

[1] Y. Tian, P. Deng, B. Li et al., "Treatment models of cardiac rehabilitation in patients with coronary heart disease and

related factors affecting patient compliance," *Reviews in Cardiovascular Medicine*, vol. 20, no. 1, pp. 27–33, 2019.

[2] Y. Xue, G. Liu, and Q. Geng, "Associations of cardiovascular disease and depression with memory related disease: a Chinese national prospective cohort study," *Journal of Affective Disorders*, vol. 266, pp. 187–193, 2020.

[3] R. M. Carney and K. E. Freedland, "Depression and coronary heart disease," *Nature Reviews. Cardiology*, vol. 14, no. 3, pp. 145–155, 2017.

[4] K. Kaul, J. M. Tarr, S. I. Ahmad, E. M. Kohner, and R. Chibber, "Introduction to diabetes mellitus," *Advances in Experimental Medicine and Biology*, vol. 771, pp. 1–11, 2012.

[5] C. Abi Khalil, J. al Suwaidi, M. Refaat, and K. Mohammedi, "Cardiac complications of diabetes," *BioMed Research International*, vol. 2018, Article ID 8578394, 2 pages, 2018.

[6] Z. K. Nekouei, A. Yousefy, H. T. Doost, G. Manshaee, and M. Sadeghei, "Structural model of psychological risk and protective factors affecting on quality of life in patients with coronary heart disease: a psychocardiology model," *Journal of Research in Medical Sciences : The Official Journal of Isfahan University of Medical Sciences*, vol. 19, no. 2, pp. 90–98, 2014.

[7] M. Beaumont, R. Tran, G. Vera et al., "Hydrogel-forming algae polysaccharides: from seaweed to biomedical applications," *Biomacromolecules*, vol. 22, no. 3, pp. 1027–1052, 2021.

[8] S. Luthuli, S. Wu, Y. Cheng, X. Zheng, M. Wu, and H. Tong, "Therapeutic effects of fucoidan: a review on recent studies," *Marine Drugs*, vol. 17, no. 9, p. 487, 2019.

[9] N. A. Chudasama, R. A. Sequeira, K. Moradiya, and K. Prasad, "Seaweed polysaccharide based products and materials: an assessment on their production from a sustainability point of view," *Molecules*, vol. 26, no. 9, p. 2608, 2021.

[10] J. E. Dalen, J. S. Alpert, R. J. Goldberg, and R. S. Weinstein, "The epidemic of the 20th century: coronary heart disease," *The American Journal of Medicine*, vol. 127, no. 9, pp. 807–812, 2014.

[11] P. H. Wirtz and R. von Känel, "Psychological stress, inflammation, and coronary heart disease," *Current Cardiology Reports*, vol. 19, no. 11, p. 111, 2017.

[12] S. V. Bădescu, C. Tătaru, L. Kobylinska et al., "The association between diabetes mellitus and depression," *Journal of Medicine and Life*, vol. 9, no. 2, pp. 120–125, 2016.

[13] K. Schütt, D. Müller-Wieland, and N. Marx, "Diabetes mellitus and the heart," *Experimental and Clinical Endocrinology & Diabetes*, vol. 127, no. S 01, pp. S102–s104, 2019.

[14] M. Clodi, C. Säly, F. Hoppichler, M. Resl, C. Steinwender, and B. Eber, "Diabetes mellitus, coronary artery disease and heart disease," *Wiener Klinische Wochenschrift*, vol. 128, Supplement 2, pp. 212–215, 2016.

[15] R. Meng, C. Yu, N. Liu et al., "Association of depression with all-cause and cardiovascular disease mortality among adults in China," *JAMA Network Open*, vol. 3, no. 2, article e1921043, 2020.

[16] D. Y. Hu, "From psycho-cardiology to "five prescriptions for cardiovascular health"," *Zhonghua Xin Xue Guan Bing Za Zhi*, vol. 49, no. 11, pp. 1061-1062, 2021.

[17] J. Wei, X. Chen, C. Wen et al., "Analysis of the application of "psycho-cardiology" model in nursing care of acute stroke patients with depression," *American Journal of Translational Research*, vol. 13, no. 7, pp. 8021–8030, 2021.

[18] A. Jiménez-Escrig, E. Gómez-Ordóñez, and P. Rupérez, "Seaweed as a source of novel nutraceuticals: sulfated polysaccharides and peptides," *Advances in Food and Nutrition Research*, vol. 64, pp. 325–337, 2011.

[19] M. Cao, Y. Li, A. C. Famurewa, and O. J. Olatunji, "Antidiabetic and nephroprotective effects of polysaccharide extract from the seaweed *Caulerpa racemosa* in high fructose-streptozotocin induced diabetic nephropathy," *Diabetes Metab Syndr Obes*, vol. 14, pp. 2121–2131, 2021.

[20] E. S. Brown, P. J. Allsopp, P. J. Magee et al., "Seaweed and human health," *Nutrition Reviews*, vol. 72, no. 3, pp. 205–216, 2014.

Hindawi
Disease Markers
Volume 2022, Article ID 6461041, 5 pages
https://doi.org/10.1155/2022/6461041

Research Article

Diffusion-Weighted Imaging Combined with Cervical Vascular Ultrasound in the Elderly Patients with Multiple Cerebral Infarction

Jinchun Lv[1] **and Jia Zhao**[2]

[1]*Radiology Department, Yueqing Hospital Affiliated to Wenzhou Medical University, Yueqing, Zhejiang 325600, China*
[2]*Department of Ultrasound, Yueqing Hospital Affiliated to Wenzhou Medical University, Yueqing, Zhejiang 325600, China*

Correspondence should be addressed to Jinchun Lv; mrcwb35@163.com

Received 5 January 2022; Revised 13 February 2022; Accepted 17 February 2022; Published 31 March 2022

Academic Editor: Yaoyao Bian

Objective. This study is aimed at evaluating the diagnostic value of diffusion-weighted imaging combined with cervical vascular ultrasound in the elderly patients with multiple cerebral infarctions and at demonstrating whether the diagnostic value is affected by the history of diabetes. *Methods.* From January 2020 to November 2021, the case data of 30 elderly patients with multiple cerebral infarction diagnosed in our hospital were included. Diffusion-weighted magnetic resonance imaging (DWI) and cervical vascular ultrasound (CAU) were performed, respectively. The diagnosis rates of the simple diffusion-weighted imaging group, the simple cervical vascular ultrasound group, and the diffusion-weighted imaging combined with cervical vascular ultrasound group were compared. *Results.* The median onset time of 30 patients was 26.5 (4.75, 43.0) hours. There were 10 hyperacute patients and 20 acute patients. The proportion of diagnosable patients in the diffusion-weighted imaging group was 83.8% (25/30), which was lower than the proportion of diagnosable patients in the diffusion-weighted imaging combined with cervical vascular ultrasound group, which was 90% (27/30). The difference was statistically significant ($\chi^2 = 16.667$; $P < 0.001$). The ratio of diagnosable patients in the cervical vascular ultrasound group alone was 66.7% (20/30), which was lower than 90% (27/30) in the diffusion-weighted imaging combined with cervical vascular ultrasound group. The difference was statistically significant ($\chi^2 = 6.7$; $P = 0.010$). In the hyperacute phase, the proportion of diagnosable patients in the diffusion-weighted imaging combined with cervical vascular ultrasound group was higher than that in the diffusion-weighted imaging group alone ($\chi^2 = 5.833$; $P = 0.016$) and the cervical vascular ultrasound group alone ($\chi^2 = 2.500$; $P = 0.004$). In the acute phase, the proportion of diagnosable patients in the diffusion-weighted imaging combined with cervical vascular ultrasound group was also higher those that in the diffusion-weighted imaging group alone ($\chi^2 = 9.474$; $P = 0.002$) and the cervical vascular ultrasound group alone ($\chi^2 = 3.158$; $P = 0.006$). The diagnostic accuracy of diffusion-weighted imaging combined with cervical vascular ultrasound was not significantly different between patients with history of diabetes and without history of diabetes ($\chi^2 = 1.014$; $P = 0.314$) *Conclusion.* The combined application of diffusion-weighted imaging and cervical vascular ultrasound has important value in improving the diagnosis rate of multiple cerebral infarction in the elderly, regardless of diabetes history, and it is worthy of clinical application.

1. Introduction

Cerebral infarction is the second most common cause of death and the third most common cause of disability worldwide, bringing heavy social and economic burdens [1]. Elderly patients are more prone to cerebral infarction, and multiple cerebral infarctions are more common [2]. The early diagnosis of elderly patients with multiple cerebral infarctions can be treated more quickly, which can help reduce the mortality and disability rates of patients with cerebral infarction and improve the prognosis [3]. Magnetic resonance is a technology based on the water content in tissues, and the diffusion-weighted imaging developed in recent years is a new type of magnetic resonance imaging

method that can mainly measure and image the diffusion of water molecules, thus indirectly reflecting the characteristics of the microstructure of the organization [4]. The use of DWI has had a huge impact in both clinical and neuroimaging fields, and it has high sensitivity and specificity for the diagnosis of multiple cerebral infarction in the elderly [4]. However, DWI-negative multiple cerebral infarction limits the further promotion of this method [5]. Cervical vascular ultrasound (CAU) is a commonly used color doppler ultrasound examination in clinical practice. It can directly reflect the direction and shape of blood vessels and assess whether there is stenosis or occlusion in the lumen and has a high diagnostic value for cerebral infarction [6]. Diabetes, significantly associated with cerebral infarction, may expand the area of cerebral infarction and increase the risk of recurrence of cerebral infarction [7]. This study is aimed at evaluating the diagnostic value of diffusion-weighted imaging combined with CAU in the diagnosis of multiple cerebral infarctions in the elderly and at demonstrating whether the diagnostic value is affected by history of diabetes, providing a theoretical basis for the combined clinical application.

2. Materials and Methods

2.1. Participants. From January 2020 to November 2021, 30 elderly patients with multiple cerebral infarction were selected in our hospital, combined with the symptoms, signs, laboratory tests, and imaging examinations of the patients to confirm the diagnosis of multiple cerebral infarction. The average age of the 30 patients was 73.5 ± 3.8 years, including 16 males (53.3%) and 14 females (46.7%). Collect the patient's height, weight, time of onset, blood pressure, past medical history, and other data. Fasting venous blood was drawn to detect liver and kidney function, electrolytes, coagulation function, blood lipids, high-sensitivity C-reactive protein, and other indicators. Exclude patients who had a clear history of atrial fibrillation, valvular disease, severe liver and kidney disease, tumor, and other malignant diseases. All patients signed an informed consent form, and the research protocol was approved by the ethics review committee of Yueqing Hospital Affiliated to Wenzhou Medical University.

2.2. Imaging Methods

2.2.1. Diffusion-Weighted Magnetic Resonance Imaging (DWI). All patients were examined with the United Imaging uMR586 magnetic resonance instrument. An eight-channel special head coil was used for routine MR scanning and DWI scanning of the head. T1WI (T1-weighted imaging) and T2WI (T2-weighted imaging) were detected by the SE (spin echo) method and fast SE (fast spin echo) method, respectively. And DWI (diffusion-weighted imaging) was detected by the SS-EPI (single-shot echo planar imaging) method.

2.3. Cervical Vascular Ultrasound (CAU). All patients underwent cervical vascular ultrasound examination, including bilateral subclavian, common cervical, external cervical, internal cervical, and vertebral arteries. The inner diameter of the patient's blood vessel and the thickness of the intima-media were measured to assess whether there was stenosis of the lumen, thickening of the intima, or carotid artery plaque.

2.4. Imaging Evaluation. Two senior radiologists and sonographers performed DWI and CAU assessments, respectively, to confirm the diagnosis of multiple cerebral infarction.

2.5. Statistical Analysis. Continuous variables were expressed as mean ± standard deviation or median (interquartile range). Categorical variables were expressed by frequency (rate), and the chi-square test was used for comparison between groups. All data were analyzed by IBM SPSS 21.0, and two-sided $P < 0.05$ was considered statistically significant.

3. Results

3.1. Clinical Characteristics of Elderly Patients with Multiple Cerebral Infarction. As shown in Table 1, the median onset time of the 30 participants was 26.5 (4.75, 43.0) hours and there were 10 hyperacute patients and 20 acute patients. The patients' average BMI, systolic blood pressure, and diastolic blood pressure were 24.5 ± 2.9 kg/m^2, 136 ± 15 mmHg, and 71 ± 11 mmHg, respectively. The proportions of plaques found in previous diabetes, hypertension, and color doppler ultrasound were 23.3%, 46.7%, and 66.7%, respectively. The average alanine aminotransferase and aspartate aminotransferase of the participants were 37 ± 13 U/L and 33 ± 12 U/L, respectively, and the average blood creatinine and average low-density lipoprotein cholesterol were 56 ± 16 μmol/L and 2.99 ± 0.65 mmol/L, respectively. The thickness of the carotid artery intima was 1.29 ± 0.29 cm.

3.2. Diffusion-Weighted Imaging Combined with Cervical Vascular Ultrasound in the Diagnosis of Multiple Cerebral Infarction in the Elderly. As shown in Table 2, the proportion of diagnosable patients in the diffusion-weighted imaging group alone was 83.8% (25/30), which was lower than the diagnosable proportion of patients in the diffusion-weighted imaging combined with cervical vascular ultrasound group, which was 90% (27/30). There was statistical significance ($\chi^2 = 16.667$; $P < 0.001$). The ratio of diagnosable patients in the cervical vascular ultrasound group alone was 66.7% (20/30), which was lower than 90% (27/30) in the diffusion-weighted imaging combined with cervical vascular ultrasound group. The difference was statistically significant ($\chi^2 = 6.7$; $P = 0.010$).

3.3. Diagnosis of Multiple Cerebral Infarction in the Elderly at Different Stages. As shown in Table 3, among patients in the hyperacute phase (<6 hours), the proportion of diagnosable patients in the DWI group alone was 70.0% (7/10), which was lower than the proportion of diagnosable patients in the combined group by 80% (8/10), and the difference was statistically significant ($\chi^2 = 5.833$; $P = 0.016$). The proportion of diagnosable patients in the CAU group alone was 50% (5/10), which was lower than the proportion of diagnosable patients in the combined group of 80% (8/10). The difference was statistically significant ($\chi^2 = 2.500$; $P = 0.004$

Table 1: Clinical characteristics of elderly patients with multiple cerebral infarction.

	People with cerebral infarction
Number of people, *n*	30
Age	73.5 ± 3.8
Proportion of males, *n* (%)	16 (53.3)
Onset time (h)	26.5 (4.75, 43.0)
Proportion of hyperacute phase, *n* (%)	10 (33.3)
Proportion in acute phase, *n* (%)	20 (66.7)
Body mass index (BMI) (kg/m^2)	24.5 ± 2.9
Systolic blood pressure (mmHg)	136 ± 15
Diastolic blood pressure (mmHg)	71 ± 11
History of diabetes, *n* (%)	7 (23.3)
History of hypertension, *n* (%)	14 (46.7)
Alanine aminotransferase (U/L)	37 ± 13
Aspartate aminotransferase (U/L)	33 ± 12
Serum creatinine (μmol/L)	56 ± 16
Low-density lipoprotein cholesterol (mmol/L)	2.99 ± 0.65
High sensitivity C-reactive protein (mg/L)	4.5 ± 2.6
Carotid artery intima thickness (cm)	1.29 ± 0.29
Proportion of carotid artery plaque, *n* (%)	20 (66.7)

). Among the patients in the acute phase (6 to 72 hours), the proportion of diagnosable patients in the DWI group alone was 90% (18/20), which was lower than the proportion of diagnosable patients in the combined group of 95% (19/20). The difference was statistically significant ($\chi^2 = 9.474$; $P = 0.002$). The proportion of diagnosable patients in the CAU group alone was 75% (15/20), which was lower than the proportion of diagnosable patients in the combined group of 95% (19/20). The difference was statistically significant ($\chi^2 = 3.158$; $P = 0.006$).

3.4. Diagnostic Value of Diffusion-Weighted Imaging Combined with Cervical Vascular Ultrasound Based on History of Diabetes. According to the history of diabetes, patients were divided into two groups: patients with history of diabetes and without diabetes history (Table 4). The diagnostic accuracy of diffusion-weighted imaging combined with cervical vascular ultrasound was 87% (20/23) in patients without diabetes and 100% (7/7) in patients with history of diabetes. The diagnostic performance of diffusion-weighted imaging combined with cervical vascular ultrasound was likely to be better in patients with history of diabetes than in patients without diabetes, but there was no significantly different among the two groups ($\chi^2 = 1.014$; $P = 0.314$).

4. Discussion

In this study, we found that in 30 elderly patients with multiple cerebral infarction, the combined use of magnetic resonance diffusion-weighted imaging and cervical vascular ultrasound can improve the diagnosis rate of cerebral infarction. Moreover, we also found that the diagnosis rate of the combined use of magnetic resonance diffusion-weighted imaging and cervical vascular ultrasound was better than that of diffusion-weighted imaging alone or cervical vascular ultrasound alone, regardless of whether it is in the hyperacute or acute phase.

Early diagnosis can reduce the number of dead brain cells and improve the severity of cerebral infarction. Timely diagnosis and treatment are essential to improve the prognosis of elderly patients with multiple cerebral infarction. Early diagnosis can reduce the mortality and disability rate of patients [8]. DWI is very sensitive to showing ischemic lesions of brain tissue, especially multiple acute ischemia, which is manifested as abnormal high signal in the lesion area, and the clarity and sensitivity of the display are better than conventional magnetic resonance [9]. Studies have shown that, compared with head CT, DWI has significantly higher sensitivity (88%-100%) and specificity (95%–100%) in the diagnosis of cerebral infarction [10]. However, it is worth noting that a meta-analysis study showed that the prevalence of DWI-negative cerebral infarction was 6.8% and DWI-negative cerebral infarction was significantly related to posterior circulation ischemia [5]. DWI-negative cerebral infarction not only is related to posterior circulation ischemia but may also be related to the following reasons: DWI may not be able to detect multiple small infarcts, especially multiple small infarcts that occur in the brain stem; in addition, DWI may not be able to detect some well hyperacute cerebral infarction [11].

Carotid vascular ultrasound, as a common clinically safe and effective examination, has the main value in diagnosing cerebral infarction in that it can accurately assess the characteristics, range, and location of intravascular plaques and show the degree of vascular stenosis and blockage [12]. In addition, according to the characteristics of the plaque shape, internal structure, and echo, it can be judged whether the plaque is stable. There are more lipid cells and inflammatory cells in unstable plaques, more irregular shapes on ultrasound, and more uneven echo [13]. The combined application of DWI and carotid vascular ultrasound can make up for each other's deficiencies, thereby increasing the diagnosis rate.

Diabetic patients have twice the risk of cerebral infarction than patients without diabetes, and diabetes is associated with the poor outcome after cerebral infarction [14]. Diabetes could accelerate the vascular aging of the brain, and it could increase the difficulty of accurate diagnosis of cerebral infarction [15]. However, in our study, the diagnostic accuracy of diffusion-weighted imaging combined with cervical vascular ultrasound is not significantly different between patients with history of diabetes and without diabetes.

The results of this study suggest that in the hyperacute and acute phases, the diagnosis rate of the combined group was superior to that of diffusion-weighted imaging alone or carotid vascular ultrasound alone. From the mechanism analysis, in the hyperacute phase of cerebral infarction, due to ischemic changes in the brain tissue, leading to cerebral edema, there is a high signal on DWI [16]. In the acute

Table 2: Diffusion-weighted imaging combined with cervical vascular ultrasound in the diagnosis of multiple cerebral infarction in the elderly.

Inspection method	Simple diffusion-weighted imaging	Simple cervical vascular ultrasound	Diffusion-weighted imaging combined with cervical vascular ultrasound
Total number of confirmed cases, *n*	30	30	30
Number of people diagnosed, *n*	25	20	27
Percentage (%)	83.8	66.7	90
χ^2	16.667*	6.7#	
P	<0.001	0.010	

*Comparison between the diffusion-weighted imaging group and the diffusion-weighted imaging combined with cervical vascular ultrasound group. #Comparison between the cervical vascular ultrasound group and the diffusion-weighted imaging combined with cervical vascular ultrasound group.

Table 3: Diagnosis results of multiple cerebral infarction in the elderly at different stages.

Inspection method	Total number of people diagnosed, *n*	Number of people diagnosed, *n*	Percentage (%)	Chi-square value	*P* value
Hyperacute phase					
Simple diffusion -weighted imaging	10	7	70	5.833*	0.016
Simple cervical vascular ultrasound	10	5	50	2.500#	0.004
Diffusion-weighted imaging combined with cervical vascular ultrasound	10	8	80	—	—
Acute phase					
Diffusion-weighted imaging	20	18	90	9.474*	0.002
Cervical vascular ultrasound	20	15	75	3.158#	0.006
Diffusion-weighted imaging combined with cervical vascular ultrasound	20	19	95	—	—

*Comparison between the diffusion-weighted imaging group and the diffusion-weighted imaging combined with cervical vascular ultrasound group. #Comparison between the cervical vascular ultrasound group and the diffusion-weighted imaging combined with cervical vascular ultrasound group.

Table 4: Diagnostic value of diffusion-weighted imaging combined with cervical vascular ultrasound based on the history of diabetes*.

		Diffusion-weighted imaging combined with cervical vascular ultrasound		Total
		Negative	Positive	
History of diabetes	No	3 (13)	20 (87)	23 (100)
	Yes	0 (0)	7 (100)	7 (100)
Total		3 (10)	27 (90)	30 (100)

The data was expressed as *n* (%). *The chi-square value was 1.014, and the *P* value was 0.314.

phase, the edema of the cerebral infarction area was aggravated and the extracellular space water increased and the DWI signal was significantly increased [16]. The combined use of DWI and cervical vascular ultrasound can effectively overcome the shortcomings of the two technologies in diagnosing hyperacute and acute multiple cerebral infarctions and better reflect the vascular lumen of the cerebral artery in patients with cerebral infarction and better evaluate the hemodynamics of blood vessels.

In short, the early diagnosis of multiple cerebral infarctions in the elderly is a clinically urgent problem. Based on the results of this study, we found that the combined use of magnetic resonance diffusion-weighted imaging and carotid vascular ultrasound can improve the diagnosis rate of multiple cerebral infarctions in the elderly.

Data Availability

The analyzed datasets generated during the study are available from the corresponding author upon reasonable request.

Conflicts of Interest

The authors declare that they have no conflicts of interest

References

[1] V. L. Feigin, B. Norrving, and G. A. Mensah, "Global burden of stroke," *Circulation Research*, vol. 120, no. 3, pp. 439–448, 2017.

[2] M. Zhou, H. Wang, X. Zeng et al., "Mortality, morbidity, and risk factors in China and its provinces, 1990-2017: a systematic analysis for the Global Burden of Disease Study 2017," *The Lancet*, vol. 394, no. 10204, pp. 1145–1158, 2019.

[3] J. D. Pandian, S. L. Gall, M. P. Kate et al., "Prevention of stroke: a global perspective," *The Lancet*, vol. 392, no. 10154, pp. 1269–1278, 2018.

[4] I. Guadilla, D. Calle, and P. Lopez-Larrubia, "Diffusion-weighted magnetic resonance imaging," *Methods in Molecular Biology*, vol. 1718, pp. 89–101, 2018.

[5] B. L. Edlow, S. Hurwitz, and J. A. Edlow, "Diagnosis of DWI-negative acute ischemic stroke: a meta-analysis," *Neurology*, vol. 89, no. 3, pp. 256–262, 2017.

[6] J. B. Naidich, A. Weiss, G. M. Grimaldi, N. Kohn, J. J. Naidich, and J. S. Pellerito, "Carotid ultrasound examinations," *Ultrasound Quarterly*, vol. 34, no. 3, pp. 183–189, 2018.

[7] R. Chen, B. Ovbiagele, and W. Feng, "Diabetes and stroke: epidemiology, pathophysiology, pharmaceuticals and outcomes," *The American Journal of the Medical Sciences*, vol. 351, no. 4, pp. 380–386, 2016.

[8] J. L. Saver, "Time is brain—quantified," *Stroke*, vol. 37, no. 1, pp. 263–266, 2006.

[9] N. Nagaraja, J. R. Forder, S. Warach, and J. G. Merino, "Reversible diffusion-weighted imaging lesions in acute ischemic stroke: a systematic review," *Neurology*, vol. 94, no. 13, pp. 571–587, 2020.

[10] E. C. Jauch, J. L. Saver, H. P. Adams Jr. et al., "Guidelines for the early management of patients with acute ischemic stroke," *Stroke*, vol. 44, no. 3, pp. 870–947, 2013.

[11] H. Kawano, T. Hirano, M. Nakajima, Y. Inatomi, and T. Yonehara, "Diffusion-weighted magnetic resonance imaging may underestimate acute ischemic lesions: cautions on neglecting a computed tomography-diffusion-weighted imaging discrepancy," *Stroke*, vol. 44, no. 4, pp. 1056–1061, 2013.

[12] C. S. G. Murray, T. Nahar, H. Kalashyan, H. Becher, and N. C. Nanda, "Ultrasound assessment of carotid arteries: current concepts, methodologies, diagnostic criteria, and technological advancements," *Echocardiography*, vol. 35, no. 12, pp. 2079–2091, 2018.

[13] S. Latha, D. Samiappan, and R. Kumar, "Carotid artery ultrasound image analysis: a review of the literature," *Proceedings of the Institution of Mechanical Engineers Part H*, vol. 234, no. 5, pp. 417–443, 2020.

[14] A. Ergul, W. Li, M. M. Elgebaly, A. Bruno, and S. C. Fagan, "Hyperglycemia, diabetes and stroke: focus on the cerebrovasculature," *Vascular Pharmacology*, vol. 51, no. 1, pp. 44–49, 2009.

[15] M. D. Hill, "Stroke and diabetes mellitus," *Handbook of Clinical Neurology*, vol. 126, pp. 167–174, 2014.

[16] R. G. Gonzalez, P. W. Schaefer, F. S. Buonanno et al., "Diffusion-weighted MR imaging: diagnostic accuracy in patients imaged within 6 hours of stroke symptom onset," *Radiology*, vol. 210, no. 1, pp. 155–162, 1999.

Hindawi
Disease Markers
Volume 2022, Article ID 9231408, 5 pages
https://doi.org/10.1155/2022/9231408

Research Article

Vitamin D is Positively Associated with Bone Mineral Density Muscle Mass and Negatively with Insulin Resistance in Senile Diabetes Mellitus

Yan Gao,[1] **Zhaoyu Chen**,[2] **and Zijian Ma**[3]

[1]*Department of Senior Official Ward, China-Japan Friendship Hospital, Beijing, China*
[2]*Arthritis Clinic and Research Center, Peking University People's Hospital, Beijing, China*
[3]*Department of Senior Official Ward, The Third Hospital of Hebei Medical University, Shijiazhuang, China*

Correspondence should be addressed to Yan Gao; dugao4@126.com

Received 23 December 2021; Revised 25 January 2022; Accepted 15 February 2022; Published 29 March 2022

Academic Editor: Hongsheng Zhang

Objective. To explore the correlations between vitamin D level and bone mineral density (BMD), insulin resistance (HOMA-IR), and muscle mass in patients with senile type 2 diabetes mellitus (T2DM). *Methods*. Totally, 80 patients with senile T2DM admitted to China-Japan Friendship Hospital from Jan 2020 to Oct 2021 were enrolled and assigned to the 25 (OH)D-deficiency group ($n = 35$) or 25(OH)D-normal group ($n = 45$) according to serum 25(OH)D level. BMD and HOMA-IR in the femur neck and muscle masses of upper and lower limbs were compared between the two groups, and Pearson's correlation analysis was performed to determine the relations between 25(OH)D and BMD, HOMA-IR, and muscle masses of upper and lower limbs. *Results*. No notable difference was found between the two groups in general data including age, gender, diabetes duration, BMI, HBA 1c, and fasting insulin (all $P > 0.05$). Compared with the 25(OH)D-normal group, the 25 (OH)D-deficiency group showed a notably lower BMD in the femur neck, notably lower muscle masses of upper and lower limbs, and a notably higher HOMA-IR level (all $P < 0.05$). The Pearson's correlation analysis revealed positive associations between 25(OH)D and BMD and muscle masses of upper and lower limbs in patients with senile T2DM and a negative correlation between 25(OH)D and HOMA-IR (all $P < 0.05$). *Conclusions*. The serum 25(OH)D decreases notably in patients with senile T2DM, and higher serum 25(OH)D level may improve insulin resistance, limb muscle masses, and bone density and thus maintain bone health.

1. Introduction

With the rapid development of social economy, the change of diet structure, and the emergence of aging trend, senile type 2 diabetes mellitus (T2DM) shows an annually growing incidence, seriously compromising patients' health and quality of life [1]. Among Chinese patients with senile T2DM, the incidence of sarcopenia reaches 21%, which hinders the physical activity and daily living ability, undermines the quality of life, and increases the hospitalization rate, medical expenses, and the risk of fractures and chronic cardiopulmonary diseases among the elderly population [2]. Patients with senile T2DM are prone to osteopenia or osteoporosis, with a prevalence of osteoporosis of 31.7% [3]. The incidence of T2DM is associated with insulin resistance (IR) induced by decreased insulin sensitivity and insufficient insulin secretion induced by islet cell destruction and dysfunction [4]. Vitamin D is a fat-soluble vitamin and plays a key role in the development of bone, maintenance of bone mineralization and regulation of the metabolism of calcium and phosphorus. Being strongly correlated with the development and progression of T2DM, vitamin D can increase insulin sensitivity, improve blood sugar control, and contribute to prevent and reduce some diabetic complications [5]. To our knowledge, vitamin D can increase the body's absorption of calcium and phosphorus and balance the calcium and phosphorus, and its deficiency can cause bone metabolic disorder, thus resulting in a decline in bone

mass and bone loss. Additionally, vitamin D also plays a role in relieving stress, restraining activity of RAAS system, regulating cell apoptosis, maintaining immunity, reducing urinary protein, and improving insulin resistance. It is reported that 25(OH)D serves as an optimal indicator to evaluate the status of vitamin D and is closely related to the occurrence and disease control of T2DM via promoting the synthesis and secretion of insulin [6]. Nevertheless, more evidence-based medical evidence is urgently required to clarify the specific relation between serum vitamin D and bone mineral density, muscle mass, and insulin resistance in senile diabetes. To fill this gap, this study evaluated the changes of serum vitamin D in patients with senile T2DM and analyzed the correlation between serum vitamin D and IR, bone mineral density BMD, and muscle mass.

2. Data and Methods

2.1. General Data. Totally, 80 patients with senile T2DM admitted to our hospital from Jan 2020 to Oct 2021 were enrolled. The written consent was obtained from all participants before enrolment. The protocol of this study was approved by the ethic committee of the China-Japan Friendship Hospital with the approved No. of 2019-11/23.

2.2. Inclusion and Exclusion Criteria

2.2.1. Inclusion Criteria. The inclusion criteria are as follows: (1) aged ≥60 years old; (2) met the diagnostic criteria of the World Health Organization (WHO) for the diagnosis of T2DM [7]; and (3) participated in the study voluntarily.

2.2.2. Exclusion Criteria. The exclusion criteria are as follows: (1) with comorbid diabetic ketoacidosis or diabetic ketosis; (2) with severe dysfunction of important organs such as heart, liver and kidney, acute infection, or tumour; and (3) had taken vitamin D for a long time.

2.3. Methods

2.3.1. General Data of Patients. All subjects were inquired by the same doctor for medical history and given physical examination by the same doctor. The body mass index (BMI) of patients was calculated, and their age, weight, height, gender, and course of disease were all recorded.

2.3.2. BMD. The BMD in the left femoral neck of each subject was measured by an American OSTEOMETER dual-energy X-ray absorptiometer (DTX-2000).

2.3.3. Muscle Mass. The muscle masses of upper and lower limbs were determined using a dual-energy X-ray absorptiometer.

2.3.4. Specimen Collection and Determination. Fasting venous blood was collected from each subject, followed by quantification of serum 25(OH)D via the enzyme-linked immunosorbent assay (ELISA). Based on the serum 25 (OH)D level, the patients were assigned to the 25 (OH)D-deficiency group (25 (OH)D < 70 nmol/L) or the 25 (OH)D-normal group (25(OH)D ≥ 70 nmol/L). The fasting insulin (FINS, μU/mL) was measured by the chemiluminescence immunoassay, and fasting plasma glucose (FPG, mmol/L) by the glucose oxidase method. HOMA-IR [8] was calculated according to the following formula: HOMA − IR = FINS × FPG/22.5, where 22.5 is the correction factor. The calculation formula indicates that 5 μU/mL plasma insulin corresponds to 4.5 mmol/L blood glucose level in a normal ideal individual. All determinations were conducted in accordance with the laboratory quality control standards.

2.4. Statistical Analysis. All data analysis was performed with SPSS 24.0. The continuous variables were expressed as mean with standard deviation ($\bar{x}\pm s$) and Shapiro-Wilk test was adopted to check the normal or nonnormal distribution. For normal distribution continuous variables, intergroup comparison was conducted via the independent-samples t test, while the intragroup comparison was conducted via the pair-sample t test. For nonnormal distribution continuous variables, t test was adopted after normal transformation. The categorical data was expressed as cases with percentage (n, %), and the difference was tested and compared using a chi-squared test. Pearson's correlation analysis was conducted for analysing the associations between 25(OH)D and BMD and HOMA-IR and muscle masses of upper and lower limbs. The conventional $P \leq 0.05$ was used to assess statistical significance.

The difference was tested and compared using a chi-squared test,

3. Results

3.1. General Data of 25(OH)D-Deficiency Group and 25(OH)D-Normal Group. In the 25(OH)D-deficiency group, the mean age was (71.42 ± 8.74) years, the course of disease was (6.54 ± 3.61) years, the BMI was (23.42 ± 3.21), the FPG was (8.56 ± 2.47) mmol/L, and the ratio of male to female was 16: 19; in the 25(OH)D-normal group, the mean age was (69.58 ± 11.03) years, the course of disease was (5.62 ± 3.33) years, the BMI was (23.52 ± 4.40), the FPG was (7.97 ± 2.31) mmol/L, and the ratio of male to female was 24: 21. No notable difference was found between the two groups in general data, fasting insulin level, HbA1c, diabetes duration, and the frequency of coexisting diseases ($P < 0.05$, Table 1).

3.2. The BMD, Muscle Mass, and HOMA-IR in 25(OH)D-Deficiency Group and 25(OH)D-Normal group. The femoral neck BMD of the two groups was shown in Table 2. The femoral neck BMD in the 25(OH)D-deficiency group was (0.72 ± 0.13) g/cm^2, while (0.81 ± 0.06) g/cm^2 in the 25(OH)D-normal group. The 25(OH)D-deficiency obtained a notably lower femoral neck BMD than the 25(OH)D-normal group ($P < 0.05$, Table 2). Femoral neck BMD is a strong predictor of hip fracture, suggesting that the 25(OH)D-deficiency group is prone to hip fracture.

In the 25(OH)D-deficiency group, the upper limb muscle mass was (4.39 ± 0.22) kg and the lower limb muscle mass was (14.78 ± 0.73) kg. In the 25(OH)D-normal group, the upper limb muscle mass was (4.77 ± 0.31) kg and the

Table 1: General data analysis.

	25(OH)D-deficiency group ($n = 35$)	25(OH)D-normal group ($n = 45$)	$t/\chi 2$	P
Mean age	71.42 ± 8.74	69.58 ± 11.03	0.809	0.421
Gender			0.457	0.676
Male	16	24		
Female	19	21		
Diabetes duration (years)	6.54 ± 3.61	5.62 ± 3.33	1.182	0.241
BMI (kg/m^2)	23.42 ± 3.21	23.52 ± 4.40	0.113	0.910
HbA1c (%)	5.58 ± 1.15	5.29 ± 1.84	0.816	0.417
Fasting insulin (mmol/L)	8.56 ± 2.47	7.97 ± 2.31	1.099	8.560
Coexisting diseases				
Hypertension	12	17	0.104	0.322
Coronary artery disease	5	11	1.270	0.260
Hyperlipidaemia	6	10	0.318	0.573

Table 2: Comparison of insulin resistance ($\bar{x} \pm s$).

	25(OH)D-deficiency group ($n = 35$)	25(OH)D-normal group ($n = 45$)	t	P
Femoral neck BMD	0.72 ± 0.13	0.81 ± 0.06	4.112	≤0.001
Upper limb	4.39 ± 0.22	4.77 ± 0.31	5.898	<0.001
Lower limb	14.78 ± 0.73	15.67 ± 0.68	5.617	≤0.001
HOMA-IR	4.85 ± 0.49	4.33 ± 0.52	4.565	≤0.001

lower limb muscle mass was (15.67 ± 0.68) kg. The 25(OH)D-deficiency group showed notably lower muscle masses of upper and lower limbs than the 25(OH)D-normal group ($P < 0.05$, Table 2). Muscle mass is important for muscle strength and quality of life, and lower muscle mass indicates a lower muscle strength in the 25(OH)D-deficiency group.

The HOMA-IR of the 25(OH)D-deficiency group was 4.85 ± 0.49 and 4.33 ± 0.52 in the 25(OH)D-normal group. The 25(OH)D-deficiency group showed a notably higher HOMA-IR than the 25(OH)D-normal group ($P < 0.05$, Table 2). Higher HOMA-IR indicates elevated insulin resistance levels of the 25(OH)D-deficiency group.

3.3. Correlations between Serum 25(OH)D Level and BMD and HOMA-IR and Muscle Mass. The Pearson's correlation analysis revealed positive associations between 25(OH)D and BMD, upper limb muscle mass, and lower limb muscle mass in patients with senile T2DM and a negative relation between 25(OH)D and HOMA-IR (all $P < 0.05$, Table 3).

4. Discussion

The vitamin D deficiency witnesses a high prevalence in elderly male population in China, among which the proportions of severe deficiency, and the deficiency and insufficiency are 20.97%, 39.20%, and 24.36%, respectively [9]. Over the past few years, many studies have confirmed the association between T2DM and vitamin D [10]. Hongxia et al. [11] revealed a lower active form of vitamin D level in T2DM patients than health enrolments. Sarcopenia is a muscle-wasting syndrome characterized by progressive and systemic degenerative loss of skeletal muscle mass (SMM) and strength, often associated with aging and many chronic diseases. In addition to muscular dystrophy, people with sarcopenia demonstrate a higher risk of fractures and metabolic diseases, compromising their quality of life. Neurological complications of diabetes and sarcopenia (metabolic disorders of diabetes, hormonal abnormalities, oxidative stress, and inflammatory response) would aggravate muscle damage [12]. Additionally, loss of muscle mass and function plays a negative role in controlling blood sugar and further leads to metabolic disorders.

In the present study, in contrast to the 25(OH)D-normal group, the 25(OH)D-deficiency group showed notably lower BMD in the femur neck, lower muscle masses of upper and lower limbs, and higher HOMA-IR level. Moreover, the Pearson's correlation analysis revealed positive associations between 25(OH)D and BMD and muscle masses of upper and lower limbs in patients with senile T2DM and a negative relation between 25(OH)D and HOMA-IR. Reportedly, the occurrence of T2DM is attributed to IR and insulin secretion dysfunction. Vitamin D level can regulate the synthesis and secretion of insulin and is related to fasting blood glucose, glycosylated hemoglobin, IR, and islet β cells. To our best understanding, active form of vitamin D level deficiency lowers the sensitivity of insulin and thus increases IR [13]. Its supplementation can reduce HOMA-IR-associated metabolic parameters and improve glucose and lipid metabolism,

Table 3: Correlations between 25(OH)D and BMD and HOMA-IR and muscle mass.

	BMD	HOMA-IR	Upper limb muscle mass	Lower limb muscle mass
r	0.372	-0.472	0.557	0.520
P	≤0.001	≤0.001	≤0.001	≤0.001

and the serum vitamin D level can lower HOMA-IR and reduce related diseases by lowering oxidative stress and improving metabolic status [14]. The mechanism of vitamin D on IR can be explained as follows: (1) vitamin D level affects insulin secretion of pancreatic β cells by regulating Ca^{2+} homeostasis and thus improves insulin sensitivity and insulin signal transduction [15]; (2) it controls the Ca^{2+} level in muscle cells and adipocytes to maintain the normal function of insulin responsive tissue, including muscle and adipose [16]; (3) it reduces low-degree chronic inflammation, with indirect antioxidant properties and immunomodulatory function [16]; (4) it controls epigenetic gene expression [17]; and (5) it affects lipid and glucose metabolism in muscle tissue and the liver [18].

The prevalence of fractures in patients with senile T2DM in China is 7.3%, and the decrease in BMD is one of the independent risk factors of fractures [19]. Serum vitamin D level plays a crucial part in bone metabolism by promoting the absorption of calcium and phosphorus to maintain stable blood calcium and phosphorus concentrations and promoting bone mineralization, stimulating osteoblasts to promote bone formation and inhibit osteoblast apoptosis, and promoting the differentiation of precursor osteoclasts into mature osteoclasts and promoting bone resorption. Serum vitamin D deficiency is frequently seen among postmenopausal women, and it is positively associated with BMD in the femoral neck, and appropriate vitamin D supplementation is of profound significance to prevent bone loss [20]. Senile T2DM is often complicated with osteopenia or even osteoporosis, and serum vitamin D deficiency in the body would result in the decrease in BMD [21].

The vitamin D can increase the synthesis of protein in muscle and the absorption of calcium in sarcoplasmic reticulum and influence the growth of muscle system by regulating various factors secreted by the muscle system itself and surrounding tissues [22]. *In vitro* assays revealed positive influences of vitamin D-based therapy on muscle cell hypertrophy, muscle fibers, and muscle strength in cultured cells. A prior study pointed out that vitamin D supplementation can regulate lipid and mitochondrial muscle metabolism and can also directly impact glucose metabolism and insulin-driven signal transduction [23]. For patients with senile T2DM, serum vitamin D level deficiency contributes to the decrease of muscle mass and function and would result in the decrease of lower limb muscle mass [24]. For patients with senile T2DM, a notable decrease of serum 25(OH)D level may trigger IR and decreased BMD and muscle mass. Serum vitamin D and BMD and muscle masses of upper and lower limbs are positively related, while serum vitamin D and HOMA-IR are negatively related. This study confirmed the correlation between vitamin D deficiency and bone mineral density, muscle mass, and insulin resistance, providing evidence-based medical basis for vitamin D supplementation in senile T2DM, but there are still the following problems. First, this study was a single-center study, with a small number of patients included and a lack of representativeness. Secondly, the effects of vitamin D supplementation on bone mineral density, muscle mass, and insulin resistance in patients with vitamin D deficiency were not observed in this study. In the future, we will enlarge the sample size and follow-up time and further explore the effect of vitamin D supplementation.

5. Conclusion

The serum 25(OH)D level correlates with bone and muscle mass as well as insulin resistance in senile T2DM patients. Vitamin D deficiency in senile T2DM may accelerate insulin resistance, loss of limb muscle masses, and bone density. Therefore, vitamin D supplementation in senile T2DM may decrease insulin resistance and the risk of bone fracture and loss of muscle mass.

Data Availability

The datasets used during the present study are available from the corresponding author upon reasonable request.

Conflicts of Interest

The authors declare that they have no conflict of interest.

References

[1] Q. Wang, X. Zhang, L. Fang, Q. Guan, L. Guan, and Q. Li, "Prevalence, awareness, treatment and control of diabetes mellitus among middle-aged and elderly people in a rural Chinese population: a cross-sectional study," *PLoS One*, vol. 13, no. 6, 2018.

[2] W. Lijuan, G. Tailin, L. Xiaoming, and L. Fan, "Meta-analysis of the prevalence and influencing factors of sarcopenia in elderly patients with type 2 diabetes in Asia," *Chinese Journal of Diabetes*, vol. 28, no. 9, pp. 651–656, 2020.

[3] L. Xiang, L. Yanhui, G. Yanping, L. Nan, M. Lichao, and L. Chunlin, "Survey of osteoporosis in elderly male patients with type 2 diabetes in outpatient department," *Chinese Journal of Healthcare and Medicine*, vol. 23, no. 3, pp. 224–226, 2021.

[4] Q. Yang, A. Vijayakumar, and B. B. Kahn, "Metabolites as regulators of insulin sensitivity and metabolism," *Nature Reviews. Molecular Cell Biology*, vol. 19, no. 10, pp. 654–672, 2018.

[5] Q. Fanfan, Z. Huimin, and Z. Yaru, "Research progress of vitamin D and diabetes," *Journal of Hebei Medical University*, vol. 38, no. 9, pp. 1099–1103, 2017.

[6] T. A. D. Association, "Executive summary: standards of medical care in Diabetes—2012," *Diabetes Care*, vol. 35, Supplement_1, pp. S4–10, 2012.

[7] WHO, *Abbreviated report of a WHO consultation. Use of glycated hemoglobin (HbA1c) in the diagnosis if diabetes mellitus*, World Health Organization, Geneva, 2011.

[8] W. Xiaohong and L. Li, "The effect of vitamin D on insulin resistance in elderly patients with type 2 diabetes," *Chongqing Medicine*, vol. 45, no. 9, pp. 1195–1197, 2016.

[9] W. Qi, L. Yanhui, L. Chunlin et al., "Investigation on the nutritional status of vitamin D in elderly men in Beijing and its correlation with cardiovascular risk factors," *Chinese Journal of Healthcare and Medicine*, vol. 17, no. 1, pp. 10–13, 2015.

[10] L. Deda, Y. Yeshayahu, S. Sud et al., "Improvements in peripheral vascular function with vitamin D treatment in deficient adolescents with type 1 diabetes," *Pediatric Diabetes*, vol. 19, no. 3, pp. 457–463, 2018.

[11] L. Hongxia, W. Jinxiu, and X. Xiaomin, "Comparison of plasma 25-hydroxyvitamin D levels in people with different glucose tolerance," *Chinese Journal of Diabetes*, vol. 29, no. 5, pp. 362–366, 2021.

[12] W. Jiamin, Z. Kexiang, S. Yue, D. Zidan, L. Cheng, and X. Qian, "Research progress on the relationship between bone mass-myomass obesity syndrome and type 2 diabetes," *Chinese General Practice*, vol. 24, no. 9, pp. 1152–1157, 2021.

[13] G. Yixing, W. Dan, W. Qingfeng et al., "Meta-analysis of the relationship between vitamin D levels and type 2 diabetes," *Journal of Gannan Medical College*, vol. 40, no. 10, pp. 1061–1067, 2020.

[14] S. Wenclewska, I. Szymczak-Pajor, J. Drzewoski, M. Bunk, and A. Śliwińska, "Vitamin D supplementation reduces both oxidative DNA damage and insulin resistance in the elderly with metabolic disorders," *International Journal of Molecular Sciences*, vol. 20, no. 12, 2019.

[15] I. Szymczak-Pajor, J. Drzewoski, and A. Śliwińska, "The molecular mechanisms by which vitamin D prevents insulin resistance and associated disorders," *International Journal of Molecular Sciences*, vol. 21, no. 18, 2020.

[16] Y. Wang, H. T. Zhang, X. L. Su et al., "Experimental diabetes mellitus down-regulates large-conductance Ca^{2+}-activated K + channels in cerebral artery smooth muscle and alters functional conductance," *Current Neurovascular Research*, vol. 7, no. 2, pp. 75–84, 2010.

[17] M. J. Berridge, "VitaminDdeficiency and diabetes," *The Biochemical Journal*, vol. 474, no. 8, pp. 1321–1332, 2017.

[18] K. Yang, J. Liu, S. Fu et al., "Vitamin D status and correlation with glucose and lipid metabolism in Gansu Province, China," *Diabetes, Metabolic Syndrome and Obesity: Targets and Therapy*, vol. 13, no. 13, pp. 1555–1563, 2020.

[19] Y. Guo, Y. Wang, F. Chen, J. Wang, and D. Wang, "Assessment of risk factors for fractures in patients with type 2 diabetes over 60 years old: a cross-sectional study from Northeast China," *Journal Diabetes Research*, vol. 2020, article 1508258, 8 pages, 2020.

[20] Z. Lei and W. Qiushi, "Analysis of the correlation between serum 25-hydroxyvitamin D levels and bone mineral density in postmenopausal women in Tianhe community, Guangzhou," *Chinese Journal of Osteoporosis*, vol. 23, no. 9, pp. 1132–1135, 2017.

[21] W. Ke Wencai and Q.,. G. Yunxia, "Correlation analysis of bone metabolism markers and bone mineral density in elderly patients with type 2 diabetes," *Laboratory Medicine*, vol. 32, no. 2, pp. 86–89, 2017.

[22] Y. Jiang, X. Wenhua, and R. Tianli, "The effect and effect of vitamin D on sarcopenia," *Chinese Journal of Osteoporosis*, vol. 24, no. 9, pp. 1246–1249, 2018.

[23] K. Romeu Montenegro, M. Amarante Pufal, and P. Newsholme, "Vitamin D supplementation and impact on skeletal muscle function in cell and animal models and an aging population: what do we know so Far?," *Nutrients*, vol. 13, no. 4, 2021.

[24] M. Zhijing, X. Shuangling, W. Li, and S. Lina, "Study on the correlation between vitamin D and grip strength and muscle mass in elderly diabetic patients," *Chinese Journal of Clinical Medicine*, vol. 36, no. 2, pp. 154–157, 2020.

Hindawi
Disease Markers
Volume 2022, Article ID 6309188, 5 pages
https://doi.org/10.1155/2022/6309188

Research Article

Clinical Effects of Exercise Rehabilitation Combined with Repaglinide in the Treatment of Diabetes

Yan Li,[1] Xi Wang,[2] and Ying Zhang[3]

[1]*Department of Nursing, China-Japan Union Hospital of Jilin University, Changchun, China*
[2]*Department of Gynecology, China-Japan Union Hospital of Jilin University, Changchun, China*
[3]*Department of Cardiology, China-Japan Union Hospital of Jilin University, Changchun, China*

Correspondence should be addressed to Ying Zhang; zhangying01@jlu.edu.cn

Received 29 December 2021; Revised 14 February 2022; Accepted 18 February 2022; Published 25 March 2022

Academic Editor: Yaoyao Bian

Objective. Diabetes, a common endocrine and metabolic disease in clinical practice, generally manifests a certain defect in insulin secretion due to several factors, thereafter leading to a metabolic disorder such as hyperglycemia. This study was conducted to explore the clinical effects of repaglinide combined with exercise rehabilitation on improving the blood glucose of patients with diabetes. *Methods*. In this retrospective study, 100 patients with diabetes treated in our hospital from January 2018 to January 2020 were assessed for eligibility and recruited. They were assigned at a ratio of 1 : 1 to receive either repaglinide (control group) or repaglinide plus exercise rehabilitation (experimental group). Outcome measures include fasting blood glucose, 2 h postprandial blood glucose, glycosylated hemoglobin, time to normal blood glucose, blood glucose fluctuation, insulin dosage, adverse reactions, and blood glucose adequate rate. *Results*. All eligible patients showed similar pretreatment fasting blood glucose, glycosylated hemoglobin, and 2 h postprandial blood glucose ($P > 0.05$). After treatment, repaglinide plus exercise rehabilitation resulted in lower levels of fasting blood glucose, glycosylated hemoglobin, and 2 h postprandial blood glucose versus repaglinide alone ($P < 0.05$). Repaglinide plus exercise rehabilitation was associated with a significantly shorter time to normal blood glucose and a milder fluctuation versus repaglinide ($P < 0.05$). The incidence of adverse reactions and blood glucose adequate rate was 6% and 94% in the experimental group and 50% and 52% in the control group, respectively ($P < 0.05$). *Conclusion*. Repaglinide plus exercise rehabilitation results in effective blood glucose control and reduced incidence of adverse reactions and yields a promising efficacy, so it is worthy of clinical promotion and application.

1. Introduction

Diabetes, a common endocrine and metabolic disease in clinical practice, generally manifests a certain defect in insulin secretion due to several factors, thereafter leading to a metabolic disorder such as hyperglycemia [1]. The elderly population is susceptible to diabetes mellitus due to reduced body functions [2]. The high blood glucose elicited by diabetes is considered detrimental to the patients' multiple organs, nervous system, and vascular system, resulting in the complications such as diabetic retinopathy, diabetic nephropathy, and diabetic foot [3–5]. At present, most clinical treatments are carried out by oral medication and insulin subcutaneous injection, coupled with self-management measures such as diet adjustment, exercise, and blood glucose monitoring. With the feature of rapid action, repaglinide lowers the blood glucose by inhibiting insulin release from the pancreas [6–8]. It is associated with short-term but promising effects on postprandial blood glucose but fails to yield a satisfactory control on fasting blood glucose. Exercise rehabilitation improves the sensitivity of insulin target cells to insulin and glucose utilization and thus contributes to lower blood glucose [9–11]. This study was aimed at exploring the clinical effects of repaglinide combined with exercise rehabilitation on improving the blood glucose of patients with diabetes.

2. Materials and Methods

2.1. General Materials. In this retrospective study, 100 patients with diabetes treated in our hospital from January

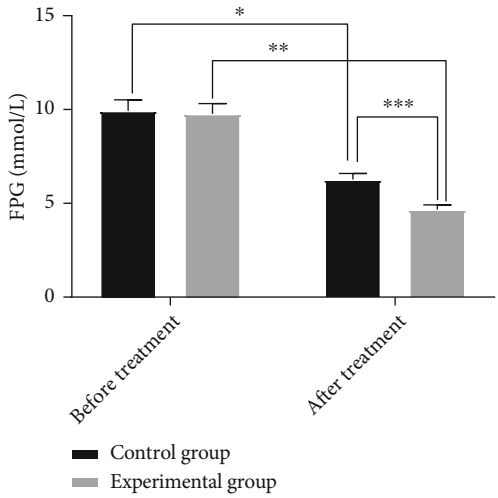

Figure 1: Comparison of FPG before and after treatment ($x \pm s$). The x-axis indicates before and after treatment, and the y-axis indicates the FPG level (mmol/L). The FPG levels of patients in the control group before and after treatment were 9.52 ± 0.83 mmol/L and 6.03 ± 0.47 mmol/L, respectively. The FPG levels of patients in the experimental group before and after treatment were 9.38 ± 0.78 mmol/L and 4.49 ± 0.36 mmol/L, respectively. $*$ indicates that there is a significant difference in FPG levels before and after treatment in the control group ($t = 25.8724$, $P = 000$). $**$ indicates that a significant difference is found in FPG levels before and after treatment in the experimental group ($t = 40.2500$, $P = 000$). $***$ indicates that a significant difference is observed in FPG levels between the experimental group and the control group after treatment ($t = 18.3934$, $P = 000$).

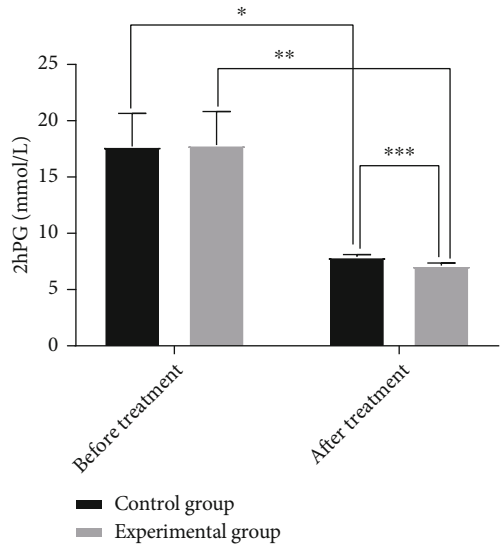

Figure 2: Comparison of 2hPG before and after treatment ($x \pm s$). The x-axis indicates before and after treatment, and the y-axis indicates the 2hPG (mmol/L). The 2hPG levels of patients in the control group before and after treatment were 15.64 ± 4.16 mmol/L and 7.78 ± 0.27 mmol/L, respectively. The 2hPG levels of patients in the experimental group before and after treatment were 15.73 ± 4.22 mmol/L and 6.97 ± 0.33 mmol/L, respectively. $*$ indicates that a significant difference is found in 2hPG levels before and after treatment in the control group ($t = 13.3322$, $P = 000$). $**$ indicates that a significant difference is observed in 2hPG levels before and after treatment in the experimental group ($t = 14.6337$, $P = 000$); $***$ indicates that a significant difference is discovered in 2hPG levels between the experimental group and the control group after treatment ($t = 13.4330$, $P = 000$).

2018 to January 2020 were assessed for eligibility and recruited. They were assigned at a ratio of 1 : 1 to a control group ($n = 50$) or experimental group ($n = 50$). The baseline characteristics of the control group (27 males and 23 females, course of disease of 2-6 years, mean course of disease of 3.6 ± 0.5, aged 35–73 years, and mean age of 50.62 ± 3.4 years) were comparable with those of the experimental group (29 males and 21 females, course of disease of 2.5-7 years, mean course of disease of 3.3 ± 0.4, aged 36–75 years, and mean age of 51.6 ± 3.2 years) ($P > 0.05$).

2.2. Inclusion Criteria. The following are the inclusion criteria: (1) patients who met the diagnostic criteria of diabetes; (2) patients without a history of severe hypoglycemia; (3) patients who stopped using other types of hypoglycemic drugs at one month before enrollment; (4) patients with certain cognitive and communication skills; and (5) the ethics committee of our hospital had approved this study, and patients and their families were informed of the purpose and process of this research and provided written informed consent.

2.3. Exclusion Criteria. The following are the exclusion criteria: (1) patients with serious insufficiency of other combined organs such as the heart, kidney, and liver; (2) patients with malignant tumors; (3) patients with limb movement disorders; (4) patients with poor compliance; and (5) patients with drug allergies to the drugs used in this study.

2.4. Methods. The control group was given repaglinide (Beijing Wansheng Pharmaceutical Co., Ltd., SFDA approval number H20133037) orally at 15 minutes before meals, 0.5 mg/time, 3 times/d. The dosage was modified based on 2 h postprandial plasma glucose (2hPG) within a maximum dosage of 2 mg. The eligible patients in the experimental group were treated with repaglinide plus exercise rehabilitation after discharge. The treatment was performed in wake of the evaluation of the patients' exercise function and cardiopulmonary function. A week of adaptive training was carried out before the formal exercise. The exercise was performed and progressively strengthened and reasonably modified based on their conditions. Before the formal intervention one week later, the patients were instructed to perform 5-10 minutes of low-intensity barehanded exercises or slow walking. Formal training mainly consists of fast and slow walking. The patients were equipped with a heart rate monitor throughout the whole exercise that lasted 30 minutes, and the heart rate was controlled at 50%-70% of the highest heart rate (220 ages), followed by 5-10 minutes of restorative exercise-slow walking or barehanded exercises. Patients started exercise about one hour after a meal and wore a name card with their name, disease, and contact on it for emergency needs. Candies or biscuits were allowed to prevent palpitation, fatigue, and hunger. Exercises were performed with an interval of less than one day and each

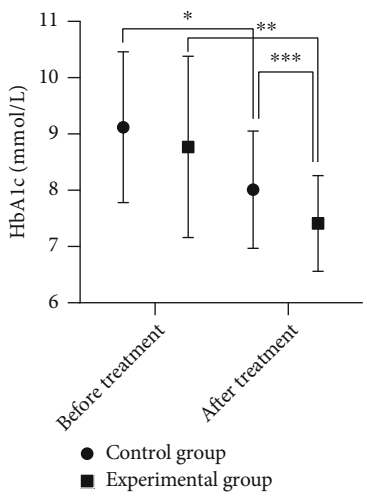

Figure 3: Comparison of HbA1c between the two groups of patients before and after treatment. The abscissa indicates before and after treatment, and the ordinate indicates the level of HbA1c, in mmol/L. The HbA1c levels of patients in the control group before and after treatment were 9.12 ± 1.34 mmol/L and 8.01 ± 1.04 mmol/L, respectively. The HbA1c levels of patients in the experimental group before and after treatment were 8.77 ± 1.61 mmol/L and 7.41 ± 0.85 mmol/L, respectively. $*$ indicates that there is a significant difference in HbA1c levels before and after treatment in the control group ($t = 4.6272$, $P = 000$). $**$ indicates significant differences in HbA1c levels before and after treatment in the experimental group ($t = 5.2821$, $P = 000$). $***$ indicates that there is a significant difference in HbA1c levels between the experimental group and the control group after treatment ($t = 3.1587$, $P = 000$).

exercise lasting 40-60 min, four times per week. The exercise rehabilitation training of the patients was closely monitored, and the patients' conditions were evaluated once a week. An exercise diary of each patient was a must for data management and analysis.

All the measurements implemented in the two groups continued for 6 months.

2.5. Evaluation Criteria. On the evening before each study day, patients consumed a meal before 7 pm. After the meal, patients fasted from solids and liquids (14 h for solids and 12 h for liquids) until the following morning. On the study day, patients attended the department at 8 am, and an intravenous catheter was inserted for blood sampling.

In this study, the fasting plasma glucose (FPG), 2hPG, glycosylated hemoglobin (HbA1c), and the blood glucose adequate rate of the two groups before and after treatment were analyzed (normal levels of FPG and 2hPG were < 5.1 mmol/L and <8.5 mmol/L, respectively).

2.6. Statistical Methods. In this study, SPSS20.0 was used for data analyses, and GraphPad Prism 7 (GraphPad Software, San Diego, USA) was for image rendering. The enumeration data were represented by n (%) and processed using the X^2 test. The measurement data were represented by $\bar{x} \pm s$ and processed by the t-test. $P < 0.05$ indicated that the difference was statistically significant.

3. Results

3.1. Comparison of FPG. There was no statistical significance in the FPG difference between the two groups before treatment ($P > 0.05$). After treatment, repaglinide plus exercise rehabilitation resulted in lower FPG levels versus repaglinide alone ($P < 0.05$). See Figure 1.

3.2. Comparison of 2hPG. The difference in 2hPG between the two groups before treatment was not statistically significant ($P > 0.05$), and the two groups both decreased in 2hPG after treatment, and the experimental group had significantly lower 2hPG as compared to the control group ($P < 0.05$). See Figure 2.

3.3. Comparison of HbA1c. The HbA1c difference between the two groups of patients before treatment was not statistically significant ($P > 0.05$). The experimental group showed significantly decreased levels of HbA1c versus the control group ($P < 0.05$). See Figure 3 for details.

3.4. Comparison of the Time to Normal Blood Glucose, Blood Glucose Fluctuation, and Insulin Dosage. After treatment, repaglinide plus exercise rehabilitation was associated with a significantly shorter time to normal blood glucose and a milder fluctuation versus repaglinide ($P < 0.05$). See Table 1.

3.5. Comparison of Blood Glucose Adequate Rate. After treatment, the blood glucose adequate rate and nonadequate rate were 26 (52%) and 24 (48%) of patients in the control group and 47 (94%) and 3 (6%) of those in the experimental group. There is a significant difference in the adequate rate between the two groups after treatment ($X^2 = 22.3744$, $P \leq 0.001$).

3.6. Comparison of Adverse Reactions. The incidence of adverse reactions was 6% in the experimental group and 50% in the control group, respectively ($P < 0.05$). See Table 2.

4. Discussion

Diabetes is induced by genetic and environmental factors, with the manifestation of high blood glucose [12, 13]. As the disease aggravates, the incidence of complications such as microvascular disease, neuropathy, and atherosclerosis also rises. Diabetes has now become the third high-risk disease that threatens the life and health of patients after cardiovascular diseases and cancers. Early detection and treatment are of great significance to the treatment and prognosis of patients [14, 15].

Repaglinide, an insulin secretion agent, improves the pancreatic β-cell function by exerting the dependence on glucose and specifically promotes insulin secretion in the early stage. High glucose results in strong effects on pancreatic β-cells. The duration of action of repaglinide is within 30 minutes. In the early stage of abnormal insulin secretion, repaglinide can minimize the incidence of postprandial hyperglycemia, without impact on the cardiovascular system, but reduces the risk of cardiovascular damage. The administration of repaglinide is considered safe in

Table 1: Comparison of the compliance time and fluctuation value of blood glucose and insulin dosage after treatment ($x \pm s$).

Group	Number	Time to reach the standard (d)	Fluctuation value (mmol/L)	Insulin dosage (U/d)
Control group	50	5.67 ± 1.05	7.54 ± 1.68	45.71 ± 7.06
Experimental group	50	4.08 ± 0.97	5.31 ± 1.04	40.06 ± 6.33
t	7.8651	7.9806	4.2133	
P		≤0.001	≤0.001	≤0.001

Table 2: Comparison of adverse reactions during treatment [n (%)].

Group	Numbers	Hypoglycemia	Hyperglycemia	Allergies	Adverse reactions
Control group	50	8 (16.00)	11 (22.00)	6 (12.00)	25 (50.00)
Experimental group	50	2 (4.00)	0 (0.00)	1 (2.00)	3 (6.00)
X^2					25.6921
P					<0.05

the elderly with comparatively weak cardiovascular systems [12, 16]; however, its efficacy on FPG control before meals is poor. Exercise rehabilitation is to accelerate the fat metabolism and reduce the psychological burden of patients through appropriate exercises, which also effectively reduces medication costs and improves their weight, thereby enhancing the overall immunity of patients. It also maintains a stable in vivo environment by increasing the number of insulin receptors in muscle cells and its sensitivity to insulin [17].

The study of Suzuki et al. [18] showed that comprehensive repaglinide therapy can effectively recover the FPG, HbA1c, and 2hPG of the patients to a normal level. In the present study, repaglinide plus exercise rehabilitation resulted in lower levels of fasting blood glucose, glycosylated hemoglobin, and 2 h postprandial blood glucose versus repaglinide alone ($P < 0.05$). Repaglinide plus exercise rehabilitation was associated with a significantly shorter time to normal blood glucose and a milder fluctuation versus repaglinide ($P < 0.05$). The incidence of adverse reactions and blood glucose adequate rate was 6% and 94% in the experimental group and 50% and 52% in the control group, respectively. Studies have shown that repaglinide plus exercise rehabilitation therapy effectively maintains the stability of FPG and postprandial glucose. During treatment, it can improve the compliance of patients and increase the blood glucose adequate rate. Furthermore, joint therapy also reduces adverse reactions. Neveen et al. [19] pointed out that aerobic exercise contributes to the control of blood glucose and blood lipids of patients, which is similar to the results of the present study.

In summary, repaglinide plus exercise rehabilitation results in effective blood glucose control and reduced incidence of adverse reactions and yields a promising efficacy, so it is worthy of clinical promotion and application.

Data Availability

The datasets used during the present study are available from the corresponding author upon reasonable request.

Conflicts of Interest

The authors declare that they have no conflicts of interest.

References

[1] S. K. Pawar and S. Jaldappagari, "Interaction of repaglinide with bovine serum albumin: spectroscopic and molecular docking approaches," *Journal of Pharmaceutical Analysis*, vol. 9, no. 4, pp. 274–283, 2019.

[2] J. Bojarska, A. Fruziński, L. Sieroń, and W. Maniukiewicz, "The first insight into the supramolecular structures of popular drug repaglinide: focus on intermolecular interactions in antidiabetic agents," *Journal of Molecular Structure*, vol. 1179, pp. 411–420, 2019.

[3] S. Zhou, Q. Xiang, G. Mu et al., "effects of CYP2C8 and SLCO1B1 genetic polymorphisms on repaglinide pharmacokinetics: a systematic review and meta-analysis," *Current Drug Metabolism*, vol. 20, no. 4, pp. 266–274, 2019.

[4] N. S. Abdelhamid, M. T. Elsaady, N. W. Ali, and W. G. Abuelazem, "Simultaneous determination of repaglinide, metformin hydrochloride and melamine by new HPLC and HPTLC chromatographic methods," *Analytical Chemistry Letters*, vol. 9, no. 3, pp. 418–429, 2019.

[5] K. Omori, H. Nomoto, A. Nakamura et al., "Reduction in glucose fluctuations in elderly patients with type 2 diabetes using repaglinide: a randomized controlled trial of repaglinide vs sulfonylurea," *Journal of Diabetes Investigation*, vol. 10, no. 2, pp. 367–374, 2019.

[6] S. Thakkar, N. More, D. Sharma, G. Kapusetti, K. Kalia, and M. Misra, "Fast dissolving electrospun polymeric films of anti-diabetic drug repaglinide: formulation and evaluation," *Drug Development and Industrial Pharmacy*, vol. 45, no. 12, pp. 1921–1930, 2019.

[7] J. Wang, Z.-Y. Zhang, S. Lu, D. Powers, V. Kansra, and X. Wang, "Effects of rolapitant administered orally on the pharmacokinetics of dextromethorphan (CYP2D6), tolbutamide (CYP2C9), omeprazole (CYP2C19), efavirenz (CYP2B6), and repaglinide (CYP2C8) in healthy subjects," *Supportive Care in Cancer: Official Journal of the Multinational Association of Supportive Care in Cancer*, vol. 27, no. 3, pp. 819–827, 2019.

[8] M. Ballmann, D. Hubert, and B. M. Assael, "Repaglinide versus insulin for newly diagnosed diabetes in patients with cystic fibrosis: a multicentre, openlabel, randomised trial (vol 6, pg 114, 2018)," *The Lancet Diabetes & Endocrinology*, vol. 7, no. 4, article E4, 2018.

[9] U. Yasar and M. O. Babaoglu, "Increased risk for cerebral ischemic stroke in diabetes: genetically polymorphic CYP mediated production of neuroprotective EETs and sulfonylurea metabolism in relation with KATP channels," *Acta Pharmacologica Sinica*, vol. 40, no. 4, pp. 569-570, 2019.

[10] G. Khairnar, V. Mokale, A. Mujumdar, and J. Naik, "Development of nanoparticulate sustained release oral drug delivery system for the antihyperglycemic with antihypertensive drug," *Materials Technology*, vol. 34, no. 14, pp. 880–888, 2019.

[11] J. Huguet, F. Gaudette, V. Michaud, and J. Turgeon, "Development and validation of probe drug cocktails for the characterization of CYP450-mediated metabolism by human heart microsomes," *Xenobiotica*, vol. 49, no. 2, pp. 187–199, 2019.

[12] V. Clermont, A. Grangeon, A. Barama et al., "Activity and mRNA expression levels of selected cytochromes P450 in various sections of the human small intestine," *British Journal of Clinical Pharmacology*, vol. 85, no. 6, pp. 1367–1377, 2019.

[13] M.-L. Tan, P. Zhao, L. Zhang et al., "Use of physiologically based pharmacokinetic modeling to evaluate the effect of chronic kidney disease on the disposition of hepatic CYP2C8 and OATP1B drug substrates," *Clinical Pharmacology & Therapeutics*, vol. 105, no. 3, pp. 719–729, 2019.

[14] E. Puris, M. Pasanen, V.-P. Ranta et al., "Laparoscopic Roux-en-Y gastric bypass surgery influenced pharmacokinetics of several drugs given as a cocktail with the highest impact observed for CYP1A2, CYP2C8 and CYP2E1 substrates," *Basic & Clinical Pharmacology & Toxicology*, vol. 125, no. 2, pp. 123–132, 2019.

[15] N. Matsunaga, A. Ufuk, B. L. Morse et al., "Hepatic organic anion transporting polypeptide-mediated clearance in the beagle dog: assessing in vitro-in vivo relationships and applying cross-species empirical scaling factors to improve prediction of human clearance," *Drug Metabolism and Disposition: The Biological Fate of Chemicals*, vol. 47, no. 3, pp. 215–226, 2019.

[16] Y. Jia, Y. Lao, H. Zhu, N. Li, and S. W. Leung, "Is metformin still the most efficacious first-line oral hypoglycaemic drug in treating type 2 diabetes A network metaanalysis of randomized controlled trials," *Obesity Reviews*, vol. 20, no. 1, pp. 1–12, 2019.

[17] M. T. Mohamed, E. A. Embaby, A. Labib et al., "Effects of exercise in combination with autologous bone marrow stem cell transplantation for patients with type 1 diabetes," *Physiotherapy Theory and Practice*, vol. 35, no. 12, pp. 1233–1242, 2019.

[18] K. Suzuki, M. Niitsu, T. Kamo, S. Otake, and Y. Nishida, "Effect of exercise with rhythmic auditory stimulation on muscle coordination and gait stability in patients with diabetic peripheral neuropathy: a randomized controlled trial," *Open Journal of Therapy and Rehabilitation*, vol. 7, no. 3, pp. 79–91, 2019.

[19] A. R. Neveen, G. N. El Nahas, M. K. Nadia, and G. M. Al Shaimaa, "Effect of intradialytic aerobic exercise on patients with diabetic nephropathy," *Bulletin of Faculty of Physical Therapy*, vol. 24, no. 1, pp. 1–7, 2019.

Hindawi
Disease Markers
Volume 2022, Article ID 7829454, 7 pages
https://doi.org/10.1155/2022/7829454

Research Article

A Randomized, Controlled Trial Exploring Collaborative Nursing Intervention on Self-Care Ability and Blood Glucose of Patients with Type 2 Diabetes Mellitus

Xi Wang,[1] Jing Liang,[2] and Wei Yang[3]

[1]*Department of Gynecology, China-Japan Union Hospital of Jilin University, Changchun, China*
[2]*Department of Gastrointestinal and Colorectal Surgery, China-Japan Union Hospital of Jilin University, Changchun, China*
[3]*Department of Hepatopancreatobiliary Surgery, China-Japan Union Hospital of Jilin University, Changchun, China*

Correspondence should be addressed to Wei Yang; jlccyangwei@jlu.edu.cn

Received 25 December 2021; Revised 20 January 2022; Accepted 10 February 2022; Published 22 March 2022

Academic Editor: Yaoyao Bian

Objective. For determining the impacts of collaborative nursing intervention (CNI) on self-care ability and blood glucose (BG) of patients with type 2 diabetes mellitus (T2DM). *Methods*. The study enrolled 72 T2DM patients, who are referred to our hospital between April 2017 and September 2019. Of them, 35 cases given routine nursing were set as the control group (CG) and 37 cases given CNI were set as the research group (RG). The Exercise of Self-Care Agency (ESCA) scale scores and the levels of fasting plasma glucose (FPG) as well as glycosylated hemoglobin (HbAlc) were observed pre- and postintervention. The scores of SAS and HAMD and Morisky pre- and postnursing intervention as well as postnursing SF-36 scores and patients' satisfaction toward the nursing content were recorded. *Results*. After intervention, RG presented notably lower serum HbAlc and FPG levels than CG ($P < 0.05$); RG presented evidently lower SAS and HAMD scores while distinctly higher Morisky, SF-36, and ESCA scores than CG ($P < 0.05$); the nursing satisfaction in RG and CG was 97.30% and 51.43%, respectively. *Conclusions*. In view of the fact that CNI can decrease HbAlc and FPG levels in patients with T2DM and enhance their self-care ability, it is worth popularizing in the clinic.

1. Introduction

Diabetes mellitus (DM) is a ubiquitous metabolic dysregulation with a terribly high incidence across the globe [1]. It is a set of metabolic diseases featured with hyperglycemia due to insulin secretion deficiency or insulin action or the two. Chronic hyperglycemia of diabetes is bound up with long-run injury, dysfunction, and organ failure, especially the nerves, kidneys, eyes, and heart as well as blood vessels [2]. DM is currently the illness with the highest incidence worldwide, and society advancement and improvement of people's living standards are driving the increasing incidence of DM [3]. According to research statistics, the proportion of diabetes worldwide reached 25.6% in 2015 [4]. DM can predispose people to complications like nervous system diseases and kidney diseases. Once the disease deteriorates because of the absence of timely therapy, it will lead to malignant tumours directly. DM, defined by elevated blood glucose (BG) markers, is a primary risk factor for cardiovascular illnesses, which bears the major responsibility for death in diabetic patients [5]. The treatment of diabetes is still a challenge. Clinically, efforts have been made to find a way to effectively prevent and treat diabetes, but no significant breakthrough has been made so far [6]. Hence, early screening and diagnosis are of utmost importance.

Patients with DM need long-time medication, and some also require insulin injections to control their BG. And during treatment, patients' compliance and awareness of the disease directly affect their BG status and mental health. Today, the major obstacle that stands in the way of nursing work is how to make patients face diabetes actively and rationally and receive professional and systematic treatment [7–9]. The concept of collaborative nursing intervention (CNI) mode is to give full play to patients' self-care ability

on the basis of accountability nursing, encourage patients and their families to take part in the process of health care, maximize patients' subjective initiative and treatment enthusiasm, and creatively utilize existing manpower and material resources [10, 11]. Such a nursing model has been applied to the care of patients with cardiovascular surgery, AIDS, depression, and schizophrenia [12][13][14], but whether it can play a role in diabetes has not been indicated. In light of this, we investigate the impacts of CNI on self-care ability and BG of type 2 diabetes mellitus (T2DM) patients, with the aim of rendering evidence and advice for future clinical practice.

2. Materials and Methods

2.1. General Information. This was a randomized, controlled trial. Totally, 72 T2DM patients admitted to our hospital between Apr. l, 2017, and Sep. 2019 were enrolled as the study population by using the continuous fixed-point sampling method, of whom 35 patients in the control group (CG) received routine nursing, and 37 patients in the research group (RG) were given CNI. The hospital Medical Ethics Committee approved the study protocol without reserves with the license no. of 2016.239.22.

2.2. Inclusion and Exclusion Criteria. Inclusion criteria include (1) patients diagnosed with diabetes according to the diagnostic guidelines for diabetes issued in 2014 [15] and treated in our hospital, (2) patients with detailed case data, (3) patients glad to cooperate and take part in the study, (4) patients between 30 and 65 years old, (5) patients without other severe organ diseases impacting this study, and (6) patients who provided informed consent signed by the patient himself/herself or his/her next of kin.

Exclusion criteria include (1) patients who died in the process of therapy, (2) patients comorbid with other tumours or other cardiac-cerebral vascular illnesses, (3) patients with physical disability, (4) pregnant patients, (5) patients comorbid with other autoimmune illnesses or other chronic illnesses, (6) referred patients, and (7) patients with mental disorders, speech disorders, or diseases that affect the results of this study.

2.3. Nursing Methods. CG received routine nursing care: diet nursing: nurses gave health education to patients and advised them to eat multiple small meals on a regular basis and follow the dietary principles of low sugar and fat, proper protein, and high fiber and vitamins; appropriate exercise: appropriate exercise was conducted to intensify the body immunity, elevate the sensitivity to insulin, and help patients keep BG under control. In addition, the nurses instructed the patients to positively take part in aerobic activities like jogging and yoga.

RG adopted cooperative nursing: RG implemented CNI based on routine nursing from the following dimensions: knowledge guidance: manuals regarding health education were distributed to patients and their families, and diabetes-related knowledge such as the effects and adverse reactions of common drugs for diabetes was explained to them, together with the guidance on daily dietary and lifestyle. Besides, the contents of electrolyte, BG, and glycosylated hemoglobin (HbAlc) were reviewed regularly by following the doctor's suggestions, and patients were guided to read examination results such as BG and blood lipid. Self-care strengthening: the responsible nurse explained diabetes knowledge to patients and their families, provided psychological counseling, and encouraged patients to actively participate in the nursing diagnosis and treatment process, so that patients can control BG at the ideal level through self-care and self-psychological adjustment. What is more, medical professionals set up files for patients, developed care plans according to the patient's condition, and hired diabetes experts to conduct learning concerning exercise, diet, and disease-related knowledge every week. The responsible nurse maintained telephone contact with patients and conducted weekly telephone follow-ups to collect and analyze patient information. Moreover, questionnaires were distributed and retrieved by specialized nursing staff on admission and one month after discharge. Psychological nursing: the responsible nurse listened to the patient's complaints carefully and patiently, coordinated with the family to give care and support to patients, and conducted psychological nursing according to the patient's individual psychological characteristics. Besides, the nurses try their best to relieve patients' psychological pressure and helped them to cope with various psychological problems in the treatment of the disease and to enhance their adaptability. In particular, for patients with excessive pressure and mood swings during hospitalization, the responsible nurse provided patients with certain psychological counseling and support and explained to patients the great role of a good state of mind and mood in conquering the disease and promoting rehabilitation, hoping that patients can cooperate with the treatment with a pleasant and relaxed attitude.

2.4. Scoring Criteria. Self-Rating Anxiety Scale 9.4 software (SAS Institute, Inc., USA) and Hamilton Depression Rating Scale (HAMD; Hamilton, 1960) were employed for mental health assessment. The SAS has a full score of 100 points with mild anxiety corresponding to a SAS value 50-70, moderate anxiety to a SAS value 71-90, and severe anxiety to a SAS value > 90. HAMD composed of 24 items evaluated patients' depression. The score was positively bound up with depression severity.

The Morisky medication adherence scale (MMAS; 2006 Donald E. Morisky) [16] was utilized to evaluate the therapy compliance of patients pre- and postnursing intervention from four respects, namely, diet control, following the doctor's advice, body mass control, and proper exercise. With a full score of 50 points, full compliance corresponded to a MMAS value of 50, partial compliance to a MMAS value between 30 and 40 points, and noncompliance to a MMAS value of less than 30 points. Self-care ability was assessed via the Exercise of Self-Care Agency (ESCA, Hanson and Bickel's 1985), which consists of 4 dimensions and 43 items, with a full score of 172 points. A higher score denotes better self-care ability. The quality of life (QOL) of patients was assessed via the SF-36, which covered physical health (role-

physical, somatic pain, overall health, and physiological function) and mental health (social function, vitality, emotional role, and mental health), with 8 dimensions, each corresponding to 100 points. A higher score denotes better QOL of the patient. The nursing satisfaction questionnaire (20 questions, 5 points each) developed by our hospital was adopted for scoring the patients' satisfaction toward nursing, with questionnaire Cronbach's alpha representing internal consistency of criteria *A* 0.93: a total score < 70: dissatisfaction; 70-89: satisfaction; ≥90: high satisfaction: Satisfaction = (high satisfaction + satisfaction)cases/the sum of cases × 100%.

2.5. Blood Sampling and Main Reagents. Morning fasting venous peripheral blood (5 mL) was placed at room temperature for 30 min before centrifuging for 10 min (3000 rpm/min), and the resulting upper serum was subpackaged into enzyme-free EP tubes. Part of the serum samples was processed for experiment, while the rest were kept at -80°C until use. Following the manufacturer's instructions, the determination of BG function (glycosylated hemoglobin: HbAlc, fasting plasma glucose: FPG) was made with an automatic biochemical analyzer (Jiaozuo Lufeifan Biotechnology Co., Ltd., Cat. No. LFF-LC-1781). An Eppendorf CryoCube F740hi ultralow temperature refrigerator was obtained from Eppendorf Ltd., China (Cat. No. ep000000).

2.6. Outcome Measures. Primary endpoints: the ESCA scores and serum HbAlc and FPG levels pre- and postnursing intervention were observed. The patients' venous blood was measured at 0 weeks and after treatment.

The scores of SAS, HAMD, and Morisky pre- and postnursing intervention as well as postnursing SF-36 scores and patients' satisfaction toward nursing were recorded.

2.7. Statistical Analyses. This study statistically analyzed the obtained data via SPSS20.0 (IBM Corp, Armonk, NY, the States) and visualized them via GraphPad 7. The K-S test was adopted for analyzing the distribution of the measurement data, among which those in normal distribution were presented by mean ± SD. The independent sample *t*-test and paired *t*-test were utilized for intragroup comparisons and intergroup comparisons, respectively. The counting data (%) were subjected to analysis by the chi-squared test (denoted by χ^2). $P < 0.05$ denotes a notable difference.

3. Results

3.1. Clinical Data. The two cohorts differed insignificantly in terms of smoking history, age, BMI, residence, dietary preference, drinking history, exercise habits, HbAlc, and FPG, which was suggestive of comparability ($P > 0.05$) (Table 1).

3.2. HbAlc and FPG Levels Pre- and Postintervention. Evident differences were absent regarding serum HbAlc (9.95 ± 1.00) and FPG (9.92 ± 2.13) between the two cohorts before intervention ($P > 0.05$); however, lower HbAlc (7.45 ± 0.45) and FPG (6.95 ± 1.50) levels were observed in RG after it ($P < 0.05$) (Figure 1).

Table 1: Basic data (*n* (%)).

	RG (*n* = 37)	CG (*n* = 35)	χ^2 or *t*	*P*
Age (years old)	42.4 ± 9.6	42.2 ± 10.2	0.086	0.932
BMI	23.05 ± 1.24	23.02 ± 1.17	0.106	0.916
History of smoking				
Yes	9 (24.32)	10 (28.57)	1.167	0.683
No	28 (75.68)	25 (71.43)		
History of drinking				
Yes	17 (45.95)	19 (54.29)	0.500	0.479
No	20 (54.05)	16 (45.71)		
Residence				
Urban	31 (83.78)	30 (85.71)	0.052	0.820
Rural	6 (16.22)	5 (14.29)		
Dietary preference				
Light	7 (18.92)	9 (25.71)	0.481	0.488
Spicy	30 (81.08)	26 (74.29)		
Exercise habits				
Yes	11 (29.73)	13 (37.14)	0.445	0.505
No	26 (70.27)	22 (62.86)		
HbAlc (%)	11.03 ± 1.18	11.05 ± 1.12	0.074	0.942
FPG (mmol/L)	11.54 ± 1.28	11.51 ± 1.23	0.101	0.920

3.3. SAS Scores Pre- and Postintervention. No difference was noted between the two cohorts in the SAS score before intervention ($P > 0.05$); however, a more evident decrease in the SAS score was observed in RG after it ($P < 0.05$) (Figure 2).

3.4. HAMD Scores Pre- and Postnursing Intervention. The two cohorts were similar in the HAMD score before intervention ($P > 0.05$), but after it, the HAMD score was significantly lower in RG than in CG ($P < 0.05$) (Figure 3).

3.5. Morisky Scores Pre- and Postnursing Intervention. The Morisky score showed no notable difference between the two cohorts before intervention ($P > 0.05$). After it, RG showed a notably higher Morisky score than CG in the following four aspects: body mass control, following the doctor's advice, proper exercise, and diet control ($P < 0.05$) (Figure 4).

3.6. SF-36 Scores after Nursing Intervention. Observation of the SF-36 scores in the two groups revealed notably better physical health (physiological function, role-physical, somatic pain, and overall health) and mental health (vitality, social function, emotional role, and mental health) in RG than in CG ($P < 0.05$) (Figure 5).

3.7. ESCA Scores Pre- and Postnursing Intervention. Observation of ESCA scores before and after intervention determined no evident difference between the two cohorts before it ($P > 0.05$), while observably higher scores of self-care concept, sense of responsibility for self-care, self-nursing skills, and health knowledge level in RG than in CG postnursing intervention ($P < 0.05$) (Figure 6).

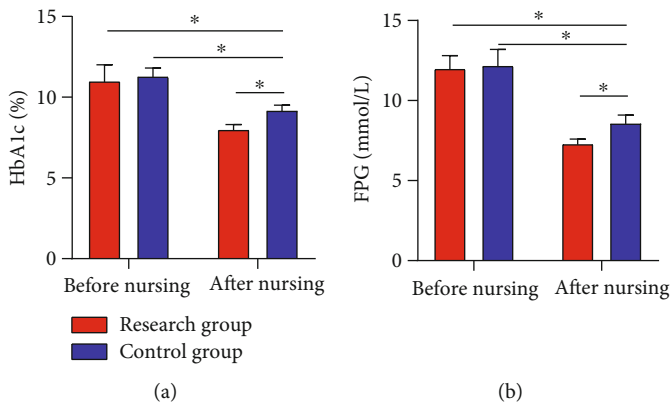

Figure 1: HbAlc and FPG levels pre- and postintervention. (a) After intervention, the HbAlc expression in the RG dropped notably and was lower than that in the CG. (b) After intervention, the FPG expression in the RG dropped notably and was lower than that in the CG. Note: $^{*}P < 0.05$ between the two groups.

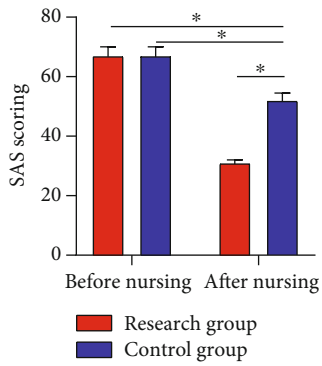

Figure 2: SAS scores pre- and postintervention. After intervention, the SAS score in the RG dropped notably and was lower than that in the CG. Note: $^{*}P < 0.05$ between the two groups.

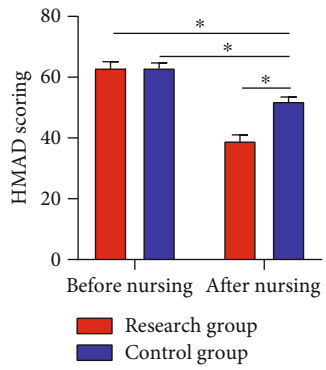

Figure 3: HAMD scores pre- and postintervention. After intervention, the HAMD score in the RG dropped notably and was lower than that in the CG. Note: $^{*}P < 0.05$ between the two groups.

3.8. Patient Satisfaction with Nursing Content. The nursing satisfaction of patients in RG was 97.30%, evidently higher than 51.43% in CG ($P < 0.05$) (Table 2).

4. Discussion

DM is a group of metabolic diseases featured with hyperglycemia due to insulin secretion deficiency/insulin action or the two [17]. In 2014, the prevalence of diabetes was estimated to be 9% worldwide [18], and approximately 1.6 million people died of the illness worldwide in 2015 [19]. The disease is also bound up with high morbidity because of extensive complications like nephropathy, retinopathy, neuropathy, and cardiovascular diseases [20, 21]; thus, preventing and managing these complications have become the primary aspect of modern diabetes care. The CNI model emphasizes that nurses, patients, and family members are integrated into nursing work, so that patients and family members can gradually learn and master the condition monitoring and nursing skills during diagnosis and treatment, which is the best nursing model to improve the QOL of patients with T2DM [22, 23].

In our study, no notable difference was observed in HbAlc and FPG levels between the two cohorts before nursing intervention, while the two parameters were notably lower in RG than in CG after intervention, which indicated that CNI could effectively control the BG level of patients. Under normal circumstances, nervous and excited mood and psychological pressure will stimulate the substantial secretion of stress hormones that are antagonistic to insulin, such as adrenocortical hormone, glucagon, and norepinephrine, making it more difficult for diabetic patients to control BG. Studies have shown that [24], compared with the nondiabetic population, people with T2DM are more susceptible to subclinical and clinical symptoms of anxiety. Traditionally, anxiety has been related to unfavorable metabolic outcomes and elevated medical complications in T2DM patients and has an adverse impact on their self-awareness of health and QOL. By observing the Morisky and ESCA scores of patients in the two cohorts, we found that the treatment compliance and self-care ability improved notably after intervention, with better parameters in RG, suggesting that CNI could effectively improve patients' self-management ability and treatment compliance. The CNI model has been used for multidisciplinary therapy of mental health problems and chronic diseases and has been proved to be successful in managing the pathology of depression,

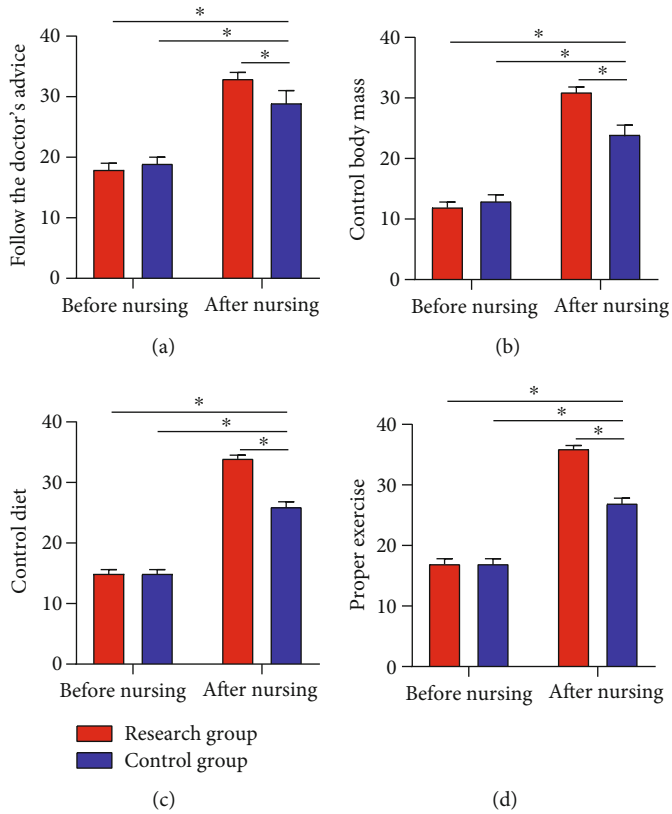

Figure 4: Morisky scores pre- and postintervention. (a) After intervention, the RG got a notably higher score of following the doctor's advice than the CG. (b) After intervention, the RG got a notably higher score of body mass control than the CG. (c) After intervention, the RG got notably higher scores of diet control than the control. (d) After intervention, the RG got a notably higher score of proper exercise than the CG. Note: $^{*}P < 0.05$ between the two groups.

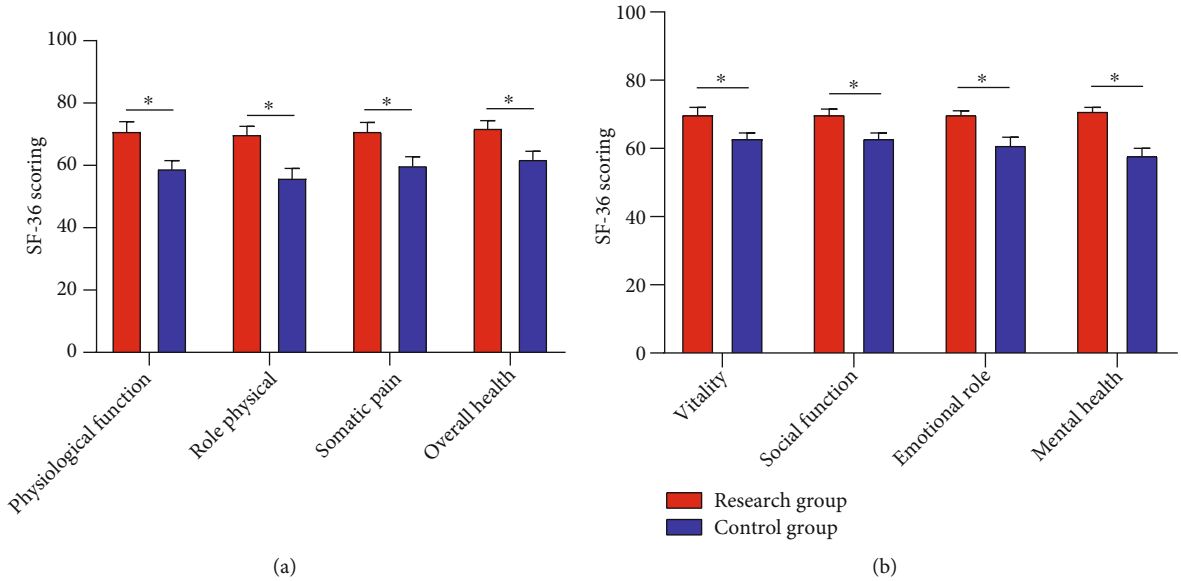

Figure 5: SF-36 scores postintervention. (a) The RG got notably higher physical health scores of SF-36 than the CG. (b) The RG got notably higher mental health scores of SF-36 than the CG. Note: $^{*}P < 0.05$ between the two groups.

which accompanies diabetes in most cases [25]. With the transformation of modern medical mode and the raise of people's health awareness, treatment is to improve and prolong the survival of patients and also to improve their QOL. CNI is a novel nursing mode, which emphasizes nurses as supporters and educators in the medical sector and deeply

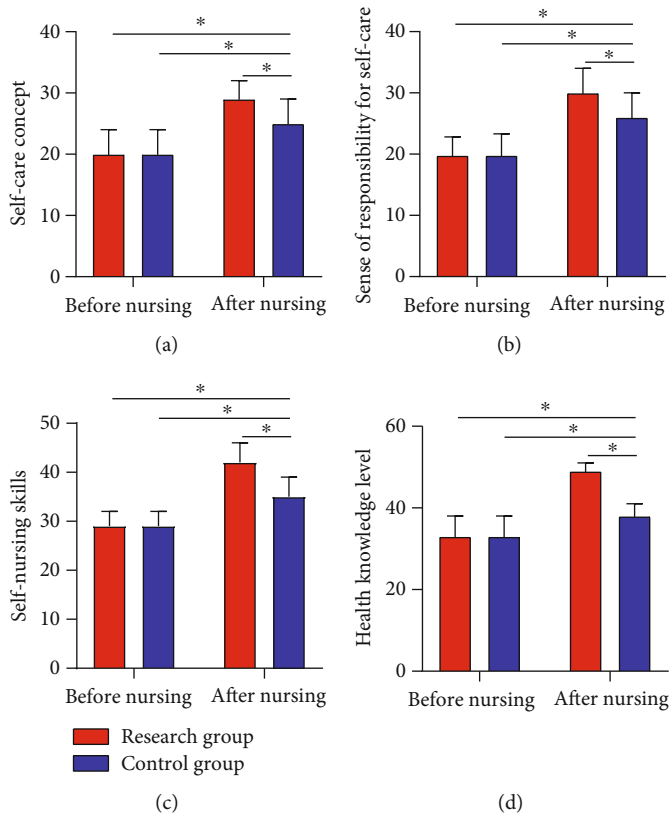

Figure 6: ESCA scores pre- and postintervention. (a) After intervention, the RG got notably higher scores of self-care concept than the CG. (b) The RG got notably higher scores of sense of responsibility for self-care than the CG after intervention. (c) The RG got notably higher scores of self-nursing skills than the CG after intervention. (d) The RG got notably higher scores of health knowledge level than the CG after nursing intervention. Note: $^{*}P < 0.05$ between the two groups.

Table 2: Nursing satisfaction scores (n (%)).

Groups	Number of cases	Satisfied	Relatively satisfied	Dissatisfied	Satisfaction (%)
RG	37	30 (81.08)	6 (16.22)	1 (2.70)	36 (97.30)
CG	35	8 (22.86)	10 (28.57)	17 (48.57)	18 (51.43)
t	—	—	—	—	20.180
P	—	—	—	—	0.001

reflects the crucial part of patients' involvement in nursing work. In addition to accountability nursing, CNI also covers other dimensions like psychological nursing and health education, aimed at encouraging patients to take part in nursing work and clinical therapy, giving enough play to patients' self-care ability, and improving their enthusiasm as well as initiative in treatment [26, 27]. Lastly, we used the self-made nursing satisfaction questionnaire of our hospital for evaluating patient satisfaction toward nursing and found 97.30% and 51.43% of nursing satisfaction in RG and CG, respectively. The results indicate that CNI is unanimously appreciated by the patients and their families, which proved the practicability of CNI and its enormous success in clinical practice future.

Based on the above research, we preliminarily proved the ability of CNI in validly controlling the BG level of patients with diabetes and improving their self-care ability. However, there are still some deficiencies. First, this study only adopts routine nursing as a control instead of other care models out there, which is relatively single. Second, patient follow-up should be supplemented in the future research design. All in all, more nursing models will be included as controls, and prognostic follow-up of patients will be added in future studies, so as to supplement the comprehensiveness of our research and support our research results.

To sum up, given that the CNI model can strongly boost the self-care ability of T2DM patients, effectively control the BG level, and improve their treatment compliance, it is worth popularizing in clinical nursing of T2DM.

Data Availability

The datasets used during the present study are available from the corresponding author upon reasonable request.

Conflicts of Interest

The authors declare that they have no conflict of interest.

References

[1] American Diabetes Association, "Standards of medical care in diabetes—2016 abridged for primary care providers," *Clinical Diabetes*, vol. 34, no. 1, pp. 3–21, 2016.

[2] American Diabetes Association, "Diagnosis and classification of diabetes mellitus," *Diabetes Care*, vol. 33, Supplement 1, pp. S62–S69, 2010.

[3] American Diabetes Association, "2. Classification and diagnosis of diabetes," *Diabetes Care*, vol. 38, Supplement_1, pp. S8–S16, 2015.

[4] B. Zinman, C. Wanner, J. M. Lachin et al., "Empagliflozin, cardiovascular outcomes, and mortality in type 2 diabetes," *The New England Journal of Medicine*, vol. 373, no. 22, pp. 2117–2128, 2015.

[5] A. S. Go, D. Mozaffarian, V. L. Roger et al., "Executive summary: heart disease and stroke statistics–2013 update: a report from the American Heart Association," *Circulation*, vol. 127, no. 1, pp. 143–152, 2013.

[6] P. O. Carlsson, E. Schwarcz, O. Korsgren, and K. le Blanc, "Preserved β-cell function in type 1 diabetes by mesenchymal stromal cells," *Diabetes*, vol. 64, no. 2, pp. 587–592, 2015.

[7] S. V. Bădescu, C. Tătaru, L. Kobylinska et al., "Effects of caffeine on locomotor activity in streptozotocin-induced diabetic rats," *Journal of Medicine and Life*, vol. 9, no. 3, pp. 275–279, 2016.

[8] W. Li, E. Huang, and S. Gao, "Type 1 diabetes mellitus and cognitive impairments: a systematic review," *Journal of Alzheimer's Disease*, vol. 57, no. 1, pp. 29–36, 2017.

[9] W. D. Strain and P. M. Paldánius, "Diabetes, cardiovascular disease and the microcirculation," *Journal of Diabetes and its Complications*, vol. 17, no. 1, p. 57, 2018.

[10] K. Pfaff and A. Markaki, "Compassionate collaborative care: an integrative review of quality indicators in end-of-life care," *BMC Palliative Care*, vol. 16, no. 1, p. 65, 2017.

[11] N. Han, S. H. Han, H. Chu et al., "Service design oriented multidisciplinary collaborative team care service model development for resolving drug related problems," *PLoS One*, vol. 13, no. 9, article e0201705, 2018.

[12] H. Y. Wu, H. S. Chao, H. C. Shih, C. C. Shih, and S. C. Chang, "The impact of open to collaborative care model in cardiovascular surgical unit," *Journal of the Chinese Medical Association*, vol. 81, no. 1, pp. 64–69, 2018.

[13] S. M. Fuller, K. A. Koester, X. A. Erguera et al., "The collaborative care model for HIV and depression: patient perspectives and experiences from a safety-net clinic in the United States," *SAGE Open Medicine*, vol. 7, 2019.

[14] E. Baker, R. Gwernan-Jones, N. Britten et al., "Refining a model of collaborative care for people with a diagnosis of bipolar, schizophrenia or other psychoses in England: a qualitative formative evaluation," *BMC Psychiatry*, vol. 19, no. 1, p. 7, 2019.

[15] D. Dabelea, A. Rewers, J. M. Stafford et al., "Trends in the prevalence of ketoacidosis at diabetes diagnosis: the search for diabetes in youth study," *Pediatrics*, vol. 133, no. 4, pp. e938–e945, 2014.

[16] D. E. Morisky, L. W. Green, and D. M. Levine, "Concurrent and predictive validity of a self-reported measure of medication adherence," *Medical Care*, vol. 24, no. 1, pp. 67–74, 1986.

[17] American Diabetes Association, "Diagnosis and classification of diabetes mellitus," *Diabetes Care*, vol. 37, Supplement 1, pp. S81–S90, 2014.

[18] World Health Organization Global Status Report on Noncommunicable Diseases, *Attaining the nine global noncommunicable diseases targets; a shared responsability.*, 2014.

[19] "Global Health Estimates 2015: Deaths by cause age sex by country and by region 2000-2015," 2016, http://www.who.int/entity/healthinfo/global_burden_disease/GHE2015_Deaths_Global_2000_2015.xls.

[20] World Health Organization, "Global Report on Diabetes," 2016, http://www.who.int/diabetes/global-report/en/.

[21] M. J. Fowler, "Microvascular and macrovascular complications of diabetes," *Clinical Diabetes*, vol. 26, no. 2, pp. 77–82, 2008.

[22] A. Beck, J. M. Boggs, A. Alem et al., "Large-scale implementation of collaborative care management for depression and diabetes and/or cardiovascular disease," *The Journal of the American Board of Family Medicine*, vol. 31, no. 5, pp. 702–711, 2018.

[23] D. M. Dumont, C. Pizzonia, S. Poulin, and P. Meddaugh, "Diabetes quality of care and maintenance in New England: can cross-state collaboration move us forward?," *Preventing Chronic Disease*, vol. 15, article E165, 2018.

[24] A. Bickett and H. Tapp, "Anxiety and diabetes: innovative approaches to management in primary care," *Experimental Biology and Medicine*, vol. 241, no. 15, pp. 1724–1731, 2016.

[25] C. Tovilla-Zárate, I. Juárez-Rojop, Y. Peralta Jimenez et al., "Prevalence of anxiety and depression among outpatients with type 2 diabetes in the Mexican population," *PLoS One*, vol. 7, no. 5, article e36887, 2012.

[26] S. V. Arnold, A. Goyal, S. E. Inzucchi et al., "Quality of care of the initial patient cohort of the Diabetes Collaborative Registry®," *Journal of the American Heart Association*, vol. 6, no. 8, 2017.

[27] S. Wu, K. Ell, H. Jin et al., "Comparative effectiveness of a technology-facilitated depression care management model in safety-net primary care patients with type 2 diabetes: 6-month outcomes of a large clinical trial," *Journal of Medical Internet Research*, vol. 20, no. 4, article e147, 2018.

Hindawi
Disease Markers
Volume 2022, Article ID 5845627, 21 pages
https://doi.org/10.1155/2022/5845627

Research Article

KLF4 Affects Acute Renal Allograft Injury via Binding to MicroRNA-155-5p Promoter to Regulate ERRFI1

Jiquan Zhao,[1] Jiqiang Zhao,[2] Zhaohui He,[1] Minzhuan Lin,[2] and Feng Huo[3]

[1]*Department of Urological Surgery, The Eighth Affiliated Hospital of Sun Yat-sen University (Shenzhen Futian), Shenzhen, 518033 Guangdong, China*
[2]*Department of Organ Transplantation, The Third Affiliated Hospital of Guangzhou Medical University, 3 Duobao Road, Liwan District, Guangzhou, 510150 Guangdong, China*
[3]*Department of Hepatobiliary Surgery, General Hospital of the PLA Southern Theater Command, Guangzhou, 510010 Guangdong, China*

Correspondence should be addressed to Jiqiang Zhao; jiqianggzmu@163.com

Received 14 January 2022; Revised 12 February 2022; Accepted 15 February 2022; Published 17 March 2022

Academic Editor: Zhaoqi Dong

Kruppel-like factor 4 (KLF4) owns the promising potential in treating kidney injury, which inevitably occurs during renal allograft. Given that, this research targets to unveil KLF4-oriented mechanism from microRNA-155-5p/ERBB receptor feedback inhibitor 1 (miR-155-5p/ERRFI1) axis in acute renal allograft injury. Mice were injected with miR-155-5p-related sequences before acute renal allograft modeling. Afterwards, serum inflammation, along with oxidative stress, renal tubular injury, and apoptosis in renal tissues were detected. HK-2 cells were processed by hypoxia/reoxygenation (H/R) and transfected with miR-155-5p- or ERRFI1-related sequences, after which cell proliferation and apoptosis were measured. KLF4, miR-155-5p, and ERRFI1 expressions and their interaction were tested. KLF4 and miR-155-5p levels were enhanced, and ERRFI1 level was repressed in mice after acute renal allograft and in H/R-treated HK-2 cells. KLF4 bound to the promoter of miR-155-5p. Depleting miR-155-5p reduced serum inflammation and attenuated oxidative stress, renal tubular injury, and apoptosis in mice with acute renal allograft injury. Downregulating miR-155-5p facilitated proliferation and repressed apoptosis of H/R-treated HK-2 cells. miR-155-5p targeted ERRFI1. Knocking down ERRFI1 antagonized the effects of downregulated miR-155-5p on acute renal allograft injury, as well as on H/R-treated HK-2 cell proliferation and apoptosis. A summary displays that silencing KLF4 suppresses miR-155-5p to attenuate acute renal allograft injury by upregulating ERRFI1, which provides a way to control acute renal allograft injury.

1. Introduction

Renal transplantation is the best treatment to improve the survival rate of patients with end-stage kidney disease [1]. Unfortunately, acute kidney injury (AKI), along with subsequent chronic allograft dysfunction, occurs unexpectedly during renal allograft, which may eventually progress to renal function loss [2]. Ischemic AKI is the most common complication following renal transplantation, which may be resulted from ischemia/reperfusion injury (I/RI) [3]. Moreover, current therapy is impossible to immediately predict acute renal allograft injury after renal transplantation [4]. Hence, the potential targets to manage acute renal allograft injury are urgently asked.

Kruppel-like factor 4 (KLF4) has been suggested as a therapeutic target in the context of chronic kidney disease [5]. Investigated by a late research, an increase presents in KLF4 expression in the kidneys of mice after I/RI [6]. Functionally, KLF4 downregulation has been proved to attenuate renal function deterioration after I/RI [7]. There is a self-activating and feedback mechanisms between transcription factors (including KLF4) and miRNAs [8], and KLF4 positively modulates miR-200b and miR-183 levels [9]. As the reported researches proved, regulation of miRNA is

conducive to attenuate I/RI during renal allograft, such as miR-378 [10]. As to miR-155, it is implied that overexpressed miR-155 is substantially connected with abnormality in human solid organ allografts and rat renal allografts [11]. Actually, enhanced miR-155 level in plasma of renal allograft recipients is linked to renal dysfunction [12]. Moreover, abnormally expressed miR-155 is promoted to stimulate inflammation and apoptosis of tubular epithelial cells in AKI [13]. In fact, the abundance of miR-155 level in hypoxia-reoxygeneration- (H/R-) treated cells disrupts the balance of renal cell apoptosis and proliferation [14]. KLF4 as a transcription factor has not yet been studied as to regulation of miR-155-5p.

ERBB receptor feedback inhibitor 1 (ERRFI1) has been studied as a target of miRNAs to modulate AKI, and inhibited ERRFI1 deteriorates the development of AKI through interfering renal cell apoptosis and inflammation [15]. Moreover, ERRFI1 has the ability to mediate IR/I-induced oxidative stress and apoptosis [16]. To our best knowledge, a little few study has revealed the combined function of miR-155-5p and ERRFI1 in diseases.

Consulted from the aforementioned researches, we know that KLF4 is of therapeutic significance in treating kidney injury. Given that, we would like to figure out whether mediating KLF4 could manage acute renal allograft injury from the axis of miR-155-5p/ERRFI1 and hope to provide a theoretical reference for treat kidney injury.

2. Methods and Materials

2.1. Ethics Statement. This study was approved by the ethics committee of the Eighth Affiliated Hospital of Sun Yat-sen University (Shenzhen Futian). Animal treatments were reviewed and supervised by the Animal Ethics of the Eighth Affiliated Hospital of Sun Yat-sen University (Shenzhen Futian). The sufferings for animals were minimized.

2.2. Establishment of Acute Renal Allograft Model and Animal Treatment. Female C57BL/6 mice (14 weeks old, 24-28 g) were accessible from SLAC Laboratory Animal (Shanghai, China). There were 25 donor mice and 25 receptor mice. A model of renal allograft was established as previously described [17]. In short, a midline incision was performed on mice who had been anesthetized by 2% isoflurane (RWD Life Science Co., Ltd., Shenzhen, China). The left kidney, aorta, inferior vena cava, and ureter of donor mice were cut off under a microscope. The donor kidney was transplanted below the primary renal artery in the recipient mice after left nephrectomy, the inferior renal artery, and inferior vena cava were anastomosed perfectly with the recipient mice. Then, the ureter was anastomosed with the bladder to reconstruct urethra. After renal allograft, mice were treated with long-term ischemia (cold ischemia for 60 min and warm ischemia for 60 min) to induce ischemic injury of allograft. The mice for sham operation were treated with left kidney reanastomosis after left nephrectomy. Antagomir-negative control (NC), miR-155-5p antagomir, and si-ERRFI1 (2.5 mg/kg) were intravenously injected into mice before renal allograft ($n = 5$/group). On the next day, a model of acute renal allograft was established [18].

Table 1: Primer sequences.

Genes	Primer sequences
KLF4	5′-GCGGGAAGGGAGAAGACAC-3′
	5′-GGGGAAGACGAGGATGAAGC-3′
miR-155-5p	5′-GCTTCGGTTAATGCTAATCGTG-3′
	5′-CAGAGCAGGGTCCGAGGTA-3′
ERRFI1	5′-CACGGCGCAGCCTCACTCTG-3′
	5′-CTTGGGGCAGGGGCTCTTGAC-3′
GAPDH	5′-TCCCATCACCATCTTCCA-3′
	5′-CATCACGCCACAGTTTTCC-3′
U6	5′-GGAACGATACAGAGAAGATTAGC-3′
	5′-TGGAACGCTTCACGAATTTGCG-3′

Note: KLF4: Kruppel-like factor 4; miR-155-5p: microRNA-155-5p; ERRFI1: ERBB receptor feedback inhibitor 1; GAPDH: glyceraldehyde-3-phosphate dehydrogenase.

2.3. Enzyme-Linked Immunosorbent Assay (ELISA). After 10 d [19], mice were anesthetized to obtain serums, in which proinflammatory cytokine interferon- (IFN-) γ, tumor necrosis factor- (TNF-) α, and interleukin- (IL-) 2 contents were evaluated by an ELISA kit (R&D Systems, Minneapolis, MN, USA) as the biomarkers of allograft function.

2.4. Renal Function Assessment. Serum creatinine content was measured by sarcosine oxidase enzymatic assay (Kehua Dongling Diagnostic Products, Shanghai, China) while estimated glomerular filtration rate (eGFR) by abbreviated Modification of Diet in Renal Disease equation. The blood samples were subjected to centrifugation at 3600 rpm to take the supernatant, which was reacted with a mixture of creatine hydrolase, sarcosine oxidase, and catalase. The optical density value ($OD_{546\ nm}$) was measured.

2.5. Hematoxylin-Eosin (H&E) Staining. Mice were euthanized to harvest their kidneys. Specially, the mice were anesthetized by 2% isoflurane and then were decapitated and killed. One-half of the renal allografts was immediately fixed in formalin buffer and embedded in paraffin, while the other half was frozen in liquid nitrogen. H&E staining was utilized to evaluate the renal tissue sections.

2.6. Transferase-Mediated Deoxyuridine Triphosphate-Biotin Nick End Labeling (TUNEL) Staining. Cell apoptosis was assessed by TUNEL staining (Roche, Mannheim, Germany). TUNEL-positive cells were counted in five random fields under a fluorescence microscope. Apoptosis index was measured as the percentage of TUNEL-positive cells in total nucleus.

2.7. Oxidative Stress-Related Parameter Detection. Oxidative stress in the kidneys was evaluated by measuring malondialdehyde (MDA) content and superoxide dismutase (SOD)

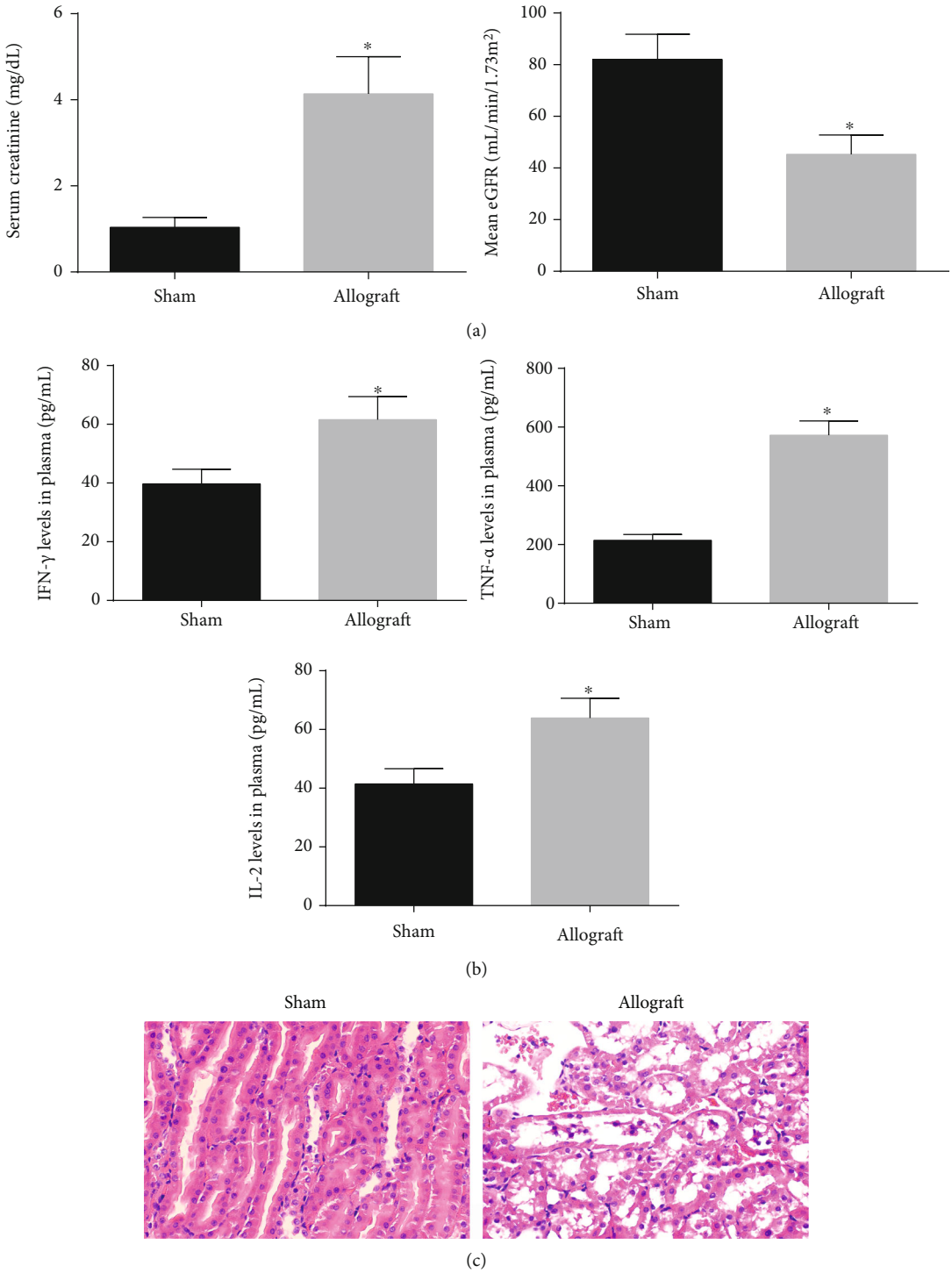

Figure 1: Continued.

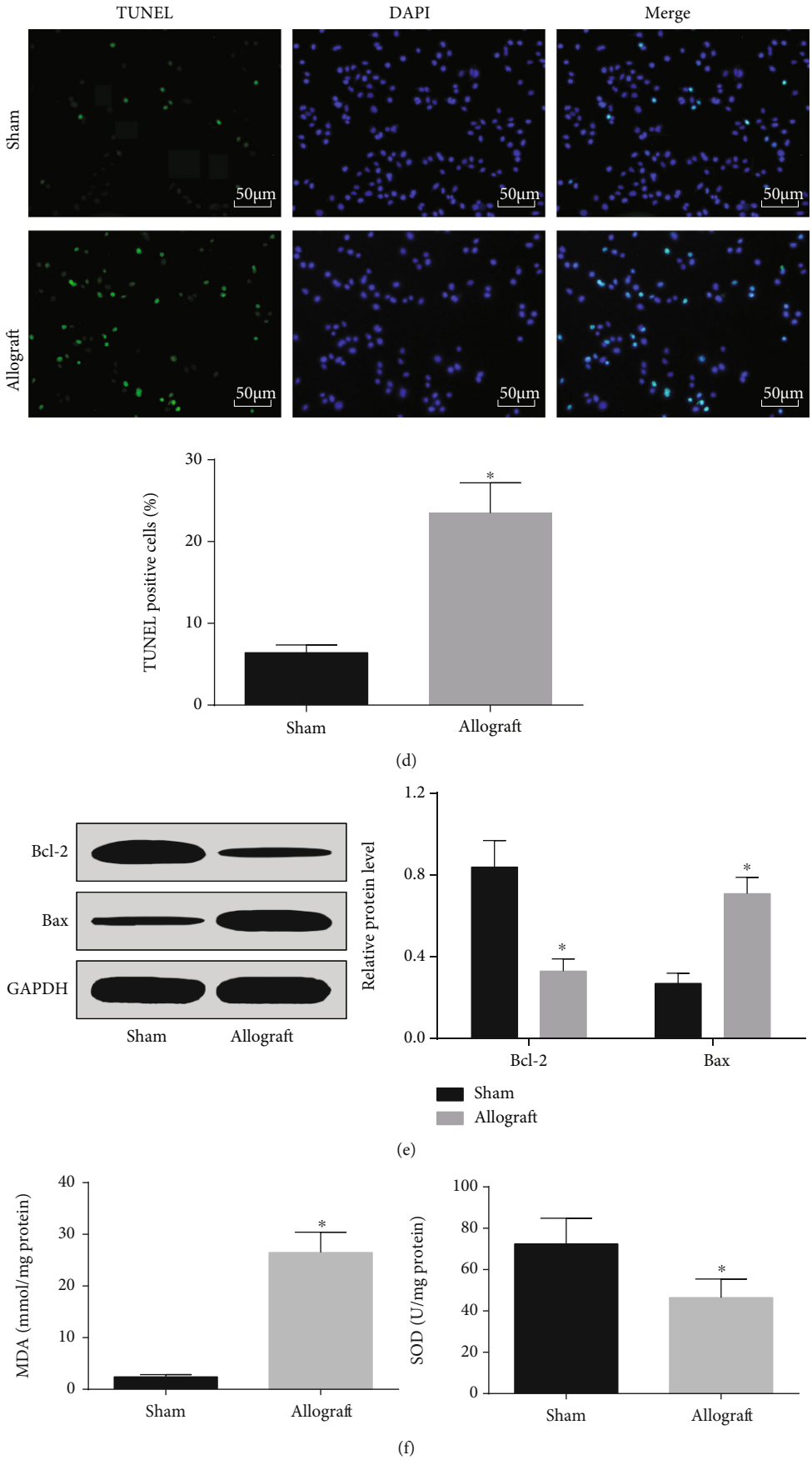

Figure 1: Continued.

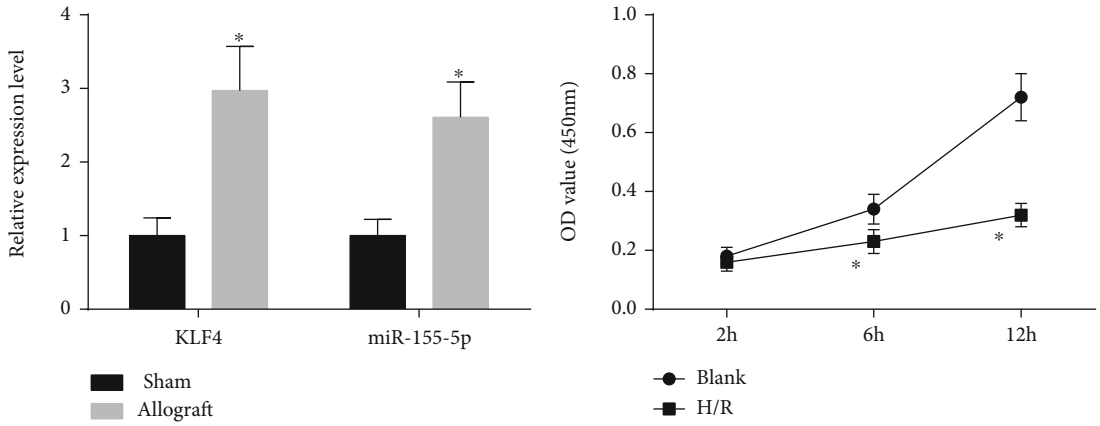

(g) (h)

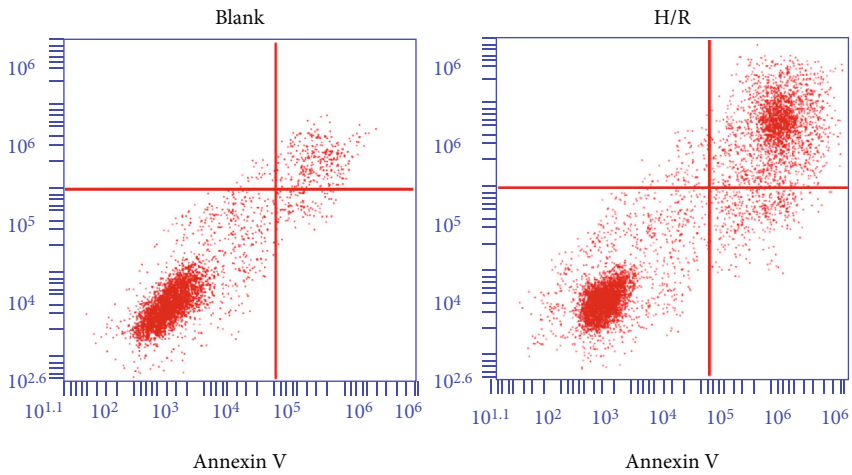

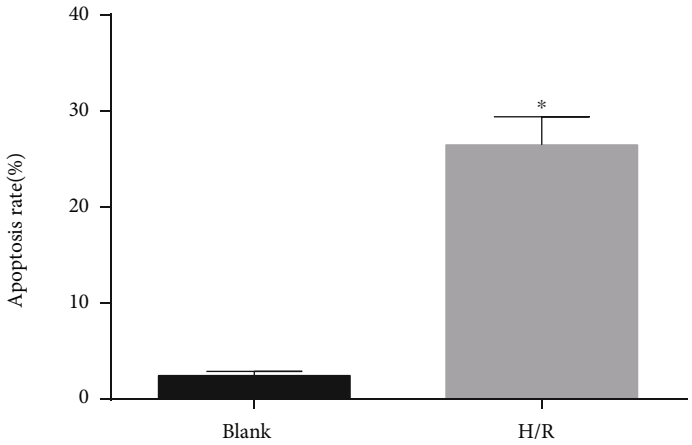

(i)

Figure 1: Continued.

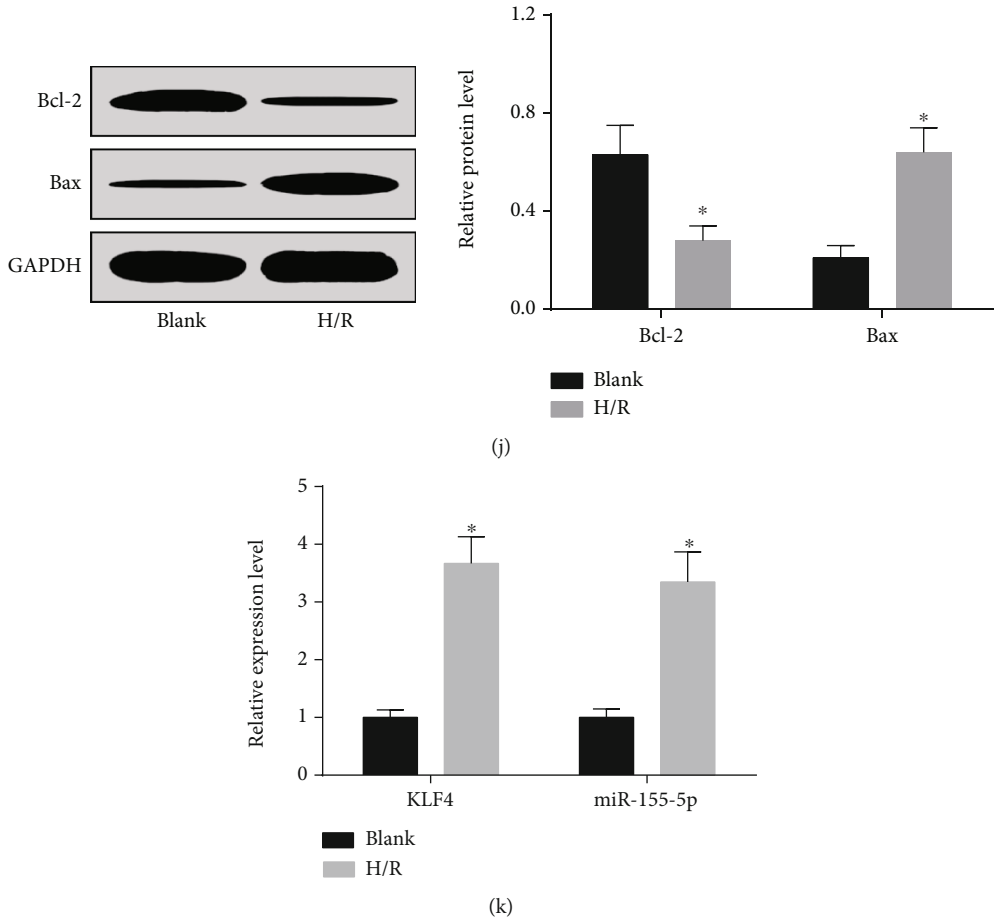

Figure 1: KLF4 and miR-155-5p are overexpressed in mice with acute renal allograft injury. (a) Serum creatinine and eGFR contents in mice. (b) ELISA detected serum IFN-γ, TNF-α, and IL-2 contents in mice. (c) H&E staining detected kidney injury of mice. (d) TUNEL staining detected renal tubular apoptosis of mice. (e) Western blot detected Bax and Bcl-2 protein expression in renal tissues of mice. (f) MDA content and SOD activity in renal tissues of mice. (g) RT-qPCR detected KLF4 and miR-155-5p expressions in renal tissues of mice. (h) CCK-8 assay detected proliferation of H/R-treated HK-2 cells. (i) Flow cytometry detected the apoptosis rate of H/R-treated HK-2 cells. (j) Western blot detected Bax and Bcl-2 protein expressions in H/R-treated HK-2 cells. (k) RT-qPCR detected KLF4 and miR-155-5p expressions in H/R-treated HK-2 cells. The data were expressed as mean ± standard deviation; $^*P < 0.05$ compared with the sham/blank group. (a–g) $n = 5$ and (h–k) $n = 3$.

activity. MDA content was measured with a kit (Beyotime, Shanghai, China) via thiobarbituric acid method and the $OD_{535\ nm}$ value was determined. The SOD assay kit (Beyotime) was applied to test SOD activity in the kidney [20].

2.8. Cell Culture and Modeling. Immortalized human renal proximal tubule (HK-2) cells, with phenotypic and functional characteristics of proximal tubule cells, were obtained from the American Type Culture Collection (VA, USA). HK-2 cells were hatched in a culture system of Dulbecco's Modified Eagle Medium/F12 supplemented with 10% fetal bovine serum (Invitrogen, Carlsbad, USA), 100 U/mL penicillin G, 100 μg/mL streptomycin and 0.25 μg/mL amphotericin B (Invitrogen). Then, the cells were cultivated in a hypoxic environment (1% O_2, 94% N_2, and 5% CO_2) for 24 h and then in an aerobic environment (21% O_2, 74% N_2, and 5% CO_2) for 3 h to establish an *in vitro* H/R model [21].

2.9. Cell Transfection. Overexpression- (Oe-) KLF4, oe-negative control (NC), sh-KLF4, sh-NC, inhibitor-NC, miR-155-5p inhibitor, and si-ERRFI1 were synthesized by RiboBio (Guangzhou, China) and transfected into cells via Lipofectamine 2000 (Invitrogen). The transfection efficiency was verified 48 h after cell transfection. The cells that had been transfected for 48 h were collected for *in vitro* experiments.

2.10. Cell Counting Kit- (CCK-) 8 Assay. CCK-8 assay was applied to assess the proliferation of HK-2 cells. HK-2 cells (10 μL/well) were added with CCK-8 solution at the 2nd, 6th, and 12th hour, respectively, and incubated for another 2 h. The $OD_{450\ nm}$ value was recorded by a microplate reader (Bio-Rad, Hercules, USA).

2.11. Flow Cytometry. HK-2 cells resuspended in phosphate-buffered saline were successively hatched with Annexin V-fluorescein isothiocyanate (5 μL) and with propidium iodide

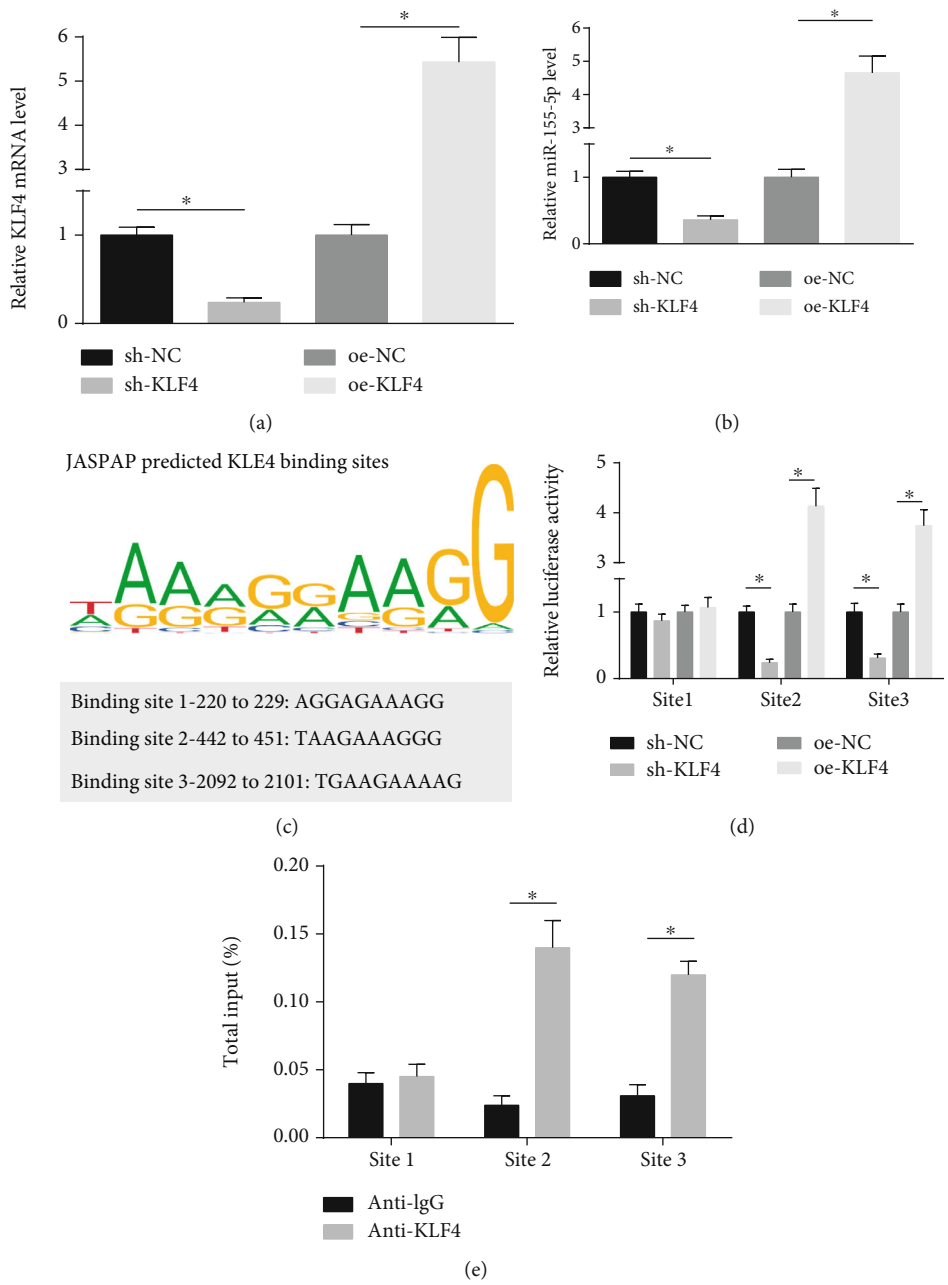

Figure 2: KLF4 binds to miR-155-5p promoter. (a and b) RT-qPCR detected KLF4 and miR-155-5p mRNA expressions in HK-2 cells. (c) JASPAR predicted the binding sites of KLF4 on miR-155-5p promoter. (d) Luciferase activity of oe-KLF4 and sh-KLF4 on miR-155-5p promoter reporters. (e) ChIP assay detected the site of KLF4 on miR-155-5p promoter. The data were expressed as mean ± standard deviation; ∗ represented $P < 0.05$; $N = 3$.

(10 μL) (both from Beyotime) without light exposure. Cell apoptosis was examined by a flow cytometer (FACSCalibur; BD Biosciences, Franklin Lakes, USA).

2.12. Reverse Transcription Quantitative Polymerase Chain Reaction (RT-qPCR). Total RNA was extracted from tissues and cells by TRIzol reagent (Invitrogen). Total RNA (1 μg) was subjected to reverse transcription by Superscript II reverse transcriptase (Invitrogen) and random primer oligonucleotides (Invitrogen). The gene-specific TaqMan miRNA detection probe (Applied Biosystems, Foster City, USA) was applied to analyze miRNA expression. Total RNA (1 mg) was reverse-transcribed through avian myeloblastosis virus (Takara, Kyoto, Japan) and stemi-loop RT primers (Applied Biosystems). The primers are shown in Table 1. Real-time PCR was conducted via 7900 HT Real-time PCR system, and gene expression levels were calculated with $2^{-\Delta\Delta Ct}$ method. Briefly, after an initial denaturation step at 95°C for 3 min, the amplifications were carried out with 40 cycles at a melting temperature of 95°C for 15 s and an annealing

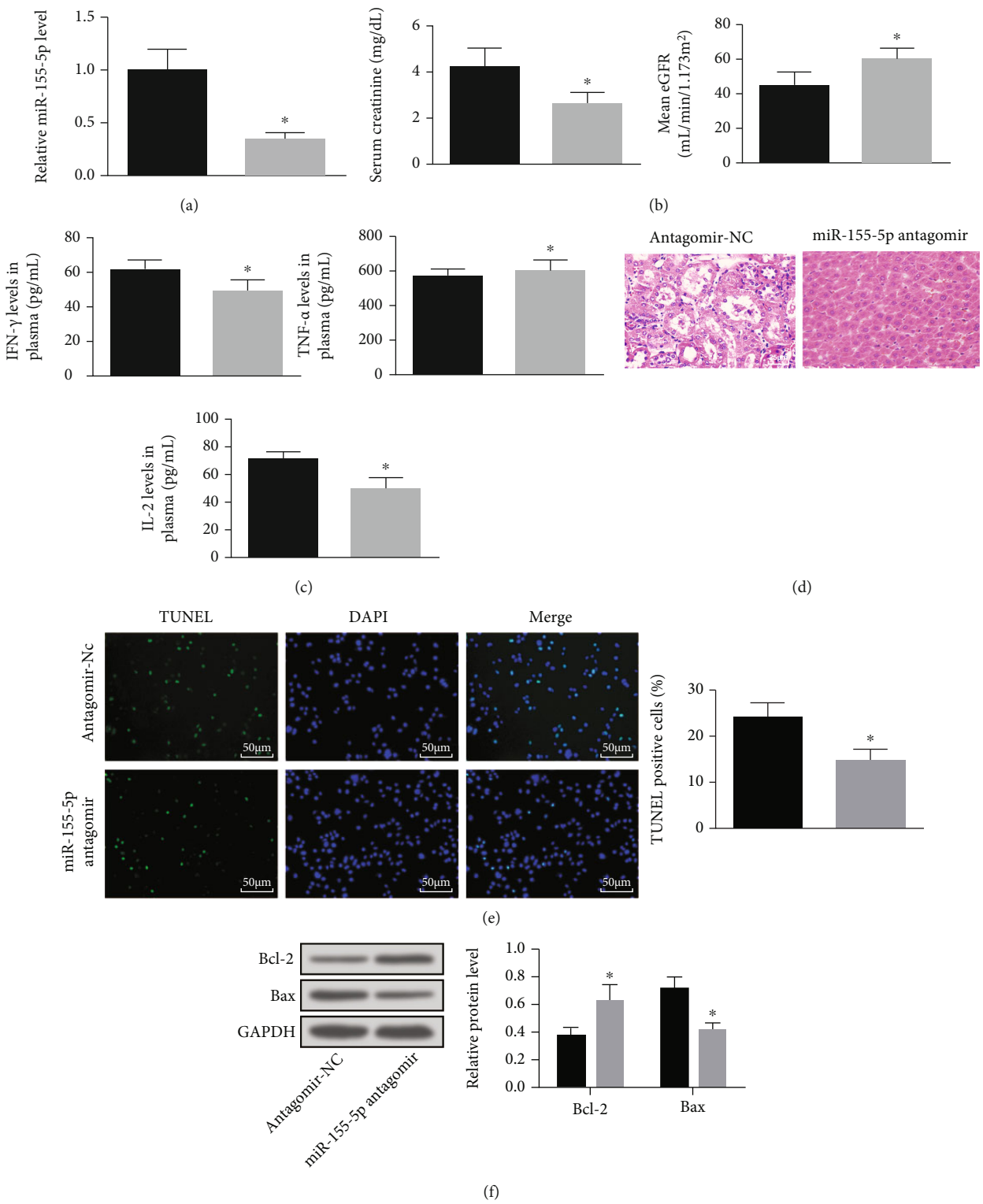

Figure 3: Continued.

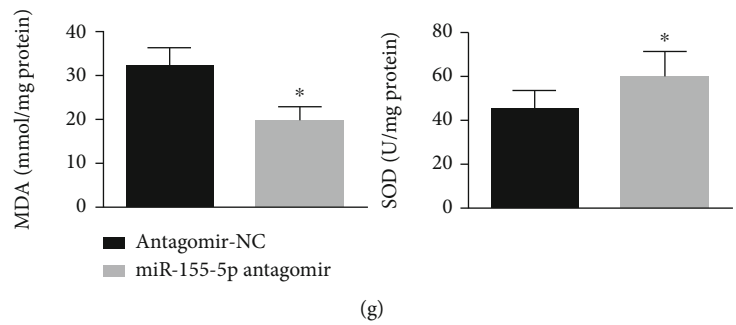

Figure 3: Depleting miR-155-5p attenuates acute renal allograft injury in mice. (a) RT-qPCR detected miR-155-5p expression in renal tissues of mice. (b) Serum creatinine and eGFR contents of mice. (c) ELISA detected serum IFN-γ, TNF-α, and IL-2 contents in mice. (d) H&E staining detected kidney injury of mice. (e) TUNEL staining detected renal tubular apoptosis of mice. (f) Western blot detected Bax and Bcl-2 protein expression in renal tissues of mice. (g) MDA content and SOD activity in renal tissues of mice. The data were expressed as mean ± standard deviation; $^*P < 0.05$ compared with the antagomir-NC group, $n = 5$.

temperature of 62°C for 34 s. KLF4 and ERRFI1 expressions were normalized to glyceraldehyde-3-phosphate dehydrogenase (GAPDH) while miR-155-5p expression to U6.

2.13. Western Blot Assay. Total protein of tissues and cells was extracted, of which the concentration was measured by bicinchoninic acid kit (Boster, Wuhan, China). Boiled (30 μg/well) with the loading buffer at 95°C, protein samples were isolated by 10% polyacrylamide gel (Boster), electroblotted onto polyvinylidene fluoride membrane, and sealed in 5% bovine serum albumin. Afterwards, the membrane was probed with primary antibodies Bax, Bcl-2, ERRFI1 (1 : 1000, Abcam, Cambridge, UK) and GAPDH (1 : 2000, Jackson Immuno Research, Pennsylvania, USA), and peroxidase-labeled secondary antibody (1 : 500, Jackson Immuno Research). Processed by the Odyssey dual-color infrared fluorescence scanning imaging system, the protein bands were assessed by Quantity One image analysis software to measure the gray value. The ratio of gray value in each target band to that in internal control band was measured.

2.14. Dual Luciferase Reporter Gene Assay. ERRFI1 luciferase vector was cloned into psiTM-Check2-control vector (GenePharma, Shanghai, China). The wild-type (WT) psitm-check2-ERRFI1-3′-untranslated region containing the predicted miR-155-5p site was generated. A mutant (MUT) miR-155-5p binding site plasmid was also cloned. All cloned plasmids were identified by sequencing (TsingKe, China). HK-2 cells were cotransfected with ERRFI1 WT or MUT and miR-155-5p mimic or mimic-NC via Lipofectamine 2000 (Thermo Fisher Scientific, MA, USA). The miR-155-5p promoter containing KLF4 binding sites was cloned into pGL3-Basic reporter vectors (Promega, WI, USA). HK-2 cells were cotransfected with luciferase vectors and high/low KLF4. A dual luciferase reporter system (Promega) was employed to measure luciferase activities.

2.15. Chromatin Immunoprecipitation (ChIP) Assay. The binding affinity of KLF4 and miR-155-5p was determined by ChIP assay based on the protocol (Beyotime). KLF4 level was increased or decreased by oe-KLF4 or sh-KLF4 vectors, respectively. HK-2 cells (1×10^6 cells) were processed by ultrasound for 48 cycles, after which cell supernatant was extracted by centrifugation. Followed by that, the beads were reacted with the target protein antibody or immunoglobulin G (IgG). The antibody-bound beads were incubated with the sample to bind the antibody to the target protein. KLF4 chromatin complex was immunoprecipitated by the anti-KLF4 antibody and then the target protein was eluted. In the experiment, anti-IgG (Santa Cruz, CA, USA) served as a control.

2.16. Statistical Analysis. The data were expressed as mean ± standard deviation. SPSS 22.0 (IBM, Armonk, USA) was utilized to data evaluation. Discrepancies between the two groups were assessed by t-test while those among multiple groups by one-way analysis of variance and Tukey's test. With $P < 0.05$, statistical significance was registered.

3. Results

3.1. KLF4 and miR-155-5p Are Overexpressed in Acute Renal Allograft Injury. Renal function was evaluated by detecting serum creatinine and eGFR. In mice with acute renal allograft, serum creatinine level was increased while eGFR level was decreased. At the same time, IFN-γ, TNF-α, and IL-2 contents in serum were detected to increase in mice after acute renal allograft (Figures 1(a) and 1(b)).

Detected by H&E staining, it was observed that renal tubules were severely damaged, some cells were arranged disorderly, renal tubules were dilated, and vacuoles were formed in mice with renal allograft (Figure 1(c)). Revealed by TUNEL staining and Western blot, mice with renal allograft showed increased TUNEL-positive rate and Bax level and reduced Bcl-2 level in renal tissues (Figures 1(d) and 1(e)), indicating cell apoptosis in mice after acute renal allograft. Oxidative stress damage of the kidney was measured by detecting MDA content and SOD activity. It was displayed that MDA content was heightened and SOD activity was impaired in mice with renal allograft injury (Figure 1(f)).

KLF4 is upregulated in AKI and knocking out KLF4 attenuates renal dysfunction and interstitial fibers in I/R

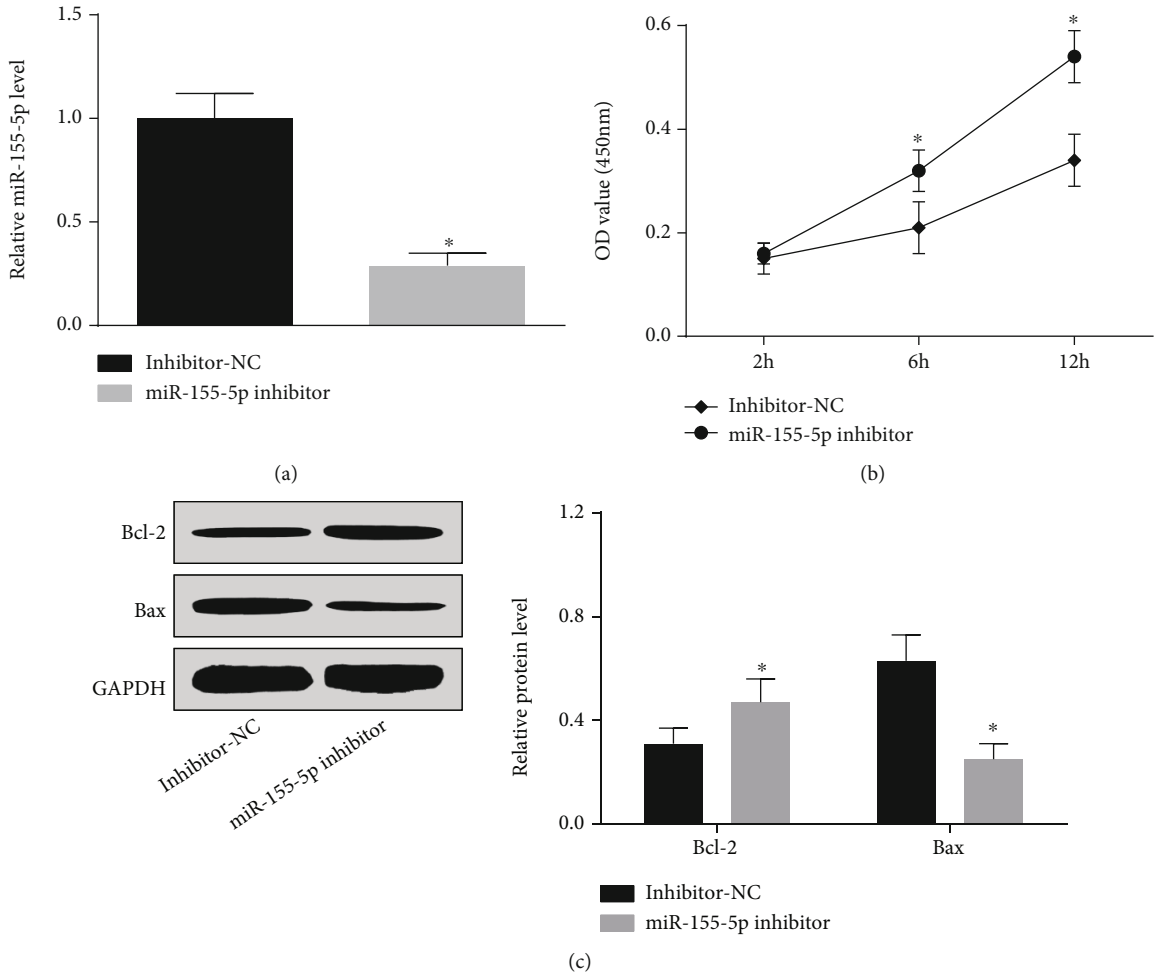

Figure 4: Continued.

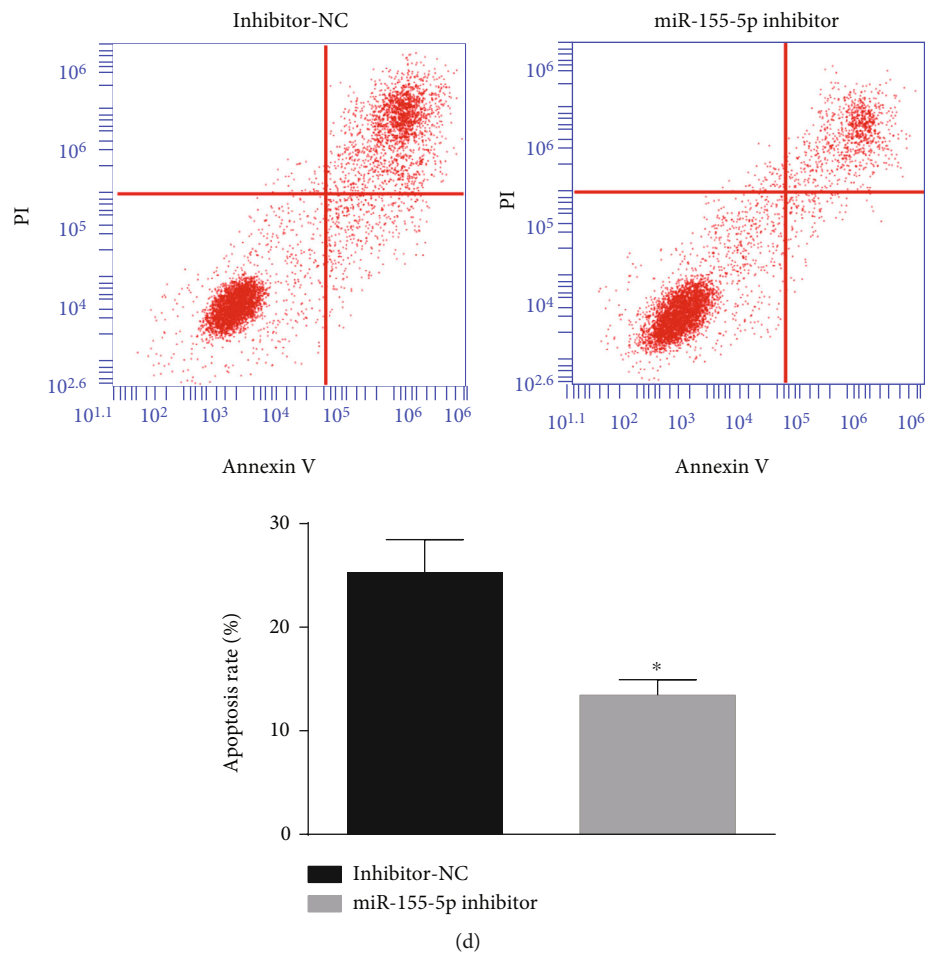

Figure 4: Downregulating miR-155-5p facilitates H/R-treated HK-2 cell proliferation and represses apoptosis. (a) RT-qPCR detected miR-155-5p expression in H/R-treated HK-2 cells. (b) CCK-8 assay detected the proliferation of H/R-treated HK-2 cells. (c) Flow cytometry detected the apoptosis rate of H/R-treated HK-2 cells. (d) Western blot detected Bax and Bcl-2 expressions in H/R-treated HK-2 cells. The data were expressed as mean ± standard deviation; $^*P < 0.05$ compared with the inhibitor-NC group, $N = 3$.

mice [7]. Also, miR-155-5p has been explored to upregulate in the injured kidneys [22]. In this study, KLF4 and miR-155-5p expressions were increased in renal tissues after acute renal allograft (Figure 1(g)).

For further validation of the effects of KLF4 and miR-155-5p on kidney injury after acute allograft, an H/R model of HK-2 cells *in vitro* was established [18]. CCK-8 assay, flow cytometry, and Western blot were utilized to examine cell proliferation, apoptosis, and apoptosis-related proteins. The results revealed that proliferation capacity was impaired, apoptosis rate and Bax level were increased, and Bcl-2 level was suppressed in H/R-treated HK-2 cells (Figures 1(h)–1(j)). Also, in H/R-treated HK-2 cells, KLF4 and miR-155-5p levels were both upregulated (Figure 1 (k)). Shortly, KLF4 and miR-155-5p were related to acute renal allograft injury.

3.2. KLF4 Binds to miR-155-5p Promoter. Though KLF4 and miR-155-5p expressions in acute renal allograft injury were determined, their internal action remained unclear. KLF4 is a transcription factor to bind to the promoter of miRNA [23]. Based on that, the same mechanism of KLF4 was speculated to work with miR-155-5p. To clarify the regulatory mechanism of KLF4 and miR-155-5p, we firstly interfered and overexpressed KLF4 in the cells (Figure 2(a)) and then observed that overexpressed/depleted KLF4 up-/downregulated miR-155-5p, proving that KLF4 positively regulated miR-155-5p (Figure 2(b)). Then, JASPAR database searched 3 potential binding sites of KLF4 on the promoter of miR-155-5p (Figure 2(c)). Subsequently, each KLF4 binding site was cloned into pGL3-Basic vector to analyze KLF4-regulated miR-155-5p promoter region. The findings suggested that KLF4 at sites 2 and 3 substantially regulated miR-155-5p while KLF4 at site 1 did not (Figure 2(d)). In addition, ChIP assay confirmed that KLF4 could directly bind to the miR-155-5p promoter and KLF4 was recruited through the binding sites 2 and 3 (Figure 2(e)).

3.3. Depleting miR-155-5p Attenuates Acute Renal Allograft Injury. To explore the effects of miR-155-5p inhibition on acute renal allograft injury, miR-155-5p expression was interfered by miR-155-5p antagomir in mice with acute renal allograft (Figure 3(a)). Then, it was found that miR-155-5p antagomir treatment could reduce serum creatinine,

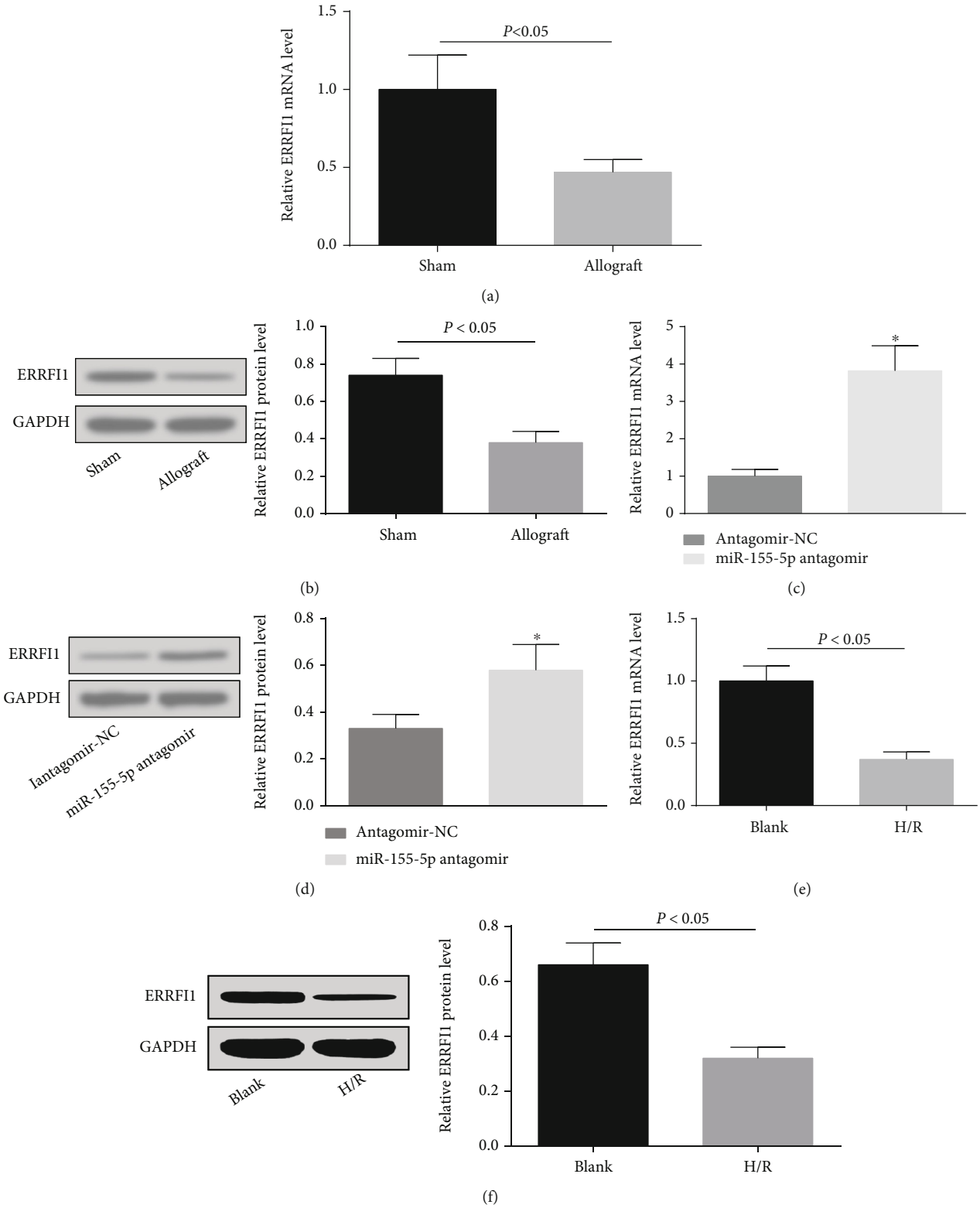

Figure 5: Continued.

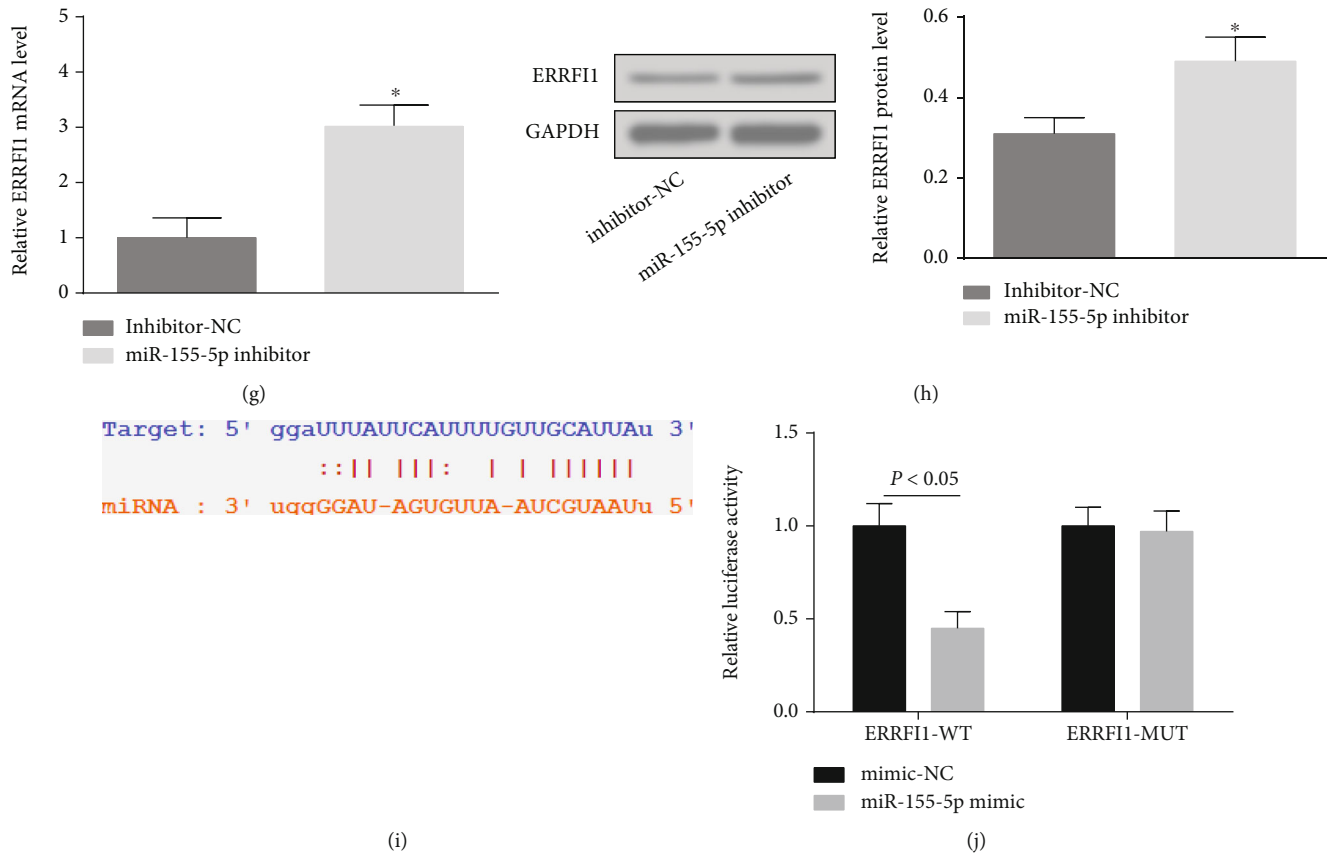

Figure 5: miR-155-5p targets ERRFI1. (a and b) RT-qPCR and Western blot detected ERRFI1 expression in renal tissues of mice after acute renal allografts. (c and d) RT-qPCR and Western blot detected ERRFI1 expression in renal tissues of mice after downregulation of miR-155-5p. (e and f) RT-qPCR and Western blot detected ERRFI1 expression in H/R-treated HK-2 cells. (g and h) RT-qPCR and Western blot detected ERRFI1 expression in H/R treated HK-2 cells after downregulation of miR-155-5p. (i) Starbase website predicted the binding site of miR-155-5p and ERRFI1. (j) Dual luciferase reporter gene assay verified the targeting relation between miR-155-5p and ERRFI1. The data were expressed as mean ± standard deviation; in mice, $^*P < 0.05$ compared with the antagomir-NC group; In H/R-treated HK-2 cells and $^*P < 0.05$ compared with the inhibitor-NC group. (a–d) $n = 5$ and (e–j) $n = 3$.

IFN-γ, TNF-α, and IL-2 levels and elevated eGFR level in serum (Figures 3(b) and 3(c)). Moreover, downregulating miR-155-5p ameliorated renal tubular injury and reduced apoptosis and oxidative stress in renal tissues (Figures 3(d)–3(g)). It was implied that miR-155-5p knockdown attenuated acute renal allograft injury.

3.4. Downregulating miR-155-5p Facilitates H/R-Treated HK-2 Cell Proliferation and Suppresses Apoptosis. The protective effects of miR-155-5p depletion on acute renal allograft injury were proved in animal models; then, its effects on H/R-treated HK-2 cells were deciphered. miR-155-5p inhibitor was transfected into the cells to successfully downregulate miR-155-5p (Figure 4(a)). Next, functional assays presented that in response to miR-155-5p inhibitor treatment, cell proliferation was reinforced, apoptosis rate and Bax level were reduced, and Bcl-2 level was heightened (Figures 4(b)–4(d)). It was found that miR-155-5p silencing relieved H/R-induced damage to HK-2 cells.

3.5. miR-155-5p Targets ERRFI1. Detected by RT-qPCR and Western blot, ERRFI1 expression was downregulated in renal tissues of mice after acute renal allograft and in H/R-treated HK-2 cells, and moreover, downregulating miR-155-5p suppressed ERRFI1 level (Figures 5(a)–5(h)). Starbase website predicted the binding sites between miR-155-5p and ERRFI1 (Figure 5(i)). Dual luciferase reporter experiment made it clear that cotransfection of ERRFI1-WT and miR-155-5p mimic weakened the luciferase activity of HK-2 cells, while that of ERRFI1-MUT and miR-155-5p mimic did not (Figure 5(j)). All of those results hinted that ERRFI1 was targeted by ERRFI1.

3.6. Knocking Down ERRFI1 Antagonizes the Effects of Downregulated miR-155-5p on Acute Renal Allograft Injury. The impacts of spontaneous knockdown of miR-155-5p and ERRFI1 on acute renal allograft injury were tested. It was uncovered that downregulating ERRFI1 impaired the effects of downregulated miR-155-5p on ERRFI1 expression. Besides, depleting ERRFI1 antagonized the impacts of miR-155-5p knockdown on serum creatinine, eGFR, IFN-γ, TNF-α and IL-2 levels, renal tubular injury, apoptosis, and oxidative stress (Figures 6(a)–6(h)).

3.7. Knocking Down ERRFI1 Offsets the Effects of Downregulated miR-155-5p on H/R-Treated HK-2 Cell

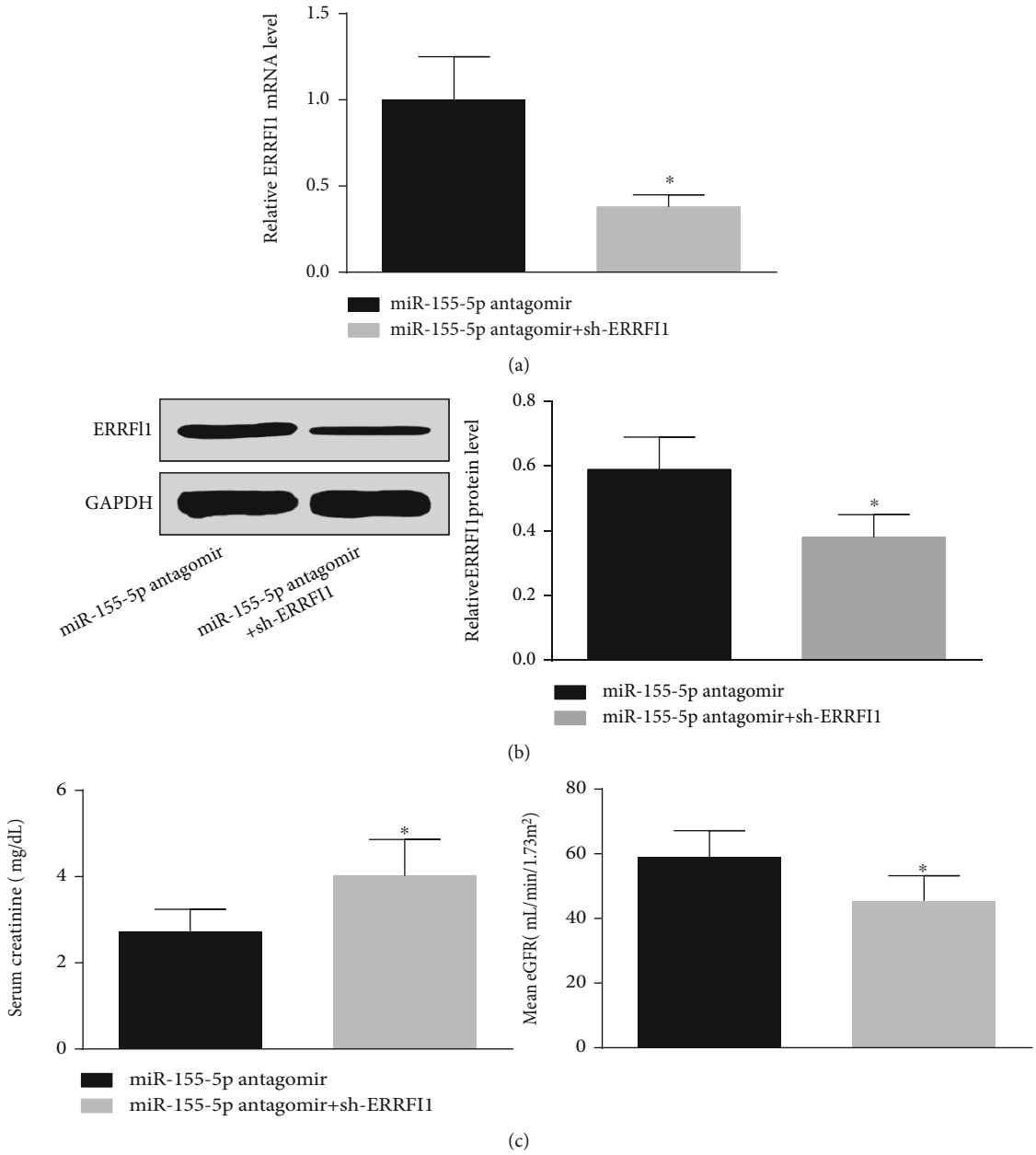

Figure 6: Continued.

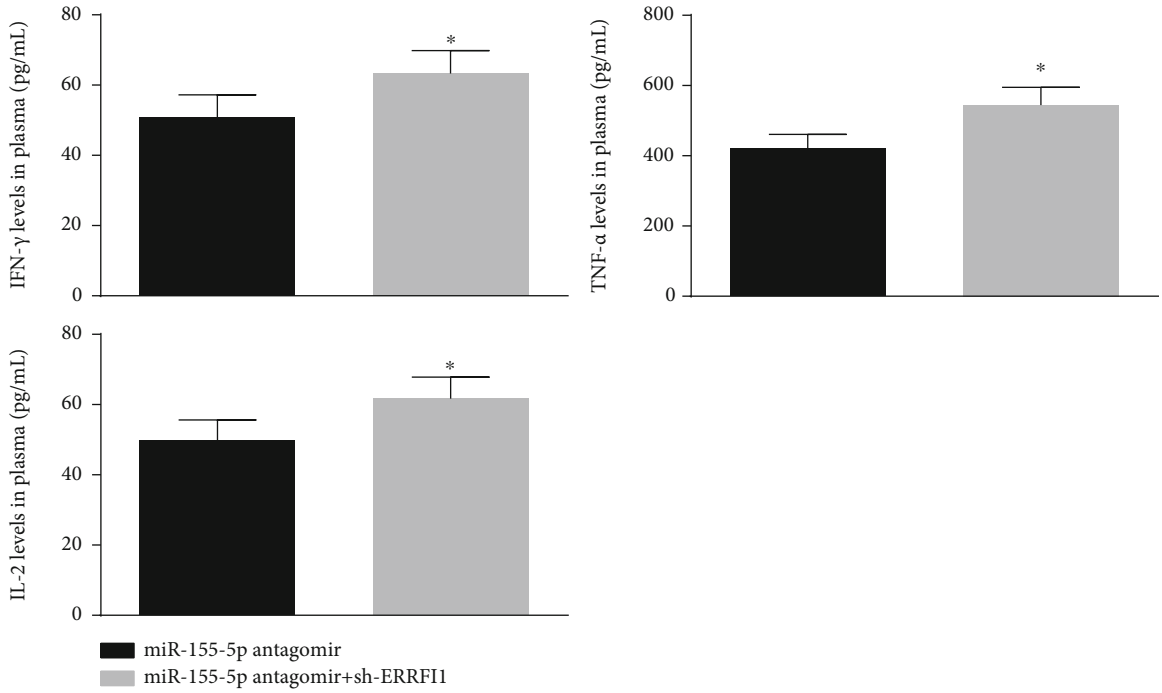

(d)

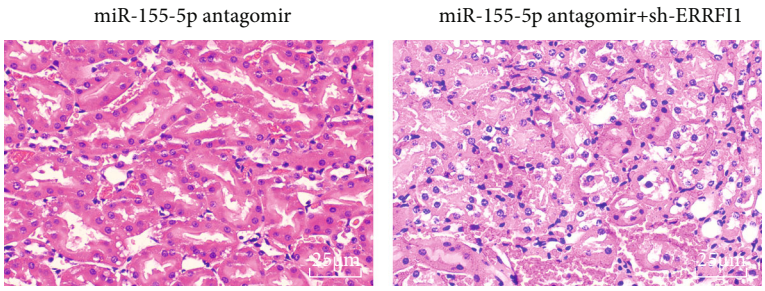

(e)

Figure 6: Continued.

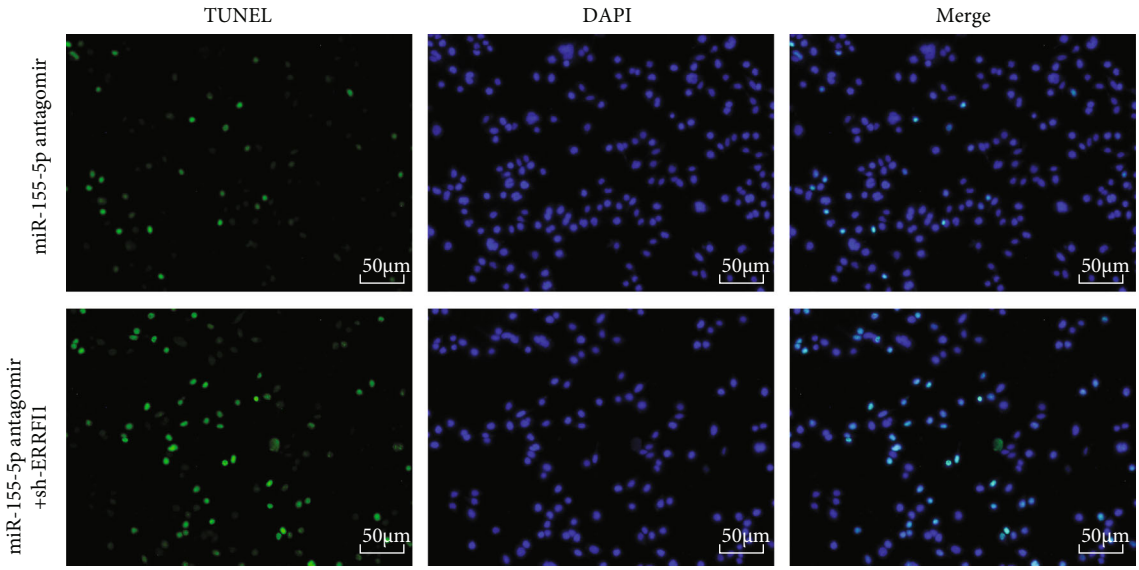

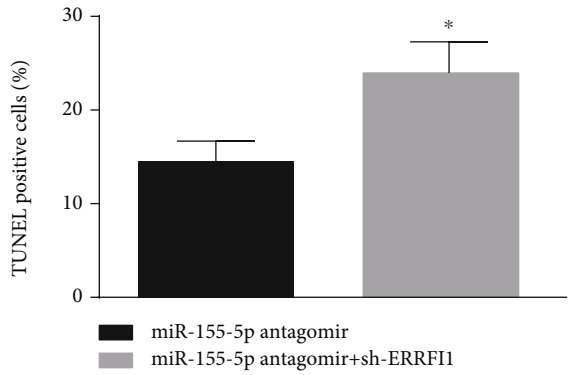

(f)

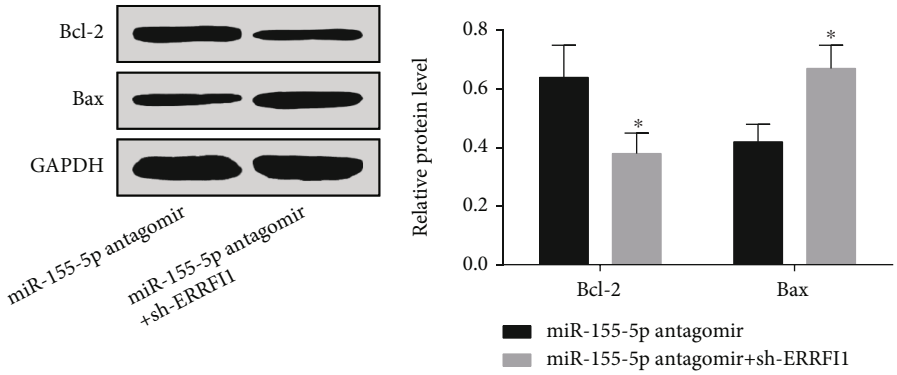

(g)

Figure 6: Continued.

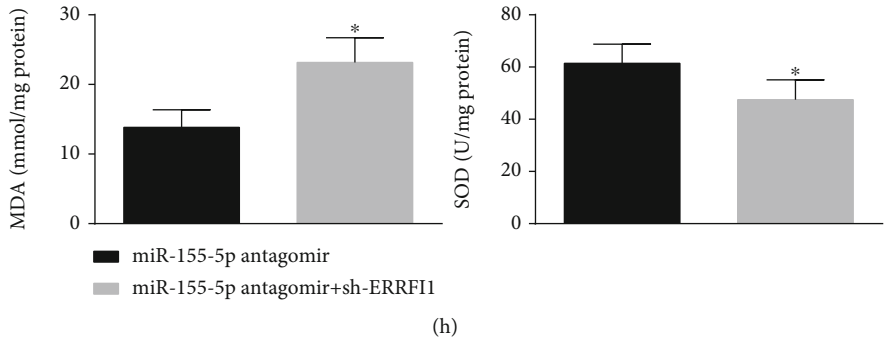

Figure 6: Knocking down ERRFI1 antagonizes the effects of downregulated miR-155-5p on acute renal allograft injury. (a and b) RT-qPCR and Western blot detected ERRFI1 expression in renal tissues of mice. (c) Serum creatinine and eGFR contents in mice. (d) ELISA detected serum IFN-γ, TNF-α, and IL-2 contents in mice. (e) H&E staining detected kidney injury of mice. (f) TUNEL staining detected renal tubular apoptosis of mice. (g) Western blot detected Bax and Bcl-2 protein expressions in renal tissues of mice. (h) MDA content and SOD activity in renal tissues of mice. The data were expressed as mean ± standard deviation; $^*P < 0.05$ compared with the miR-155-5p antagomir group, $n = 5$.

Proliferation and Apoptosis. Lastly, the changes of HK-2 cell proliferation and apoptosis after depletion of miR-155-5p and ERRFI1 were observed. It was manifested that on the basis of miR-155-5p downregulation, further treatment of ERRFI1 depletion lowered ERRFI1 expression. Meanwhile, ERRFI1 knockdown rescued the effects of miR-155-5p downregulation on the proliferation and apoptosis of H/R-treated HK-2 cells (Figures 7(a)–7(f)).

4. Discussion

Kidney injury, specially IR/I-induced kidney injury, is the common result during acute renal allograft [24]. In this manuscript, we navigated and unveiled the mechanism of KLF4 in acute renal allograft injury. To begin with, we checked KLF4 and miR-155-5p expressions, and the findings presented that both the two were overexpressed in mouse renal allografts and H/R-treated HK-2 cells. Afterwards, we explored the interaction between KLF4 and miR-155-5p and found that KLF4 bound to the promoter of miR-155-5p. Subsequently, functional experiments discovered that depleting miR-155-5p reduced serum inflammation and attenuated oxidative stress, renal tubular injury, and apoptosis in mice with acute renal allograft injury, as well as facilitated proliferation and repressed apoptosis of H/R-treated HK-2 cells. After that, the downstream targets of miR-155-5p were predicted, and eventually ERRFI1, the downregulated gene in mice with acute renal allograft injury, was picked. Finally, knocking down ERRFI1 was detected to antagonize the effects of downregulated miR-155-5p on mice with acute renal allograft injury, as well as on H/R-treated HK-2 cell proliferation and apoptosis.

KLF4 level was examined to upregulate in mice with IR/I in the kidney, and knocking down KLF4 prevented kidney from further dysfunction, while overexpressing KLF4 oppositely worked [7]. Also, another work has elucidated that in response to IR/I, KLF4 level went to an upregulation in the kidney of mice [6]. KLF4 expression in astrocytes was induced within 3 d of ischemia, as well as in oxygen-glucose deprivation-treated rat primary cortical astrocytes [25]. As to the interaction between KLF4 and miR-155-5p, nearly no study has reported the binding of KLF4 on the promoter of miR-155-5p, which requires further validation.

Impressively, raised miR-155-5p expression in urine suggested the rejection after renal transplantation [26]. Also, miR-155-5p was overexpressed in oxalate-/calcium-induced oxidative stress injury in the kidney, and downregulating miR-155-5p attenuated oxidative stress, as suggested by reduced MDA content [27]. In a similar way, miR-155 inhibition could partially encourage viability and hinder inflammation, oxidative stress, and apoptosis of HK-2 cells in sepsis-induced AKI [28]. In compliance with the discoveries, in LPS-induced AKI, elevated miR-155 expression was recognizable in tubular epithelial cells, and miR-155 suppression partially attenuated inflammation and apoptosis, which was reflected by decreased TNF-α content [13]. Experimentally, miR-155 expression suggested an increase in rats with I/R-induced AKI and H/R-treated cells, and moreover, restored miR-155 enhanced apoptosis and discouraged proliferation of H/R-treated NRK-52E cells, while depleted miR-155 had the opposite functions [14]. In the context of abnormal allograft, miR-155 level in plasma was elevated, which was connected with acute rejection of renal allografts in rats [11]. Besides, the upregulated miR-155 accelerated LPS-induced tubular cell apoptosis, while suppressing miR-155 at least contributed to attenuated AKI [29]. Further echoed without research, another literature has elaborated that miR-155 expression reached a high level in renal tissues and HK-2 cells after chronic intermittent hypoxia treatment, and elevating miR-155 augmented oxidative stress in renal tubular cells [30]. In renal I/RI, miR-155 expression went toward an increase in rat renal tissues and HR-treated HK-2 cells, and restoring miR-155 strengthened inflammation response in HR-treated HK-2 cells [20]. At present, no reported research has declared the relation between miR-155-5p and ERRFI1. In fact, ERRFI1 level was insufficiently expressed in AKI, and ERRFI1 elevation mediated by miR-152-3p was inhibitory for the apoptotic and inflammatory activities of renal cells [15]. However, the more specific mechanism of ERRFI1 in kidney injury

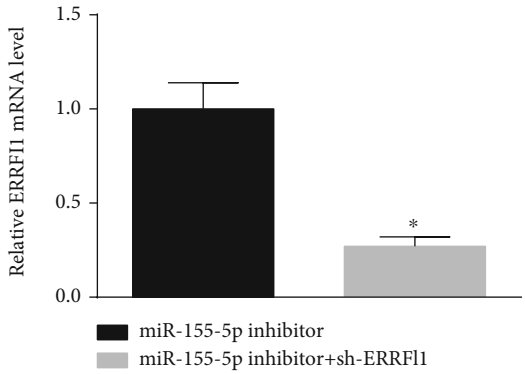

(a)

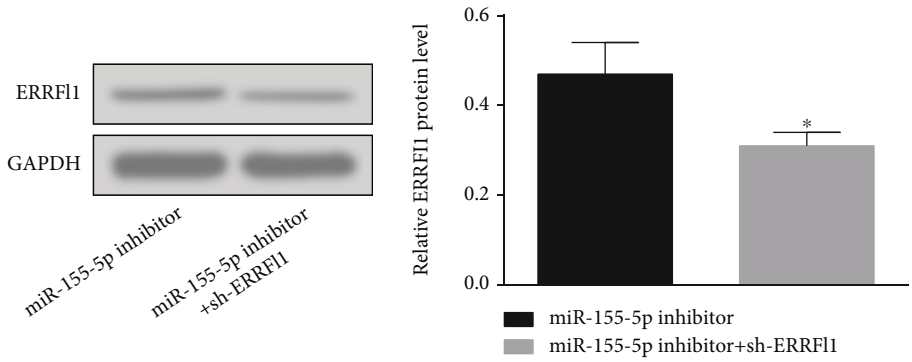

(b)

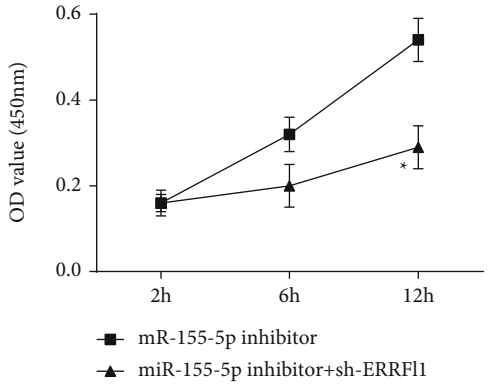

(c)

Figure 7: Continued.

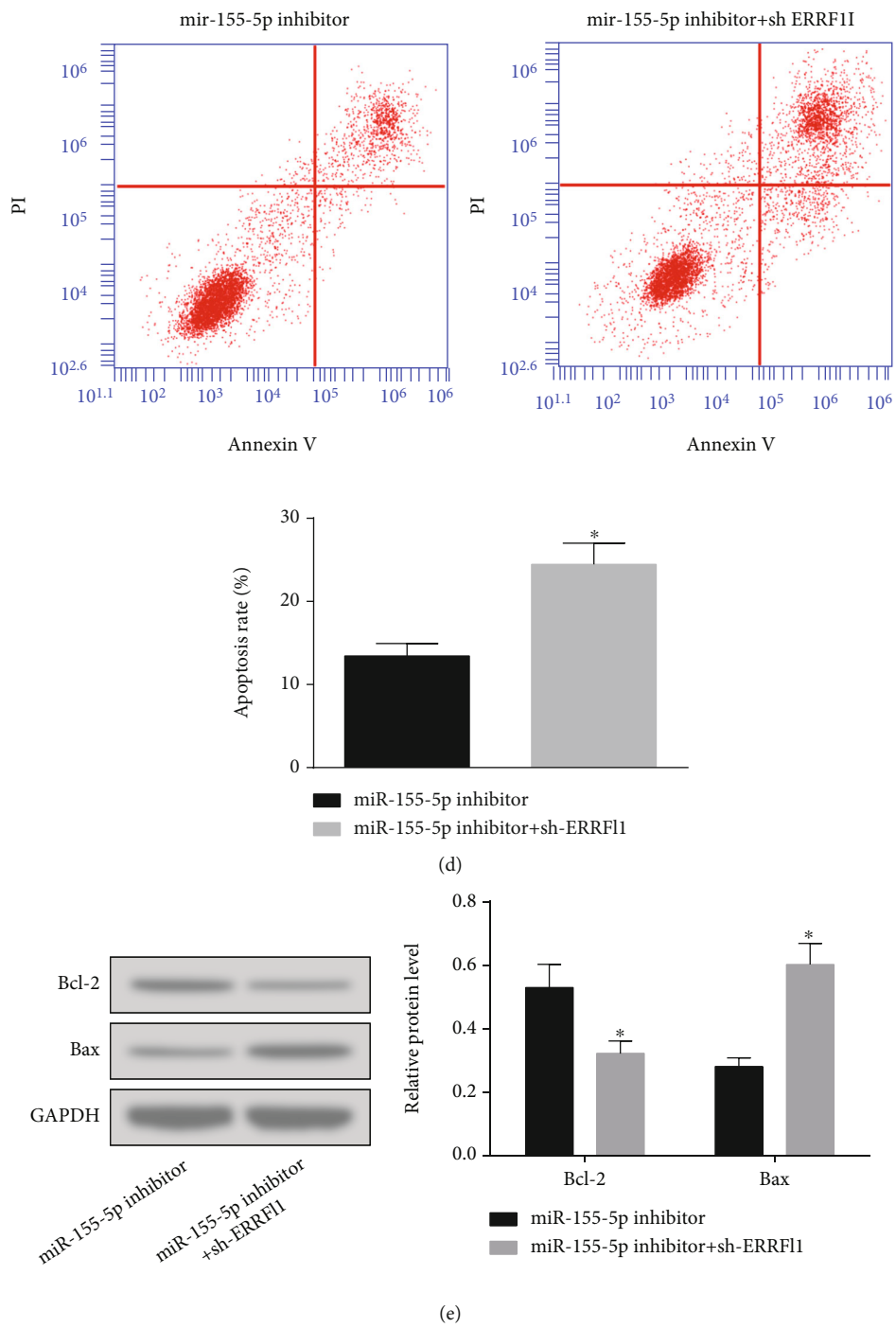

Figure 7: Knocking down ERRFI1 offsets the effects of downregulated miR-155-5p on H/R-treated HK-2 cell proliferation and apoptosis. (a and b) RT-qPCR and Western blot detected ERRFI1 expression in H/R-treated HK-2 cells. (c) CCK-8 assay detected the proliferation of H/R-treated HK-2 cells. (d) Flow cytometry detected the apoptosis rate of H/R-treated HK-2 cells. (e) Western blot detected Bax and Bcl-2 protein expression in H/R-treated HK-2 cells. The data were expressed as mean ± standard deviation; ∗ compared with the miR-155-5p inhibitor group, $N = 3$.

after acute renal allograft needs more researches for comprehensive explanation.

All in all, it was elucidated that silencing KLF4 mediated miR-155-5p to enhance ERRFI1 expression, thereby attenuating acute renal allograft injury in mice, as well as promoting proliferation and suppressing apoptosis of H/R-treated HK-2 cells. This work more or less widened our horizon to the mechanism of KLF4/miR-155-5p/ERRFI1 axis in acute renal allograft injury, which supplied a novel approach to manage acute renal allograft injury. However, whether the KLF4/miR-155-5p/ERRFI1 axis works in other diseases needs more explorations.

Data Availability

The analyzed data sets generated during the study are available from the corresponding author on reasonable request.

Conflicts of Interest

The authors declare that there is no conflict of interest.

Acknowledgments

This research was supported by the Health Public Welfare Scientific Research Project in Futian District of Shenzhen (Grant No. FTWS2018077) and Open Project of Key Laboratory of Organ Donation and Transplantation Immunity in Guangdong (Grant No. 2016002).

References

[1] C. Thongprayoon, P. Hansrivijit, N. Leeaphorn et al., "Recent advances and clinical outcomes of kidney transplantation," *Journal of Clinical Medicine*, vol. 9, no. 4, p. 1193, 2020.

[2] C. Yang, R. Qi, and B. Yang, "Pathogenesis of chronic allograft dysfunction progress to renal fibrosis," *Advances in Experimental Medicine and Biology*, vol. 1165, pp. 101–116, 2019.

[3] F. Panah, A. Ghorbanihaghjo, H. Argani, M. Asadi Zarmehri, and S. Nazari Soltan Ahmad, "Ischemic acute kidney injury and klotho in renal transplantation," *Clinical Biochemistry*, vol. 55, pp. 3–8, 2018.

[4] M. Tepel, C. Borst, C. Bistrup et al., "Urinary calprotectin and posttransplant renal allograft injury," *PLoS One*, vol. 9, no. 11, article e113006, 2014.

[5] A. Hishikawa, K. Hayashi, and H. Itoh, "Transcription factors as therapeutic targets in chronic kidney disease," *Molecules*, vol. 23, no. 5, p. 1123, 2018.

[6] N. M. Rogers, Z. J. Zhang, J. J. Wang, A. W. Thomson, and J. S. Isenberg, "CD47 regulates renal tubular epithelial cell self-renewal and proliferation following renal ischemia reperfusion," *Kidney International*, vol. 90, no. 2, pp. 334–347, 2016.

[7] D. Xu, P. P. Chen, P. Q. Zheng et al., "KLF4 initiates sustained activation of YAP after AKI to promote renal fibrosis," *Acta Pharmacologica Sinica*, vol. 42, no. 3, pp. 436–450, 2020.

[8] C. J. Stavast, P. J. M. Leenen, and S. J. Erkeland, "The interplay between critical transcription factors and microRNAs in the control of normal and malignant myelopoiesis," *Cancer Letters*, vol. 427, pp. 28–37, 2018.

[9] Z. Wang, Y. Chen, Y. Lin et al., "Novel crosstalk between KLF4 and ZEB1 regulates gemcitabine resistance in pancreatic ductal adenocarcinoma," *International Journal of Oncology*, vol. 51, no. 4, pp. 1239–1248, 2017.

[10] L. Xiong, S. Ding, and T. Yang, "The protective function of miR-378 in the ischemia-reperfusion injury during renal transplantation and subsequent interstitial fibrosis of the renal allograft," *International Urology and Nephrology*, vol. 52, no. 9, pp. 1791–1800, 2020.

[11] J. Liang, Y. Tang, Z. Liu et al., "Increased expression of miR-155 correlates with abnormal allograft status in solid organ transplant patients and rat kidney transplantation model," *Life Sciences*, vol. 227, pp. 51–57, 2019.

[12] S. Zununi Vahed, A. Poursadegh Zonouzi, H. Ghanbarian et al., "Differential expression of circulating miR-21, miR-142-3p and miR-155 in renal transplant recipients with impaired graft function," *International Urology and Nephrology*, vol. 49, no. 9, pp. 1681–1689, 2017.

[13] S. Lu, L. Dong, X. Jing, C. Gen-Yang, and Z. Zhan-Zheng, "Abnormal lncRNA CCAT1/microRNA-155/SIRT1 axis promoted inflammatory response and apoptosis of tubular epithelial cells in LPS caused acute kidney injury," *Mitochondrion*, vol. 53, pp. 76–90, 2020.

[14] X. B. Zhang, X. Chen, D. J. Li et al., "Inhibition of miR-155 ameliorates acute kidney injury by apoptosis involving the regulation on TCF4/Wnt/β-catenin pathway," *Nephron*, vol. 143, no. 2, pp. 135–147, 2019.

[15] P. Ma, C. Zhang, P. Huo, Y. Li, and H. Yang, "A novel role of the miR-152-3p/ERRFI1/STAT3 pathway modulates the apoptosis and inflammatory response after acute kidney injury," *Journal of Biochemical and Molecular Toxicology*, vol. 34, no. 9, p. e22540, 2020.

[16] W. Wang, Y. Zheng, M. Wang, M. Yan, J. Jiang, and Z. Li, "Exosomes derived miR-126 attenuates oxidative stress and apoptosis from ischemia and reperfusion injury by targeting ERRFI1," *Gene*, vol. 690, pp. 75–80, 2019.

[17] K. Hueper, B. Hensen, M. Gutberlet et al., "Kidney transplantation: multiparametric functional magnetic resonance imaging for assessment of renal allograft pathophysiology in mice," *Investigative Radiology*, vol. 51, no. 1, pp. 58–65, 2016.

[18] X. Pang, G. Feng, W. Shang et al., "Inhibition of lncRNA MEG3 protects renal tubular from hypoxia-induced kidney injury in acute renal allografts by regulating miR-181b/TNF-α signaling pathway," *Journal of Cellular Biochemistry*, vol. 120, no. 8, pp. 12822–12831, 2019.

[19] Y. Lei, B. Ehle, S. V. Kumar et al., "Cathepsin S and protease-activated receptor-2 drive alloimmunity and immune regulation in kidney allograft rejection," *Frontiers in Cell and Development Biology*, vol. 8, p. 398, 2020.

[20] H. Wu, T. Huang, L. Ying et al., "MiR-155 is involved in renal ischemia-reperfusion injury via direct targeting of FoxO3a and regulating renal tubular cell pyroptosis," *Cellular Physiology and Biochemistry*, vol. 40, no. 6, pp. 1692–16705, 2016.

[21] D. Xu, W. Li, T. Zhang, and G. Wang, "miR-10a overexpression aggravates renal ischemia-reperfusion injury associated with decreased PIK3CA expression," *BMC Nephrology*, vol. 21, no. 1, p. 248, 2020.

[22] C. Lu, B. Chen, C. Chen et al., "CircNr1h4 regulates the pathological process of renal injury in salt-sensitive hypertensive mice by targeting miR-155-5p," *Journal of Cellular and Molecular Medicine*, vol. 24, no. 2, pp. 1700–1712, 2020.

[23] Q. Xu, M. Liu, J. Zhang et al., "Overexpression of KLF4 promotes cell senescence through microRNA-203-survivin-p21 pathway," *Oncotarget*, vol. 7, no. 37, pp. 60290–60302, 2016.

[24] K. Kreimann, M. S. Jang, S. Rong et al., "Ischemia reperfusion injury triggers CXCL13 release and B-cell recruitment after allogenic kidney transplantation," *Frontiers in Immunology*, vol. 11, p. 1204, 2020.

[25] J. H. Park, T. R. Riew, Y. J. Shin, J. M. Park, J. M. Cho, and M. Y. Lee, "Induction of Krüppel-like factor 4 expression in reactive astrocytes following ischemic injury in vitro and in vivo," *Histochemistry and Cell Biology*, vol. 141, no. 1, pp. 33–42, 2014.

[26] O. Millán, K. Budde, C. Sommerer et al., "Urinary miR-155-5p and CXCL10 as prognostic and predictive biomarkers of rejection, graft outcome and treatment response in kidney

transplantation," *British Journal of Clinical Pharmacology*, vol. 83, no. 12, pp. 2636–2650, 2017.

[27] K. Jiang, J. Hu, G. Luo et al., "miR-155-5p promotes oxalate- and calcium-induced kidney oxidative stress injury by suppressing MGP expression," *Oxidative Medicine and Cellular Longevity*, vol. 2020, Article ID 5863617, 14 pages, 2020.

[28] M. Wang, J. Wei, F. Shang, K. Zang, and T. Ji, "Long noncoding RNA CASC2 ameliorates sepsis-induced acute kidney injury by regulating the miR-155 and NF-κB pathway," *International Journal of Molecular Medicine*, vol. 45, no. 5, pp. 1554–1562, 2020.

[29] J. Du, S. Jiang, Z. Hu et al., "Vitamin D receptor activation protects against lipopolysaccharide-induced acute kidney injury through suppression of tubular cell apoptosis," *American Journal of Physiology. Renal Physiology*, vol. 316, no. 5, pp. F1068–F1077, 2019.

[30] X. Wu, S. C. Chang, J. Jin, W. Gu, and S. Li, "NLRP3 inflammasome mediates chronic intermittent hypoxia-induced renal injury implication of the microRNA-155/FOXO3a signaling pathway," *Journal of Cellular Physiology*, vol. 233, no. 12, pp. 9404–9415, 2018.

Hindawi
Disease Markers
Volume 2022, Article ID 7319277, 7 pages
https://doi.org/10.1155/2022/7319277

Research Article

Study on Correlation between Type 2 Diabetes and No-Reflow after PCI

Su-Rui Zhao,[1] **Rui Huang**,[2] **Fang Liu**,[2] **Ya Li**,[2] **Yue Gong**,[2] **and Jun Xing**[3]

[1]*Department of Cardiology IV, Cangzhou Central Hospital, Cangzhou, 061001 Hebei Province, China*
[2]*Department of Cardiology II, Cangzhou Central Hospital, Cangzhou, 061001 Hebei Province, China*
[3]*Department of Gynecology and Obstetrics, Cangzhou Peace Hospital, Cangzhou, 061001 Hebei Province, China*

Correspondence should be addressed to Su-Rui Zhao; surongsui83854@126.com

Received 29 December 2021; Revised 1 February 2022; Accepted 7 February 2022; Published 17 March 2022

Academic Editor: Hongsheng Zhang

Diabetes, a serious chronic disease globally, is often complicated with cardiovascular diseases for which percutaneous coronary intervention (PCI) is the mainstay. The no-reflow rate of diabetic patients after PCI is 2-4 times higher than that of nondiabetic patients, yet the specific mechanism is still unclear. This study was designed to investigate the correlation between the duration of diabetes, preoperative blood glucose level, coronary angiographic blood flow, coronary artery stenosis level, and no-reflow after PCI. A total of 131 patients with type 2 diabetes who underwent PCI in our hospital from 2019 to 2020 were divided into control group and observation group. The disease duration, preoperative blood glucose level, coronary angiographic blood flow, and coronary artery stenosis level of the two groups were calculated. There were differences in the duration of diabetes between the two groups; the blood glucose level of the control group was about 3.8%, which was lower than 5.8% of the observation group; the thrombolysis in myocardial infarction (TIMI) value of the control group was 18.46 ± 4.6, which was lower than 20.67 ± 3.9 of the observation group; The degree of coronary stenosis in the control was $63\% \pm 2\%$, which was lower than $76\% + 3\%$ in the observation group. Binary logistic stepwise regression analysis was performed on these indicators and no-reflow after PCI to explore the correlation between these indicators and no-reflow after PCI in diabetic patients. The study found that the diabetes duration, higher preoperative blood glucose level, coronary angiography blood flow, and coronary artery were positively associated with no-reflow after PCI.

1. Introduction

Diabetes is a globally serious chronic disease, with approximately 425 million patients worldwide, and 114 million adults in China [1, 2]. Studies have shown that diabetes patients aged over 50 years are susceptible to coronary heart disease with 12%-31.7% probability [3]. The United States spends as much as 348 billion dollars on diabetes treatment research every year, of which cardiovascular complications of diabetes accounts for 1/4, indicating that the cardiovascular disease (CVD) complicated by diabetes has imposed substantial burden to patients and society [4]. At present, CVD tops the causes of death among urban and rural residents in China, accounting for 40% [5]. Percutaneous coronary intervention (PCI) is commonly applied in the treatment of CVD, and it alleviates the patient's pain and improves the prognosis [6]. However, bare-metal stent (BMS) is prone to restenosis in the stent following PCI, leading to nonreflow. The incidence of such event is as high as 16%-44%, and it is the most daunting obstacle for PCI [7]. It is proved that the incidence of in-stent restenosis in diabetes patients after PCI is 2-4 times higher than that of nondiabetic patients [8, 9], but the exact mechanism remains unclear. To this end, this study aims at exploring the correlation between disease duration, preoperative blood glucose levels, coronary angiographic blood flow conditions, coronary stenosis levels, and no-reflow after PCI.

2. Materials and Methods

2.1. Subjects. A total of 131 patients with type 2 diabetes who underwent PCI in our hospital from 2019 to 2020 were divided into 2 groups: control group (reflow, $n = 60$) and observation group (no-reflow, $n = 71$). The flowchart of enrollment was shown in Figure 1. Before enrollment, the general data including demographic characteristics, medical history, and blood pressure were collected by doctors. The diagnostic criteria for acute myocardial infarction (AMI) were in accordance with the Diagnostic and Therapeutic Guidelines for AMI developed by the Cardiovascular Branch of the Chinese Medical Association and the Editorial Board of Chinese Journal of Cardiovascular Disease and Chinese Journal of Circulation [10]. The diabetes is diagnosed according to the 2017 American Diabetes Association Diabetes Diagnosis and Treatment Standard.

2.2. Inclusion and Exclusion Criteria. Inclusion criteria are as follows: (1) patients aged 18 years or older; (2) patients had chest pain and distress in the emergency department; (3) patients had segment elevation myocardial infarction (STEMI) diagnosed according to the Acute Myocardial Infarction Diagnosis and Treatment Guide; (4) patients developed symptoms within 24 hours before consultation; (5) patients signed the PCI informed consent; and (6) patients complicated with diabetes. Exclusion criteria are as follows: (1) patients rejected PCI; (2) patients with STEMI diagnosed in other hospitals; (3) patients underwent thrombolysis and reopened before admission; (4) patients had severe liver and kidney diseases, had no previous left main disease, or had a history of coronary bypass; (5) patients had preexcitation syndrome; and (6) patients presented severe dissection, thromboembolism in other parts, and vasospasm.

2.3. Institutional Review Board Statement. This study was approved by the Ethics Committee of Cangzhou Central Hospital and was in accordance with the Helsinki Declaration [11], all participants and their families signed informed consent forms before enrollment.

2.4. PCI Procedure. All patients were punctured by the radial artery or femoral artery within 12 hours of onset and underwent coronary angiography and PCI treatment. Coronary angiography was used to determine the location, stenosis, or occlusion range of the infarcted vessel. According to the specific circumstances, the lesion site was superselected; and thrombus aspiration, balloon dilation, or stent placement was performed. Residual stenosis ≤ 10% was used as the standard to judge successful vascular opening. After the operation, the catheter was withdrawn, and the patients who underwent radial artery puncture were locally compressed to stop bleeding for 6 hours, and those who underwent femoral artery puncture were locally compressed to stop bleeding for 24 hours. Before PCI, ticagrelor (AstraZeneca Pharmaceutical Co., Ltd., specification: 90 mg) 180 mg and aspirin (Bayer Health Care Company, specification: 100 mg) 300 mg were administered via chewing. Postoperatively, ticagrelor, 90 mg/time, 2 times/d and aspirin 100 mg/time, 1 time/d were administered orally until 1 year after surgery. Some patients with severe myocardial ischemia received intravenous infusion of tirofiban (Lunan Pharmaceutical Factory, specification: 12.5 mg) for 3 days after operation, and beta-blocker Betaloc (AstraZeneca Pharmaceutical Co., Ltd., specification: 25 mg), ACEI/ARB irbesartan (Zhejiang Huahai Pharmaceutical Co., Ltd., specification: 75 mg), or benazepril (Shenzhen Xinlitai Pharmaceutical Co., Ltd., specification: 5 mg) were orally administered for a long run.

2.5. Criteria of No-Reflow. The coronary angiographic blood flow classification was applied by two senior cardiac interventional experts to determine the no-reflow phenomenon. No-reflow means that although the occlusioned coronary artery has been opened after emergency PCI treatment after excluding vascular spasm, dissection, and other related factors, there is no effective blood reperfusion in the ischemic myocardial tissue, that is, the coronary blood flow is slowed down or there is no blood flow. TIMI blood flow grading: TIMI 0 indicates that there is no forward blood flow outside the occlusion point. TIMI 1 indicated weak forward blood flow at the distal end of the coronary artery and incomplete filling at the distal end of the coronary bed. TIMI 2 represents complete distal coronary artery filling with delayed or slow forward flow. TIMI 3 indicates normal blood flow with the distal coronary artery fully filled. TIMI blood flow was recorded in the last frame of coronary angiography after stent implantation during PCI, and TIMI blood flow < level 2 was judged as no cardiac reflow; otherwise, it was considered as cardiac reflow.

The diabetes time, preoperative blood glucose levels, coronary angiographic blood flow, and coronary CT stenosis levels were monitored and compared. The number of patients with no-reflow and the number of deaths were compared between the two groups.

2.6. Statistical Analysis. The sample size was determined by power analysis (statistical power of 0.80, α of 0.05) with a moderate effect size (0.25) and an allocation ratio of 1 using the G∗Power, yielding 40 patients per group for a total of 80 patients. More than 40 patients were enrolled in each group. Primary and secondary outcome continuous variables were analyzed using the Student t-test. The Mann–Whitney U test was used when data were not equally distributed. Nominal variables were analyzed using χ^2 tests. Binary logistic stepwise regression analysis was performed on these indicators and no-reflow after PCI to explore the correlation between these indicators and no-reflow after PCI in diabetic patients. Receiver Operating Characteristic (ROC) curve was conducted and Area Under the Curve (AUC) was calculated. All p values were 2-tailed, and the significance level was set at 0.05. All analyses were performed using the SPSS version 25.0 software.

3. Results

3.1. Clinical Data of Participants. There were no significant differences in age, gender, family history of coronary heart disease, history of cerebrovascular disease, history of angina pectoris, systolic blood pressure, diastolic blood pressure,

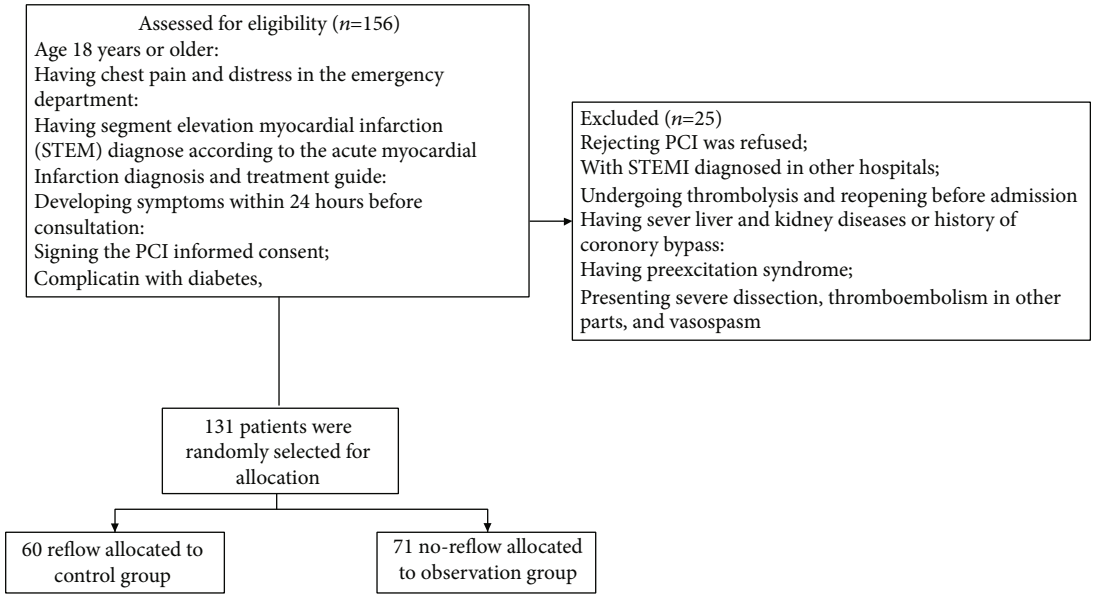

Figure 1: Flowchart of enrollment.

Table 1: The comparison of baseline information.

	Overall ($n = 131$)	Control group ($n = 60$)	Observation group ($n = 71$)	$t/\chi 2$	p
Age	64.73 ± 5.06	64.25 ± 4.81	65.13 ± 5.26	0.992	0.323
Male	71	31	40	0.286	0.593
Female	60	29	31		
SYNTAX score	15.15 ± 5.96	14.35 ± 6.23	15.82 ± 5.68	1.412	0.160
CHD family history	31	14	17	0.007	0.934
Cerebrovascular disease history	48	21	27	0.128	0.720
Systolic blood pressure	129.16 ± 23.15	129.96 ± 23.31	128.49 ± 23.16	0.361	0.719
Diastolic blood pressure	77.82 ± 14.35	78.02 ± 14.91	77.66 ± 13.97	0.143	0.887
Pulse pressure	51.33 ± 16.32	51.94 ± 16.09	50.82 ± 16.61	0.390	0.697

pulse pressure, etc. between the two groups (Table 1), indicating that the baseline information in the two groups at the initial assessment was well balanced.

3.2. Correlation between the Duration of Type 2 Diabetes and the Incidence of No-Reflow. There were differences in the duration of diabetes between the two groups, but the differences were not statistically significant. The duration of disease in the control group was 10 ± 2.8 years, and the duration of observation group was 11.2 ± 1.9 years (Figure 2(a)). Correlation analysis showed that duration of diabetes was positively correlated with no-reflow after PCI (Figure 2(b)).

3.3. Correlation between Blood Glucose Levels and the Incidence of No-Reflow. HbA1c reflects the blood glucose level of patients, the blood glucose level of the control group was about 3.8%, which was lower than 5.8% of the observation group (Figure 3(a)). Correlation analysis revealed that the blood glucose level was positively correlated with no-reflow after PCI (Figure 3(b)).

3.4. Correlation between Coronary Blood Flow and Incidence of No-Reflow. The thrombolysis in myocardial infarction (TIMI) value could accurately reflect the coronary blood flow of the patient, and the higher the value, the slower the blood flow. As shown in Figure 4(a), the TIMI value of the control group was 18.46 ± 4.6, which was lower than 20.67 ± 3.9 of the observation group. The correlation between the TIMI value and the case of no-reflow after PCI showed TIMI value and the no-reflow was positively correlated (Figure 4(b)).

3.5. Correlation between the Degree of Coronary Stenosis and the Incidence of No-Reflow. There is also a correlation between the degree of coronary stenosis and the incidence of no-reflow after PCI. The degree of coronary stenosis in the control was 63% ± 2%, which was lower than 76% + 3%

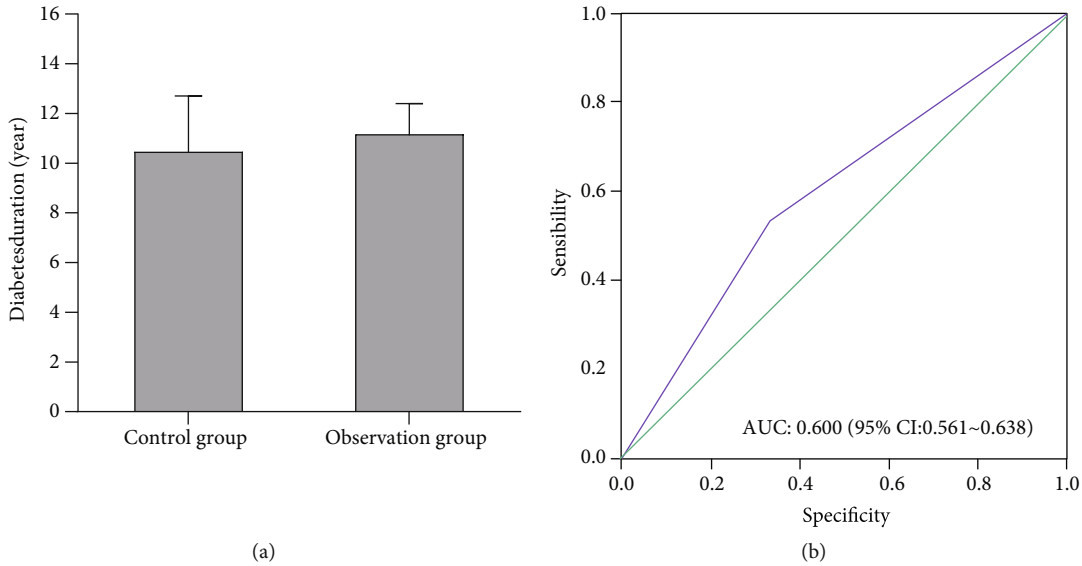

Figure 2: Correlation between the duration of type 2 diabetes and the incidence of no-reflow.

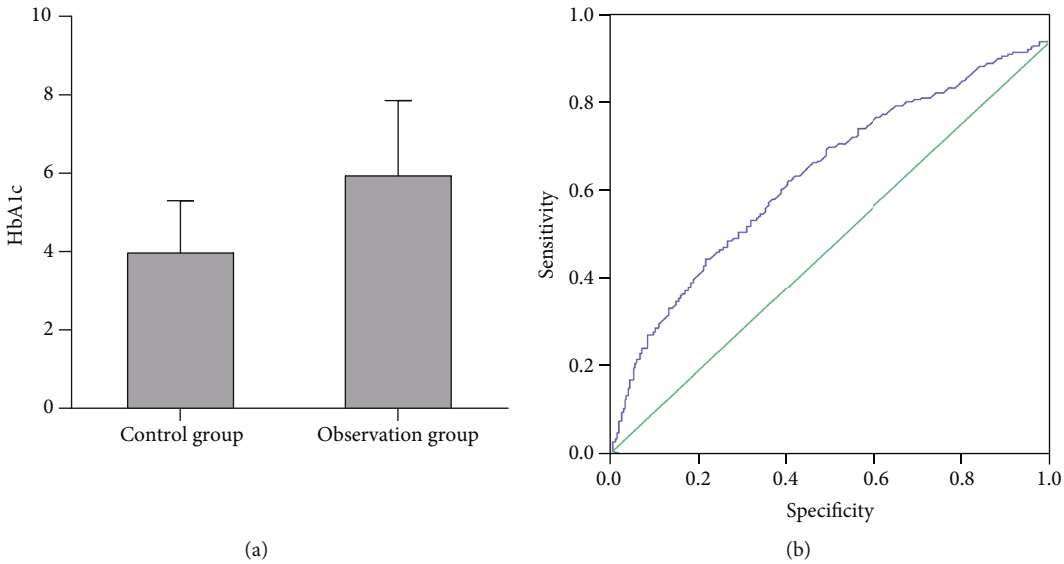

Figure 3: Correlation between blood glucose levels and the incidence of no-reflow.

in the observation group. The correlation between the degree of coronary stenosis and the incidence of no reflow after PCI showed that the degree of coronary stenosis was positively correlated with the incidence of no reflow after PCI, i.e., the higher the degree of coronary stenosis, the easier the occurrence of no-reflow (Figure 5).

4. Discussion

Diabetes causes metabolic disorder, atherosclerosis of large and medium blood vessels, and microvascular disease, and the prevalence of diabetes has been on a rise [12]. Therefore, patients with diabetes often complicate with coronary heart disease, and many severe coronary artery diseases also occur in multiple blood vessels and single blood vessels. PCI is a widely used treatment for cardiovascular disease, yet no-reflow might occur in diabetic patients after PCI [13, 14], and the correlation between these two remains unclear. Thus, the purpose of this study was to investigate the correlation between the diabetes course, preoperative blood glucose levels, coronary angiographic blood flow, coronary CT stenosis, and no-reflow after PCI.

The study found that the longer the diabetes duration, the higher the preoperative blood glucose level, the slower the coronary angiography blood flow, the narrower the coronary artery, and the more likely they were to have no-reflow after PCI. The longer the time of diabetes, the more serious the impact on cardiovascular complications thus more likely to induce no-reflow after PCI [15]. Insulin can mediate antilipolysis, but adipose tissue insulin resistance can reduce this effect, lowering lipoprotein lipase activity and further triggering hyperlipidemia. It serves as one of

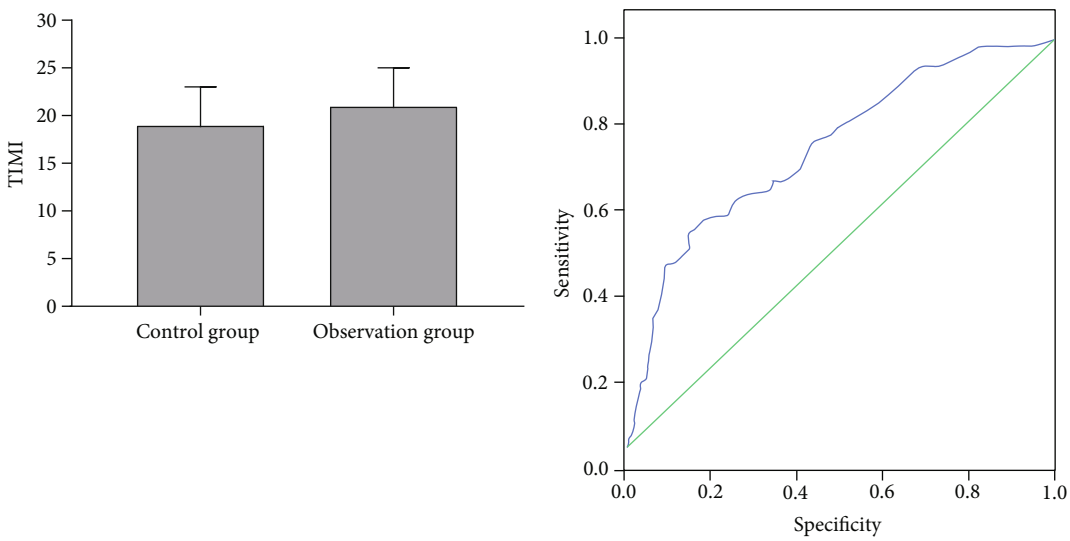

(a) (b)

Figure 4: Correlation between coronary blood flow and incidence of no-reflow.

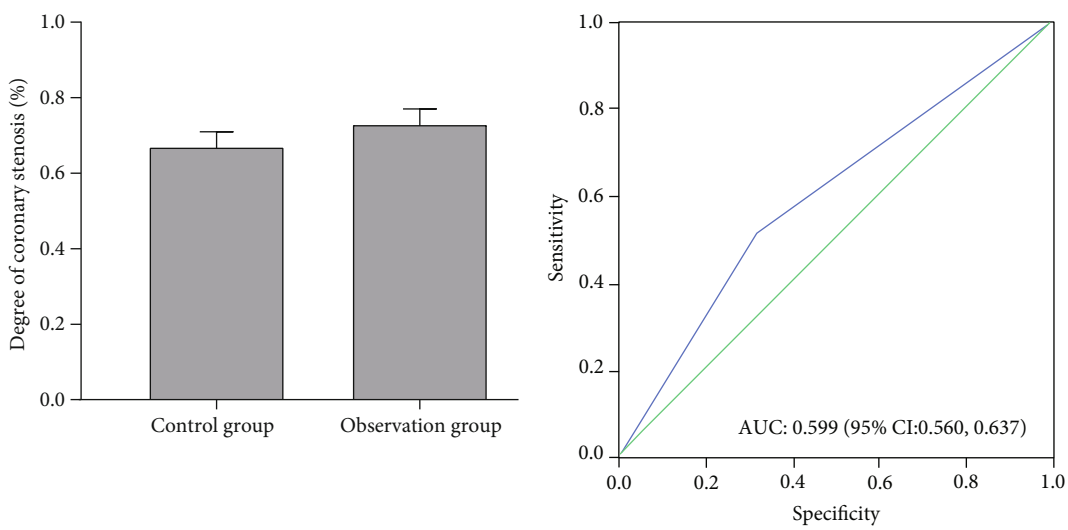

(a) (b)

Figure 5: Correlation between the degree of coronary stenosis and the incidence of no-reflow.

the main causes of dyslipidemia in diabetic patients and can aggravate coronary atherosclerosis [16]. After PCI, the application of the stent would destroy the coronary artery endothelial cell layer, cause platelet activation and aggregation, and promote the infiltration of leukocytes and monocytes to the injured site [17]. Excessive platelets and some inflammatory factors can induce macrophages to phagocytose and clear cellular debris from damaged cells. These processes further stimulate the migration and proliferation of resting vascular smooth muscle cells and endothelial cells, which may further narrow coronary artery [18–22], and lead to no-reflow after PCI. Consistently, our study showed that the longer the duration of diabetes, the higher the lipid concentration, which leads to narrower coronary arteries, reduces blood flow, and induces no-reflow after PCI. Moreover, in our study, patients with high HbA1c were found to have a higher incidence of no-reflow after PCI. HbA1c concentration and blood glucose concentration are positively correlated; this indicator has become the gold standard for judging diabetes control, due to its accurate reflection of the average level 8-12 weeks before taking the blood [23]. To our knowledge, insulin resistance in patients with diabetes causes metabolic disorders such as chronic hyperglycemia, which in turn affects vascular endothelial metabolism [24]. This can also lead to the migration and proliferation of vascular smooth muscle intimal cells, further narrowing coronary arteries [25]. Overall, the blood glucose level of diabetic patients would also induce no-reflow after PCI. After analysis, the following can be attributed to the increase of probability of nonrecurrence. The longer the course of

type 2 diabetes, the longer the development time of vascular endothelial injury and oxidative stress response caused by hyperglycemia, and the more serious the harm, the more difficult the recanalization of vessels during PCI, and the higher the risk of nonrecurrence [26]. Patients who do not follow hypoglycemic treatment are more likely to suffer cardiovascular and cerebrovascular damage due to poor blood glucose level control, which aggravates the condition and increases the probability of nonrelapse [27]. Previous study has confirmed that IRI > 2.5 is an important marker of insulin resistance, and insulin insensitivity means that the body's ability to regulate blood glucose is weakened, and the harm caused by hyperglycemia is more serious, and the incidence of nonrelapse increases significantly [28]. PCI is inconvenient for patients with proximal coronary artery embolism, which is easy to cause damage to the vascular wall, difficult to recover hemodynamics, and easy to cause no recurrence due to vascular endothelial injury and inflammatory reaction [29]. Therefore, the above factors increase the probability of nonrecurrence during PCI in AMI patients with T2MD to a certain extent.

5. Conclusion

In summary, the prevalence of no-reflow in patients with diabetes after PCI is affected by multiple factors. The duration of the disease, preoperative blood glucose level, coronary blood flow, and coronary stenosis were positively correlated with the incidence of no-reflow after PCI in patients with diabetes.

6. Study Limitations

However, our study has certain limitations, i.e., it was a single-centered study with relatively small sample size which may result in biased results and conclusions. The prevalence of no-reflow in patients with diabetes mellitus after PCI is a complex disorder, in which multiple factors are involved. Therefore, more cases needed to be enrolled to explore the influence of multiple factors on the incidence of no-reflow in patients with diabetes mellitus after PCI. Still, some other relevant factors should be considered in the future study, including delay in procedure and local protocol.

Data Availability

The datasets used during the present study are available from the corresponding author upon reasonable request.

Conflicts of Interest

The authors declare that they have no conflicts of interest.

References

[1] G. De Luca, H. Suryapranata, and P. Marino, "Reperfusion strategies in acute ST-elevation myocardial infarction: an overview of current status," *Progress in Cardiovascular Diseases*, vol. 50, no. 5, pp. 352–382, 2008.

[2] G. Niccoli, F. Burzotta, L. Galiuto, and F. Crea, "Myocardial no-reflow in humans," *Journal of the American College of Cardiology*, vol. 54, no. 4, pp. 281–292, 2009.

[3] K. M. Abbo, M. Dooris, S. Glazier et al., "Features and outcome of no-reflow after percutaneous coronary intervention," *The American Journal of Cardiology*, vol. 75, no. 12, pp. 778–782, 1995.

[4] R. Jaffe, T. Charron, G. Puley, A. Dick, and B. H. Strauss, "Microvascular obstruction and the no-reflow phenomenon after percutaneous coronary intervention," *Circulation*, vol. 117, no. 24, pp. 3152–3156, 2008.

[5] R. W. Harrison, A. Aggarwal, F. Ou et al., "Incidence and outcomes of no-reflow phenomenon during percutaneous coronary intervention among patients with acute myocardial infarction," *The American Journal of Cardiology*, vol. 111, no. 2, pp. 178–184, 2013.

[6] K. Peter Rentrop, M. Cohen, H. Blanke, and R. A. Phillips, "Changes in collateral channel filling immediately after controlled coronary artery occlusion by an angioplasty balloon in human subjects," *Journal of the American College of Cardiology*, vol. 5, no. 3, pp. 587–592, 1985.

[7] G. Ndrepepa, J. Mehilli, S. Schulz et al., "Prognostic significance of epicardial blood flow before and after percutaneous coronary intervention in patients with acute coronary syndromes," *Journal of the American College of Cardiology*, vol. 52, no. 7, pp. 512–517, 2008.

[8] R. H. Mehta, K. J. Harjai, J. Boura et al., "Prognostic significance of transient no-reflow during primary percutaneous coronary intervention for ST-elevation acute myocardial infarction," *The American Journal of Cardiology*, vol. 92, no. 12, pp. 1445–1447, 2003.

[9] H. K. Yip, M. C. Chen, H. W. Chang et al., "Angiographic Morphologic Features of Infarct-Related Arteries and Timely Reperfusion in Acute Myocardial Infarction: Predictors of Slow-Flow and No- Reflow Phenomenon," *Chest Journal*, vol. 122, no. 4, pp. 1322–1332, 2002.

[10] G. De Luca, H. Suryapranata, F. Zijlstra et al., "Symptom-onset-to-balloon time and mortality in patients with acute myocardial infarction treated by primary angioplasty," *Journal of the American College of Cardiology*, vol. 42, no. 6, pp. 991–997, 2003.

[11] A. Y. Malik and C. Foster, "The revised declaration of Helsinki: cosmetic or real change?," *Journal of the Royal Society of Medicine*, vol. 109, no. 5, pp. 184–189, 2016.

[12] A. Tomaszuk-Kazberuk, B. Sobkowicz, K. Kaminski et al., "Correlation entre la perfusion myocardique evaluee par l'echocardiographie de contraste et les parametres angiographiques de perfusion chez des patients ayant subi un premier infarctus aigu du myocarde, traite par angioplastie," *Canadian Journal of Cardiology*, vol. 24, no. 8, pp. 633–639, 2008.

[13] G. J. Horszczaruk, P. Kwasiborski, A. Rdzanek, K. J. Filipiak, J. Kochman, and G. Opolski, "TIMI myocardial perfusion grade and ST-segment resolution in the assessment of coronary reperfusion after primary angioplasty," *Kardiologia Polska*, vol. 72, no. 1, pp. 27–33, 2014.

[14] H. Zhou, X. Y. He, S. W. Zhuang et al., "Clinical and procedural predictors of no-reflow in patients with acute myocardial infarction after primary percutaneous coronary intervention," *World Journal of Emergency Medicine*, vol. 5, no. 2, pp. 96–102, 2014.

[15] C. Kirma, A. Izgi, C. Dundar et al., "Clinical and procedural predictors of no-reflow phenomenon after primary percutaneous coronary interventions Experience at a Single Center," *Circulation Journal*, vol. 72, no. 5, pp. 716–721, 2008.

[16] G. N. Levine, E. R. Bates, J. C. Blankenship et al., "2011 ACCF/AHA/SCAI guideline for percutaneous coronary intervention," *Catheterization and Cardiovascular Interventions*, vol. 82, no. 4, pp. E266–E355, 2013.

[17] C. M. Gibson, J. A. de Lemos, S. A. Murphy et al., "Combination therapy with abciximab reduces angiographically evident thrombus in acute myocardial infarction," *Circulation*, vol. 103, no. 21, pp. 2550–2554, 2001.

[18] H. S. Mueller, A. Dyer, and M. A. Greenberg, "The thrombolysis in myocardial infarction (TIMI) trial. Phase I findings," *New England Journal of Medicine*, vol. 312, no. 14, pp. 932–936, 1985.

[19] C. M. Gibson, C. P. Cannon, S. A. Murphy et al., "Relationship of TIMI myocardial perfusion grade to mortality after administration of thrombolytic drugs," *Circulation*, vol. 101, no. 2, pp. 125–130, 2000.

[20] J. M. Dizon, S. J. Brener, A. Maehara et al., "Relationship between ST-segment resolution and anterior infarct size after primary percutaneous coronary intervention: analysis from the INFUSE-AMI trial," *European Heart Journal Acute Cardiovascular Care*, vol. 3, no. 1, pp. 78–83, 2014.

[21] J. R. Le Gall, S. Lemeshow, and F. Saulnier, "A new simplified acute physiology score (SAPS II) based on a European/North American multicenter study," *JAMA*, vol. 270, no. 24, pp. 2957–2963, 1993.

[22] E. Braunwald, "Myocardial reperfusion, limitation of infarct size, reduction of left ventricular dysfunction, and improved survival. Should the paradigm be expanded?," *Circulation*, vol. 79, no. 2, pp. 441–444, 1989.

[23] W. H. Leung and C. P. Lau, "Correlation of quantitative angiographic parameters with changes in left ventricular diastolic function after angioplasty of the left anterior descending coronary artery," *The American Journal of Cardiology*, vol. 67, no. 13, pp. 1061–1066, 1991.

[24] H. D. White, R. M. Norris, M. A. Brown, P. W. Brandt, R. M. Whitlock, and C. J. Wild, "Left ventricular end-systolic volume as the major determinant of survival after recovery from myocardial infarction," *Circulation*, vol. 76, no. 1, pp. 44–51, 1987.

[25] I. Sheiban, G. Fragasso, C. Lu, S. Tonni, G. P. Trevi, and S. L. Chierchia, "Influence of treatment delay on long-term left ventricular function in patients with acute myocardial infarction successfully treated with primary angioplasty," *American Heart Journal*, vol. 141, no. 4, pp. 603–609, 2001.

[26] B. E. Kurtul, A. Kurtul, and F. Yalçın, "Predictive value of the SYNTAX score for diabetic retinopathy in stable coronary artery disease patients with a concomitant type 2 diabetes mellitus," *Diabetes Research and Clinical Practice*, vol. 177, p. 108875, 2021.

[27] K. B. Michels and S. Yusuf, "Does PTCA in acute myocardial infarction affect mortality and reinfarction rates?," *Circulation*, vol. 91, no. 2, pp. 476–485, 1995.

[28] M. J. de Boer, H. Suryapranata, J. C. Hoorntje et al., "Limitation of infarct size and preservation of left ventricular function after primary coronary angioplasty compared with intravenous streptokinase in acute myocardial infarction," *Circulation*, vol. 90, no. 2, pp. 753–761, 1994.

[29] A. Rodriguez, V. Bernardi, M. Fernández et al., "In-hospital and late results of coronary stents versus conventional balloon angioplasty in acute myocardial infarction (GRAMI trial)," *The American Journal of Cardiology*, vol. 81, no. 11, pp. 1286–1291, 1998.

Hindawi
Disease Markers
Volume 2022, Article ID 7553670, 9 pages
https://doi.org/10.1155/2022/7553670

Research Article

Thyroid-Stimulating Hormone Inhibits Insulin Receptor Substrate-1 Expression and Tyrosyl Phosphorylation in 3T3-L1 Adipocytes by Increasing NF-κB DNA-Binding Activity

Yajing Zhang[1] **and Ling Feng**[2]

[1]*NHC Key Laboratory of Hormones and Development, Tianjin Key Laboratory of Metabolic Diseases, Chu Hsien-I Memorial Hospital & Tianjin Institute of Endocrinology, Tianjin Medical University, Tianjin 300134, China*
[2]*People's Hospital of Guangxi Zhuang Autonomous Region, China*

Correspondence should be addressed to Yajing Zhang; lianyajing@163.com

Received 22 January 2022; Revised 21 February 2022; Accepted 24 February 2022; Published 14 March 2022

Academic Editor: Yaoyao Bian

Background. Abundant evidence indicates that thyroid-stimulating hormone (TSH) levels are associated with insulin resistance in adipocytes. However, the potential mechanism of the association remains uncertain. The objective of this study was to determine the potential role of TSH in the suppression of insulin receptor substrate-1 (IRS-1) expression and IRS-1 tyrosyl phosphorylation, which might contribute to insulin resistance. *Methods*. Mouse 3T3-L1 preadipocytes were differentiated into adipocytes. After treatment with 0.01, 0.1, and 1.0 mIU/ml bovine TSH, the TNF-α concentration in the medium was determined by enzyme-linked immunosorbent assay (ELISA). Nuclear factor-kappa B (NF-κB) DNA-binding activity was quantified by electrophoretic mobility shift assay (EMSA). IRS-1 levels in adipocytes were quantified by Western blotting, and tyrosine phosphorylation was measured by immunoprecipitation. *Results*. TSH induced TNF-α secretion in a dose-dependent manner. There was a significant positive correlation between NF-κB DNA-binding activity and TNF-α secretion. This effect and correlation were weakened by BAY 11-7082 (a nuclear NF-κB inhibitor) and H89 (an inhibitor of cyclic adenosine monophosphate- (cAMP-) dependent protein kinase A (PKA)). Treatment of cultured adipocytes with TSH inhibited insulin-stimulated IRS-1 tyrosyl phosphorylation but promoted TSH-dependent secretion of TNF-α and activation of NF-κB DNA-binding activity. The effects of TSH were significantly inhibited by BAY 11-7082 and H89 and were completely blocked by the TNF-α antagonist WP9QY. *Conclusion*. TSH inhibited IRS-1 protein expression and tyrosyl phosphorylation in 3T3-L1 adipocytes by stimulating TNF-α production via promotion of NF-κB DNA-binding activity. TSH might play a pivotal role in the development of insulin resistance.

1. Introduction

Diabetes mellitus (DM) is a major chronic disease affecting humans. More than 95% of all cases of diabetes are type 2 DM (T2DM) [1]. The etiology of T2DM is associated with insulin resistance; specifically, insulin resistance in adipose tissue is a prominent T2DM feature. This insulin resistance results from decreased insulin sensitivity in tissues such as adipose, skeletal muscle, and liver tissues. Adipose tissue secretes numerous cytokines (adipokines), such as leptin [2], tumor necrosis factor-alpha (TNF-α), and interleukin 6 (IL-6) [3, 4]. The association between adipokines and insulin resistance is well known. It has been reported that TNF-α is the key mediator of insulin resistance in obesity because it suppresses insulin activity [5] by potently inhibiting the expression and tyrosyl phosphorylation of insulin receptor substrate-1 (IRS-1, the major insulin-like growth factor-I receptor), which might reduce the ability of IRS-1 to transduce signals in the insulin signaling system [6].

Thyroid-stimulating hormone receptor (TSHR) is expressed not only in thyrocytes but also in adipocytes. Thyroid-stimulating hormone (TSH) may activate TSHR in adipose cells [7, 8]. We previously reported that TSH stimulates TNF-α secretion from adipocytes via a cyclic

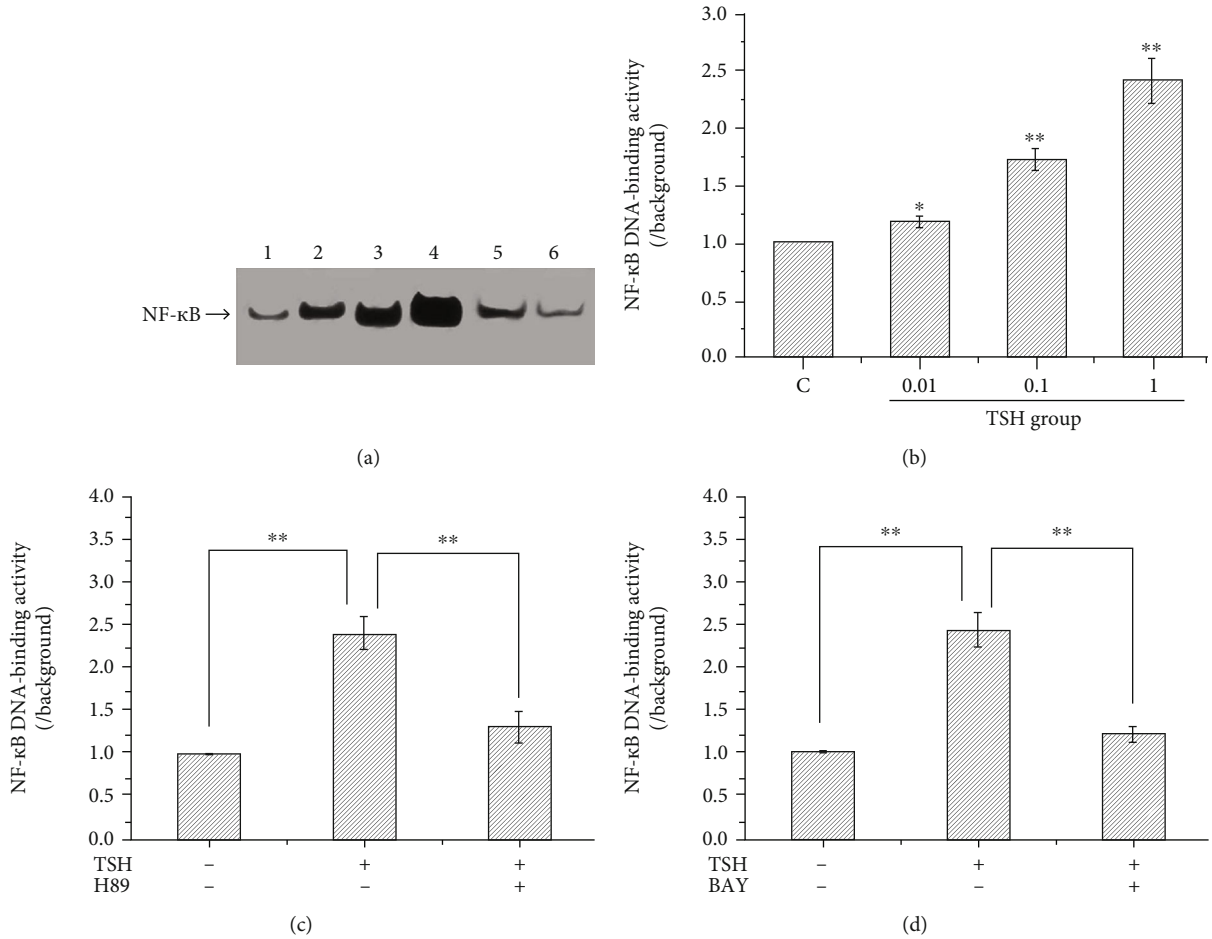

Figure 1: Effect of TSH on the DNA-binding activity of NF-κB in 3T3-L1 adipocytes. (a) Representative autoradiogram showing the NF-κB DNA-binding activity in each group. 1: the control, 2: the TSH concentration of 0.01 mIU/ml, 3: the TSH concentration of 0.1 mIU/ml, 4: the TSH concentration of 1 mIU/ml, 5: after H89; and 6: after BAY 11-7082. (b) NF-κB DNA-binding activity was significantly and dose-dependently upregulated in cells treated with different concentrations of TSH (0.01, 0.1, and 1 mIU/ml) compared with control cells ($P < 0.05$), especially in cells stimulated with 0.1 mIU/ml and 1 mIU/ml TSH ($P < 0.01$). (c) Effects of H89 on NF-κB DNA binding. (d) Effects of BAY 11-7082 on NF-κB DNA-binding. Cells cultured under the same conditions were pretreated with H89 (an inhibitor of cAMP-dependent PKA) or BAY 11-7082 (a nuclear NF-κB inhibitor). NF-κB DNA-binding activity was suppressed after treatment with H89 and BAY 11-7082. The DNA-binding activity of NF-κB was quantified by densitometric analysis. The band intensities were normalized relative to the internal control and background. The number 1 represents the control group; 2, 3, and 4 represent the 0.01, 0.1, and 1 mIU/ml TSH groups, respectively; and 5 and 6 represent the H89- and BAY 11-7082-pretreated groups, respectively. The data are presented as the mean ± SD from three independent experiments ($^{**}P < 0.01$ vs. the 1 mIU/ml TSH group).

adenosine monophosphate- (cAMP-) protein kinase A- (PKA-) dependent pathway [9]. Recently, increasing clinical evidence of the association between TSH and insulin resistance has been obtained [10–12]. However, a few basic studies on the mechanism and signaling pathways of the association between TSH and insulin resistance have been reported. The present study was designed to assess the changes in NF-κB DNA-binding activity, IRS-1 expression, and IRS-1 tyrosyl phosphorylation in 3T3-L1 adipocytes after treatment with TSH and then to determine the potential role of TSH in the suppression of IRS-1 expression and tyrosyl phosphorylation, which might contribute to insulin resistance.

2. Materials and Methods

2.1. Cell Culture and Induced Differentiation of Adipocytes. Mouse 3T3-L1 preadipocytes (ATCC, China) were seeded at a density of 1.5×10^4 cells/cm^2 in Corning polystyrene culture dishes and cultured in Dulbecco's modified Eagle's medium (DMEM) supplemented with 10% calf serum (CS), 100 U/ml penicillin, and 0.1 mg/ml streptomycin (KeyGEN, Nanjing, China) in a humidified 5% CO_2 incubator at 37°C. The medium was replaced every two days. Upon reaching 60-70% confluence, the cells were seeded for experiments and were passaged a maximum of three times. The 3T3-L1 preadipocytes were differentiated as described previously [9].

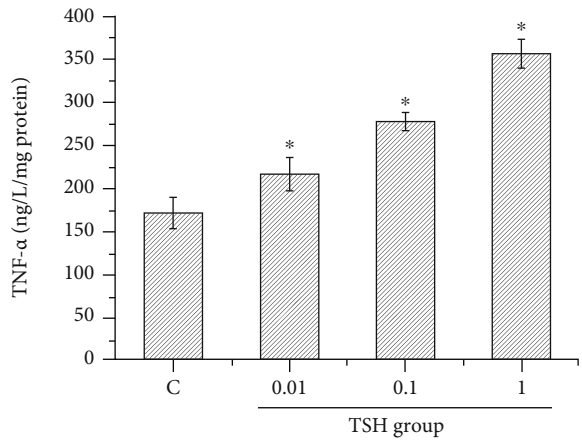

Figure 2: TSH-stimulated 3T3-L1 adipocytes produce TNF-α. Differentiated adipocytes were treated with different concentrations of TSH (0.01, 0.1, and 1 mIU/ml) for 4 h, and the TNF-α concentration in the medium was measured by ELISA. Increasing doses of TSH stimulated 3T3-L1 adipocytes to secrete TNF-α. The data are presented as the mean ± SD ($n = 3$) ($P < 0.05$ for all comparisons).

The adipocytes were starved overnight in serum-free DMEM and treated with different concentrations of TSH (0.01, 0.1, and 1 mIU/ml) or pretreated with 5 μM BAY 11-7082 (a nuclear factor-kappa B (NF-κB) inhibitor, Biyuntian Institute of Biological Technology, China) or 10 μM H89 (an inhibitor of cAMP-dependent PKA, Sigma, CA, USA) for 15 min. The cells and medium were harvested for enzyme-linked immunosorbent assay (ELISA), electrophoretic mobility shift assay (EMSA), or Western blot analysis.

2.2. ELISA. After treatment, the TNF-α concentration in the medium was determined using an ELISA kit (R&D Systems) according to the manufacturer's instructions.

2.3. Nuclear Extract Preparation. Nuclear extracts were prepared from cells using an NE-PER Nuclear and Cytoplasmic Extraction Reagent Kit according to the manufacturer's directions (KeyGEN, Nanjing, China) with some modifications. After two washes with 10 ml of phosphate-buffered saline (PBS), the cells were harvested into 75-cm^2 culture flasks and pelleted by centrifugation at $500 \times g$ for 3 min at 4°C. Each cell pellet was resuspended by gentle pipetting in 1.3 ml of buffer A (10 mM HEPES-KOH (pH 7.9), 10 mM KCl, 1.5 mM MgCl2, 2 mM EDTA, 1 mM dithiothreitol (DTT), 1 mM phenylmethanesulfonyl fluoride, and 1 μM pepstatin). After centrifugation at $12{,}000 \times g$ for 15 sec at 4°C, the cells were lysed via incubation on ice for 10 min in 100 μl of buffer B and then centrifuged at $16{,}000 \times g$ for 5 min. The pellet was washed with PBS(−), resuspended in 100 μl of buffer C (20 mM HEPES-KOH (pH 7.9), 0.4 M KCl, 2 mM EDTA, 1 mM DTT, 1 mM phenylmethanesulfonyl fluoride, and 1 μM pepstatin) and lysed by freezing and thawing. After centrifugation at $16{,}000 \times g$ for 10 min at 4°C, the supernatant was used as a nuclear extract. The protein concentration in each lysate was measured by bicinchoninic acid (BCA) assay. The extracts were aliquoted and stored at -80°C until analysis by EMSA.

2.4. EMSA. EMSA was performed using a Chemiluminescent EMSA Kit (Biyuntian Institute of Biological Technology, China) according to the manufacturer's protocol with double-stranded oligonucleotides encoding the NF-κB consensus sequence (5′-AGT TGA GGG GAC TTT CCC AGG C-3′ and 3′-TCA ACT CCC CTG AAA GGG TCC G-5′), which were end-labeled with biotin (Biyuntian Institute of Biological Technology, China). Nuclear extracts (2.5 μg) were added to 10 μl of binding reagent and incubated for 20 min at room temperature. The bound complexes were resolved by electrophoresis on nondenaturing 6% polyacrylamide gels using 0.5× TBE as the running buffer and assessed by autoradiography. To establish the specificity of the reaction, negative controls without cell extracts were used. In a cold probe competition reaction, 50-fold corresponding unlabeled probe was added for preincubation.

2.5. Western Blotting. The procedures used for preparation of cytosolic extracts and Western blot analysis have been described previously [9]. In brief, the protein concentration in each lysate was measured by BCA assay. Equal amounts of protein were separated by SDS-PAGE. After electrophoresis, the proteins were transferred onto nitrocellulose membranes. The membranes were incubated with an anti-IRS-1-pTyr^{15} antibody (1 : 500, Biyuntian Institute of Biological Technology, China) or an anti-β-tubulin antibody (1 : 1000, Sungene Biotech Co., Ltd., Tianjin, China). The membranes were then incubated with a peroxidase-conjugated secondary antibody (1 : 5000, Santa Cruz Biotechnology). After rinsing, chemiluminescent detection was performed using an ECL Western blot detection kit followed by exposure and development of X-ray film. The Western blot results were analyzed by densitometry. Where indicated, the membranes were stripped according to the manufacturer's directions before reblotting.

2.6. Immunoprecipitation. 3T3-L1 adipocytes were lysed in RIPA buffer on ice for 10 min. The cytosolic extracts were prepared by centrifuging the lysates twice at 12,000 rpm for 10 min at 4°C. The cytosolic extracts were incubated with an anti-IRS-1 antibody overnight at 4°C with shaking. The immunocomplexes were captured by adding protein A/G-agarose and gently rotating the samples for 2 h at 4°C. The immunocomplex precipitates were washed with PBS three times, and the immunoprecipitated proteins were subjected to Western blot analysis using an anti-IRS-1 antibody.

2.7. Statistical Analyses. Each experiment was performed at least in triplicate. Statistical analyses were performed using Student's t-test or analysis of variance (ANOVA). All the data are presented as the mean ± SD, and $P < 0.05$ was considered to indicate significance.

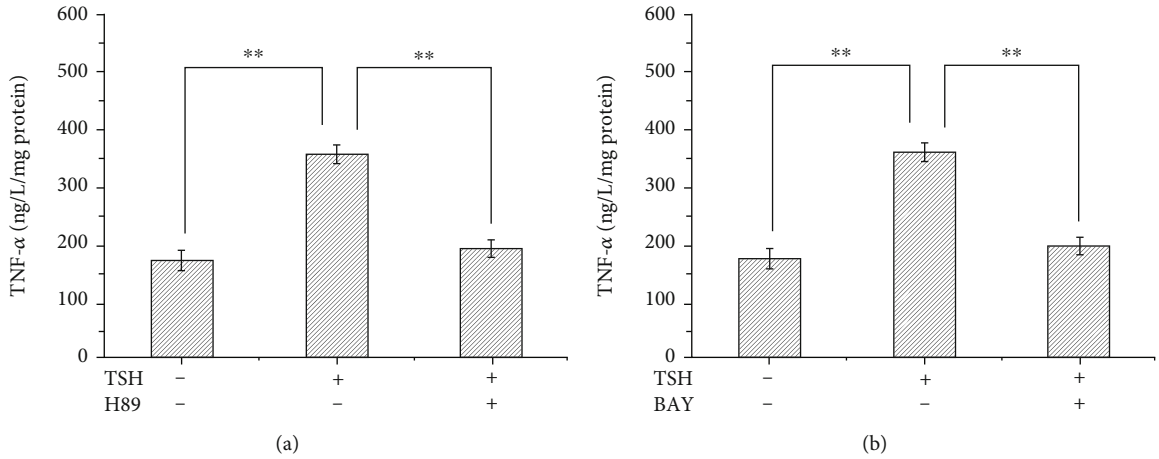

Figure 3: Factors that affect TNF-α secretion from 3T3-L1 adipocytes. (a) Pretreatment of cells with the PKA inhibitor H89 (10 μM) for 15 minutes before treatment with 1 mIU/ml bovine TSH decreased TNF-α levels. (b) Pretreatment with the nuclear NF-κB inhibitor BAY 11-7082 (5 μM) reduced TSH-stimulated TNF-α production. These results suggested that H89 and BAY 11-7082 inhibited the effect of TSH on TNF-α secretion. The data demonstrated that TSH stimulated 3T3-L1 adipocytes to secrete TNF-α via the cAMP-PKA pathway. The data are presented as the mean ± SD ($n = 3$) ($^{**}P < 0.01$).

3. Results

In a previous study, we detected the IκBα/PKAc complex in lysates of 3T3-L1 adipocytes treated with bovine TSH by coimmunoprecipitation and Western blotting [9]. To investigate whether TSH activates NF-κB, we measured the NF-κB DNA-binding activity in 3T3-L1 adipocytes treated with different concentrations of TSH (0.01, 0.1, and 1 mIU/ml) or pretreated with 5 μM BAY 11-7082 (a nuclear NF-κB inhibitor) or 10 μM H89 (an inhibitor of cAMP-dependent PKA). Nuclear extracts were used to analyze NF-κB DNA-binding activity via EMSA. It was found that NF-κB DNA-binding activity was significantly and dose-dependently upregulated in cells treated with different concentrations of TSH (0.01, 0.1, and 1 mIU/ml) compared with control cells, especially in cells stimulated with 0.1 mIU/ml and 1 mIU/ml TSH ($P < 0.01$) (Figures 1(a) and 1(b)). These results indicated that TSH increased NF-κB DNA-binding activity in adipocytes. Pretreatment with H89 significantly suppressed the TSH-dependent activation of the slow-migrating complex (Figures 1(a) and 1(c)). No apparent protein-κBwt complex was observed when the nuclear extracts prepared from cells pretreated with 5 μM BAY 11-7082 were examined (Figures 1(a) and 1(d)). This result indicated that BAY 11-7082 and H89, especially BAY 11-7082, significantly blocked TSH-stimulated NF-κB activation. This binding reaction was shown to be specific since an excess of unlabeled NF-κB probe decreased the signals of the slow-migrating bands.

We have previously reported that TSH stimulates TNF-α secretion from adipocytes in a dose-dependent manner by elevating the levels of phospho-NF-κBp65 Ser276 via the PKA signaling pathway [9]. To investigate the effects of NF-κB DNA-binding activity on TSH-stimulated TNF-α secretion, adipocytes were treated with different concentrations of TSH (0.01, 0.1, and 1 mIU/ml) for 4 h. Some cells were pretreated with 10 μM H89 or 5 μM BAY 11-7082 for 15 min and then treated with 1 mIU/ml TSH for 4 h; the TNF-α concentration in the medium was measured by ELISA. These experiments showed the same results as our previous study: TNF-α secretion increased with increasing doses of TSH ($P < 0.01$ or $P < 0.05$) (Figure 2). H89 and BAY 11-7082 reduced TSH-stimulated TNF-α production by ~46% (Figures 3(a) and 3(b)). Previous research has shown that free NF-κB translocates into the nucleus, binds to specific DNA regions, and triggers numerous transcriptional events and cellular responses [13]. Since TNF-α transcription is positively regulated by NF-κB, the experimental results indicated that TSH-stimulated NF-κB DNA-binding activity resulted in enhanced TNF-α transcriptional activity via the PKA signaling pathway.

Previously, Shen et al. [6] have reported that TNF-α inhibits IRS-1 expression and tyrosyl phosphorylation. Since TSH can stimulate the production of TNF-α, we next tested whether TSH can suppress the protein expression and tyrosine phosphorylation of IRS-1. IRS-1 levels in adipocytes were quantified by Western blotting, and tyrosine phosphorylation was measured by immunoprecipitation after pretreatment with 100 nM insulin for 10 min and subsequent treatment with different concentrations of TSH (0.01, 0.1, and 1 mIU/ml) for 24 h. Tyrosine phosphorylation of IRS-1 decreased with increasing doses of TSH ($P < 0.01$ or $P < 0.05$) (Figure 4) and was inhibited by H89 and BAY 11-7082 (Figures 5(a) and 5(b)). The opposite effects were observed for TSH-dependent secretion of TNF-α and activation of NF-κB DNA-binding activity.

IRS-1 is the major insulin-like growth factor-I receptor (IGF-IR). Insulin resistance is associated with a reduced ability of insulin to activate a variety of events in the insulin signaling system, such as tyrosine phosphorylation of IRS-1 [14]. It has been reported that TNF-α is the key mediator of insulin resistance because it can reduce insulin signaling by potently inhibiting insulin receptor (IR) tyrosine kinase, which might reduce the ability of IRS-1 to transduce signals in the insulin signaling system [5, 14]. Next, we aimed to

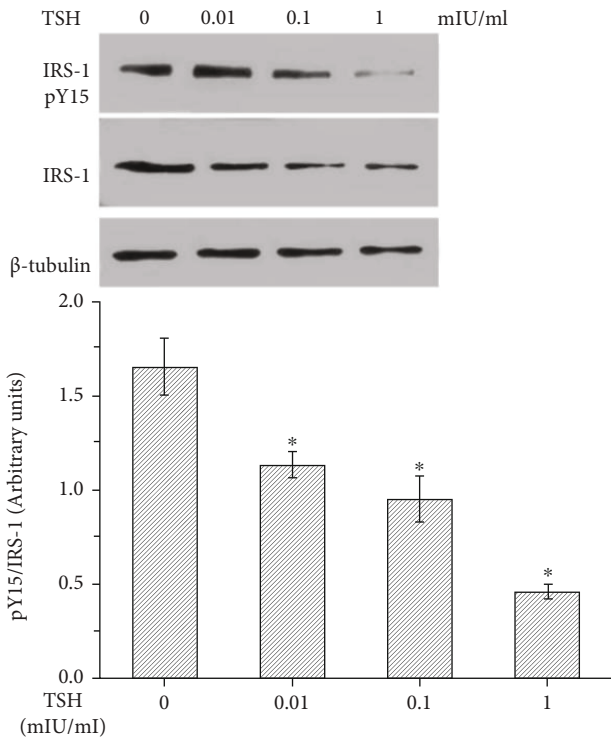

Figure 4: TSH decreased tyrosine phosphorylation of IRS-1 in 3T3-L1 adipocytes. Cells were pretreated with 100 nM insulin for 10 min and then treated with different concentrations of TSH (0.01, 0.1, and 1 mIU/ml) for 24 h. IRS-1 levels in adipocytes were quantified by Western blotting, and tyrosine phosphorylation was measured by immunoprecipitation. The relative expression levels of IRS-1 and IRS-1-tyr in each treatment group were calculated using β-tubulin as the standard. Treatment with various concentrations of bovine TSH (0.01, 0.1, and 1 mIU/ml) increased the ratio of phosphorylated IRS-1 to total IRS-1 in a dose-dependent manner in 3T3-L1 adipocytes. These data indicated that TSH suppressed IRS-1 tyrosyl phosphorylation in 3T3-L1 adipocytes ($P < 0.05$ for all comparisons).

identify the underlying molecular mechanisms responsible for TSH-mediated inhibition of IRS-1 tyrosyl phosphorylation (Tyr^{15}). We investigated the effects of TSH on IRS-1 tyrosyl phosphorylation in adipocytes treated with 100 nM insulin and then coincubated with 1 mIU/ml TSH in the absence or presence of WP9QY. In the present study, cells treated with insulin (the positive control group) exhibited ~61% higher IRS-1 tyrosyl phosphorylation than the untreated control cells (Figure 6). IRS-1 tyrosyl phosphorylation was ~72% lower in TSH-treated 3T3-L1 adipocytes than in positive control cells (insulin-treated cells). WP9QY is a TNF-α antagonist designed to mimic the most critical tumor necrosis factor (TNF) recognition loop on TNF receptor I. It prevents interactions of TNF with its receptor. Pretreatment with WP9QY significantly reversed the TSH-induced decrease in IRS-1 tyrosyl phosphorylation (Figure 6). Taken together, these observations strongly suggest that TSH plays an important role in downregulating IRS-1 tyrosyl phosphorylation by inducing TNF-α secretion in 3T3-L1 adipocytes.

4. Discussion

As dietary structures and lifestyles change, the incidence and prevalence of T2DM continue to increase. In 2010, there were approximately 220 million DM patients worldwide, and the rates of T2DM are expected to reach epidemic levels before 2030 [1]. The increases in incidence and prevalence will be associated with significant increases in the numbers of patients with diabetes complications, which could lead to disastrous outcomes. Insulin resistance is a characteristic feature in most patients with T2DM.

Insulin is a pleiotropic hormone that has diverse functions; for example, it stimulates nutrient transport into cells, regulates glycometabolism, modifies enzymatic activity, and regulates energy homeostasis via actions in the arcuate nucleus [15, 16]. Reduced insulin action is associated with reduced insulin-stimulated activity of enzymes such as glycogen synthase and hexokinase [17, 18], and adipose tissue insulin resistance (adipo-IR) plays important roles [19, 20]. Adipose tissue functions not only as an energy depot [21] but also as an organ that exerts its effects through both paracrine and endocrine mechanisms [22]. Adipose tissue is understood to secrete numerous cytokines (adipokines), such as leptin [2], TNF-α, and IL-6 [3, 4]. It has been reported that these adipokines are the key mediators of insulin resistance because they suppress insulin activity (especially TNF-α) [5].

Recently, increasing numbers of studies have focused on the correlation between TSH and insulin resistance. An elevated risk for insulin resistance appears to be independently associated with subclinical hypothyroidism [23]. In addition, numerous reports have suggested that serum TSH levels are significantly associated with the homeostasis model assessment index for insulin resistance (HOMA-IR) [10] and negatively associated with the insulin sensitivity index [12, 23, 24]. Moreover, high-normal TSH levels are significantly associated with increased insulin resistance [10]. Currently, controversy exists regarding the upper limit of normal serum TSH values (above which treatment should be indicated), and it has been suggested that baseline thyrotropin concentrations greater than 2.2 mIU/L may be predictive of hypothyroidism in patients with DM [11]. In a previous study, we found that serum levels of TSH were higher in T2DM patients than in nondiabetic volunteers. Overall, there is an abundance of evidence that TSH levels are associated with insulin resistance, although the mechanisms of this association are unknown.

Many studies have shown that TSHR is expressed in thyrocytes as well as in extrathyroidal cells [7, 8]. The extrathyroidal effects of TSH on adipocytes have also been extensively studied [25, 26]. TSH, which is secreted by the anterior pituitary gland, not only regulates the endocrine function of the thyroid gland but also acts on adipocytes by binding directly to TSH receptors (TSHRs) expressed on adipocytes [7, 27–29]. Lisboa et al. [30] reported that TSH stimulates leptin secretion by adipocytes. It has also been reported that TSH stimulates 3T3-L1 adipocytes to release cAMP and glycerin in a dose-dependent manner [31]. We have reported previously that TSH stimulates TNF-α secretion from adipocytes

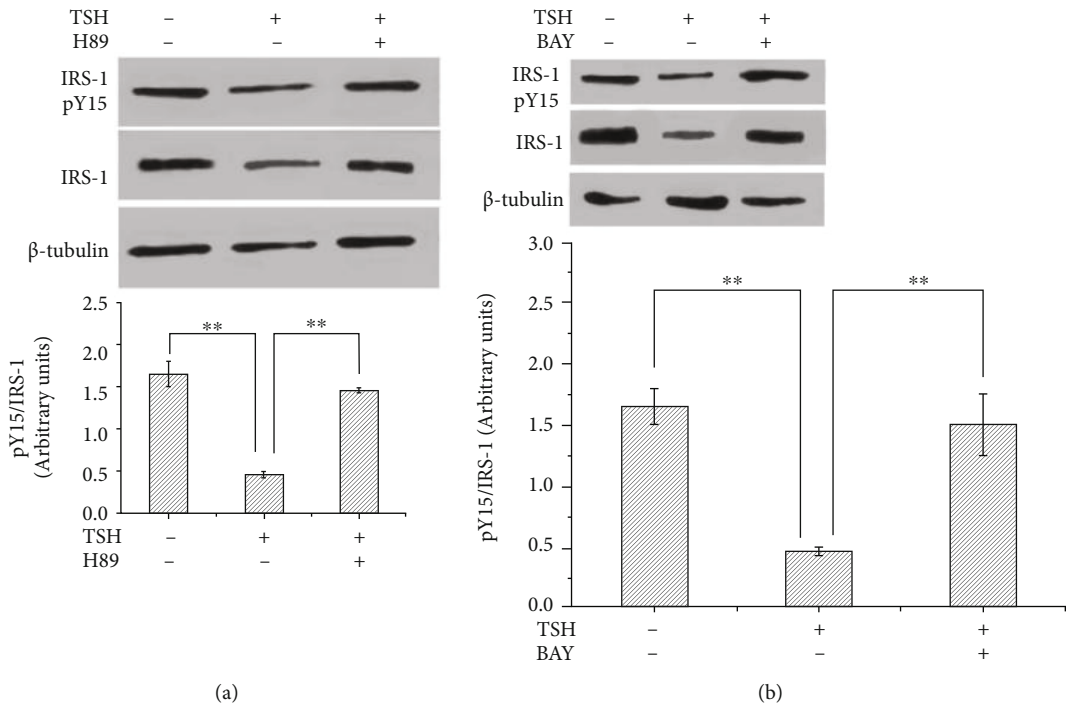

Figure 5: BAY 11-7082 and H89 inhibited the TSH-mediated downregulation of tyrosine phosphorylation of IRS-1 in 3T3-L1 adipocytes. (a) After pretreatment with 10 μM H89 for 15 minutes and treatment with 1 mIU/ml bovine TSH, phosphorylated IRS-1 levels were unchanged in 3T3-L1 adipocytes. (b) Pretreatment of cells with BAY 11-7082 inhibited the TSH-dependent increases in phosphorylated IRS-1 levels. The data are presented as the mean ± SD ($n = 3$) ($^{*}P < 0.05$, $^{**}P < 0.01$).

via a cAMP-PKA-dependent pathway [9]. Likewise, in our present study, we found that TSH increased NF-κB DNA-binding activity in adipocytes and that TNF-α secretion increased with increasing doses of TSH. However, all of these effects were alleviated by BAY 11-7082 (a nuclear NF-κB inhibitor) and H89 (an inhibitor of cAMP-dependent PKA). NF-κB is a multidirectional transcription factor that is involved in regulating the transcription of inflammatory mediators, cytokines, and growth factors, among other molecules. Transcriptional activation of NF-κB increases the mRNA expression of NF-κB target genes such as TNFα. Our data demonstrate that TSH-stimulated NF-κB DNA-binding activity results in enhanced TNF-α transcriptional activity via the PKA signaling pathway.

The functions of insulin are exerted across a variety of insulin target tissues through several intracellular signaling cascades. Under normal conditions, insulin binds to IR in cell membranes to activate IR tyrosine kinase and triggers a series of insulin signal transduction responses in cells. The insulin signaling cascade branches into two main pathways. The first is the phosphatidylinositol 3-kinase- (PI3K-) AKT pathway, which is largely responsible for the effect of insulin on glucose uptake as well as other metabolic actions of insulin, including suppression of gluconeogenesis. The second pathway is the Ras-mitogen-activated protein kinase (MAPK) pathway, which mediates gene expression [32]. IRS-1 is a cellular signaling carrier protein involved in the modulation of intracellular bioinformation and recognizes messages from insulin receptors. Insulin binding induces receptor tyrosine autophosphorylation, which is followed by the tyrosine phosphorylation of IRS-1 and IRS-2 [33]. Tyrosyl phosphorylation of IRS-1 and IRS-2 activates downstream molecules and subsequently modulates blood glucose levels. It has been suggested that IRS-1 functions in glycometabolism by regulating insulin signals in the muscle and adipose tissues, whereas IRS-2 is a major participant in hepatic insulin action [34]. IRS-1 is the main IGF-IR, as defects in insulin signaling typically involve this insulin receptor substrate. Notably, IRS-1-deficient mice show a phenotype of peripheral insulin resistance (mainly in muscle and white adipose tissue) [35, 36]. Tyrosine phosphorylation of IRS-1 initiates signal transduction. However, the serine/threonine phosphorylation of IRS-1 subsequently suppresses tyrosine phosphorylation and blocks insulin signaling [37].

Proinflammatory cytokines can cause insulin resistance in adipose, skeletal muscle, and liver tissue by inhibiting insulin signal transduction. The sources of cytokines in insulin-resistant states are the insulin target tissue themselves. TNF-α is a proinflammatory cytokine secreted partly by adipocytes. TNF-α is an important mediator of insulin resistance. The possible mechanisms by which TNF-α impairs insulin signal transduction involve downregulation of IR and IRS-1 expression, inhibition of tyrosyl phosphorylation of IR and IRS-1, increased serine/threonine phosphorylation of IRS-1, decreased activity of IR kinase and protein tyrosine phosphatases (PTPs), and inhibition of insulin-stimulated glucose transporters [38, 39]. A previous study has revealed that treatment of cultured 3T3-L1 adipocytes with TNF-α leads to reduced expression of the IR, IRS1, and glucose transporter 4 (GLUT4) genes as well as a

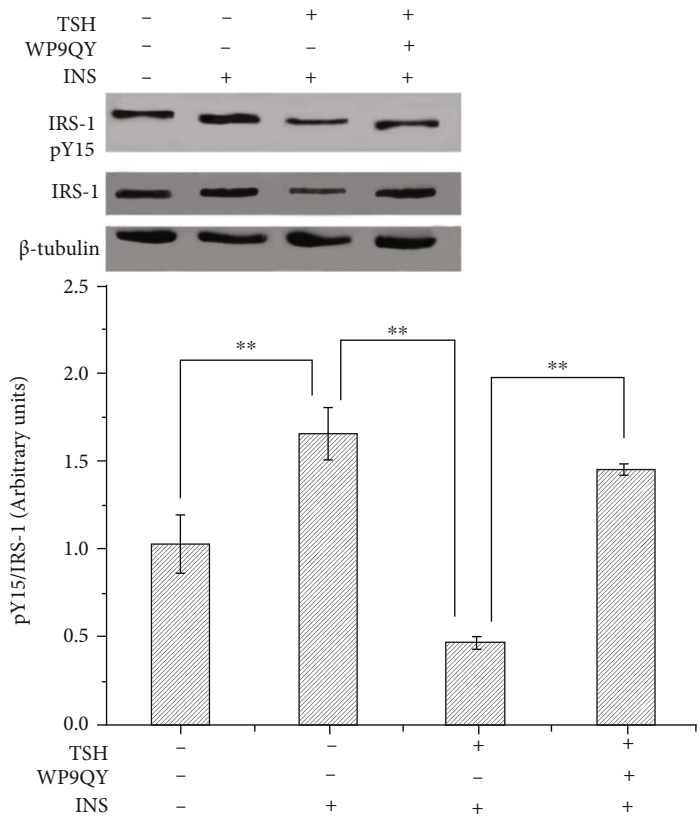

Figure 6: Effect of TSH on TNF-α-induced inhibition of insulin signals in 3T3-L1 adipocytes. Adipocytes were treated with 100 nM insulin and then coincubated with 1 mIU/ml TSH in the absence or presence of WP9QY. (a) Cells treated with insulin (the positive control group) exhibited higher IRS-1 tyrosyl phosphorylation levels than untreated control cells (the negative control group). TSH decreased IRS-1 tyrosyl phosphorylation. (b) Pretreatment with WP9QY significantly reversed the TSH-induced decrease in IRS-1 tyrosyl phosphorylation. The data are presented as the mean ± SD ($n = 3$) ($^{**}P < 0.01$).

decrease in insulin-stimulated glucose uptake. [40]. The initiating factors of this inflammatory response remain to be fully determined. Our current results demonstrate that treatment of cultured adipocytes with TSH inhibited insulin-stimulated IRS-1 tyrosyl phosphorylation. Pretreatment with BAY 11-7082 or H89 significantly reversed the TSH-induced decrease in IRS-1 tyrosyl phosphorylation. The opposite effects were observed for TSH-dependent secretion of TNF-α and activation of NF-κB DNA-binding activity. WP9QY, a TNF-α antagonist, was designed to mimic the most critical TNF recognition loop on TNF receptor I. It prevents interactions of TNF with its receptor. Pretreatment with WP9QY prevented the TSH-induced decreased in IRS-1 expression and tyrosyl phosphorylation in 3T3-L1 adipocytes. The present results demonstrate that TSH can inhibit IRS-1 tyrosyl phosphorylation in adipocytes by stimulating the production of TNF-α via TSH-mediated promotion of NF-κB DNA-binding activity.

Downregulation of IRS-1 expression and tyrosyl phosphorylation suppresses the activity of PI3K. Suppression of PI3K activity might reduce insulin sensitivity and the efficiency of translocation of glucose transporters, leading to inhibition of glycogen synthesis-related gene modulation [41]. On the basis of our previous results indicating that TSH can downregulate GLUT4 expression and inhibit GLUT4 translocation to the plasma membrane [9], we speculate that TSH might play a pivotal role in the development of insulin resistance and that TSH is an important therapeutic target for improvement of insulin resistance.

Currently, the biological effects of TSH on adipocytes are likely underappreciated. The novelty of our study resides in the identification of TSH as a potentially novel mediator of the development of insulin resistance in adipocytes. However, the mechanism of insulin resistance is complicated. The results of this study are limited to in vitro cultures of 3T3-L1 adipocytes and cannot fully explain the role of TSH in human adipose tissue. Further studies on this topic may be warranted.

Data Availability

The analyzed datasets generated during the study are available from the corresponding author on reasonable request.

Ethical Approval

This study does not involve any human or animal testing. The study was approved by the ethics committee of Tianjin Medical University Chu Hsien-I Memorial Hospital & Tianjin Institute of Endocrinology.

Conflicts of Interest

There are no conflicts of interest to declare.

Acknowledgments

This study was supported by the NHC Key Laboratory of Hormones and Development, Tianjin Key Laboratory of Metabolic Diseases, Tianjin Medical University Chu Hsien-I Memorial Hospital & Tianjin Institute of Endocrinology. The authors also thank the support from National Natural Science Foundation of China (81972899).

References

[1] H. Karimi, M. Nezhadali, and M. Hedayati, "Association between adiponectin rs 17300539 and rs 266729 gene polymorphisms with serum adiponectin level in an Iranian diabetic/pre-diabetic population," *Endocrine Regulations*, vol. 52, no. 4, pp. 176–184, 2018.

[2] A. Andres-Hernando, M. A. Lanaspa, M. Kuwabara et al., "Obesity causes renal mitochondrial dysfunction and energy imbalance and accelerates chronic kidney disease in mice," *American Journal of Physiology. Renal Physiology*, vol. 317, no. 4, pp. F941–F948, 2019.

[3] A. K. Azad, S. Chakrabarti, Z. Xu, S. T. Davidge, and Y. Fu, "Coiled-coil domain containing 3 (CCDC3) represses tumor necrosis factor-α/nuclear factor κB-induced endothelial inflammation," *Cellular Signalling*, vol. 26, no. 12, pp. 2793–2800, 2014.

[4] M. Y. Chung, S. J. Hong, and J. Y. Lee, "The influence of obesity on postoperative inflammatory cytokine levels," *The Journal of International Medical Research*, vol. 39, no. 6, pp. 2370–2378, 2011.

[5] G. Atila Uslu and H. Uslu, "Evaluating the effects of *Juglans regia* L. extract on hyperglycaemia and insulin sensitivity in experimental type 2 diabetes in rat," *Archives of Physiology and Biochemistry*, vol. 128, no. 1, pp. 121–125, 2022.

[6] S.-C. Shen, W.-C. Chang, and C.-L. Chang, "Fraction from wax apple [Syzygium samarangense (Blume) Merrill and Perry] fruit extract ameliorates insulin resistance via modulating insulin signaling and inflammation pathway in tumor necrosis factor α-treated FL83B mouse hepatocytes," *International Journal of Molecular Sciences*, vol. 13, no. 7, pp. 8562–8577, 2012.

[7] S. Neumann, A. Pope, E. Geras-Raaka, B. M. Raaka, R. S. Bahn, and M. C. Gershengorn, "A drug-like antagonist inhibits thyrotropin receptor-mediated stimulation of cAMP production in Graves' orbital fibroblasts," *Thyroid*, vol. 22, no. 8, pp. 839–843, 2012.

[8] A. Sorisky, T. T. Antunes, and A. Gagnon, "The adipocyte as a novel TSH target," *Mini Reviews in Medicinal Chemistry*, vol. 8, no. 1, pp. 91–96, 2008.

[9] Y. J. Zhang, W. Zhao, M. Y. Zhu, S. S. Tang, and H. Zhang, "Thyroid-stimulating hormone induces the secretion of tumor necrosis factor-α from 3T3-L1 adipocytes via a protein kinase A-dependent pathway," *Experimental and Clinical Endocrinology & Diabetes*, vol. 121, no. 8, pp. 488–493, 2013.

[10] H. Xiao, Y. Lu, X. Cheng et al., "Correlation of thyroid-stimulating hormone with metabolic syndrome in euthyroid male elders," *Zhonghua Yi Xue Za Zhi*, vol. 94, no. 14, pp. 1055–1059, 2014.

[11] S. Kouidhi, R. Berhouma, M. Ammar et al., "Relationship of thyroid function with obesity and type 2 diabetes in euthyroid Tunisian subjects," *Endocrine Research*, vol. 38, no. 1, pp. 15–23, 2013.

[12] M. S. Saleem, T. A. Shirwany, and K. A. Khan, "Relationship of thyroid-stimulating hormone with metabolic syndrome in a sample of euthyroid Pakistani population," *Journal of Ayub Medical College, Abbottabad*, vol. 23, no. 2, pp. 63–68, 2011.

[13] X. Zheng, W. Zheng, S. Liu et al., "Crosstalk between JNK and NF-κB in the KDO2-mediated production of TNFα in HAPI cells," *Cellular and Molecular Neurobiology*, vol. 32, no. 8, pp. 1375–1383, 2012.

[14] M. Y. Ali, S. Zaib, M. M. Rahman et al., "Didymin, a dietary citrus flavonoid exhibits anti-diabetic complications and promotes glucose uptake through the activation of PI3K/Akt signaling pathway in insulin-resistant HepG2 cells," *Chemico-Biological Interactions*, vol. 305, pp. 180–194, 2019.

[15] K. Sharabi, C. D. J. Tavares, and P. Puigserver, "Regulation of hepatic metabolism, recent advances, and future perspectives," *Current Diabetes Reports*, vol. 19, no. 10, p. 98, 2019.

[16] M. Ahmad, L. He, and N. Perrimon, "Regulation of insulin and adipokinetic hormone/glucagon production in flies," *Wiley Interdisciplinary Reviews*, vol. 9, no. 2, article e360, 2020.

[17] A. Abulizi, J. P. Camporez, M. J. Jurczak et al., "Adipose glucocorticoid action influences whole-body metabolismviamodulation of hepatic insulin action," *The FASEB Journal*, vol. 33, no. 7, pp. 8174–8185, 2019.

[18] K. Rufinatscha, C. Ress, S. Folie et al., "Metabolic effects of reduced growth hormone action in fatty liver disease," *Hepatology International*, vol. 12, no. 5, pp. 474–481, 2018.

[19] B. S. Mühlhäusler, C. Toop, and S. Gentili, "Nutritional models of type 2 diabetes mellitus," *Methods in Molecular Biology*, vol. 2076, pp. 43–69, 2020.

[20] L. Vishvanath and R. K. Gupta, "Contribution of adipogenesis to healthy adipose tissue expansion in obesity," *The Journal of Clinical Investigation*, vol. 129, no. 10, pp. 4022–4031, 2019.

[21] J. S. Flier, "The adipocyte: storage depot or node on the energy information superhighway?," *Cell*, vol. 80, no. 1, pp. 15–18, 1995.

[22] R. S. Ahima, "Adipose tissue as an endocrine organ," *Obesity*, vol. 14, Suppl 5, pp. 242S–249S, 2006.

[23] J. M. Fernández-Real, A. López-Bermejo, A. Castro, R. Casamitjana, and W. Ricart, "Thyroid function is intrinsically linked to insulin sensitivity and endothelium-dependent vasodilation in healthy euthyroid subjects," *The Journal of Clinical Endocrinology and Metabolism*, vol. 91, no. 9, pp. 3337–3343, 2006.

[24] S. A. Chubb, W. A. Davis, and T. M. Davis, "Interactions among thyroid function, insulin sensitivity, and serum lipid concentrations: the Fremantle diabetes study," *The Journal of Clinical Endocrinology and Metabolism*, vol. 90, no. 9, pp. 5317–5320, 2005.

[25] M. K. Moon, G. H. Kang, H. H. Kim et al., "Thyroid-stimulating hormone improves insulin sensitivity in skeletal muscle cells via cAMP/PKA/CREB pathway-dependent upregulation of insulin receptor substrate-1 expression," *Molecular and Cellular Endocrinology*, vol. 436, pp. 50–58, 2016.

[26] A. Bell, A. Gagnon, and A. Sorisky, "TSH stimulates IL-6 secretion from adipocytes in culture," *Arteriosclerosis, Thrombosis, and Vascular Biology*, vol. 23, no. 12, pp. e65–e66, 2003.

[27] S. Lu, Q. Guan, Y. Liu et al., "Role of extrathyroidal TSHR expression in adipocyte differentiation and its association with

obesity," *Lipids in Health and Disease*, vol. 11, no. 1, p. 17, 2012.

[28] S. Gormez, A. Demirkan, F. Atalar et al., "Adipose tissue gene expression of adiponectin, tumor necrosis factor-α and leptin in metabolic syndrome patients with coronary artery disease," *Internal Medicine*, vol. 50, no. 8, pp. 805–810, 2011.

[29] M. Pomerance, H. B. Abdullah, S. Kamerji, C. Correze, and J. P. Blondeau, "Thyroid-stimulating hormone and cyclic AMP activate p38 mitogen-activated protein kinase cascade:," *The Journal of Biological Chemistry*, vol. 275, no. 51, pp. 40539–40546, 2000.

[30] P. C. Lisboa, E. Oliveira, A. T. Fagundes et al., "Postnatal low protein diet programs leptin signaling in the hypothalamic-pituitary-thyroid axis and pituitary TSH response to leptin in adult male rats," *Hormone and Metabolic Research*, vol. 44, no. 2, pp. 114–122, 2012.

[31] D. Jiang, S. Ma, F. Jing et al., "Thyroid-stimulating hormone inhibits adipose triglyceride lipase in 3T3-L1 adipocytes through the PKA pathway," *PLoS One*, vol. 10, no. 1, article e0116439, 2015.

[32] C. M. Taniguchi, B. Emanuelli, and C. R. Kahn, "Critical nodes in signalling pathways: insights into insulin action," *Nature Reviews Molecular Cell Biology*, vol. 7, no. 2, pp. 85–96, 2006.

[33] R. M. Evans, G. D. Barish, and Y. X. Wang, "PPARs and the complex journey to obesity," *Nature Medicine*, vol. 10, no. 4, pp. 355–361, 2004.

[34] S. B. Biddinger and C. R. Kahn, "From mice to men: insights into the insulin resistance syndromes," *Annual Review of Physiology*, vol. 68, no. 1, pp. 123–158, 2006.

[35] E. Araki, M. A. Lipes, M. E. Patti et al., "Alternative pathway of insulin signalling in mice with targeted disruption of the *IRS-1* gene," *Nature*, vol. 372, no. 6502, pp. 186–190, 1994.

[36] H. Tamemoto, T. Kadowaki, K. Tobe et al., "Insulin resistance and growth retardation in mice lacking insulin receptor substrate-1," *Nature*, vol. 372, no. 6502, pp. 182–186, 1994.

[37] H. Kwon, J. Lee, K. Jeong, D. Jang, and Y. Pak, "Fatty acylated caveolin-2 is a substrate of insulin receptor tyrosine kinase for insulin receptor substrate-1-directed signaling activation," *Biochimica et Biophysica Acta*, vol. 1853, no. 5, pp. 1022–1034, 2015.

[38] L. F. del Aguila, K. P. Claffey, and J. P. Kirwan, "TNF-alpha impairs insulin signaling and insulin stimulation of glucose uptake in C2C12 muscle cells," *The American Journal of Physiology*, vol. 276, no. 5, pp. E849–E855, 1999.

[39] Y. N. Liu, J. H. Jung, H. Park, and H. Kim, "Olive leaf extract suppresses messenger RNA expression of proinflammatory cytokines and enhances insulin receptor substrate 1 expression in the rats with streptozotocin and high-fat diet-induced diabetes," *Nutrition Research*, vol. 34, no. 5, pp. 450–457, 2014.

[40] J. M. Stephens, J. Lee, and P. F. Pilch, "Tumor necrosis factor-α-induced insulin resistance in 3T3-L1 adipocytes is accompanied by a loss of insulin receptor substrate-1 and GLUT4 expression without a loss of insulin receptor-mediated signal transduction∗," *The Journal of Biological Chemistry*, vol. 272, no. 2, pp. 971–976, 1997.

[41] M. V. Vijayakumar, S. Singh, R. R. Chhipa, and M. K. Bhat, "The hypoglycaemic activity of fenugreek seed extract is mediated through the stimulation of an insulin signalling pathway," *British Journal of Pharmacology*, vol. 146, no. 1, pp. 41–48, 2005.

Hindawi
Disease Markers
Volume 2022, Article ID 1579928, 7 pages
https://doi.org/10.1155/2022/1579928

Research Article

Analysis of Rehabilitation Effect of Neurology Nursing on Stroke Patients with Diabetes Mellitus and Its Influence on Quality of Life and Negative Emotion Score

Yanhong Yang,[1] Guixia Niu,[2] Qing Mi,[1] Feifei Hong,[1] and Guiqin Zhang[3]

[1]*Second Department of Neurology, People's Hospital Affiliated to Shandong First Medical University, Jinan 271199, Shandong Province, China*
[2]*Second Department of Rehabilitation Medicine, People's Hospital Affiliated to Shandong First Medical University, Jinan 271199, Shandong Province, China*
[3]*Department of Science Teaching, People's Hospital Affiliated to Shandong First Medical University, Jinan 271199, Shandong Province, China*

Correspondence should be addressed to Guiqin Zhang; jiaoyou253uf@126.com

Received 14 January 2022; Revised 16 February 2022; Accepted 24 February 2022; Published 10 March 2022

Academic Editor: Yaoyao Bian

Objective. To explore and analyze the rehabilitation effect of neurology nursing on stroke patients with diabetes mellitus (DM) and its influence on quality of life and negative emotion score. *Methods*. In this experiment, 110 stroke patients with DM diagnosed and treated in our hospital from 2018 to 2020 were randomly selected and assigned to the study group (SG) and the control group (CG) according to different nursing methods, with 55 cases in each group. In SG, they were given neurology nursing. In CG, they were given routine nursing. The rehabilitation efficacy, quality of life, and negative emotion scores were compared between the two groups. *Results*. Compared with the CG, the levels of fasting blood glucose, 2 h postprandial blood glucose, and urinary microalbumin in SG were obviously better after treatment. In SG, the proportion of patients with basic recovery and significant improvement after treatment was higher, and the proportion of patients without treatment effect was significantly lower. Overall, the nursing effect of the SG after treatment was better than that of the CG. There was no striking difference in the quality of life and Morisky scores between the two groups before nursing intervention ($P > 0.05$), but the quality of life and Morisky scores of patients in SG were obviously higher than those in CG after nursing intervention. After nursing intervention, SAS and SDS scores of patients in SG were obviously lower than those of patients in CG, and patients in SG were less affected by negative emotions. Questionnaires were used to investigate the satisfaction of patients in both groups, and the results showed that the satisfaction of patients in SG was higher (all $P < 0.05$). *Conclusion*. Neurology nursing has better clinical efficacy for stroke patients with DM and has obvious rehabilitation effect. The quality of life and negative emotion score of patients are better, which is worthy of extensive clinical promotion and application.

1. Introduction

Cerebral stroke is a cardiovascular and cerebrovascular disease, commonly known as "stroke," also known as "cerebrovascular accident" (CVA), which is mainly caused by abnormal blood circulation in the brain. It is a sudden and rapid cerebral hemorrhage or cerebral ischemia disease with high morbidity, disability, recurrence, and mortality [1]. A survey shows that stroke has become the first cause of death and the leading cause of disability among Chinese adults in China. DM is a group of metabolic diseases characterized by chronic increase of blood glucose level. Long-term hyperglycemia will lead to dysfunction of various tissues such as the eyes, kidneys, heart, blood vessels, and nerves [2]. DM is the disease with the highest incidence in the world at present. With the social progress and improvement of living standards, the incidence trend is increasing. Some research statistics show that the number of diabetic patients in the

Table 1: Comparison of baseline data between the two groups ($\bar{x} \pm s$).

Groups	Cases	Gender	Age	Average age	Medical history	Average course	Levels of blood glucose
SG	55	28/27	40-69	55.87 ± 5.64	2-8	5.13 ± 1.24	8.13 ± 2.45
CG	55	30/25	43-71	56.39 ± 5.82	2-8	5.51 ± 1.03	8.41 ± 2.05
t	—	—	—	0.476	—	1.748	0.620
P	—	—	—	0.635	—	0.083	0.537

Table 2: Comparison of blood sugar level between the two groups after treatment ($\bar{x}$±s).

Groups	Cases	FPG (mmol/L)	2hFPG (mmol/L)	ALB (mg/L)
SG	55	6.01 ± 1.02	11.18 ± 1.21	41.65 ± 6.07
CG	55	6.93 ± 1.95	12.79 ± 1.87	20.02 ± 5.68
t	—	3.100	5.361	19.296
P	—	0.002	<0.001	<0.001

world is as high as 25.6% in 2015 [3]. DM is easy to cause various complications, and stroke is a common complication of DM [4]. According to relevant studies, the relative risk of stroke patients with DM is 1.8-6.0, and the combined disability rate and mortality rate are higher [5, 6]. Stroke complicated with DM is quite common in clinic, mostly developing in middle-aged and elderly people. Patients need to take drugs for a long time. Compliance and knowledge of the disease directly affect the blood sugar status and mental health of patients [7, 8]. At present, how to make patients face DM actively and rationally and receive professional and systematic treatment is the most important problem to be solved in a nursing work. If nursing intervention is not carried out in time, it is easy to induce other complications and cause incalculable consequences [9, 10]. Studies have shown that positive intervention should be carried out to further ensure the diagnosis and treatment effect of stroke patients with DM. Neurology nursing is a systematic, comprehensive, and targeted method, which can better meet the patients' physiological and psychological nursing needs. Based on the characteristics of the patient's condition and their own specific situation, they can be given psychological, diet, medication, complications, body and language function exercise, and other aspects of better nursing intervention [11]. This research is aimed at providing references and opinions for future clinical practice by exploring and analyzing the rehabilitation effect of neurology nursing on stroke patients with DM and its influence on the quality of life and negative emotion score. The report is as follows.

2. Materials and Methods

2.1. Baseline Data. In this experiment, 110 stroke patients with DM diagnosed and treated in our hospital from 2018 to 2020 were randomly selected and assigned to SG and CG according to different nursing methods, with 55 cases in each group. In SG, the ratio of male to female is 28 : 27, the age range is 40-69 years old, the average age is 55.87 ± 5.64 years, and the history of DM is 2-8 years with an average course of 5.13 ± 1.24 years. In CG, the ratio of male to female is 30 : 25, the age range is 43-71 years, the average age is 56.39 ± 5.82 years, and the history of DM is 2-8 years with an average course of 5.51 ± 1.03 years. The two groups are of comparative value ($P > 0.05$, Table 1).

2.2. Inclusion and Exclusion Criteria. The inclusion criteria were as follows: (1) patients met the criteria for the diagnosis of stroke and the indications of DM; (2) patients were informed of this research and voluntarily affixed the consent form; and (3) this research has been ratified by the Ethics Committee of our hospital.

The exclusion criteria were as follows: (1) history of drug allergy, (2) liver and kidney dysfunction, and (3) cognitive dysfunction.

2.3. Nursing Methods. In CG, patients were given routine nursing intervention, including blood sugar observation, basic nursing, daily ward rounds, and medication according to doctor's advice.

In SG, patients were given neurology nursing intervention, which was mainly divided into four aspects:

(1) Basic intervention: medical staff needed to help patients turn over on time and do not squeeze the patient's skin to prevent pressure sores; Medical staff needed to regularly clean up foreign bodies in the respiratory tract to avoid obstructing breathing and pay attention to catheter blockage and slippage. Medical staff needed to help the patient lift his or her lower limbs to prevent venous thrombosis.

(2) Psychological care: patients with DM need to take medicine for a long time, and the possibility of recurrence is extremely high, and they worry about the occurrence of stroke disease and do not understand the condition, which will easily cause serious psychological burden to the patients. Therefore, medical staff should communicate with family members and patients more according to the patient's situation, help patients clearly understand their symptoms, establish the source of their negative emotions, and enhance patients' confidence in recovery.

(3) Limb rehabilitation nursing: in the early stage, massage rehabilitation was used, and active training was changed according to the patient's recovery condition, slowly improving the patient's activity intensity, carrying out sitting, migration, and other sports, and slowly carrying out the training of

Table 3: Comparison of nursing effects between the two groups after treatment (%).

Groups	Cases	Basic rehabilitation	Significant improvement	Improvement	Ineffectiveness	Total effective rate
SG	55	21 (38.18)	27 (49.09)	6 (10.91)	1 (1.81)	54 (98.19)
CG	55	11 (20.00)	17 (30.91)	15 (27.27)	12 (21.82)	43 (78.18)
x^2	—	—	—	—	—	10.555
P	—	—	—	—	—	0.001

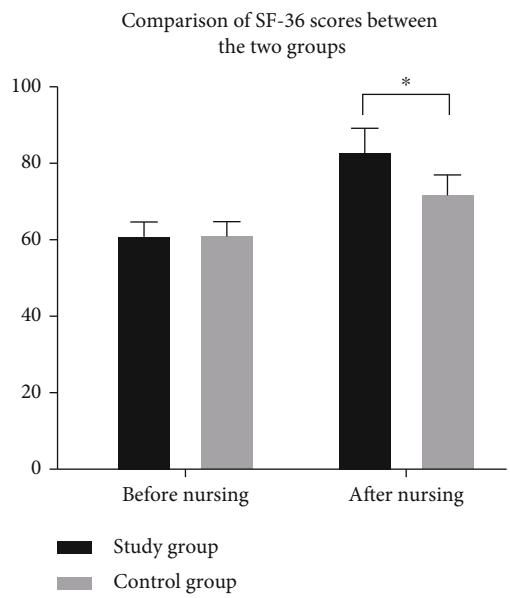

Figure 1: Comparison of SF-36 scores between the two groups before and after nursing intervention. * indicates that there is a difference between the two groups.

standing and walking on a foot walking vehicle. All training intensity is subject to patient tolerance to prevent secondary injury.

(4) Language rehabilitation training: according to the patient's own situation and education level, language training should be conducted on time, and listening training should be carried out with radio or TV equipment until the patient can communicate simply.

2.4. Scoring Standards. The following indicators were collected on the day of admission and discharge:

(1) The blood (200 ml) was taken from the patient's vein on an empty stomach and two hours after a meal, respectively. The changes of blood sugar and the occurrence of adverse diseases in the two groups were observed and compared after treatment. Also, morning urine of patients was taken

(2) The Nursing Effect Table developed by our hospital was used to analyze the nursing effect of patients, comprising four levels: basic rehabilitation, obvious improvement, improvement, and ineffectiveness. The total effective rate of each group was calculated according to the number of people in each level

(3) The quality of life of patients was assessed by SF-36, which was assigned to eight dimensions: physical health (physiological function, physiological role, physical pain, and general health) and mental health (vitality, social function, emotional role, and mental health). The total score of each dimension was 100 points. The higher the score, the better the patient's quality of life

(4) The Morisky Compliance Scale was used to evaluate the treatment compliance of patients before and after nursing intervention from four aspects: medication according to doctor's advice, body quality control, diet control, and appropriate exercise, with a full score of 50 [full compliance: 50, partial compliance: 30-40, and noncompliance: less than 30]

(5) Self-rating Anxiety Scale (SAS) and self-rating Depression Scale (SDS) were used to evaluate and compare the psychological states of patients in both groups. A score below 55 is normal, 56-65 is mild anxiety or depression, 66-75 is moderate anxiety or depression, and 76 or above is severe anxiety or depression. The lower the score, the better the psychological state of the patient

(6) The Nursing Satisfaction Questionnaire developed by our hospital (including the attitude of medical staff, the efficiency of medical staff, and the explanation of diseases by medical staff) was divided into four options (very satisfied, satisfied, not very satisfied, and dissatisfied) to understand the satisfaction of patients in both groups. Then, the results of the two groups were analyzed to determine which treatment was more effective

2.5. Data Analysis. The image was processed by GraphPad Prism 8. SPSS22.0 was used to process the data. A chi-square test and T-test were performed on the enumeration data [n (%)] and the measuring materials ($\bar{x} \pm s$), respectively. The difference was statistically significant ($P < 0.05$).

3. Results

3.1. Blood Glucose Level. Compared with the CG (6.93 ± 1.95, 12.79 ± 1.87, and 20.02 ± 5.68), the levels of fasting blood glucose, 2 h postprandial blood glucose, and urinary micro-albumin in SG (6.01 ± 1.02, 11.18 ± 1.21, and 41.65 ± 6.07) were obviously better after treatment. The results showed that the blood glucose level in SG was better ($P < 0.05$) (Table 2).

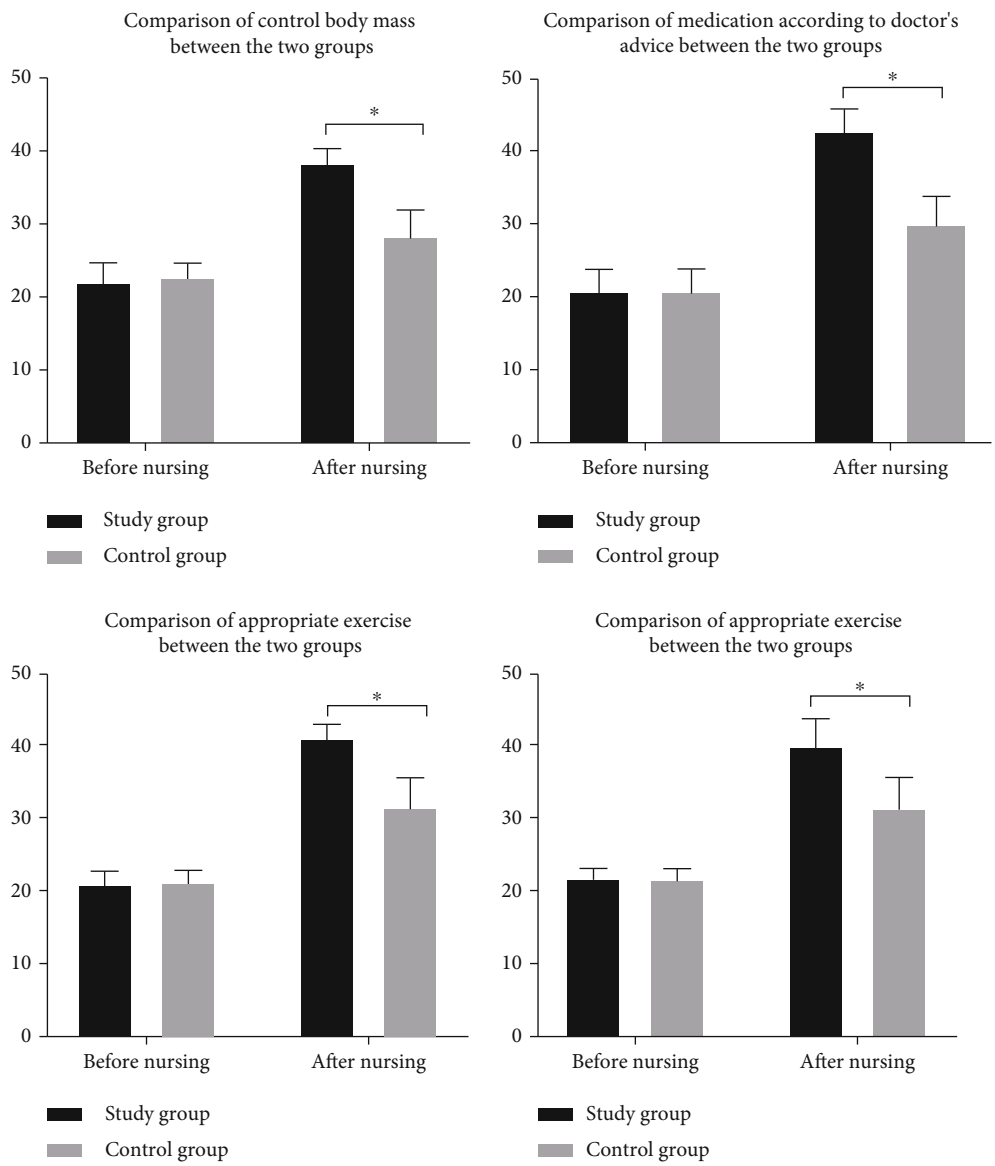

Figure 2: Comparison of Morisky scores between the two groups before and after nursing intervention. ∗ indicates that there is a difference between the two groups.

Table 4: Comparison of negative emotion scores between the two groups after nursing intervention ($\bar{x} \pm s$).

Groups	Cases	SAS	SDS
SG	55	37.12 ± 2.01	35.96 ± 2.34
CG	55	48.49 ± 3.65	49.21 ± 3.17
t	—	20.236	24.940
P	—	<0.001	<0.001

3.2. Nursing Effect. After treatment, the proportion of patients in SG who basically recovered and had obvious improvement (38.18%, 49.09%) was higher than that in CG (20.00%, 30.91%), and the proportion of patients without treatment effect (1.81%) was obviously lower than that in CG (21.82%). Overall, the nursing effect of the SG (98.19%) after treatment was better than that of the CG (78.18) ($P < 0.05$) (Table 3).

3.3. Quality of Life. There was no significant difference in the SF-36 score between the two groups before nursing intervention ($P > 0.05$). After the intervention, the quality of life score of patients in SG (83.23 ± 5.87) was obviously higher than that in CG (72.14 ± 4.79) ($P < 0.05$) (Figure 1).

3.4. Morisky Score. There was no significant difference in the Morisky score between the two groups before nursing intervention ($P > 0.05$). After the nursing intervention, the patients in SG (38.21 ± 2.14, 42.85 ± 3.02, 41.21 ± 1.84, and 40.07 ± 3.78) were obviously higher than those in CG (28.25 ± 3.68, 30.02 ± 3.87, 31.65 ± 4.17, and 31.56 ± 4.25) in terms of controlling body weight, taking medicine

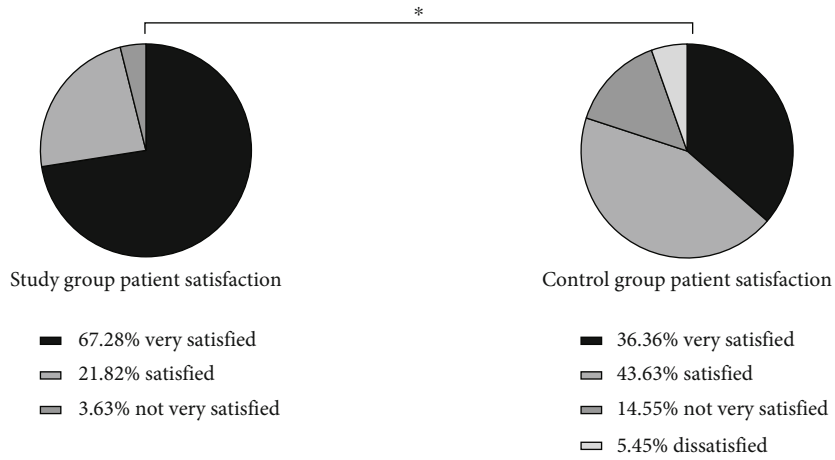

Figure 3: Comparison of SF-36 scores between the two groups before and after nursing intervention. ∗ indicates that there is a difference between the two groups.

according to doctor's advice, exercising properly and controlling diet ($P < 0.05$) (Figure 2).

3.5. Negative Emotion Score. After nursing intervention, SAS and SDS scores of patients in SG (37.12 ± 2.01 and 35.96 ± 2.34) were obviously lower than those of patients in CG (48.49 ± 3.65 and 49.21 ± 3.17), and patients in SG were less affected by negative emotions ($P < 0.05$) (Table 4).

3.6. Nursing Satisfaction. Questionnaires were used to investigate the satisfaction of patients in both groups. The results showed that 37 (67.28%) patients were very satisfied, 12 (21.82%) patients were satisfied, 2 (3.63%) patients were not very satisfied, 0 (0.00%) patients were not satisfied, and the total satisfaction was 53 (96.37%) patients in SG. In CG, 20 (36.36%) patients were very satisfied, 24 (43.63%) patients were satisfied, 8 (14.55%) patients were not very satisfied, 3 (5.45%) patients were not satisfied, and the total satisfaction was 44 (80.00%) patients. In SG, patient's satisfaction was higher ($P < 0.05$) (Figure 3).

4. Discussion

Cerebral stroke is a common cardiovascular and cerebrovascular disease in clinic, which is mainly caused by abnormal blood circulation in the brain. It has the characteristics of high morbidity, disability, recurrence, and mortality and has a great impact on the physical and mental health of patients [12]. A survey shows that stroke has become the first cause of death and the leading cause of disability among Chinese adults in China [13]. DM is a metabolic disease with the highest incidence in the world at present. Hyperglycemia is most common, and its pathogenic principle is caused by abnormal insulin secretion or impaired biological effects [14]. Statistics show that the number of diabetic patients in the world was as high as 25.6% in 2015 [15]. DM is easy to cause various complications. Stroke is a common complication of DM, which is a severe complication [16], with a high mortality and morbidity rate. It develops in middle-aged and elderly people over 40 years and has an impact on multiple body functions of patients, requiring long-term drug use. Compliance and awareness of diseases directly affect patients' blood glucose status and mental health [17, 18]. At present, routine nursing intervention is often used in clinical treatment, but the effect is not obvious. Studies have shown that neurology nursing can improve this issue. Neurology nursing is the key nursing method of stroke complicated with DM at present. It can intervene the patient according to their different condition, simultaneously observe patients' blood sugar level, effectively improve their limb function, and accelerate the process of disease rehabilitation [19, 20]. The results showed that compared with the CG (6.93 ± 1.95, 12.79 ± 1.87, and 20.02 ± 5.68), the levels of fasting blood glucose, 2 h postprandial blood glucose, and urinary microalbumin in SG (6.01 ± 1.02, 11.18 ± 1.21, and 41.65 ± 6.07) were obviously better after treatment. Neurology nursing can observe patients' blood glucose level synchronously and control patients' blood glucose better ($P < 0.05$). After treatment, the proportion of patients in SG who basically recovered and had obvious improvement (38.18%, 49.09%) was higher than that in CG (20.00%, 30.91%), and the proportion of patients without treatment effect (1.81%) was obviously lower than that in CG (21.82%). Overall, the nursing effect of the SG (98.19%) after treatment was better than that of the CG (78.18%) ($P < 0.05$). There was no significant difference in SF-36 score between the two groups before nursing intervention ($P > 0.05$). After the intervention, the quality of life score of patients in SG (83.23 ± 5.87) was obviously higher than that in CG (72.14 ± 4.79) ($P < 0.05$). There was no significant difference in Morisky score between the two groups before nursing intervention ($P > 0.05$). After the nursing intervention, the patients in SG (38.21 ± 2.14, 42.85 ± 3.02, 41.21 ± 1.84, and 40.07 ± 3.78) were obviously higher than those in CG (28.25 ± 3.68, 30.02 ± 3.87, 31.65 ± 4.17, and 31.56 ± 4.25) in terms of controlling body weight, taking medicine

according to doctor's advice, exercising properly, and controlling diet. These may be due to the fact that neurology nursing can accelerate the recovery of patients themselves and gradually recover the corresponding limb functions through limb rehabilitation training. Language exercise can repair the patients' language function and promote the recovery of expression ability. Basic nursing can restrain complications, thus accelerating the recovery process of patients and the speed of body recovery ($P < 0.05$). After nursing intervention, SAS and SDS scores of patients in SG ($37.12 \pm 2.01, 35.96 \pm 2.34$) were obviously lower than those of patients in CG ($48.49 \pm 3.65, 49.21 \pm 3.17$), and patients in SG were less affected by negative emotions. Neurological nursing also pays attention to psychological nursing. Nurses can communicate in time, explain patiently and enlighten patients, make patients understand more about their own condition, pay attention to their emotional changes, and mobilize their enthusiasm for treatment and cooperation, which is conducive to the recovery of patients' mental health ($P < 0.05$). Questionnaires were used to investigate the satisfaction of patients in both groups. The results showed that 37 (67.28%) patients were very satisfied, 12 (21.82%) patients were satisfied, 2 (3.63%) patients were not very satisfied, 0 (0.00%) patients were not satisfied, and the total satisfaction was 53 (96.37%) patients in SG. In CG, 20 (36.36%) patients were very satisfied, 24 (43.63%) patients were satisfied, 8 (14.55%) patients were not very satisfied, 3 (5.45%) patients were not satisfied, and the total satisfaction was 44 (80.00%) patients. The results showed that the neurology nursing was more meticulous and comprehensive, and the patient satisfaction in SG was higher ($P < 0.05$), which was consistent with the previous conclusions obtained by scholars.

To sum up, neurology nursing has better clinical effect on stroke patients with DM, has obvious rehabilitation effect, can improve patients' quality of life, and can reduce their negative emotions, which is worthy of extensive clinical promotion and application.

Data Availability

The datasets used during the present study are available from the corresponding author upon reasonable request.

Conflicts of Interest

The authors declare that they have no conflicts of interest.

References

[1] M. J. Cipolla, D. S. Liebeskind, and S. L. Chan, "The importance of comorbidities in ischemic stroke: impact of hypertension on the cerebral circulation," *Journal of Cerebral Blood Flow and Metabolism*, vol. 38, no. 12, pp. 2129–2149, 2018.

[2] M. K. Cho and M. Y. Kim, "Self-management nursing intervention for controlling glucose among diabetes: a systematic review and meta-analysis," *International Journal of Environmental Research and Public Health*, vol. 18, no. 23, article 12750, 2021.

[3] G. R. S. Ferreira, L. R. C. Viana, C. J. L. Pimenta et al., "Self-care of elderly people with diabetes mellitus and the nurse-patient interpersonal relationship," *Revista Brasileira de Enfermagem*, vol. 75, no. 1, article e20201257, 2021.

[4] H. B. Lin, F. X. Li, J. Y. Zhang et al., "Cerebral-cardiac syndrome and diabetes: cardiac damage after ischemic stroke in diabetic state," *Frontiers in Immunology*, vol. 12, article 737170, 2021.

[5] Z. Bloomgarden and R. Chilton, "Diabetes and stroke: an important complication," *Journal of Diabetes*, vol. 13, no. 3, pp. 184–190, 2021.

[6] S. Nannoni, R. de Groot, S. Bell, and H. S. Markus, "Stroke in COVID-19: a systematic review and meta-analysis," *International Journal of Stroke*, vol. 16, no. 2, pp. 137–149, 2021.

[7] A. H. Katsanos, L. Palaiodimou, R. Zand et al., "The impact of SARS-CoV-2 on stroke epidemiology and care: a meta-analysis," *Annals of Neurology*, vol. 89, no. 2, pp. 380–388, 2021.

[8] P. Tran, L. Tran, and L. Tran, "Nonadherence in diabetes care among US adults with diabetes by stroke status," *PLoS One*, vol. 16, no. 12, article e0260778, 2021.

[9] M. J. Krinock and N. S. Singhal, "Diabetes, stroke, and neuroresilience: looking beyond hyperglycemia," *Annals of the New York Academy of Sciences*, vol. 1495, no. 1, pp. 78–98, 2021.

[10] M. Iwase, Y. Komorita, T. Ohkuma et al., "Incidence of stroke and its association with glycemic control and lifestyle in Japanese patients with type 2 diabetes mellitus: the Fukuoka diabetes registry," *Diabetes Research and Clinical Practice*, vol. 172, article 108518, 2021.

[11] D. J. M. Isaman, W. H. Herman, and W. Ye, "Prediction of transient ischemic attack and minor stroke in people with type 2 diabetes mellitus," *Journal of Diabetes and its Complications*, vol. 35, no. 7, article 107911, 2021.

[12] B. J. MacIntosh, E. Cohen, J. Colby-Milley et al., "Diabetes mellitus is associated with poor in-hospital and long-term outcomes in young and midlife stroke survivors," *Journal of the American Heart Association*, vol. 10, no. 14, article e019991, 2021.

[13] E. Esposito, G. Shekhtman, and P. Chen, "Prevalence of spatial neglect post-stroke: a systematic review," *Annals of Physical and Rehabilitation Medicine*, vol. 64, no. 5, p. 101459, 2021.

[14] M. Lorber, S. Kmetec, N. Mlinar Reljić, and Z. Fekonja, "Diabetes management of older adults in nursing homes: a retrospective study," *Journal of Nursing Management*, vol. 29, no. 5, pp. 1293–1301, 2021.

[15] J. Huang, Y. Yang, M. Yang, X. Liu, J. Wang, and Y. Huang, "Study on the effect of whole-course education and nursing mode on quality of life and blood glucose level of patients with diabetes mellitus," *Minerva Medica*, vol. 112, no. 5, pp. 674–676, 2021.

[16] F. F. Oliveira, M. Beuter, M. D. Schimith et al., "Therapeutic itinerary of elderly people with diabetes mellitus: implications for nursing care," *Revista Brasileira de Enfermagem*, vol. 74, no. 3, article e20200788, 2021.

[17] W. N. Kernan and S. E. Inzucchi, "Treating diabetes to prevent stroke," *Stroke*, vol. 52, no. 5, pp. 1557–1560, 2021.

[18] B. Riegel, H. Westland, P. Iovino et al., "Characteristics of self-care interventions for patients with a chronic condition: a scoping review," *International Journal of Nursing Studies*, vol. 116, article 103713, 2021.

[19] H. Jiang, L. Liu, H. Wang, and G. Sun, "Observation on the effect of short-term intensive insulin pump therapy combined with early rehabilitation nursing in patients with type 2 diabetes mellitus complicated with stroke," *Minerva Medica*, 2021.

[20] K. Hu, M. Jiang, Q. Zhou et al., "Association of diabetic retinopathy with stroke: a systematic review and meta-analysis," *Frontiers in Neurology*, vol. 12, article 626996, 2021.

Hindawi
Disease Markers
Volume 2022, Article ID 6516246, 9 pages
https://doi.org/10.1155/2022/6516246

Research Article

Glaucocalyxin A Attenuates IL-1β-Induced Inflammatory Response and Cartilage Degradation in Osteoarthritis Chondrocytes via Inhibiting the Activation of NF-κB Signaling Pathway

Weidong Zhu,[1] Yi Zhang,[2] Yueshan Li,[3] and Hao Wu[1]

[1]*The Department of Orthopedics, The Second Affiliated Hospital of Xi'an Jiaotong University, Xi'an, 710004 Shaanxi Province, China*
[2]*The Department of Ophthalmology, The Second Affiliated Hospital of Xi'an Jiaotong University, Xi'an, 710004 Shaanxi Province, China*
[3]*The Department of Stomatology, The First Affiliated Hospital of Xi'an Jiaotong University, Xi'an, 710061 Shaanxi Province, China*

Correspondence should be addressed to Hao Wu; dihaoji62588049@126.com

Received 20 December 2021; Revised 18 January 2022; Accepted 26 January 2022; Published 26 February 2022

Academic Editor: Yaoyao Bian

Glaucocalyxin A (GLA) is a bioactive natural compound with anti-inflammatory activity. Herein, the role of GLA in osteoarthritis (OA) was evaluated. Our results demonstrated that the IL-1β-induced inducible nitric oxide synthase (iNOS) and cyclooygenase-2 (COX-2) expression, two enzymes resulting in the release of nitric oxide (NO) and PGE2, were also prevented by GLA in chondrocytes. Moreover, GLA suppressed inflammatory cytokines production in chondrocytes. In addition, the elevated expressions of MMPs and ADAMTSs and the degradation of aggrecan and collagen II were reversed by GLA in chondrocytes. Furthermore, GLA decreased p-p65 level and suppressed the nuclear p65 accumulation in the nucleus of chondrocytes. Collectively, we concluded that GLA attenuated inflammatory response in chondrocytes via NF-κB pathway. These findings suggested that GLA might become an effective agent for OA treatment.

1. Introduction

Osteoarthritis (OA) is a frequent inflammation-related disease affecting individuals over 60 years of age [1]. OA is clinically presented with crepitus, joint pain, stiffness, tenderness, and limited movement [2]. Thus, OA patients commonly suffer with functional decline as well as loss of life quality, accompanied by heavy health care and society costs. Although osteoarthritis management consists of joint replacement for end-stage disease, the prevention and the treatment of early OA are still limited [1].

The identification of risk factors and understanding of the pathogenesis are central for selecting targets for OA therapy. It is evident for the role of chronic inflammation in the development of OA [3, 4]. Inflammation contributes to the evolution of joint tissue degradation and remodeling as well as joint pain [5]. A plethora of inflammatory mediators and signaling pathways are involved in the OA pathogenesis, which become potential biomarkers or therapeutic targets [6]. It is increasingly evident that interleukin-1β- (IL-1β-) mediated signaling pathways play central roles in OA pathology [7]. It is believed that components in the IL-1β signaling may be developed into novel drugs for OA.

Glaucocalyxin A (GLA), a bioactive natural compound, possesses important biological activities including anti-inflammatory activity [8–12]. Its chemical structure is shown in Figure 1(a). The administration of GLA reduces inflammation and mortality in lipopolysaccharide- (LPS-) induced septic-shock mouse model through regulating NLRP3 inflammasome activation [13]. Another study has proven that the LPS-stimulated increased production of pro-inflammatory cytokines in microglia is inhibited by GLA

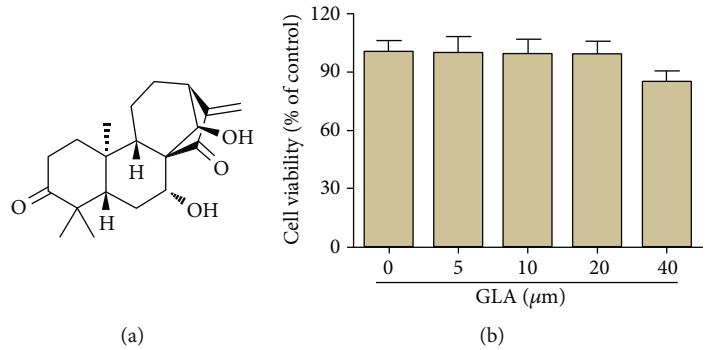

Figure 1: Examination of cytotoxicity effect of GLA on human OA chondrocytes. (a) The chemical structure of GLA. (b) Primary human OA chondrocytes were prepared and incubated with different concentrations of GLA (0, 5, 10, 20, and 40 μM) for 24 h. Subsequently, cells were processed to test the cell viability using CCK-8 assay. Experiments were performed at least in triplicate. $^{*}p < 0.05$ versus the control group.

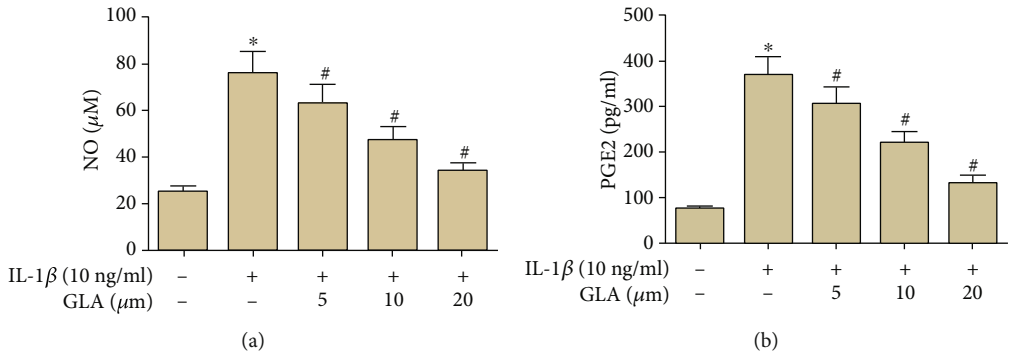

Figure 2: GLA inhibits the production of NO and PGE2 in IL-1β-stimulated OA chondrocytes. Primary human OA chondrocytes were incubated with different concentrations of GLA (0, 5, 10, and 20 μM) for 2 h and then stimulated with IL-1β (10 ng/ml) for 24 h. (a) NO production was evaluated using the Griess reaction. (b) PGE2 content in culture supernatant was determined using ELISA. $^{*}p < 0.05$ versus the control group; $\#p < 0.05$ versus the IL-1β group.

treatment [14]. Moreover, treatment with GLA reduces the inflammatory response in hydrogen peroxide- (H_2O_2-)induced smooth muscle cells [15].

Herein, we examined the potential role of GLA in OA. Evidence has been building that the inflammatory process in chondrocytes plays crucial role in the joint injury. Thus, IL-1β-induced chondrocytes are generally applied for in vitro model of OA [7]. Herein, we examined the effect of GLA on inflammation in chondrocytes.

2. Materials and Methods

2.1. Cell Culture and Treatment. Articular cartilage samples were obtained from articular joints of OA patients undergoing total knee replacement surgery. Primary human OA chondrocytes were then harvested from these clinical samples as previously described [16]. The resulting cells were centrifuged and cultured for our following study.

The experiments were divided into five groups: control, IL-1β, IL $-$ 1β + GLA (5 μM), IL $-$ 1β + GLA (10 μM), and IL $-$ 1β + GLA (20 μM).

2.2. Cell Viability Assay. We performed cell viability assay using CCK-8 kit (Promega Corp, Madison, WI). After the treatment with GLA (0, 5, 10, 20, and 40 μM; Yuanye Bio-Tech, Shanghai, China), the cells were treated with CCK-8 for 4 h. The OD value was measured at 450 nm.

2.3. Measurement of Nitric Oxide (NO). Primary human OA chondrocytes were incubated with different concentrations of GLA (0, 5, 10, and 20 μM) for 2 h and then stimulated with IL-1β (10 ng/ml) for 24 h. NO accumulation was measured using a commercial assay kit (Dojindo Laboratories, Kumaoto, Japan). The absorbance at 550 nm was measured and calculated for NO accumulation.

2.4. qRT-PCR. The total RNA from human OA chondrocytes was used for cDNA synthesis with cDNA Reverse Transcription Kit. The obtained cDNA was used for qRT-PCR. The primer sequences used are listed as follows: inducible nitric oxide synthase (iNOS), 5′-GAA ACT TCT CAG CCA CCT TGG-3′, and 5′-CCG TGG GGC TTG TAG TTG AC-3′; cyclooygenase-2 (COX-2), 5′-GGT GAA AAC TGT ACT ACG CCG A-3′, and 5′-ACT CCC TTG AAG TGG GTC AG-3′; TNF-α, 5′-CAT CTT CTC AAA ATT CGA GTG ACA A-3′, and 5′-TGG GAG TAG ACA AGG TAC AAC CC-3′; IL-6, 5′-AGA AAT CCC TCC

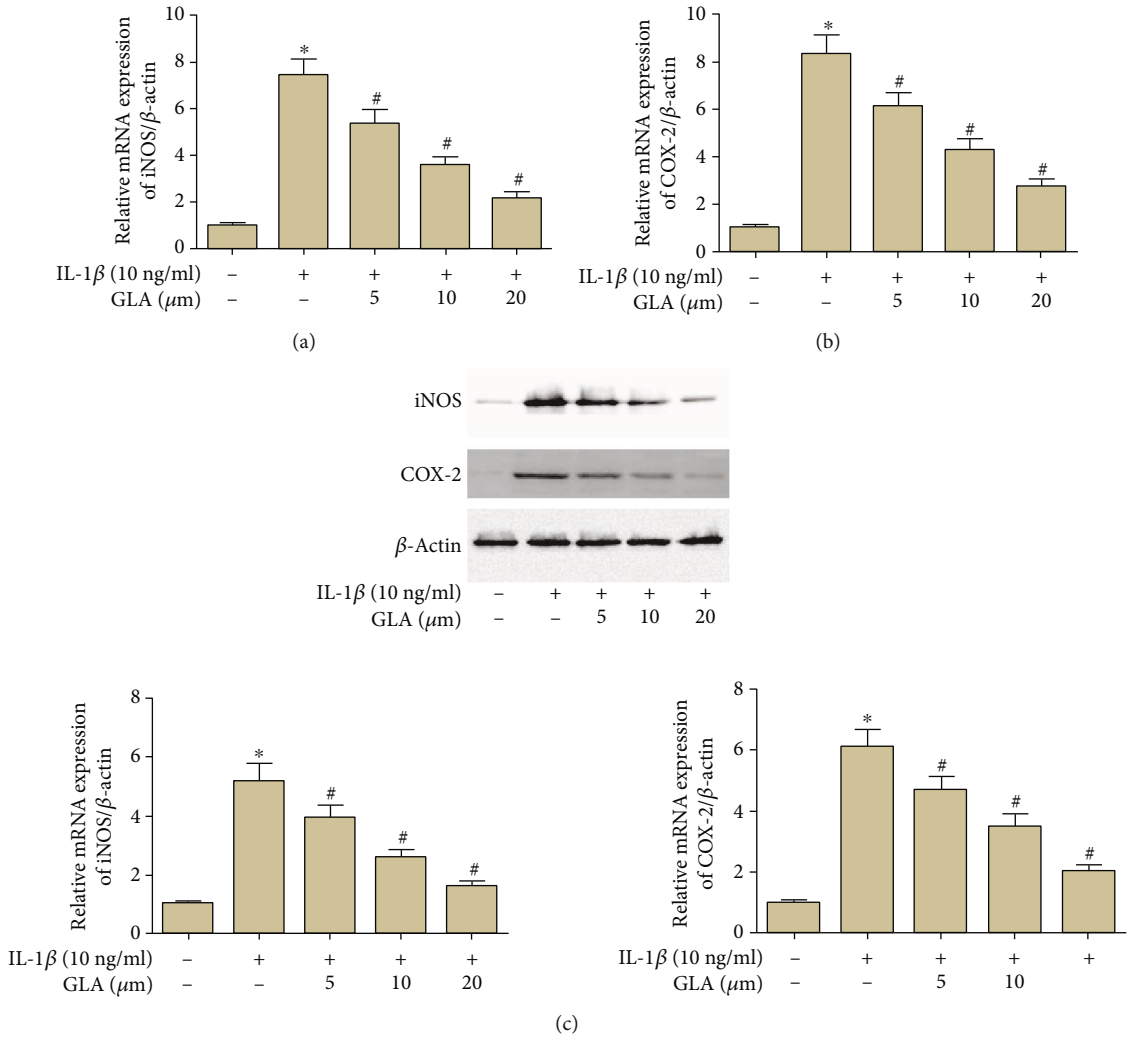

Figure 3: GLA inhibits the expression of iNOS and COX-2 in IL-1β-stimulated OA chondrocytes. Primary human OA chondrocytes were incubated with different concentrations of GLA (0, 5, 10, and 20 μM) for 2 h and then stimulated with IL-1β (10 ng/ml) for 24 h. (a and b) The mRNA levels of iNOS and COX-2 were evaluated using qRT-PCR. (c) The protein levels of iNOS and COX-2 were evaluated using western blot. $^{*}p < 0.05$ versus the control group; $\#p < 0.05$ versus the IL-1β group.

TCG CCA AT-3′, and 5′-AAA TAG CGA ACG GCC CTC A-3′; IL-8, 5′-GCC CTC CTC CTG GTT TCA G-3′, and 5′-TGG CAC CGC AGC TCA TT-3′; matrix metalloproteinase (MMP)-3, 5′-TGA GGA CAC CAG CAT GAA CC-3′, and 5′-ACT TCG GGA TGC CAG GAA AG-3′; MMP-13, 5′-GCC ATT ACC AGT CTC CGA GG-3′, and 5′-TAC GGT TGG GAA GTT CTG GC-3′; A disintegrin-like and metalloproteinase with thrombospondin type I motifs (ADAMTS)-4, 5′-CAT CCT ACG CCG GAA GAG TC-3′, and 5′-AAG CGA AGC GCT TGT TTC TG-3′; ADAMTS-5, 5′-CCC AAA TAC GCA GGT GTC CT-3′, and 5′-ACA CAC GGA GTT GCT GTA GG-3′; aggrecan, 5′-AAG TGC TAT GCT GGC TGG TT-3′, and 5′-GGT CTG GTT GGG GTA GAG GT-3′; collagen II, 5′-CTC AAG TCG CTG AAC AAC CA-3′, and 5′-GTC TCC GCT CTT CCA CTC TG-3; and β-actin, 5′-ACT CTT CCA GCC TTC CTT CC-3′, and 5′-TGT TGG CGT ACA GGT CTT TG-3′.

2.5. Western Blot. Control and treated chondrocytes were lysed, followed by SDS-PAGE electrophoresis as previously described [13]. The primary antibodies used were listed: anti-iNOS, anti-COX-2, anti-β-actin, and HRP-conjugated secondary antibody from Santa Cruz Biotechnology, Santa Cruz, CA; and anti-ADAMTS-4, anti-ADAMTS-5, anti-aggrecan, anti-collagen II, anti-p65, anti-p-p65, anti-p-IκBα, and anti-IκBα from Abcam. Finally, the bands were visualized with the ECL reagent.

2.6. Elisa. The culture supernatants of chondrocytes were collected, centrifugated, and frozen at -80°C until assayed. Prostaglandin E2 (PGE2), TNF-α, IL-6, IL-8, and MMP-3 and MMP-13 contents were measured by ELISA (Boster Immunoleader, Pleasanton, CA).

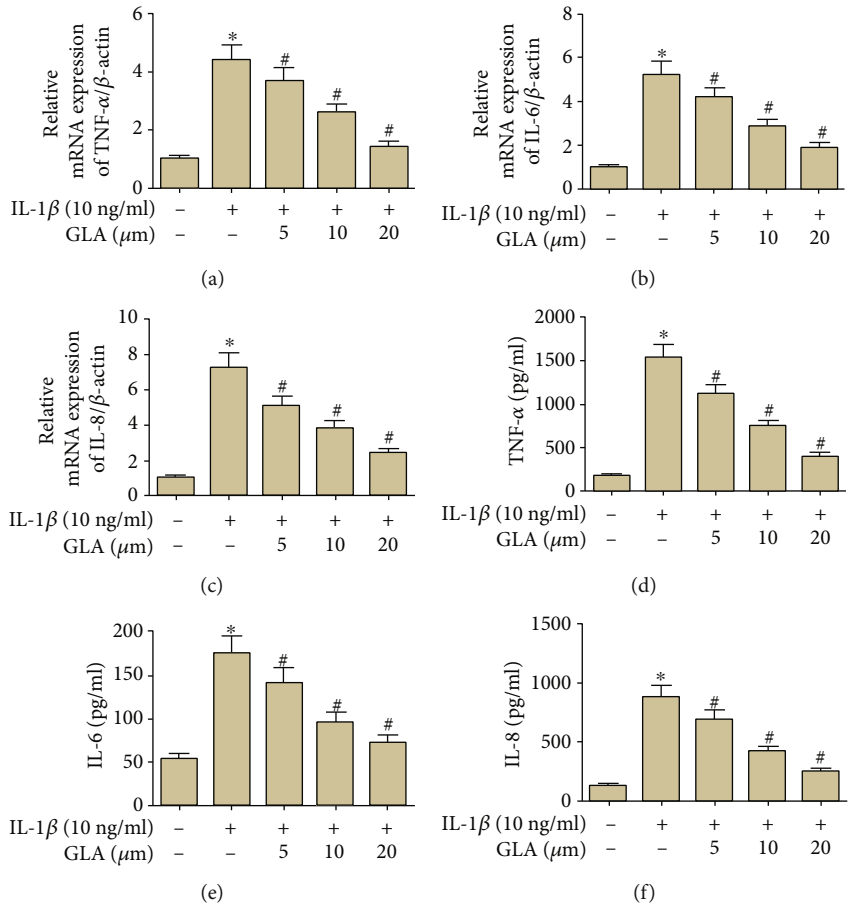

Figure 4: Modulation of TNF-α, IL-6, and IL-8 production by GLA in human OA chondrocytes. Primary human OA chondrocytes were incubated with different concentrations of GLA (0, 5, 10, and 20 μM) for 2 h and then stimulated with IL-1β (10 ng/ml) for 24 h. (a–c) The mRNA levels of TNF-α, IL-6, and IL-8 were evaluated using qRT-PCR. (d–f) The contents of TNF-α, IL-6, and IL-8 in culture supernatant were determined using ELISA. $^*p < 0.05$ versus the control group; $\#p < 0.05$ versus the IL-1β group.

2.7. Immunofluorescence Staining. After the completion of treatment, chondrocytes were fixed, permeabilized, and blocked for 1 h. Then, cells were probed with anti-p65 antibody (Abcam) overnight, followed by an incubation with ant-rabbit Alexa Fluor 546 secondary antibodies for 2 h. Cells were then mounted with DAPI and visualized by Olympus FV1000 confocal microscope (Olympus, Tokyo, Japan).

2.8. Statistical Analysis. Experimental data are presented as mean ± S.E.M. ANOVA was performed to show the difference between groups. $p < 0.05$ was considered as significant difference.

3. Results

3.1. Effect of GLA on OA Chondrocyte Viability. According to the results of Figure 1(b), GLA did not exhibit obvious cytotoxic effect on chondrocytes at the doses of 5, 10, and 20 μM. Hence, these three concentrations were used for the next experiments.

3.2. Effect of GLA on NO and PGE2 Production. A rapid increase in the NO production was observed in IL-1β-induced chondrocytes, and this response was mitigated in the GLA-treated groups (Figure 2(a)). Besides, an acute increase in PGE2 content was noted in response to induction with IL-1β, while the GLA-treated chondrocytes showed significant mitigation in PGE2 content (Figure 2(b)).

3.3. Effect of GLA on iNOS and COX-2 Expression. IL-1β could increase the mRNA levels of iNOS and COX-2, these effects were reversed by GLA (Figures 3(a) and 3(b)). Chondrocytes in the IL-1β-treated group had significant higher protein levels of iNOS and COX-2, while GLA suppressed these proteins expression (Figure 3(c)).

3.4. Effect of GLA on Inflammatory Cytokine Production. QRT-PCR demonstrated that the mRNA levels of TNF-α, IL-6, and IL-8 were upregulated evidently in the IL-1β-stimulated group. However, in comparison with the IL-1β group, the mRNA levels were markedly decreased in the GLA-treated chondrocytes (Figures 4(a)–4(c)). Similarly, the contents of inflammatory factors were significantly induced by

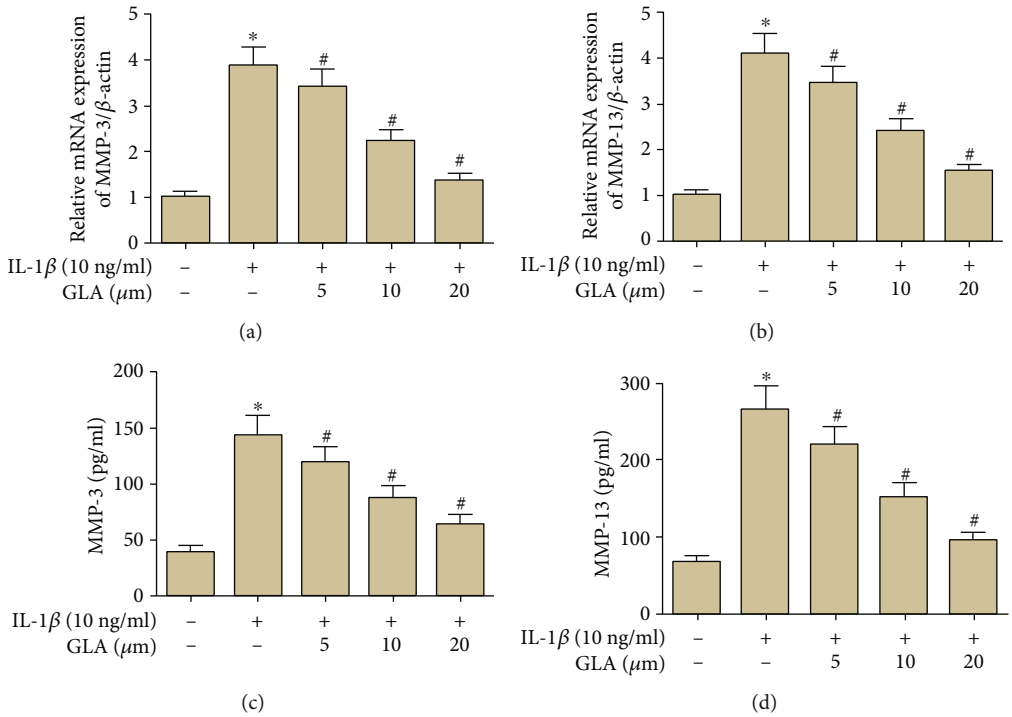

Figure 5: GLA inhibits the expression of MMP-3 and MMP-13 in IL-1β-stimulated OA chondrocytes. Primary human OA chondrocytes were incubated with different concentrations of GLA (0, 5, 10, and 20 μM) for 2 h and then stimulated with IL-1β (10 ng/ml) for 24 h. (a and b) The mRNA levels of MMP-3 and MMP-13 were evaluated using qRT-PCR. (c and d) The productions of MMP-3 and MMP-13 were evaluated using ELISA. $^*p < 0.05$ versus the control group; $\#p < 0.05$ versus the IL-1β group.

IL-1β, which were attenuated in the GLA-treated chondrocytes (Figures 4(d)–4(f)).

3.5. Effect of GLA on the Expression of MMPs. According to the results of qRT-PCR, chondrocytes in the IL-1β-stimulated group had increased mRNA levels of MMP-3 and MMP-13. While compared to the IL-1β-treated group, chondrocytes in the GLA-treated group had lower expressions of MMPs at mRNA level (Figures 5(a) and 5(b)). In addition, the results of ELISA assay indicated that GLA greatly inhibited the production of MMPs in chondrocytes (Figures 5(c) and 5(d)).

3.6. Effect of GLA on the Expression of ADAMTSs. Compared to the control group, the mRNA levels of ADAMTS-4 and ADAMTS-5 in the chondrocytes from the IL-1β-treated group were significantly increased, which were suppressed by GLA treatment (Figures 6(a) and 6(b). In addition, we observed that IL-1β greatly increased the protein levels of ADAMTS-4 and ADAMTS-5, which were downregulated after the pretreatment with GLA (Figure 6(c)).

3.7. Effect of GLA on the Expression of Aggrecan and Collagen II. IL-1β could decrease the mRNA expression levels of aggrecan and collagen II. However, GLA upregulated the mRNA expression levels of aggrecan and collagen II in OA chondrocytes (Figures 7(a) and 7(b)). Similarly, the western blot assay revealed comparable results in aggrecan and collagen II protein expression levels (Figure 7(c)).

3.8. Effect of GLA on the NF-κB Pathway. The results from immunofluorescence indicated that IL-1β induced p65 nuclear accumulation, whereas the p65 accumulation was prevented by GLA (Figure 8(a)). The phosphorylation levels of p65 and IκBα were increased in the IL-1β-treated chondrocytes, while IκBα level was greatly decreased by IL-1β treatment. However, GLA prevented NF-κB activation in the IL-1β-treated chondrocytes (Figures 8(b) and 8(c)).

4. Discussion

The recent work in OA-associated field has implicated inflammatory chemokines in OA pathogenesis. Interleukins are a big family of cytokines that comprises 11 members that shared similar gene structure [17]. IL-1β is involved in the pathology of OA [7]. IL-1β binds to the type I IL-1RI [18]. It was reported that increased levels of IL-1RI are detected in isolated chondrocytes. It is evident that during inflammatory processes, increased IL-1β increases IL-1RI expression. The extracellular domain of IL-1RI causes IL-1 receptor accessory protein recruitment, which is considered a coreceptor for IL-1β signal transduction [7]. Next, the signal transduction causes the activation of MAPK pathways and eventually results in various transcription factors activation, such as NF-κB [7]. Collectively, IL-1β signaling is necessary for the development of OA and serves as a therapeutic target.

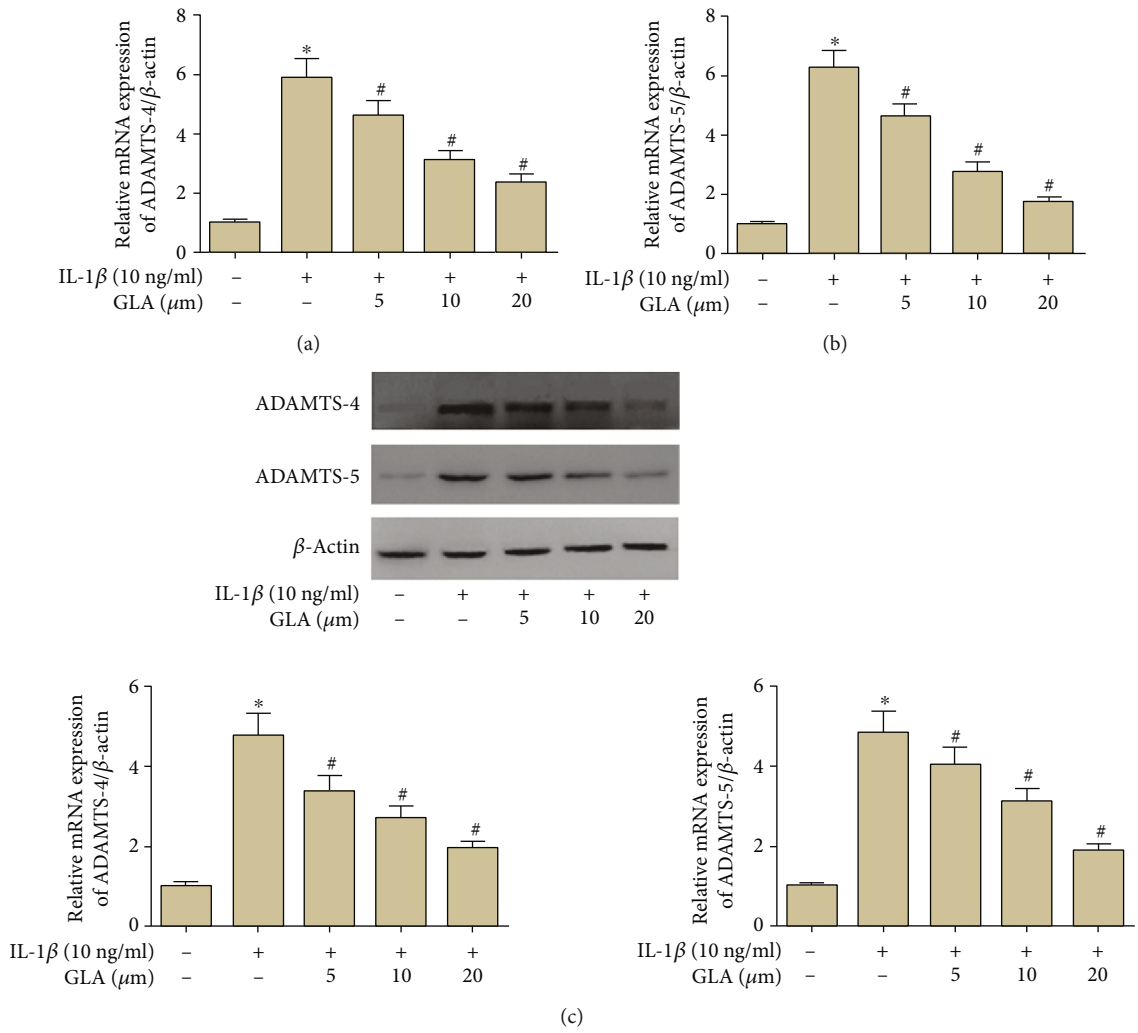

Figure 6: Modulation of ADAMTS-4 and ADAMTS-5 expression by GLA in human OA chondrocytes. Primary human OA chondrocytes were incubated with different concentrations of GLA (0, 5, 10, and 20 μM) for 2 h and then stimulated with IL-1β (10 ng/ml) for 24 h. (a and b) The mRNA levels of ADAMTS-4 and ADAMTS-5 were evaluated using qRT-PCR. (c) The protein levels of ADAMTS-4 and ADAMTS-5 were evaluated using western blot. $^{*}p < 0.05$ versus the control group; $\#p < 0.05$ versus the IL-1β group.

Here, we used IL-1β to induce an in vitro inflammatory OA model in chondrocytes, thereby exploring the anti-inflammatory effect of GLA exposed to IL-1β induction. IL-1β produces the production of proinflammatory cytokines, further induces iNOS expression, which results in NO accumulation [19]. Moreover, NO level is highly increased in OA chondrocytes as well as cartilage tissues [20]. NO inhibits the synthesis of proteoglycan and collagen and activates MMPs [21, 22]. Our results proved that GLA suppressed iNOS expression and NO release in chondrocytes. Like NO, PGE2, a predominant product of COX-2, is also increased during the progression of OA [19]. In human chondrocytes, the induction with IL-1β causes increased PGE2 release via regulating p38 MAPK pathway [23]. We also found that GLA suppressed the COX-2 expression and PGE2 release in IL-1β-induced chondrocytes.

In addition to acting as a key proinflammatory cytokine, IL-1β also contributes to the OA progression via mediating other events, such as inducing the expression of MMPs and ADAMTSs, which are cartilage-degrading enzymes [24–26]. IL-1β stimulates chondrocytes to release several types of MMPs, and these three proteases become a strategy to prevent OA [27, 28]. Moreover, the ADAMTS family of proteins, especially ADAMTS-4 and ADAMTS-5, is also

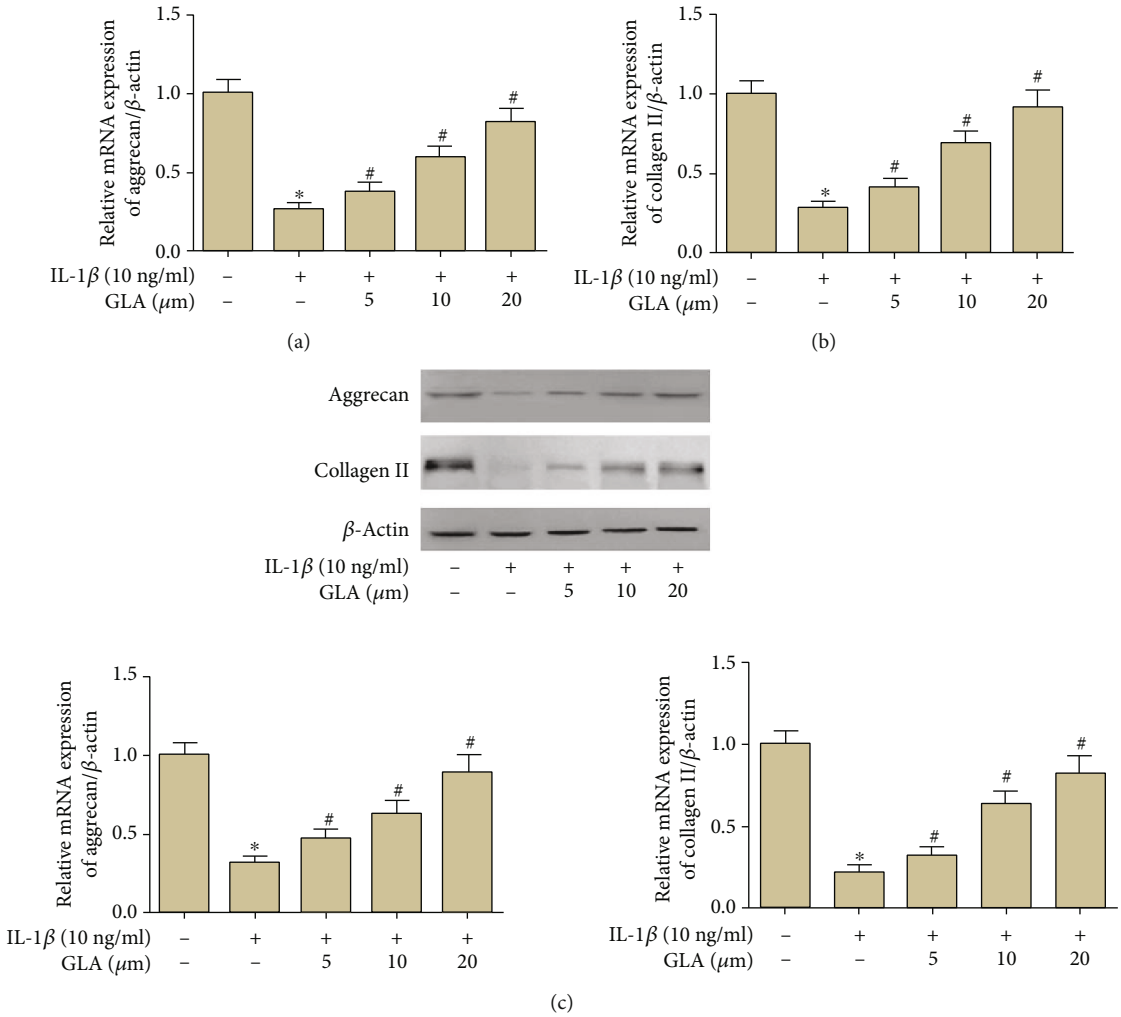

Figure 7: GLA inhibited the degradation of aggrecan and collagen II induced by IL-1β. Primary human OA chondrocytes were incubated with different concentrations of GLA (0, 5, 10, and 20 μM) for 2 h and then stimulated with IL-1β (10 ng/ml) for 24 h. (a and b) The mRNA levels of aggrecan and collagen II were evaluated using qRT-PCR. (c) The protein levels of aggrecan and collagen II were evaluated using western blot. $^*p < 0.05$ versus the control group; $\#p < 0.05$ versus the IL-1β group.

important in cartilage degradation [29]. We found that the elevated expression of MMPs and aggrecan and collagen II degradation were reversed by GLA in chondrocytes.

The NF-κB plays a crucial role in inflammation through modulating activation or repression of target gene expression [30]. Consequently, NF-κB is essential in various inflammatory diseases including OA [31]. NF-κB mediates critical inflammatory events by modulating chondrocytes, results in progressive extracellular matrix (ECM) damage [32]. The NF-κB signaling was found to be regulated by IL-1β in OA chondrocytes [33]. Thus, we evaluated the role of GLA in NF-κB pathway. NF-κB is commonly presented in an inactive form in the cytoplasm associated with the inhibitory κB proteins (IκB) [34]. The IκBα is an important mechanism for the activation and repression of NF-κB [35]. We found that GLA decreased the levels of p-p65 and suppressed the p65 accumulation in nucleus, which indicated that GLA prevented NF-κB pathway activation [36].

There existed several limitations in this study. A major limitation is that our results are based on the in vitro experiments. Future in vivo experiments are needed to verify the role of GLA in OA. Secondly, the exact molecular mechanisms by which GLA regulates NF-κB pathway need to be further explored in the future study.

In light of this, we concluded that GLA attenuated the inflammatory response and cartilage degradation in

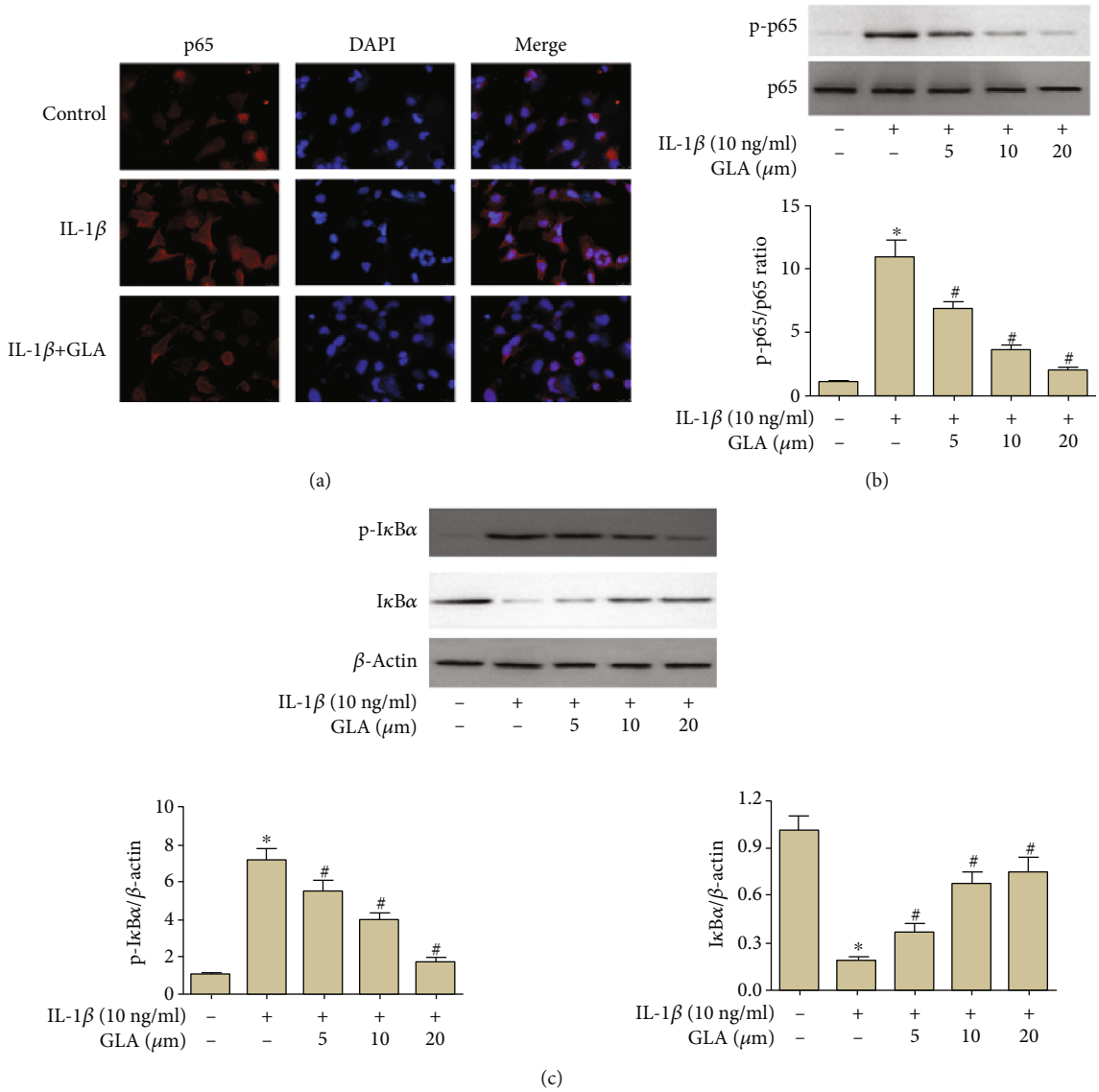

Figure 8: Modulation of NF-κB signaling pathway by GLA in human OA chondrocytes. Primary human OA chondrocytes were incubated with GLA for 2 h and then stimulated with IL-1β. (a) The immunofluorescence was performed to assess p65 accumulation. (b and c) The levels of p-p65, p65, p-IκBα, and IκBα were evaluated using western blot. $^{*}p < 0.05$ versus the control group; $\#p < 0.05$ versus the IL-1β group.

chondrocytes via the regulation of NF-κB. Thus, GLA might become an effective therapeutic agent for OA.

Data Availability

The datasets used during the present study are available from the corresponding author upon reasonable request.

Conflicts of Interest

The authors declare that they have no conflicts of interest.

References

[1] S. Glyn-Jones, A. J. Palmer, R. Agricola et al., "Osteoarthritis," *Lancet*, vol. 386, no. 9991, pp. 376–387, 2015.

[2] D. Pereira, E. Ramos, and J. Branco, "Osteoarthritis," *Acta Médica Portuguesa*, vol. 28, no. 1, pp. 99–106, 2015.

[3] C. R. Scanzello, "Chemokines and inflammation in osteoarthritis: insights from patients and animal models," *Journal of Orthopaedic Research*, vol. 35, no. 4, pp. 735–739, 2017.

[4] S. Vila, "Inflammation in osteoarthritis," *Puerto Rico Health Sciences Journal*, vol. 36, no. 3, pp. 123–129, 2017.

[5] J. Shen, Y. Abu-Amer, R. J. O'Keefe, and A. McAlinden, "Inflammation and epigenetic regulation in osteoarthritis," *Connective Tissue Research*, vol. 58, no. 1, pp. 49–63, 2017.

[6] M. Kapoor, J. Martel-Pelletier, D. Lajeunesse, J. P. Pelletier, and H. Fahmi, "Role of proinflammatory cytokines in the pathophysiology of osteoarthritis," *Nature Reviews Rheumatology*, vol. 7, no. 1, pp. 33–42, 2011.

[7] Z. Jenei-Lanzl, A. Meurer, and F. Zaucke, "Interleukin-1β signaling in osteoarthritis - chondrocytes in focus," *Cellular Signalling*, vol. 53, pp. 212–223, 2019.

[8] Z. Xiang, X. Wu, X. Liu, and Y. Jin, "Glaucocalyxin a: a review," *Natural Product Research*, vol. 28, no. 24, pp. 2221–2236, 2014.

[9] X. Jiang, Z. Zhang, C. Song et al., "Glaucocalyxin A reverses EMT and TGF-β1-induced EMT by inhibiting TGF-β1/Smad2/3 signaling pathway in osteosarcoma," *Chemico-Biological Interactions*, vol. 307, pp. 158–166, 2019.

[10] X. Liu, D. Xu, Y. Wang et al., "Glaucocalyxin a ameliorates myocardial ischemia-reperfusion injury in mice by suppression of microvascular thrombosis," *Medical Science Monitor*, vol. 22, pp. 3595–3604, 2016.

[11] W. Li, X. Tang, W. Yi et al., "Glaucocalyxin a inhibits platelet activation and thrombus formation preferentially via GPVI signaling pathway," *PLoS One*, vol. 8, no. 12, article e85120, 2013.

[12] M. Mao, T. Zhang, Z. Wang et al., "Glaucocalyxin A-induced oxidative stress inhibits the activation of STAT3 signaling pathway and suppresses osteosarcoma progression in vitro and in vivo," *Biochimica et Biophysica Acta - Molecular Basis of Disease*, vol. 1865, no. 6, pp. 1214–1225, 2019.

[13] X. Hou, G. Xu, Z. Wang et al., "Glaucocalyxin a alleviates LPS-mediated septic shock and inflammation via inhibiting NLRP3 inflammasome activation," *International Immunopharmacology*, vol. 81, article 106271, 2020.

[14] B. W. Kim, S. Koppula, S. S. Hong et al., "Regulation of microglia activity by glaucocalyxin-a: attenuation of lipopolysaccharide-stimulated neuroinflammation through NF-κB and p38 MAPK signaling pathways," *PLoS One*, vol. 8, no. 2, article e55792, 2013.

[15] S. Zhu, J. Zhang, and Y. Lv, "Glaucocalyxin a inhibits hydrogen peroxide-induced oxidative stress and inflammatory response in coronary artery smooth muscle cells," *Clinical and Experimental Pharmacology & Physiology*, vol. 47, no. 5, pp. 765–770, 2020.

[16] M. Scotece, J. Conde, V. Abella et al., "Oleocanthal inhibits catabolic and inflammatory mediators in LPS-activated human primary osteoarthritis (OA) chondrocytes through MAPKs/NF-κB pathways," *Cellular Physiology and Biochemistry*, vol. 49, no. 6, pp. 2414–2426, 2018.

[17] T. Yoshimoto, N. Morishima, M. Okumura, Y. Chiba, M. Xu, and J. Mizuguchi, "Interleukins and cancer immunotherapy," *Immunotherapy*, vol. 1, no. 5, pp. 825–844, 2009.

[18] M. Bujak and N. G. Frangogiannis, "The role of IL-1 in the pathogenesis of heart disease," *Archivum Immunologiae et Therapiae Experimentalis (Warsz)*, vol. 57, no. 3, pp. 165–176, 2009.

[19] S. B. Abramson, "Osteoarthritis and nitric oxide," *Osteoarthritis and Cartilage*, vol. 16, Supplement 2, pp. S15–S20, 2008.

[20] S. B. Abramson, "Nitric oxide in inflammation and pain associated with osteoarthritis," *Arthritis Research & Therapy*, vol. 10, Supplement 2, p. S2, 2008.

[21] D. Taskiran, M. Stefanovicracic, H. Georgescu, and C. Evans, "Nitric oxide mediates suppression of cartilage proteoglycan synthesis by interleukin-1," *Biochemical and Biophysical Research Communications*, vol. 200, no. 1, pp. 142–148, 1994.

[22] F. J. Blanco, R. L. Ochs, H. Schwarz, and M. Lotz, "Chondrocyte apoptosis induced by nitric oxide," *The American Journal of Pathology*, vol. 146, no. 1, pp. 75–85, 1995.

[23] A. M. Badger, A. K. Roshak, M. N. Cook et al., "Differential effects of SB 242235, a selective p38 mitogen-activated protein kinase inhibitor, on IL-1 treated bovine and human cartilage/chondrocyte cultures," *Osteoarthritis and Cartilage*, vol. 8, no. 6, pp. 434–443, 2000.

[24] C. Tu, Y. Ma, M. Song, J. Yan, Y. Xiao, and H. Wu, "Liquiritigenin inhibits IL-1β-induced inflammation and cartilage matrix degradation in rat chondrocytes," *European Journal of Pharmacology*, vol. 858, article 172445, 2019.

[25] X. Huang, Y. Xi, Q. Pan et al., "Caffeic acid protects against IL-1β-induced inflammatory responses and cartilage degradation in articular chondrocytes," *Biomedicine & Pharmacotherapy*, vol. 107, pp. 433–439, 2018.

[26] C. J. Malemud, "Inhibition of MMPs and ADAM/ADAMTS," *Biochemical Pharmacology*, vol. 165, pp. 33–40, 2019.

[27] N. Cui, M. Hu, and R. A. Khalil, "Biochemical and biological attributes of matrix metalloproteinases," *Progress in Molecular Biology and Translational Science*, vol. 147, pp. 1–73, 2017.

[28] E. E. Mehana, A. F. Khafaga, and S. S. El-Blehi, "The role of matrix metalloproteinases in osteoarthritis pathogenesis: an updated review," *Life Sciences*, vol. 234, article 116786, 2019.

[29] P. Verma and K. Dalal, "ADAMTS-4 and ADAMTS-5: key enzymes in osteoarthritis," *Journal of Cellular Biochemistry*, vol. 112, no. 12, pp. 3507–3514, 2011.

[30] J. P. Mitchell and R. J. Carmody, "NF-κB and the Transcriptional Control of Inflammation," *International Review of Cell and Molecular Biology*, vol. 335, pp. 41–84, 2018.

[31] M. C. Choi, Jo, Park, Kang, and Park, "NF-B signaling pathways in osteoarthritic cartilage destruction," *Cell*, vol. 8, no. 7, p. 734, 2019.

[32] J. A. Roman-Blas and S. A. Jimenez, "NF-kappaB as a potential therapeutic target in osteoarthritis and rheumatoid arthritis," *Osteoarthritis and Cartilage*, vol. 14, no. 9, pp. 839–848, 2006.

[33] E. X. Xue, J. P. Lin, Y. Zhang et al., "Pterostilbene inhibits inflammation and ROS production in chondrocytes by activating Nrf2 pathway," *Oncotarget*, vol. 8, no. 26, pp. 41988–42000, 2017.

[34] M. Karin and M. Delhase, "The IκB kinase (IKK) and NF-κB: key elements of proinflammatory signalling," *Seminars in Immunology*, vol. 12, no. 1, pp. 85–98, 2000.

[35] M. D. Jacobs and S. C. Harrison, "Structure of an IkappaBalpha/NF-kappaB complex," *Cell*, vol. 95, no. 6, pp. 749–758, 1998.

[36] J. Wu, X. Zhang, S. Hu, S. Pan, and C. Wang, "Polygonatum sibiricum polysaccharide inhibits IL-1β-induced inflammation in human chondrocytes," *Food Science and Technology*, 2021.